

# **PROCEEDINGS OF THE THIRTEENTH ANNUAL PACIFIC CLIMATE (PACLIM) WORKSHOP**

Asilomar, California — April 14-17, 1996

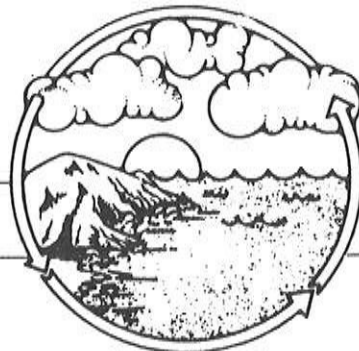
Edited by  
Caroline M. Isaacs and Vera L. Tharp

Technical Report 53  
of the  
Interagency Ecological Program  
for the  
Sacramento-San Joaquin Estuary

---

**PACLIM**

---



**Climate Variability  
of the  
Eastern North Pacific  
and  
Western North America**



## Sponsors

---

The Thirteenth Annual Pacific Climate Workshop is sponsored by:

The U.S. Geological Survey Global Change Program (Michael Carr)

The U.S. Geological Survey Water Resources Division (Harry Lins)

The U.S. Geological Survey Geological Research Division (Richard Poore)

The American Geophysical Union (A. F. Spilhaus, Jr.)

The State of California Department of Water Resources (Randy Brown)

The Naval Postgraduate School (Tom Murphree)

California State University, Monterey Bay (John Stamm)

Publication of this proceedings has been sponsored by the

INTERAGENCY ECOLOGICAL PROGRAM

for the

SACRAMENTO-SAN JOAQUIN ESTUARY

A Cooperative Program of:

California Department of Water Resources  
State Water Resources Control Board  
U.S. Bureau of Reclamation  
U.S. Geological Survey

California Department of Fish and Game  
U.S. Fish and Wildlife Service  
U.S. Army Corps of Engineers  
U.S. Environmental Protection Agency  
National Marine Fisheries Service

These proceedings were published by the Interagency Ecological Program for the Sacramento-San Joaquin Estuary (Interagency Program) in a cooperative effort with the United States Department of the Interior, Geological Survey, Menlo Park, California. Information generated by the PACLIM Workshop provides the Interagency Program with a climatological perspective that cannot be obtained from its own studies. Views and conclusions contained in this publication do not necessarily reflect the opinions of the Interagency Program or its member agencies.



# Contents

Sponsors . . . . .	iii
Authors . . . . .	vii
Acknowledgments . . . . .	ix
Statement of Purpose . . . . .	xi
Introduction . . . . . <i>Caroline M. Isaacs</i>	1
The Top Ten California Floods of the 20th Century . . . . . <i>Maurice Roos</i>	9
Daily Rainfall Along the United States Pacific Coast Appears to Conform to a Square-Root Normal Probability Distribution . . . . . <i>Raymond C. Wilson</i>	19
An Uncommon Period of Cold and Change of Lapse Rate in the Rocky Mountains of Colorado and Wyoming. . . . . <i>Mark Losleben</i>	33
Southern California's Megaflood Event of ca. 1605 AD Linked to Large-scale Atmospheric Forcing . . . . . <i>Arndt Schimmelmann, Carina B. Lange, Meixun Zhao, and Colin Harvey</i>	39
A Late-Holocene Pollen Record from Lower Pahranaagat Lake, Southern Nevada, USA: High Resolution Paleoclimatic Records and Analysis of Environmental Responses to Climate Change. . . . . <i>Peter E. Wigand</i>	63
Decadal Hydroclimatic Variability in the Western Coastal United States: Temporal and Spatial Variations in Precipitation, Streamflow, and Lake Level . . . . . <i>Hong-Chun Li and Teh-Lung Ku</i>	79
Monte Carlo Simulation of Streamflow of the Salt River, Arizona . . . . . <i>Marina Timofeyeva and Rachael Craig</i>	93
The Influence of Climate on Phytoplankton Communities in the Upper San Francisco Estuary . . . . . <i>Peggy W. Lehman</i>	105
Potential Solar Radiation at H.J. Andrews Experimental Forest, Oregon . . . . . <i>David Greenland</i>	121
Quantifying Global Terrestrial Carbon Influx and Storage as Stimulated by an Increase in Atmospheric CO <sub>2</sub> Concentration . . . . . <i>Yiqi Luo</i>	129
Long-Term Response of Torrey Pine to Coastal Climate: Precipitation, Temperature, and Fog. . . . . <i>Franco Biondi, Daniel R. Cayan, and Wolfgang H. Berger</i>	141

Tree-Ring Reconstructions of Winter Climate and Circulation Indices for the Southwestern United States. . . . .	161
<i>Connie A. Woodhouse</i>	
The Near-AD 1600 Multi-Proxy Puzzle . . . . .	169
<i>Franco Biondi, Carina B. Lange, Malcolm K. Hughes, and Wolfgang H. Berger</i>	
Some Perspectives on the Late Quaternary Paleoclimate of Beringia . . . . .	193
<i>Cary J. Mock and Patricia M. Anderson</i>	
Addendum I: Paleoclimate and the Solar-Insolation / Tidal-Resonance Climate Model. . . . .	201
<i>Thor Karlstrom</i>	

## **Abstracts**

---

Oral Presentations . . . . .	227
Poster Presentations . . . . .	241

## **Appendixes**

---

A	Agenda . . . . .	261
B	Poster Presentations . . . . .	267
C	Attendees . . . . .	271

## Authors

Patricia M. Anderson  
Quaternary Research Center  
University of Washington  
Seattle, WA 98195

Wolfgang H. Berger  
Geosciences Research Division  
Scripps Institution of Oceanography  
La Jolla, CA 92093-0215

Franco Biondi  
Geosciences Research Division  
Scripps Institution of Oceanography  
La Jolla, CA 92093-0215

Daniel R. Cayan  
Climate Research Division  
Scripps Institution of Oceanography  
La Jolla, CA 92093-0220  
619/534-4507  
dcayan@ucsd.edu

Rachel C. Craig  
Department of Geology  
Kent State University  
Kent, OH 44240  
330/672-7987; Fax 330/672-7949  
rcraig@geology.kent.edu

David Greenland  
Department of Geography  
University of Oregon  
Eugene, OR 97405  
503/346-4541  
greenlan@oregon.uoregon.edu

Colin Harvey  
Biogeochemical Laboratories  
Indiana University  
Bloomington IN 47405-1403  
812/855-7645

Malcolm K. Hughes  
Laboratory of Tree-Ring Research  
University of Arizona  
Tucson, AZ 85721

Teh-Lung Ku  
Department of Earth Sciences  
University of Southern California  
Los Angeles, CA 90089-0740

Carina B. Lange  
Scripps Institution of Oceanography  
Geological Resources Division  
9500 Gilman Drive  
La Jolla, CA 92093-0215  
619/534-4605

Hong-Chun Li  
Department of Earth Sciences  
University of Southern California  
Los Angeles, CA 90089-0740

Mark Losleben  
Mountain Research Station  
University of Colorado  
Nederland, CO 80466  
303/492-8841  
markl@culter.colorado.edu

Yiqi Luo  
Biological Sciences Center  
Desert Research Institute  
7010 Dandini Boulevard  
Reno, NV 89512  
702/674-7562  
yluo@maxey.dri.edu

Cary J. Mock  
Department of Geography  
University of Oregon  
Eugene OR 97403  
541/346-0466  
cmock@oregon.uoregon.edu

Maurice Roos  
California Department of Water Resources  
P.O. Box 942836  
Sacramento, CA 94236-0001  
916/574-2625

Arndt Schimmelmann  
Biogeochemical Laboratories  
Indiana University  
Bloomington IN 47405-1403  
812/855-7645

Marina Timofeyeva  
Department of Geology  
Kent State University  
Kent, OH 44240  
330/672-7987; Fax 330/672-7949  
mtimofey@geology.kent.edu

Peter E. Wigand  
Quaternary Sciences Center  
Desert Research Institute  
University and Community College System  
of Nevada  
P.O. Box 60220  
Reno, NV 89506  
702/673-7387  
pwigand@maxey.dri.edu

Connie A. Woodhouse  
818 County Road 116  
Nederland, CO 80466  
303/492-8841  
woodhous@cultur.colorado.edu

Meixun Zhao  
Department of Earth Sciences  
Dartmouth College  
Hanover, NH 03755-3571  
603/646-2150

Raymond C. Wilson  
U. S. Geological Survey  
345 Middlefield Road, Mail Stop 998  
Menlo Park, CA 94025  
415/329-4892  
rwilson@mojave.wr.usgs.gov

## Acknowledgments

---

The PACLIM workshops are produced by an array of enthusiastic volunteers. For 1996, thanks go to Don Gautier as the general workshop chairman, and to his able assistant Tim Klett for his multitudinous behind-the-scenes activities. Special thanks also go to Barb Johnson for registration at the meeting (and much other assistance), and Tom Murphree for providing the audiovisual equipment.

Sponsorship and funding for the workshops comes from a wide variety of sources. In addition to the agencies and programs responsible (listed separately), we also thank all those who helped in the funding process, including Michael Carr, Harry Lins, Dick Poore, Fred Spilhaus, and Randy Brown.

For the scientific agenda of the workshop, we thank the indomitable Dan Cayan, with secretarial assistance from Nicki Pyles and logistic support from Larry Riddle. Gary Sharp was also invaluable in rounding up speakers for the theme session and the evening session on the Salinas River Flood. The meeting chairs and moderators are also gratefully acknowledged — Dan Cayan, Caroline Isaacs, David Blackbourn, John Dracup, and Peter Wigand. Finally, we thank all our speakers and poster presenters for their contributions and enthusiasm — Michelle Wood, Genevieve Atwood, Arndt Schimmelmann, David Blackbourn, Tom Murphree, Jim Goodridge, Maurice Roos, Noah Knowles, Ray Wilson, Scott Stine, Dick Parrish, Nathan Mantua, Daniel Lluch-Cota, Frank Schwing, Bob Francis, Art Miller, Yiqi Luo, Charles Keeling, Kelly Redmond, Thomas Piechota, John McGowan, John Oliver, Lynn Ingram, Franco Biondi, Cary Mock, Lowell Stott, Peter Wigand, David Adam, Roger Anderson, Platt Bradbury, Daniel Cayan, Walt Dean, Patricia Dell'Arciprete, Stewart Fallon, Jim Gardner, David Greenland, Katherine Hirschboeck, David Jones, Thor Karlstrom, Carina Lange, Peggy Lehman, Jo Chiu-Fang Lin, Hong-Chun Li, Mark Losleben, Harry Rowe, Gary Sharp, Jacqueline Shinker, Leila Shiozawa, Jim Speer, Marina Timofeyeva, Amy Weinheimer, and Connie Woodhouse.

For the Proceedings volume, enormous thanks go to Vera Tharp for her patience with diverse format types and her incredible expertise with technical editing, graphics, tables, and highly skilled pasting. Invaluable precedents for the 1996 volume were established by the previous editors of the PACLIM Proceedings — Dave Peterson (1984-1988) with the able assistance of Lucenia Thomas, Julio Betancourt and Ana MacKay (1989-1990), and Kelly Redmond and Vera Tharp (1991-1993). Special thanks also go to all the authors who contributed.

Caroline Isaacs  
U.S. Geological Survey  
Menlo Park, California



## **STATEMENT OF PURPOSE**

### **Pacific Climate (PACLIM) Workshops**

---

In 1984, a workshop was held on "Climatic Variability of the Eastern North Pacific and Western North America". From it has emerged an annual series of workshops held at the Asilomar Conference Center, Monterey Peninsula, California. These annual meetings, which involve 80-100 participants, have come to be known as PACLIM (Pacific Climate) Workshops, reflecting broad interests in the climatologies associated with the Pacific Ocean and western Americas in both the northern and southern hemispheres. Participants have included atmospheric scientists, hydrologists, glaciologists, oceanographers, limnologists, and both marine and terrestrial biologists. A major goal of PACLIM is to provide a forum for exploring the insights and perspectives of each of these many disciplines and for understanding the critical linkages between them.

PACLIM arose from growing concern about climate variability and its societal and ecological impacts. Storm frequency, snowpack, droughts and floods, agricultural production, water supply, glacial advances, stream chemistry, sea surface temperature, salmon catch, lake ecosystems, and wildlife habitat are among the many aspects of climate and climatic impacts addressed by PACLIM Workshops. Workshops also address broad concerns about the impact of possible climate change over the next century. From observed changes in the historical record, the conclusion is evident that climate change would have large societal impacts through effects on global ecology, hydrology, geology, and oceanography.

Our ability to predict climate, climate variability, and climate change critically depends on an understanding of global processes. Human impacts are primarily terrestrial in nature, but the major forcing processes are atmospheric and oceanic in origin and transferred through geologic and biologic systems. Our understanding of the global climate system and its relationship to ecosystems in the Eastern Pacific area arises from regional study of its components in the Pacific Ocean and western Americas, where ocean/atmosphere coupling is strongly expressed. Empirical evidence suggests that large-scale climatic fluctuations force large-scale ecosystem response in the California Current and in a very different system, the North Pacific central gyre. With such diverse meteorologic phenomena as the El Niño-Southern Oscillation and shifts in the Aleutian Low and North Pacific High, the Eastern Pacific has tremendous global influences and particularly strong effects on North America. In the western United States, where rainfall is primarily a cool-season phenomenon, year-to-year changes in the activity and tracking of North Pacific winter storms have substantial influence on the hydrological balance. This region is rich in climatic records, both instrumental and proxy. Recent research efforts are beginning to focus on better paleoclimatic reconstructions that will put present-day climatic variability in context and allow better anticipation of future variations and changes.

The PACLIM Workshops address the problem of defining regional coupling of multifold elements, as organized by global phenomena. Because climate expresses itself throughout the natural system, our activity has been, from the beginning, multidisciplinary in scope. The specialized knowledge from different disciplines has brought together climatic records and process measurements to synthesize an understanding of the complete system. Our interdisciplinary group uses diverse time series, measured both directly and through proxy indicators, to study past climatic conditions and current processes in this region. Characterizing and linking the geosphere, biosphere, and hydrosphere in this region provides a scientific analogue and, hence, a basis for understanding similar linkages in other regions, as well as for anticipating the response to future climate variations. Our emphasis in PACLIM is to study the interrelationships among diverse data. To understand these interactive phenomena, we incorporate studies that consider a broad range of topics both physical and biological, time scales from months to millennia, and space scales from single sites to the entire globe.

An overview of the PACLIM Workshops was published in the December 30, 1986, issue of *EOS*.  
Proceedings of PACLIM Workshops are published annually by the  
California Department of Water Resources as Technical Reports of the  
Interagency Ecological Program for the Sacramento-San Joaquin Estuary.  
A multi-disciplinary collection of research papers, spawned at least partially by interactions in the  
initial PACLIM Workshops, was published as *AGU Geophysical Monograph 55* (Peterson, ed., 1989).

Caroline M. Isaacs

The Thirteenth Annual PACLIM Workshop was held at the Asilomar Conference Center on April 14-17, 1996. Attended by about 100 registered participants (see Appendix C, Attendees), the workshop included 27 talks and 26 poster presentations. The talks consisted of a one-day theme session of seven 45-minute talks and two featured evening talks (see Appendix A, Agenda). Throughout the remainder of the meeting were nearly 20 shorter, 20-minute presentations. Poster presenters gave a short 1-2 minute introduction to their posters, which were displayed during the entire meeting (see Appendix B, Poster Presentations).

All presenters were invited to expand their abstracts into a manuscript for inclusion in the Proceedings volume, and nearly all presentations are included in manuscript or abstract form. In this Proceedings volume, manuscripts are presented first, and abstracts of talks and then posters follow.

### **Workshop Theme — Unusual Events and Uncommon Episodes**

---

The 1996 PACLIM workshop focused on extremes — with a theme session entitled “Unusual Events and Uncommon Episodes”. Many of the presentations emphasized flooding. The societal impacts and predictive complexities of flooding were well-illustrated by Genevieve **Atwood**’s presentation (talk abstract, this volume) on the Great Salt Lake of Utah. After historical high lake levels in the 1870s, the Great Salt Lake retreated to persistently lower lake levels assumed to reflect increased consumptive use, and these low levels were used as a basis for development and planning. Then, after rising about 10 feet in the 1960s-1970s and a 4-year wet cycle in the drainage basin beginning in 1982, the lake rose rapidly to the level of the 1870s highstand. The cresting of the lake in 1986-1987 disrupted lifelines and industries on the lake and caused hundreds of millions of dollars in damage. To mitigate such damage in the future, Atwood outlines the scientific information needed by decision-makers, including (1) detailed knowledge of lake morphology to predict elevations where the level may stabilize, and (2) weather and wind patterns that locally cause lake set-up and wave run-up. Decision-makers also need to know (3) the expected highstand having a recurrence interval on the order of a hundred to several hundred years, and (4) how to tell when a 4- to 6-year wet cycle has begun. Because recurrence intervals cannot be determined from historical data, detailed study of shoreline morphology and sediment cores are needed to estimate these intervals from the paleohydrologic record. To be effective, then, research on Salt Lake flooding hazards requires study at a variety of spatial and temporal scales, with an interdisciplinary

mix of geomorphology, sedimentology, meteorology, climatology, and statistics — an excellent example of the PACLIM *modus operandi*.

In one of the featured evening sessions, John **Oliver** presented a brief account of an extensive interdisciplinary study by a group at Moss Landing Marine Laboratories and California State University, Monterey Bay, highlighting the Salinas River flood of 1995. This presentation retraced modifications to the drainage system over the last century, showing that much of the very damaging flooding in that year utilized natural flood control areas that had been modified in the 19th century and brought under cultivation or urbanized in recent decades.

In California, notable flood hazards result from short-term high precipitation events. Maurice **Roos** (paper, this volume) discusses the top ten major floods in California in the 20th century. Worst floods derive from the “pineapple connection” — slow-moving weather systems with long southwestern fetches over the ocean from Hawaii. One of the reasons that floods are a persistent predictive problem is the spatial variability of unusually high precipitation events. Based on daily rainfall records from 3000 stations, Jim **Goodridge** (talk abstract, this volume) reviews historical storms of California with extremely high precipitation, from the major flood of 1862 up to 1995. Rainfall events in excess of 10 inches/day are focused on the windward slopes of orographic barriers, but storm events with estimated return periods in excess of 1000 years were found to be distributed in a random spatial pattern over the entire state. Detailed maps of these historical storms are being published by the California Department of Water Resources (Goodridge, in press).

Short-term high precipitation events are a major cause of damaging landslides, as Ray **Wilson** graphically illustrated at the 1995 PACLIM workshop. For accurately predicting the frequency of extreme rainfall events, the probability distribution model assumed for precipitation is critical. Ray Wilson (paper, this volume) shows that although rainfall is usually modeled as a log-normal probability distribution, for Pacific coastal stations precipitation is predicted only fairly by that model ( $r^2 = 0.83-0.90$ ) and — of particular importance — deviates significantly at extremes. Precipitation in the Pacific coastal region actually conforms much better to a square-root normal probability distribution ( $r^2 = 0.98-0.99$ ). Wilson also shows how the square-root normal probability function neatly contrasts precipitation regimes related to different elevations and orographic features.

An uncommon 6-year episode of anomalously cold temperatures is the subject Mark **Losleben**'s study (paper, this volume) on Niwot Ridge in the Front Range, Colorado. The accuracy of the record is verified by comparison with temperature data at other sites, suggesting that the anomalously cold temperatures were confined to elevations above 3000 meters in a

restricted region north of 40°N and speculatively linked to the sequential occurrence of explosive volcanic eruptions 1981-1983. Dendrochronological studies indicate that such cold periods have been rare in the 20th century but were relatively common in the 19th century.

In addition to data from instrumental records, proxy records also yield rich evidence of unusual events and uncommon episodes in the paleoclimate record. For paleofloods, Arndt **Schimmelmann** and Carina **Lange** (paper, this volume) discuss evidence from Santa Barbara Basin varved sediment for a distinct flood deposit in AD 1605 ± 5 of major proportions, Southern California's "Flood of the Millennium". Comparing data from unusual events recorded in other regional studies (including evidence of a perennial lake at the terminus of the Mojave River and very high precipitation in the Santa Barbara area from tree-ring records) and global events (including severe flooding in Mexico City, evidence of a dense cluster of severe winters in northern Italy, and a large volcanic eruption in 1601), the authors speculate on aberrations in atmospheric circulation over North America that might have been responsible. **Hirschboek et al** (talk abstract, this volume) describe the Global Paleoflood Database Project, a project to compile existing paleoflood information, assemble a bibliographic database, and provide a communication forum on hydrologic extremes in the paleoclimate record.

Paleodroughts also receive considerable attention. Scott Stine (talk abstract, this volume) describes evidence from relict tree stumps of two major droughts in late Medieval time (AD 900-1120 and 1200-1350) throughout the Sierra Nevada in California. These droughts, corroborated by the dendroclimatic record in the Sierras, seem to have extended to the Rocky Mountains and the plains of Nebraska and eastern Colorado. Such a marked Medieval Climatic Anomaly in the western United States has major socio-economic implications for potential future hydrologic trends in this water-poor region. On a longer time scale, pollen studies by Peter **Wigand et al** (paper, this volume) from southern Nevada suggest numerous alternations over the last 4,000 years between wet and dry periods having rapid onsets and terminations. Compared to the rest of the late Holocene in the area, droughts have been much more severe in the last 2 ka, particularly during the period 1.9-1.6 ka (AD 100-400) and 0.9-0.3 ka (AD 1100-1700). During the pre-Holocene, Roger **Anderson** and Bruce **Allen** (poster abstract, this volume) discuss the generation of eolian and shoreline landforms resulting from desiccation of Lake Estancia in central New Mexico during the period of glacial termination and Younger Dryas climate episode (11,000-9,650 radiocarbon YBP). In the western Great Basin during the late glacial to deglacial period, **Lin et al** (poster abstract, this volume) date the timing of the last major pluvial event (16,500 YBP) and six distinct desiccation events (23-35,000 YBP) and correlate them with millennial-scale climates recorded by Dansgaard-Oeschger events in Greenland ice cores.

## **Hydrology, Climate, and Ocean-Atmosphere System**

---

Hydrology, climate, and the ocean-atmosphere system are examined at a variety of spatial and temporal scales. For streamflow modeling, Thomas **Piechota** and John **Dracup** (talk abstract, this volume) present a probabilistic streamflow forecast model for eastern Australia based on an optimal linear combination of climatology, persistence, Southern Oscillation Index phase, and Linear Discriminant Analysis forecasts. In Arizona, Marina **Timofeyeva** and Rachel **Craig** (paper, this volume) simulate streamflow for the Salt River drainage by Monte Carlo techniques, using a stochastic Local Climate Model (LCM) linked with a Snow and Surface Hydrology Model (SSHM). In California, Hong-Chun **Li** and Teh-Lung **Ku** (paper, this volume) analyzed streamflow variations for the past 90 years at 15 gauging stations, suggesting that variations in runoff are associated with ENSO at a decadal scale but not at an annual scale. Noah **Knowles** *et al* (poster abstract, this volume) present an intertidal simulation of current velocities and salinity in the San Francisco Bay on daily to interannual time scales and formulate a predictive scheme to forecast these properties from winter-spring runoff and snowpack.

Kelly **Redmond** (talk abstract, this volume) discusses spatial patterns of winter temperature and precipitation related to ENSO. Previously established spatial patterns show that positive summer/autumn SOI (Southern Oscillation Index) is followed by wet and cool winters in the Pacific Northwest and dry and warm winters in the Desert Southwest — with negative summer/autumn SOI followed by the opposite pattern. New data show that these patterns extend well into Mexico and western Canada, and that a relationship opposite (but weaker) to the Pacific Northwest relationship then extends along the Pacific coast from Queen Charlotte Island northward and westward. David **Jones** and Rachel **Craig** (poster abstract, this volume) present calibration by multiple linear regression analysis of a local climate model (LCM) for northwestern Mexico. Based on 252 stations for the period 1961-1985, the model successfully predicts mean monthly maximum and mean monthly minimum temperature but is less successful with temperature range and precipitation.

Dan **Cayan** and Larry **Riddle** (poster abstract, this volume) examine decadal variability of high elevation snow accumulation in the western United States from a set of 200 snow course records (1930s-1990). Much of the variability over these multi-year time scales is captured by two key patterns, centered in the Northwest and in the Southwest. Each of these is linked to distinct hemispheric-global scale patterns of atmospheric circulation and sea surface temperature (SST), indicating that snow accumulation contains a global climate signal.

---

## Fisheries, Marine and Estuarine Ecosystems

---

The complex relationships between climate and fish populations is discussed in a number of presentations, with an emphasis on the need for new principles for resource management. In the North Pacific, Richard **Parrish** (talk abstract, this volume) discusses variations of the Japanese and California sardine and mackerel fisheries and the North American albacore fishery, suggesting that population declines of major stocks are associated with basinwide regime changes affecting the productivity of feeding grounds. Based on assessment of populations of marine mammals, birds, and fish resources in the Bering Sea, Robert **Francis** (talk abstract, this volume) discusses new views on sequential changes in marine ecosystems and new principles implied for fishery management. In the Gulf of California, where the Mexican sardine fishery increased tenfold from the mid-1970s to late 1980s and then collapsed, Daniel **Lluch-Cota et al** (talk abstract, this volume) relate increases in the sardine population to low levels of upwelling activity and a sustained decrease in sea surface temperature. In the northeast Pacific, Nathan **Mantua et al** (talk abstract, this volume) compare salmon production in 10 geographical regions with climate variability, showing coherence between some regions and linkages with Pacific-wide SST and atmospheric circulation including warm and cold ENSO years. Off British Columbia, David **Blackbourn** (talk abstract, this volume) examines the relationship between climate variability and the spawning of salmon species.

In the estuarine environment, Peggy **Lehman** (paper, this volume) discusses the relation between biologic community composition and climate variables for the upper San Francisco Bay estuary during 1975-1993, when physical, chemical, and phytoplankton data were collected monthly at 16 stations throughout the estuary. Long-term changes in chlorophyll *a* concentration and a shift in phytoplankton community composition mainly reflect interannual variation associated with water year type (wet, average, dry, critical), and covariance analysis suggests mechanisms by which climate contributes to long-term changes in phytoplankton communities.

---

## Land Vegetation and the Carbon Cycle

---

One of the most important impacts of climate and climate variability relate to land vegetation and the carbon cycle. Several studies detail these impacts for key plant species. Jacqueline **Shinker** and J.C. **King** (poster abstract, this volume) examine the chronology of the release of krummholz leaders in whitebark pine, which signals the change from shrub-like krummholz to upright tree forms. The study finds a sharp increase in stem releases in the Yosemite area during the late 1940s and early 1950s, corresponding to an increase in recorded June-August

temperature. Dendrochronological techniques are also used by Jim **Speer** *et al* (poster abstract, this volume) to identify defoliation events in ponderosa pine in the Deschutes National Forest. Leila **Shiozawa** and Rachel **Craig** (paper, this volume) use simulations of a Local Climate Model to link climate with growth and dispersal of saguaro in the Sonoran Desert.

In the H.J. Andrews Experimental Forest, a Long-Term Ecological Research site in central Oregon, David **Greenland** (paper, this volume) models seasonal variations in potential clear-sky radiation on a closely spaced topographic grid to (1) estimate of heat energy input, (2) establish relationships between solar input and net primary productivity, and (3) identify areas of high potential for the initiation of forest fires. Spatial variability in potential radiation is found to be highest in February and seems to be associated with the presence of debris flows and zones of predominant tree species such as Pacific silver fir.

For the global carbon cycle, Yiqi **Luo** (paper, this volume) presents a global terrestrial carbon sequestration model based on (1) a leaf-level function found to be an invariant function of atmospheric CO<sub>2</sub> concentration, and (2) global mean residence time of photosynthetically fixed carbon. Luo's model estimates that the potential global terrestrial carbon sink is 2.5 times the "missing sink". Charles **Keeling** and T. **Whorf** (talk abstract, this volume) suggest that climate variability affects the global carbon cycle on all time scales that can be explored with existing records. On an interannual scale, they discuss evidence indicating that variations reflect imbalances between the uptake and release of CO<sub>2</sub> by vegetation and soils, which affect both the seasonally-adjusted concentration of atmospheric CO<sub>2</sub> and the amplitude of its seasonal cycle.

## **Proxy Records: Paleoclimate**

---

Dendrochronological proxy records are the focus of two presentations. Franco **Biondi** *et al* (paper, this volume) examine the underutilized Torrey Pine of Southern California to reconstruct climate parameters, and they present a 128-year chronology based on 28 increment cores from 17 trees. Using principal component analysis, tree growth was found to be not significantly related to temperature but highly and directly related to precipitation falling between the previous November and current April. At seasonal scale, tree growth was closely related only to winter and spring precipitation. Connie **Woodhouse** (paper, this volume) uses a network of 75 tree-ring chronologies located throughout the Southwest to reconstruct winter climate and circulation indices for the region over the last several hundred years. Results suggest that the 1800s included more dry extremes than either the 1700s or 1900s.

For the sediment record in southern California, Carina **Lange** *et al* (poster abstract, this volume) examine fluxes of biogenic debris from sediment traps deployed in the Santa Barbara Basin during August 1993-August 1994. For the last 100 years, Amy **Weinheimer** *et al* (poster abstract, this volume) focus on reconstruction of climate and circulation of the California Current System from radiolarian assemblages in the sediment record of the Santa Barbara Basin. Also in the Santa Barbara Basin, Franco **Biondi**, Carina **Lange**, *et al* (paper, this volume) examine variations in varve thickness over the last 1000 years using singular spectrum analysis. They find statistically significant oscillatory periods at ~100, ~58, ~25, and ~12 years and an abrupt change in frequency and amplitude of varve thickness near A.D. 1600. Lowell **Stott** (talk abstract, this volume) examines anoxic episodes inferred from the sediment record in the Santa Monica Basin, and Walter **Dean** *et al* (poster abstract, this volume) compare geochemical characteristics of Holocene sediments on the Peru and California margins.

Reconstructions of climate from coral aragonite are generally based on proxies such as  $\delta^{18}\text{O}$  and Sr/Ca ratios. Stewart **Fallon** *et al* (poster abstract, this volume) examines the use and reliability of a new proxy — the uranium/calcium ratio — for corals from Fiji and Hawaii 5-100 years old.

For the marine sediment record on longer time-scales, Lynn **Ingram** and James **Kennett** (talk abstract, this volume) discuss oceanographic circulation changes deduced from radiocarbon data in the Santa Barbara Basin sediment record over the last 20,000 years. Jim **Gardner** (poster abstract, this volume) correlates laminated sequences in late Pleistocene sediments deposited on the open continental slope off central California during the period 15,000-40,000 YBP. Pollen and lake-level evidence from Beringia (Alaska and eastern Siberia) are compared to results from General Circulation Models for the last 18,000 years by Cary **Mock** (paper, this volume). This comparative study suggests that synoptic climatic features such as the East Asian trough, Siberian high, and Pacific subtropical high may explain some spatially heterogeneous patterns observed in the proxy data.

Paleosecular variation of the geomagnetic field is the focus of sediment studies by Harold **Rowe** *et al* (poster abstract, this volume) on late Pleistocene Lake Estancia in New Mexico. David **Adam** and A. **Roberts** (poster abstract, this volume) present a new dating model for a 102-meter core from Butte Valley California — extending the core's coverage through the last 3 million years — and compare the pollen records with Tule Lake pollen records.

Synthesizing numerous proxy series, Karlstrom (1995, 1996) in previous papers at PACLIM workshops has presented detailed analyses of more

than 40 time series from the literature that appear to define cyclical elements of solar insolation/tidal resonance climate model. Thor **Karlstrom** (paper, this volume) presents an addendum comprising analysis of 20 or so additional proxy records of climate and volcanic time series. These range in length from 400 to 90,000 years and range spatially from Alaska to Tierra del Fuego, including records from both Old World and New World sites.

## Last Word

---

Finally, Gary **Sharp** (poster abstract, this volume) asks some fundamental questions about whether global warming is a bad thing — pointing out that humans have historically thrived during warm wet periods and suffered tremendous problems during cool, dry epochs — and reviews the many climate and ecosystem changes of the last two decades, including the 1976 regime shift (*eg*, Ebbesmeyer *et al* 1991), rise and fall of the Pacific sardine, warming and cooling of the Gulf of Alaska, *etc.* Looking back to PACLIM's AGU Monograph of 1989 (*eg*, Baumgartner *et al* 1989; Peterson 1989), Sharp exhorts PACLIM participants to update and review their datasets in view of more recent changes.

## References

---

- Baumgartner, T.R., J. Michaelsen, L.G. Thompson, G.T. Shen, A. Soutar, and R.E. Casey. 1989. The recording of interannual climatic change by high-resolution natural systems: Tree-rings, coral bands, glacial ice layers, and marine varves. Pages 1-14 in *Aspects of Climate Variability in the Pacific and the Western Americas*. D.H. Peterson, editor. Geophysical Monograph 55, American Geophysical Union, Washington, D.C.
- Ebbesmeyer, C.C., D.R. Cayan, D.R. McLain, F.H. Nichols, D.H. Peterson, and K.T. Redmond. 1991. 1976 step in the Pacific climate: Forty environmental changes between 1968-1975 and 1977-1984. Pages 115-126 in *Proceedings of the Seventh Annual Pacific Climate (PACLIM) Workshop, April 1990*. J.L. Betancourt and V.L. Tharp, editors. California Department of Water Resources, Interagency Ecological Studies Program Technical Report 26.
- Goodridge, J., in press, *Historic Rain Storms in California*: California Department of Water Resources.
- Karlstrom, T. 1995. A 139-year dendroclimatic cycle, cultural/environmental history, sunspots, and longer-term cycles. Pages 137-159 in *Proceedings of the Eleventh Annual Pacific Climate (PACLIM) Workshop, April 19-22, 1994*. C.M. Isaacs and V.L. Tharp, editors. California Department of Water Resources, Interagency Ecological Studies Program Technical Report 40.
- Karlstrom, T. 1996. The QBO, El Niño, and Tidal Resonance Model. Pages 241-253 in *Proceedings of the Twelfth Annual Pacific Climate (PACLIM) Workshop, May 2-5, 1995*. C.M. Isaacs and V.L. Tharp, editors. California Department of Water Resources, Interagency Ecological Studies Program Technical Report 46.
- Peterson, D.H., editor, 1989. *Aspects of Climate Variability in the Pacific and the Western Americas*. Geophysical Monograph 55, American Geophysical Union, Washington, D.C.

# **The Top Ten California Floods of the 20th Century**

---

Maurice Roos

The purpose of this paper is to summarize the biggest northern California floods of the 20th century. Flooding in California can occur from different causes. At least three types of floods occur:

- Winter general floods, which cover a large area.
- Spring and early summer snowmelt floods unique to the higher-elevation central and southern Sierra Nevada, which occur about once in 10 years on the average.
- Local floods from strong thunderstorms, with intense rain over a relatively small area. These originate in moist tropical or subtropical air and include the flash floods of the desert and other areas of southern California when remnants of eastern Pacific hurricanes get carried into the state.

In recent years, we have also seen intense cells develop at times in the warm sector of major winter storms. An example was the local flooding northeast of Sacramento during January 1995, when up to 6 inches fell in 24 hours.

## **Flood Factors**

---

The most feared flooding comes from general winter storms covering a wide area. These storms are slow moving, with a long southwesterly fetch extending toward Hawaii, the so-called "pineapple connection" (Figure 1). Often there is a near balance between a high pressure area to the south of California and a strong low pressure area off the northern California or Oregon coast. The greater the pressure difference, the stronger the southwesterly winds, which can reach speeds of 100 km/hr or more at 3000 meters over the San Francisco Bay area. The line of strongest air mass contrast, the frontal zone, can ripple back and forth several hundred kilometers but produces almost continuous rain to fairly high elevations over a broad zone in northern or central California (and less commonly in southern California). This warm southwesterly flow pattern is evident in practically all of our large general floods.

An important factor is the mountain barriers. As moisture-laden air is blown over mountains such as the Sierra Nevada, the air is lifted and cooled with additional rain and snow (Figures 2 and 3). Typically the

---

In: C.M. Isaacs and V.L. Tharp, Editors, 1997. *Proceedings of the Thirteenth Annual Pacific Climate (PACCLIM) Workshop, April 15-18, 1996*. Interagency Ecological Program, Technical Report 53. California Department of Water Resources.

orographic precipitation is 3 to 4 times the amount in the lowlands. For example, the 1600-meter elevation Blue Canyon weather station, northeast of Sacramento, averages around 1600 mm of precipitation per year, about 3.5 times the 450 mm expected at Sacramento, in the middle of the Central Valley. The multiplier ratio on some of the steeper ocean-facing mountain fronts of southern California can be even greater.

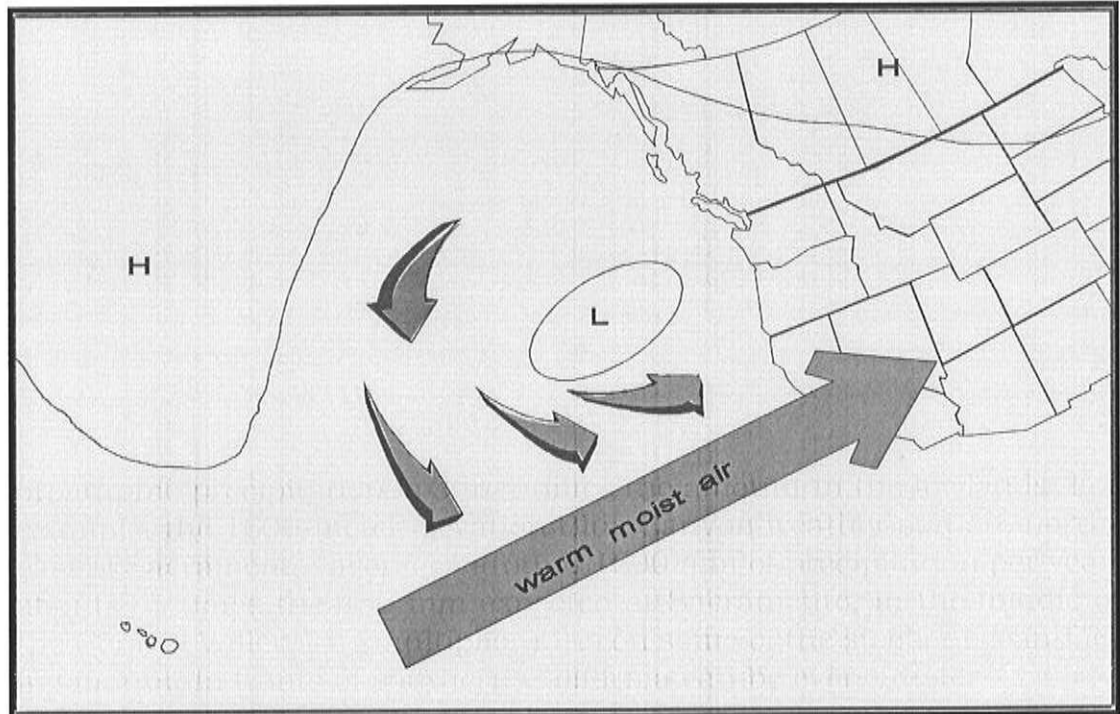


Figure 1. Warm Storm System

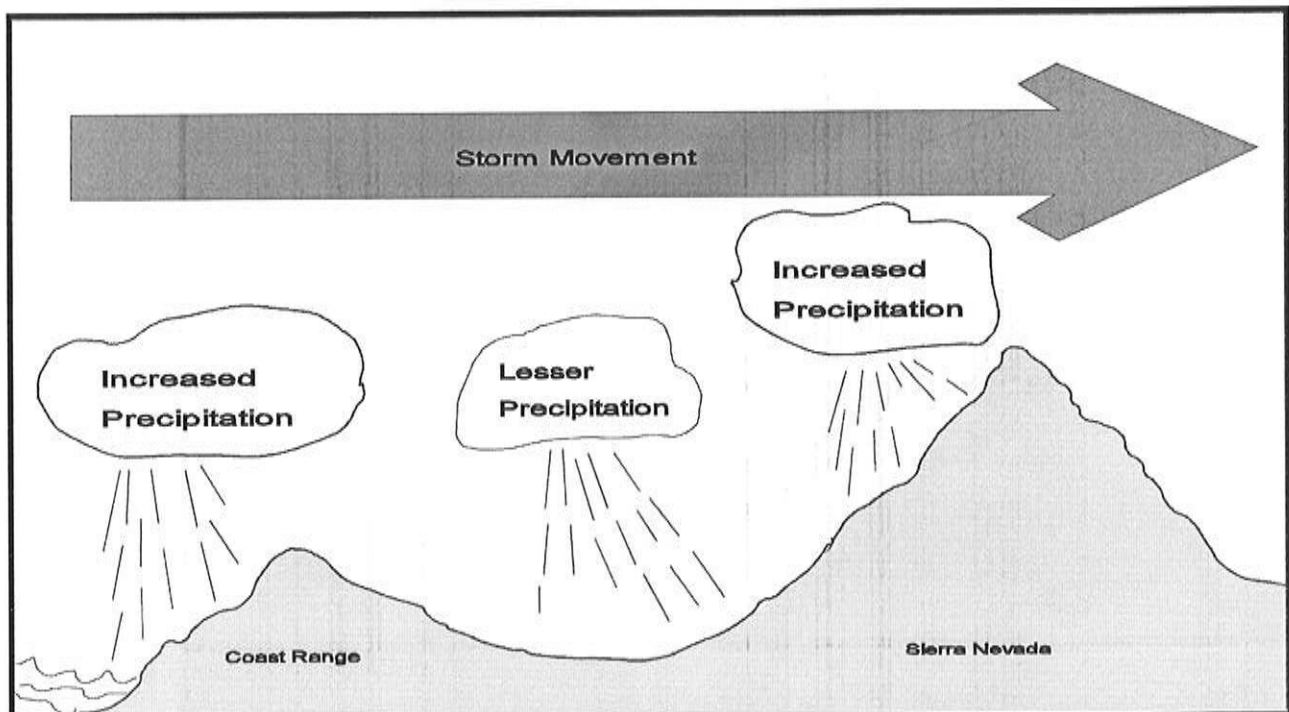


Figure 2. Orographic Precipitation

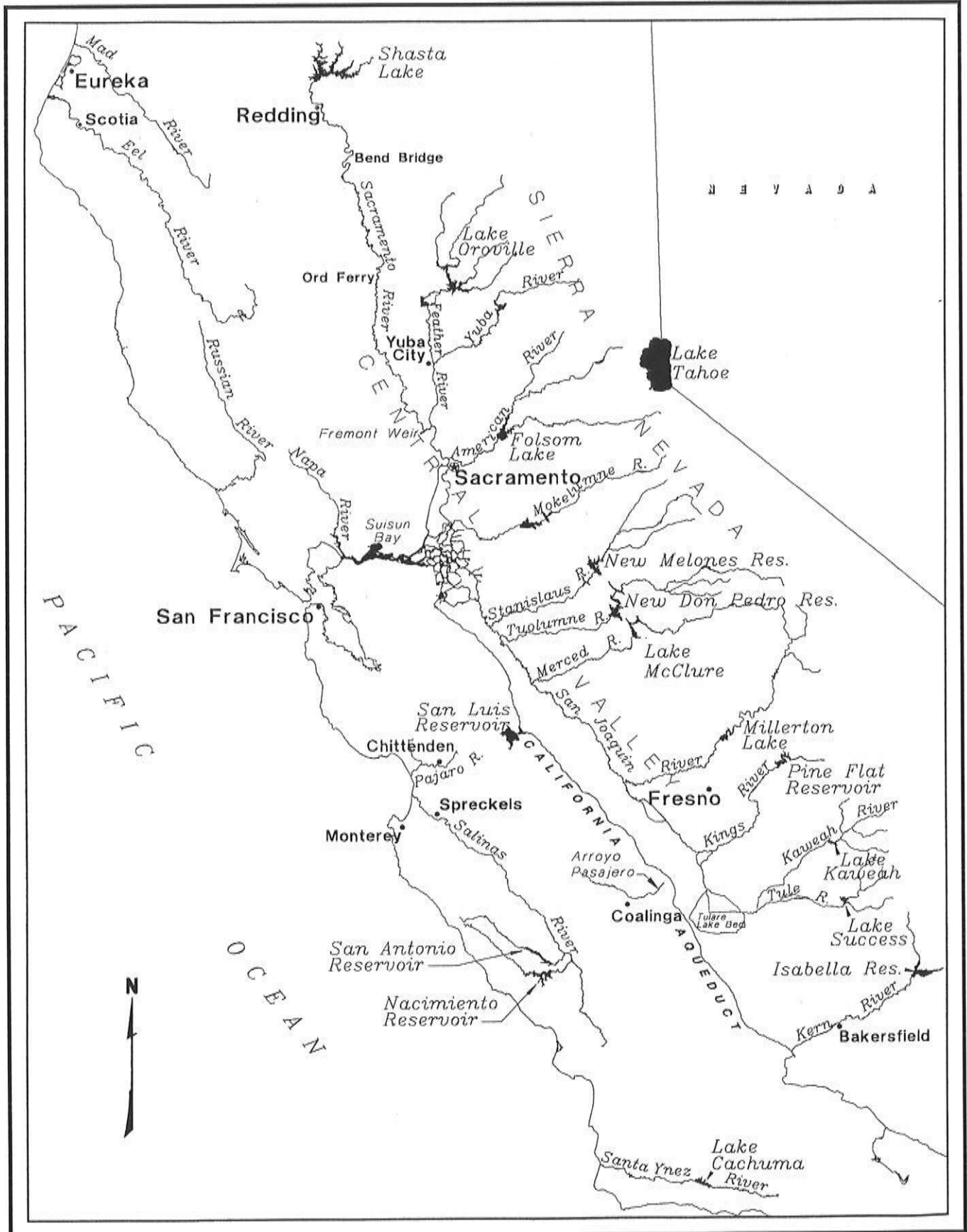


Figure 3. Major Rivers and Lakes in Northern and Central California

The direction of orographic wind flow is important. The greatest amount of water is extracted when the wind flow is at right angles to the mountain barrier, or from the southwest for the Sierra Nevada. A southerly wind direction does not produce such large amounts in the Sierra, but often concentrates precipitation at the north end of the Sacramento Valley, and even the normally rain-shadowed eastern slopes of the northern Coast Ranges if there is a small easterly component. Of course, many storms start out with a more southerly flow during the early phases and shift into a southwesterly and eventually westerly direction as the storm progresses. A west or northwest direction means the flood threat is passing for two reasons: cooler air has less moisture content; and cooler temperatures mean snow at lower elevations, which curtails direct runoff.

A lot of people think snowmelt is the cause of the flooding during the big southwesterly winter storms, but melting snow is only a small portion of runoff during these events, perhaps 10 to 15 percent. Most of the flow is direct rain runoff from intense rain falling to high elevations.

One other factor is necessary to produce large floods in northern California — wet ground, which requires antecedent precipitation. The most striking example is the Columbus Day storm of 1962. This storm produced rainfall comparable to “standard project flood” amounts<sup>1</sup>, yet runoff was less than a 10-year annual flood event because the rain fell on dry ground. It produced only a moderate flood, unusually early in the season, but not big enough to make the list of top ten floods.

Folks have generally underestimated the size of the flood threat in our rivers. An exception was John Sutter, who built his Sacramento fort on high ground after ascertaining from the Indians how high the water could get. The early pioneers mostly came from the humid east and just simply couldn't grasp that a river could expand 100 to 1,000 times its low-flow discharge. They just didn't recognize the risk; some say we still don't.

## **Flood History**

---

With that background let us look at some of the historic floods. The first is the big one of March 1907. It was a monster flood, with huge outflows of water from the mountains —beyond what anyone had experienced except the few old folks who could remember the legendary inundations of 1862, 45 years earlier.

There had been a 50-year debate over what to do for flood control in the Sacramento Valley. A smaller flood (about half as big as 1907) in 1904 was a wake-up call and stimulated much flood control planning activity. In 1905, in cooperation with the U.S. Geological Survey, the State of

---

1 Standard project flood refers to a return period of more than 1 in 200 years.

California began to put in stream gages to measure flow in the Central Valley. In 1904, a commission of leading river engineers was appointed, headed by Major T. G. Dabney, a distinguished U.S. Corps of Engineers engineer with 20 years experience in the lower Mississippi River. Relying on that experience, the Dabney Commission rejected the concept of bypasses and recommended that the Sacramento River be confined within levees (wider apart than the present ones) that would allow it to carry 250,000 cubic feet per second. The main river channel would then scour, helping to restore navigability. The report was published in 1905, and the “powers that be” set out to construct the plan as a joint local-state-federal project.

Then, in 1907, the flood struck. The Feather River burst out of its banks a few miles south of Oroville to rush southwesterly, north of Sutter Buttes, and poured into the Sacramento River above and below the town of Colusa, overwhelming levees and inundating much of the land between the Sacramento and Feather rivers. In all, 300,000 acres was flooded in the Sacramento Valley. By the time the Geological Survey got through analyzing its records, they found that about 600,000 cfs had poured out of the Sacramento River into Suisun Bay.

Two years later, in January 1909, another large flood reinforced this conclusion, with a comparable 3-day volume but not as high an instantaneous peak, at least on the Feather River. This record flood removed lingering doubts about the design flood for the Sacramento River Flood Control Project. It was fortunate that these floods happened before the Dabney Report’s project could be constructed; it would have been mostly wasted money.

A gifted engineer, Thomas H. Jackson, from the Corps of Engineers, became a leading spirit in the California Debris Commission. Captain Jackson and the Debris Commission got right to work and produced a new plan in 1910, which included overflow weirs and bypasses. This plan has become the Sacramento River Flood Control Project (Figure 4). At the latitude of Sacramento, it can handle about 600,000 cubic feet per second — 110,000 in the Sacramento River and 500,000 in the Yolo Bypass, with the design based largely on a blend of the 1907 and 1909 flood events. This design has served well, including the monster 1986 flood. Remember, however, that the plan did not include flood control reservoirs in the foothills — but was built to contain the largest expected flood — maybe about 50-year flood protection. The big flood control reservoirs were added later to further improve protection.

After 1909, no really big regional flood seems to have occurred until the 1950s. There was a moderate-sized flood in March 1928, another in December 1937, and again in late-February 1940. Those from San Diego County may remember the January 1916 floods, supposedly set off by rainmaker Charles Hatfield. Also, I believe 1938 was impressive in the coastal mountains of Los Angeles County.

But we have to move to water year 1951, specifically November 1950, to see a resurgence of heavy southwesterly-origin downpours. This storm was especially heavy in the southern Sierra (with 91,000 cfs peak flow on the Kings River east of Fresno) and was further impetus to complete the four Tulare Lake Basin flood control reservoirs from the Kings to Kern rivers: Pine Flat, Terminus (Lakd Kaweah), Success, and Isabella reservoirs (and also Folsom Reservoir on the American River near Sacramento). The 1950 storm was not particularly impressive in the northern Sacramento Valley. Pine Flat and Isabella dams were completed in 1954; Folsom in 1956 (but the dam was ready for flood control in 1955), and Success and Terminus dams were completed in 1961 and 1962.

As several of these new flood control projects became operational, an even larger flood was unleashed a few days before Christmas 1955. The storm ranged over most of the central and northern part of California from Bakersfield to the Oregon border. It was larger than the 1907 flood on the upper Sacramento and American rivers, but not quite as big on the Feather River. The North Coast was hit heavily, with the greatest flow of record (to that time), 541,000 cfs, on the Eel River. A break in the Feather River levee at Yuba City caused 38 deaths.

Nine years later, in December 1964, a still bigger flood hit. Again a large area was affected, from about Fresno northward into coastal Oregon. The runoff of the North Coast rivers was enormous, with a peak flow shooting past the 1955 record to around 750,000 cfs on the Eel River at Scotia. The area was devastated. Three-day runoff on the Feather River exceeded the 1907 peak and the nearly comparable 1955 peak, with a 3-day flow rate of 165,000 cubic feet per second, but the partially completed Oroville Dam reduced the peak and undoubtedly prevented severe flood damage in the Sacramento Valley.

Except for the December 1966 intense flood in the southern Sierra, most of the middle part of California had a respite for two decades. But 1969 was a very wet water year, with a large snowmelt flood on the San Joaquin River from a snowpack that was 210% of average statewide on April 1. Santa Barbara County also saw amazing record flows of 80,000 cfs on the Santa Ynez River near Lompoc in January of that year.

In January 1970 and the same month in 1974 we saw a pair of very large floods on the upper Sacramento River, with 3-day unimpaired flow rates exceeding 200,000 cfs near Red Bluff. These appear to be the largest floods of record here, slightly exceeding the December 1964 event and another large flood in 1940, and definitely more than the 1907 flood on which the system design was patterned. But these two floods were upper Sacramento floods and, although large, were not unusual on other northern California rivers.

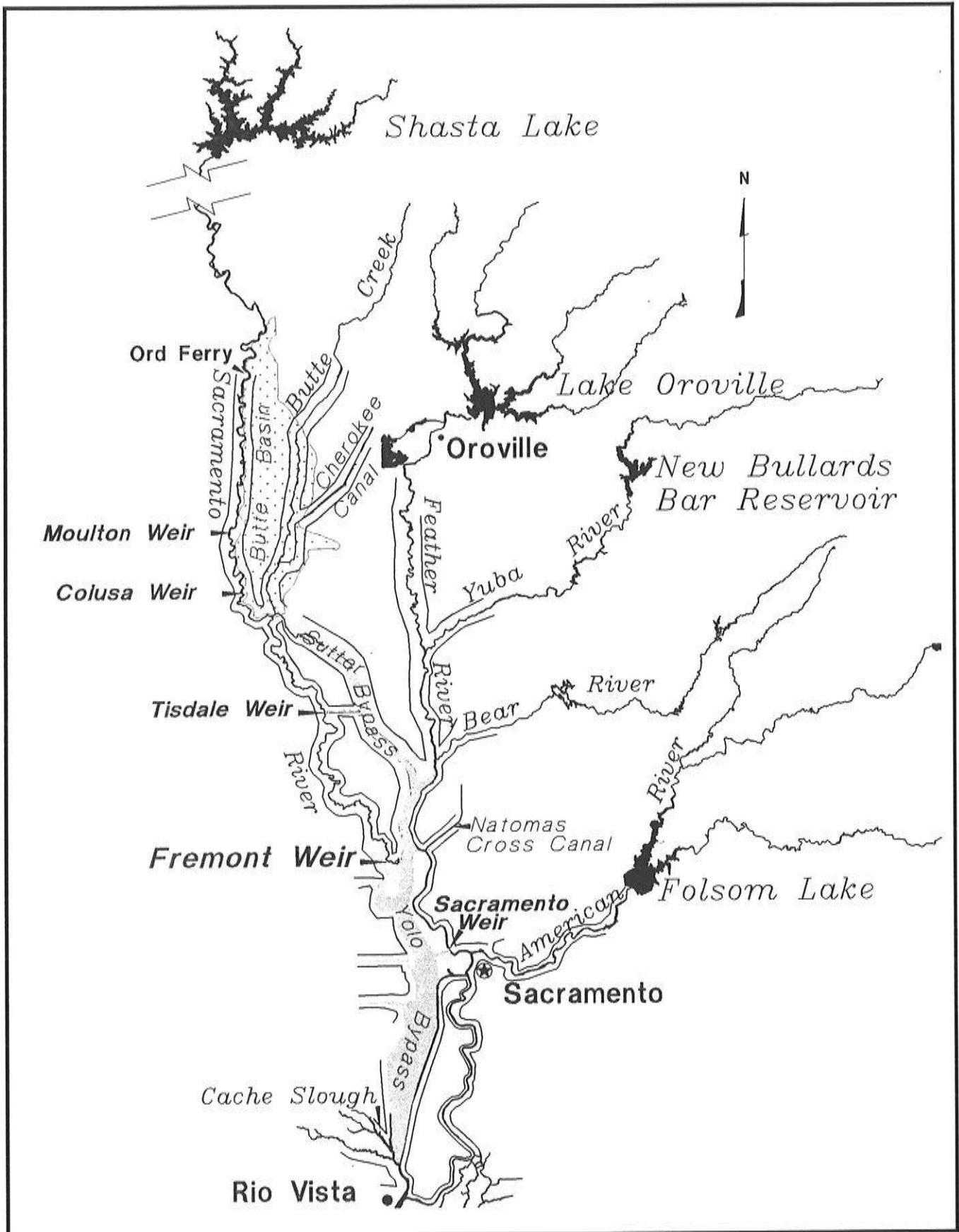


Figure 4. Sacramento River Flood Control System

Water year 1983 was the wettest this century, but did not produce any major river floods, although rivers ran high for an extended period. Once again, the high Sierra accumulated an enormous snowpack, over twice average. But shrewd operation of the reservoir system averted major snowmelt flood damage. Tulare Lake even became California's largest fresh water body again for a short time.

Now we come to the big one for the north-central part of California — the February 1986 flood. Until nearly the middle of February in that water year, conditions were a little drier than average. Then we got about a half-year's precipitation in 10 days. Again it was a classical warm, subtropical southwesterly flow situation. The heaviest rain areas were from the northern San Francisco Bay area across the central Sierra. Although flooding occurred on the North Coast and on the upper Sacramento River, floods were not unusually large in those regions. The Eel River, for example, peaked at 364,000 cfs. But the sheer volume of flow in the mid-Sierra from the Feather River on down through Mokelumne River was astounding, as shown by flood size comparisons (Figure 5). (The 3-day floodflow rate is shown because that time period better indicates the need for foothill reservoir flood control storage.)

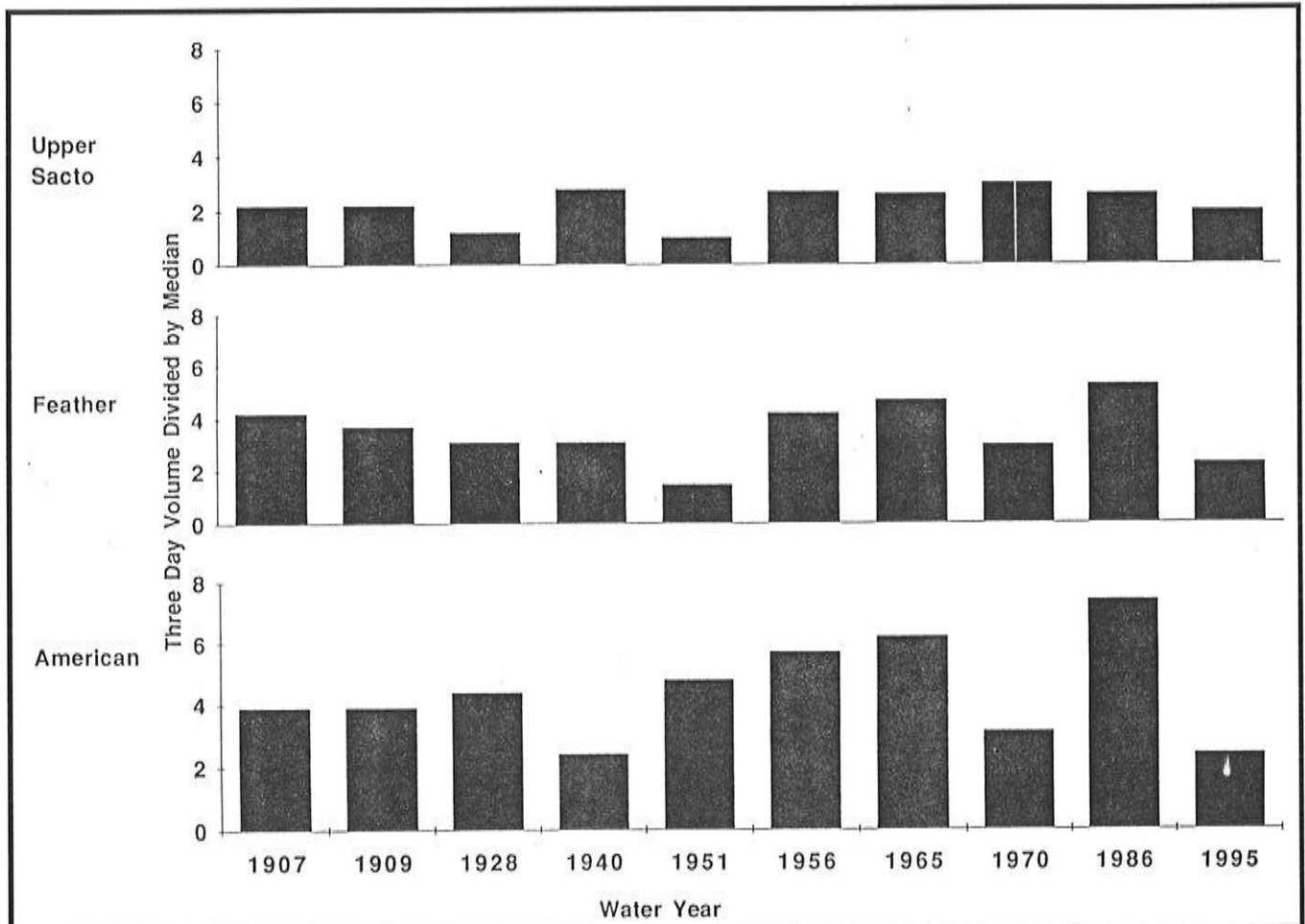


Figure 5. Comparison of Flood Sizes to Median

The lower Sacramento River floodway system was taxed to near design levels. In fact, Fremont Weir and Yolo Bypass stages actually went over design. Once again the American River was shown to be bigger than expected (Figure 6) leading to proposals for more flood control. A few hours more of the steady rain of 0.3 inch per hour on the watershed could have been disastrous to the Sacramento area.

From there, the scene shifted into drought, and it was 1995 before significant high water recurred. However, the 1995 floods were not that big on the major rivers of northern California, except near the coast. The Russian River approached its 1986 peak in January, and the Napa River reached a new peak of record in March. The real surprise was the Salinas River, which crested at 30.3 feet near Spreckels and exceeded the 1952 record of 26.2 feet by about 4 feet in March. This was within 1 or 2 feet of the estimated stage of 31 to 32 feet back in the legendary 1862 flood — long before Nacimiento and San Antonio dams were built. The Pajaro River, while exceeding its flood stage of 32 feet at Chittenden gage, did not quite reach the peak of record, 33.1 feet, set in 1958. Arroyo Pasajero flows near Coalinga, which collapsed the Interstate-5 crossing, probably were close to a 100-year event.

## **Conclusion**

---

There you have the 10 biggest California floods of this century. There seems to be a trend for bigger events. Is it real? We would like to be sure we are not under-designing, but large water and flood control projects are costly.

There are always strange quirks. Water year 1996 was not especially noteworthy in the flood department, mostly a “normal” year. But during a west-northwest flow pattern with relatively high pressure at the end of December 1995, we saw the Mad River near Arcata (in the Eureka area) rise above flood stage for the highest level since the big North Coast flood of 1964. Stay tuned, be alert, be prepared!

## **References**

---

- California Department of Water Resources. 1980. *California Flood Management: An Evaluation of Flood Damage Prevention Programs*. Sacramento.
- Kelley, Robert. 1989. *Battling the Inland Sea*. University of California Press, Berkeley and Los Angeles.
- U.S. Army Corps of Engineers. 1987. *Folsom Dam and Lake, American River, California, Water Control Manual*. Sacramento District, Sacramento.
- U.S. Army Corps of Engineers. 1996. *American River Watershed Project, California. Part I Main Report; Part II Final Supplemental EIS/EIR*. Sacramento District. Co-Sponsors: The Reclamation Board and Sacramento Area Flood Control Agency. Sacramento.

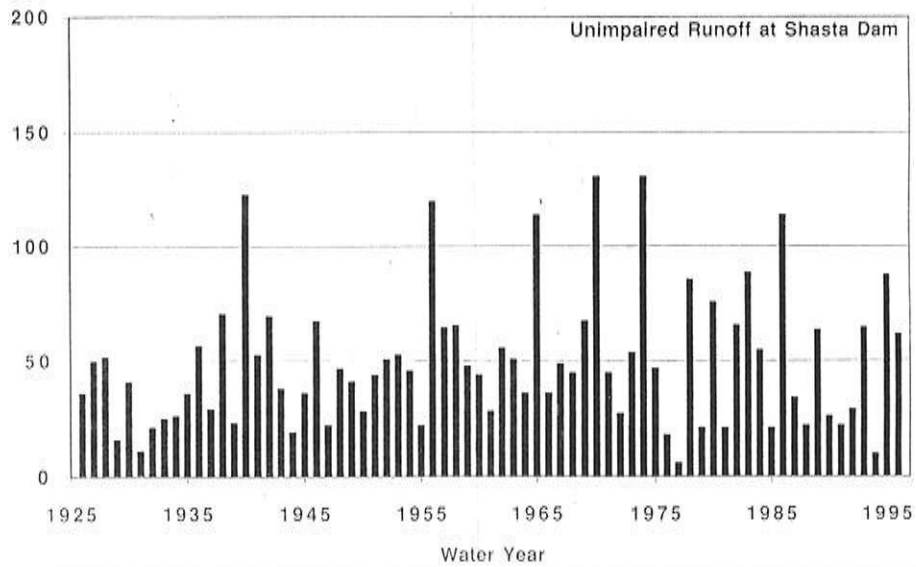
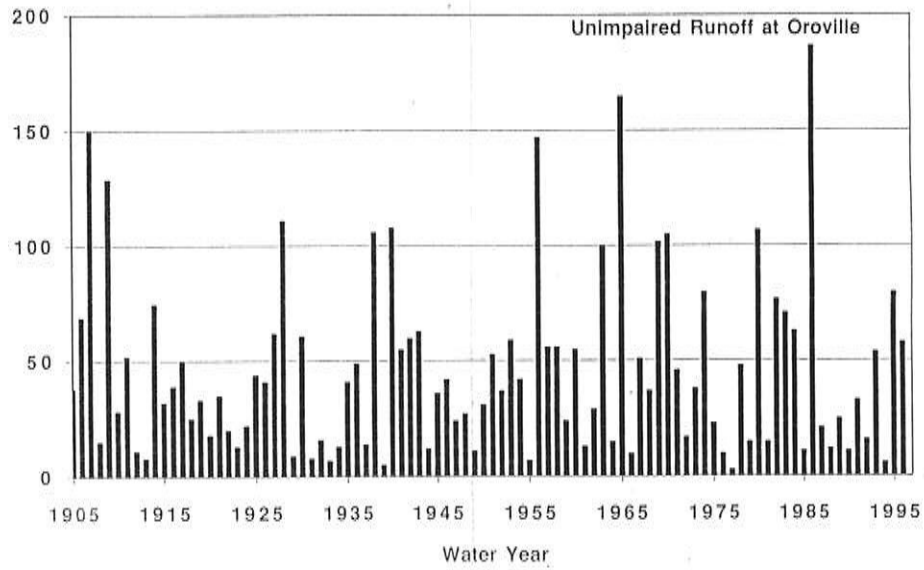
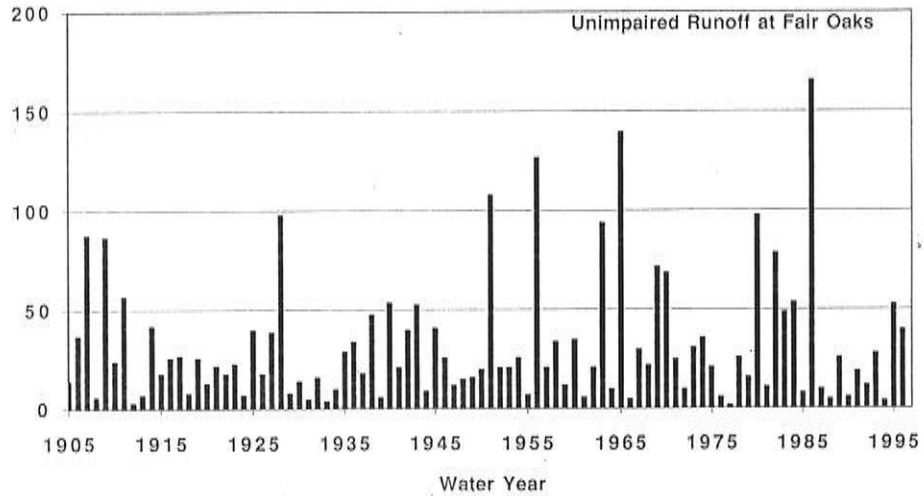


Figure 6. Annual maximum 3-day flow for the American River (top), Feather River (center), and upper Sacramento River (bottom).  
Flow is expressed as 1,000 cubic feet per second.

# Daily Rainfall Along the United States Pacific Coast Appears to Conform to a Square-Root Normal Probability Distribution

Raymond C. Wilson

**ABSTRACT:** As part of a study of climatic influences on landslide initiation, a statistical analysis of long-term (>40 years) records of daily rainfall from 24 Pacific coastal stations, from San Diego to Cape Flattery, disclosed an unexpected result — the square root of the daily rainfall closely approximates a normal distribution function. The fit from a square-root normal distribution is significantly better than that provided by the conventional log-normal distribution. This greater precision enables meaningful, quantitative comparisons of rainfall records from gauges in different locations and provides a sharper tool for delineating both spatial and temporal variations in precipitation. The paper illustrates the use of the square-root-normal distribution to analyze variations in precipitation along the mainland United States Pacific Coast with examples of orographic enhancement, rain shadows, and increase in precipitation frequency with geographic latitude.

## Introduction

In areas instrumented with rain gauges, the most common way to describe the precipitation climate is to calculate the mean annual precipitation (MAP), the total annual accumulation of rain (and snow) averaged over the years of record. For many applications dealing with the annual water budget, MAP is generally a sufficient description, although monthly means may be more useful in regions where rainfall is strongly seasonal, such as the west coast of the United States. The MAP alone, however, is insufficient for applications requiring a knowledge of the precipitation that can fall in a single storm, such as urban storm-water drainage design, flood control, and estimating thresholds for triggering debris flows (mud slides). While unsuitable for detailed description of individual storms, a long-term record of daily rainfall totals provides a description adequate to discern rainfall patterns on a climatological scale. This paper deals with an improved statistical description of the frequency distribution of daily rainfall at a gauged location.

I became interested in statistical rainfall models while studying debris flows triggered by heavy rains in California. Following the disastrous storm of January 3-5, 1982 (Ellen and Wiczorek 1988), rainfall thresholds for debris-flow initiation were developed in the San Francisco Bay region (Cannon and Ellen 1985) and used as the basis for a real-time warning system, operated by the U.S. Geological Survey and the National Weather Service (Keifer and others 1987) from 1986 until 1995. Because

In: C.M. Isaacs and V.L. Tharp, Editors. 1997. *Proceedings of the Thirteenth Annual Pacific Climate (PACCLIM) Workshop, April 15-18, 1996*. Interagency Ecological Program, Technical Report 53. California Department of Water Resources.

of the strong orographic gradients in the region, the threshold values were normalized by dividing by the MAP (Cannon 1988), and later (Wilson and others 1993), by the winter rainy day normal (RDN) — the mean monthly rainfall divided by the mean monthly number of days with >0.1 inch of rain (Barbato 1988).

While investigating the possibility of applying the rainfall/debris-flow thresholds to regions outside the San Francisco area, I realized that, although RDN and MAP are proportional within a limited area (<1° of latitude), they diverge for areas separated by greater distances (Wilson in press). Further, the storms that trigger hazardous debris flows, with return periods of a decade or more, represent the large, rare end-member of the magnitude spectrum; the bulk of the total rainfall, represented by the MAP, is supplied by the far smaller, far more frequent (10s of days/year) “normal” rainy days. Because the distribution of daily rainfall values has a marked asymmetry, an adequate description of the entire rainfall magnitude spectrum may require more than a simple arithmetic average like the RDN. Thus, whether one is dealing with debris flows, flash floods, or other “extreme storm” events, further development of predictive models will require a better statistical description of long-term rainfall distribution to accommodate significant differences in climate.

Mapping the climatology of precipitation depends on comparing and extrapolating rainfall records from one gauge to another. Rainfall records are complex and highly variable, both from gauge to gauge at a given time, or from one season to another at the same gauge. Meaningful comparisons, either spatial or temporal, have to be made on a common basis, with uniform standards over the entire field. On a practical level, this requires a rigorously defined, yet compact description wherein a complex historical record of rainfall values can be expressed with a minimum of precise, well-defined parameters. This is the role of the frequency distribution model.

## **Distribution Models for Daily Rainfall**

Frequency distributions portray the relative abundance of a large number of items of variable size in terms of a compact, idealized mathematical description. With only two parameters, for example, the classical normal, or Gaussian, distribution well describes many natural systems where most of the items fall within a relatively narrow range of a central value and become progressively less numerous with values that depart from the center, either above or below. The first parameter is the mean,  $\mu$ , which describes the “central tendency” of the population; the second, the standard deviation,  $\sigma$ , measures the decrease in frequency of occurrence above or below the mean.

A number of frequency distribution models have been used to describe precipitation, generally based on various adaptations of the normal distribution. If a particular collection of measurements does not appear to fit the normal distribution, a number of possible adaptation strategies may provide a satisfactory statistical description. One strategy is a mathematical transformation of the data, such as the log-normal distribution, where the logarithm of the variable fits a normal distribution. Another strategy is to relax the strict symmetry required by the normal distribution by using a more general mathematical form, such as the Pearson distributions.

Rainfall statistics may also be compressed by selecting a subset of the data, such as the peak rainfall recorded during the year. Selection of annual extremes is attractive for some purposes, such as debris-flow or flash-flood mitigation, where large, rare rainfall events are of principal interest. Several frequency distribution models have been used to describe extremal data, including the Gumbel and Pearson Type III distributions (Elderton 1953). For broadest utility, however, a climatological description should portray the entire spectrum of rainfall events, from the minimum measurable to the rainfall of record.

### **Limitations of the Log-Normal Distribution**

Along the U.S. Pacific Coast, the statistical distribution of daily rainfall values is highly asymmetrical. Many days of the year are completely dry and sunny, and those days with measurable rainfall tend toward relatively low values (0.01 to 0.25 inch). Yet, there is a small but significant number of days with relatively high rainfall (several inches). Because these rare, large storms supply an important fraction of the total annual rainfall, they cannot be ignored. While annual precipitation data are closely fit by the log-normal distribution and a logarithmic transformation helps correct some of the asymmetry in the daily rainfall data, some problems still remain.

As an illustration, plots of the frequency distribution of daily rainfall data for the San Francisco Mission Dolores rain gauge are shown in Figures 1 and 2. The data, shown as dots connected with heavy line, were derived from size-sorting 15,583 days of measurements, taken during a continuous period, 1948-1991. The plots are scaled so that a population of values derived from a normal distribution will plot as a straight line. (The X-axis, cumulative percentage, is actually a linear scale in probits, but is labeled in terms of absolute probability, %.) The intersection with the 50% (0 probits) line defines the median ( $\mu$ ), and the slope of the line defines the standard deviation ( $\sigma$ ), the two parameters that define the normal distribution.

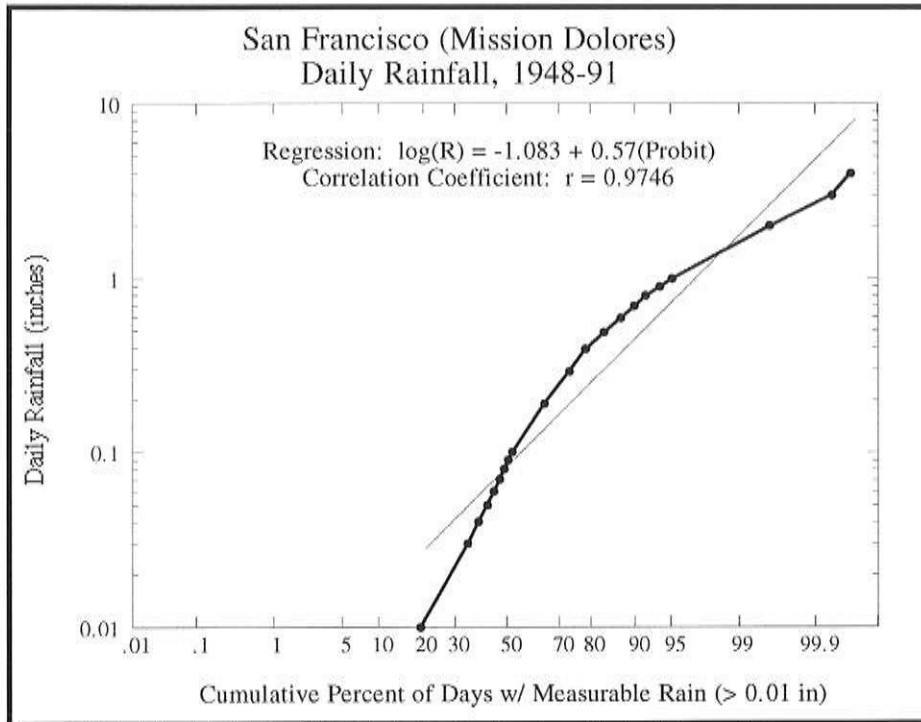


Figure 1. Probability plot of daily rainfall data for the San Francisco, Mission Dolores rain gauge.

Data from every day with measurable rainfall in the period 1948-1991 were sorted into size bins. The upper value of each bin was then plotted (dots connected with a heavy line) against the cumulative percentage of rainfall days in that and smaller bins. The X-axis is scaled so that a population of values derived from a normal distribution will plot as a straight line. The Y-axis is logarithmically scaled,  $\log(R)$ .

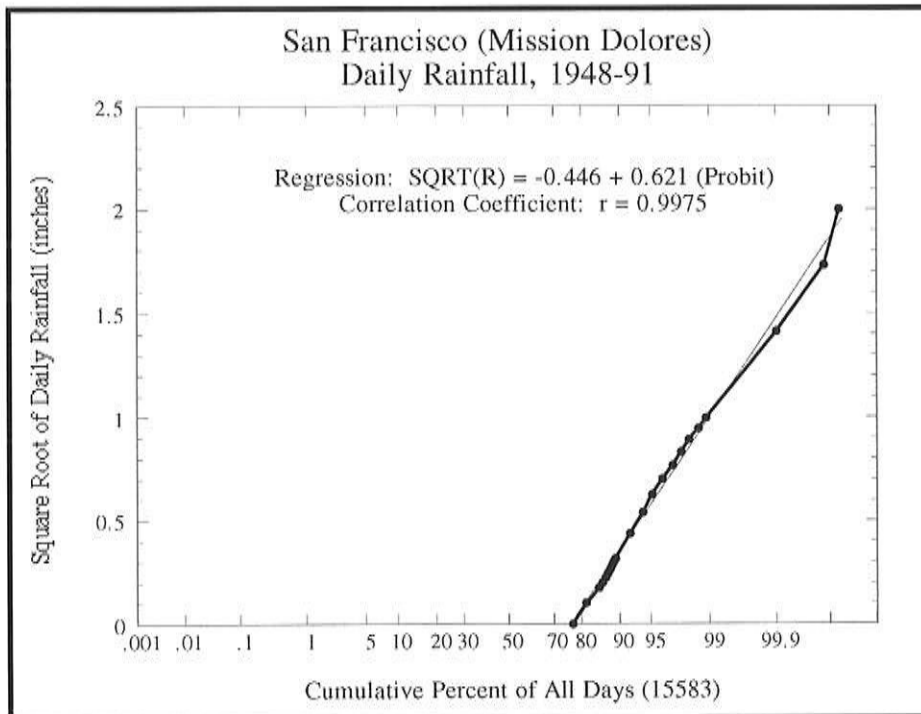


Figure 2. Probability plot of binned daily rainfall data for the San Francisco, Mission Dolores rain gauge.

The plot is similar to Figure 1 except that: (a) the square root of the upper limit of each rainfall bin,  $\sqrt{R}$ , is plotted against the cumulative percent (dots connected with a heavy line); and (b) all of the daily values, rainy or dry (zero), are included, a total of 15,583 days over the period 1948-1991. The lighter straight line is a least-squares linear regression to the data, yielding values for the mean,  $\mu = -0.446$  and standard deviation,  $\sigma = 0.621$ , of the square-root-normal distribution.

In Figure 1, the Y-axis is scaled to the logarithm of the daily rainfall (inches) and the straight line is the least-squares linear regression to the data, shown as solid circles. The correlation coefficient is high,  $r = 0.975$ , but the data appear to outline a distinctly curvilinear relationship, rather than the straight line assumed by the normal distribution. Also, because  $\log(0) = -\infty$ , there is no way to represent zero rainfall on dry days, so the number of days with measurable rainfall must be specified as a separate parameter, in addition to the log-normal frequency distribution.

**The Square-Root Normal Distribution**

In Figure 2, the Y-axis is defined as the square-root of the daily rainfall. Now, the data are closely fit by the least-squares straight line defining the square-root normal distribution (SQRND), as measured by the coefficient of determination,  $r^2=0.995$ , versus  $r^2=0.950$  for the log-normal distribution (Figure 1). Daily rainfall data from other gauges along the Pacific Coast also show excellent fits by the SQRND (Table 1).

Table 1  
DAILY RAINFALL DISTRIBUTION PATTERNS FOR 24 RAIN GAUGES  
ALONG THE PACIFIC COAST OF CALIFORNIA, OREGON, AND WASHINGTON

Station	Latitude	Longitude	Mean ( $\mu$ )	Standard Deviation ( $\sigma$ )	Goodness of Fit ( $r^2$ )	Number of Rainfall Days >0	MAP (inches)
<b>California</b>							
San Diego	32.73	117.17	-0.654	0.636	0.994	55.5	10.13
Los Angeles, LAX	33.93	118.40	-0.9395	0.798	0.994	43.7	11.46
Santa Maria	34.90	120.45	-0.563	0.608	0.991	64.7	12.01
Morro Bay	35.37	120.85	-0.573	0.6441	0.988	68.3	15.72
Big Sur State Park	36.25	121.78	-0.837	1.002	0.997	73.7	39.45
Santa Cruz	36.98	122.02	-0.606	0.787	0.994	80.8	29.72
Half Moon Bay	37.47	122.45	-0.509	0.709	0.998	86.3	26.42
San Francisco (MD)	37.77	122.43	-0.446	0.621	0.995	86.3	19.96
Kentfield	37.95	122.55	-0.838	1.05	0.996	77.7	49.18
Fort Ross	38.52	123.25	-0.447	0.7615	0.997	101.8	38.49
Point Arena	38.90	123.70	-0.463	0.788	0.996	101.8	40.50
Fort Bragg	39.50	123.78	-0.284	0.664	0.996	122.3	38.59
Eureka	40.80	124.17	-0.163	0.582	0.9989	141.0	38.66
Klamath	41.52	124.03	-0.212	0.817	0.996	145.2	81.25
<b>Oregon</b>							
Brookings	42.03	124.25	-0.095	0.716	0.997	163.3	78.72
Bandon	43.15	124.40	-0.0224	0.6003	0.998	177.2	59.22
Canary	43.92	124.03	0.116	0.575	0.9989	211.8	83.10
Newport	44.58	124.05	0.0875	0.5397	0.9991	206.2	68.03
Otis	45.03	123.93	0.1294	0.6066	0.9993	213.5	97.40
Astoria	46.15	123.88	0.142	0.487	0.9991	224.6	67.69
<b>Washington</b>							
Hoquiam	46.98	123.93	0.128	0.513	0.9996	218.6	70.32
Forks	47.95	124.37	0.179	0.671	0.9991	221.1	118.21
Neah Bay	48.37	124.62	0.148	0.602	0.997	218.1	104.34
Tatoosh Island	48.38	124.73	0.153	0.519	0.996	224.9	77.51

In addition to having long records, these gauges were chosen to be as close to the shoreline as possible to minimize disturbance of the marine storm systems by orographic effects and other inland processes. Values for  $\mu$  and  $\sigma$  describe the mean and standard deviation, respectively, for the square-root-normal distribution (SQRND) of daily rainfall for each gauge. Goodness-of-fit is measured by the coefficient of determination,  $r^2$ , the square of the correlation coefficient. Number of rainfall days >0 is derived from the SQRND (Figure 3). Mean annual precipitation (MAP) for each gauge is a simple average of annual rainfall totals.

Another distinction between the two plots concerns the definition of the X-axis. In Figure 1, the log-normal model, the X-axis is the cumulative percentage of days with measurable rainfall ( $R > 0.01$  inch), so that the proportion of rainy days to the total number of days must be determined separately. In Figure 2, the square-root normal model, the X-axis is the cumulative percentage, referenced to the total number of days — 365.25 days/year. The relative proportion of rainy days is determined by the point where the square-root-normal line intersects the X-axis (*ie*,  $R=0$ ). For San Francisco Mission Dolores, this intersection lies at 76.4%, which means that this proportion of days in San Francisco are dry. Rain falls on only 23.6% of the days (86.3 days/year) at this location. At this zero rainfall intersection, the probability, in probits, is determined by the ratio of the mean to the slope,  $\mu/\sigma$ , so that the frequency of rainy days is described by the SQRND relationship itself, not as an external parameter.

## Applications

### Estimating Precipitation Frequency

To illustrate the use of the SQRND to estimate the frequency of various levels of daily rainfall, a hypothetical SQRND was created with  $\mu = -0.3$  and  $\sigma = 0.6$ , values typical of the Sonoma coast in northern California. This SQRND is shown in Figure 3 as a plot of  $\sqrt{r}$  versus frequency.

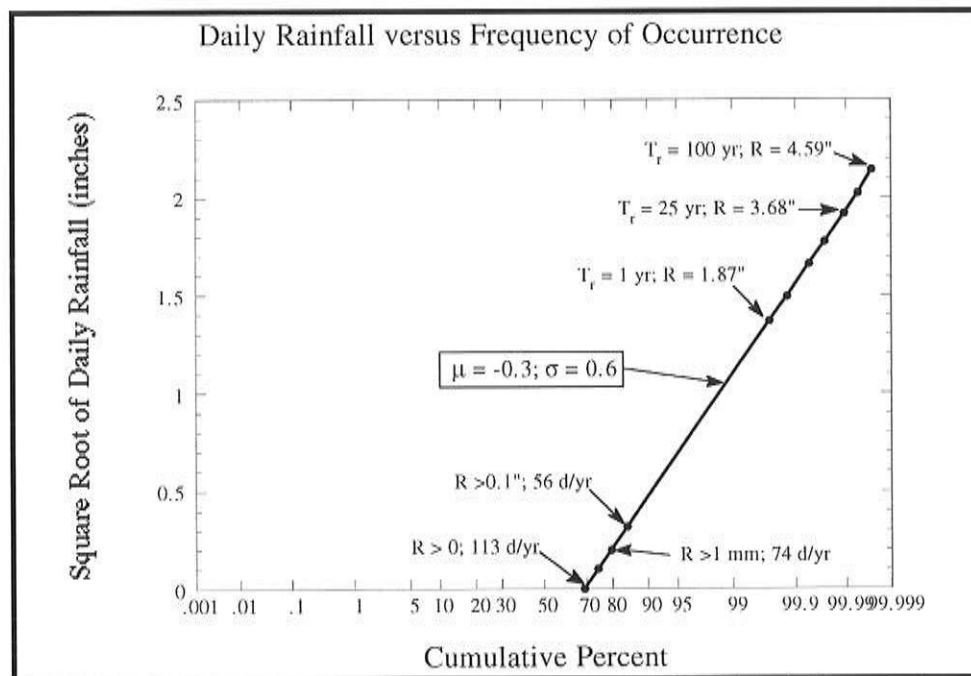


Figure 3. Illustration of the use of the square-root-normal distribution (SQRND) to estimate the frequency of occurrence of a given amount of daily rainfall.

The graph is a probability plot of a hypothetical rainfall record represented by a SQRND with a mean,  $\mu = -0.3$  and a standard deviation,  $\sigma = 0.6$ . The frequency of occurrence (X-axis) may be expressed as cumulative percent, days/year, or a return period in years, and is found by selecting a rainfall value, taking the square root, and using the plot to find the corresponding probability. The value of rainfall expected for a certain frequency or return period is found by the reverse procedure.

Rainfall frequency may be expressed in different ways, depending on which end of the frequency spectrum is examined. At the low-rainfall end of the plot, the frequency is high enough to be expressed in days per year. For the example in Figure 3, there are 113 days/year with some rainfall ( $R > 0$ ). However, the number of rainy days depends on the definition of minimum rainfall. Different agencies use different minimum rainfall amounts to measure precipitation frequency. In the United States, NOAA (eg, Baldwin 1973) defines a rainy day as  $R > 0.01$  inch (92 days/year in this case), some international entities use 1 mm (74 days/year), and in northern California, a “rainy day normal” is defined by the National Weather Service (eg, Barbato 1988) in terms of the number of days where  $R > 0.1$  in (56 days/year). In our example, therefore, only half the number of days with measurable rainfall ( $R > 0$ ) would exceed the 0.1 inch NWS standard.

Why not simply count the number of days with zero rainfall and subtract from the total number of days in the record? The problem is that standard rainfall measurements are subject to error at low rainfall values ( $< 0.1$  inch). Diurnal condensation (dew), radiation fog, and other effects may give “false positive” rainfall values. Virga, precipitation that is reabsorbed in the lower atmosphere before it reaches the ground, may give “false negatives.” Using a SQRND model, fit to the entire dataset, to back-calculate the number of days with non-zero rainfall, should produce a more stable result.

For high rainfall values, the frequency is low enough to be defined in terms of return periods, expressed in years. In our example in Figure 3, a 25-year return period (1 day in 25 years) corresponds to a rainfall of 3.68 inches, and a “100-year storm” would produce a daily rainfall of 4.59 inches. Because the frequency base is actually days, it is possible to define a 1-year storm, about 1.87 inches. These estimates are based on a statistical model calibrated from every day of rainfall in the record, not just the largest storm each year. Thus, SQRND magnitude estimates of the largest, rarest storms, needed for flood control design, urban storm-water management, and similar applications, are based on the entire precipitation record for the site.

### **Orographic Effects**

By comparing  $\mu$  and  $\sigma$  values for two or more rain gauge records, the SQRND model may be used to explore the processes by which Pacific storms are modified as they move inland. In Figure 4, coastal and upland gauges are compared to illustrate the effect of orographic enhancement. Data are plotted for two gauges near San Luis Obispo, California: Morro Bay, located near the coast at an elevation of 120 feet, and Santa Margarita Booster, located on Cuesta Ridge at an elevation of 1100 feet. Although the two gauges are only about 12 miles apart, Santa Margarita

Booster has nearly twice the mean annual rainfall (31.2 inches) as Morro Bay (15.7 inches). The two plots intersect the zero rainfall axis at the same place, indicating the two gauges have the same precipitation frequency. This is not surprising, given the close proximity of the two gauges relative to the large winter storm fronts that provide most of the precipitation in this area. However, the plot for the upland gauge, Santa Margarita Booster, has a significantly steeper slope, indicating a higher variance in daily rainfall so that, for a given frequency (or return period), the upland gauge will have a higher value of the square-root of the daily rainfall, thus a much higher value of the rainfall itself.

A simple interpretation of the plots in Figure 4 is that, at least in this location, orographic enhancement acts as a “linear amplifier” multiplying all rain systems, large and small, by a constant factor. While the ratio that determines the rainfall frequency,  $\mu/\sigma$ , remains equal for both the coastal and upland gauges, the  $\mu$  and  $\sigma$  values for the upland gauge are both equal to a common multiple of the corresponding  $\mu$  and  $\sigma$  values for the coastal gauge, increasing the rainfall at the upland gauge. In this case, the common multiple equals 1.41, which is very close to  $\sqrt{2}$ , so the net effect is to double all daily rainfall from Morro Bay to Santa Margarita — thus doubling the MAP. Similar linear amplification effects have been noted for a number of other rain gauge pairs.

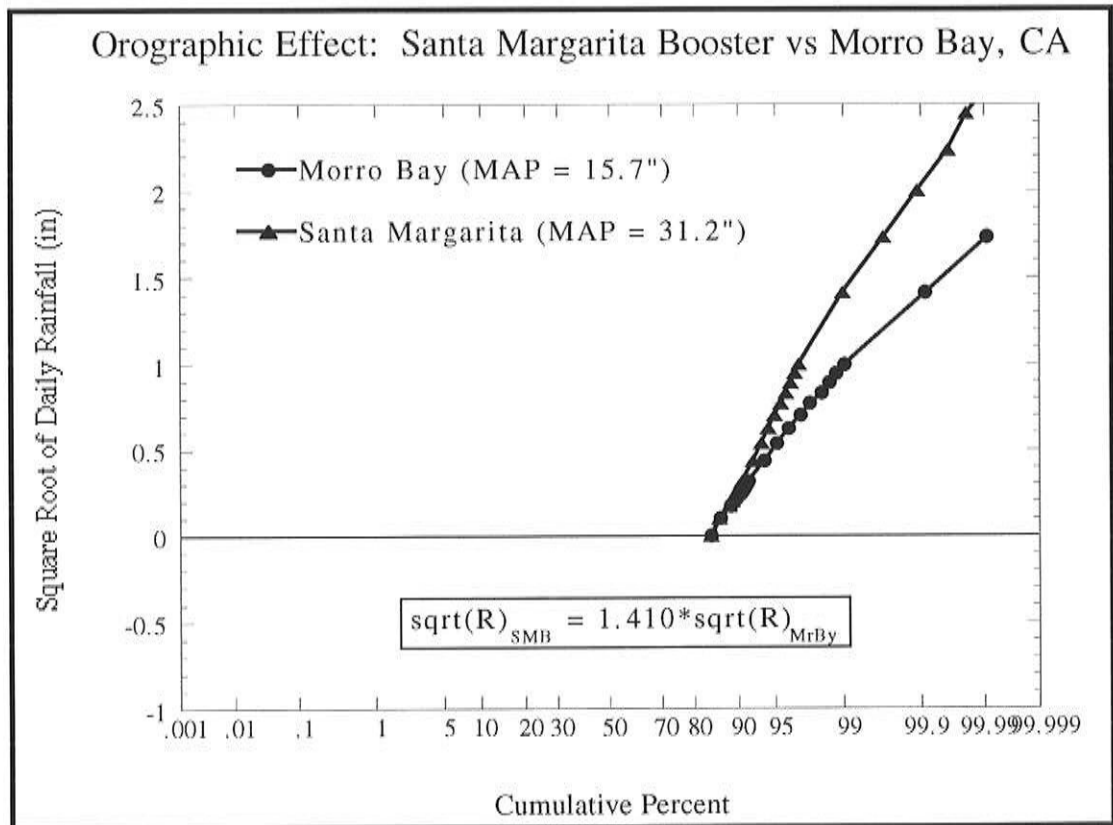


Figure 4. Illustration of the use of the SQRND model to examine the orographic enhancement of rainfall.

The probability plots compare data for a rain gauge, Morro Bay Fire Station, on the central California coast with data from the Santa Margarita Booster gauge on a ridgetop, 12 miles away. In this case, as summarized by the formula in the box, orographic enhancement acts as a “linear amplifier” that multiplies all storms, large and small, by a constant factor.

### Rain-Shadow Effects

By comparing rainfall distributions for coastal and inland sites, the SQRND model may also be used to investigate the “rain shadow” effect, the reduction of precipitation in the lee of a topographic ridge. In Figure 5, data is plotted for two rain gauges in central Oregon: Canary, near the coast, and Eugene (Airport) located in the Willamette Valley, some 42 miles to the ENE. The two gauges are both at low elevations, but they are separated by the Oregon Coast Range, with elevations up to 2500 feet. The two plots have similar slopes, and thus similar variances, but the plot for Eugene, the inland gauge, is offset to the right from Canary, the coastal gauge. This means that the inland gauge has a smaller precipitation frequency (160 days/year) than the coastal gauge (212 days/year), as well as a reduction in the MAP — 46 inches for Eugene versus 83 inches for Canary.

The principal effect of the rain shadow, at least in this location, appears to be to subtract a constant amount from all rainfall systems passing over the Oregon Coast Range (Figure 5, formula in box). I describe this as a “tollgate effect”, since the same “toll” is subtracted from each system, large or small, as it crosses the mountains. Large storms pass over the range with some reduction in yield, decreasing the MAP at inland gauges. Small rain systems that reach the coast with less than the critical amount

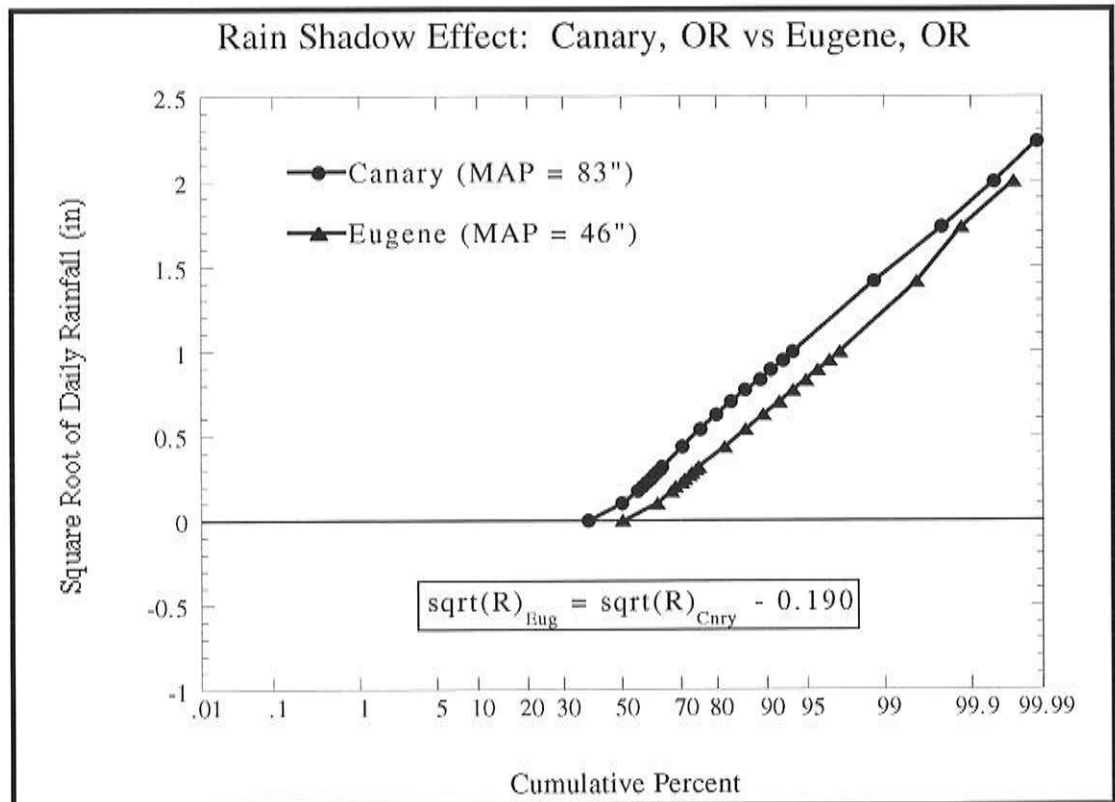


Figure 5. Illustration of the use of the SQRND model to examine the “rain shadow” effect.

Data are plotted for two rain gauges in central Oregon: Canary, near the coast, and Eugene (Airport) in the Willamette Valley, some 42 miles to the ENE. The formula in the box shows that, in this case, the net effect of the “rain shadow” is to subtract a constant amount from all storms, large or small, passing over the Oregon Coast Range.

of rainfall ( $\sqrt{r} < 0.19$ ) are blocked completely, thus reducing the rainfall frequency. In terms of the SQRND parameters, the rain shadow decreases  $\mu$ , but leaves  $\sigma$  unchanged, reducing both #RDs and MAP. Similar patterns have been noted for other areas, although variations in the  $\sigma$  parameter between the inland and coastal gauges are a frequent complication.

By showing the relative changes in the SQRND patterns, these comparisons reveal significant differences in the workings of orographic enhancement versus rain-shadow effects. In the simplest cases (Figures 4 and 5), the orographic effect involves a constant multiplier; the rain shadow effect, a constant decrement. These two effects may also be combined, of course, particularly where multiple mountain ranges and valleys are involved. The uneven distribution of wind directions during storms provides an additional source of variation because both orographic and rain shadow effects depend on the location of the site relative to topography and wind direction. In practice, it may be difficult to unravel the relative importance of orography, shadowing, and various other modifications at many inland gauge locations.

### **Precipitation Frequency versus Latitude**

That precipitation increases as one moves north along the U.S. Pacific Coast has long been known and is fairly obvious on national-scale precipitation maps (eg, Baldwin 1973, maps 20 and 21). Weaver and Denney (1964), for example, attempted to develop quantitative relationships between precipitation frequency, latitude, and distance inland for California. The National Weather Service Forecast Offices in California still rely on these relationships for their quantitative precipitation forecasts (Barbato 1988).

This regional variation of precipitation frequency with latitude was examined using the SQRND model as a tool. Daily rainfall data was collected from 24 gauges, scattered along the Pacific Coast from San Diego, California, to Tatoosh Island, Washington (Table 1), and analyzed to estimate  $\mu$  and  $\sigma$  values and the number of rainy days ( $R > 0$ ). In Figure 6, the precipitation frequency at each gauge was plotted against the geographic latitude of the gauge location. The plot shows a general increase in precipitation frequency with latitude from ~50 days/year in southern California to ~225 days/year in the Pacific Northwest. This relationship appears to "level off" near the northern (latitude  $> 46^\circ\text{N}$ ) and southern (latitude  $< 34^\circ\text{N}$ ) limits of the dataset. Between latitudes  $34^\circ\text{N}$  and  $46^\circ\text{N}$ , there is a strong, continuous gradient in precipitation frequency. This gradient appears to be associated with the mid-latitude storm track across the North Pacific, which recent satellite microwave precipitation measurements (Spencer 1993) portray as trending from south of Japan northeastward into the waters off British Columbia.

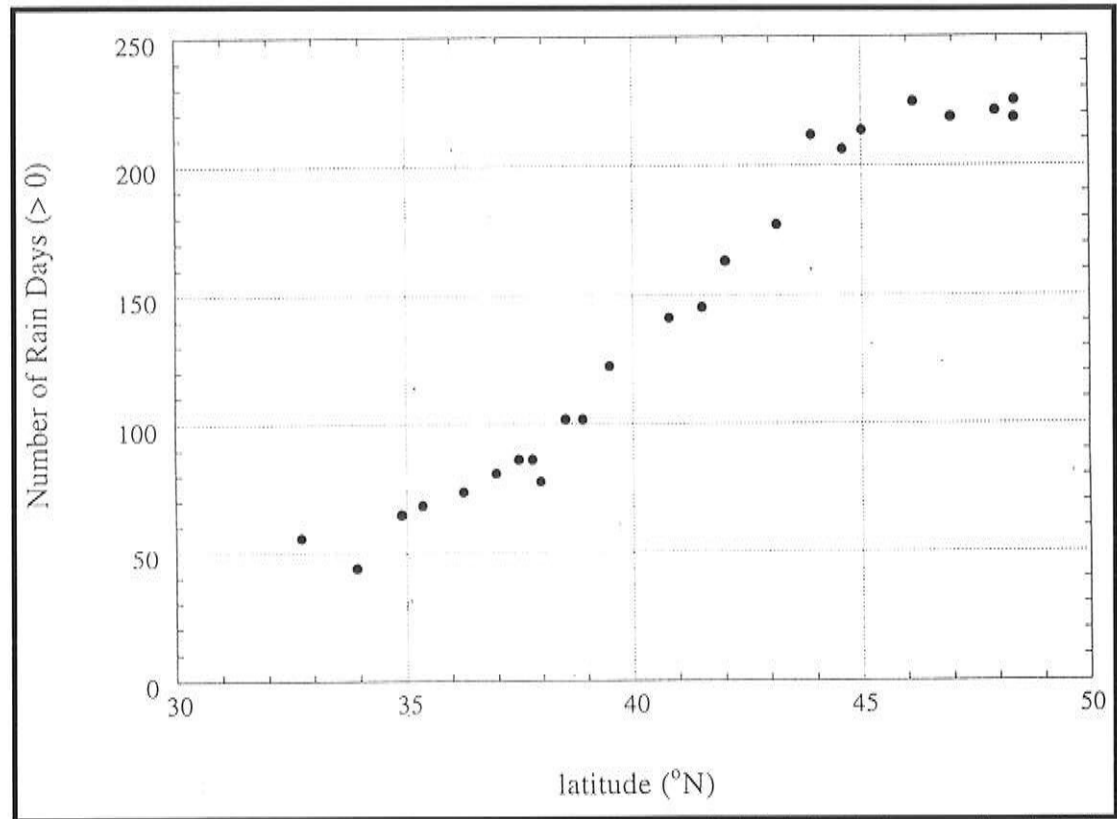


Figure 6. Plot of storm frequency, estimated from the SQRND, versus the geographic latitude, for 24 rain gauges along the Pacific Coast (Table 1).

The plot shows a general increase in storm frequency with latitude from ~50 days/year in southern California to ~225 days/year in the Pacific Northwest, with a steeper gradient between latitudes 34°N and 46°N.

## Discussion

### A Physical Mechanism?

At this time, the physical explanation for the square-root-normal frequency distribution of daily rainfall remains unknown. Assigning physical causes to statistical distributions is an awkward enterprise, at best. Originally developed to describe the distribution of errors in repeated measurements, a normal distribution can be produced by a summation process with many irregular additions (and subtractions). Similarly, many log-normal distributions result from a multiplication process with a series of irregularly varying factors. In both cases, the mean represents the net result of many, largely self-canceling, transactions and the variance represents the range of sizes of the perturbations.

One way to produce a square-root normal distribution is to take the product of two normally distributed variables. The two normal variables may be completely independent, indirectly correlated, or may represent a single variable multiplied by itself (squared). Although the two constituent variables may each result from numerous additions and

subtractions, the process involves only one multiplication between them. These conditions still provide a wide range of possibilities. Many alternatives exist, but plausible candidates for the constitutive variables include: (1) the atmospheric moisture content, perhaps related to the sea surface temperature, and (2) the vertical air motion, related to the distribution of barometric pressure. Further, even if the constituent normal variables could be identified, they may exert their influence on the rainfall at a point some distance upwind of the rain gauge site, making it difficult to obtain useful measurements.

### **Limitations**

The SQRND appears to function best for the cyclonic marine systems typical of winter precipitation along the U.S. Pacific Coast. It may perform less well in describing rainfall produced by other processes, such as the convective thunderstorms that produce much of the summer rainfall in the Midwest. Other problems may arise in areas where different precipitation mechanisms co-exist. Rainfall is produced on Oahu, Hawaii, for example, both by "Kona" storms associated with regional low-pressure systems, and "trade-wind" showers produced by local, diurnal wind and temperature cycles (Blumenstock and Price 1967). Rainfall records from Oahu produce concave plots of  $\sqrt{r}$  versus probability, rather than the straight lines predicted by the SQRND. Although it appears to be limited to describing a single, simple precipitation process, the SQRND model might provide a starting point for later work in more complex climatic situations.

### **Utility of the SQRND**

By allowing meaningful comparisons to be made between spatially related rain gauge records, the SQRND can reveal patterns that otherwise appear obscure. The orographic enhancement of precipitation depicted in Figure 4, for example, is seen to be a simple linear amplification process, whereas the rain shadow effect depicted in Figure 5 represents a constant decrement in rainfall. Precipitation frequency is shown to be strongly correlated with latitude (Figure 6), increasing northward from southern California (~50 days/year) to the Pacific Northwest (~225 days/year). Therefore, while its underlying physical mechanisms remain undetermined, the square-root normal distribution improves the ease and precision of the description of rainfall frequency distributions, compared to conventional methods, and provides a useful tool for mapping climatological variations in precipitation along the U.S. Pacific Coast.

### **Note Added in Review**

In his review of this manuscript, Dan Cayan (written comm., 10/96) called my attention to the previous work of C.K. Stidd. Stidd (1953) proposed a cube-root model for rainfall frequency distributions and speculated that this distribution resulted from the product of three normally distributed parameters: vertical motion, moisture content, and duration. Later, Stidd (1970, 1973) conducted computer simulation experiments intended to relate the cube-root normal distribution to the spectrum of atmospheric turbulence. Based on the cube-root model, Stidd (1968, 1973) built a comprehensive, quantitative model for the distribution of precipitation on time scales ranging from hourly to annual. While pleased to acknowledge this pioneering work, I must note that, after reanalyzing the daily rainfall datasets from West Coast rain gauges (Table 1) with both square-root and cube-root distribution models, I conclude that the square-root distribution model provides the superior description of the daily rainfall data on the West Coast.

### **References**

---

- Barbato, G.E. 1987. *Quantitative precipitation forecasting in northern and central California by the National Weather Service*. National Weather Service, Redwood City, CA, 9 pp.
- Baldwin, J.L. 1973. *Climates of the United States*. U.S. Department of Commerce, National Oceanic and Atmospheric Administration, Environmental Data Service, 113 pp.
- Blumenstock, D.I., and S. Price. 1967. Hawaii. in *Climates of the States*. Climatography of the United States No. 60-51, U.S. Department of Commerce, Environmental Science Services Administration, 27 pp.
- Cannon, S.H. 1988. Regional rainfall-threshold conditions for abundant debris-flow activity. in *Landslides, Floods, and Marine Effects of the Storm of January 3-5, 1982, in the San Francisco Bay Region, California*. S.D. Ellen and G.F. Wiczorek, editors. U.S. Geological Survey Professional Paper 1434, 310 pp.
- Cannon, S.H., and S.D. Ellen. 1985. Rainfall conditions for abundant debris avalanches, San Francisco Bay Region, California. *California Geology* 38:267-272.
- Elderton, W.P. 1953. *Frequency Curves and Correlation*. Fourth Edition, Harren Press. Washington, DC.
- Ellen, S.D., and G.F. Wiczorek. 1988. *Landslides, floods, and marine effects of the storm of January 3-5, 1982, in the San Francisco Bay region, California*. U.S. Geological Survey Professional Paper 1434, 310 pp.
- Keefer, D.K., R.C. Wilson, R.K. Mark, E.E. Brabb, W.M. Brown, S.D. Ellen, E.L. Harp, G.F. Wiczorek, C.S. Alger, and R.S. Zatkun. 1987. Real-time landslide warning during heavy rainfall. *Science*. 238:921-925.
- Spencer, R.W. 1993. Global oceanic precipitation from the MSU during 1979-91 and comparisons to other climatologies. *Journal of Climate* 6:1301-1326.
- Stidd, C.K. 1953. Cube-root-normal precipitation distributions. American Geophysical Union, *Transactions* 34:31-35.
- Stidd, C.K. 1968. A three-parameter distribution for precipitation data with a straight-line plotting method. American Meteorological Society, *Proceedings of the First Statistical Meteorological Conference* 158-162.

- Stidd, C.K. 1970. The nth root normal distribution of precipitation. *Water Resources Research* 6:1095-1103.
- Stidd, C.K. 1973. Estimating the precipitation climate. *Water Resources Research* 9:1235-1241.
- Weaver R., and W. Denney. 1964. *Normalized quantitative precipitation forecasting in California*. U.S. Weather Bureau Manuscript, for 230th National Meeting of the American Meteorological Society, 11 pp. (Available from National Weather Service Forecast Office, Monterey, CA.)
- Wilson, R.C. (in press). Broad-scale climatic influences on rainfall thresholds for debris flows: adapting thresholds for northern California to southern California. in *Effects of the 1992-93 Winter Storms on the Southwestern Cordillera*. R.A. Larson and J.E. Slosson, editors. Geological Society of America, *Reviews in engineering geology* 25 ms. pp.
- Wilson, R.C., R.K. Mark, and G.E. Barbato. 1993. Operation of a real-time warning system for debris flows in the San Francisco Bay area, California. Pages 1908-1913 in *Hydraulic Engineering '93*. H.W. Shen, S.T. Su, and F. Wen, editors. American Society of Civil Engineers, Hydraulics Division, Proceedings of the 1993 Conference, July 25-30, 1993, San Francisco, CA.

# An Uncommon Period of Cold and Change of Lapse Rate in the Rocky Mountains of Colorado and Wyoming

Mark Losleben

**ABSTRACT:** Temperature and lapse rate show extreme departures from mean values for May 1981 through October 1986 at the high-elevation station D1 on Niwot Ridge in the Front Range, Colorado. If the D1 record is accurate, this period may present an opportunity to identify factors that influence temperature at high elevations, but not necessarily at low elevations. This paper focuses on four questions: (1) Is the D1 temperature record accurate? (2) What is the geographical extent of this anomalous cold period? (3) Are there any identifiable contributing factors or physical events relating to this period? (4) Is there evidence of a similar anomalous period in the past? Review of temperature data from other sites supports the accuracy of the D1 record and suggests that this cold period occurred at elevations above 3,000 meters at latitudes north of Berthoud Pass, Colorado, or roughly 40°N latitude. Additional data suggest that temperatures at these high-elevation locations may be related to conditions in the lower stratosphere as well as extreme temperature anomalies in the eastern Pacific Ocean. A possible physical explanation for this cold event is the sequential occurrence of the explosive volcanic eruptions of Alaid in 1981, then El Chichon in 1982, followed by the strong El Niño event of 1982-83. Tree-ring width chronologies from a high-elevation northern Colorado site suggest that the frequency of such cold periods is rare in the 20th century but was relatively common in the 19th century.

## Introduction

The D1 climatological station is an alpine site at 3749 meters on Niwot Ridge, in the Front Range, Colorado, about 2 kilometers east of the Continental Divide and 27 kilometers west of Boulder and Longmont, Colorado (Figure 1). Annual temperature at D1 is variable, with a mean of  $-3.92^{\circ}\text{C}$ , standard deviation of  $1.10^{\circ}\text{C}$ , and no significant long-term trend ( $p < 0.40$ ).

Mean annual temperature (Figure 2) for 1982-1985 is 2.5 standard deviations less than the 45-year mean. The lapse rate, defined here as the temperature difference between D1 and Longmont as a function of elevation, increased more than 20% during this same period. An examination of records from several climate stations at lower elevations, just a few kilometers east of D1, including Longmont and Waterdale, indicate no similar decrease in temperature. Lapse rate changes are climatically important because they reflect changes in atmospheric water vapor, cloud cover, and atmospheric stability; all are factors in feedback processes involving precipitation and temperature.

Evaluation of temperature and geophysical data validate the D1 cold period and suggests the following working hypothesis: high-elevation temperatures in the northern Colorado/southern Wyoming Rockies are

inversely related to lower stratospheric temperature anomalies (LST) and atmospheric turbidity (TB) and directly related to the Southern Oscillation Index (SOI). Further, this relationship is enhanced when it occurs during the positive phase of the quasi-biennial oscillation (QBO).

## Data

Surface temperatures: The D1 and C1 data are from the University of Colorado, Mountain Research Station, Mountain Climate Program. Periods of record are 1951-1995 for D1 and 1953-1995 for C1. Other Colorado temperature data were provided by the Colorado Climate Center, Colorado State University, Department of Atmospheric Sciences. Wyoming temperature data were provided by the University of Wyoming, Wyoming Water Resources Center. The periods of record for the other Colorado and Wyoming data are variable and generally shorter than the D1 record length.

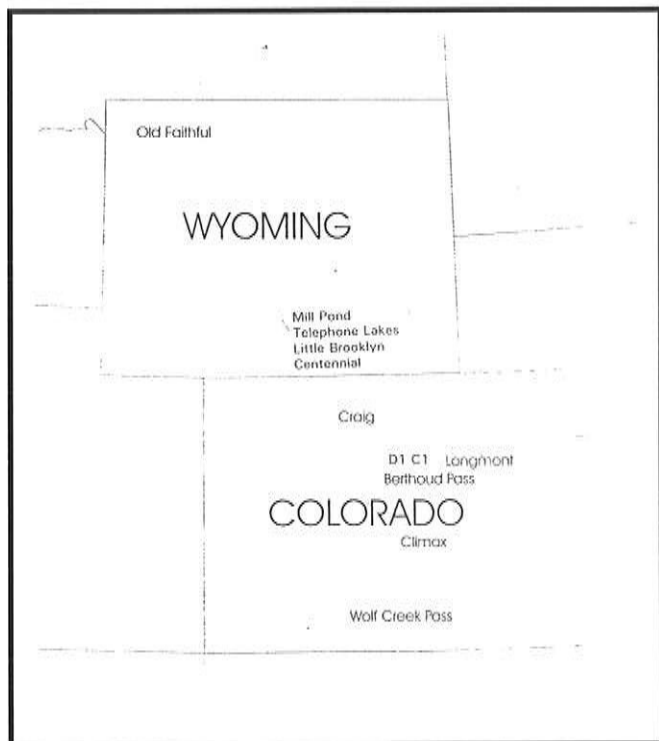


Figure 1. Map showing the areal extent of the cold period.

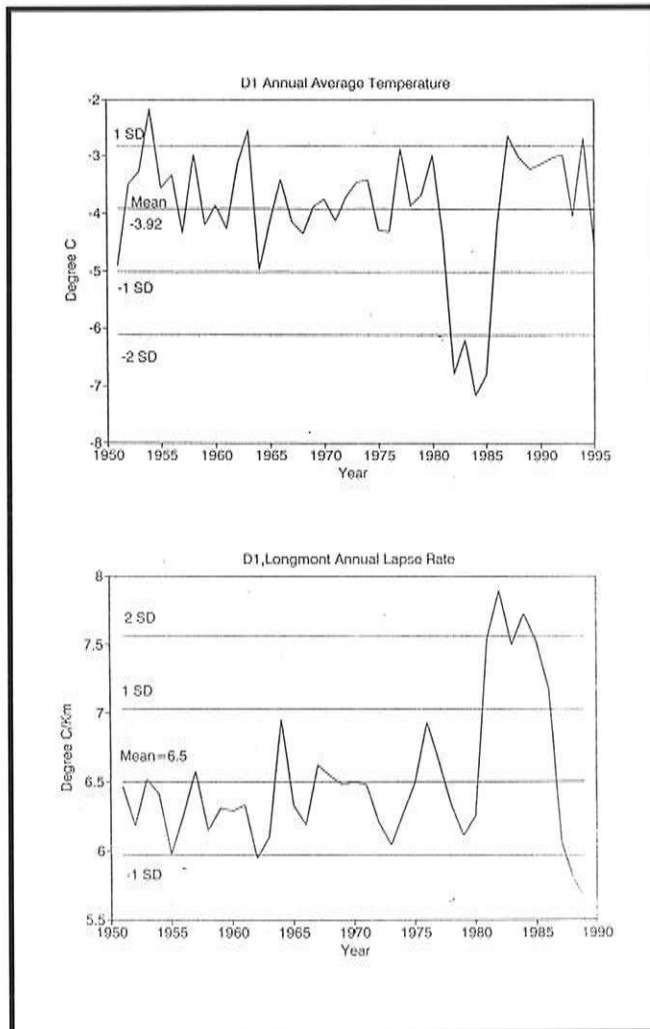


Figure 2 Temperature and lapse rate records.

Top: D1 Mean Annual Temperature (3749 meters).  
 Bottom: Lapse rate, D1 minus Longmont, in °C/Km.

Annual atmospheric Linke Turbidity (TB) index, Tucson, Arizona (Wm. Sellers, Institute of Atmospheric Physics, University of Arizona): This index is a general measure of aerosols and water vapor in the total atmospheric column and is greatly affected by volcanic activity. The TB index at Tucson is more sensitive to high-latitude volcanic eruptions than the Mauna Loa index (Sellers and Liu 1988). The period of this record is 1957-1995.

Lower stratospheric temperature anomalies (LST): These are northern hemisphere annual temperature anomalies at the 100-50 millibar height. The period of this record is 1959-1989 (Oort *et al* 1994).

Southern Oscillation Index (SOI): This index is the Tahiti-Darwin sea level pressure, obtained from the University of Washington Joint Institute for the Study of the Atmosphere and Ocean. A seasonal running mean of 3 months is used for the period of this record, 1951-1996.

Quasi-biennial oscillation (QBO): This phenomenon is represented by the 50-mb winds at Singapore. This paper uses a winter average (DJF). The period of this record is 1954-1995.

## **Results and Discussion**

---

Anomalously cold temperatures occurred at D1 in 61 of the 66 months from May 1981 through October 1986. Twelve months are more than two standard deviations colder than the 45-year mean. Annually, the 1981-1985 temperatures average 2.5 standard deviations below this mean. Monthly maximum and minimum temperatures were equally depressed during this period. Thus, this cold period appears to have occurred evenly over all seasons and all diurnal cycles. In contrast, this cold period is not recorded at stations only 20-30 kilometers east and two kilometers lower than D1. This dichotomy is reflected in an increase in the D1-Longmont lapse rate of more than 20% in the early 1980s (Figure 2), and suggests a change in the overall climate regime of the area for this period.

This cold period is recorded at the following sites above 3,000 meters: Berthoud Pass, D1, and C1, Niwot Ridge, in Colorado, and Mill Pond, Little Brooklyn, and Telephone Lakes in Wyoming (Figure 3). This cold period is not recorded at the following mountain sites, which are below 3000 meters: Centennial, Wyoming, and Estes Park and Grand Lake, Colorado. The four Wyoming sites illustrate the elevational character of this cold period, as all are very close; however only Centennial is below 3000 meters, and the cold period is absent only at Centennial. The D1, C1, Berthoud Pass, Estes Park, Grand Lake, Longmont, and Waterdale records exhibit the same elevational departure; all are spatially close, but D1, C1, and Berthoud Pass are above 3000 meters and show the cold period whereas Estes Park, Grand Lake, Longmont, and Waterdale are below 3000 meters and the cold period is absent.

Latitudinally, Climax and Wolf Creek Pass stations are south of 40°N latitude and are higher than 3000 meters. The cold period is absent in these two records. In summary, a review of the 23 records in the Colorado/southern Wyoming area suggests that this cold period occurred above 3000 meters elevation and north of about 40°N latitude.

The working hypothesis — that high elevation temperatures in the northern Colorado/southern Wyoming Rocky Mountains are inversely related to lower stratospheric temperature anomalies and atmospheric turbidity and directly related to the SOI, with an enhanced relationship during the positive phase of the QBO — is based on several geophysical indices. Figure 4 shows temperature anomalies at the 100-50 millibar height in the Northern Hemisphere, anomalies of atmospheric turbidity, the SOI, and the phase of the QBO. Extreme departures occur in the SOI, TB, and LST in the early 1980s. At no other time of period of common record are all these anomalies so extreme and in near-synchrony. This period coincides with the cold period of the high-elevation Rocky Mountain locations discussed here, as well as two explosive volcanic eruptions, Alaid in 1981 and El Chichon in 1982, and the powerful El Niño event of 1982-83. This sequence of physical events may have perturbed the climate system sufficiently to result in this cold period.

A question, then, is how frequently do such extreme conditions occur? Due to the short record of instrumented data, a proxy temperature record has been used — the Fool Creek (Fraser, Colorado) tree-ring chronology. This chronology, recently developed by Brown and Shepperd (1995), is at a treeline site between D1 and Berthoud Pass and correlates with late spring temperature ( $r^2=0.36$ ). The tree-ring record reflects the cold period of the early 1980s and shows that other cold periods have not occurred since 1906 but may have been relatively frequent between 1800 and 1906.

## Summary

---

There are four main points to this study:

- The 1981-1985 cold period presents an opportunity to investigate factors that may influence climate at high elevations in the Rocky Mountains of northern Colorado and southern Wyoming.
- The D1 temperature record is validated, indicating the cold period is not due to instrumental error or microsite conditions. Results of analysis also show a greater than 20% increase of the lapse rate in the study region. This anomalous cold period appears to have occurred in the Rocky Mountains above 3000 meters, approximately bounded on the south at 40°N latitude, but the northern boundary is yet to be determined.

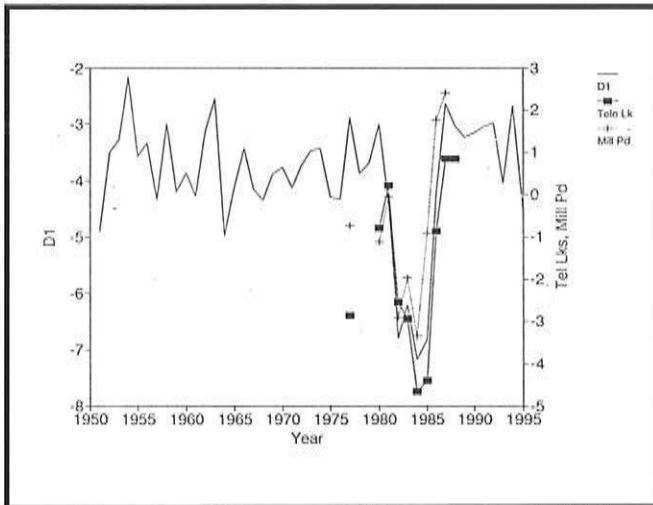


Figure 3. A selection of three mean annual temperature records that show the cold period.

The D1 record is plotted against the left side abscissa;  
 Telephone Lakes and Mill Pond are plotted against the right side abscissa.

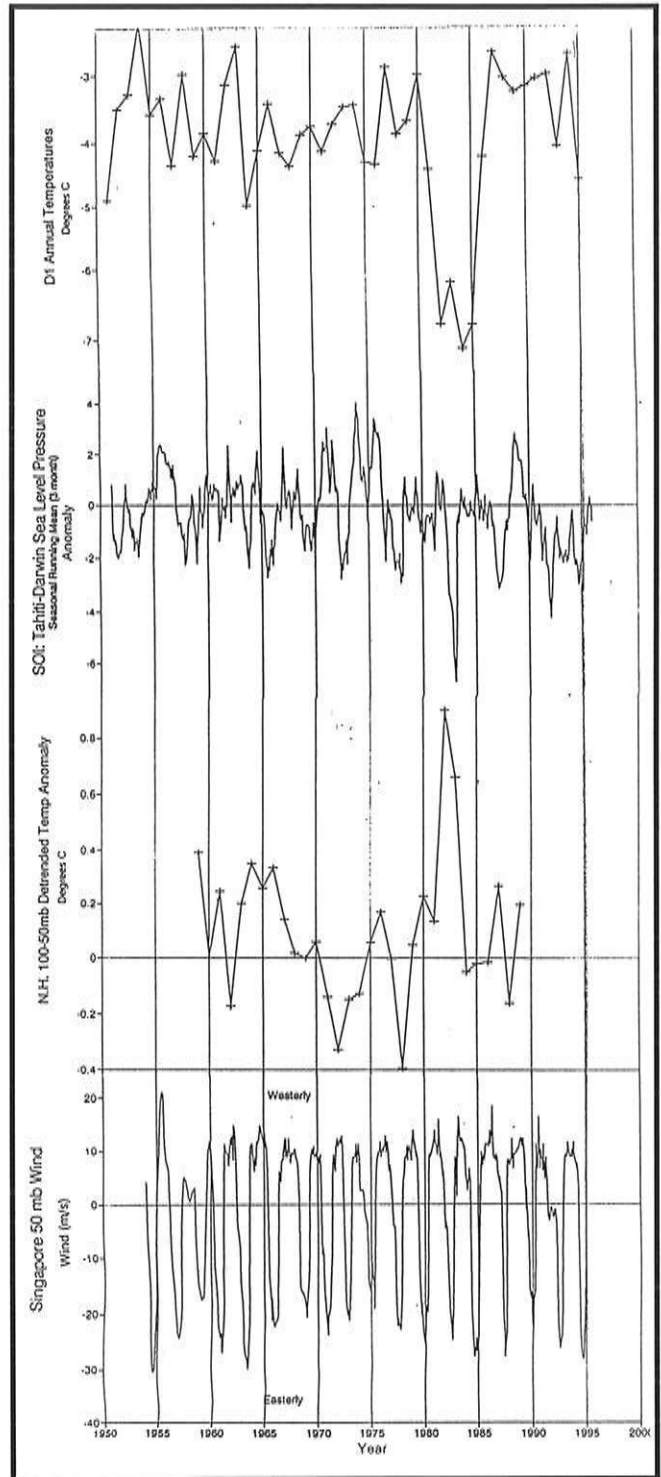


Figure 4 Geophysical Indices. From top to bottom: Atmospheric turbidity index at Tucson, Arizona; SOI; lower stratospheric temperature anomalies ( $^{\circ}\text{C}$ ); Singapore 50-mb wind (meters/second) representing the QBO. Turbidity and SOI are standardized values.

- A measurable relationship may exist between these high-elevation temperatures and conditions in the lower stratosphere and temperature extremes in the eastern Pacific Ocean, as indicated by the SOI. Additionally, the positive phase of the QBO appears to be related to these relationships.
- Evidence from a tree-ring chronology suggests that such cold periods have been rare in the 20th century but relatively frequent in the 19th century.

Implications of this study include the suggestion that climatic conditions at high elevations can differ from those at lower elevations; therefore, caution should be exercised when adjusting for the paucity of high-elevation data by extrapolating from low-elevation data. Also, physical events such as volcanic eruptions and shifting positions of the Pacific Ocean equatorial warm pool may contribute to climate changes in this study region by destabilizing the upper atmosphere, a result of colder temperatures aloft.

Future work includes better defining the geographical extent of this cold period by analyzing more surface site records and comparing surface conditions to radiosonde data at 700 millibars. Also, analysis of synoptic-scale patterns using daily surface and 500-mb maps and pressure anomaly maps may be informative.

## References

---

- Brown, Peter and Wayne Shepperd, 1995. Engelmann spruce tree-ring chronologies from Fraser Experimental Forest, CO: Potential for a long-term temperature reconstruction in the central Rocky Mountains. *Proceedings of the Interior West Global Change Workshop*, Fort Collins, CO April 24-26, 1995. USDA Forest Service, Rocky Mountain Forest and Range Experiment Station General Technical Report RM-000.
- Oort, A.H., H. Liu, and M. Rosenstein. 1994. Global and hemispheric anomalies derived from rawinsonde records. Pages 673-684 in *Trends '93: A Compendium of Data on Global Change*. ORNL/CDIAC-65.
- Sellers, W.D., and Wen Liu. 1988. Temperature patterns and trends in the upper and lower stratosphere. *Journal of Climate* (1):6.

# Southern California's Megaflood Event of ca. 1605 AD Linked to Large-scale Atmospheric Forcing

Arndt Schimmelmann, Carina B. Lange, Meixun Zhao, and Colin Harvey

**Abstract:** A distinct, 1- to 2-cm-thick flood deposit found in Santa Barbara Basin with a varve-date of 1605 AD  $\pm$  5 years testifies to an intensity of precipitation that remains unmatched for later periods when historical or instrumental records can be compared against the varve record. The 1605 AD  $\pm$  5 event correlates well with Enzel's (1992) finding of a Silver Lake playa perennial lake at the terminus of the Mojave River ( $^{14}\text{C}$ -dated 1560 AD  $\pm$  90 years), in relative proximity to the rainfall catchment area draining into Santa Barbara Basin. According to Enzel, such a persistent flooding of the Silver Lake playa occurred only once during the last 3,500 years and required a sequence of floods, each comparable in magnitude to the largest floods in the modern record. To gain confidence in dating of the 1605 AD  $\pm$  5 event, we compare Southern California's sedimentary evidence against historical reports and multi-proxy time-series that indicate unusual climatic events or are sensitive to changes in large-scale atmospheric circulation patterns. The emerging pattern supports previous suggestions that the first decade of the 17th century was marked by a rapid cooling of the Northern Hemisphere, with some indications for global coverage. A burst of volcanism and the occurrence of El Niño seem to have contributed to the severity of the events. The synopsis of the 1605 AD  $\pm$  5 years flood deposit in Santa Barbara Basin, the substantial freshwater body at Silver Lake playa, and much additional paleoclimatic, global evidence testifies for an equatorward shift of global wind patterns as the world experienced an interval of rapid, intense, and widespread cooling.

## Introduction

The most obvious economic impact of climate on society results from extreme weather events rather than from gradually shifting climatic averages (Katz and Brown 1992). Modern extreme events act as a catalyst for public awareness about changing climate. California's 20th century floods made news mostly because the effects of peak runoff and mudslides interfered with the sprawling urbanization of coastal areas, but there is abundant evidence that floods of earlier centuries were occasionally much more severe. For example, historical sources described the 1861/62 "Noachian Deluge" when all rivers from Oregon to the Mexican border were above flood stage, rainfall was 300-400 percent above normal in many parts of California, and the Sacramento Valley became navigable. Steamboats and barges were the only means of connecting the flooded city of Sacramento with surrounding higher ground. Subsequently, a much reduced tax basis forced the State of California into bankruptcy (Farquhar 1966, p. 241ff; Roden 1989).

Pre-19th century floods in California have little or no historical documentation. An earlier report of extreme, prehistoric flood events in Southern California was based on laminated lake deposits in the Mojave Desert, at the terminus of the Mojave River at Silver Lake playa, with  $^{14}\text{C}$ -dates of 1560

In: C.M. Isaacs and V.L. Tharp, Editors. 1997. *Proceedings of the Thirteenth Annual Pacific Climate (PACLIM) Workshop, April 15-18, 1996*. Interagency Ecological Program, Technical Report 53. California Department of Water Resources.

AD  $\pm$  90 years and 3620  $\pm$  70 years BP (Enzel *et al* 1989). Enzel (1992) concluded that each lake had persisted for at least a few decades and that a sequence of severe floods originating from intense precipitation in the San Bernardino Mountain area was necessary for their generation. By comparison, none of the 20th century major precipitation events of the area resulted in severe enough flooding to produce a perennial lake.

Here we document a flood deposit from the nearby Santa Barbara Basin that testifies to the worst regional flooding of this millennium and correlates well with the last Silver Lake playa episode and with other, multi-proxy regional evidence for unusual cool, moist conditions in the early part of the 17th century. Extreme climatic events in one region are frequently expressed by anomalous climates in neighboring areas, and may even be "teleconnected" to remote regions of the globe via changes in quasi-stationary atmospheric waves and storm track patterns (Trenberth 1993). Climatic teleconnections in the form of documented extreme and unusual climatic conditions around 1605 AD are indicated on a global scale, to support our hypothesis that a catastrophic Southern California flood was climatically linked to an equatorward shift of earth's major wind patterns during the most severe global cold spell of the last millennium.

### **Description of the Santa Barbara Basin Flood Deposit of About 1605 AD and Adjacent Layers**

---

Extreme precipitation in the Mojave River catchment of Southern California around 1560 AD  $\pm$  90 years should also have resulted in flooding of other regional rivers and creeks, carrying increased loads of detritus into the Pacific Ocean. At a distance of about 250 km to the west of the San Bernardino Mountains lies the center of the Santa Barbara Basin, where below a water column of 590 meters, laminated, annually varved sediments have been accumulating for much of the Holocene (Kennett *et al* 1995). The preservation of laminae is due to the oxygen-deficiency of the bottom water that makes the center of Santa Barbara Basin inhospitable for large, sediment-dwelling and bioturbating benthos (Thunell *et al* 1995) combined with high export production of the surface waters. Kasten cores were recovered between 1987 and 1989 and the annual varves documented and counted down-core using thinsections and X-radiography of sediment slabs (Lange *et al* in press). The resulting varve-chronology of Santa Barbara Basin was independently verified by isotope-geochronological methods and by correlation with local tree-ring records (reviewed by Lange *et al* in press). Santa Clara River and Ventura River have been identified as the main sources of terrigenous detritus for the modern Santa Barbara Basin (Soutar and Crill 1977).



At the 1605 AD  $\pm$  5 years level, at a sediment depth of about 1.18 meters, we observe a distinct, 1- to 2-cm-thick, clay-rich, gray layer (Munsell Soil Color 5Y 5/1) with sharp upper and lower boundaries against regular, varved sediment (color 5Y 4/2). An X-radiograph of this sediment interval indicates that the flood deposit may be the result of one or more closely spaced floods (Figure 1). All other identified flood deposits since 1420 AD have compacted to thicknesses below 1 mm (Lange *et al* in press), including the 1969 flood deposit in Santa Barbara Basin (Drake *et al* 1971), which resulted from intense precipitation in California in 1968/69 (Namias 1971). In contrast to normal olive-colored varves in Santa Barbara Basin, the gray flood deposit contains abundant terrigenous minerals that reduce the overall pore water content and the content of organic carbon (Figure 2). The depletion of  $^{13}\text{C}$  in the organic carbon in the flood deposit is consistent with non-marine, continentally derived detritus in Santa Barbara Basin (Figure 2; Schimmelmann and Kastner 1993). A distinction between graded gray turbidites and gray flood deposits is important, because only flood deposits are caused by precipitation on land. By comparison to regular varves and to gray turbidite layers in the Santa Barbara Basin sedimentary record (Schimmelmann *et al* 1990) we found that flood deposits dated 1605 and 1418 AD have a significantly finer particle size and higher smectite content (Figure 3). These data are supported by studies of transported sediment in Santa Clara River during a severe flood in 1969 (Drake *et al* 1971).

Light-microscope analyses of smear-slides of acid-treated sediment permit the quantification of biogenic components (Figure 4). The interval 1603-1605, including the flood deposit, shows the highest non-carbonate proportion of terrigenous pollen and plant remains. The interval 1606-1611 above the flood deposit stands out with its large relative abundance of diatoms, which may indicate a burst in productivity following the flood event. A sudden increase in productivity could have been the result of strong upwelling after years with frequent or lasting El Niño conditions.

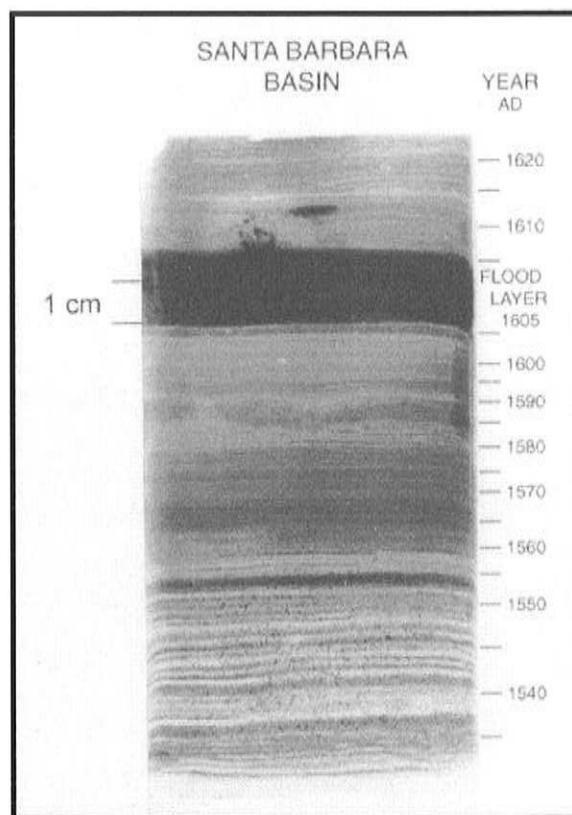
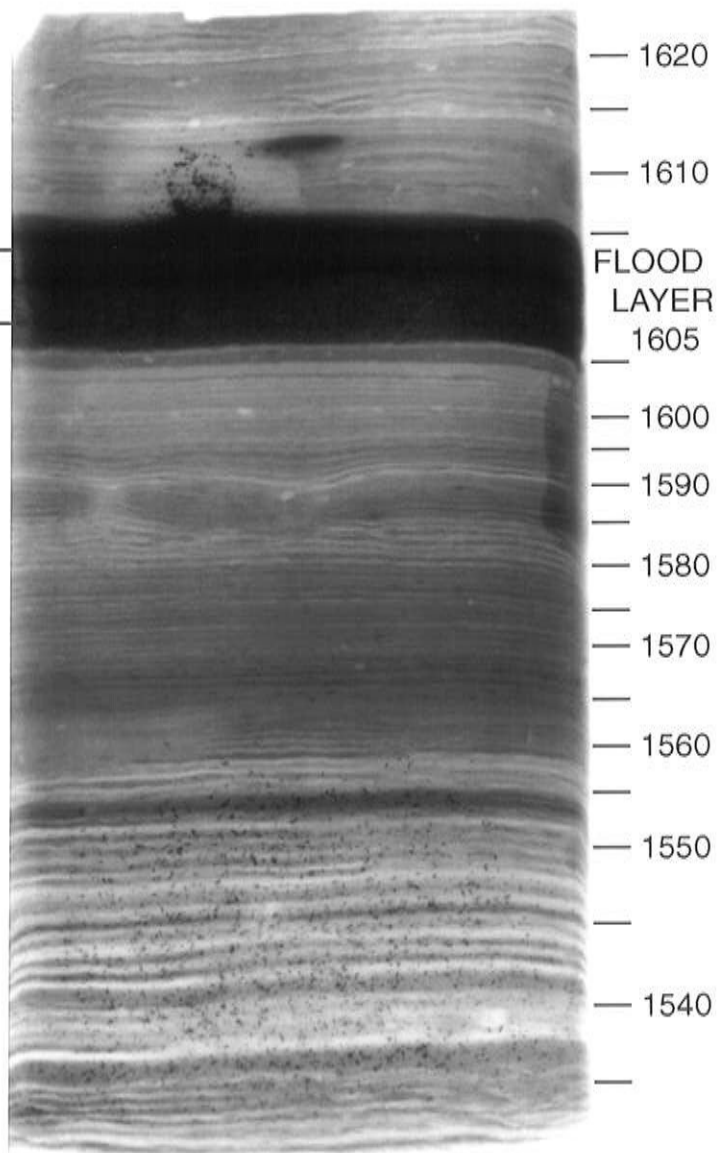


Figure 1. X-radiograph of a 1-cm-thick Santa Barbara Basin sediment slab (interval ca. 1530-1625 AD) from core KC4, cruise SABA 1993 (34°13.24'N, 120°03.66'W; 590m water depth). Dark color indicates mineral-rich, less porous sediment.

SANTA BARBARA  
BASIN

YEAR  
AD

1 cm



At the 1605 AD  $\pm$  5 years level, at a sediment depth of about 1.18 meters, we observe a distinct, 1- to 2-cm-thick, clay-rich, gray layer (Munsell Soil Color 5Y 5/1) with sharp upper and lower boundaries against regular, varved sediment (color 5Y 4/2). An X-radiograph of this sediment interval indicates that the flood deposit may be the result of one or more closely spaced floods (Figure 1). All other identified flood deposits since 1420 AD have compacted to thicknesses below 1 mm (Lange *et al* in press), including the 1969 flood deposit in Santa Barbara Basin (Drake *et al* 1971), which resulted from intense precipitation in California in 1968/69 (Namias 1971). In contrast to normal olive-colored varves in Santa Barbara Basin, the gray flood deposit contains abundant terrigenous minerals that reduce the overall pore water content and the content of organic carbon (Figure 2). The depletion of  $^{13}\text{C}$  in the organic carbon in the flood deposit is consistent with non-marine, continentally derived detritus in Santa Barbara Basin (Figure 2; Schimmelmann and Kastner 1993). A distinction between graded gray turbidites and gray flood deposits is important, because only flood deposits are caused by precipitation on land. By comparison to regular varves and to gray turbidite layers in the Santa Barbara Basin sedimentary record (Schimmelmann *et al* 1990) we found that flood deposits dated 1605 and 1418 AD have a significantly finer particle size and higher smectite content (Figure 3). These data are supported by studies of transported sediment in Santa Clara River during a severe flood in 1969 (Drake *et al* 1971).



Figure 1. X-radiograph of a 1-cm-thick Santa Barbara Basin sediment slab (interval ca. 1530-1625 AD) from core KC4, cruise SABA 1993 (34°13.24'N, 120°03.66'W; 590m water depth). Dark color indicates mineral-rich, less porous sediment.

reduce the overall pore water content and the content of organic carbon (Figure 2). The depletion of  $^{13}\text{C}$  in the organic carbon in the flood deposit is consistent with non-marine, continentally derived detritus in Santa Barbara Basin (Figure 2; Schimmelmann and Kastner 1993). A distinction between graded gray turbidites and gray flood deposits is important, because only flood deposits are caused by precipitation on land. By comparison to regular varves and to gray turbidite layers in the Santa Barbara Basin sedimentary record (Schimmelmann *et al* 1990) we found that flood deposits dated 1605 and 1418 AD have a significantly finer particle size and higher smectite content (Figure 3). These data are supported by studies of transported sediment in Santa Clara River during a severe flood in 1969 (Drake *et al* 1971).

Light-microscope analyses of smear-slides of acid-treated sediment permit the quantification of biogenic components (Figure 4). The interval 1603-1605, including the flood deposit, shows the highest non-carbonate proportion of terrigenous pollen and plant remains. The interval 1606-1611 above the flood deposit stands out with its large relative abundance of diatoms, which may indicate a burst in productivity following the flood event. A sudden increase in productivity could have been the result of strong upwelling after years with frequent or lasting El Niño conditions.

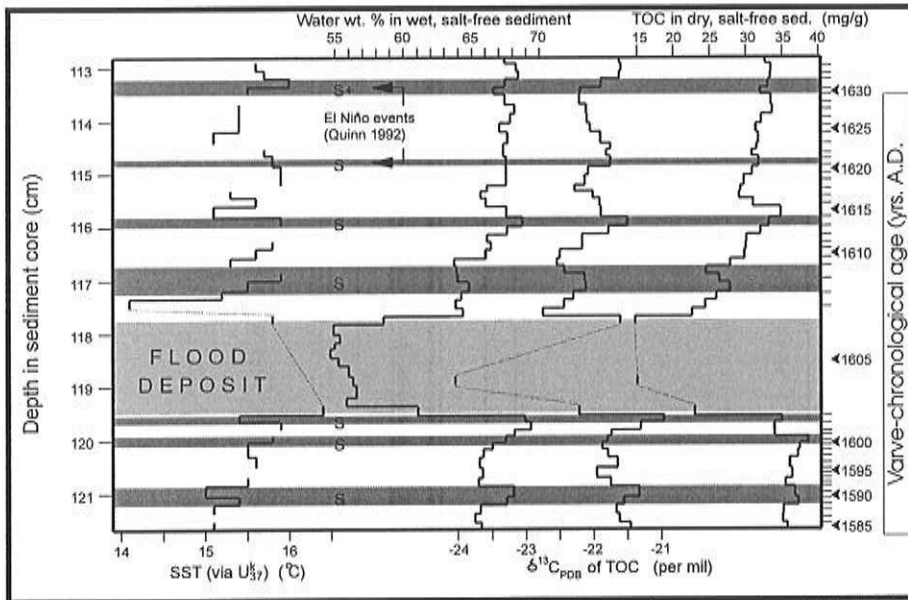


Figure 2. Geochemical time-series 1585-1635 AD from Santa Barbara Basin sediment, from left to right: alkenone-based sea surface temperature (SST); sediment water content; carbon stable isotope ratio  $\delta^{13}\text{C}_{\text{PDB}}$  of total organic carbon (TOC); TOC content. Weighing of sediment samples before and after freeze-drying permitted the calculation of the water content in wet sediment. Samples were stored freeze-dried until aliquots were analyzed for TOC and their carbon stable isotope ratios (Schimmelmann and Tegner 1991). The determination of alkenone abundances followed Parry's (1993) description. SST was calculated from the  $U^k_{37}$  index using Prahl *et al's* (1988) equation:  $\text{SST } (^\circ\text{C}) = (U^k_{37} - 0.039) / 0.034$ . The analytical precision of alkenone-based SST is about  $\pm 0.5^\circ\text{C}$ . Quinn's (1992) historical strong El Niño events are indicated by shading.

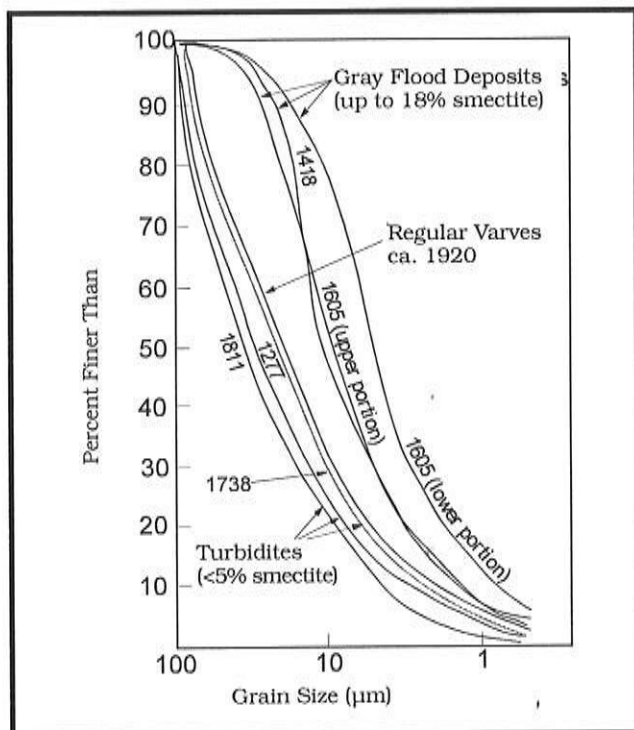


Figure 3. Particle size distribution in gray flood deposits (1605 and 1418 AD) in comparison with those of turbidites (1811, 1738, and 1277 AD) and of regular varves (ca. 1920). The smectite content was determined using the methylene blue method (American Petroleum Institute 1985).

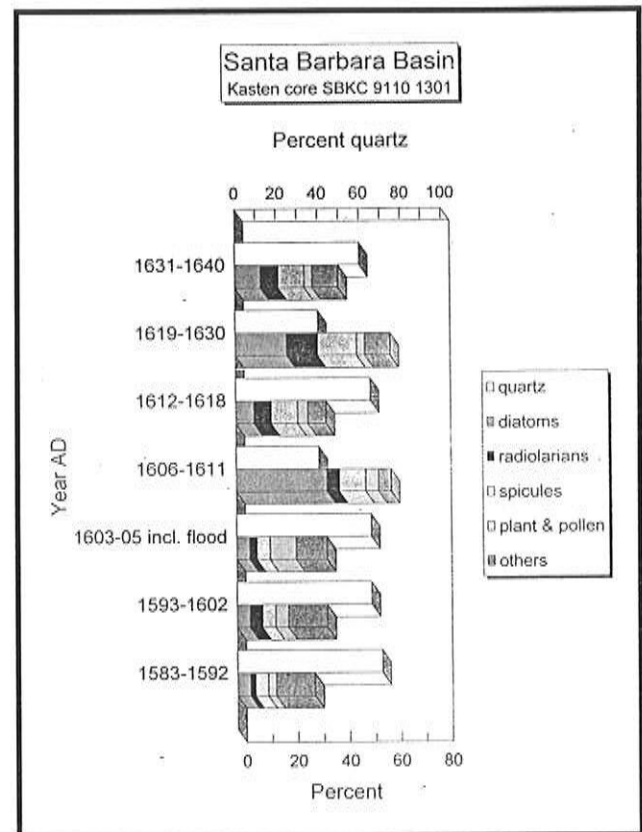


Figure 4. Light-microscope analyses of non-carbonate biogenic components (lower axis: diatoms, radiolarians, sponge spicules, pollen and plant debris) and quartz (upper axis) from smear slides of acid-treated sediment, as percent of total. "Others" include clay, silt, and non-identifiable particles that were not removed by the acid treatment. Sample resolution for varved intervals is about 5 to 10 years.



## Matching Santa Barbara Basin Time-Series with Paleo-El Niño Events, 1585-1635 AD

---

Over much of the middle to lower latitudes, anomalies in the atmosphere and ocean circulation and temperature known as “El Niño-Southern Oscillation” (ENSO) events are an eminent source of year-to-year climate variability. During the Southern Oscillation phase, when the surface pressure is low in the southeastern tropical Pacific, warm water replaces the usually cool surface waters of the central and eastern Pacific — an event known as “El Niño” (Whetton and Rutherford 1994). Off the Americas, a strong El Niño event is typically characterized by anomalously warm sea surface temperatures, weakened circulation in the California Current system along the eastern margin of the Pacific, and reduced upwelling along the Californian and Peruvian coasts. The influence of ENSO extends to higher latitudes, mostly in winter, and changes the jet stream and storm track locations (Trenberth 1993) to more southerly locations over North America, such as documented for the 1982/83 ENSO event (Enfield 1992).

Quinn’s (1992) latest compilation of historical ENSO events compares well with ENSO proxies from North China, Java, and India, because it bears more supraregional relevance in comparison to its earlier, South American-centered predecessors (Whetton *et al* 1996). For the 1585-1635 AD interval, Quinn’s strong (S and S+) ENSO events include 1589-1591 (S), 1600/01 (S), 1604 (S), 1607/08 (S), 1614 (S), 1621 (S), and 1630/31 (S+) (see horizontally shaded intervals in Figure 2). Other, independent ENSO-sensitive time-series support specific ENSO occurrences for 1605  $\pm$  5 years. The year 1600 is suggested by New Zealand tree-ring data (D’Arrigo *et al* 1995, with references therein).

Quinn’s strong ENSO events around 1605 AD appear to be recorded in other high-resolution records, in part with a minor lag. The year 1607 AD was suggested as an ENSO-year by Lough’s (1992) North American tree-ring record and by Dunbar’s *et al* (1994) oxygen isotope record from Galápagos corals, making 1607 a most likely year for a widespread ENSO event. Further support for the relevancy of Quinn’s (1992) ENSO data to Santa Barbara Basin around 1605 comes from detailed reports of the expedition of the Spanish explorer Sebastian Vizcaino, who sailed along the west coast of North America in the winter of 1602/03. Vizcaino’s pilot (Wagner 1929) and an accompanying clergy (Wagner 1928) portray a rather benign California coastal climate without symptoms of an ENSO event. Santa Barbara Basin was calm, and abundant kelp beds were reported for off Point Loma, near San Diego, and adjacent to Isla Cedros, off Baja California, Mexico, at 28°N. Kelp beds are frequently reduced during strong ENSO events (Schimmelmann and Tegner 1991).

A comparison of Quinn's (1992) record with geochemical time-series from the 1585-1635 AD interval of Santa Barbara Basin sediment reveals that six of the seven S and S+ historical ENSO events are represented by  $^{13}\text{C}$ -enrichment in total organic carbon (Figure 2). The comparable correspondence between modern, strong El Niño events and  $^{13}\text{C}$ -spikes in an upper, 1845-1986 interval of Santa Barbara Basin varves was interpreted to be the result of El Niño-induced disturbances of  $^{13}\text{C}$ -enriched, local kelp forests (Schimmelmann and Tegner 1991). It is highly unlikely that the 1585-1635 AD ENSO/ $^{13}\text{C}$  match is fortuitous. We obtained an independent proxy for paleo-sea surface temperature in Santa Barbara Basin by measuring the relative abundances of long-chain alkenone molecules, commonly expressed by the  $U_{37}^k$  index (Brassell *et al* 1986; Prah *et al* 1988; Eglinton *et al* 1992), in selected samples, 1585 to 1635 AD (Figure 2). Kennedy and Brassell (1992) had successfully used alkenone abundances to correlate warming in Santa Barbara Basin with ENSO events of the 20th century. The highest sea surface temperature of the 50-year interval shown in Figure 2 was measured in the lowest part of the 1605 AD sample, containing the transition from olive, regularly varved sediment to the gray flood deposit. In contrast, the olive 1606 AD sample above the flood deposit features the coldest sea surface temperature. The high sea surface temperature suggests that the flood occurred in association with an ENSO event, followed by resumed upwelling, lowered sea surface temperature, and high productivity (as recorded by diatoms, Figure 4). The remarkable contrast between high and low sea surface temperature across the flood deposit seems to be resolved analytically because the flood deposit physically separates the opposing signals. In regularly varved sediment, where stratigraphic sample boundaries typically do not coincide with tightly spaced varve boundaries, the amplitude of geochemical signals may be dampened by uneven spacing of samples. For example, the warm season will be underrepresented in a sample encompassing 15 months of material from fall to winter, whereas the adjacent samples then tend to overrepresent warm seasons. These limitations, together with the analytical precision of  $\pm 0.5^\circ\text{C}$  for reconstructed sea surface temperature, reduce the significance of smaller, warm sea surface temperature signals in varves assigned to Quinn's (1992) ENSO years 1589, 1600, 1608, 1614, and 1631 (Figure 2).

The fit between the historical paleo-ENSO pattern and the geochemical evidence suggests an accuracy of about  $\pm 2$  years for our Santa Barbara Basin varve-chronology at the 1600 AD level. The base of the flood layer seems to be linked to a strong ENSO event, probably Quinn's 1604 AD event. We caution against overconfidence in year-to-year comparisons, because oceanographic changes in the strong upwelling areas of the eastern equatorial Pacific are sometimes not in synchrony with variations in other features of the Southern Oscillation (Diaz and Pulwarty 1992).

## Additional Multi-Proxy and Historical Evidence for Unusual Climates around 1605 AD

The following paragraphs present major paleoclimatic evidence in light of general circulation theory. Tables 1-3 give a brief overview including other, additional paleoclimatic evidence.

### Regional Evidence from Southwestern USA

Regional reconstructions of precipitation and temperature from the southwestern USA include sites near Santa Barbara, the larger Sacramento Basin catchment area, the Sierra Nevada, northeastern Nevada, and northwestern New Mexico (Table 1). The existence of a perennial lake in the Mojave Desert for at least a few decades requires not only initial, extreme rainfall, but subsequently also occasional replenishing floods in addition to cool summers to reduce evaporation. Abundant evidence for moist winters and cool summers in the southwestern USA during the early 17th century, in part extending into the 1640s (Table 1), fulfills

Table 1  
REGIONAL EVIDENCE FOR UNUSUALLY WET, COLD CLIMATE AROUND 1605 AD

Time (AD)	Location and Evidence	Method	Source
1604; 1601-1611	Santa Barbara area, California; 1604 is the fourth wettest year, and 1601-1611 is the third wettest 11-year period in the entire 1366-1985 reconstruction of precipitation.	tree-ring width	Haston & Michaelsen 1994
1597-1613	Larger Sacramento Basin, California; maximum reconstructed streamflow for 1660-1980, peaking around 1601 to 1606.	tree-ring width	Earle & Fritts 1986
1602	Sierra Nevada; end of a 1566-1602 drought.	tree-ring width	Graumlich 1993
1580-1637	Sierra Nevada; no wide-spread drought recorded.	tree-ring width	Hughes & Brown 1992
1595-1644	Sierra Nevada; cold summer temperatures, especially 1604-1623 as the second largest 20-year temperature anomaly of the 800-1989 record.	tree-ring width	Graumlich 1993
1601, 1605	Sierra Nevada; two unusually narrow tree-rings suggest cold growing seasons; 1605 is even narrower than 1601.	tree-ring width	Scuderi 1990
about 1600-1650	Mono Lake fills rapidly to the record level of the past millennium.	sediment structural evidence	Stine 1990
1598; 1609-1623	Northwestern New Mexico; 1598 ended the worst decadal drought, followed in 1609-1623 by the fourth wettest decadal-scale interval in a 985-1970 reconstructed record of winter precipitation.	tree-ring width	D'Arrigo & Jacoby 1991
1601-1610	Northeastern Nevada; fifth wettest 10-year period in a 1601-1982 record, with a 1605/06 peak.	tree-ring width	Nichols 1989

these requirements. Especially noteworthy is a tree-ring-based reconstruction of overall annual streamflow in the larger Sacramento Basin since 1560 AD (Figure 5; Earle and Fritts 1986, p. 114) where an extremely wet spell occurred between 1599 and 1606. Each year's flow in 1599, 1603, 1604, and 1606 exceeded the annual flow data of the devastating flood years of 1861 and 1862. Increased wetness between 1601 and 1611, with a peak at 1604, is also indicated for the Santa Barbara area (Haston and Michaelsen 1994). A long-lasting drought in the Sierra Nevada ended in 1602 (Graumlich 1993), and 1601-1610 is among the five wettest 10-year periods in a 1601-1982 northeastern Nevada precipitation record (Nichols 1989). On the northwestern plateau of New Mexico, 1598 marked the end of the worst decadal drought of a millennial record (985-1971 AD), to be followed in 1609-1623 with the fourth wettest decadal-scale interval of winters (D'Arrigo and Jacoby 1991). Tree-ring data may severely underestimate the amount of precipitation when extreme events cause intensive runoff and/or detrimental waterlogging of the root system, whereas the water level record of the closed Mono Lake offers a more quantitative, cumulative measure of flood intensity. Mono Lake filled rapidly in the first half of the 17th century to briefly reach the highest level of the past millennium (Stine 1990). The  $^{14}\text{C}$ -date of 1650 AD for the 17th century highstand of Mono Lake is corroborated by additional geological evidence (Stine 1987, pers comm).

A strong cooling trend in Sierra Nevada summer temperatures had started in 1595 and lowered the mean, smoothed summer temperature during the first half of the 17th century, to reach an absolute minimum for the entire 800-1989 AD time-series. The period 1604-1623 marks the second largest 20-year low temperature anomaly of the record (Graumlich 1993; see also Table 1). Scuderi (1990) finds tree-ring evidence for very cold growing seasons in the Sierra Nevada in 1601 and especially in 1605 (Figure 5).

The cited evidence agrees well with Enzel's (1992) hypothesis that winter atmospheric circulation patterns during the Silver Lake playa flood episodes were associated with an extreme southerly displacement of winter storm tracks and the Polar Jet over western North America and with a southerly shift of the central North Pacific winter low pressure zone (Figure 6). Major frontal cyclones would thus be steered into the southwestern USA, raising the potential for large floods. Much of the precipitation in the Mojave River basin falls in the high-elevation San Bernardino Mountains, which are ideally located to lift moist southwesterly airflow of winter cyclones (Ely *et al* 1994). Along with increasing regional winter precipitation, an equatorward shift of quasi-stationary planetary waves would have brought a decline in temperatures (Roden 1989; Hurrell 1995). For comparison, the "Noachian Deluge" of 1861/62 also was accompanied by an extreme cold spell in the Pacific Northwest that froze the mouths of the Fraser and Columbia rivers (Roden 1989).

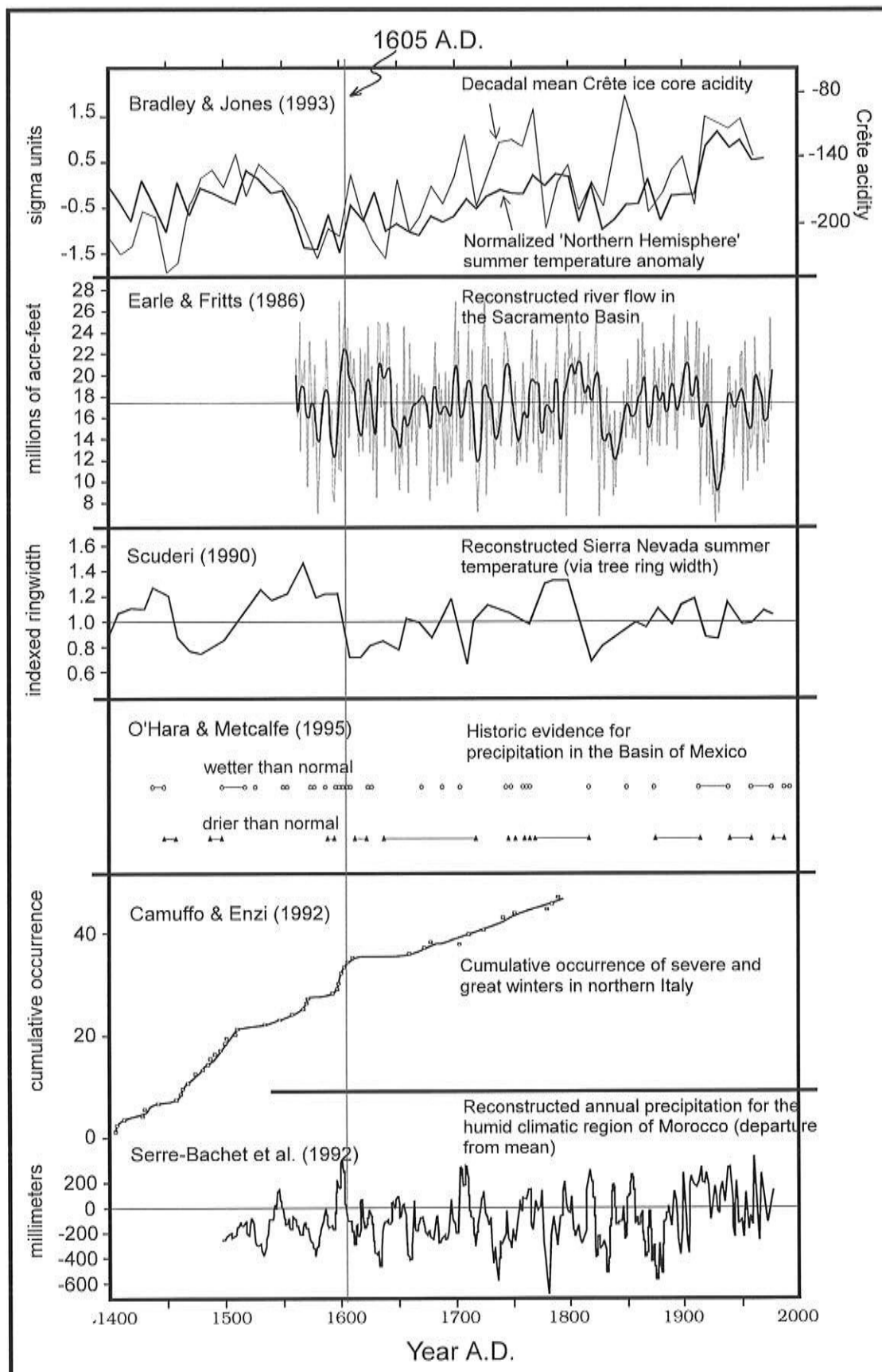


Figure 5. Selected paleoclimatic time-series with relevance to extreme events around 1605 AD.

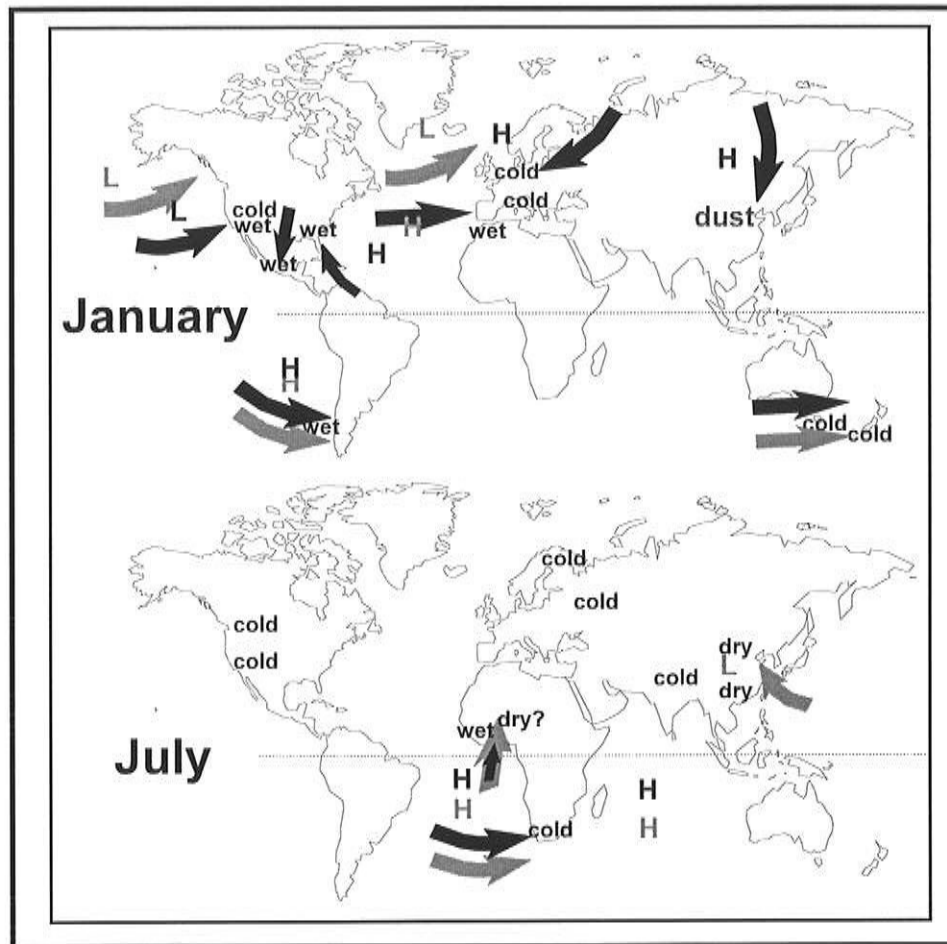


Figure 6. Suggested equatorward displaced atmospheric circulation for ca. 1605 AD (black arrows and black text). For comparison, modern mean conditions are displayed in gray tone.

### **Supraregional Evidence from the Northern Hemisphere**

Supraregionally teleconnected climatic events frequently differ in their expression. For example, the southerly displacement of the westerlies and jet stream pattern over the Northern Hemisphere that brought intense precipitation to Southern California may have caused drought in parts of China. The unifying link in the following discussions is an equatorward shift in wind patterns. Observations are summarized in Table 2.

An accumulation of five unusually wet spring seasons in the southeastern USA, an occurrence rate more than five times higher than the long-term mean, was suggested to be linked to a westward shift of the North Atlantic subtropical high, or “Bermuda high” (Stahle and Cleveland 1994). This implies that large-scale atmospheric circulation over eastern North America may have been amplified around 1596-1613 AD and was perhaps causally linked with climatic anomalies elsewhere in the Northern Hemisphere during the most consistent and extensive cold episode of the “Little Ice Age” (Stahle and Cleveland 1994). A southerly displacement of atmospheric circulation patterns around 1605 AD is also

Table 2  
SUPRAREGIONAL EVIDENCE FOR NORTHERN HEMISPHERE UNUSUAL CLIMATES AROUND 1605 AD

Time (AD)	Location and Evidence	Method	Source
1600-1609	Northern Hemisphere, comprehensive summer temperature evaluation; exceptionally cold decade.	multi-proxy	Bradley & Jones 1993
1580-1610	Canadian Rocky Mountains, cold summers. 1595 shows minimum for entire 1505-1970 record.	tree-ring width	Smith et al 1995
1607/08	Severe winter in Maine, Virginia (Jamestown), and Lake Superior	historical records	Lamb 1982, p. 230
ca. 1590-1610	Northern Mexico, unusually dry period in area between 23 and 30°N where summer precipitation predominates.	tree-ring width	O'Hara & Metcalfe 1995
1604, 1607	Basin of Central Mexico, Mexico City; following a 1590s drought, severe flooding occurred in 1604 and 1607; the severity of the 1607 flood prompted excavation of a drainage canal out through the northern part of the basin.	historical records	O'Hara & Metcalfe 1995
1596-1613	Southeastern USA; 5 of the 48 wettest spring rainfall years in a 1,053-year-long record fall between 1596 and 1613, namely 1596, 1600, 1602, 1605, and 1613.	tree-ring width	Stahle & Cleaveland 1994
1604-1614	Central Europe; increased precipitation, with a wet peak from winter 1608 through the very wet summer of 1609.	historical records	Rüdiger Glaser, pers comm
1600-1608	Central Europe; all seasons of the years 1600, 1601, 1606 and 1608 were significantly colder than the long-term mean.	historical records	Rüdiger Glaser, pers comm
1608	Europe; "great" winter.	historical records	Lamb 1985
1595-1608	Netherlands; densest cluster of unusual winters on record, since 1408; winters were cold [c], severe [s] or very severe [vs]: 1595vs, 1599c, 1600s, 1602c, 1603c, 1608vs.	historical records	Buisman 1984
1590s to 1610	Northern Fennoscandia; very cold July/August temperatures; 1600/1601 absolute minimum for entire record (1580-1975).	tree-ring width and maximum latewood density	Briffa & Schweingruber 1992
1601-1620	Fennoscandia; third-coldest 20-year interval in a 1,400-year record of summer temperatures, 500 to 1975.	tree-ring width and maximum latewood density	Briffa et al 1990
1595-1608	Northern Italy; densest cluster of severe and great winters in recorded history (since 1406): 1595, 1599, 1600, 1602, 1603, 1605, 1608.	historical records	Camuffo & Enzi 1992
1601-1603	Russia, "Great Famine", with "Godunov Hunger Riot"; reportedly "one third of the Moscow Tzardom" population died, 120,000 people perished from hunger in Moscow alone.	historical records	Borisenkov 1992
1590-1620	Mid-Russia; unusually low spring/summer temperatures.	historical records	Borisenkov 1992
ca. 1610 (?)	Africa, Lake Chad; most dramatic lake level decline of the last millennium? The radiocarbon dating is imprecise.	sediment records, pollen	Maley 1973

Table 2 (continued)  
SUPRAREGIONAL EVIDENCE FOR NORTHERN HEMISPHERE UNUSUAL CLIMATES AROUND 1605 AD

Time (AD)	Location and Evidence	Method	Source
1602-03	Africa, Timbuktu (Mali), great flood from unusually heavy rains over the upper basin of River Niger.	historical records	Lamb 1982, p. 226
ca. 1610	North China; substantial increase in dust fall indicates increase in aridity and windiness; this record has decadal resolution.	historical records	Liu Tungsheng et al 1989
shortly before 1600	Tibet Plateau and Qilianshan Mountains east of the Tibet Plateau begin strong cooling; southern China became drier and the Yangtze River level declined.	tree-ring width; historical evidence	Zhaodong Feng et al 1993
1602-1611; 1620-1629	Algeria experiences the worst episodes of famine since 1500 AD (reasons were not reported).	historical evidence	Nicholson 1980
1598-1604; 1602	Morocco; 1598-1604 unusually large amount of annual precipitation, with 1602 representing the absolute maximum of the 1499-1878 record.	tree-ring width	Serre-Bachet et al 1992
1601	Unknown location, but probably in the Northern Hemisphere: large volcanic eruption; recorded in Greenland ice sheet, tree-rings, and by historical accounts.	multi-disciplinary	Lamb 1970; Hammer et al 1980; Scuderi 1990; Briffa & Schweingruber 1992; Pavese et al 1992

in agreement with O'Hara and Metcalfe's (1995) historical climate record from central Mexico. Devastating drought conditions during the 1590s in the basin of central Mexico, which is climatically distinct from northern Mexico, ended about 1600 (Figure 5). In 1604 and 1607, flooding was so severe around Mexico City that a drainage canal was excavated through the northern part of the basin. At present, the regional precipitation pattern in central and part of northern Mexico is influenced primarily by seasonal shifts in the latitudes of the trade winds in summer and the subtropical high pressure belt in winter. During the Northern Hemisphere summer, a monsoon-type easterly flow brings the main rainfall to central Mexico. However, in late winter and early spring, with the Intertropical Convergence Zone<sup>1</sup> displaced equatorward, outbreaks of cold polar air, called "nortes", can bring rains as far south as the Yucatan Peninsula of southern Mexico (O'Hara and Metcalfe 1995). We suggest that after 1600 AD frequent nortes originated from a much colder North American continent, picked up moisture on their paths across the Gulf of Mexico, and brought intense precipitation to central Mexico (Figure 6).

With regard to summer temperatures, the decade 1600-1609 stands out as exceptionally cold in a comprehensive 1400-1970 Northern Hemisphere composite record based on historical, tree-ring, and ice core data

1 Zone of equatorial rainfall maximum where the two hemispheric wind systems adjoin.

(Figure 5; Bradley and Jones 1993). The largest effects are seen at higher latitudes such as in Svalbard, Northern Scandinavia, and South Greenland (Bradley and Jones 1993). The 1607/08 AD winter was severe in eastern North America. In Maine, “persistent northerly winds and such severe frosts ... [killed] many people ... both among the Europeans and the Indian population. At Jamestown it was reported that ‘the extraordinary frost in most of Europe ... was as extreme in Virginia’. And Samuel Champlain, the founder of Quebec, found bearing ice on the edges of Lake Superior in June 1608.” (Lamb 1982, p. 230). Lamb suspects that “there seems to have been a general reduction of the westerlies, which were shifted to a lower latitude over the Pacific.” European archives document a unique concentration of severe winters near the turn of the 16th century (Table 2). The year 1608 is one of the few “great” winters listed in Lamb’s (1985) classification of European historical winters. Between 1599 and 1608, Northern Italy experienced its densest cluster of severe and great winters since 1406 (Figure 5; Camuffo and Enzi 1992). Eyewitness accounts in 1603 describe “the Lagoon and all the canals in Venice froze over for 8 to 10 days” and in 1608 “the winter [in Venice] was so severe, as had never occurred from time immemorial. Due to an exceptional snowfall, it was impossible to walk in the streets or go out through the door” (Camuffo 1987, p. 60). A large central European database identifies 1600, 1601, 1606, and 1608 as extremely cold (Rüdiger Glaser, pers comm). Pfister *et al* (1994) interpret decadal cooling of western Europe as due to the shrinking of the Hadley cell, a zonal-mean tropospheric circulation linking the lower and middle latitudes. The influence of the westerlies with their warm, Atlantic air masses would be diminished, whereas polar air masses from the northeast would gain more access (Rogers 1985).

The proposed shift of wind patterns is consistent with a southerly displacement and/or weakening of the westerlies (Figure 6). Further evidence for this hypothesis is found in the humid climatic region of Morocco, where 1598-1604 AD brought unusually large annual precipitation, with 1602 reaching an absolute maximum in the 1499-1978 record (Figure 5; Serre-Bachet *et al* 1992). The Mediterranean winter/spring climate of Morocco apparently came under temporary influence of the equatorwardly displaced westerlies (Jinjun Ji *et al* 1993; Tyson and Lindesay 1992). Between 1602 and 1611 and again between 1620 and 1629, Algeria suffered through its worst 30-year period of famine in recorded history, since 1500 AD (Nicholson 1980). Climatic changes were likely responsible, although the actual reasons for the famine are not reported.

A change in northeast Asian wind patterns is indicated by substantially increased dustfall due to higher aridity around 1610 on the Loess Plateau of central China (record with decadal resolution shown in Liu Tungsheng *et al* 1989; also discussed in Zhaodong Feng *et al* 1993). Strong cooling

trends starting shortly before 1600 are evident from tree-rings on the southern Tibet Plateau and the Qilianshan Mountains east of the Tibet Plateau. At the same time, southern China became drier and the water level of the Yangtze River declined (Zhaodong Feng *et al* 1993). During periods when the strong Mongolian winter high moves southward and reduces the strength of the Southern Pacific high, temperature and precipitation in China are relatively low (Zhaodong Feng *et al* 1993). The increased dustiness can be interpreted in the context of global cooling associated with an increase of the meridional temperature gradient, an increase in the intensity of the wind field over northern desert regions and the Chinese Loess Plateau, an expansion and strengthening of the Mongolian winter high, a decline of the humid summer monsoon influence, and a southward expansion of the north China desert (Liu Tungsheng *et al* 1989). This scenario of north Chinese drought is consistent with equatorward shifts of the polar jet stream (Zhang Linyuan *et al* 1995) and the Intertropical Convergence Zone (Jinjun Ji *et al* 1993).

A great flood in 1602-03 AD in the city of Tombouctoo (Timbuktu) in Mali resulted from unusually heavy rains in the previous summer over the upper basin of the River Niger in westernmost Africa in latitudes 10-12°N (Lamb 1982, p. 226). Summer rains in 1602 AD in west Africa fell much closer to the equator, rather than migrating seasonally to 15-20°N or beyond, as in this century before 1960. Geological and pollen evidence suggests an early 17th century low stand of Lake Chad in north Africa (Maley 1973) as the consequence of a severe drought caused by a displacement of the Intertropical Convergence Zone near west Africa closer to the equator (Jinjun Ji *et al* 1993). We caution, however, that Maley's (1973) underlying radiocarbon dates do not offer high precision, and that some sparse historical information indicates that droughts set in later, during the 1680s (Nicholson 1980).

### **Supraregional Evidence from the Southern Hemisphere**

Southern Hemisphere climatic changes and extremes around 1605 are summarized in Table 3. Between 1590 and 1630, the seasonal oscillations of the oxygen isotope ratios of precipitation on the Quelccaya glacier in the Peruvian Andes are much lower than during adjacent centuries, marking 1590 and 1630 as times of rapid alternation of climate or environmental conditions (Thompson 1992).

Precipitation in central Chile is related to a northward shift of westerly storm tracks along the coast of Chile, in response to the latitudinal position and intensity of the Southeastern Pacific High (Figure 6). A northerly shifted position is characterized with a "weak" index, or "high index" (*ie*, weaker subtropical pressure) and is sometimes associated with El Niño conditions (Villalba 1994). Tree-ring studies suggest that summer precipitation on Chiloe Island, off south-central Chile at 42°S, increased

dramatically between 1601 and 1604, synchronously with a minor shift of the anticyclone position toward the equator (Boninsegna 1992).

Tree-ring data from Tasmania indicate a rapid cooling of summer temperatures (November-April) between 1600 and 1610 (Cook *et al* 1992), parallel to similar observations in tree-rings from Patagonia, Argentina (Boninsegna 1992; Bradley and Jones 1993 show the two graphs in comparison). On the South Island of New Zealand, under the influence of the middle-latitude southern westerlies, extreme growth of silver pine in 1600 AD was followed by an abrupt, deep decline through 1604/05 (D'Arrigo *et al* 1995). Similarly, mean annual temperatures in southern Africa declined sharply around 1600 (Tyson and Lindesay 1992). The Southern Hemisphere mid-latitude climatic change around 1600 was suggested to be the result of an equatorward expansion of the Antarctic circumpolar vortex, together with a northward displacement of the westerlies in the Southern Hemisphere, and northward-shifted high pressure systems in the south Atlantic and south Indian oceans (Tyson and Lindesay 1992; Cohen and Tyson 1995; Figure 6).

Table 3  
SUPRAREGIONAL EVIDENCE FOR SOUTHERN HEMISPHERE UNUSUAL CLIMATES AROUND 1605 AD

Time (AD)	Location and Evidence	Method	Source
1607 ± 5 year	Galápagos Islands.; second largest <sup>18</sup> O-depletion in 1607-1950 record of annual coral aragonite bands, suggesting strong El Niño conditions.	oxygen isotope ratios	Dunbar et al 1994
ca. 1600-1620	South Africa; decline of mean temperature in coastal water and in continental air. This study has relatively low time resolution.	oxygen isotope ratios	Tyson & Lindesay 1992
ca. 1590-1630	Peru, Quelccaya glacier; the oxygen isotope ratio in annual ice core layers shows distinctly reduced variability.	oxygen isotope ratio	Thompson 1992
1606; 1604-1628	Tasmania; summer temperature (Nov-Apr);1606 was cold, the only tree-ring year with especially notable "narrow and light" character in entire series 900-1988; 1604-1628 is the fifth-coldest 25-year interval of the summer temperature record.	tree-ring width	Cook et al 1992
ca. 1603-1610	South-central Chile, Chiloa island; unusually strong summer precipitation.	tree-ring width	Boninsegna 1992
1600	Southeastern Pacific Ocean; third highest winter anticyclone belt index for entire record (AD 1450-1972), suggesting El Niño conditions.	tree-ring width	Boninsegna 1992
1600; 1601-1605	New Zealand, South Island; 1600 AD absolute maximum growth in entire record (1350-1991); this is followed by a dramatic decline until about 1604/05, suggesting cooling.	tree-ring width	D'Arrigo et al 1995

## **Potential 1600-1610 AD Climatic Forcing Factors**

---

Causes of decade- to century-scale climate variability, such as solar variability, volcanic aerosol loading, fluctuations in ocean circulation, and natural unforced variability interact at varying spatial and temporal scales to provide the climatic complexity of the last millennium (reviewed by Crowley and Kim 1993 and by Rind and Overpeck 1993). In addition to ENSO events (discussed above), we consider a few other likely causes that may have contributed to climatic anomalies around 1605 AD.

### **Solar Variability**

The reconstructed solar irradiance was declining in the early 17th century (Lean *et al* 1995). The dramatic climatic changes around 1605 AD, including the observed cold temperatures during the first decades of the 17th century, clearly predate the 1650-1715 Maunder Minimum (Meko 1991; Stuiver and Braziunas 1993) when the absence of sunspots decreased the solar radiation influx to a long-term minimum (Eddy 1976). It appears that the Spörer Minimum low solar irradiance, which lasted into the 16th century, may have cooled the earth and thus contributed to the ca. 1605 AD extreme climatic events. However, 1604 AD marks the minimum of atmospheric  $\Delta^{14}\text{C}$  between the Spörer and Maunder Minima, which indicates temporarily increased solar activity and shielding of the earth from  $^{14}\text{C}$ -producing galactic cosmic rays (Stuiver and Braziunas 1993). This argues against a direct, major role of solar-induced cooling for the ca. 1605 AD events.

### **Explosive Volcanism**

Explosive volcanism increases the stratospheric aerosol load and reduces solar radiation receipts in the lower troposphere. It is now recognized as a major factor for short-term atmospheric and continental cooling (Nesje and Johannessen 1992; Bradley and Jones 1993; Stuiver *et al* 1995), although the actual temperature effects differ geographically and over the few years following an eruption (Robock and Mao 1995; Portman and Gutzler 1996). Clusters of intense volcanism may cause a decadal-scale thermal excursion (Crowley and Kim 1996). The acid fallout from a large 1601 AD, albeit geographically unidentified, volcanic eruption is evident from the Crête ice core record in Greenland (Hammer *et al* 1980). Lamb (1970, p. 501) noted: "The sun greatly dimmed by a constant haze over southern Scandinavia in 1601... The Sun and Moon appeared 'reddish, faint and lacked brilliance' in central Europe all through the year 1601 and up to the end of July 1602". The spring of 1601 was anomalously cold in northern Italy (Pavese *et al* 1992). Cold temperatures are evident in western USA tree rings for 1601 AD (LaMarche and Hirschboeck 1984; Scuderi 1990) and in northern Fennoscandian tree-rings where

1600/1601 indicates the lowest reconstructed July/August temperature of the entire 1580-1975 record (Briffa and Schweingruber 1992).

Other known volcanic eruptions in 1600 to 1610 include Mount Etna in Italy, which was active from 1603 to 1610, with a climax around 1606/07 (Lamb 1970). In the Southern Hemisphere, eyewitness accounts noted the eruption of Huaynaputina in Peru, the most explosive event ever recorded in the central Andes of Peru. Its February/March 1600 eruption provided an absolute date for a prominent volcanic ash layer in the nearby Quelccaya glacier ice core (Thompson and Mosley-Thompson 1989). In the same year, the Ecuadorian volcano Quilotoa erupted (Bradley and Jones 1992). An unknown eruption around 1605/06 with influence on the Southern Hemisphere may have caused a 1606 AD “especially notable narrow and light” tree-ring in Huon pine in Tasmania, the only one of this character in a 900-1988 data series (Cook *et al* 1992).

The North Atlantic zone of main cyclonic activity tends to shift south in the summers after great eruptions, this accounting for many, perhaps most, of the coldest, wettest summers of the last 300 years in western Europe and eastern North America (Lamb 1982, p. 63). The severity of the 1600/01 eruptions seems to have caused a series of disastrous harvests in Russia, leading to the 1601-1603 “Great Famine” with a subsequent “Godunov Hunger Riot”; reportedly “one third of the Moscow Tzardom” population died — 120,000 people perished from hunger in Moscow alone (Borisenkov 1992).

## **Large-Scale Cooling, Meridional Shifts of Midlatitude Storm Tracks, and ENSO**

---

The quasi-stationary planetary waves and the transient component of atmospheric heat transport (*eg*, frontal cyclones) are mainly forced by patterns of temperature gradients and by orography. Therefore, an alteration of global temperature gradients greatly influences the planetary waves, the storm track pattern of the transients, and ultimately is linked to changes in regional precipitation patterns (Trenberth 1993). More specifically, global cooling decreases the Hadley circulation and causes a southward shift of storm tracks in midlatitudes in the Northern Hemisphere, with severe socio-economic repercussions on human cultures (Bryson and Murray 1977).

With regard to the southwestern USA, several authors have noted a connection between precipitation, upper air pressure anomalies, elevated sea surface temperature in the eastern North Pacific, and ENSO events (Cayan and Webb 1992; Haston and Michaelsen 1994; Ely *et al* 1994; Graham *et al* 1994). ENSO is only one of many factors that affect the occurrence of winter floods in the southwest, but an increased frequency of large winter floods during multiple-year periods dominated by a

negative Southern Oscillation Index and the near absence of large floods during the intervening periods led Ely *et al* (1994) to suggest that the warm phase of ENSO is influential in producing the most extreme winter floods. The ca. 1605 occurrences of ENSO-related, near-coastal, relatively warm sea surface temperature off California during a decade of very cold mean Northern Hemisphere continental summer temperatures are not contradictory. In fact, reconstructions of summer temperature using tree-ring data from the western USA correlate relatively poorly with the overall Northern Hemisphere summer temperature reconstruction (Bradley and Jones 1993). Presumably this is because western North American summer temperatures are strongly buffered by winds from the Pacific Ocean.

### **Synthesis of Paleoenvironmental Evidence: What Led to the ca. 1605 AD Flood Event?**

---

Starting around 1550 AD, large-scale cooling had set in, covering much of the Northern Hemisphere (Bradley and Jones 1993). One may speculate that the cooling was in response to reduced solar irradiance, based on a strong correlation between reconstructed solar irradiance and Northern Hemisphere surface temperature that was shown for the subsequent, pre-industrial period 1610-1800 (Lean *et al* 1995; Crowley and Kim 1996). Although the concept of a global "Little Ice Age" is no longer supported by the available evidence (Hughes and Diaz 1994), the first decade of the 17th century stands out as having exceptionally cold conditions that were sufficiently widespread to represent a large-scale climatic signal (Bradley and Jones 1993). Our suggested paleoclimatic scenario for 1600-1610 is illustrated in Figure 7. Starting in 1600/01, pre-existing cool conditions were exacerbated in many regions by a cluster of large volcanic activities that caused further, excessive short-term cooling. Strong El Niño conditions in the eastern Pacific, probably around 1604, increased the sea surface temperature and the moisture loading of vigorous cyclones that were forced to travel eastward along southerly displaced storm tracks into Southern California. The major flooding likely occurred in 1605 AD  $\pm$  1 year. The region was just recovering from a severe, late-16th-century drought (Graumlich 1993; D'Arrigo and Jacoby 1991; Biondi *et al* this volume), which had left the soil vulnerable to erosion and may thus have contributed to the remarkable thickness of the flood deposit in Santa Barbara Basin.

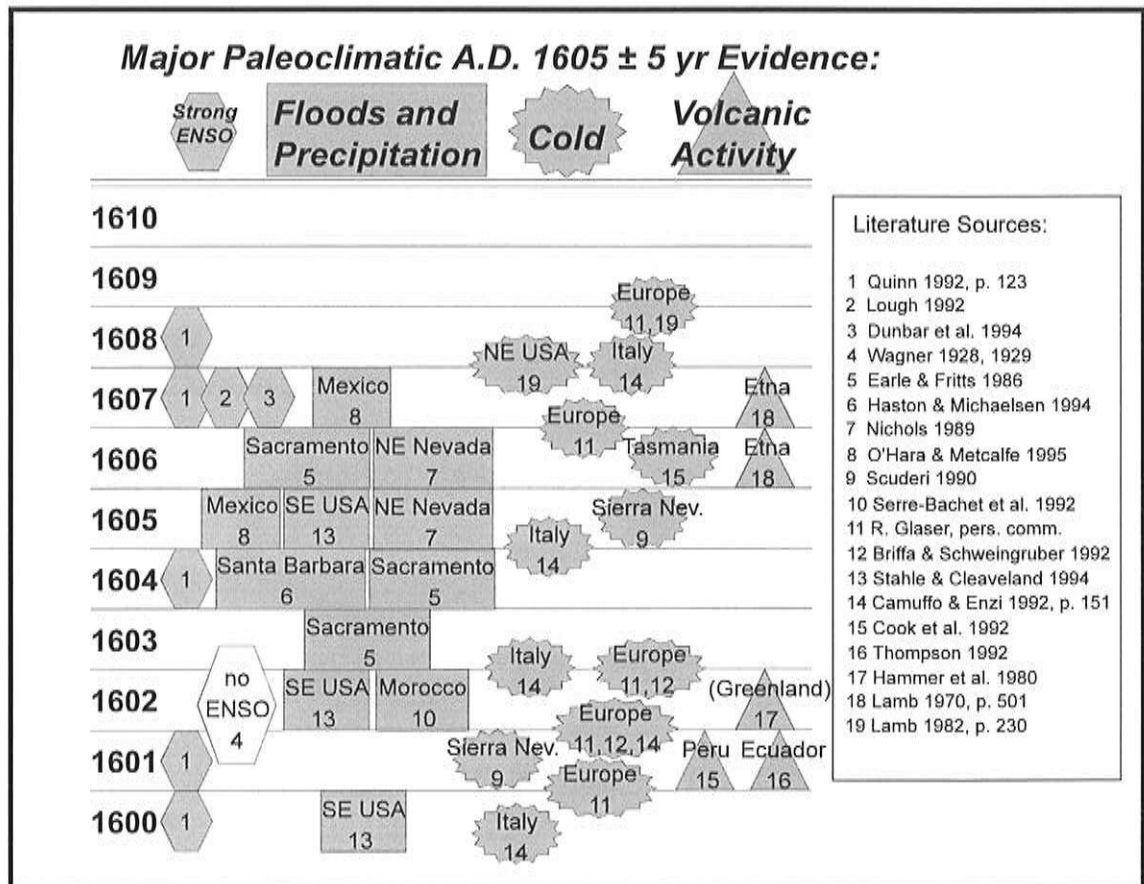


Figure 7. Chronology of major climatic evidence and relevant historical observations, 1600-1610 AD.

## Conclusion

The paleoclimatic contrasts around 1605 AD from many regions in both hemispheres seem to be consistent with an equatorward displacement of major wind patterns and associated storm tracks. A relatively cool mean global temperature around the turn of the 16th century was exacerbated after 1600 AD by a sharp volcanic-induced cold spell. With the additional influence of a strong ENSO event around 1604 AD, precipitation in Southern California from vigorous, southerly displaced cyclones climaxed and resulted in highly unusual and distinctive flood and lake deposits in Santa Barbara Basin and at the terminus of the Mojave River.

## Acknowledgments

Funding was provided by National Science Foundation grant OCE-9301438; by Western Regional Center of the National Institute for Global Environmental Change (WESTGEC) grant 92-007; by NATO Collaborative Research Grant 930391; and by National Oceanic and Atmospheric Administration grant NA16RC0083-01.

## References

- American Petroleum Institute. 1985. Standard procedure for field testing drilling fluids. API RP 13B, Washington DC, 47 pp.
- Boninsegna, J.A. 1992. South American dendroclimatological records. Pages 446-462 in *Climate Since A.D. 1500*. R.S. Bradley and P.D. Jones, editors. Routledge, London.
- Borisenkov, Ye.P. 1992. Documentary evidence from the U.S.S.R. Pages 171-183 in *Climate Since A.D. 1500*. R.S. Bradley and P.D. Jones, editors. Routledge, London.
- Bradley, R.S., and P.D. Jones. 1992. Records of explosive volcanic eruptions over the last 500 years. Pages 606-622 in *Climate Since A.D. 1500*. R.S. Bradley and P.D. Jones, editors. Routledge, London.
- Bradley, R.S., and P.D. Jones. 1993. "Little Ice Age" summer temperature variations: their nature and relevance to recent global warming trends. *The Holocene*, 3:367-376.
- Brassell, S.C., G. Eglinton, I. Marlowe, M. Sarnthein, and U. Pflaumann. 1986. Molecular stratigraphy: a new tool for climatic assessment. *Nature*, 320:129-133.
- Briffa, K.R., and F.H. Schweingruber. 1992. Recent dendroclimatic evidence of northern and central European summer temperatures. Pages 366-392 in *Climate Since A.D. 1500*. R.S. Bradley and P.D. Jones, editors. Routledge, London.
- Briffa, K.R., T.S. Bartholin, D. Eckstein, P.D. Jones, W. Karlén, F.H. Schweingruber, and P. Zetterberg. 1990. A 1,400-year tree-ring record of summer temperatures in Fennoscandia. *Nature*, 346:434-439.
- Bryson, R.A., and T.J. Murray. 1977. *Climates of Hunger*. University of Wisconsin Press, Madison, Wisconsin, 171 pp.
- Buisman, J. 1984. *Bar en Boos, Zeven Eeuwen Winterweer in de Lage Landen*. Bosch and Keuning, Baam, Netherlands.
- Camuffo, D. 1987. Freezing of the Venetian lagoon since the 9th century A.D. in comparison to the climate of western Europe and England. *Climatic Change*, 10:43-66.
- Camuffo, D., and S. Enzi. 1992. Reconstructing the climate of northern Italy from archive sources. Pages 143-154 in *Climate Since A.D. 1500*. R.S. Bradley and P.D. Jones, editors. Routledge, London.
- Cayan, D.R., and R.H. Webb. 1992. El Niño/Southern Oscillation and streamflow in the western United States. Pages 29-68 in *El Niño. Historical and Paleoclimatic Aspects of the Southern Oscillation*. H.F. Diaz and V. Markgraf, editors. Cambridge University Press, Cambridge.
- Cohen, A.L., and P.D. Tyson. 1995. Sea-surface temperature fluctuations during the Holocene off the south coast of Africa: implications for terrestrial climate and rainfall. *The Holocene*, 5:304-312.
- Cook, E., T. Bird, M. Peterson, M. Barbetti, B. Buckley, R. D'Arrigo, and R. Francey. 1992. Climatic change over the last millennium in Tasmania reconstructed from tree-rings. *The Holocene*, 2:205-217.
- Crowley, T.J., and K.-Y. Kim. 1993. Towards development of a strategy for determining the origin of decadal-centennial scale climate variability. *Quaternary Science Reviews*, 12:375-385.
- Crowley, T.J., and K.-Y. Kim. 1996. Comparison of proxy records of climate change and solar forcing. *Geophysical Research Letters*, 23:359-362.
- D'Arrigo, R., and G.C. Jacoby. 1991. A 1000-year record of winter precipitation from northwestern New Mexico, USA: a reconstruction from tree-rings and its relation to El Niño and the Southern Oscillation. *The Holocene*, 1:95-101.
- D'Arrigo, R.D., B.M. Buckley, E.R. Cook, and W.S. Wagner. 1995. Temperature-sensitive tree-ring width chronologies of pink pine (*Halocarpus biformis*) from Stewart Island, New Zealand. *Palaeogeography, Palaeoclimatology, Palaeoecology*, 119:293-300.

- Diaz, H.F., and R.S. Pulwarty. 1992. A comparison of Southern Oscillation and El Niño signals in the tropics. Pages 175-192 in *El Niño. Historical and Paleoclimatic Aspects of the Southern Oscillation*. H.F. Diaz and V. Markgraf, editors. Cambridge University Press, Cambridge.
- Drake, D.E., P. Fleischer, and R.L. Kolpack. 1971. Transport and deposition of flood sediment, Santa Barbara Channel, California. Pages 95-113 of Vol. 2, Chapter 5 in *Survey of the Santa Barbara Channel Oil Spill 1969-1970*. R.L. Kolpack, editor. Allan Hancock Foundation, University of Southern California, Los Angeles.
- Dunbar, R.B., G.M. Wellington, M.W. Colgan, and P.W. Glynn. 1994. Eastern Pacific sea surface temperature since 1600 A.D.: The  $\delta^{18}\text{O}$  record of climate variability in Galápagos corals. *Paleoceanography*, 9:291-315.
- Earle, C.J., and H.C. Fritts. 1986. *Reconstructing river flow in the Sacramento Basin since 1560*. Report to the California Department of Water Resources; Laboratory of Tree-Ring Research, University of Arizona, Tucson, Arizona, 122 pp.
- Eddy, J.A. 1976. The Maunder Minimum. *Science*, 192:1,189-1,202.
- Eglinton, G., S.A. Bradshaw, A. Rosell, M. Sarnthein, U. Pflaumann, and R. Tiedemann. 1992. Molecular record of secular sea surface temperature changes on 100-year timescales for glacial terminations I, II, and IV. *Nature*, 356:423-426.
- Ely, L.L., Y. Enzel, and D.R. Cayan. 1994. Anomalous North Pacific atmospheric circulation and large winter floods in the Southwestern United States. *Journal of Climate*, 7:977-987.
- Enfield, D.B. 1992. Historical and prehistorical overview of El Niño/Southern Oscillation. Pages 95-118 in *El Niño: Historical and Paleoclimatic Aspects of the Southern Oscillation*. H.F. Diaz and V. Markgraf, editors. Cambridge University Press, Cambridge.
- Enzel, Y. 1992. Flood frequency of the Mojave River and the formation of late Holocene playa lakes, southern California, USA. *The Holocene*, 2:11-18.
- Enzel, Y., D.R. Cayan, R.Y. Anderson, and S.G. Wells. 1989. Atmospheric circulation during Holocene lake stands in the Mojave Desert: Evidence of regional climate change. *Nature*, 341:44-48.
- Farquhar, F.P. (editor). 1966. *Up and Down California in 1860-1864. The Journal of William H. Brewer*. Univ. of Calif. Press, 2nd edition, 583pp.
- Graham, N.E., T.P. Barnett, and R. Wilde. 1994. On the roles of tropical and midlatitude SST's in forcing interannual to interdecadal variability in the winter Northern Hemisphere circulation. *Journal of Climate*, 7:1,416-1,441.
- Graumlich, L.J. 1993. A 1000-year-record of temperature and precipitation in the Sierra Nevada. *Quaternary Research*, 39:249-255.
- Hammer, C.U., H.B. Clausen, and W. Dansgaard. 1980. Greenland ice sheet evidence of post-glacial volcanism and its climatic impact. *Nature*, 288:230-235.
- Haston, L., and J. Michaelsen. 1994. Long-term central coastal California precipitation variability and relationships to El Niño-Southern Oscillation. *Journal of Climate*, 7:1,373-1,387.
- Hughes, M.K., and P.M. Brown. 1992. Drought frequency in central California since 101 B.C. recorded in giant sequoia tree rings. *Climate Dynamics*, 6:161-167.
- Hughes, M.K., and H.F. Diaz. 1994. Was there a 'Medieval Warm Period', and if so, where and when? *Climatic Change*, 26:109-142.
- Hurrell, J.W. 1995. Decadal trends in the North Atlantic oscillation: Regional temperatures and precipitation. *Science*, 269:676-679.
- Jinjun Ji., N. Petit-Maire, and Zhongwei Yan. 1993. The last 1000 years: climatic change in arid Asia and Africa. *Global and Planetary Change*, 7:203-210.
- Katz, R.W., and B.G. Brown. 1992. Extreme events in a changing climate: variability is more important than averages. *Climatic Change*, 21:289-302.
- Kennedy, J.A., and S.C. Brassell. 1992. Molecular records of twentieth century El Niño events in laminated sediments from the Santa Barbara basin. *Nature*, 357:62-64.

- Kennett, J.P., J.G. Baldauf, and M. Lyle. 1995. *Proceedings of the Ocean Drilling Program, Scientific Results, 146 (Pt. 2)*, College Station, Texas, 360pp.
- LaMarche, V.C., and K.K. Hirschboeck. 1984. Frost rings in trees as records of major volcanic eruptions. *Nature*, 307:121-126.
- Lamb, H.H. 1970. Volcanic dust in the atmosphere; with a chronology and assessment of its meteorological significance. *Philosophical Transactions of the Royal Society of London, A* 266: 425-533.
- Lamb, H.H. 1982. *Climate, History and the Modern World*. Methuen & Co. 1982, London, 387pp.
- Lamb H.H. 1985. *Climatic History and the Future*. Princeton University Press, Princeton, New Jersey, 835 pp. (reprinted volume 2 of *Climate: Present, Past and Future*, originally published in 1977 by Methuen, New York).
- Lange, C.B., A. Schimmelmann, M.K. Yasuda, and W.H. Berger. Paleoclimatic significance of marine varves off southern California. In: *Southern California Climate: Trends and Extremes of the Past 2000 Years*. P. Wigand and M. Rose, editors. Los Angeles County Natural History Museum, Los Angeles. *In press*.
- Lean, J., J. Beer, and R. Bradley. 1995. Reconstruction of solar irradiance since 1610: Implications for climate change. *Geophysical Research Letters*, 22:3195-3198.
- Liu Tungsheng, Ding Zhongli, Chen Mingyang, and An Zhisheng. 1989. The global surface energy system and the geological role of wind stress. *Quaternary International*, 2:43-54.
- Lough, J.M. 1992. An index of the Southern Oscillation reconstructed from western North American tree-ring chronologies. Pages 215-226 in *El Niño. Historical and Paleoclimatic Aspects of the Southern Oscillation*. H.F. Diaz and V. Markgraf, editors. Cambridge University Press, Cambridge.
- Maley, J. 1973. Mecanisme des changements climatiques aux basses latitudes. *Palaeogeography, Palaeoclimatology, Palaeoecology*, 14:193-227.
- Meko, D.M. 1991. Inter-regional correlation in tree-growth variations in the western United States, 1513-1964, at ENSO, sunspot, and longer frequency bands. Pages 179-185 in *Proceedings of the Seventh Annual Pacific Climate (PACLIM) Workshop, April 1990*. J.L. Betancourt and V.L. Tharp, editors. California Department of Water Resources, Interagency Ecological Studies Program Technical Report 26.
- Namias, J. 1971. The 1968-69 winter as an outgrowth of sea and air coupling during antecedent seasons. *Journal of Physical Oceanography*, 1:65-81.
- Nesje, A., and T. Johannessen. 1992. What were the primary forcing mechanisms of high-frequency Holocene climate and glacier variations? *The Holocene*, 2:79-84.
- Nichols, W.D. 1989. Reconstructed drought history, north-central Great Basin: 1601-1982. Pages 61-67 in *Aspects of Climate Variability in the Pacific and the Western Americas, Geophysical Monograph 55*. D.H. Peterson, editor. American Geophysical Union, Washington D.C.
- Nicholson, S.E. 1980. Saharan climates in historic times. Pages 173-200 in *The Sahara and the Nile*. M.A.J. Williams and H. Faure, editors. A.A. Balkema, Rotterdam, Netherlands.
- O'Hara, S.L., and S.E. Metcalfe. 1995. Reconstructing the climate of Mexico from historical records. *The Holocene*, 5:485-490.
- Parry, A.T. 1992. *Automation of the  $U^k_{37}$  method*. M.S. Thesis, School of Chemistry, University of Bristol, England, 64pp.
- Pavese, M.P., V. Banzon, M. Colacino, G.P. Gregori, and M. Pasqua. 1992. Three historical data series on floods and anomalous climatic events in Italy. Pages 155-170 in *Climate Since A.D. 1500*. R.S. Bradley and P.D. Jones, editors. Routledge, London.
- Pfister, C., Yan Z., and H. Schüle. 1994. Climatic variations in western Europe and China, AD 1645-1715: a preliminary continental-scale comparison of documentary evidence. *The Holocene*, 4:206-211.
- Portman, D.A., and D.S. Gutzler. 1996. Explosive volcanic eruptions, the El Niño-Southern Oscillation, and U.S. climate variability. *Journal of Climate*, 9:17-33.

- Prahl, F.G., L.A. Muehlhausen, and D.L. Zahnle. 1988. Further evaluation of long-chain alkenones as indicators of paleoceanographic conditions. *Geochimica et Cosmochimica Acta*, 52:2303-2310.
- Quinn, W.H. 1992. A study of southern oscillation-related climatic activity for A.D. 622-1900 incorporating Nile River flood data. Pages 119-149 in *El Niño. Historical and Paleoclimatic Aspects of the Southern Oscillation*. H.F. Diaz and V. Markgraf, editors. Cambridge University Press, Cambridge.
- Rind, D., and J. Overpeck. 1993. Hypothesized causes of decade-to-century-scale climate variability: climate model results. *Quaternary Science Reviews*, 12:357-374.
- Robock, A., and J. Mao. 1995. The volcanic signal in surface temperature observations. *Journal of Climate*, 8:1,086-1,103.
- Roden, G.I. 1989. Analysis and interpretation of long-term climatic variability along the west coast of North America. Pages 93-111 in *Aspects of Climate Variability in the Pacific and the Western Americas, Geophysical Monograph 55*. D.H. Peterson, editor. American Geophysical Union, Washington D.C.
- Rogers, J.C. 1985. Atmospheric circulation changes associated with the warming over the northern North Atlantic in the 1920s. *Journal of Climate and Applied Meteorology*, 24:1,303-1,310.
- Schimmelmann, A., and M. Kastner. 1993. Evolutionary changes over the last 1000 years of reduced sulfur phases and organic carbon in varved sediments of the Santa Barbara Basin, California. *Geochimica et Cosmochimica Acta*, 57:67-78.
- Schimmelmann, A., and M.J. Tegner. 1991. Historical oceanographic events reflected in  $^{13}\text{C}/^{12}\text{C}$  ratio of total organic carbon in laminated Santa Barbara Basin sediment. *Global Biogeochemical Cycles*, 5:173-188.
- Schimmelmann, A., C.B. Lange, J. Michaelsen, and W.H. Berger. 1990. Climatic changes reflected in laminated Santa Barbara Basin sediments. Pages 97-99 in *Proceedings of the Sixth Annual Pacific Climate (PACCLIM) Workshop, March 5-8, 1989*. J.L. Betancourt and A.M. MacKay, editors. California Department of Water Resources, Interagency Ecological Studies Program Technical Report 23.
- Scuderi, L.A. 1990. Tree-ring evidence for climatically effective volcanic eruptions. *Quaternary Research*, 34:67-85.
- Serre-Bachet, F., J. Guiot, and L. Tessier. 1992. Dendroclimatic evidence from southwestern Europe and northwestern Africa. Pages 349-365 in *Climate Since A.D. 1500*. R.S. Bradley and P.D. Jones, editors. Routledge, London.
- Serre-Bachet, F. 1994. Middle Ages temperature reconstructions in Europe, a focus on Northeastern Italy. *Climatic Change*, 26:213-224.
- Smith, D.J., D.P. McCarthy, and M.E. Colenutt. 1995. Little Ice Age glacial activity in Peter Lougheed and Elk Lakes provincial parks, Canadian Rocky Mountains. *Canadian Journal of Earth Sciences*, 32:579-589.
- Soutar, A., and P.A. Crill. 1977. Sedimentation and climatic patterns in the Santa Barbara Basin during the 19th and 20th Centuries. *Geological Society of America Bulletin*, 88:1,161-1,172.
- Stahle, D.W., and M.K. Cleaveland. 1994. Tree-ring reconstructed rainfall over the southeastern U.S.A. during the Medieval Warm Period and Little Ice Age. *Climatic Change*, 26:199-212.
- Stine, S. 1987. *Mono Lake: The Past 4,000 Years*. Ph.D. dissertation, University of California, Berkeley, 615 pp. (unpublished).
- Stine, S. 1990. Late Holocene fluctuations of Mono Lake, eastern California. *Palaeogeography, Palaeoclimatology, Palaeoecology*, 78:333-381
- Stuiver, M., and T.F. Braziunas. 1993. Sun, ocean, climate and atmospheric  $^{14}\text{CO}_2$ : an evaluation of causal and spectral relationships. *The Holocene*, 3:289-305.
- Stuiver, M., P.M. Grootes, and T.F. Braziunas. 1995. The GISP  $\delta^{18}\text{O}$  climate record of the past 16,500 years and the role of the sun, ocean, and volcanoes. *Quaternary Research*, 44:341-354.

- Thompson, L.G. 1992. Ice core evidence from Peru and China. Pages 517-548 in *Climate Since A.D. 1500*. R.S. Bradley and P.D. Jones, editors. Routledge, London.
- Thompson, L.G., and E. Mosley-Thompson. 1989. One-half millennia of tropical climate variability as recorded in the stratigraphy of the Quelccaya ice cap, Peru. Pages 15-31 in *Aspects of Climate Variability in the Pacific and the Western Americas, Geophysical Monograph 55*. D.H. Peterson, editor. American Geophysical Union, Washington D.C.
- Thunell, R.C., E. Tappa, and D.M. Anderson. 1995. Sediment fluxes and varve formation in Santa Barbara Basin, offshore California. *Geology*, 23:1,083-1,086.
- Trenberth, K. E. 1993. Northern Hemisphere climate change; physical processes and observed changes. Pages 35-59 in *Earth System Responses to Global Change: Contrasts between North and South America*. H.A. Mooney, E.R. Fuentes, and B.I. Kronberg, editors. Academic Press, San Diego.
- Tyson, P.D., and J.A. Lindesay. 1992. The climate of the last 2000 years in southern Africa. *The Holocene*, 2:271-278.
- Villalba, R. 1994. Tree-ring and glacial evidence for the Medieval Warm Epoch and the Little Ice Age in southern South America. *Climatic Change*, 26:183-197.
- Wagner, H.R. 1928. Spanish voyages to the Northwest coast in the sixteenth century. Chapter XI: Father Antonio de la Ascension's account of the voyage of Sebastian Vizcaino. *California Historical Society Quarterly*, 7:295-394.
- Wagner, H.R. 1929. Spanish voyages to the Northwest coast in the sixteenth century. Appendix G: The Bolaños-Ascension derrotero. *California Historical Society Quarterly*, 8:55-68.
- Whetton, P., and I. Rutherford. 1994. Historical ENSO teleconnections in the eastern hemisphere. *Climatic Change*, 28:221-253.
- Whetton, P., R. Allan, and I. Rutherford. 1996. Historical ENSO teleconnections in the eastern hemisphere: comparison with latest El Niño series of Quinn. *Climatic Change*, 32:103-109.
- Zhang Linyuan, Jiang Zhaoli, and Lu Pengnan. 1995. Zur Genese des Trockenklimas in Nordwestchina. *Naturwissenschaften*, 82:370-374 (in German).
- Zhaodong Feng, L.G. Thompson, E. Mosley-Thompson, and T.Yao. 1993. Temporal and spatial variations of climate in China during the last 10000 years. *The Holocene*, 3:174-180.

# A Late-Holocene Pollen Record from Lower Pahranaagat Lake, Southern Nevada, USA: High Resolution Paleoclimatic Records and Analysis of Environmental Responses to Climate Change

Peter E. Wigand

**ABSTRACT:** High resolution paleobotanical records provide sufficient detail to correlate events regionally. Once correlated events can be examined in tandem to determine the underlying inputs that fashioned them. Several localities in the Great Basin have paleobotanical records of sufficient detail to generate regional reconstructions of vegetation changes for the last 2 ka and provide conclusions as to the climates that caused them. In southern Nevada, analysis of 266 pollen samples from the upper two-thirds of a 15-meter-long, 10-cm-diameter set of overlapping cores retrieved from Lower Pahranaagat Lake (elevation 975 meters), Lincoln County, Nevada, is providing a detailed record of vegetation change at an interval of every 14 years over the last 3.8 ka. Samples, averaging about 3.8 years of pollen deposition with about 10.4 year gaps between each, outline a record of dry and wet periods with rapid onsets and terminations. Periodic increases in the values of sagebrush (*Artemisia*) pollen, sometimes coincident with increases in juniper pollen reflect intervals of cooler and/or wetter climate. Occasional, sometimes severe, drought is marked by increased bur sage (*Ambrosia*-type) and saltbush (*Chenopodiaceae*) pollen and decreased regional conifer pollen. Drier climates between 3.0 and 2.5 ka, 2.4 and 2.0 ka are eclipsed in magnitude by the severe droughts of the last 1.9 ka. In particular, the droughts between 1.9 and 1.6 ka and at 0.9 and 0.3 ka have little parallel during the late Holocene (last 4.0 ka) in southern Nevada. The ratio of aquatic to littoral pollen types indicates generally deeper water conditions about 1.6 to 1.3 ka (also characteristic of most of the early part of the record from 3.7 to 2.0 ka) and more variable, but predominantly more marshy, conditions during most of the last 1.3 ka. Ongoing geomorphic investigations in the Lower Pahranaagat Lake area suggest that the sudden shift from lake to marsh conditions around 1.2 to 1.4 ka may be linked to the impact of extreme rainfall events. These may have eroded a spillway through the alluvial fans that impounded the lake during the early portion of the Late Holocene (3.7-1.4 ka), thereby reducing the effective lake level after 1.4 ka. Increasing *Pinus* (pine) pollen values with respect to *Juniperus* (juniper) pollen values indicate that piñon pine is now more abundant in the southern Great Basin than at any time since the beginning of the "Neoglacial", about 4.0 ka. This is due not only to a shift from harsher winters about 2.0 ka (in part evidenced by the decline of juniper dominance in the woodland), but also to periods of summer-shifted rainfall (increased summer rainfall often with decreased winter rainfall), which favored seedling survival during the summer. In southern Nevada, evidence of summer-shifted precipitation during the first millennium of the Christian Era is seen in the expansion of grasses (reflected in *Poaceae* pollen) preceding expansions of piñon pine without coincident expansions of winter precipitation-loving species such as sagebrush and juniper. To the north, pollen and woodrat midden records from the Carson Sink of the central Great Basin (Lead Lake, Nevada) evidence summer-shifted rainfall in contemporaneous expansion of piñon pine into semi-arid woodlands. Pollen records from the northern Great Basin (in particular, the high-resolution pollen record from Diamond Pond, south-central Oregon) indicate grass expansion at the expense of juniper at the same time, providing further evidence of a major period of summer-shifted precipitation that characterized much of the Intermountain West.

## **Introduction**

---

Most paleoenvironmental proxy data have inherent time lags that limit their utility in reconstruction of paleoclimatic records of sufficient detail and synchronicity for deriving understandings of environmental processes. With the exception of dendroclimatology, and perhaps studies of varved lake sediments containing invertebrates, algae, and pollen, significant periods ranging from several years to millennia may intervene between climatic change and its first manifestation in most paleoclimatic proxy records as traditionally analyzed.

Efforts to recover high-resolution paleoenvironmental records from the Great Basin have been dominated by high-elevation bristlecone pine dendroclimatological research (Graybill *et al* 1994). Through measurements of the tree-rings (an indirect assessment of the climate-driven productivity of the sampled trees) otherwise unattainable reconstructions of the exact timing and magnitude of past precipitation and, to a lesser extent, of past temperature extremes can be achieved. Although these records indicate the physiological response of bristlecone pine trees to changing climates, they give no indication of the response of the rest of the botanical community to these changes. This role is filled by both pollen and woodrat midden records.

Both fossil pollen and woodrat midden records traditionally have been used to reveal past plant/climate interactions through reconstruction of past **terrestrial** plant community composition (Wigand 1987; Spaulding 1985). Although this may reveal an ultimate response to climate, the composition and structure of a plant community at a particular time in the past might not actually reflect an immediate link to the climate of that period. Instead, a community reconstruction might mirror the conditions of a previous climate state.

The response rate of plant communities to climate change is constrained by many factors including:

- Distance to the plant source area.
- Intervening geographical barriers along the path to the plant source area.
- Seed dispersal mechanisms of the plant species.
- Availability of niches opened through disturbance phenomena (insect infestations, disease, fire).

In addition, an apparent lag may occur in the paleobotanical record because evidence of a plant might not appear until well after its arrival. For example, it might be many years before a plant is mature enough to become a significant contributor to the regional pollen rain. On the other

hand, its abundance might be low and, therefore, it might not be located near areas (paleobotanical repositories) where its macrofossils (leaves, twigs, *etc*) can be preserved. As a result, even if plants have already become established in an area they might be absent from the fossil woodrat midden, bog, dry cave, or other paleobotanical record.

Changes in **aquatic** plant community composition, however, can reflect the contemporaneous climate state because these communities spread and proliferate rapidly and their remains are almost immediately deposited in localities where they are preserved. Only rarely will aquatic plant communities lag climate change by some interval because their response might mirror longer-term changes in lake or marsh water levels and/or chemistry. Occasionally lagged response in the water chemistry of spring-fed aquatic plant communities reflects the long travel times of regional deep ground water, which evidences the climates of past periods (Smiley and Mehringer no date; Mehringer and Warren 1976; Mehringer and Sheppard 1978).

Finally, no model exists for integrating the various paleobotanical data available to reveal the processes linking climate, biotic response, and its appearance in the paleoenvironmental record. If our understanding of processes of change in the biotic sphere were more complete, we could apply it more rigorously to prediction of potential impacts of future climate changes. Keys to such understanding lie in the promise of combining dendroclimatological data with other high-resolution paleobotanical dataset(s) and in validation of models with both modern and past analogue data.

### **The Great Basin as a Sensitive Indicator of Past Western Climates**

Today, the Great Basin is characterized by semi-arid to arid climates (Houghton 1969; Houghton, Sakamoto, and Gifford 1975). Except for a few mountain summits and the more northerly quarter of the region where ~20 inches is the norm, mean annual precipitation averages less than 10 inches. Due to the effects of latitude and elevation, the cold (10-40°F) winters and hot (50-80°F) summers of the northern Great Basin contrast with the mild winters (40-50°F) and very hot summers (80-90°F) of the southern Great Basin.

Today, as in the past, the Great Basin lies at the intersection of the Pacific, Arctic and Gulf of Mexico pressure systems. Displacement of winter and summer storm-tracks, and penetration of the summer monsoon are all affected by the realignment of these pressure systems through time. Past movements of these systems and their impact on local and regional climate are reflected in the paleoenvironmental record as changes in hydrology, erosional and depositional processes, and vegetation. Evidence that these movements and responses are a reflection of

changes occurring on the global level is clear (Thompson *et al* 1993). In addition, the effect of topographic diversity in the Great Basin on the distribution of precipitation has complicated the effects of the major pressure systems through formation of a multiplicity of habitats within close proximity of each other.

The dramatic year-to-year vegetative response of individual plants within the Great Basin to changing weather arises as the result of millions of years (since late Miocene and early Pliocene times over 5 million years ago) of adaptation to arid and semi-arid conditions (Axelrod 1976). Plants that grow in the Great Basin are often opportunistic, having evolved to quickly take advantage of increased precipitation. Numerous species respond to wetter conditions through rapid vegetative growth and increased pollen and seed production. For example, annual production of biomass in arid and semiarid environments is linearly related to effective precipitation up to 600 cm (Walter 1954), so even moderate increases in rainfall can result in dramatic spurts in biomass production.

In the Great Basin, changes in the areal extent and elevational distribution of plant species through time are accentuated by topographic relief. Climate changes are emphasized by the rainfall forcing effect of north-south trending mountain chains that lie across the paths of Pacific storms. Rapid changes in plant distributions in the Great Basin occur because many plants disperse their seeds with the wind or by animals that feed on them and carry them within their digestive tracts great distances to favorable locations. In addition, long-term seed and plant dormancy, characteristic of many of the plants found in the Great Basin, provides a supply of seeds in most plant communities that can span the periods between favorable conditions and respond rapidly to them. Vegetation response to even single precipitation events can be dramatic, and changed patterns of plant distribution can be noted within one or two years. Reflection of these changes in the paleobotanical record is equally striking and is evidenced in high-frequency pollen records (Wigand 1987; Mehringer and Wigand 1990).

Finally, low effective precipitation has favored the preservation of plant macro- and microfossils in dry cave deposits and woodrat middens. These can provide records of local vegetation spanning tens of thousands of years. Wood from long-dead trees, preserved by dry conditions that characterize upper and lower tree-lines in the Great Basin, provide continuous long-term evidence of climatic variation that has the potential to extend the record obtained from living trees into the early Holocene. Although lakes with lifetimes spanning the Holocene are rare in the Great Basin, especially in the southern portion, desert springs and marshes with long but complex records are available to provide continuous records of local and regional vegetation change for much of the last 11 ka. Often these highly organic sediments have rapid deposition rates from which high-frequency terrestrial and aquatic

pollen and local aquatic plant macrofossil records can be obtained and compared with tree-ring data for the generation of long, detailed records of regional climate and vegetation response.

## **High Resolution Pollen Records from the Great Basin**

Typically in the arid West, reconstructed vegetation history reflecting general trends in changing precipitation and temperature has been based on low-resolution analyses of pollen from stratified deposits in lakes, marshes, and alluvium and on plant remains preserved in ancient woodrat dens (middens) (Mehringer 1985; Mehringer 1986; Betancourt *et al* 1990). Whereas woodrat midden studies result in intermittent records of the appearance and disappearance of specific indicator species that characterized changing plant communities, analyses of pollen records result in the reconstruction of more continuous, long-term shifts in the gross composition of plant communities. In part, this focus has been dictated by techniques available to investigators and by limitations of time and money.

During the last two decades, techniques more amenable to the investigation of past plant response to climate change at the organismal level have been inaugurated in Great Basin paleobotanical analyses to extend our knowledge of plant community history and to reveal differences and/or similarities in the physiological response of plants during the Holocene and the Pleistocene (Long *et al* 1990; Van de Water 1993, Mehringer and Wigand 1990, Wigand and Rose 1990). Thus far, integration of past and ongoing late Holocene paleobotanical research in the Great Basin reveal widespread, contemporaneous, short-term temperature and precipitation changes (Wigand 1987; Wigand *et al* 1995).

Southern Nevada pollen records investigated to date include:

- Those of P.J. Mehringer (1967) from Tule Springs in the Las Vegas Valley and from Saratoga Springs (Smiley and Mehringer no date) in the Panamint Valley.
- Our own from the Oasis Valley northeast of Beatty, Nevada, and Lower Pahranaagat Lake south of Alamo, Nevada (Wigand and Rose 1990; Wigand *et al* 1995; and this report).

These form the basis of relatively continuous late Holocene and intermittent early Holocene and late Pleistocene reconstructions of vegetation history for the northern Mojave Desert. Of these, the pollen sequence from Lower Pahranaagat Lake is providing one of the most important records of vegetation response to past climate currently available in the Great Basin. It has the potential to provide a record of vegetation response to climate change of comparable resolution and time span as the pollen record from Diamond Pond in the Harney Basin of southern Oregon. As

such, it will serve in comparisons of climate change and vegetation response for the northern and southern Great Basin.

Comparison of two such high-resolution records with the dendroclimatic records from the Intermountain West makes it possible to examine vegetation responses to decadal or near-decadal climate shifts, *eg*, El Niño cycles. In addition, the charcoal from these records can provide a means of extending current records of fire history (Swetnam and Betancourt 1990) into previous millennia.

## Lower Pahrnanagat Lake Record

Lower Pahrnanagat Lake lies in one of the many low areas in the fill currently accumulating between the truncated alluvial fans lining the White River Valley in southeastern Nevada (Figure 1). Located about 152 km (92 miles) northeast of Las Vegas, the shallow (~2m deep) lake is lined with tamarisk thickets, sedge marsh, and heliotrope and lizard-tail meadows. In most areas the “green belt” surrounding the lake is no wider

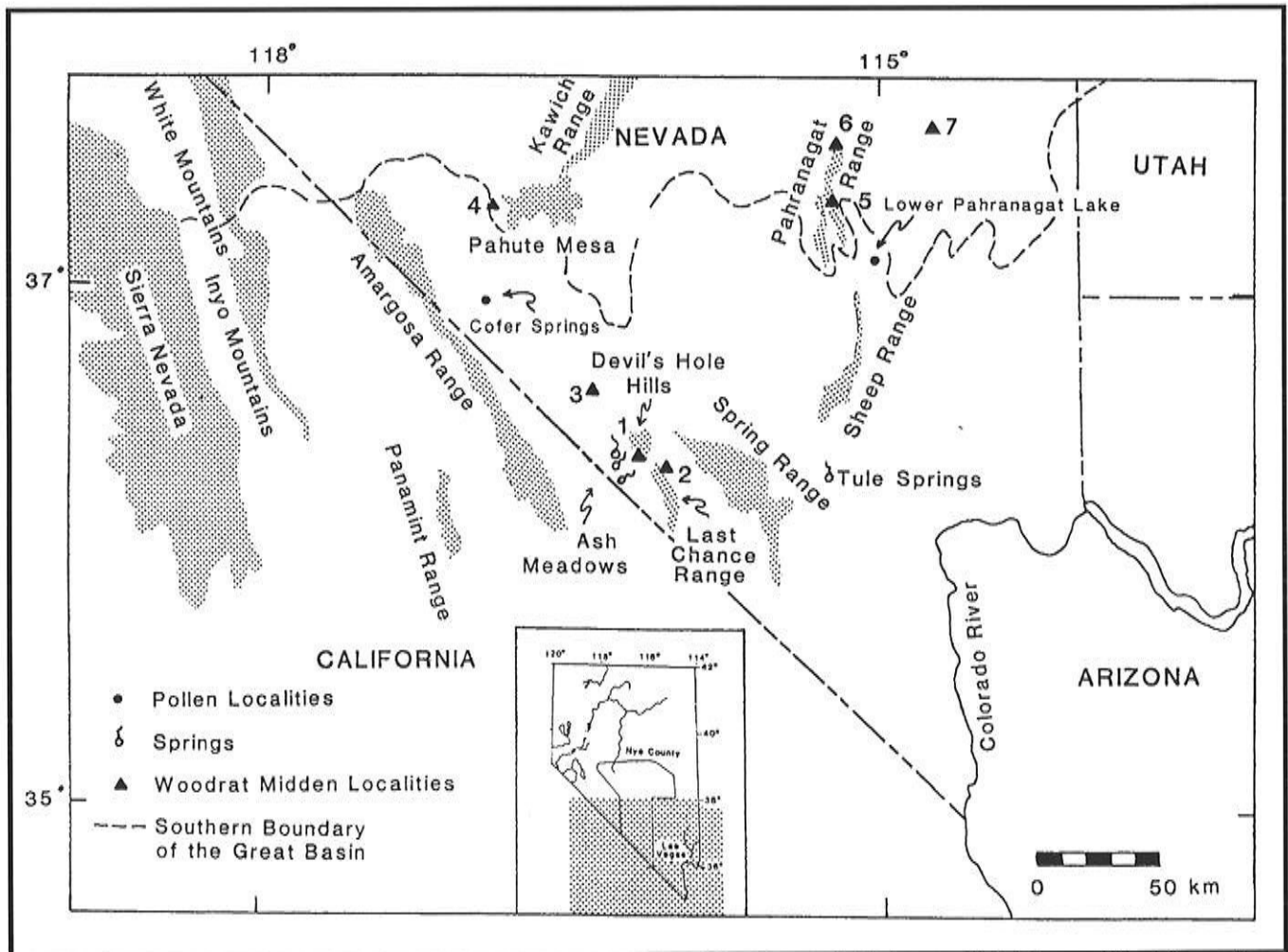


Figure 1 Southern Nevada with pollen localities mentioned in the text and woodrat middens sites studied in the area: (1) Owl Canyon; (2) Last Chance Range; (3) Little Skull Mountain; (4) Ribbon Cliffs; (5) and (6) Pahrnanagat Range, and (7) Pahroc Springs.

than 10 to 30 meters. Areas subjected to annual water fluctuation are characterized by saltgrass. Today the broad alluvial fans surrounding Lower Pahranaagat Lake are covered by creosote bush dominated scrub. Other common components include white bur sage, Mojave yucca, Joshua-tree, purple sage (alluvial channels), Fremont dalea (sandy areas), and many species of cactus.

Sediments from two sets of overlapping cores retrieved in 1988 and 1993 span 5 and 15 meters respectively and contain a radiocarbon-dated environmental record of the last 5.6 ka. Although some of the radiocarbon dates in the upper portion of the cores are contaminated by old carbon, when taken together with the remaining uncontaminated dates taken from sedge peats in the lower portion of the cores, the two dozen radiocarbon dates distributed through the cores indicate an almost continuous rate of sediment accumulation. Based on this chronology, each centimeter-high sample incorporates about 3.8 years of sediment spaced about 14 years apart. The intervening unsampled sediment represents about 10.4 years. Ongoing analyses address the ostracode, diatom, and mollusk records in addition to the pollen and plant macrofossil contents. Variations in charcoal abundance and size in the core are revealing changes in local and regional fire history.

Pollen of terrestrial, littoral and aquatic plants record both local and regional vegetation dynamics and local water table fluctuation in response to climate change during the last 2 ka (eventually to 6 ka) (Figure 2). Increases in juniper (*Juniperus*), and to some extent pine (*Pinus*), pollen values reflect increased winter precipitation and its impact

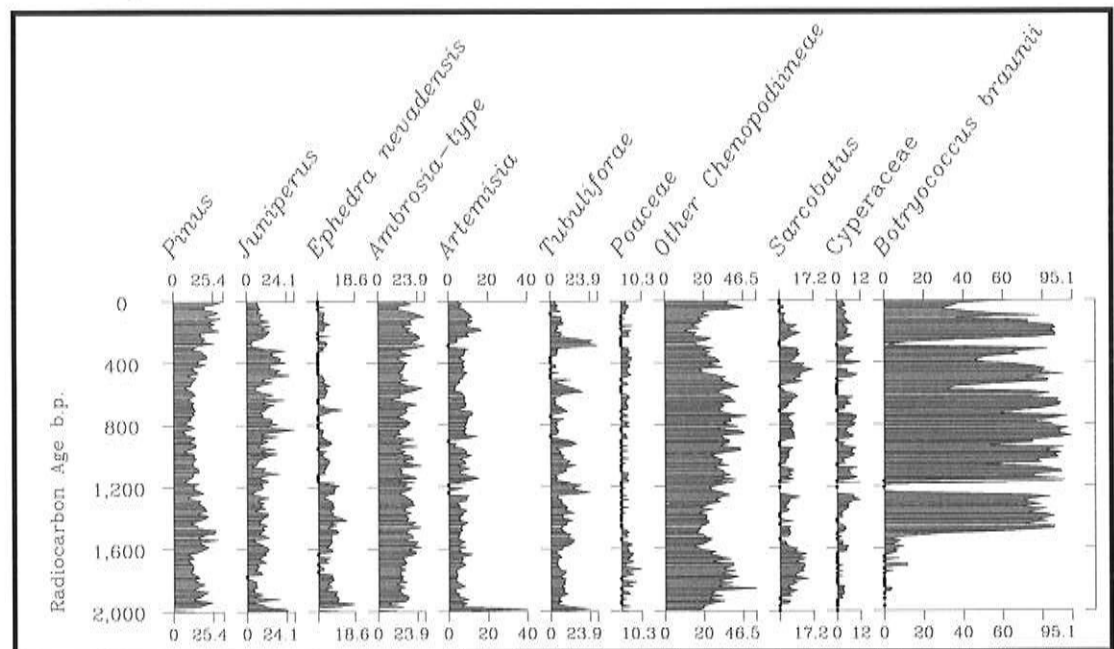


Figure 2 Summary relative percentage diagram of the major pollen types and one algae from Lower Pahranaagat Lake for the upper 2 ka of the record. Percentages are based on the sum of all terrestrial pollen types. Both long- and short-term shifts in vegetation are clear. Sample spacing is about one per 14 years. A dot indicates relative percentages of less than 2%.

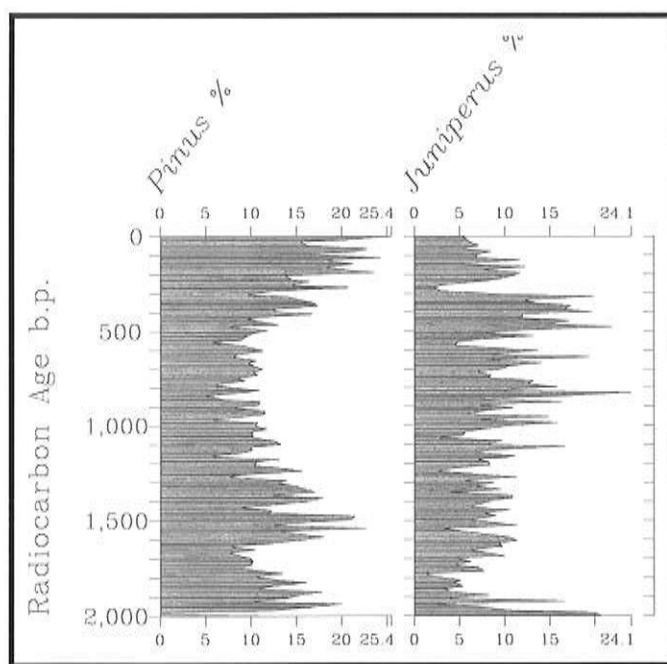


Figure 3 The pine (primarily piñon) and juniper pollen records reflect the history of the semi-arid woodlands in the mountains surrounding Lower Pahrnanagat Lake. Pine seems to have been greatly affected during the drought following the "Neoglacial" (~1.6 to 1.8 ka) and during the "Medieval Warm Period" and the severe droughts recorded in the tree-ring records of the Sierras (~1.0 to .4 ka). Juniper seems to have fared much better.

on the health and composition of intermediate elevation semi-arid woodlands. Juniper pollen values during the last 2 ka vary between 5 and 22 percent (Figure 3). High pollen values reflect major increases in the productivity, density, and distribution of juniper on the landscape.

High frequency variations of juniper (and other) pollen values throughout the Lower Pahrnanagat Lake record on the order of 10 to 14 years apparently mirror differences in pollen production, not increased numbers of trees. These variations can serve as a proxy for past interdecadal climate variations. Long-term, low frequency increases in mean juniper (and other) pollen values reflect initial response to such events through increased biomass and, in the later stages, increased local density and/or expansions of juniper (or these other species) into adjacent vegetation communities.

Such an increase in the Lower Pahrnanagat Lake record of juniper pollen suggests that this species may briefly have grown at slightly lower elevations about 2 ka than they currently do (Wigand and Rose 1990). This would evidence a drop in lower tree-line of from tens to a few hundred meters. Woodrat midden data from the Sheep Range south of Lower Pahrnanagat Lake suggest there may have been as much as a 200m depression in lower tree-line prior to 2 ka (Spaulding 1981, 1985).

Reconstructed deposition rates of the Lower Pahrnanagat Lake record together with dramatic changes in relative pollen values indicate that at times the transition to wetter, or conversely drier, conditions took less than a decade or two. The local increase in effective precipitation necessary to accomplish this change, based on the difference in the minimal annual rainfall requirements between sagebrush (Mozingo 1987) and Utah juniper (Leonard *et al* 1987), must have been at least 10-20 mm per year and could have been as much as 70 mm per year at elevations around 1500 meters. Reduced evaporation rates due to reduced mean annual temperature may also have played a significant role in increasing effective precipitation.

At Lower Pahrnanagat Lake, additional increases in juniper pollen, indicating greater effective precipitation resulting from increased winter precipitation and/or reduced evaporation rates, occur about 1.5, 0.9, 0.7,

and after 0.5 ka (Figure 3). Increased juniper values climaxing at about 0.8 and between 0.4 and 0.3 ka approach relative values that occurred about 2 ka. The times when these pollen values begin to increase roughly coincide to times when Stine (1990) indicates the drowning of trees in the basins and valleys surrounding Mono Lake. These periods are mirrored in the marsh pollen records from Cofer Spring north of Beatty, Nevada (Wigand and Rose 1990), at Warm Sulfur Springs in the Panamint Valley (Smiley and Mehringer no date), and in the timings of the latest dune and peat layers from Ash Meadows (Mehringer and Warren 1976). The regional nature of some of these events is confirmed by comparison with pollen and woodrat midden records farther north.

In contrast to the general increase in juniper pollen values, which climaxed about 0.3 ka and has plunged since, there have been at least three significant increases in pine pollen values over the last 2 ka. Of these, a period of increased pine pollen values between about 1.6 and 1.2 ka (Figure 3) is characterized by minimal corresponding increases in juniper pollen values and a distinct period of increased grass pollen values immediately preceding (Figure 4). Based upon ongoing analysis of woodrat midden data from the Pahranaagat Range and the pollen data from Lower Pahranaagat Lake, this regional expansion of piñon may evidence a period of summer-shifted rainfall (increased summer rainfall with reduced winter rainfall). Juniper, which favors winter precipitation, responds little during this period. Sagebush (*Artemisia*), another plant favored by winter precipitation, did not respond during this period (Figure 4). The grass expansion evident just prior to the beginning of this period, at a time when according to saltbush (*Chenopodiaceae*) and greasewood (*Sarcobatus*) pollen (Figure 5) drier climate was prevalent, suggests summer-shifted rainfall. This would have favored the establishment of piñon seedlings through more reliable supply of moisture during the hot summer months.

The relatively greater abundance of pondweed (*Potamogeton*) pollen in relationship to sedge (*Cyperaceae*) pollen (Figure 6) from 1.6 to 1.4 ka indicates the development of a shallow, fluctuating lake system. Maintenance of a shallow perennial lake at a time contemporaneous with the expansion of piñon pine despite the apparent reduction of winter precipitation provides additional evidence of summer-shifted precipitation. Increased dominance of sedge pollen after 1.4 ka indicates the expansion of littoral plant communities at the expense of shallow lake plant communities. This might have occurred either as the result of in-filling of the basin, breaching of the alluvial fans that dammed the lake, or through reduced hydrologic input.

Expansion of piñon pine in the Great Basin was further favored by reduction in harshness of winter conditions following the end of the "Neoglacial" about 2 ka. Piñon pine is readily subject to winter-kill during

times of extreme cold. Even today its distribution in the northern Great Basin is characterized by distributions on lower mountain ranges sheltered behind larger chains that effectively block the direct impact of winter storms.

An index generated by placing conifer pollen against saltbush pollen recovered from Lower Pahrnanagat appears to be an excellent measure of regional drought when compared with a bristlecone pine tree-ring record from Methuselah Walk in the White Mountains of southern California (Graybill *et al* 1994) (Figure 7). Except for the extreme drought centered around 1.9 ka, the correspondence for the last 2 ka is very close. The discrepancy around 1.9 might reflect the variable effect of summer-shifted precipitation at high and low elevations. At lower elevations, summer rainfall had limited impact on the conifer pollen record from Lower Pahrnanagat Lake because the semi-arid woodlands had already

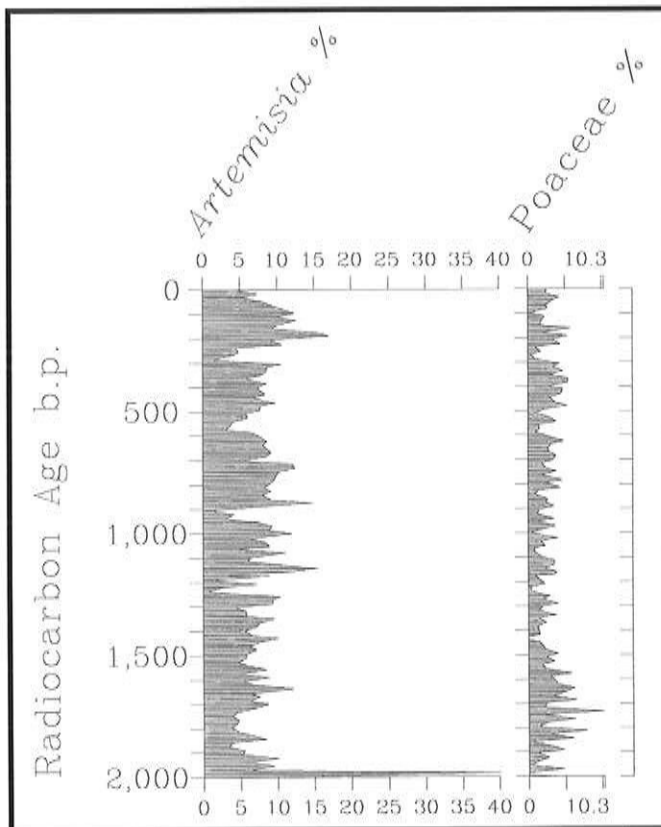


Figure 4 Comparison of the sagebrush (*Artemisia*) and grass (*Poaceae*) pollen records from Lower Pahrnanagat Lake. In general, sagebrush (which generally grows above 1,700 m in the surrounding mountains) and grasses respond similarly. They seem to have been less impacted (except during the most extreme events) by the droughts that have characterized the last 2 ka. However, one period centered around 1.8 ka is characterized by dramatic grass expansion. Pine and juniper both suffer during this period. We suggest that this is a time of summer-shifted precipitation when grasses could benefit from summer rainfall, but the semi-arid woodland species (already having stopped growing for the year) could not respond to the input of additional precipitation.

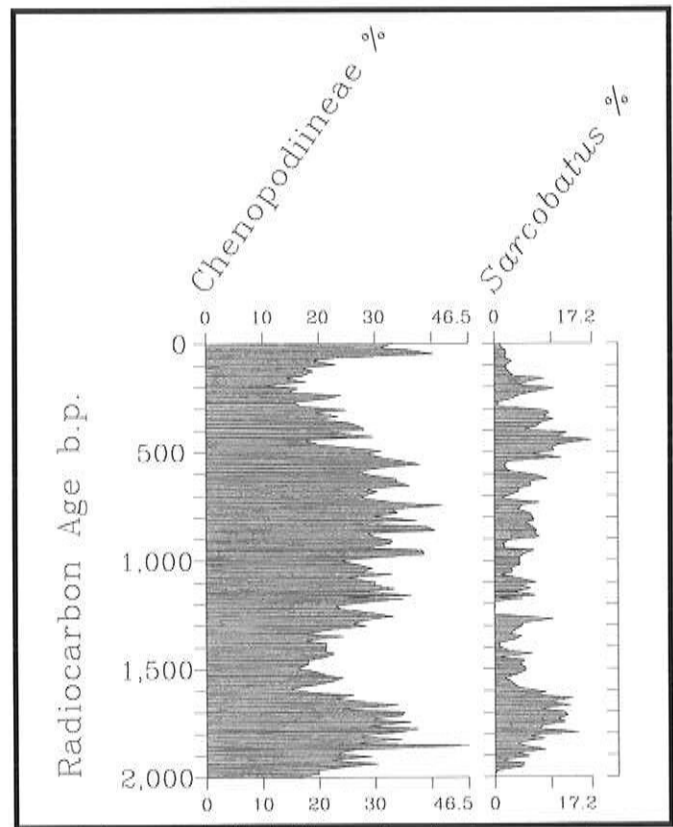


Figure 5 Increases of saltbush (*Chenopodiineae*) and greasewood (*Sarcobatus*) pollen at Lower Pahrnanagat Lake highlight the major droughts of the last 2 ka. Saltbushes (*Atriplex* spp.) demonstrate vigorous response to drought shifted climate. It is clear that both the onsets and the termination of these droughts are very rapid. Again the terminal "Neoglacial" and "Medieval Warm Period" droughts are clear. In particular the droughts of about 0.5 to 0.6 ka documented in the Sierran tree-ring record (Graumlich 1993) are among the worst of the last 2 ka.

completed their annual growth and pollen production. However, the high-elevation bristlecone pine forest was still in the growing season and could easily respond to summer rainfall inputs, which would be reflected in wider tree-ring growth.

The Lower Pahranaagat Lake pollen record provides an additional dimension to the climatic index that is generated from the tree-ring record, *ie*, the response of various plant species to climate can be assessed. The tree-ring record only provides a measure of the climate and the response of one plant species (bristlecone pine, *Pinus longaeva*). It is apparent from this comparison that the response of semi-arid woodlands and desert scrub communities are potentially just as sensitive and immediate as the tree-ring record even in comparisons of the relative magnitudes of the variations. Thus, the regional nature of the climate changes reflected in the Lower Pahranaagat Lake record is clear.

In north-central Nevada, a pollen record from Lead Lake in the Carson Sink records the same dramatic expansion of piñon pine seen in the Lower Pahranaagat Lake record between 1.6 and 1.2 ka just prior to the

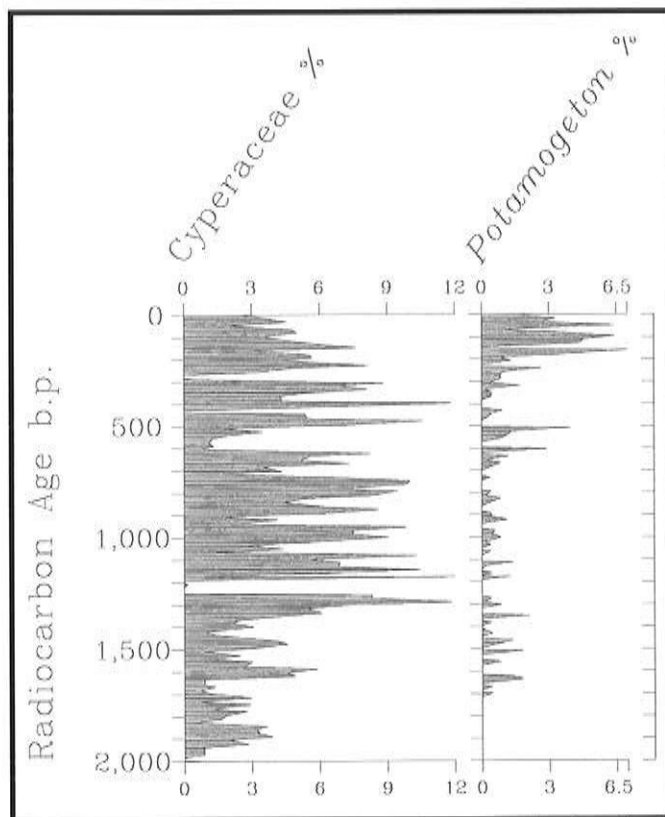


Figure 6 Sedge (*Cyperaceae*) and pondweed (*Potamogeton*) pollen reflects Lower Pahranaagat Lake/Marsh history. Rapid shifts in this vegetation result from the shallowness of the lake (a 1- or 2-meter change in water depth can expose or drown huge areas). In general, the "Medieval Warm Period" and the early part of the millennium were characterized by marsh. However, the "Little Ice Age" and a period between 0.6 and 0.7 ka seems indicative of two brief deeper lake episodes.

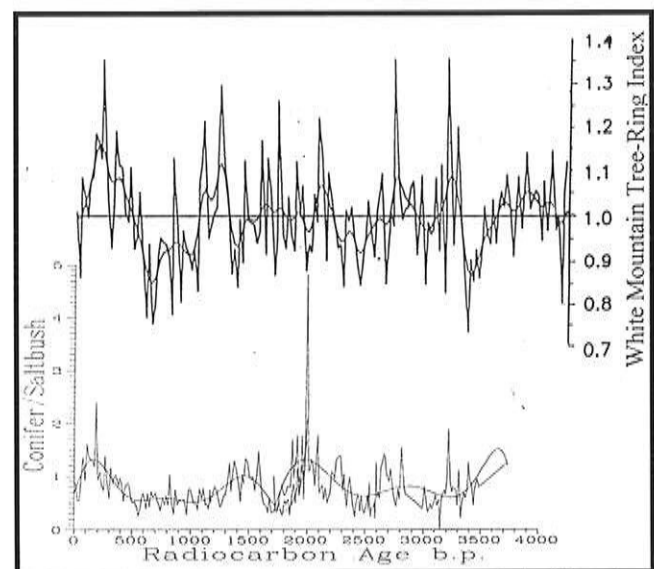


Figure 7 Comparison of an effective precipitation index derived from the Lower Pahranaagat Lake pollen record (lower line plotted against the age scale as radiocarbon age b.p.) and the White Mountain bristlecone pine tree-ring record (upper line plotted against the age scale as calendar years b.p.) (Graybill *et al* 1994). The (Juniper + Pine)/All Chenopodiaceae ratio reflects regional precipitation. Increases in this ratio indicate wetter periods (primarily winter precipitation). Decreases indicate reduced winter precipitation. The tree-ring index from the White Mountains also reflects regional precipitation, though temperature may also play a role. Wider ring width (up) corresponds with greater precipitation, while narrower ring width (down) corresponds with reduced precipitation.

“Medieval Optimum” (Wigand *et al* 1995) (Figures 8 and 9). The earliest record of piñon pine in the woodrat midden record from northwestern Nevada west of the Lahontan Basin, thus far, is 2.1 ka (Wigand and Nowak 1992). However, around 1.4 ka, based upon both the pollen and woodrat midden records, it expands both northward (Figure 8) and downward in elevation (Figure 9). Reduced numbers of dated piñon pine-containing middens and decreased pine pollen abundance after 1.0 ka reflect the same conifer retrenchment pattern seen at Lower Pahranaगत Lake during the early and mid-millennial droughts. Increased occurrence of pine in the pollen record of Lead Lake during the last 0.15 ka corresponds to the unprecedented, post “Little Ice Age” expansion of piñon pine recorded in stand establishment records (Tausch *et al* 1981).

Finally, at Diamond Pond in the Harney Basin of south-central Oregon, an early post “Neoglacial” expansion of grass between 1.9 and 1.0 ka overlaps with both grass and piñon pine expansions seen at Lower Pahranaगत Lake and the piñon pine expansion at Lead Lake (Wigand 1987) (Figure 10). Because juniper is not increasing in abundance, grass expansion at Diamond Pond also seems to indicate summer-shifted rainfall. Radiocarbon dates plotted with standard deviations on bison remains from archaeological sites in the northern Great Basin (Marwitt 1973) and the plateau of eastern Washington (Schroedl 1973) show remarkable coincidence with this period of grass expansion (Figure 10).

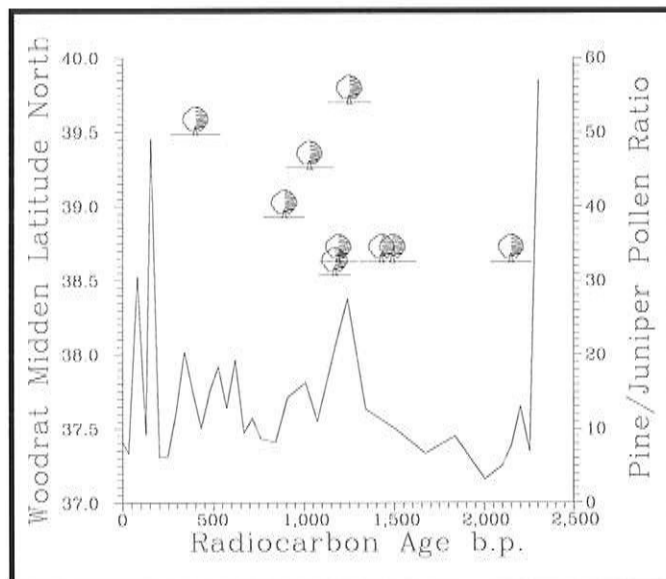


Figure 8 In north-central Nevada, the pollen record from Lead Lake in the Carson Sink records the dramatic expansion of piñon pine with respect to juniper prior to the “Medieval Warm Period”. The pine-to-juniper pollen ratio from Lead Lake indicates that around 1.4 ka, increased pine pollen abundance records a dramatic, regional expansion of pine. Elevational distribution of directly dated piñon pine from woodrat middens around the Lahontan Basin indicates that it is single-needle piñon pine (*Pinus monophylla*) that is making significant headway northward at this time. Retrenchment of piñon pine after about 1.1 ka and subsequent re-expansion around 0.15 ka is also documented in the pine to juniper pollen ratio from Lead Lake.

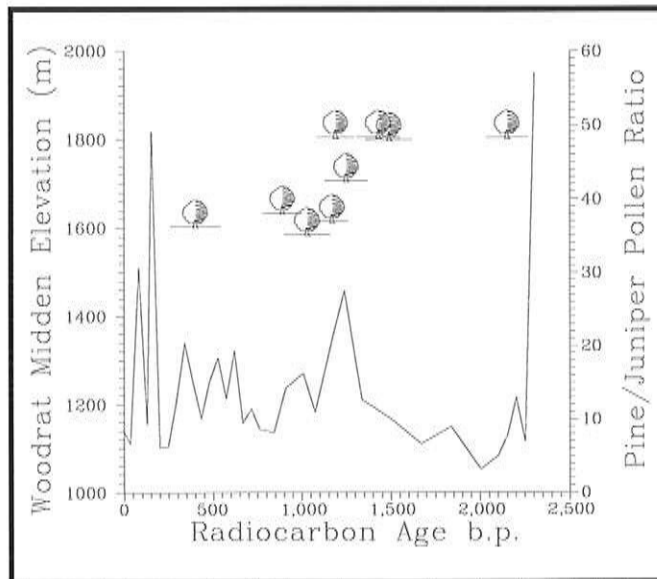


Figure 9 At the same time that the pollen record from Lead Lake indicates a dramatic, regional expansion of pine, directly dated piñon pine from woodrat middens around the Lahontan Basin indicates that single-needle piñon pine is also lowering its lower elevational distribution by as much as 200 meters.

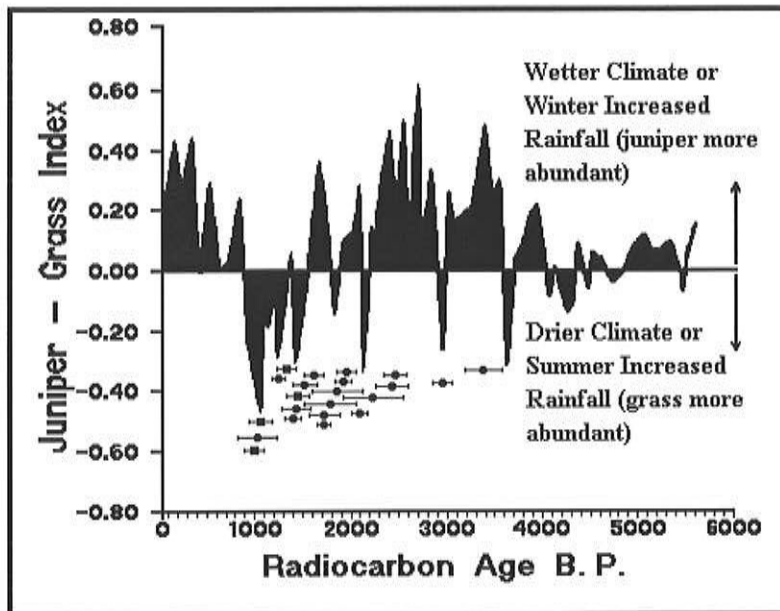


Figure 10. At Diamond Pond, the juniper-to-grass index records an early post "Neoglacial" expansion of grass. This expansion mirrors both the regional increase of grass and pine at Lower Pahranaagat Lake and the piñon pine movements recorded in pollen at Lead Lake and Lahontan Basin woodrat middens. Grass expansion at Diamond Pond, indicating summer-shifted rainfall, coincides with radiocarbon-dated bison remains from archaeological sites in the northern Great Basin and the plateau of eastern Washington. The dates are plotted with one standard deviation dashes.

Containing the greatest concentration of dated middle to late Holocene bison from archaeological contexts in the Intermountain West, this period also corresponds with the expansion of Fremont corn horticulturists in the eastern Great Basin (Marwitt 1973). Corn, in a horticultural society, requires summer rainfall to grow. Expansion of the practice of growing corn as far north as the Snake River plain, Idaho, and apparently as far northwest as the Ruby Valley, central Nevada, between 1.6 and 0.9 ka is more than coincidental.

## Conclusions

Integration of high-resolution pollen sequences and woodrat midden macrofossil records from the Great Basin offer an opportunity to examine climate change and subsequent plant community response not offered by the tree-ring record alone. Although the resolution and precision of the pollen record is not as great as that of the tree-ring record, at near decadal resolution, it provides unique information on plant response to climate both at the community and the organismal level.

Great Basin paleobotanical records discussed above indicate that considerably wetter, as well as drier, conditions have occurred during the last few millennia, resulting in dramatic responses in vegetation communities. Highly variable responses in woodland and shrub species and in the grasses that grew among them provide evidence of significantly wetter periods of climate sometimes with strong seasonal shifts in precipitation that in most cases were regional in extent.

Variations in the duration (ranging from a few dozen to a few hundred years) and the rapidity of the onset and demise of these shifts (some on the order of a decade or less) are clear in the pollen record. Hydrologic impacts from rapid shifts to wetter climates are obvious. Initial inability of local vegetation to accommodate such increases in precipitation would

result in abundant surface water that would yield considerable runoff and recharge.

Finally, although the Holocene as a whole has been drier than the late Pleistocene (last 12 ka), higher resolution sampling of paleoclimatic proxy records (12-24 ka) indicate that there have been events of short duration that have approached the extremes recorded during the Pleistocene. However, the shorter duration of Holocene events has averted the responses in regional vegetation that were seen during the Pleistocene.

## Literature

---

- Axelrod, D.I. 1976. History of the conifer forests, California and Nevada. *University of California Publications in Botany* 70. 62 pp.
- Betancourt, J.L., T.R. Van Devender, and P.S. Martin (eds.). 1990. *Fossil Packrat Middens: The Last 40,000 Years of Biotic Change*. University of Arizona Press, Tucson.
- Graumlich, L.J. 1993. A 1000-year record of temperature and precipitation in the Sierra Nevada. *Quaternary Research* 39:249-255.
- Graybill, D.A., M.R. Rose, and F.L. Nials. 1994. Tree-rings and climate: Implications for Great Basin paleoenvironmental studies. Pages 2569-2573 in *Proceedings of the fifth Annual International High-Level Radioactive Waste Management Conference and Exposition, May 22-26, 1994, Las Vegas, NV*.
- Houghton, J.G. 1969. Characteristics of rainfall in the Great Basin. University of Nevada, Desert Research Institute, Reno, Nevada.
- Houghton, J.G., C.M. Sakamoto, and R.O. Gifford. 1975. Nevada's weather and climate. *Nevada Bureau of Mines and Geology, Special Publication 2*. Reno, Nevada.
- Leonard, S., R. Miles, and H. Summerfield. 1987. Soils of the Pinyon-Juniper woodlands. Pages 227-230 in *Proceedings Pinyon-Juniper Conference, Reno, Nevada, January 13-16, 1986, General Technical Report, INT-215*. R. Everett, editor. U.S.D.A. Intermountain Forest Research Station Publication.
- Long, A., L.A. Warneke, J.L. Betancourt, and R.S. Thompson. 1990. Chapter 17: Deuterium variations in plant cellulose from fossil packrat middens. Pages 380-396 in *Fossil Packrat Middens: The Last 40,000 Years of Biotic Change*. J.L. Betancourt, T.R. Van Devender, and P.S. Martin, editors. University of Arizona Press, Tucson.
- Marwitt, J.P. 1973. Median village and Fremont culture regional variation. *University of Utah Anthropological Papers* 95. University of Utah Press, Salt Lake City, Utah.
- Mehring, P.J. Jr. 1967. Pollen analysis of the Tule Springs area, Nevada. Pages 129-200 in *Pleistocene Studies in southern Nevada*. H.M. Wormington and D. Ellis, editors. *Nevada State Museum Anthropological Papers* 13. Carson City, Nevada.
- Mehring, P.J. Jr. 1985. Late-Quaternary pollen records from the interior Pacific Northwest and northern Great Basin of the United States. Pages 167-189 in *Pollen Records of Late-Quaternary North American Sediments*. V.M. Bryant Jr. and R.G. Holloway, editors. American Association of Stratigraphic Palynologists, Dallas.
- Mehring, P.J. Jr. 1986. Prehistoric environments. Pages 31-50 *Volume 11: Great Basin, Handbook of North American Indians*. W.L. D'Azevedo, editor. Washington, D.C.
- Mehring, P.J. Jr., and J.C. Sheppard. 1978. Holocene history of Little Lake, Mojave Desert, California. Pages 153-176 *The Ancient Californians: Rancholabrean Hunters of the Mojave Lakes Country*. E.L. Davis, editor. Natural History Museum of Los Angeles County, Science Series 29. Los Angeles, California.

- Mehring, P.J. Jr., and C.N. Warren. 1976. Marsh, dune and archaeological chronology, Ash Meadows, Amargosa Desert, Nevada. Pages 120-150 in *Holocene Environmental Change in the Great Basin*. R.G. Elston and P. Headrick, editors. Nevada Archeological Survey Research Papers 6. Reno.
- Mehring, P.J. Jr., and P.E. Wigand. 1990. Comparison of Late Holocene environments from woodrat middens and pollen: Diamond Craters, Oregon. Pages 294-325 in *Fossil Packrat Middens: The Last 40,000 Years of Biotic Change*. J.L. Betancourt, T.R. Van Devender and P.S. Martin, editors. University of Arizona Press, Tucson.
- Mozingo, H.N. 1987. *Shrubs of the Great Basin: a Natural History*. University of Nevada Press, Reno.
- Schroedl, G.F. 1973. *The archaeological occurrence of bison in the southern Plateau*. Reports of Investigations 51. Laboratory of Anthropology, Washington State University, Pullman, Washington.
- Smiley, T.L., and P.J. Mehring, Jr. No date. Report to National Science Foundation for research supported by NSF Grant GB-8646. *Post-pluvial history of the spring-fed salt marshes of the Amargosa drainage*. 35 pp.
- Spaulding, W.G. 1981. *The late Quaternary vegetation of a southern Nevada mountain range*. Unpublished Ph.D. dissertation. University of Arizona, Tucson. 271 pp.
- Spaulding, W.G. 1985. *Vegetation and climates of the last 45,000 years in the vicinity of the Nevada Test Site, south-central Nevada*. U.S. Geological Survey Professional Paper 1329. 83 pp.
- Stine, S. 1990. Late Holocene fluctuations of Mono Lake, eastern California. *Palaeogeography, Palaeoclimatology, Palaeoecology* 78:333-381.
- Swetnam, T.W. and J.L. Betancourt. 1990. Fire-southern oscillation relations in the southwestern United States. *Science* 249:1017-1020.
- Tausch, R.J., N.E. West and A.A. Nabi. 1981. Tree age and dominance patterns in Great Basin pinyon-juniper woodlands. *Journal of Range Management* 34:259-264.
- Thompson, R.S., C. Whitlock, P.J. Bartlein, S.P. Harrison, and W.G. Spaulding. 1993. Climatic changes in the western United States since 18,000 yr B.P. Pages 468-513 in *Global Climates Since the Last Glacial Maximum*. H.E. Wright Jr., J.E. Kutzbach, T. Webb III, W.F. Ruddiman, F.A. Street-Perrott, and P.J. Bartlein, editors. University of Minnesota Press, Minneapolis, MN.
- Van de Water, P.K. 1993. *Ecophysiological response of Pinus flexilis to atmospheric CO2 enrichment during deglaciation*. Unpublished M.S. thesis, University of Arizona, Tucson.
- Walter, H. 1954. Le facteur eau dans les regions arides et sa signification pour l'organisation de la vegetation dans les contrees sub-tropicales. Pages 27-39 in *Les Divisions Ecologiques du Monde*. CNRS, Paris.
- Wigand, P.E. 1987. Diamond Pond, Harney County, Oregon: Vegetation history and water table in the eastern Oregon desert. *Great Basin Naturalist* 47(3):427-458.
- Wigand, P.E., and M.K. Rose. 1990. Calibration of high frequency pollen sequences and tree-ring records. In *Proceedings of the International Highlevel Radioactive Waste Management Conference and Exposition, April 8-12, 1990*. American Nuclear Society, La Grange Park, Illinois.
- Wigand, P.E., and C.L. Nowak. 1992. Chapter 3: Climate/Climate Indicators, Dynamics of northwest Nevada plant communities during the last 30,000 years. Pages 40-62 in *The History of Water: Eastern Sierra Nevada, Owens Valley, White-Inyo Mountains, White Mountain Research Station Symposium 4*. C.A. Hall Jr., V. Doyle-Jones, and B. Widawski, editors. University of California, White Mountain Research Station, Los Angeles.
- Wigand, P.E., M.L. Hemphill, S.E. Sharpe, and S. Patra. 1995. Great Basin woodland dynamics during the Holocene. Pages 51-69 in *Proceedings of the Workshop-Climatic Change in the Four Corners and Adjacent Regions: Implications for Environmental Restoration and Land-Use Planning*. W.J. Waugh, editor. CONF-9409325. U.S. Department of Energy, Grand Junction, Colorado.



# Decadal Hydroclimatic Variability in the Western Coastal United States: Temporal and Spatial Variations in Precipitation, Streamflow, and Lake Level

Hong-Chun Li and Teh-Lung Ku

**Abstract:** We have analyzed streamflow variations recorded at 15 USGS gauging stations in California during the past 90 years or so. The anomalies (departures from the 1960-1990 mean discharge) of streamflow on annual-to-decadal time scales are strongly correlated with precipitation anomalies in each drainage basin. The temporal variations of the 5-year running averages of these records clearly show high/low runoff cycles with a periodicity of about  $11 \pm 3$  years, representing a decadal climate (precipitation) variability. High runoff periods (wet climate) centered around 1982, 1969, 1956, 1940, and 1915. Low runoff periods (dry climate) centered around 1989, 1976, 1962, 1946, and 1932. In addition, streamflow intensity during the high runoff periods reveals different spatial patterns. For example, runoff around 1956 was much stronger at the northern California stations than at the southern California stations. In 1993, all stations (four) in southern California showed very high runoff, while the other stations showed weakly increased runoff. Although causes of the decadal climate (precipitation) variability are not known with certainty, the use of streamflow records may help us understand the relative strengths of moisture sources and shift of the jet stream in atmospheric circulation. Precipitation regimes in California are influenced by three moisture sources: northwesterly flow (polar front) related to the Pacific/North America anomaly, southwesterly flow controlled by the tropic ENSO pattern, and southeasterly flow governed by the summer monsoon. A preliminary assessment shows that variations of California runoff on decadal time scale, but not on annual time scale, are strongly correlated with ENSO. This implies that the northwesterly flow may be blocked by the subtropical high-pressure system with descending, dry air in mid-latitude zones when the Southern Oscillation is strong, causing drought in California. When the Southern Oscillation is weak, the northwesterly flow can penetrate farther south and the El Niño event can bring more precipitation from the equatorial Pacific to California. Summer monsoon mainly affects the climate and streamflow in southern California. Strong runoff in 1969 and 1993 recorded by gauging stations in the south may indicate the strengthening of the summer monsoon.

## Data

This study uses annual precipitation data along the climatic divisions in the west coast regions of the United States, including Washington, Oregon, and California (Figure 1). The data are extracted from the WeatherDisc Associates, Inc., World WeatherDisc CD-ROM 1994. The climatic division boundaries are defined by the National Climatic Data Center, including stations subjectively considered to exhibit similar climatic properties. Precipitation data are the averages of several stations in each division so that they can represent the best feature of each division. All divisions are along the coast regions so that the effect of topography on precipitation pattern is minimized. Records employed for precipitation extend from 1895 to 1991. Three other rainfall records

In: C.M. Isaacs and V.L. Tharp, Editors. 1997. *Proceedings of the Thirteenth Annual Pacific Climate (PACLIM) Workshop, April 15-18, 1996*. Interagency Ecological Program, Technical Report 53. California Department of Water Resources.

extended farther back are those of Los Angeles (1887), the southern San Joaquin Valley (1872), and Nevada City (1864), for longer time comparison. All data are expressed as departure from 1895-1991 mean precipitation.

The Southern Oscillation Index, defined as the sea level pressure difference Tahiti minus Darwin shown as departure from 1951-1980 annual mean of 2.8 mb, are adopted from bimonthly values in Hastenrath (1991). A low (negative) value of the index corresponds to a weaker east-west pressure gradient and correlates to a high sea surface temperature anomaly in the equatorial Central Pacific. The SOI data extend from 1902 to 1988.

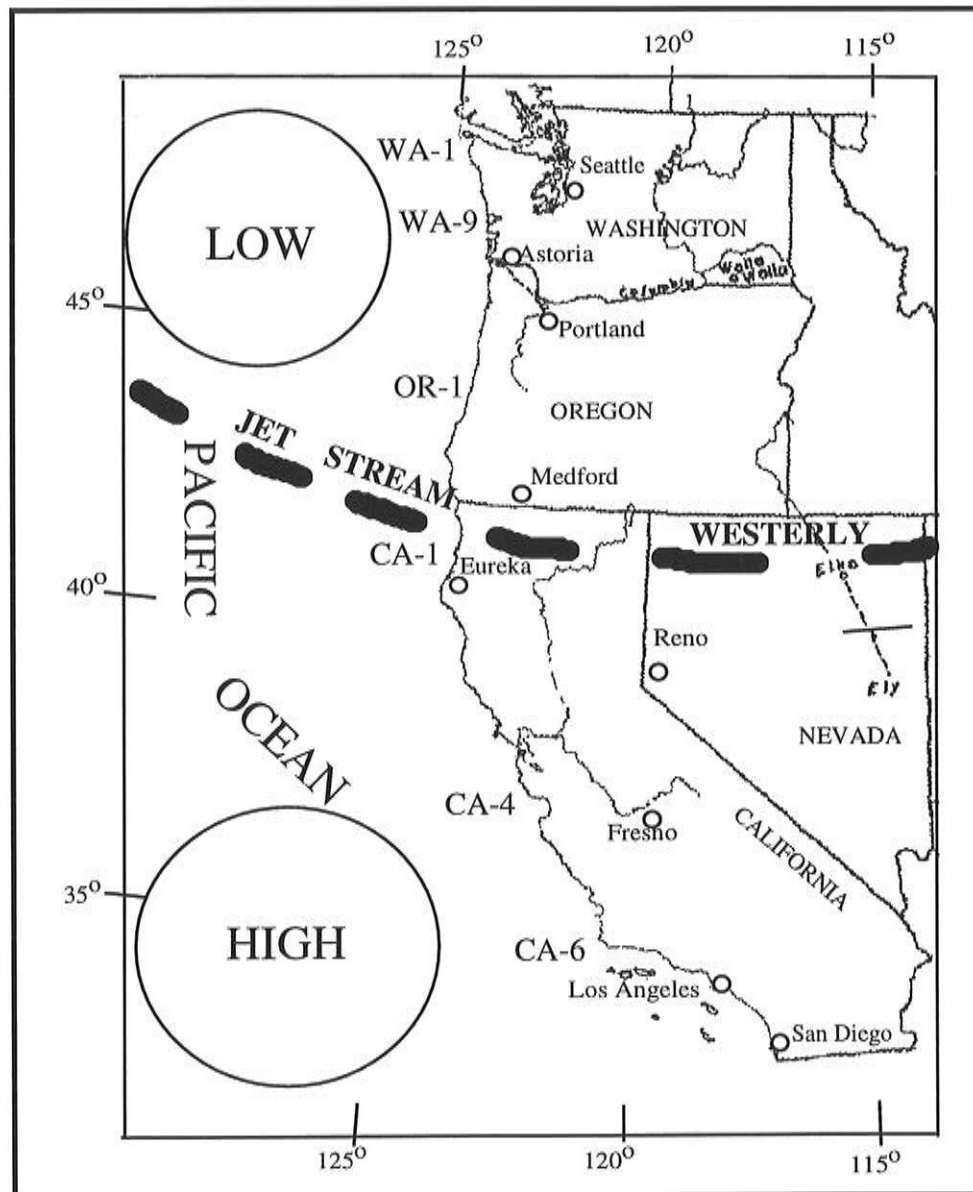


Figure 1. Map of western United States showing six precipitation regions along the coast and climatic pattern of jet stream westerly.

Subtropics High and North American/Pacific Low are simplified.

The streamflow data are recorded at 14 U.S. Geological Survey gauging stations in California. They are classified as three groups from the coastal region (west) to inland area (east) — coast, central valley, and mountain — and one group in southern California. In each group, three to four gauging stations are listed from north to south (or from west to east). These records extend from as early as 1902 to 1994 (Water Resources Data — California, 1994). The data are expressed as departure from 1960-1990 mean discharge.

Mono Lake is a hypersaline, alkaline lake in the Mono Basin at the eastern base of the California Sierra Nevada (Figure 1). Its lake-volume history since 1912 has been recorded instrumentally, showing dramatic fluctuations due to climatic variations and large decline of lake-surface elevations initiated by the 1941 artificial diversion of stream inflow (Blevins *et al* 1987). A 76-cm-long sediment core was collected in 1991 from the deepest part of Mono Lake at 39 meters, using a rectangular freeze corer (Li *et al* 1996). We have made high-resolution (0.5- to 3-year intervals) oxygen isotopic measurements on total carbonates of the deionized water washed lake sediments. The sedimentary chronology was determined from the distributions of  $^{210}\text{Pb}$  and  $^{239+240}\text{Pu}$  in the sediments and extended from 1991 to about 1840 with 5 to 10% uncertainty (Li *et al* 1996). Our previous study shows that the  $\delta^{18}\text{O}$  record simulates the lake-volume fluctuations rather well. The objective of using the lake volume and the  $\delta^{18}\text{O}$  record is to demonstrate that closed-basin lake sediment  $\delta^{18}\text{O}$  provides an effective means of probing decadal climatic variability in the past while historical records are absent.

## **Precipitation Anomalies, ENSO, and Jet Stream Shift**

---

The comparison of annual rainfall records of Los Angeles and south coast region of California with El Niño events and SOI variations shows that only half of the strong El Niño (weak SOI) years correspond to precipitation anomalies above average (Figure 2). Some of the strong El Niño years actually show precipitation anomalies below average. Some non-ENSO years (*eg*, 1889, 1909, 1938, 1978, 1980) have strong positive precipitation anomalies. This observation raises questions regarding how the ENSO system influences climatic variability in mid-latitude, and on what time scale we can correlate ENSO pattern with the climatic variability in a better way.

Five-year running averages of rainfall records in the western United States reveal apparently decadal/interdecadal climatic variability (Figure 3). In coastal California, with wet periods corresponding to the weak SOI except during 1917-1927, when the entire west coast was dry. Dry periods in this region correlate with the strong SOI. Therefore, on the interannual-to-decadal time scales, precipitation anomalies in coastal

California, but not limited to southern California, can be well correlated to the ENSO pattern.

The spatial variations of the decadal precipitation patterns on the west coast show opposite trends between the southern and northern parts except in two periods, 1917-1927 and 1978-1984. When the northern part is wet, the southern part tends to be dry, and vice versa. This observation may indicate that Jet Stream Westerly has migrated south or north depending on the intensity of the Southern Oscillation. Normally, Jet Stream Westerly meets the cold, moist air of the polar easterly at about 45-50°N above the west coast. Low pressure systems in the polar front zone generate most winter precipitation, which is the dominant rainfall along the west coast. During weak Southern Oscillation periods, the warm water of El Niño at the equatorial Pacific causes the inter-tropical convergence zone (ITCZ) to shift south from its usual position. Hence, positions of the Subtropic Highs (high pressure) and the Pacific/North America Lows (low pressure) probably migrate southward and cause Jet Stream Westerly to shift south. Under this condition, perhaps both polar front and subtropic jet streams bring more moisture to the southern part,

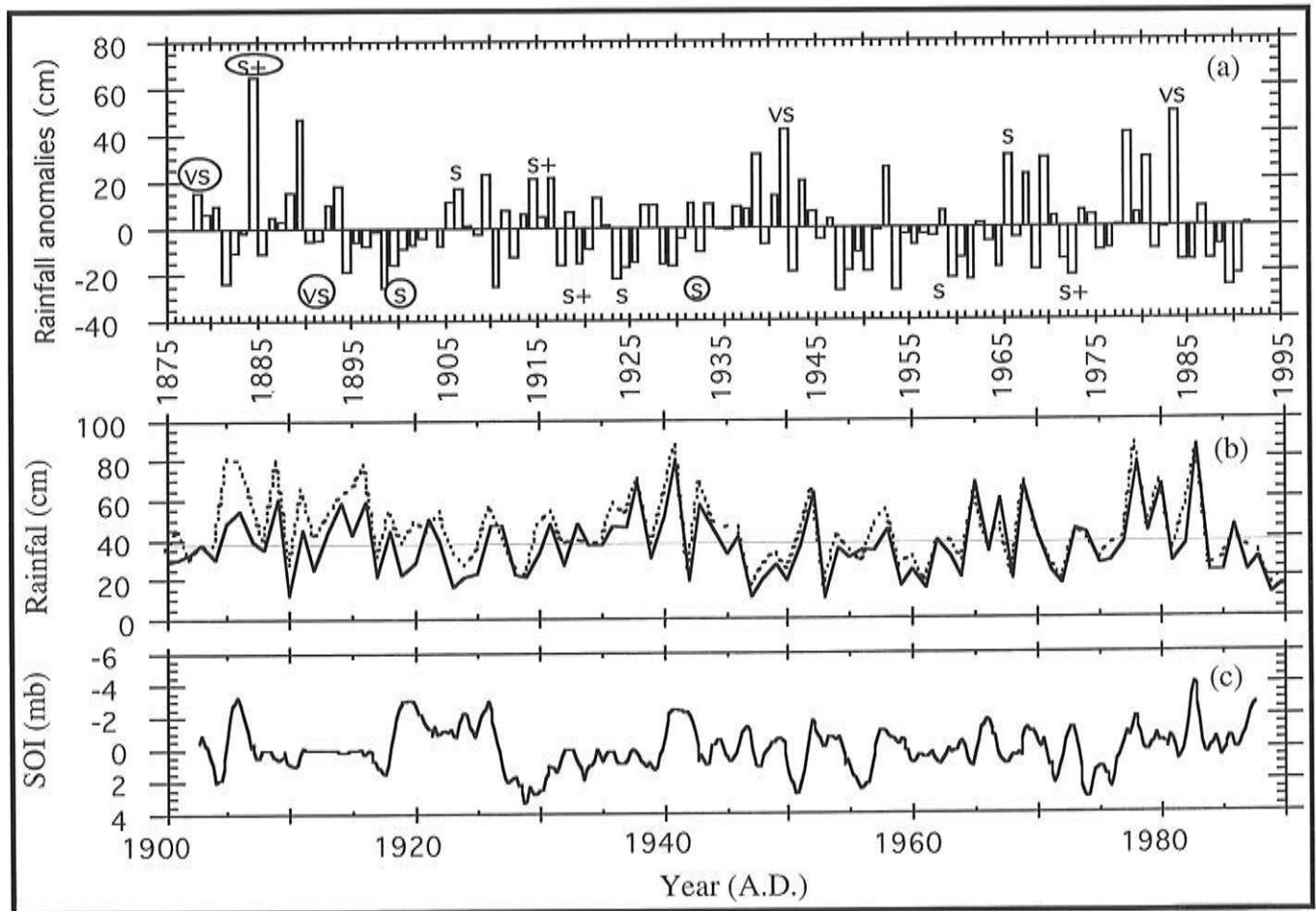


Figure 2. Comparisons of El Niño events and Southern Oscillation indexes with precipitation anomalies in southern California: (a) rainfall anomalies in Los Angeles compared with El Niño events classified by Quinn and Neal (1987) (S=strong, VS=very strong); (b) historical precipitation records in Los Angeles (solid) and southern California (dashed); (c) mean annual Southern Oscillation Index averaged from bimonthly values as departure from 1951-1980 mean of 2.8 mb.

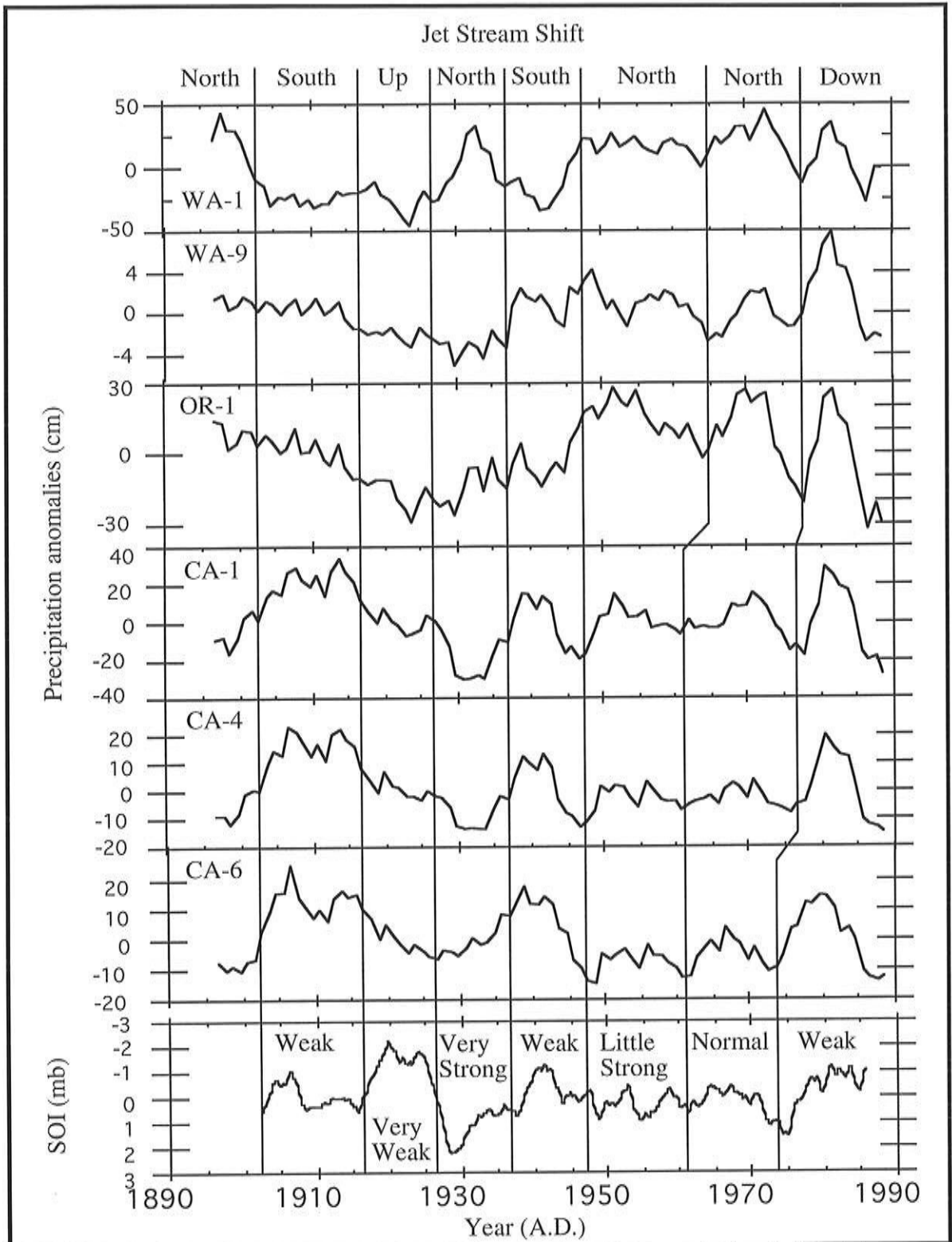


Figure 3. Comparison of 5-year running average precipitation anomalies with 5-year running average Southern Oscillation Index.

Precipitation stations (eg, WA-1, CA-6) shown in Figure 1 are plotted from north to south. North/south and up/down shifts of jet stream are indicated on the top of the plot.

so that the southern part is wet and the northern part is dry. In contrast, during strong Southern Oscillation periods, the cold water of La Niña at the equatorial Pacific causes ITCZ to shift north. This shift leads to the Jet Stream Westerly persisting in the northern part and causes more storm activity there. The northwesterly moisture from the northern part is diminished when it migrates southward, perhaps blocked by the subtropical high-pressure system with descending, dry air in mid-latitude zones when the Southern Oscillation is strong, so the southern part tends to be drought.

Two specific periods (1917-1927 and 1978-1984) are different from the above observation and cannot be explained by horizontal shift of the Jet Stream Westerly (Figure 3). Close examination indicates that both periods show very weak Southern Oscillation patterns. However, while the entire west coast experienced a dry climatic regime during 1917-1927, the entire region experienced a very wet climatic regime during 1978-1984. A hypothesis that has been made for understanding this observation is probably the vertical movement of the atmospheric circulation. Although the mechanism caused the vertical movement of the atmospheric circulation is unclear, drought along the entire west coast of the United States may reflect an upward shift of low pressure systems (polar jet and subtropic jet?), and the situation reverses when extreme wetness occurs along the entire west coast.

### **Correlation Between Streamflow and Precipitation Anomalies**

The anomalies (departures from the 1960-1990 mean discharge) of streamflow recorded at 14 USGS gauging stations in California during the past 90 years or so are strongly correlated with precipitation anomalies in each drainage basin on annual-to-decadal time scales (Figures 4-7). This means the streamflow anomaly on annual-to-decadal time scales reflects chiefly precipitation change in this arid-semiarid region. The temporal variations of the 5-year running averages of these records clearly show high/low runoff cycles with a periodicity average of  $11 \pm 3$  years, representing a decadal climate (precipitation) variability. High runoff periods (wet climate) are centered around 1982, 1969, 1956, 1940, and 1915. Low runoff periods (dry climate) are centered around 1989, 1976, 1962, 1946, and 1932. The high and low runoff periods correspond well to weak and strong Southern Oscillation, respectively, in all of California. Again, this indicates that variations of California runoff on decadal time scale, but not on annual time scale, correlate well with ENSO pattern. On such time scale (decadal), the study of ENSO may not be limited in southern California. In addition, the streamflow intensity during the high runoff periods reveals different spatial patterns, which are similar to the precipitation patterns. The temporal and spatial vari-

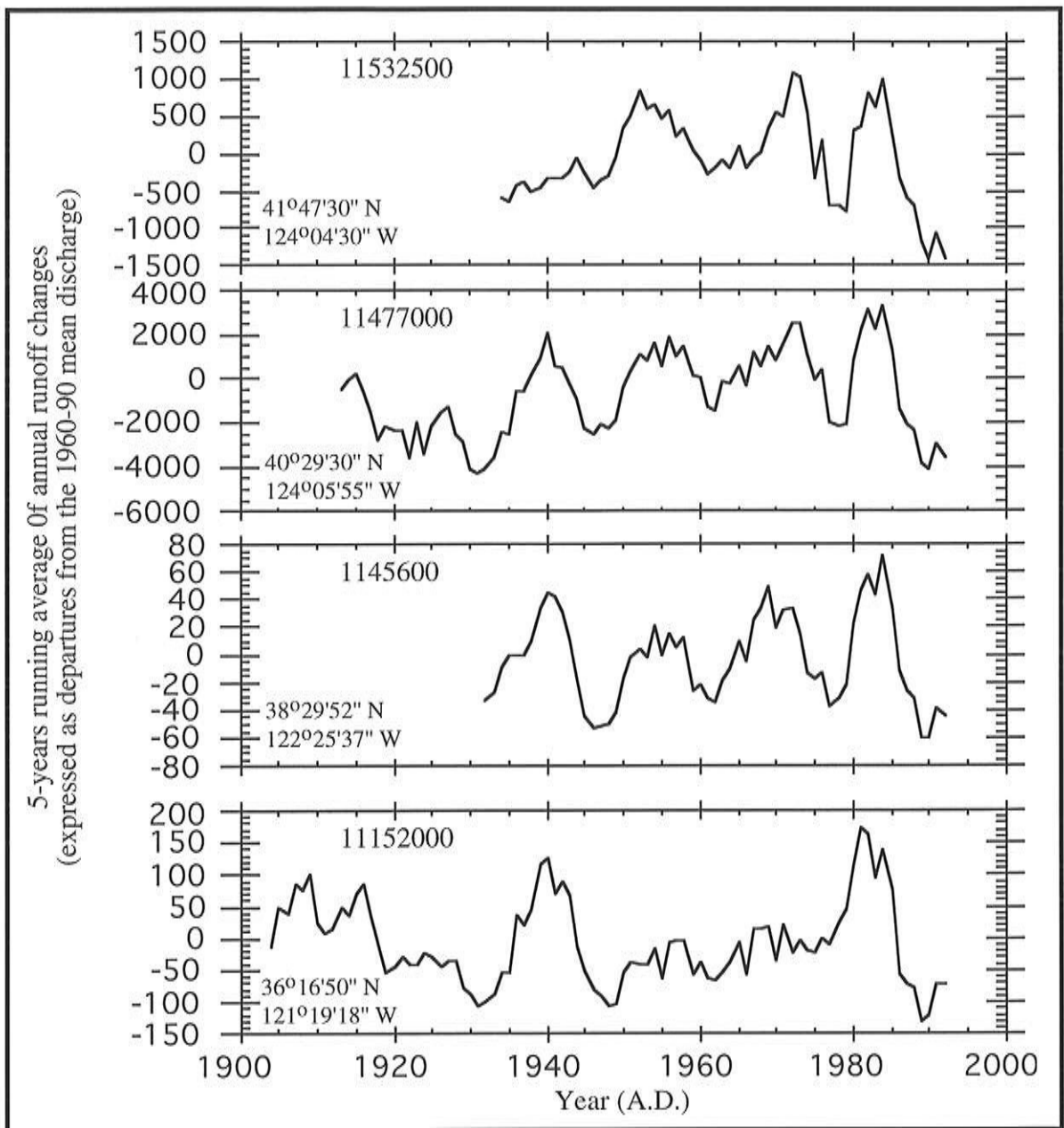


Figure 4. Temporal and spatial variations in streamflow in the coastal area of California.

Stations are plotted from north to south.

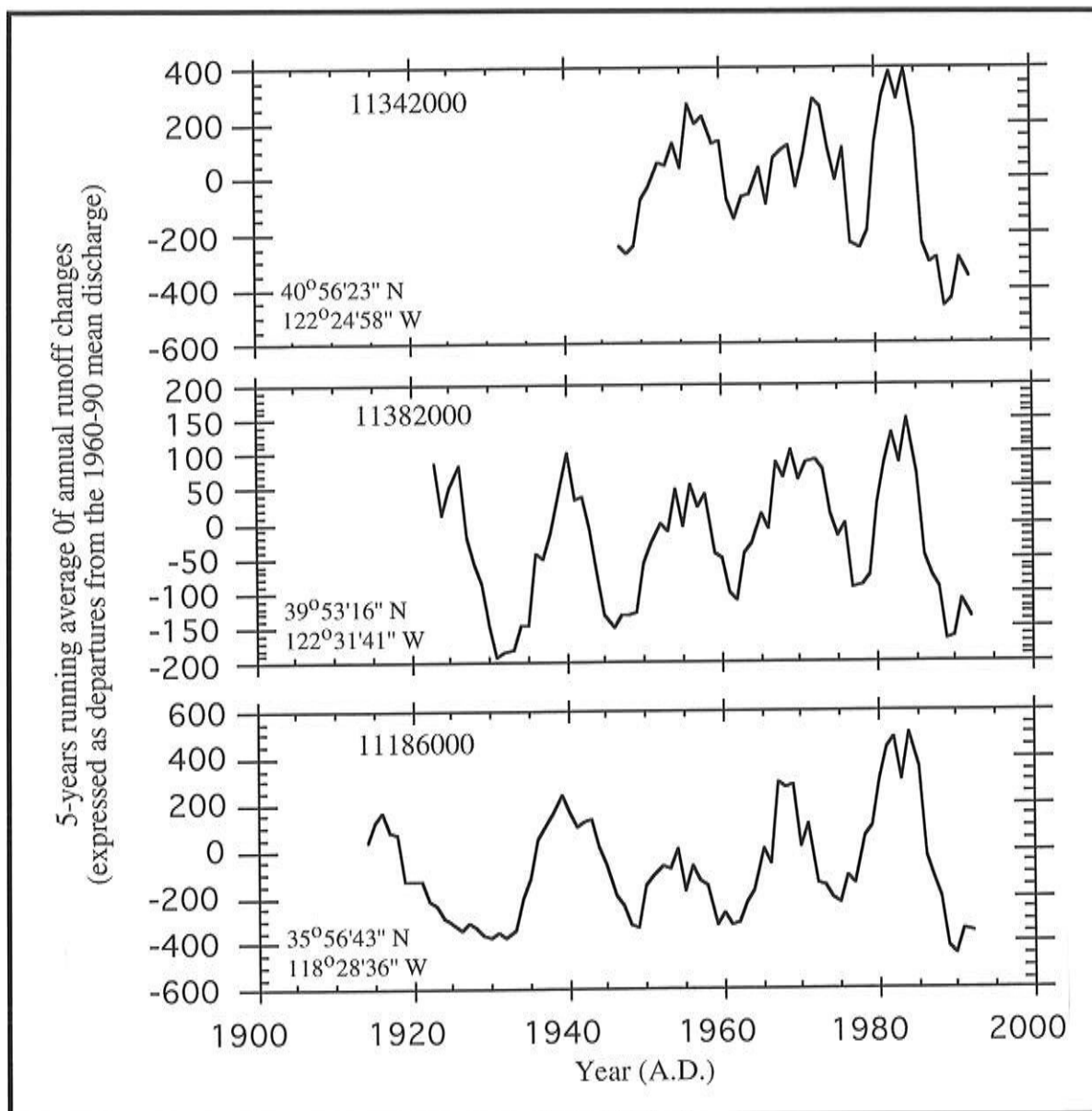


Figure 5 . Temporal and spatial variations in streamflow in the central valley of California.

Stations are plotted from north to south.

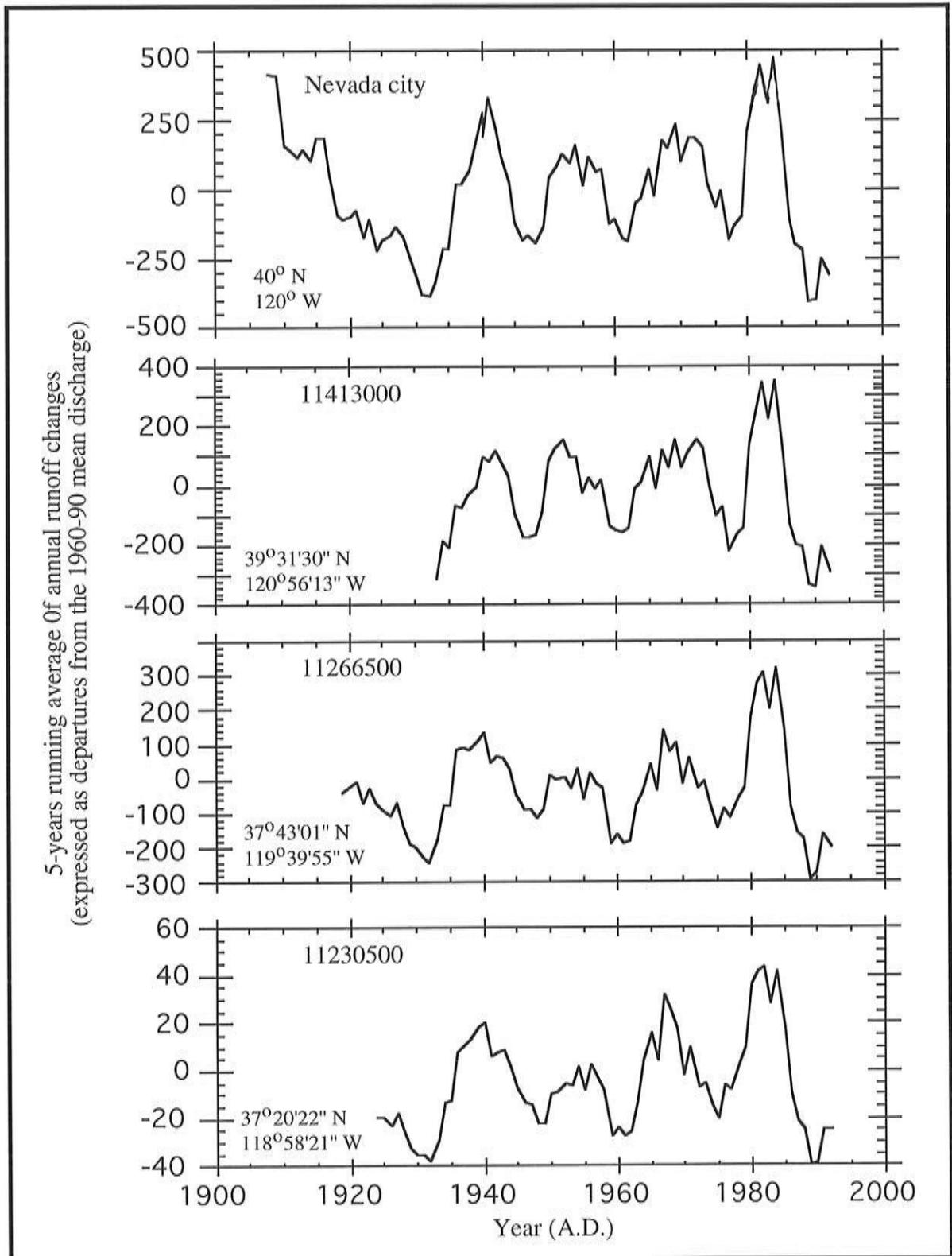


Figure 6. Temporal and spatial variations in streamflow in the mountain area of California.

Stations are plotted from north to south.

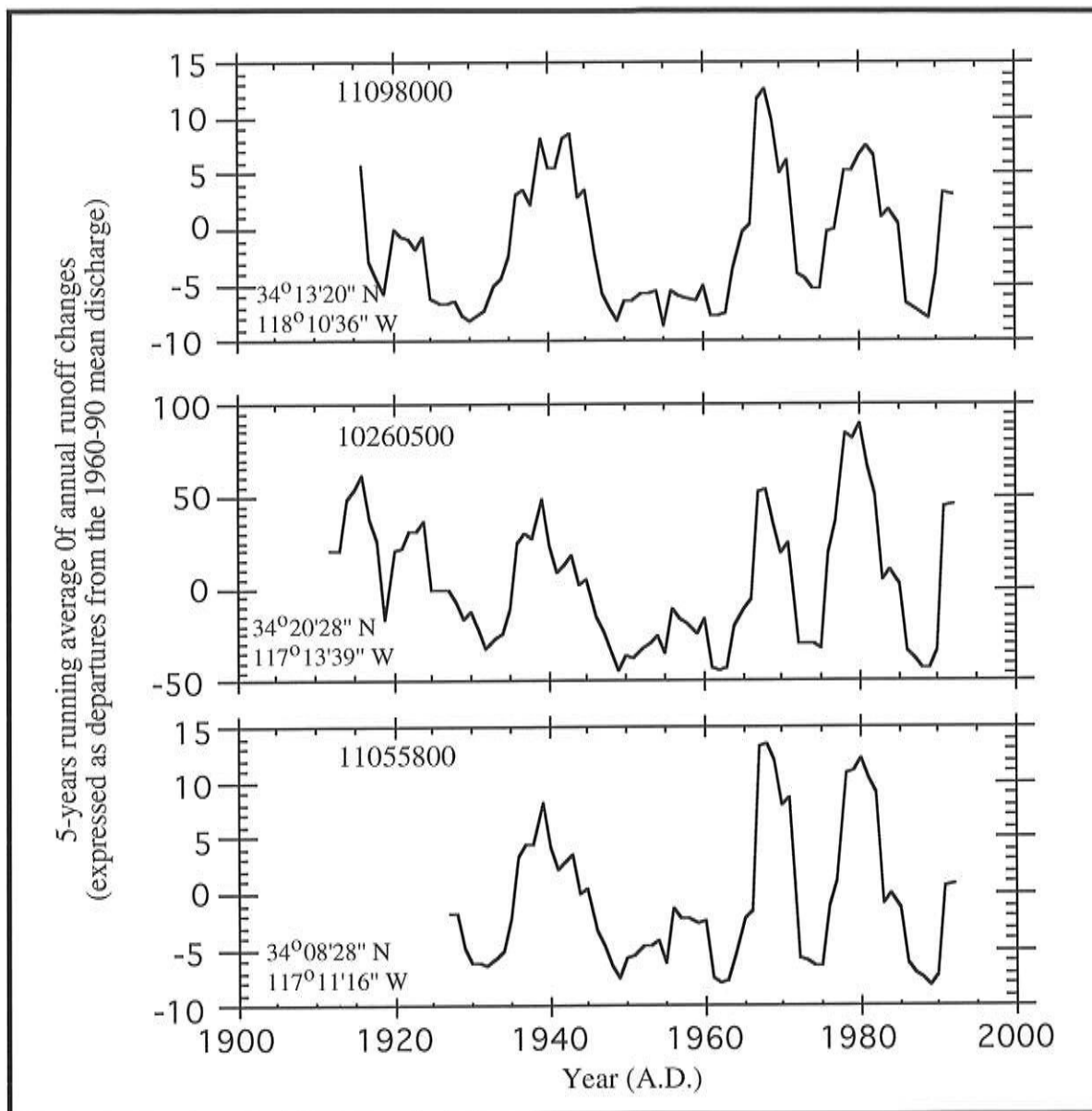


Figure 7. Temporal and spatial variations in streamflow in the Los Angeles Basin of California. Stations are plotted from west to east.

ations of California runoff can also be explained by the north-south and up-down shifts of polar and subtropic jet streams illustrated in Figure 3.

Runoff variations in the Los Angeles Basin and southern desert area of California are somewhat different from other regions (Figure 7). Precipitation in this region can be strongly influenced by southeasterly flow governed by the summer monsoon. Strong runoff in 1969 and 1993 recorded by gauging stations in this region may indicate the strengthening of the summer monsoon.

### **Lake Level Fluctuation and Anomalies of Streamflow and Precipitation**

---

Fluctuations in lake level and volume of closed-basin lakes should serve to indicate changes in the moisture budget associated with climatic change. Water entering closed-basin lakes via rain and runoff mostly leaves by evaporation. As evaporation is highly temperature dependent, one may surmise that relatively constant average annual temperature imparts little to the runoff fluctuation. Hence, changes in the effective wetness (P-E) mainly reflect changes in precipitation on interannual-to-decadal time scales.

The level and volume fluctuations of a closed-basin lake can be recorded by the  $\delta^{18}\text{O}$  of authigenic carbonates in lake sediments that is in equilibrium with the  $\delta^{18}\text{O}$  of lake water. The lake  $\delta^{18}\text{O}$  of a closed-basin lake gets progressively heavier as evaporation proceeds. Thus,  $\delta^{18}\text{O}$  of input water is always lighter than that of the lake water. When precipitation rate increases in a closed basin, runoff and lake storage in the basin will increase and the lake  $\delta^{18}\text{O}$  will be depleted. We have made high-resolution  $\delta^{18}\text{O}$  measurements on the sediments of Mono Lake, a hypersaline, alkaline closed-basin lake at the eastern base of the California Sierra Nevada. The  $\delta^{18}\text{O}$  record simulates the measured lake-level fluctuations rather well. From the comparison of the Mono Lake  $\delta^{18}\text{O}$  record with the precipitation and streamflow records in the vicinity (Figure 8), one can see that closed-basin lake sediment  $\delta^{18}\text{O}$  of relatively small lakes such as Mono Lake provides an effective means of probing decadal precipitation variations in arid-to-semiarid regions. A multi-lake study may enable us to reconstruct decadal variability of ENSO pattern and jet stream shift in the western United States.

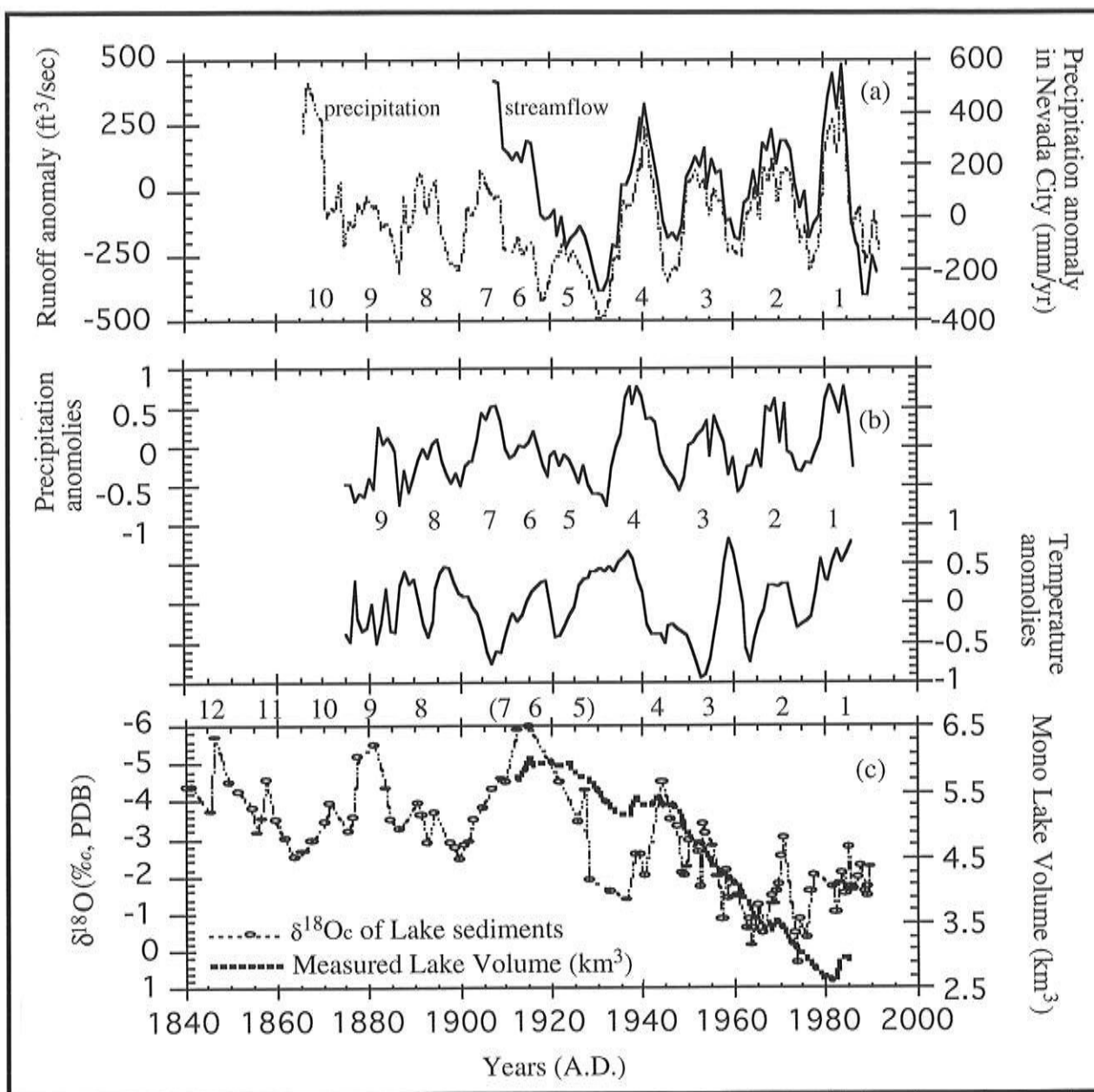


Figure 8. Comparison of the anomalies of precipitation and streamflow in Nevada City, California (top) and precipitation and temperature anomalies in the Central Valley (center) with Mono Lake fluctuations indicated by measured lake volumes and sedimentary  $\delta^{18}\text{O}$  (bottom).

## Summary

---

The teleconnection of ocean-atmospheric circulation in North Pacific and the west coastal region of the United States involves westerly flow influenced by the Pacific/North America Lows and the Subtropic Highs and southeasterly flow governed by the summer Monsoon. The dominant winter precipitation regime associated with the Jet Stream Westerly exhibits decadal variability. The temporal and spatial variability of the precipitation regime can be explained by the horizontal and vertical shifts in westerly flow. Although causes of the vertical shifts remain unknown, the south-north shifts are probably related to the intensity of the Southern Oscillation. A preliminary assessment shows that variations of California rainfall and runoff on a decadal time scale, but not on an annual time scale, are strongly correlated with ENSO. Positive SOI may cause the jet stream westerly to shift north more than normal, hence the northwestern coast is wet and the southwestern coast is dry, and vice versa. Both up and down shifts in westerly flow occur during very weak Southern Oscillation periods. This vertical shift controls a broad region of precipitation anomaly.

Streamflow anomalies in California are strongly correlated with precipitation anomalies in each drainage basin on annual-to-decadal time scales. This means that streamflow anomaly on annual-to-decadal time scales reflects chiefly precipitation change in this arid-semiarid region. The temporal and spatial variations of California runoff can also be explained by the north-south and up-down shifts of jet stream westerlies. However, strong runoff in 1969 and 1993 recorded by gauging stations in the Los Angeles Basin and the desert area of California may indicate strengthening of the summer monsoon.

Closed-basin lake sediment  $\delta^{18}\text{O}$  of relatively small lakes such as Mono Lake provides an effective means of probing decadal precipitation variations in arid-to-semiarid regions. Multi-lake study may be used to reconstruct decadal variability of ENSO pattern and jet stream shift in the western United States.

## Literature

---

- Blevins, M.L., E.L. Coufal, L.M. Watanabe, M.R. Garcia, C.J. Foley. 1987. *Mono Basin Geology and Hydrology*. LADWP, Aqueduct Division-Hydrology Section. 108 pp.
- Hastenrath, S. 1991. *Climate Dynamics of the Tropics*. Kluwer Academic Publishers. 488 pp.
- Li, H.-C., T.-L. Ku, L.D. Stott, R.F. Anderson. 1996. Stable isotope study in Mono Lake (California) — I:  $\delta^{18}\text{O}$  in lake sediments as proxy of climatic change during the last 150 years. *Limnol. Oceanogr.* (in press).
- Quinn, W.H., and V.T. Neal. 1987. El Niño occurrences over the past four and a half centuries. *Jour. Geophys. Res.* 92:14,449-14,461.
- U.S. Geological Survey. 1994. *Water Resources Data — California*. Volume 1-5, 1994.



# Monte Carlo Simulation of Streamflow of the Salt River, Arizona

Marina Timofeyeva and Rachael Craig

**Abstract:** Evaluations of the impact of climate change (such as a greenhouse effect) upon water resources should represent both the expected change and the uncertainty in that expectation. Since water resources such as streamflow and reservoir levels depend on a variety of factors, each of which is subject to significant uncertainty, it is desirable to formulate methods of representing that uncertainty in the forcing factors and from this determine the uncertainty in the response variables of interest. We report here progress in the representation of the uncertainty in climate upon the uncertainty in the estimated hydrologic response. These uncertainties are represented in Monte Carlo simulations of local climate and hydrology. For illustration we show solutions for a 5 km x 5 km grid over an area of about 30,000 km<sup>2</sup> that contains the drainage of the Salt River, Arizona. This river forms a critical water supply for the greater Phoenix area and the utility of the water supply is dependent upon wintertime snowfall and timing of snowmelt.

Results of the Local Climate Model are monthly mean maximum daily temperature (TMAX) and total monthly precipitation (PREC). We also derive standard deviations for TMAX and log(PREC) as the standard error of the regression of the canonical correlation model. Together they form the spatially-varying parameters of frequency distributions of TMAX (normal) and PREC (lognormal) at each point of a grid. Monte Carlo perturbation of climate using these parameters provides stochastic input into a mainly deterministic (mass balance) hydrology model. Results of the hydrology model with this stochastic input are long-term monthly runoff over each grid cell, and discharge at selected sites which can be compared to observed discharges at the same point.

Comparison of 78 years of modeled and observed streamflow at Roosevelt Lake shows that modeled mean discharges are very close to the observed values; but, the modeled standard deviation of discharge can differ from observed by a factor of two or three. Analysis of standard deviation of precipitation at 14 stations within the solution domain has shown long-term variations from one 10-year period to another of 2x to 5x, which may explain these discrepancies. Another explanation of the discrepancies in the standard deviation of discharges may arise from use of boundary conditions for average conditions rather than the same time period being tested.

## Introduction

Water resources may be one of the most vulnerable components of the earth system when considering future climate change associated with a greenhouse effect (Lins *et al* 1991). The sensitivity of the hydrologic system to climatic change makes our society vulnerable to impacts on various critical facilities such as reservoirs, hydroelectric plants, and irrigation and flood control structures. There is considerable debate whether the uncertainties in existing models of climate change allow clear statements of expected hydrologic impacts. We report here a method to represent the uncertainty in computed hydrology given the uncertainty in the controlling climate.

Various approaches are available to estimate the characteristics of a regional hydrologic system that can be expected in a different climate (Arnell 1992; Bultot *et al* 1992; Gleick 1987; Kite *et al* 1994; Panagoulia 1992; Cole *et al* 1991; McCabe and Ayers 1989). Typical of the current state of methods is the work of Kwadijk and Middelkoop (1994), who use monthly temperature and precipitation solved from a coarse resolution GCM to compute discharge of the Rhine River for a 2xCO<sub>2</sub> scenario. Examination of the uncertainties in such estimates of discharge typically is achieved through sensitivity analysis (Lettenmaier and Gan 1990).

Richardson (1981) shows a method of stochastic simulation of climate variables, and Ming-Ko Woo (1992) extends this idea by using stochastic simulation to represent climate and climate variability under a 2xCO<sub>2</sub> scenario. We know of no examples where a stochastic model of climate has been used to compute both the expected value and variance of streamflow under a climate change scenario. Our purpose here is to illustrate a method to achieve this, and we illustrate this method with an example from the Salt River, Arizona, which is a critical water supply for Phoenix and which derives much of its flow from snowmelt.

Our method makes use of a stochastic model of climate called the Local Climate Model (CGM). An earlier version of the LCM has been described by Craig and Stamm (1990), and results of validation of that model were reported by Stamm and Craig (1992). Orndorff, Craig, and Stamm (1993) linked the climate model to a calculation of hydrologic mass balance in a model with one soil layer, and Orndorff and Craig (1994) illustrated application of a two-layer version of that model (Orndorff 1994) in the Truckee River drainage. In this study we use a more recent version of the LCM described by Stamm and Gettelman (1995) to calculate climate.

The LCM computes mean monthly maximum daily temperature (TMAX) and total monthly precipitation (PREC) using a canonical-regression function (Stamm and Gettelman 1995). Solution of the canonical-regression function requires computation of a set of predictor variables which represent the influence of five boundary conditions: terrain, sea surface temperature, wind fields, atmospheric CO<sub>2</sub> concentration, and solar radiation. The values of these boundary conditions define the climate scenario solved by the model.

The snow and surface hydrology model (SSHM) used in this study is mostly deterministic and based on linkage of separate models reported by Orndorff (1994). SSHM uses climate as the forcing factor in the monthly runoff and streamflow discharge computation. Runoff is computed for each grid cell of the solution domain, and discharge is computed for specific locations of the watershed.

## Method

---

The climate model used was described by Stamm and Gettelman (1995). We have used that model to compute TMAX (°C) and PREC (mm) for drainage basins of the Salt River and Verde River in Arizona at a horizontal grid resolution of 5 km by 5 km (Figure 1). These values (Figure 2a,b) represent the expected value of a canonical regression model at each grid cell based on the values of 22 independent variables calculated at that grid cell by the climate model based on the General Circulation Model calculated history of air masses reaching that cell in January and July. These expected values are supplemented by estimates of the standard deviation of TMAX and of PREC at each grid cell (Figure 2c,d) by calculation of the *standard error of the regression* (Draper and Smith 1981) using the same independent variables at that cell.

We have linked together the LCM, with the hydrology and snow models modified from those reported by Orndorff (1994). Our modification of Orndorff's models joins the snow and hydrology models into one and adds a Monte Carlo element to perturb the input climate parameters so that the long-term statistical variability of climate becomes the input to a sequence of simulated years of runoff and streamflow. Variance of TMAX and PREC is computed as the standard error of the regression for the regression equations from which climate is solved. We assume TMAX is normally and independently distributed and that PREC is log-normally and independently distributed. Successive draws from these distributions represent the seasonal cycle of climate at a monthly time step through a sequence of years. From that input we calculate the hydrologic properties of a grid of points within a drainage basin. For our example, we use 78 years of simulated record, which matches the length of discharge record of the Salt River available at Roosevelt Lake, Arizona, where we computed discharge. Computed runoff is totaled for all grid points in a drainage basin to yield an estimate of streamflow, and the variability of the predicted streamflow through the sequence of simulated years gives a measure of the uncertainty in the hydrologic response as a function of the uncertainty in climate.

Runoff is calculated for each grid cell using a parameterized mass-balance approach. PREC is partitioned into snow and rain according to TMAX and assumed values for the environmental lapse rate and the fall velocity of snow. Snowpack can accumulate through the season, and snowmelt is calculated using an index method dependent upon TMAX. Infiltration may be stored in a surface (soil) layer and from there may be used to satisfy evapotranspiration needs (calculated with the Blaney-Criddle equation and a depletion term) or may recharge a groundwater layer from which baseflow is extracted at a fixed rate limited by a depletion term. Parameter values are the same as those derived by Orndorff (1994). Calculations are iterative through each simulated year

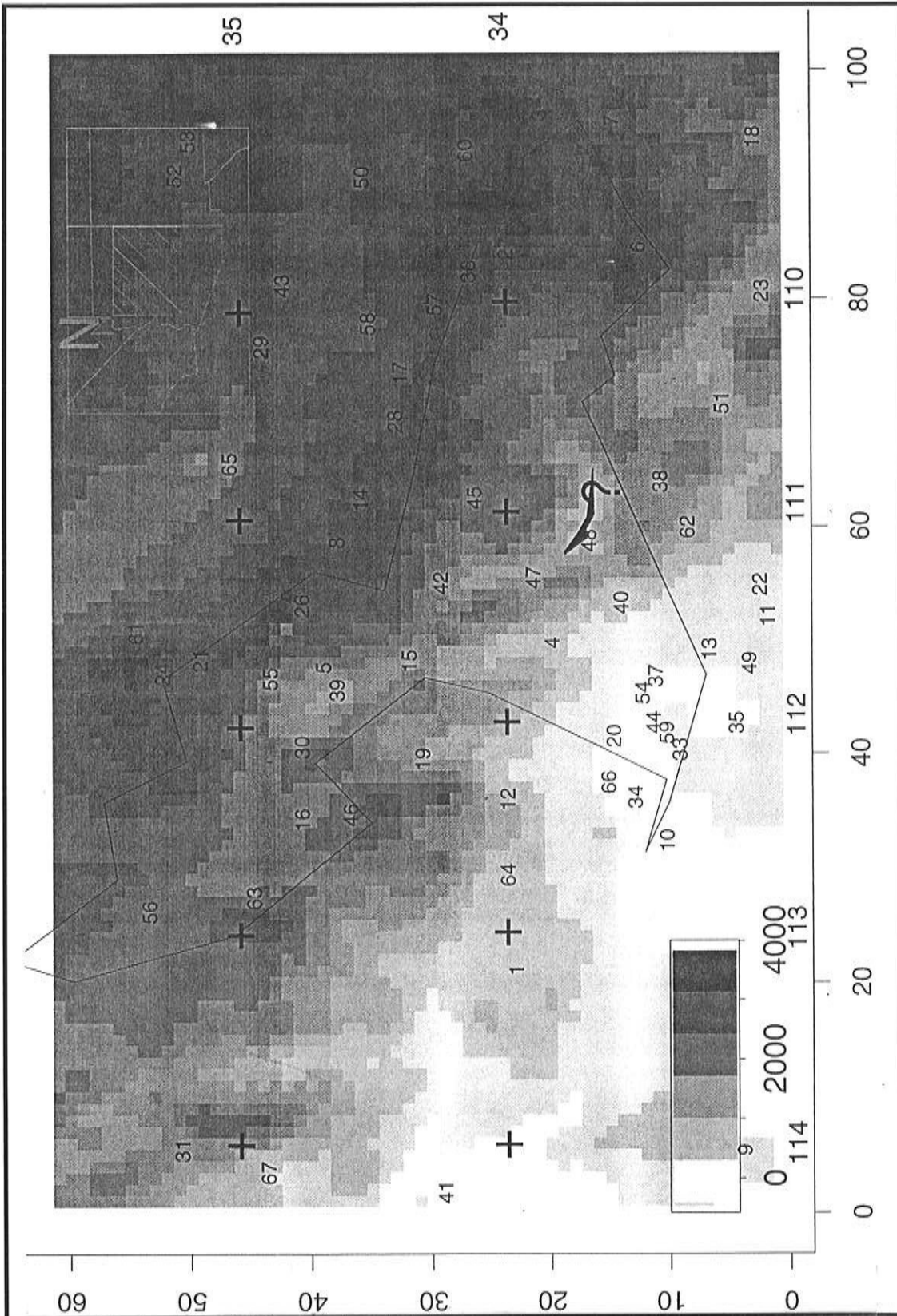


Figure 1 Solution domain for calculation of climate and hydrology.

Shades represent elevation (m) as shown in the accompanying legend. The drainage basin outline of the Salt and Verde rivers is shown schematically. Grid cell numbers are shown on the outer axis, and each cell is 15 km square. Dark tick marks within the figure mark latitude-longitude intersections, which are labeled at the inner margins. Numbers within the figure show locations of climate stations referred to in the text. The Roosevelt Lake gaging station is shown by a "?". Index map gives the setting of the grid within Arizona.

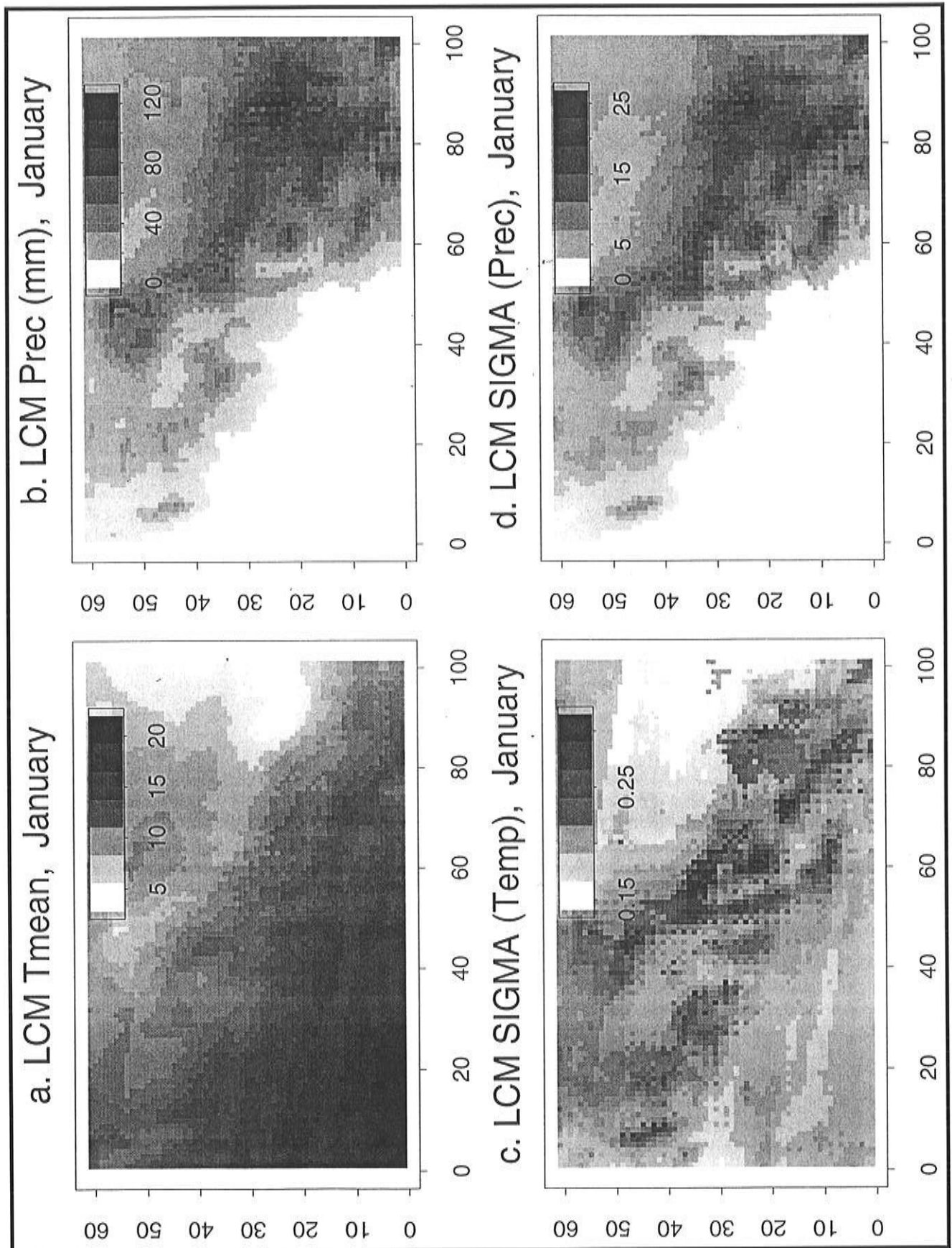


Figure 2 Example solutions of climate (for the same area as in Figure 1) for January.

until the soil moisture equilibrates. We use the method of Singer (1985) to calculate those grid cells draining to the grid cell representing the Salt River gaging station at Roosevelt Lake. Runoff for all grid cells draining to the Salt River at Roosevelt Lake (Figure 3, top) is summed to estimate discharge.

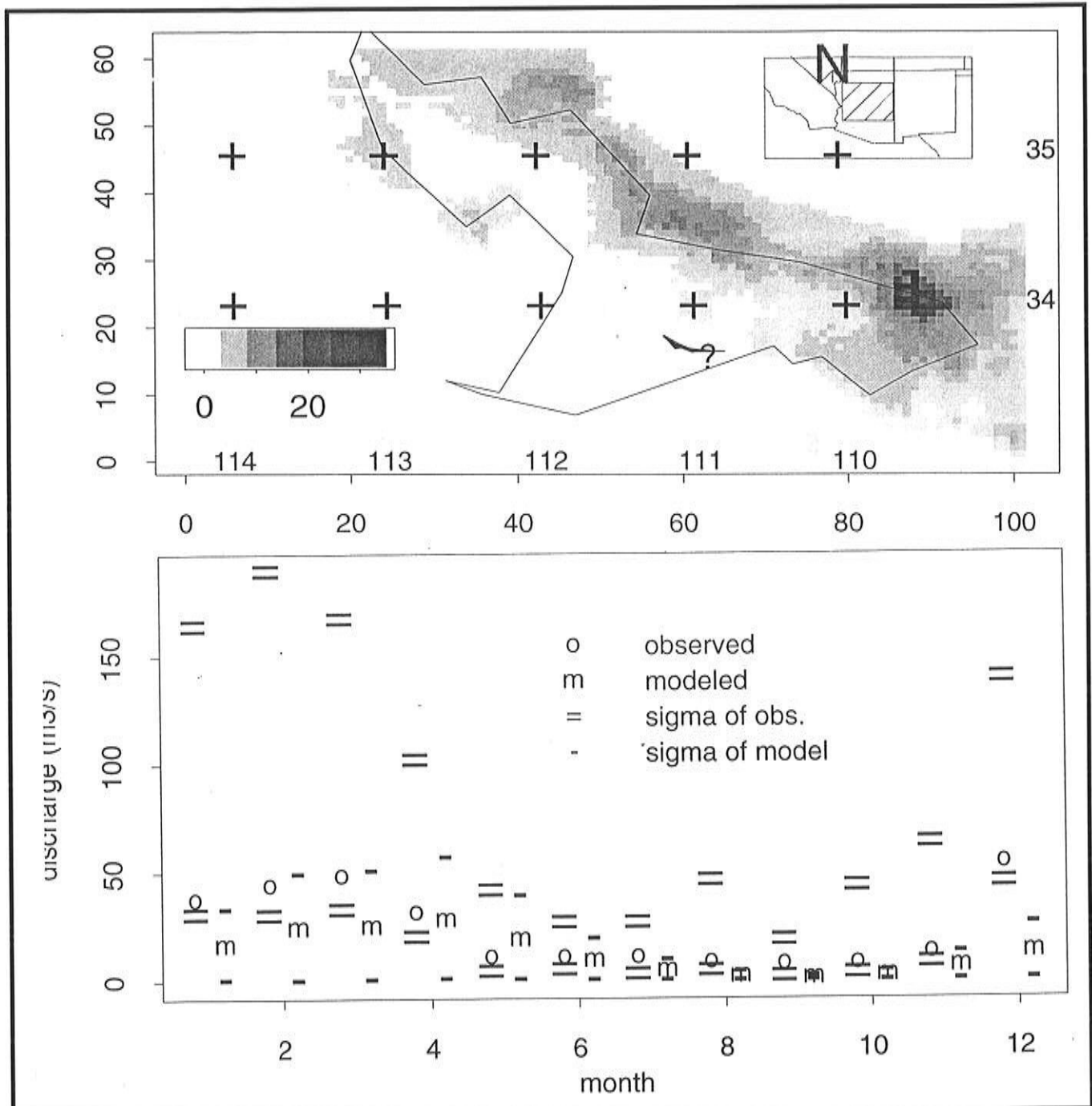


Figure 3 (Top) Calculated annual runoff (cm) for the same area as shown in Figure 1. (Bottom) graphical representation of discharge statistics at Roosevelt Lake for 78 years simulated and observed. Numbers represent mean discharge for the corresponding month and the ticks above and below the corresponding number represents the mean plus or minus one standard deviation.

## Results

---

Before evaluating the hydrologic simulation, we first examine results of the climate model and of the Monte Carlo simulations based on the expected climate. Our examination of the calculated climate is made by comparing model solutions to observed instrumental records of climate at 67 stations in the solution domain for 1975-1979. Here we report comparisons for January and July. Figure 4a compares the expected value of temperature estimated by the model to that observed. There is a close correspondence between observed and predicted, although there is a constant bias of about 1-2°C, with the model tending to estimate temperatures that are too cool. This may be because the climate model was calibrated primarily with instrumental records from more northerly locations in the western United States, which may have biased the model to cooler temperatures. The means calculated from a Monte Carlo simulation of 5 years of January temperature (Figure 4b) based on these expected values and the standard error of the prediction show the same bias and, in general, reproduces the average statistics very well.

The model estimate of July temperature provides an even closer match to observed (Figure 4c) and (unlike January) with no constant bias. The closer match may be due to the smaller north-to-south temperature gradient in the western United States during summer. In Figure 4c we do see a small linear bias in which the model is too warm at the low temperatures (high-elevation sites) and too cool at high temperature (low-elevation) sites. We assume this bias arises because the model estimates are calculated for the average elevation of the 5 km by 5 km grid cell rather than for the exact elevation of the climate station. Because of this, the model computes a temperature for an elevation higher (lower) than the climate station and therefore cooler (warmer).

Model estimates of mean precipitation are less satisfactory (Figure 4d). In this case there is the same constant bias in estimates of January PREC as was seen for January TMAX; but, the model tends to estimate a wetter climate than observed — consistent with the cooler temperatures and probably due to the same calibration bias. Except for a few stations, the correspondence is within a factor of two (Figure 4e). Considering that observed January precipitation can vary by a factor of two, or even five, from one 5-year period to another (Figure 5) this discrepancy may be attributable to actual variability. The fact that the model tends to overestimate PREC could be because the model was calibrated for a relatively wet period in the record (hatched box in Figure 5). For the Monte Carlo estimates of PREC, the model calculates the expected value and standard error of the prediction of the natural log of PREC. We exponentiate each estimate and report the mean of these values. The Monte Carlo estimates of January PREC (Figure 4e) again suggest that the model tends to slightly overestimate PREC, this time with a slight systematic bias. The

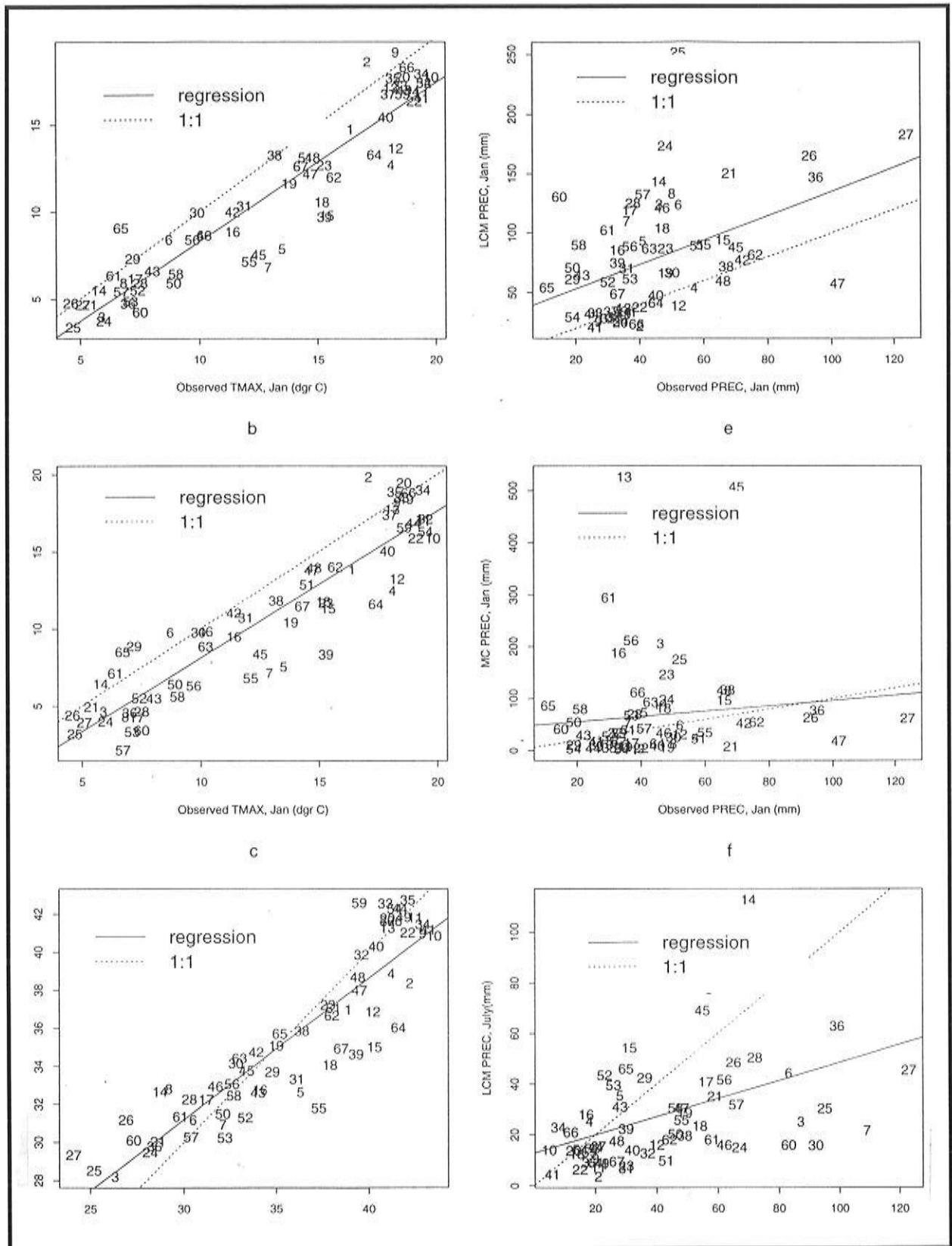


Figure 4. Comparison of observed mean TMAX and total PREC with:

- (a) modeled mean TMAX for January, (b) mean of Monte Carlo estimates of TMAX for January, (c) modeled mean TMAX for July,
- (d) modeled total PREC for January, (e) mean of Monte Carlo estimates of PREC for January, (f) modeled PREC for July.

Numbers on each plot correspond to stations shown in Figure 1. Also shown are the 1:1 line (dashed) and a line based on a simple linear regression with "observed" as the independent variable.

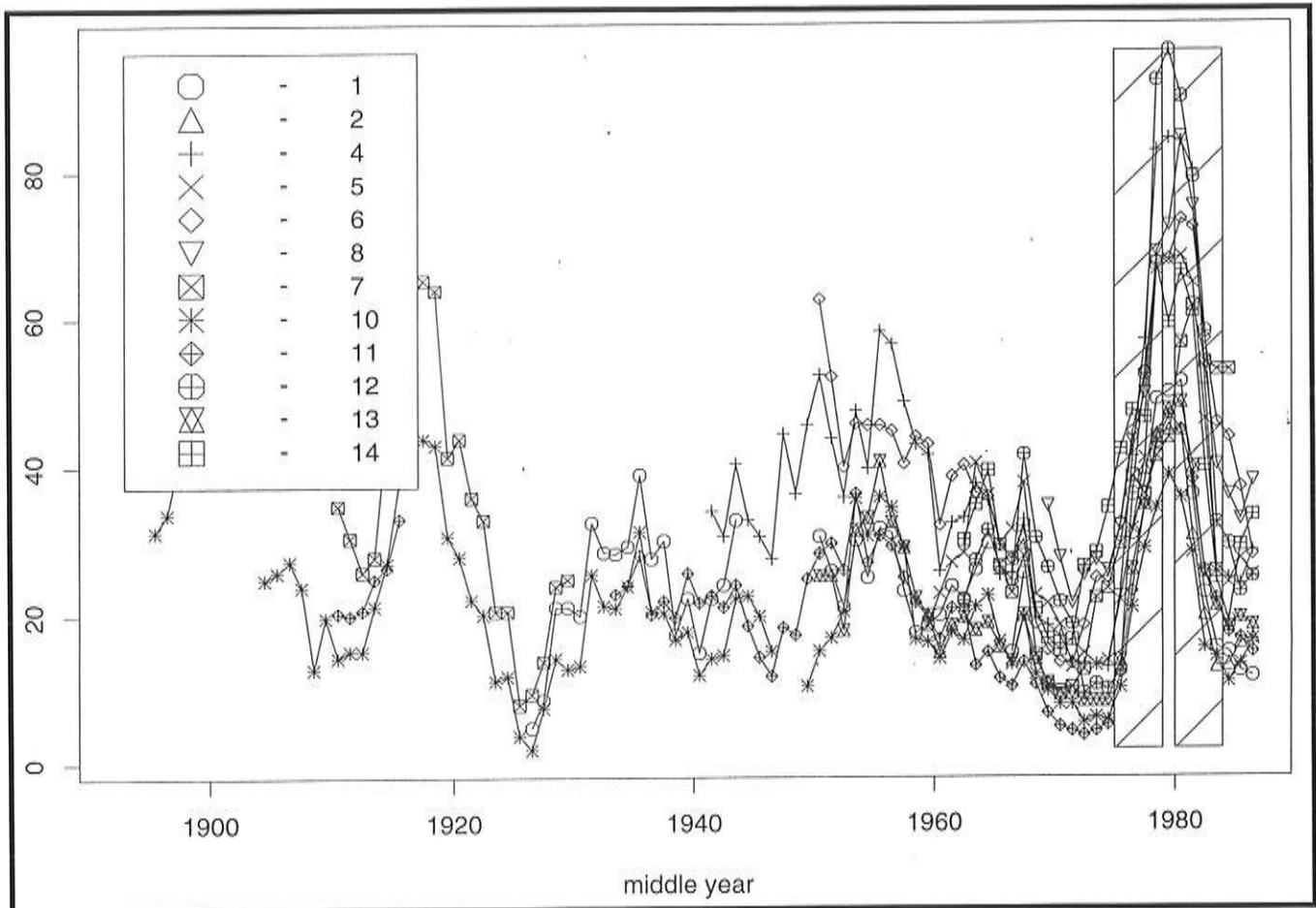


Figure 5. Temporal patterns of PREC for 12 climate stations in Arizona computed as 5-year running averages.

The hatched boxes enclose the periods 1975-1979 and 1980-1984 used for calibration of the LCM. Station numbers correspond to those in Figure 1. Five-year averages are plotted at the location of the middle year.

greatest errors occur at stations 13, 45, and 61, which are at low, intermediate, and high elevations, respectively. Thus, no systematic bias with elevation is apparent. In general, the stations with very low calculated PREC are those at the lowest elevation sites, so the simulation seems to capture the orographic effect well. For July, the pattern is similar to that for July TMAX estimates (Figure 4f); there is a tendency for a linear bias with a slope less than one leading to estimates of PREC that are slightly too high in dry areas and too low in wetter (high elevation) areas, suggesting that the grid cell elevations for which solutions are made are not as high (or low) as the actual climate station elevations, which is consistent with the bias seen in Figure 4c.

Calculated annual runoff (Figure 3 top) shows the strong spatial pattern expected in an area dominated by orographic precipitation (compare to Figure 1). Most of the runoff in this area is generated by winter rainfall and spring snowmelt, with a minor contribution from summer monsoons. The model predicts that most runoff is generated along the topographic transition between the desert of the southwest and the high plateau of the northeast, and this corresponds to the actual case.

---

## Discussion

---

A comparison between observed and calculated discharge for the gaging station at Roosevelt Lake is shown in Figure 3 (bottom). A bias toward too low estimates of discharge in winter (months 12, 1, 2, 3) and toward too high estimates of discharge in the melt season (months 4, 5, 6) can be seen. Observed annual discharge averaged (unweighted) across months is 25.5 cms, whereas the modeled average discharge is 18.8 cms. Considering the coarseness of the climate solution and the simplicity of the hydrologic model, the correspondence (*ie*, mass balance) is quite remarkable.

Figure 3 (bottom) also provides a visual representation of the variability of observed and modeled discharge. The ticks surrounding each month's average value correspond to the values of mean  $\pm$  one standard deviation calculated with the lognormal model (Aitchison and Brown 1957, equation 2.7). The variability modeled for April, May, and June (high snowmelt months) corresponds nearly perfectly to that observed. Winter months have greater variability than modeled, and the warmer (and drier) months have less variability than is modeled. In general the variability is captured within a factor of two, as was true for precipitation. It is interesting that calculation of mean discharge at this site using the output of the LCM directly and so without Monte Carlo perturbations and inclusion of the standard deviation relationship of Aitchison and Brown (1957) gives a mean discharge of 17, which is at greater deviance from observed than the value obtained by the simulation technique, as would be expected according to theory. This supports the concept that proper estimates of the mean discharge require knowledge of both mean and variance of the climate parameters.

Why is the estimated discharge too high in winter and too low in the snowmelt months? This could be explained by the constant bias toward too low temperatures in winter, as suggested in Figure 4a, which would tend to lead to a greater fraction of precipitation estimated to fall as snow in winter. This snow would be stored as snowpack in the winter, leading to lower discharge in winter and overestimation of discharge when it melts in spring. The estimate of winter snow fraction is based on a relationship to mean monthly temperature. Orndorff (1994) estimated mean monthly temperature by subtracting a constant (12°C) from TMAX, and that constant was determined by calibration using records from 52 stations in California and Nevada. However, the data of Orndorff (1994, Figure 4.4) show that the "constant" is never greater than 11°C and may be as low as 9°C in winter, with a mean of 10.5°C. If we modify the correction parameter of Orndorff (1994) to correspond to the observed values that he reports in his Figure 4.4, there is a slight decrease in modeled streamflow in winter but a great decrease in spring, so that the modeled discharge in spring closely matches observed and overall the fit is improved.

## Acknowledgments

---

We thank Rik Orndorff and John Stamm for making their computer codes available to us. This manuscript has benefited from discussions with Julio Betancourt of the USGS Desert Laboratory in Tucson and with Jim Young of Southern California Edison Company. This work has been performed with support from the Salt River Project, Phoenix, Arizona.

## References

---

- Aitchison, J., and J.A.C. Brown. 1957. *The Lognormal Distribution*. Cambridge Univ. Press, 176 p.
- Arnell, N.W. 1992. Factors controlling the effects of climate change on river flow regimes in a humid temperate environment. *Journal of Hydrology*, 132:321-342.
- Bultot, F., D. Grllens, M. Spreafico, and B. Schadler. 1992. Repercussions of a CO<sub>2</sub> doubling on the water balance — a case study in Switzerland. *Journal of Hydrology*, 137:199-208.
- Cole, J.A., S. Slade, P.D. Jones, and J.M. Gregory. 1991. Reliable yield of reservoirs and possible effects of climate change. *Hydrological Sciences Journal*, 36:579-598.
- Craig, R.G., and J.F. Stamm. 1990. A statistical model of climates in the southwestern U.S. Pages 27-31 in *Proceedings of the Sixth Annual Pacific Climate (PACCLIM) Workshop*. J.L. Betancourt and A.M. Mackay, eds., Calif. Dept. Water Resources, Inter. Ecol. Stud. Prog. Tech. Rept. 23.
- Draper, N., and H. Smith. 1981. *Applied Regression Analysis*, 2<sup>nd</sup> Ed. John Wiley, NY, 709 pp.
- Gleick, P.H. 1987. Regional hydrologic consequences of increases in atmospheric CO<sub>2</sub> and other trace gases. *Climatic Change*, 10:137-161.
- Kite, G.W., A. Dalton, and K. Dion. 1994. Simulation of streamflow in a macroscale watershed using general circulation model data. *Water Resources Research*, 30:1547-1559.
- Kwadijk, J., and H. Middelkoop. 1994. Estimation of impact of climate change on the peak discharge probability of river Rhine. *Climatic Change*, 27:199-224.
- Lettenmaier, D.P., and T.Y. Gan. 1990. Hydrologic sensitivities of the Sacramento-San Joaquin river basin, California, to global warming. *Water Resources Research*, 26:69-86.
- Lins, H.F., I.A. Shiklomanov, and E.Z. Stakhiv. 1991. Impacts on Hydrology and Water Resources. Pages 87-97 in *Climate Change: Science, Impacts and Policy*. J. Jager and H.L. Ferguson eds. Proceedings of the Second World Climate Conference, Cambridge University Press.
- McCabe, G., and M.A. Ayers. 1989. Hydrologic effects of climate change in the Delaware River basin. *Water Resources Bulletin*, 25:1231-1241.
- Ming-Ko Woo. 1992. Application of stochastic simulation to climatic-change studies. *Climatic Change*, 20:313-330.
- Orndorff, R.L. 1994. Development of a Surface Hydrologic Model and its Application to Modern and Last Glacial Conditions. Unpublished Ph.D. Dissertation, Kent State University, Kent, OH, p. 178.
- Orndorff, R.L., and R.G. Craig. 1994. Modeling the effect of snow on seasonal runoff within the Truckee River Drainage Basin. Pages 107-116 in *Proceedings of the Tenth Annual Pacific Climate (PACCLIM) Workshop*. K.T. Redmond and V.L. Tharp, eds. California Department of Water Resources, Interagency Ecological Studies Program, Technical Report 36.
- Orndorff, R.L., R.G. Craig, and J.F. Stamm. 1993. A stochastic model of temporal variations in monthly temperature, precipitation, snowfall, and resulting snowpack. Pages 165-172 in *Proceedings of the Ninth Annual Pacific Climate (PACCLIM) Workshop*. K.T. Redmond, ed., California Department of Water Resources, Interagency Ecological Studies Program, Technical Report 34.

- Panagoulia, D. 1992. Impacts of GISS-modelled climate changes on catchment hydrology. *Hydrological Sciences Journal*, 37:141-163.
- Richardson, C.W. 1981. Stochastic simulation of daily precipitation, temperature, and global radiation. *Water Resources Research*, 29:2335-2344.
- Singer, M.P. 1985. A Computer Simulation Model of the Growth and Desiccation of Pluvial Lakes in the Western Great Basin, U.S. Unpublished M.S. thesis, Kent State University, p. 436.
- Stamm, J.F., and R.G. Craig. 1992. Validation of a semi-Lagrangian, canonical regression model of climates in the southwestern United States. Pages 163-171 in *Proceedings of the Eighth Annual Pacific Climate (PACLIM) Workshop*, K.T. Redmond, ed. California Department of Water Resources, Interagency Ecological Studies Program, Technical Report 31.
- Stamm, J.F., and A. Gettelman. 1995. Simulation of the effect of doubled atmospheric CO<sub>2</sub> on the climate of Northern and Central California. *Climatic Change*, 30:295-325.

# The Influence of Climate on Phytoplankton Communities in the Upper San Francisco Estuary

Peggy W. Lehman

**ABSTRACT:** The 1977 climate shift was characterized by low chlorophyll *a* concentrations and a shift in phytoplankton community composition throughout the upper San Francisco Bay estuary. Average chlorophyll *a* concentration decreased by a factor of 2 and was associated with a loss of diatoms, particularly pennate diatoms, and an increase in flagellates. These changes in phytoplankton biomass and community composition reflected interannual variations in water-year types. Water-year types are a function of climate, which changed to very dry conditions after the 1977 climate shift. For climate to be a driving force in phytoplankton communities, it must affect mechanisms that control biomass and community composition. The influence of climate on environmental conditions and phytoplankton community composition among water-year types was examined using 19 years of physical, chemical, and phytoplankton data collected monthly at 15 stations throughout the estuary. Environmental variation associated with the ENSO climatic signal for different water-year types was isolated using covariance analysis and summarized using principal component axes. Correlations between the principal component axes describing climatically-related environmental variation and chlorophyll *a* concentration plus phytoplankton density and biovolume for individual species and species groups suggest dry conditions produced by the 1977 climate shift were at least partly responsible for the changes in phytoplankton biomass and community composition measured between 1975 and 1993.

## Introduction

Average annual chlorophyll *a* concentration decreased by a factor of 2 for most regions in the upper San Francisco estuary after 1976 (Lehman 1996a, 1992). The lower chlorophyll *a* concentrations after 1976 were accompanied by a loss of diatoms and a shift in the composition of the phytoplankton community toward more greens, bluegreens, and flagellates (Lehman and Smith 1991; Lehman 1996a). Many factors can influence phytoplankton biomass such as management practices that affect downstream transport (Jassby and Powell 1994) and grazing by introduced clams (Nichols 1985). The role of toxic substances is unclear but suspected to be important for changes in biomass and community composition. Natural environmental change associated with the 1977 climate shift may also be important. That climate was important is suggested by coincident changes in chlorophyll *a* concentration, phytoplankton community composition, and environmental variables with the 1977 climate shift (Lehman and Smith 1991). Recent studies also suggest that chlorophyll *a* concentration and community composition vary with water-year type, which is directly related to the climate (Lehman 1996a).

The purpose of this study was to determine if climate-related changes in environmental conditions may have influenced the changes in phytoplankton community composition and biomass measured among

water-year types between 1975 and 1993 in the upper San Francisco Bay estuary.

## Methods

Environmental and biological variables were measured monthly or semi-monthly at 15 stations between 1975 and 1993 (Figure 1). Chlorophyll *a* concentrations were measured since 1971. Physical and chemical measurements of the water and water samples for nutrient concentrations, chlorophyll *a* concentration, and phytoplankton enumeration and identification were collected at 1-meter depth. Phytoplankton cell volumes ( $\mu\text{m}^3$ ) were calculated from cell dimensions and corrected to account for the large vacuole in diatoms (Strathmann 1967). Details of the analytical methods for physical, chemical, and biological variables are described in Lehman (1996a, 1996b).

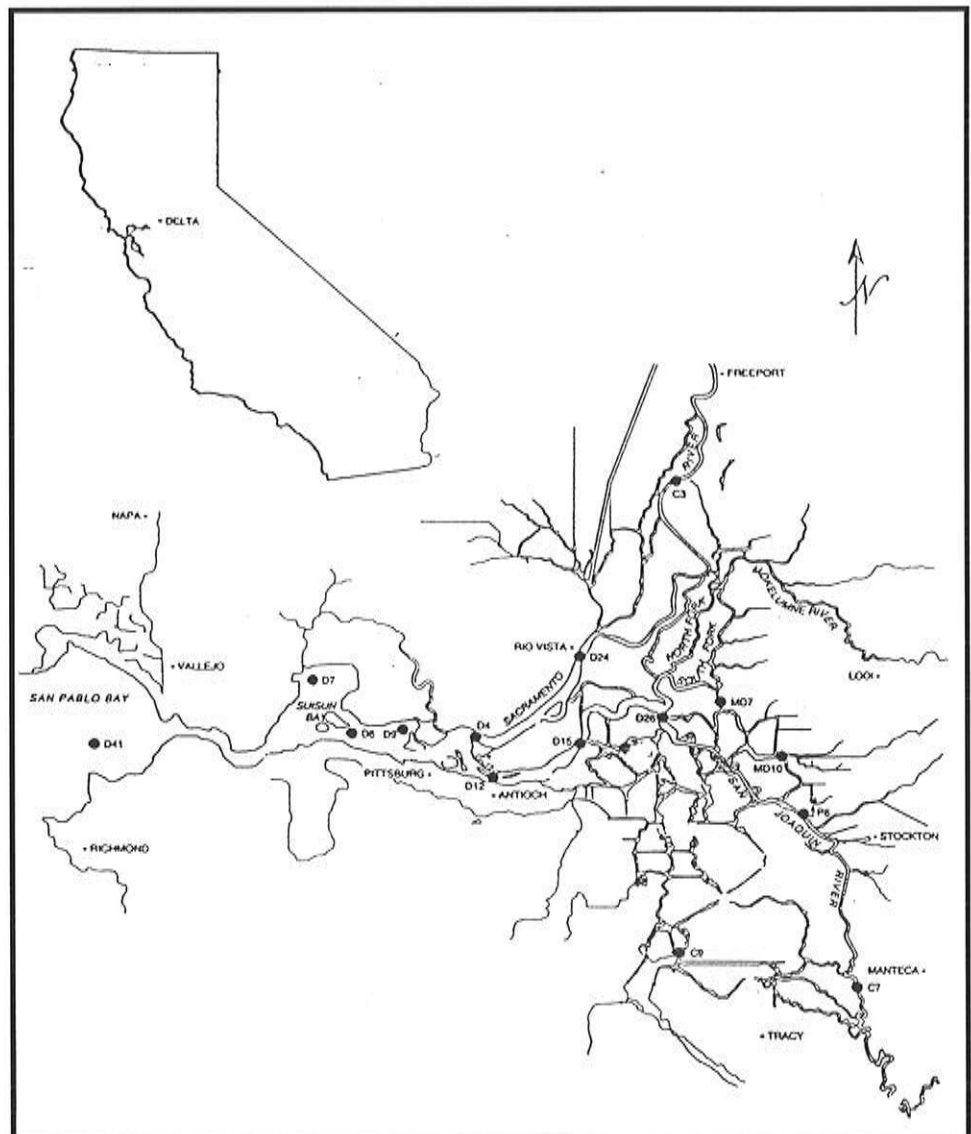


Figure 1 Sampling stations in the upper San Francisco Bay estuary.

Changes in climate were described using the CASLP (California sea level pressure) climate index developed by Dan Cayan. The index is derived from sea level pressure at 40°N and 120°W and separates wet and very dry conditions.

Each year was indexed by water-year type. Water years since 1906 have been classified as wet, above normal, below normal, dry, or critical (very dry) based on the Sacramento River index, which is an estimate of the combined unimpaired runoff of four rivers that flow into the delta. For this study, below- and above-normal years were coded as normal years because only 3 years were in these two water-year types since 1975.

All analyses were conducted with seasonally corrected standard deviation units. These units were calculated for each station and variable as the monthly average minus the average for that month over all years divided by the standard deviation for that month over all years. Only the spring and summer months April through September were used in the analysis.

Differences among environmental and biological variables among water-year types were determined using the nonparametric technique, the Kruskal-Wallis test. Significant differences were at the 0.05 significance level or higher. The conservative nature of a nonparametric statistical technique was used to compensate for the presence of significant correlations by chance alone when a large number of correlations are calculated.

Climatically related environmental change was calculated as the covariance between monthly values of the CASLP climate index and environmental variables at each station among water-year types. This climatically related environmental variation was summarized by four principal component axes. Correlations between the principal component scores of these axes and phytoplankton density or biomass variables were computed with Pearson correlation coefficients.

### **Phytoplankton Density, Biovolume, and Chlorophyll *a* Concentration**

Phytoplankton density, chlorophyll *a* concentration, and biovolume were lower than average for most of the years after 1976. For biovolume and chlorophyll *a* concentration, which are estimates of phytoplankton biomass, 9 to 11 of the 17 years after 1976 were below average (Figure 2). Biovolume and chlorophyll *a* concentration also changed in a similar fashion among years, with values higher than average in the high-outflow years 1982 and 1986. Chlorophyll *a* concentrations measured since 1971 suggest the frequency of lower-than-average values after 1976 is part of a long-term decline. Total density was lower than average for 8 of the years after 1976 and higher than average in 1982. Unlike the other variables, total density was consistently at or slightly above average during the 1987-1992 drought.

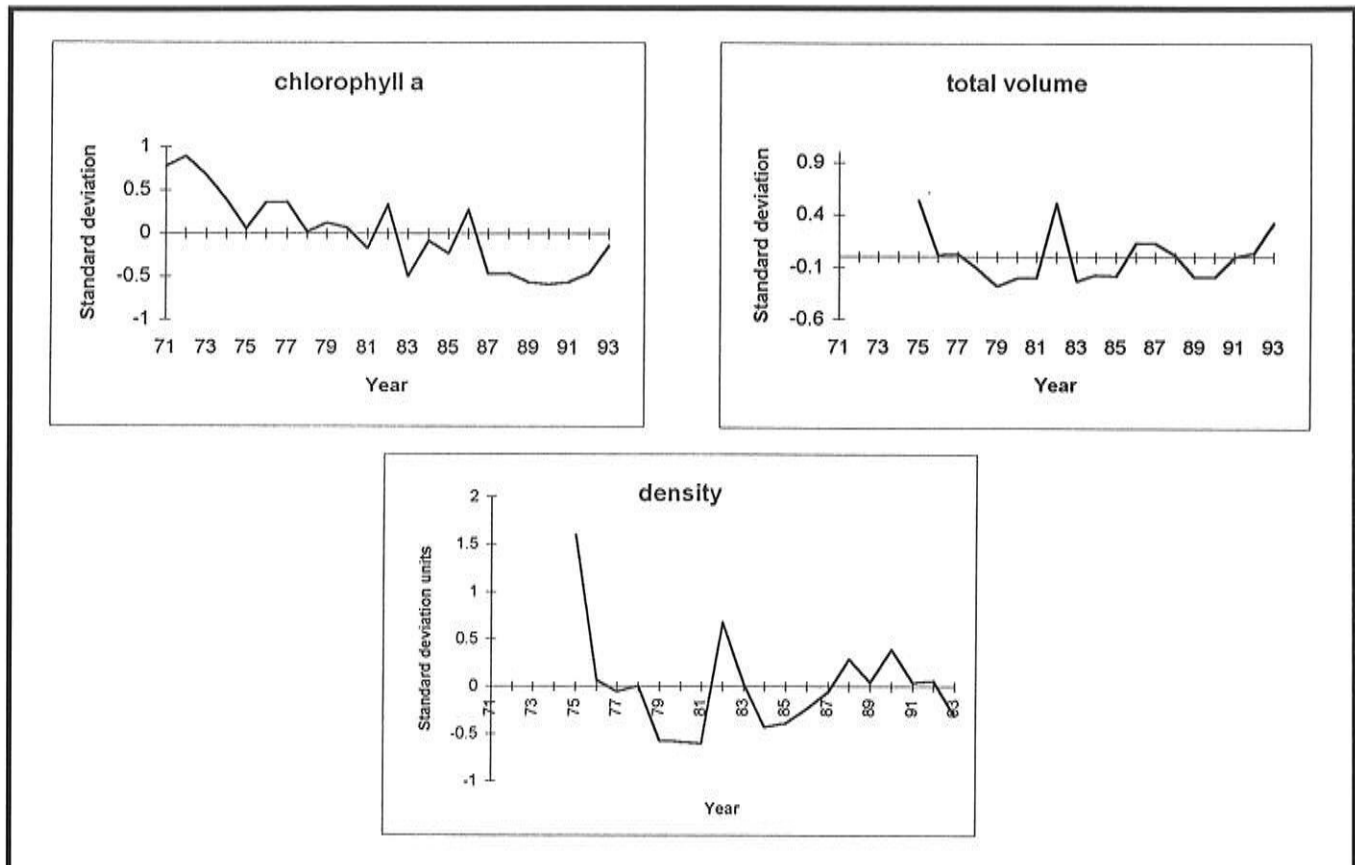


Figure 2 Average standard deviation units for phytoplankton total density, chlorophyll *a* concentration, and biovolume during spring and summer for 15 stations.  $n=90/\text{year}$ .

## Percent Community Composition

The decreased chlorophyll *a* concentration, total density, and biovolume after 1976 were associated with a decrease in the percentage of diatoms in the phytoplankton community. For total density, the percent diatoms decreased from a maximum of about 75% in the late 1970s and early 1980s to a minimum of 30% in 1990 (Figure 3). Percentages increased to near 50% in the early 1990s. For biovolume, the percentage of diatoms decreased from maxima of near 85% in the late 1970s and early 1980s to a minimum of 55% in 1990 before increasing to near maximum values in the early 1990s. The decrease in percent diatoms was accompanied by an increase in greens, bluegreens, and all flagellate groups — cryptophytes, miscellaneous flagellates, dinoflagellates, chrysophytes, and green flagellates. Each of these phytoplankton groups increased by 10-20% in the late 1970s and early 1980s and reached a maximum in the drought period of the late 1980s or 1990.

The decrease in the percentage of diatoms occurred in all regions of the upper estuary. Percent biovolume data suggest the percentage of diatoms among regions was 80-95% in the late 1970s and decreased to as low as 20% in 1990 (Figure 4). The largest decrease was in the northern, lower

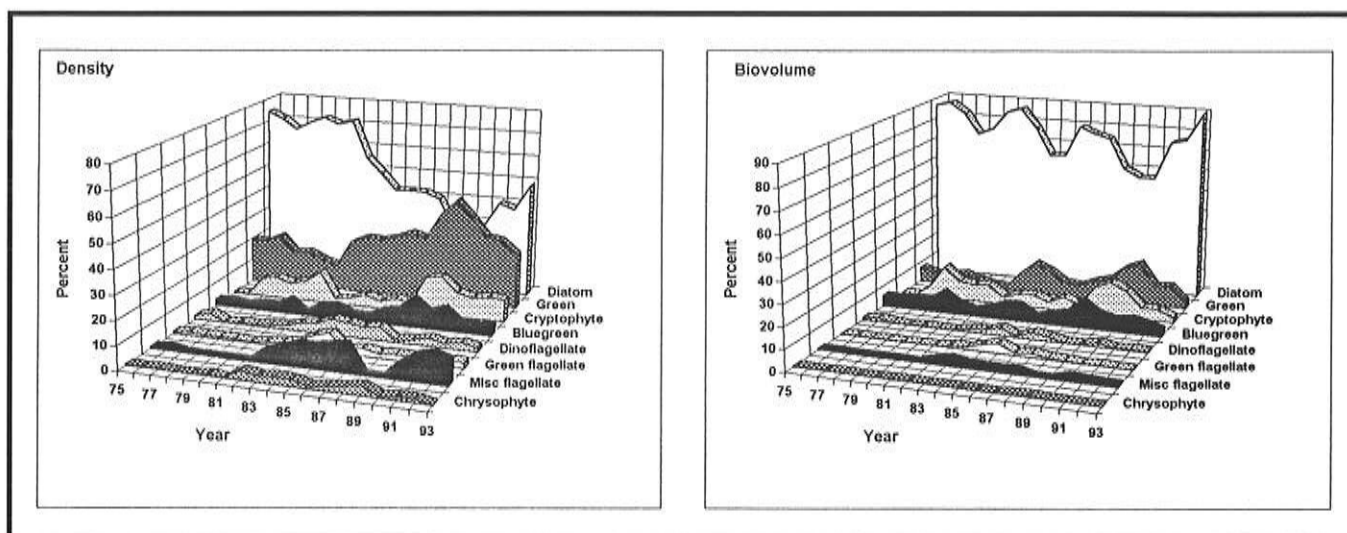


Figure 3 Average percent composition of phytoplankton groups, by density and biovolume.

San Joaquin River, Suisun Bay, and San Pablo Bay regions. For all regions, there was a coincident increase in greens, bluegreens, and flagellates, especially cryptophytes, which each increased to 20-30% of the total biovolume.

### **Pennate and Centric Diatoms**

Among the diatoms, there was a greater loss of pennate than centric biovolume. Average pennate biovolume decreased after 1976 and was consistently lower than average after 1982 (Figure 5). Although biovolume increased consistently after the minimum in 1984, it did not reach above-average values. Average centric biovolume also decreased to below-average values for most years after 1976, reaching a minimum in 1990, but increased to above-average values during the wet years 1982, 1986, 1987, and 1993. Pennate and centric biovolume often varied in an opposite fashion.

The greater loss of pennate than centric diatoms was reflected in percent composition data, with pennate biovolume decreasing to only a few percent of total diatom biovolume in the mid- to late-1980s. Pennate biovolume decreased from a maximum of 35% of the total diatom biovolume in 1978 to less than 5% of the total in 1987 (Figure 6). Although the percentage increased between 1989 and 1990, it decreased again in 1991 to 1993. Percent composition data also demonstrated the strong inverse association between centric and pennate diatom biovolume.

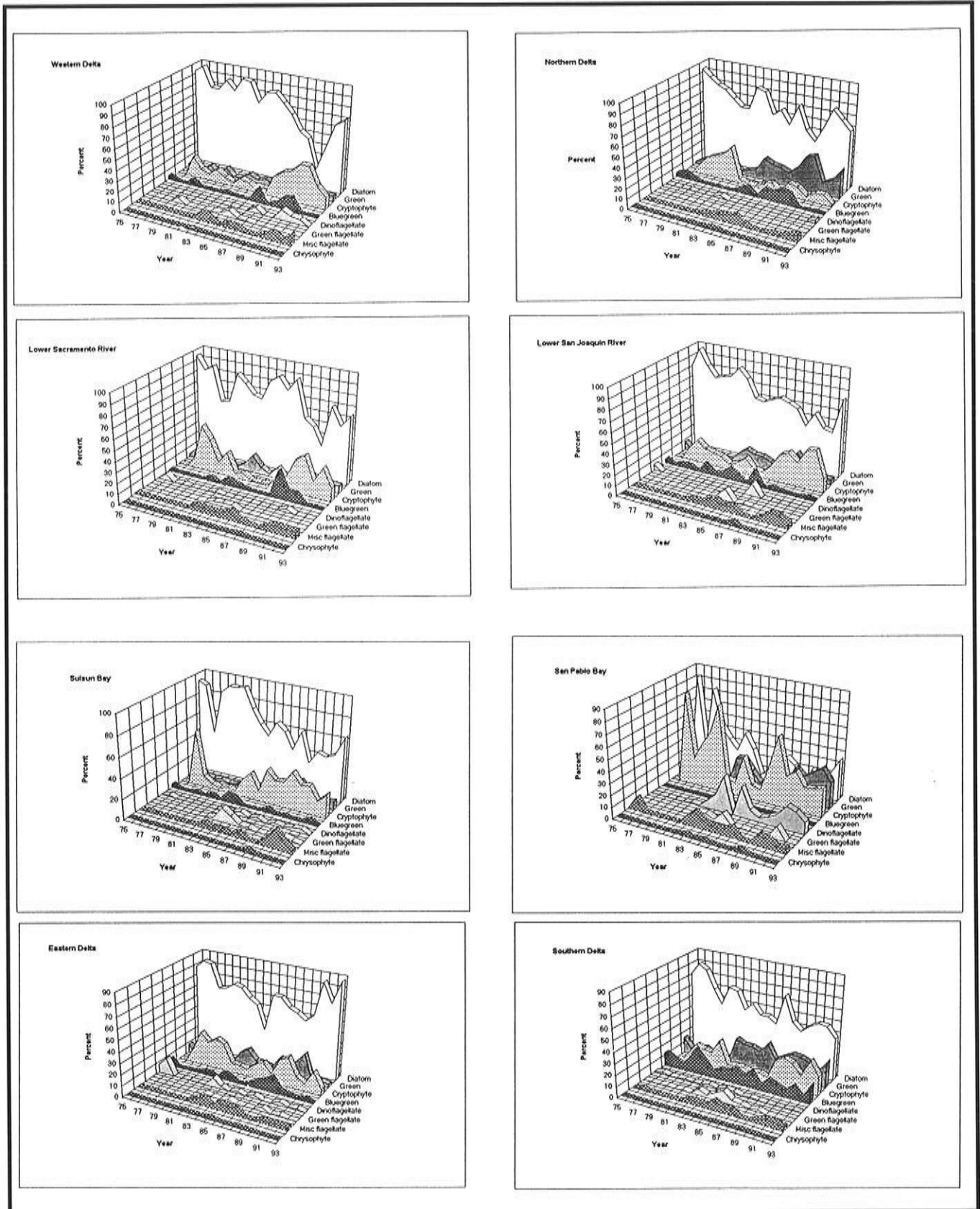


Figure 4 Average percent biovolume of phytoplankton groups among stations in the upper estuary for the spring and summer.

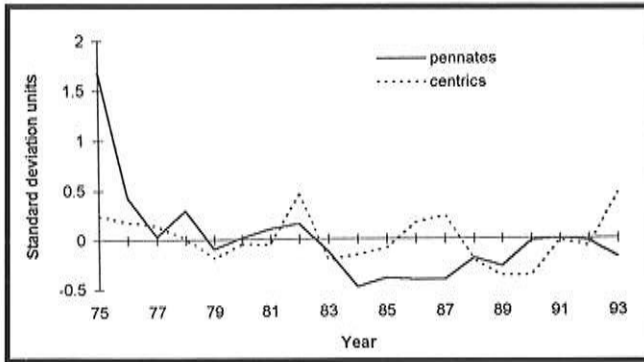


Figure 5 Average standard deviation units for pennate and centric diatoms.

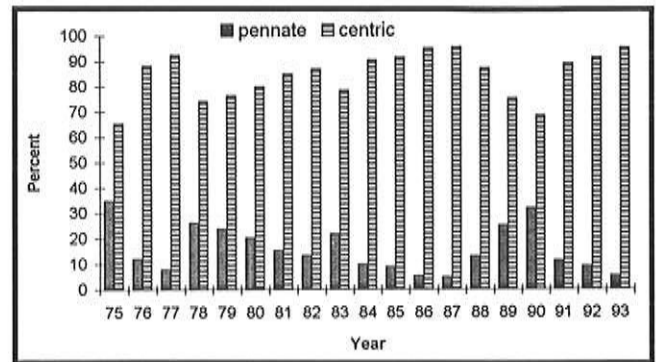


Figure 6 Average percent composition of pennate and centric biovolume.

### Changes with Water-Year Type

The climate shift in 1977 increased the frequency of wet and critical water-year types. Dry and critical water-year types comprised 10 of the 19 years 1975-1993 and were accompanied by 7 wet years (Figure 7). This high frequency of dry and critical water-year types is unmatched over the nearly 100 years of record.

Water-year types have significantly different environmental conditions and phytoplankton communities. The nonparametric statistical test, the Kruskal-Wallis test, was used to determine significant ( $p < 0.05$ ) differences between water-year types for physical, chemical, and biological variables measured monthly at 15 stations. Nearly all physical and chemical variables were significantly different for the water-year type

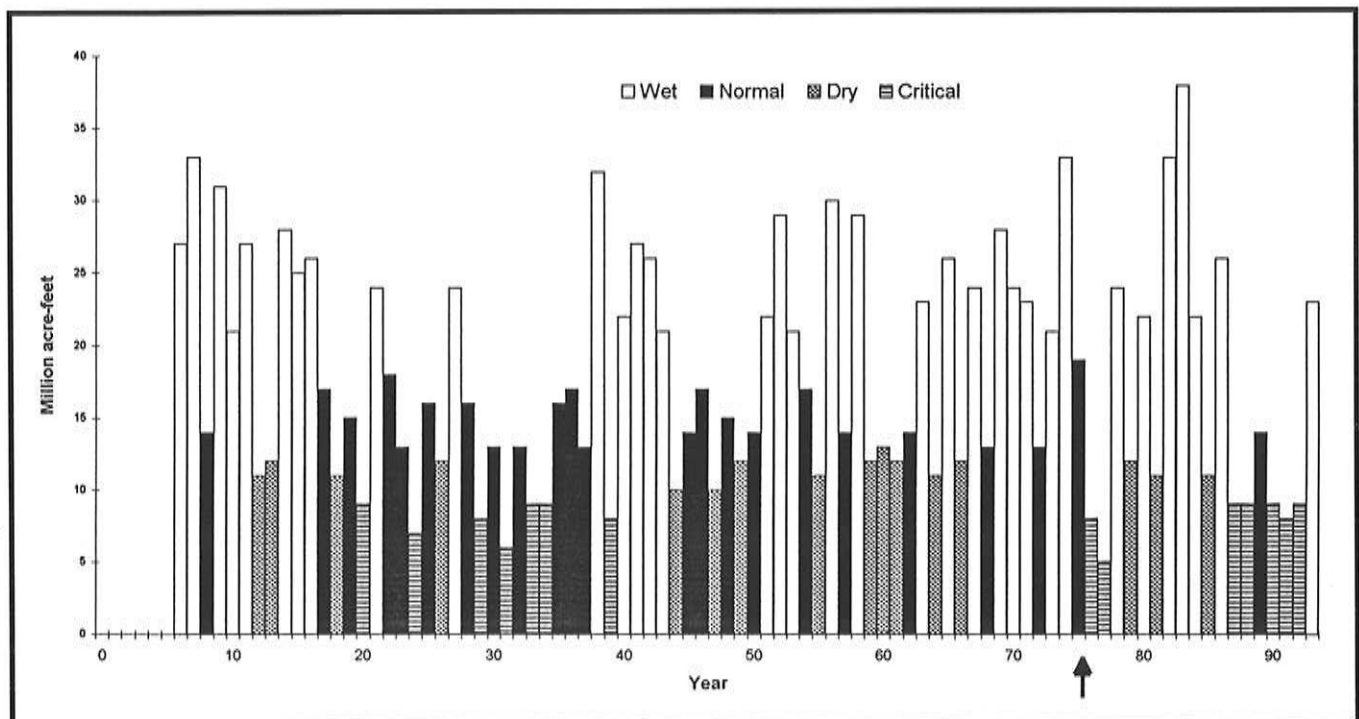


Figure 7 Sacramento Basin unimpaired streamflow, 1906-1993.

comparisons wet/critical, normal/critical, and wet/dry (Table 1). Most differences were also significant for comparisons of water-year types with similar conditions: normal/wet and dry/critical. Differences in environmental conditions among water-year types were matched by those for phytoplankton community composition, with over half of the phytoplankton groups differing for each water-year type comparison.

Table 1  
SIGNIFICANT DIFFERENCES IN ENVIRONMENTAL AND BIOLOGICAL VARIABLES AMONG WATER-YEAR TYPES

Significant differences at the  $p < 0.05$  level or higher are marked with an X.

VARIABLE	SPRING - SUMMER					
	WET / NORMAL	WET / DRY	WET / CRITICAL	NORMAL / DRY	NORMAL / CRITICAL	DRY / CRITICAL
<b>PHYSICAL</b>						
Air temperature		X	X	X	X	
Secchi disk depth		X	X	X	X	X
Water temperature		X	X	X	X	
Turbidity		X	X	X	X	X
Wind velocity			X		X	X
<b>NUTRIENTS</b>						
Total phosphate		X	X	X	X	X
Silica	X	X	X	X	X	
Organic nitrogen		X	X	X	X	
Ammonia nitrogen	X	X	X	X	X	
Nitrate		X	X		X	X
Ortho-phosphate	X	X	X	X	X	X
<b>CHEMICAL</b>						
Dissolved oxygen		X	X	X	X	
Specific conductance	X	X	X	X	X	X
pH	X	X	X		X	X
Suspended solids		X	X	X	X	X
Total dissolved solids	X	X	X	X	X	X
Volatile solids	X	X	X	X	X	X
<b>STREAM FLOW</b>						
Sacramento River		X	X		X	X
San Joaquin River	X	X	X		X	X
Mokelumne River	X	X	X		X	X
Consumnes River			X			
Miscellaneous flow						
Rio Vista flow		X	X	X	X	X
Outflow	X	X	X	X	X	X
Delta export pumping		X				X
Tracy export pumping					X	
<b>BIOLOGICAL</b>						
Chlorophyll a	X		X		X	X
Diatoms	X	X		X	X	
Greens	X	X	X	X	X	X
Chrysophytes		X		X	X	
Cryptophytes	X		X	X		X
Bluegreens	X	X	X	X	X	X
Dinoflagellates						
Green flagellates	X		X	X		X
Miscellaneous flagellates	X	X			X	X

### Environmental Variables

Environmental conditions differed among water-year types. Critical years were characterized by higher-than-average air and water temperature, wind velocity, specific conductance, pH, water transparency, and nutrient concentrations but lower-than-average streamflow and export (Figure 8). All of these conditions were opposite to those in wet years, except for exports, which were also lower than average. Environmental conditions during normal and dry years were a mixture of those for critical and wet years. Normal years, like wet years, had lower-than-average air and water temperature, specific conductance, wind velocity, and nitrate and orthophosphate concentration. Normal years differed from wet years in having higher-than-average water transparency, pH, and silica concentration. Precipitation and outflow were lower than for wet years, but exports were higher. Dry years were similar to critical years except for lower-than-average nitrate concentrations, turbidity, and suspended solids. Dry years also had higher-than-average exports compared with lower-than-average exports during critical years.

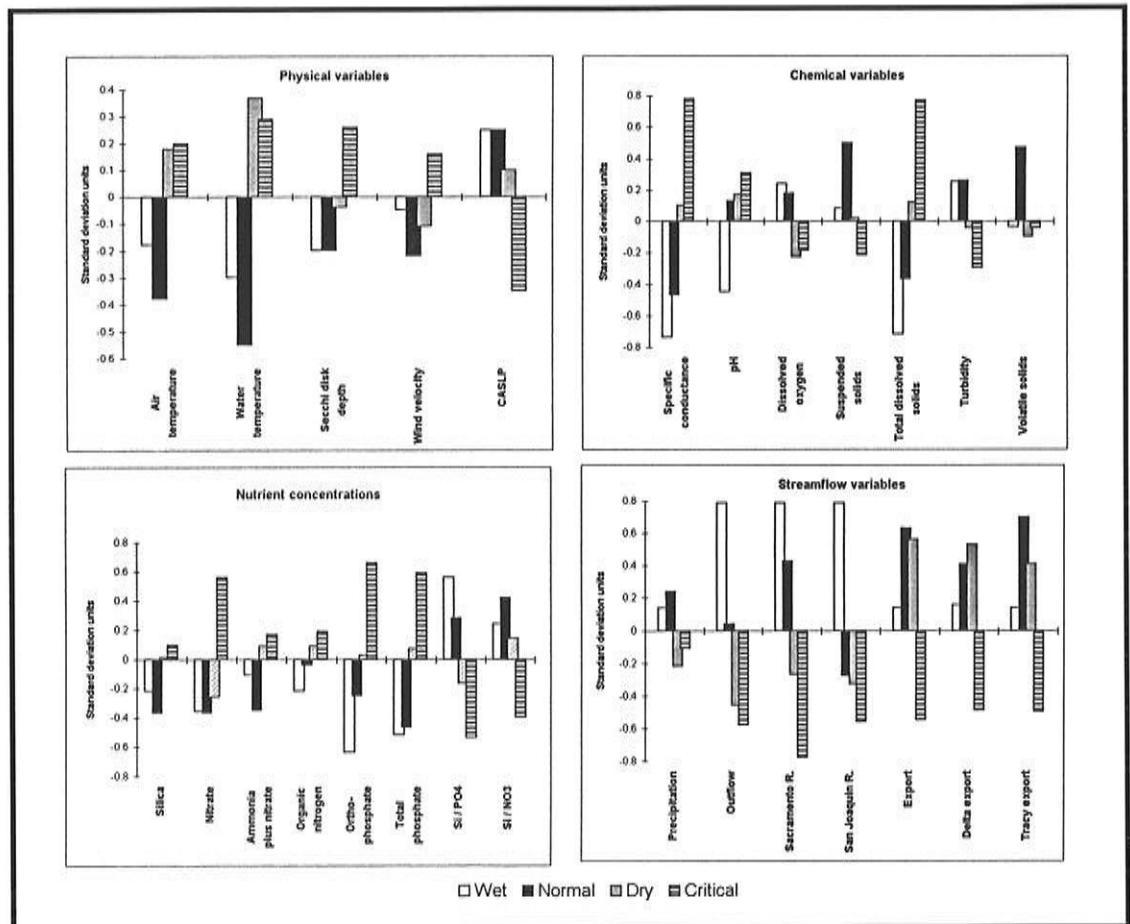


Figure 8 Average standard deviation units for environmental variables among water-year types.

### **Chlorophyll *a* Concentration, Biovolume, and Total Density**

The largest differences in chlorophyll *a* concentration, biovolume and total density occurred between wetter versus drier water-year types. Average chlorophyll *a* concentration, phytoplankton biovolume, and total density were well above average during wet and normal years but only slightly above average during critical years (Figure 9). The poorest phytoplankton growth was probably during dry years, when total density and biovolume were well below average.

### **Community Composition**

Changes in chlorophyll *a* concentration, biovolume, and total density among water-year types were associated with a shift in community composition. Biovolume and total density (not shown) of diatoms, greens, and bluegreens were higher during wet and normal years; flagellate groups (cryptophytes, dinoflagellates, green flagellates, and miscellaneous flagellates) were higher during dry and critical years (Figure 10). In addition, some phytoplankton groups increased in opposite water-year types; miscellaneous flagellates increased in critical/dry and wet years, and greens increased in normal and critical years.

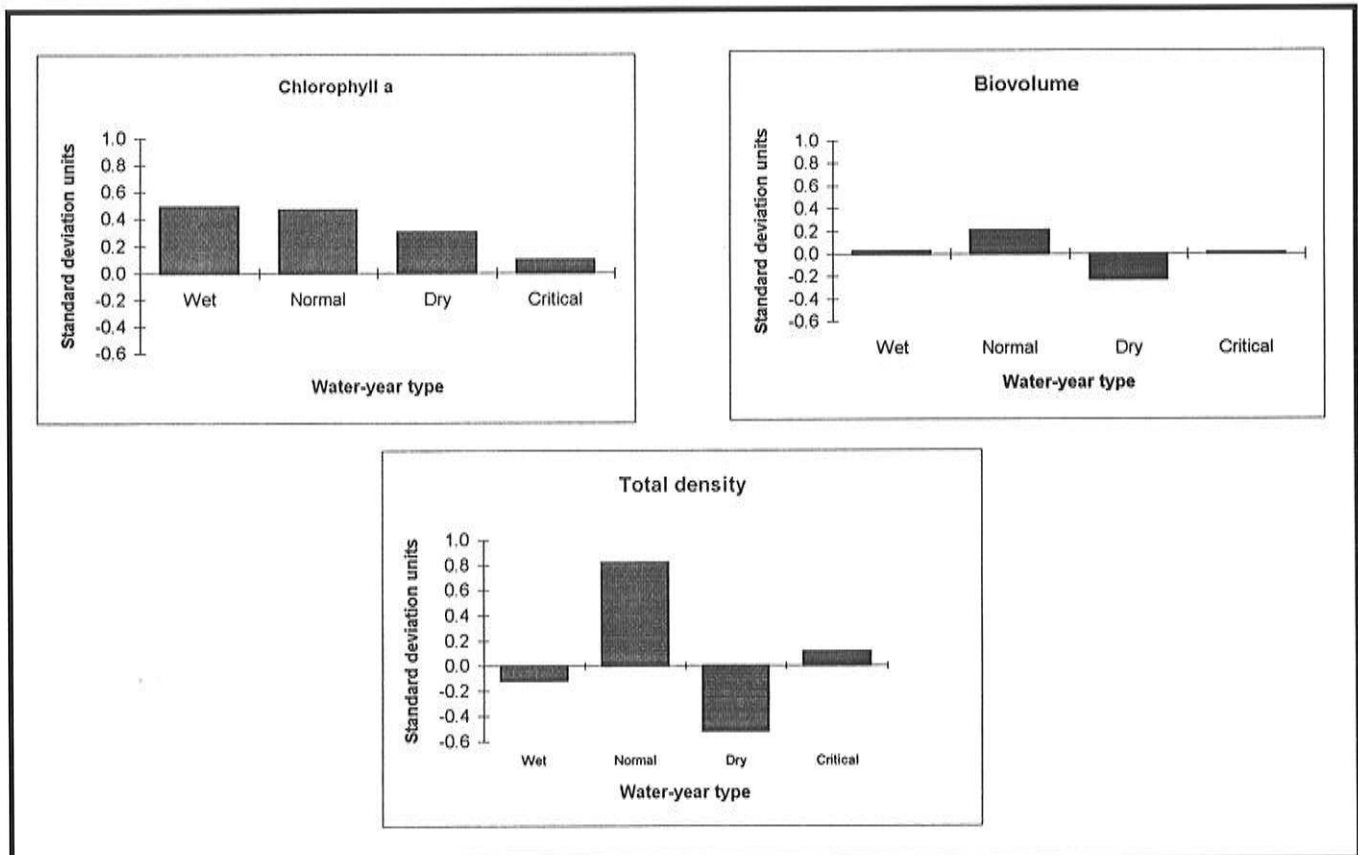


Figure 9 Average standard deviation units for chlorophyll *a* concentration, biovolume, and total density among water-year types.

### Pennate and Centric Diatoms

Among the diatoms, biovolume and density (not shown) were higher for pennate and centric diatoms during wet and normal years (Figure 11). However, biovolume and density of these two types of diatoms differed for drier years, with centrics being more abundant or having higher biovolume during dry and critical years. The direction of change for these diatom groups among water-year types persisted at the species level. Normal and wet years had more pennate diatoms; wet years and dry or critical years had more centric diatoms (Figure 12).

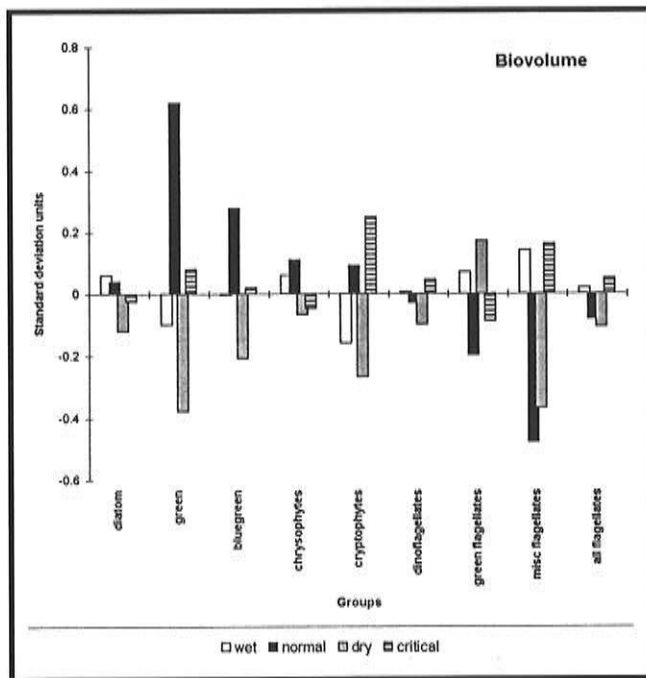


Figure 10 Average standard deviation units for biovolume of phytoplankton groups among water-year types.

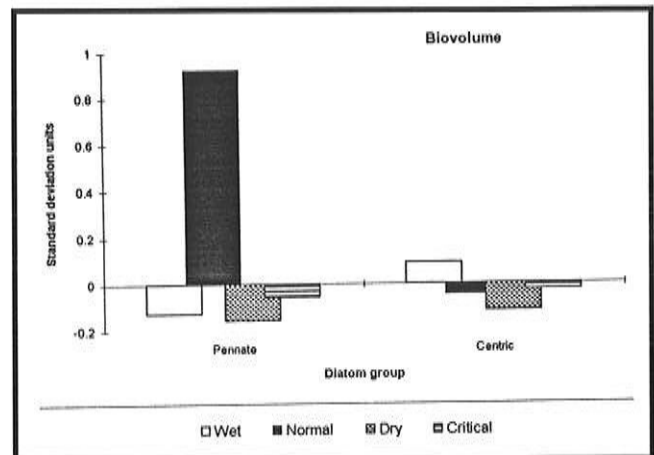


Figure 11 Average standard deviation units for biovolume of pennate and centric diatoms among water-year types.

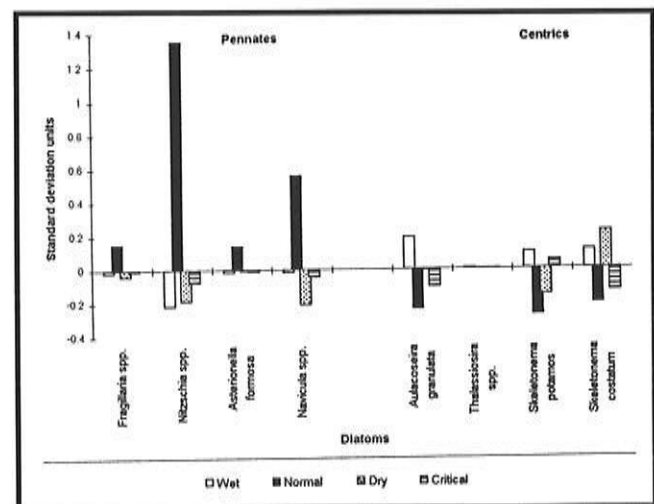


Figure 12 Average standard deviation units for biovolume of pennate and centric diatom species among water-year types.

## Associations between Climate-Related Environmental Variables and Phytoplankton Biomass and Community Composition

Principal component analysis was computed from a station by water-year type covariance matrix developed for the CASLP climate index and a suite of environmental variables. Uncorrelated ( $r < 0.70$ ) variables within the covariance matrix were summarized by three axes using principal component analysis (Table 2). Together these axes described 69% of the environmental variation. Most of the climate-related environmental variation was associated with Axis 1, which described conditions associated with very dry conditions: high water temperature, water transparency, specific conductance, wind velocity, nutrient concentrations, and export but low outflow. Axis 2 described dry conditions with low silica and high wind, while Axis 4 described conditions of average flow, high water temperature and low specific conductance.

Table 2  
PRINCIPAL COMPONENT ANALYSIS COMPUTED FOR  
CLIMATICALLY RELATED ENVIRONMENTAL VARIABLES

Variable	Principal Component Axes		
	Axis 1	Axis 2	Axis 3
Outflow	-0.44	-0.31	-0.03
Export	0.39	0.01	-0.30
Secchi disk depth	0.29	0.35	0.29
Water temperature	0.27	-0.07	0.42
Wind	0.13	0.45	0.21
Specific conductance	0.22	0.34	-0.48
pH	-0.40	0.15	-0.07
Dissolved oxygen	-0.27	0.39	0.47
Nitrate	0.37	-0.19	-0.01
Silica	0.24	-0.50	0.37
<b>Percent variation</b>	<b>38</b>	<b>17</b>	<b>14</b>

Correlations between principal component axes scores and phytoplankton variables were often highly significant for Axis 1. The very dry environmental conditions described by Axis 1 were negatively correlated with total biovolume and total density but not chlorophyll *a* concentration (Table 3). Among phytoplankton groups, correlations with Axis 1 and biovolume or density were negative for diatoms, greens, and bluegreens but positive for green and miscellaneous flagellates. Among the diatoms, Axis 1 was negatively (biovolume) or more negatively (density) correlated with pennates than centrics.

Correlations between the other principal component axes and phytoplankton variables were less consistent than for Axis 1. Correlations with Axis 2 were negative for most of the diatoms and total density or biovolume, but positively or not significantly correlated with flagellates, which do not require silica. Correlations with Axis 3 were negative for centric diatoms and flagellates, which are common when specific conductance is high in the delta.

Correlations between environmental axes and phytoplankton groups persisted at the species level (Table 4) and provided more information on variation within each group. Positive correlations with the dry conditions of Axis 1 and centric diatoms were primarily associated with chain-forming species. Cryptophytes increased when specific conductance was high, but not the common form, *Rhodomonas lacustrus*. *Skeletonema costatum* increased with dry and warm conditions, but not if silica was low. Green species decreased with dry and warm conditions, but not the flagellated species *Carteria* spp.

Table 3  
CORRELATIONS BETWEEN  
PRINCIPAL COMPONENT AXES SCORES AND  
PHYTOPLANKTON GROUP DENSITY AND BIOMASS

n=60

Biovolume		Principal component axes		
Variables	Axis 1	Axis 2	Axis 3	
Chlorophyll a		-0.26		
Total volume	<b>-0.35</b>	-0.29		
Diatom - all		-0.31		
centric				
pennate	<b>-0.80</b>	-0.34		
Green	<b>-0.65</b>	-0.27	-0.29	
Chrysophyte				
Cryptophyte			<b>-0.42</b>	
Bluegreen	<b>-0.60</b>		-0.31	
Dinoflagellate				
Green flagellate	0.46			
Misc flagellate	0.43		<b>-0.47</b>	
Density		Principal Component Axes		
Variables	Axis 1	Axis 2	Axis 3	
Total density	<b>-0.74</b>	-0.30	-0.26	
Diatom - all	<b>-0.74</b>	<b>-0.35</b>		
centric	-0.30	-0.30	-0.27	
pennate	<b>-0.81</b>	<b>-0.33</b>		
Green	<b>-0.71</b>	0.30		
Chrysophyte				
Cryptophyte	<b>-0.50</b>	0.29	<b>-0.37</b>	
Bluegreen	<b>-0.50</b>		-0.33	
Dinoflagellate			-0.28	
Green flagellate	0.40			
Misc flagellate	0.45		<b>-0.46</b>	

significance is at the .01 (bold type) or .05 (regular type) level

Table 4  
CORRELATIONS BETWEEN  
PRINCIPAL COMPONENT AXES SCORES AND  
PHYTOPLANKTON SPECIES BIOVOLUME

n=60

Biovolume	Species	Principal Component Axes		
		Axis 1	Axis 2	Axis 3
Diatom - centric	<i>Aulacoseira granulata</i>	<b>0.48</b>		
	<i>Skeletonema costatum</i>	<b>0.37</b>	<b>-0.34</b>	0.32
	<i>Skeletonema potamos</i>	0.31		<b>-0.36</b>
Diatom - pennate	<i>Thalassiosira</i> spp.			
	<i>Cyclotella</i> spp.	<b>-0.54</b>	-0.27	
	<i>Stephanodiscus</i> spp.	<b>-0.64</b>	-0.32	
	<i>Asterionella formosa</i>	<b>-0.66</b>		
	<i>Nitzschia</i> spp.	<b>-0.79</b>	-0.33	
	<i>Achnanthes</i> spp.	<b>-0.64</b>	0.27	
	<i>Gomponema</i> spp.	<b>-0.45</b>		
	<i>Tabellaria fenestra</i>			-0.29
	<i>Cymbella</i> spp.	<b>-0.63</b>		
	<i>Rhoicosphenia</i> spp.	<b>-0.66</b>		
Green	<i>Fragilaria</i> spp.	<b>-0.43</b>		
	<i>Carteria</i> spp.	0.29		-0.35
	<i>Chlamydomonas</i> spp.	<b>-0.80</b>	<b>-0.34</b>	
	<i>Pediastrum</i> spp.	<b>-0.44</b>		
Chrysophyte	<i>Chroomonas</i> spp.			
Cryptophyte	<i>Rhodomonas lacustrus</i>	<b>-0.66</b>		
Bluegreen	<i>Anacystis</i> spp.	<b>-0.70</b>		
	<i>Anabaena</i> spp.		<b>-0.34</b>	
Dinoflagellate	<i>Gymnodinium</i> spp.			
Green flagellate	<i>Euglena</i> spp.			0.28
	<i>Phacus</i> spp.			<b>-0.46</b>
Misc flagellate		<b>0.53</b>		
		0.45		

Significance is at the <0.01 level (bold type) or <0.05 level (regular type).

---

## Discussion

---

Climate-related changes in environmental conditions were significantly correlated with long-term changes in phytoplankton density, biovolume, and chlorophyll *a* concentration among water-year types. These findings support previous studies that demonstrated that interannual changes in phytoplankton community composition and chlorophyll *a* concentration since 1976 were correlated with or coincided with changes in environmental factors influenced by climate (Lehman and Smith 1991; Lehman 1992). The current study suggests this interannual variability is strongly linked to dry and critical water-year types after 1976. Climate has a major effect on precipitation and streamflow in California (Cayan and Peterson 1989). Many of the climate effects on phytoplankton are probably a function of streamflow, which affects nutrient concentrations, salinity, turbidity, and residence time in San Francisco Bay (Conomos 1979; Cloern *et al* 1983; Peterson *et al* 1986, 1989).

Mechanisms by which dry climatic conditions may have influenced the loss of diatoms and shift in the centric/pennate ratio are suggested by phytoplankton physiology and ecology. Diatoms are generally more abundant during the spring, when water temperature is cool and wind and turbidity are high, and decrease in the summer, when conditions are dry, like the climatic conditions after 1976. In the delta, however, some chain-forming centric diatoms — *Skeletonema potamos*, *Aulacoseira granulata*, and *Thalassiosira spp.* — bloom in the lower San Joaquin River during the summer, when water temperature and salinity are high. These centric diatoms contrast with pennate diatoms, which often characterize cold freshwater habitats (Kingston *et al* 1983), and may partly explain the larger negative correlation between dry conditions and pennate diatoms than centric diatoms. Single-celled diatoms in the upper estuary are also large cells (Lehman 1996a) with rapid settling rates (Ball 1981) that rely on vertical mixing to maintain position in the euphotic zone. During dry conditions, high residence times promote the settling of diatoms to the bottom, where they also become susceptible to grazing by benthos (Nichols 1985). The stable water column in the summer, however, may also promote blooms of chain-forming diatoms, which have increased buoyancy because of their large surface area. Some diatoms may also respond negatively to the increased water transparency during very dry conditions, because they usually occur in turbid environments where high accessory pigment content provides a competitive advantage. Lastly, reduced nutrient loading during dry conditions affects nutrient ratios, which affect diatom abundance and community composition, even when nutrients are in excess (Sommer 1994; Kilham *et al* 1996).

The potential for climate to influence diatom density and biomass is an important factor for the estuarine food web. Large single-celled diatoms have a high cellular carbon content (Lehman 1996a) and are a common

food of large zooplankton, like *Neomysis mercedis* (Kost and Knight 1975). In fact, adult zooplankton select for large cells. Adult zooplankton grazing and ingestion are higher when phytoplankton cell diameter is larger than 8 to 11  $\mu\text{m}$  (Paffenhoffer and Knowles 1978; Peterson *et al* 1991; Kiorboe *et al* 1990) and is a function of the linear size ratio between predator and prey (Hansen *et al* 1994). Absence of large-diameter cells can lead to intra- and inter-species competition for food quantity (Paffenhoffer 1971; Paffenhoffer and Knowles 1978) and quality (Peterson *et al* 1991). The importance of the greater loss of pennate than centric diatoms to the food web is unclear, because the utility of chain-forming centric diatoms as food varies (Paffenhoffer 1971; Gliwicz 1980). Most of the blooms in the delta are long-chain-forming centric diatoms, including *Aulacoseira granulata*, but grazing is low when chains are long (Fulton 1988).

## Literature

---

- Cayan, D.R., and D.H. Peterson. 1989. The influence of North Pacific atmospheric circulation on streamflow in the west. Pages 375-397 In D. H. Peterson, ed., *Aspects of Climate Variability in the Pacific and Western Americas*. Geophys. Monogr. 55. Amer. Geophys. Union, Washington, DC.
- Cloern, J.E., A.E. Alpine, B.E. Cole, R.L. J. Wong, J.F. Arthur, and M.D. Ball. 1983. River discharge controls phytoplankton dynamics in Northern San Francisco Bay estuary. *Est. Coast Shelf Sci.* 12:415-429.
- Conomos, J.T. 1979. Properties and circulation of San Francisco Bay waters. Pages 47-84 in *San Francisco Bay: The Urbanized Estuary*. T.J. Conomos, ed. Pac. Div. Amer. Assoc. Adv. Sci., San Francisco.
- Fulton, R.S. III. 1988. Grazing on filamentous algae by herbivorous zooplankton. *Freshwater Biology* 20:263-271.
- Gliwicz, Z.M. 1980. Filtering rates, food size selection, and feeding rates in cladocerans—Another aspect of interspecific competition in filter-feeding zooplankton. Pages 283-291 in *Evolution and Ecology of Zooplankton Communities*. W.C. Kerfoot, ed. Univ. Press of New England. London.
- Hansen, B., P.K. Bjornsen, P.J. Hansen. 1994. The size ratio between planktonic predators and their prey. *Limnol. Oceanogr.* 39:395-403.
- Jassby, A.D. And T.M. Powell. 1994. Hydrodynamic influences on interannual chlorophyll variability in an estuary: Upper San Francisco Bay-Delta (California, U.S.A.). *Est. Coast Shelf Sci.* 39:595-618.
- Kilham, S.S., E.C. Theriot, and S.C. Fritz. 1996. Linking planktonic diatoms and climate change in the large lakes of the Yellowstone ecosystem using resource theory. *Limnol. Oceanogr.* 41:1052-1062.
- Kingston, J.C., R.L. Lowe, E.F. Stoermer, and T.B. Ladewski. 1983. Spatial and temporal distribution of benthic diatoms in northern Lake Michigan. *Ecology* 64:1566-1580.
- Kiorboe, T., H. Kaas, B. Kruse, F. Mohlenberg, P. Tiselius, and G. Aertebjerg. 1990. The structure of the pelagic food web in relation to water column structure in the Skagerrak. *Mar. Ecol. Prog. Ser.* 59:19-32.
- Kost, A.L.B., and A.W. Knight. 1975. The food of *Neomysis mercedis* in the Sacramento-San Joaquin Estuary. *Cal. Fish Game* 61:35-46.
- Lehman, P.W. 1992. Environmental factors associated with long-term changes in chlorophyll concentration in the Sacramento-San Joaquin Delta and Suisun Bay, California. *Estuaries* 15:335-348.

- Lehman, P.W. 1996a. Changes in chlorophyll *a* concentration and phytoplankton community composition with water-year type in the upper San Francisco Bay estuary. Pages 351-374 in *San Francisco Bay: The Ecosystem*. J.T. Hollibaugh, ed. Pac. Div. Amer. Assoc. Adv. Sci. , San Francisco.
- Lehman, P.W. 1996b. *Water Quality Conditions in the Sacramento-San Joaquin Delta, 1970-1993*. Department of Water Resources, Environmental Services Office, Sacramento. 102 pp.
- Lehman, P.W., and R.W. Smith. 1991. Environmental factors associated with phytoplankton succession for the Sacramento-San Joaquin Delta and Suisun Bay Estuary, California. *Est. Coast Shelf Sci.* 32:105-128.
- Nichols, F.J. 1985. Increased benthic grazing: An alternative explanation for low phytoplankton biomass in northern San Francisco Bay during the 1976-1977 drought. *Est. Coast Shelf Sci.* 21:379-388.
- Paffenhofer, G. 1971. Grazing and ingestion rates of nauplii, copepodids and adults of the marine planktonic copepod *Calanus helgolandicus*. *Mar. Biol.* 11:286-298.
- Paffenhofer, G., and S.C. Knowles. 1978. Feeding of marine planktonic copepods on mixed phytoplankton. *Mar. Biol.* 48: 143-152.
- Peterson, D.H., D.R. Cayan, and J.F. Festa. 1986. Interannual variability in biogeochemistry of partially mixed estuaries: Dissolved silicate cycles in northern San Francisco Bay. Pages 123-138 in *Estuarine Variability*. D.A. Wolfe, editor. Academic Press, New York.
- Peterson, D.H., D.R. Cayan, J.F. Festa, F.H. Nichols, R.A. Walters, J.V. Slack, S.E. Hager, and L.E. Schemel. 1989. Climate variability in an estuary: effects of river flow on San Francisco Bay. Pages 419-442 in *Aspects of Climate Variability in the Pacific and Western Americas*. D.H. Peterson, ed. Geophys. Monogr. 55. Amer. Geophys. Union, Washington, DC.
- Peterson, W.T., P. Tiselius, and T. Kiorboe. 1991. Copepod egg production, molting and growth rates, and secondary production in the skagerrak in August 1988. *J. Plank. Res.* 13:131-154.
- Sommer, U. 1994. The impact of light intensity and daylength on silicate and nitrate competition among marine phytoplankton. *Limnol. Oceanogr.* 39:1680-1688.
- Strathmann, R.R. 1967. Estimating the organic carbon content of phytoplankton from cell volume or plasma volume. *Limnol. Oceanogr.* 12:411-418.

# Potential Solar Radiation at H.J. Andrews Experimental Forest, Oregon

David Greenland

**ABSTRACT:** Potential (clear-sky) radiation receipt is modeled for the slopes of the H.J. Andrews Experimental Forest Long-Term Ecological Research site in the foothills of the southern Cascade mountains of central Oregon. The modeling method developed by Williams is selected and applied to the forest area for the times of the solstices and equinox as well as mid-month times in January, February, April, and May in order to completely characterize the seasonal change of potential radiation at the location. The method uses an 82×111 point grid with a 120-meter spacing interval. Resulting maps reveal areas of the forest with extremely steep gradients of potential radiation. These steep gradients have higher absolute values in summer compared to winter. The south-facing slopes that have the highest potential radiation values tend to be at the highest elevations. There are places that receive no direct radiation as far into the year as February. Standard deviation values of potential radiation across the Andrews show the maximum spatial variability to occur in February. There is a decrease in the ratio of diffuse to direct plus diffuse potential radiation from 0.66 at December 21 to 0.23 at June 21. It seems that Lookout Creek approximately divides the Andrews Forest into an area of relatively high potential radiation to the north of the creek and relatively lower potential radiation values to the south of the creek. Potential radiation values seem to be associated with the Andrews GIS data layers of debris flows and predominant tree species zones.

## The Andrews Forest

H.J. Andrews Experimental Forest is a 6400-hectare forest of Douglas fir (*Pseudotsuga menziesii* (Mirb.) Franco), western hemlock (*Tsuga heterophylla* (Raf.) Sarg.), and Pacific silver fir (*Abies amabilis* Doug. ex Forbes) located in, and typical of, the central portion of the western slope of the Cascade mountain range of Oregon (Figure 1). The forest has a complex topography (Figure 2) and ranges in elevation from 410 to 1630 meters (1350 to 5340 feet). The research site is one of 18 sites in the Long-Term Ecological Research program currently sponsored by the National Science Foundation.

## Objective

The purpose of this study is to produce maps of seasonal potential insolation (*ie*, solar radiation receipt under clear sky conditions) for H.J. Andrews Experimental Forest. These maps will have value for:

- Making future estimates of heat energy input to the various slopes of the forest.
- Establishing relationships between solar input and net primary productivity.

In: C.M. Isaacs and V.L. Tharp, Editors. 1997. *Proceedings of the Thirteenth Annual Pacific Climate (PACLIM) Workshop, April 15-18, 1996*. Interagency Ecological Program, Technical Report 53. California Department of Water Resources.

- Identifying areas of greatest potential heat input — a process that has implication for driving mesoscale wind circulations in the area, and possibly also for establishing areas of potential forest fire initiation danger.

## The Williams Model

The Williams *et al* (1972) model, selected for this study, is based on work by Garnier and Ohmura (1968) who estimated potential global solar radiation ( $K\downarrow$ ) on slopes by:

$$K\downarrow = S_x p^m \cos(i) + D_h \cos^2(s/2) + \alpha (S_h + D_h) \sin^2(s/2) \quad (1)$$

where:  $S_x$  is incoming shortwave radiation at the top of the atmosphere; *ie*, extraterrestrial radiation  
 $p$  is the mean zenith angle path transmissivity  
 $m$  is the optical depth  
 $D_h$  is the diffuse radiation on a horizontal surface  
 $\alpha$  is the albedo of the surface  
 $S_h$  is the direct radiation on a horizontal surface

The first and second terms represent  $S$  (direct radiation) and  $D$  (diffuse radiation), respectively, and the third term represents  $D_{tr}$  (terrain reflected radiation). Garnier and Ohmura suggested using actual site measurements to determine the value of  $p$  at the site and that  $p$  should be approximated by  $\sec Z_s$  (zenith angle). This suggestion was followed in this study. The second and third terms assume an isotropic distribution of  $D$ . The third term was not used in practice or in this study.

$\cos(i)$  is given by:

$$i = \cos^{-1} \{ \cos(s) \cos(Z_s) + \sin(s) \sin(Z_s) \cos(A_z + A_s) \} \quad (2)$$

where:  $s$  is the slope of the surface  
 $A_z$  is the solar azimuth  
 $A_s$  is the slope azimuth (aspect)

Williams *et al* (1972) provide estimates of  $K\downarrow$  for complex terrain that treat the terrain as a matrix of elevation points and allow for the shading of an individual point, where appropriate, by those points surrounding it. Their estimate of  $D$  is given by:

$$D = (I_o / d^2) (0.91 - p^m) \cos(Z_s) \cos^2(s/2) \quad (3)$$

The 0.91 represents the proportion of radiation that has not been absorbed by atmospheric constituents. This model corrects the value of  $m$  for the elevation of the observation point. Daily total values are produced using integration of 20-minute values of  $Z_s$  and a grid of 82×111 points over the Andrews area with a 120-meter grid spacing.

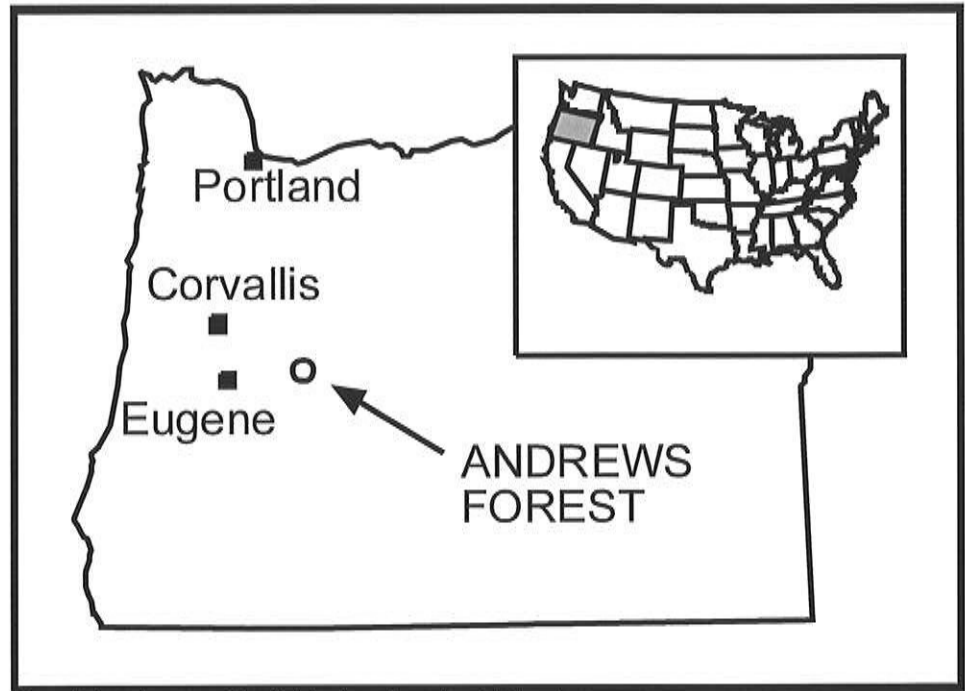


Figure 1. Location map of the H.J. Andrews Experimental Forest.

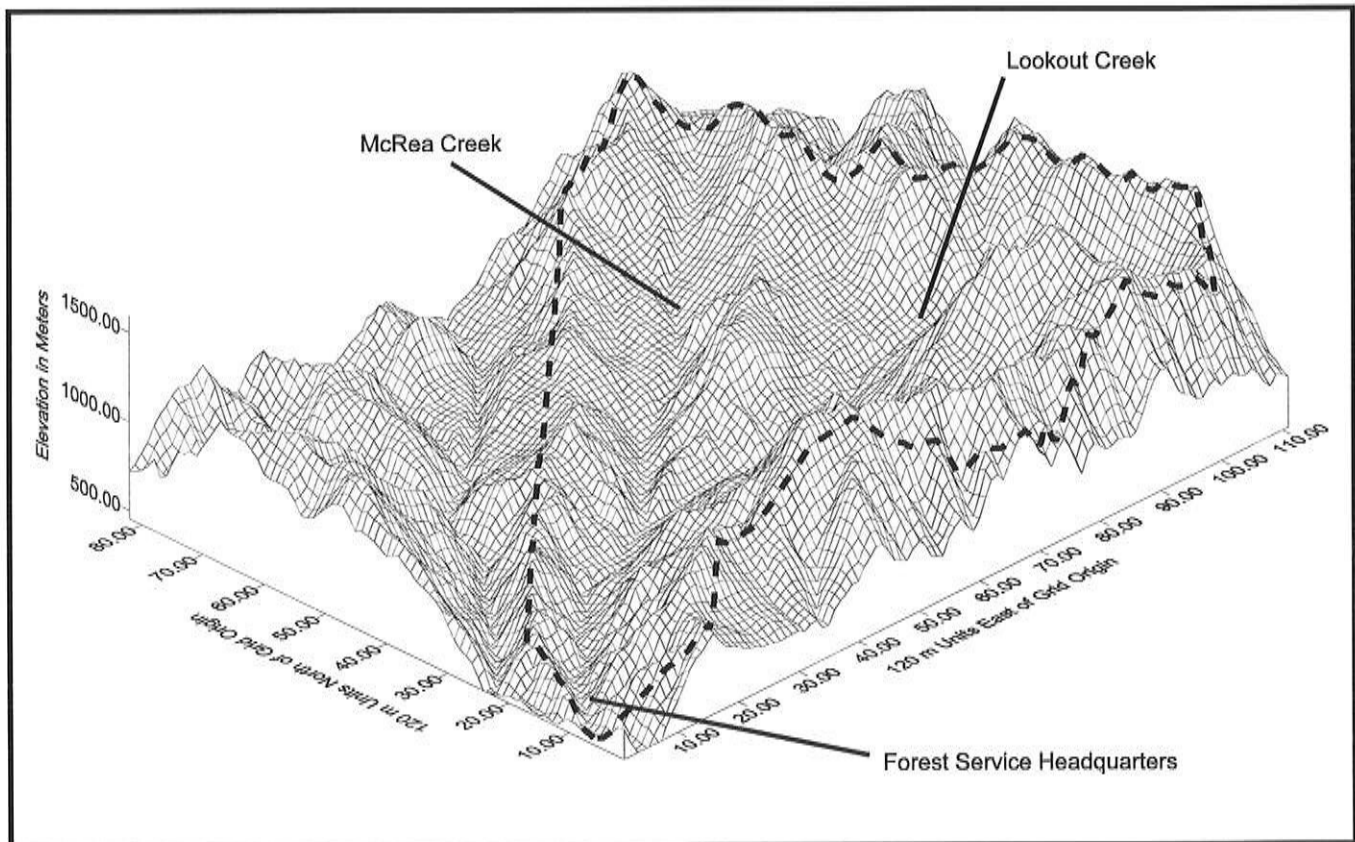


Figure 2. Three dimensional topographical map of the Andrews Forest.

## Results

Provided here is a contour map of the Andrews topography (Figure 3) and an example of the potential direct and diffuse radiation values for April 15 (Figure 4). The latter figure may not reproduce well, and interested persons should contact the author if they require further details. Complete results and maps are documented in Greenland (1996). Based on the complete set of maps in Greenland 1996, the principal results are as follows.

Potential direct and diffuse radiation received at the Andrews Forest is spatially and temporally highly variable.

Results we might expect include the higher values of potential radiation in summer than in winter and on south-facing compared to north-facing slopes and the greater relative importance of diffuse, compared to direct, radiation in the winter months.

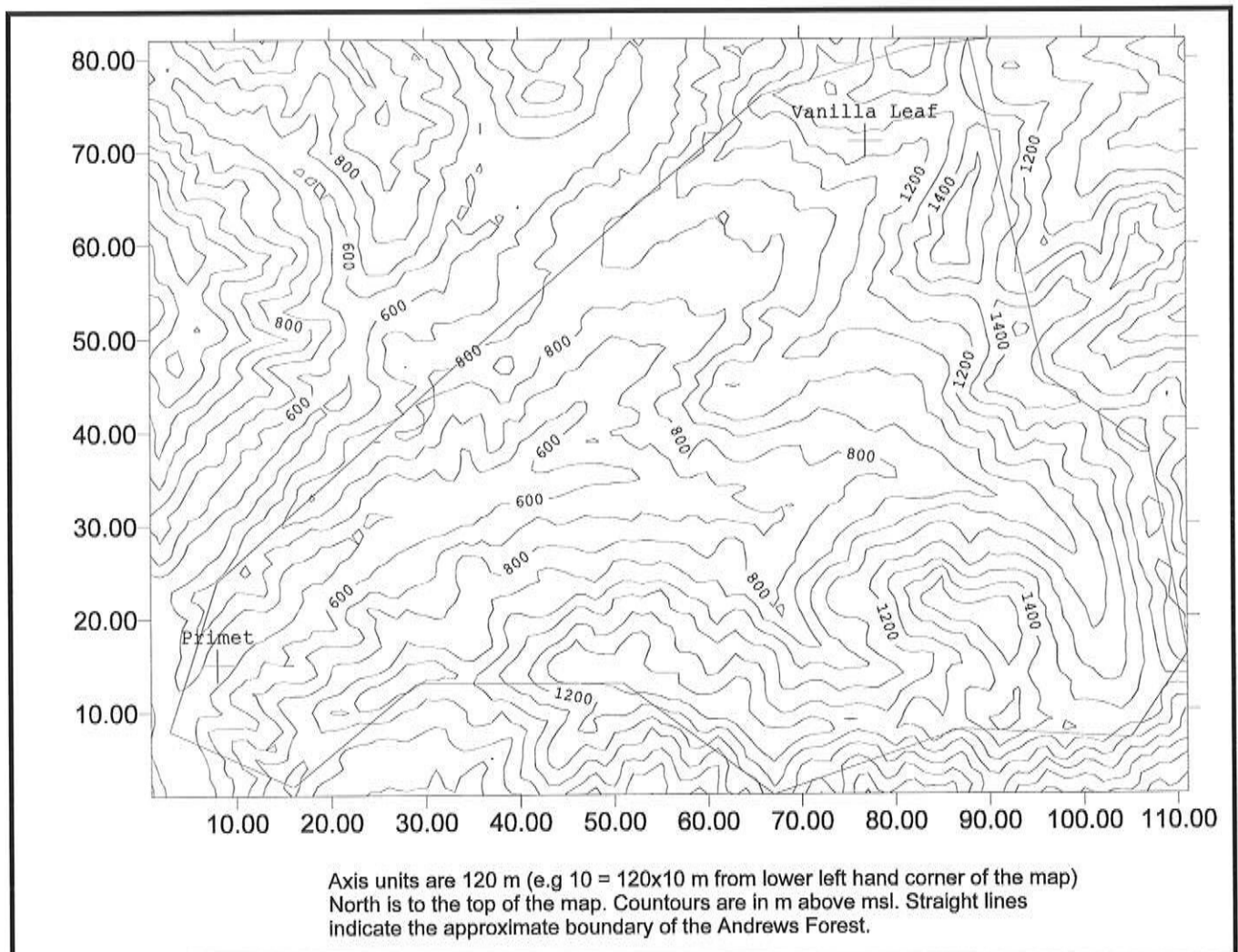


Figure 3. Contour topographical map of the Andrews Forest.

More surprising results include the identification of areas of steep potential radiation gradients and the greater receipt of potential radiation at the higher elevations than the lower ones. It could also be argued that Lookout Creek approximately divides Andrews Forest into an area of relatively high potential radiation to the north of the creek (with the exception of the north-facing slopes of McRea Creek Valley) and relatively lower potential radiation values to the south of the creek. This pattern holds throughout the change of seasons.

Counter-intuitive results also include the fact that the greatest amount of spatial variability of potential radiation occurs in late winter and early spring.

Potential radiation values seem to be associated with the spatial distributions shown on the Andrews GIS data layers of debris flows (flows are absent in low potential radiation value areas) and predominant tree species zones. In the latter case, one of the Andrews GIS layers shows the distribution of predominant tree zones (*ie*, areas dominated by one or more species). This

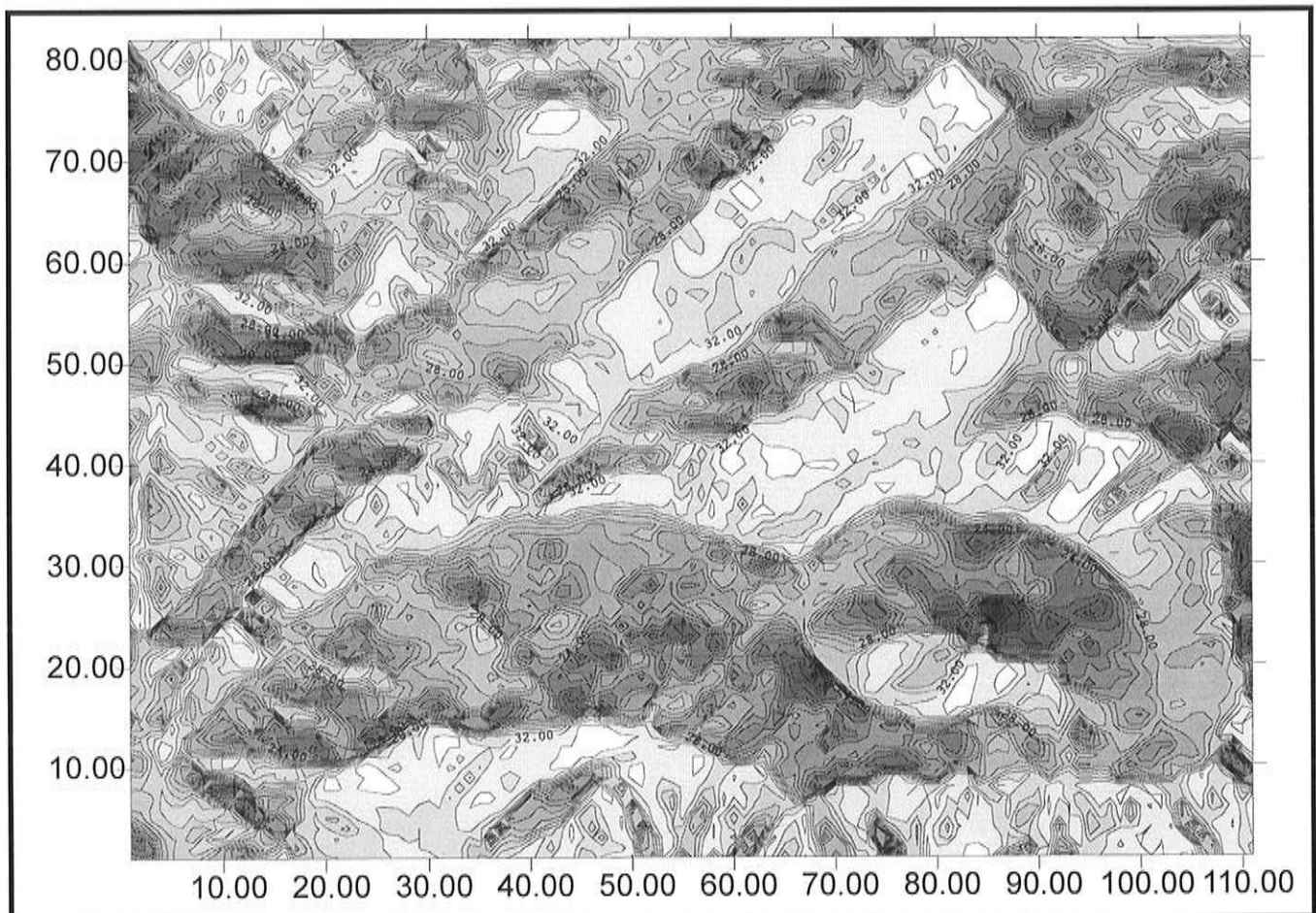


Figure 4. Potential (cloud-free) direct and diffuse radiation arriving on the slopes of the Andrews Forest on April 15.

Axis units are 120m (eg 10=120x10m from lower lefthand corner of map).  
North is to the top of the map. Isolines are in MJ/sq.m/day. Isoline interval is 1 MJ/sq.m/day.  
Highest and lowest isoline values are 33 and 13 MJ/sq.m/day, respectively.  
Lighter shading indicates more potential solar radiation.

GIS layer indicates that Pacific silver fir is mainly distributed at higher elevations. The current study demonstrates that within these higher elevations, Pacific silver fir occurs in areas of less than highest maximum possible potential solar radiation. There may also be relationships acting in concert with other processes and the distributions of other variables such as precipitation (precipitation is highest and potential radiation is low south of Lookout Creek. Forest fire frequency is least in this location).

## **Future Work**

---

This study in many ways represents a beginning. Solar radiation is itself the beginning of a cascade of energy flow through the atmospheric system and the ecosystem. Future work should continue to follow the cascade to successive levels. Specifically the following steps will be of value.

- Spatial analysis of the data will be continued by using geostatistical techniques. In particular, a semivariogram analysis will not only give greater information on the key spatial scales on which potential radiation varies.
- It is important to establish the effects of clouds and aerosols in attenuating the amount of potential radiation to determine finally how much radiation arrives at the surface.
- Values of absorbed radiation will be estimated and will likely be related even more closely to other biophysical variables of the forest.
- Establishment of potential global solar radiation ( $K\downarrow$ ) and albedo values will aid in establishment of other variables of the radiation and surface energy balance. These variables include incoming and outgoing longwave radiation, substrate heat flow, and sensible and latent heat flow. These are the fundamental components of the physical climate and are the important linking factors to the ecosystem. Saunders and Bailey (1994) noted that "the energy budgets of sloping surfaces remain a largely untouched research problem, and nowhere is this more important than in mountainous regions".
- The processes modeled in the above items must be integrated with key variables available from remote sensing technology. When this has been done, a powerful set of tools will be available to provide researchers with important bioclimatic information that can be used at a number of different scales.

## Acknowledgments

---

This study has been greatly benefited by the help and encouragement of Dr. Fred Swanson. Funding was provided in part by the USDA Forest Service, Pacific Northwest Research Station, Cooperative Agreement PNW 93-0477. Datasets for H.J. Andrews Forest were provided by the Forest Science Data Bank, a partnership between the Department of Forest Science, Oregon State University, and the U.S. Forest Service Pacific Northwest Research Station, Corvallis, Oregon. Funding for these data was provided by the Long-Term Ecological Research Program and other National Science Foundation programs, Oregon State University, and U.S. Forest Service Pacific Northwest Research Station. NSF grants: DEB-7611978, BSR-9011663.

## References

---

- Garnier, B.J., and A. Ohmura. 1968. A method of calculating direct solar radiation on slopes. *Journal of Applied Meteorology*, 7:796-800.
- Greenland, D. 1996. *Potential solar radiation at the H.J. Andrews Experimental Forest*. Interim Report on research performed under USDA Forest Service, Pacific Northwest Research Station. Cooperative Agreement PNW 93-0477. 35 pp. + Appendices.
- Saunders, I.R., and W.G. Bailey. 1994. Radiation and energy budgets of alpine tundra environments in North America. *Progress in Physical Geography*, 18(4):517- 538.
- Williams, L.D., R.D. Barry, and J.T. Andrews. 1972. Application of computed global radiation for areas of high relief. *Journal of Applied Meteorology*, 11:526-533.



# Quantifying Global Terrestrial Carbon Influx and Storage as Stimulated by an Increase in Atmospheric CO<sub>2</sub> Concentration

Yiqi Luo

**Abstract:** Measurements of spatial and temporal distributions of CO<sub>2</sub> concentration ( $C_a$ ) and  $^{13}\text{C}/^{12}\text{C}$  ratio in the atmosphere suggest a strong biospheric carbon sink in terrestrial ecosystems. Quantifying the sink, however, has become an enormous challenge for Earth system scientists because of great uncertainties associated with biological variation and environmental heterogeneity in the ecosystems. This paper presents an approach that uses two driving parameters to bound terrestrial carbon sequestration associated with an increase in  $C_a$ . The first parameter is a leaf-level function ( $\mathcal{L}$ ), the normalized photosynthetic response to a small change in  $C_a$ , which has been found to be: (1) insensitive to light, nutrient environment, and species characteristics; (2) slightly influenced by measurement temperature, and (3) a function of  $C_a$ . Since  $\mathcal{L}$  is approximately constant at a given  $C_a$ , it can cut across spatial heterogeneity of biotic and abiotic variables to quantify the  $C_a$ -induced increment of global photosynthetic carbon influx ( $P_G$ ). The second parameter is the global mean residence time ( $\tau_G$ ) of photosynthetically fixed carbon, which is used to project global respiration ( $R_G$ ), that is the return of carbon to the atmosphere through biology, from  $P_G$ . A model linking the two parameters provides a preliminary estimate that global terrestrial carbon sink approximates  $5.0 \text{ GtC yr}^{-1}$  in year 2000.

## Introduction

Modeling studies of global carbon cycling have long suggested that the global carbon budget cannot be balanced without storage of carbon in terrestrial ecosystems (Bacastow and Keeling 1973). Recently, evidence has been presented to support the idea that terrestrial ecosystems play a critical role in modulating the carbon balance of the Earth system. For example, Tans *et al* (1990) analyzed spatial and temporal distributions of atmospheric CO<sub>2</sub> concentration ( $C_a$ ) and concluded that a large amount of carbon is absorbed by terrestrial ecosystems. Other research has found that temporal variations and latitudinal gradients of  $^{13}\text{C}/^{12}\text{C}$  ratios in the atmosphere result, at least partly, from carbon isotope discrimination in plants, again indicating a possibility of terrestrial ecosystems to sequester carbon (Ciais *et al* 1995; Francey *et al* 1995; Keeling *et al* 1995, 1996; Tans *et al* 1993).

Quantifying terrestrial carbon sequestration has been exceedingly difficult with either experimental or modeling approaches for two reasons. First, this quantification demands tremendously high precision. The annual terrestrial carbon sink, which has been suggested to be 1-2 GtC (1 Gt =  $10^{15}$  g)  $\text{yr}^{-1}$  (Sarmiento *et al* 1995), is about 2-4% of net primary production, 1-2% of gross primary production, and 0.1% of global terrestrial

carbon content. Conventional research approaches, including both field experiments and simulation models, cannot detect such a small change. Second, uncertainties in ecological predictions are rooted in two general sources: interspecific variation and environmental heterogeneity. Although dividing geographical maps of world vegetation and soils into grids with relatively uniform environmental conditions and species composition helps reduce spatial variability, difficulties in model parameterization and vegetation delineation make such quantification still unsatisfactory (Schimel 1995). Therefore, new approaches with improved precision and reduced uncertainties are urgently needed to address the issue of the terrestrial carbon sink.

This paper presents a new approach that uses two parameters to bound potential terrestrial carbon influx and sink. The first parameter is a leaf-level function ( $\mathcal{L}$ ) found to be independent of species characteristics and environmental factors of light, nutrients, and water (Luo and Mooney 1995, 1996). As a result,  $\mathcal{L}$  is invariant for  $C_3$  plants<sup>1</sup> in the Earth system (Luo *et al* 1996). The function, thus, enables us to cut across environmental heterogeneity and species variation to quantify an increment of global photosynthetic carbon influx ( $P_G$ ; *ie*, gross primary productivity) stimulated by a small increase in atmospheric  $CO_2$  concentration ( $C_a$ ). The increment is estimated to be 0.21-0.45 GtC in 1993 compared to that in 1992 (assuming  $P_G = 120$  GtC yr<sup>-1</sup>) due to a 1.5-ppm  $C_a$  increase. The second parameter is the global mean residence time of carbon ( $\tau_G$ ) in terrestrial ecosystems as a parameter to project global respiration ( $R_G$ ) from  $P_G$ . Differential increases of  $P_G$  and  $R_G$  with rising  $C_a$ , caused by a delay between fixation and release, has been suggested as a major mechanism of net carbon storage in global terrestrial ecosystems. Thus, the two parameters,  $\mathcal{L}$  and  $\tau_G$ , can be used to bound global terrestrial carbon sequestration associated with an increase in  $C_a$ .

## **The $\mathcal{L}$ Function and Global Photosynthetic Carbon Influx**

Photosynthesis is almost the exclusive pathway through which carbon flows from the atmosphere to terrestrial ecosystems (Mooney *et al* 1987) and one of the primary processes, in the whole ecosystem, directly responsive to an increase in  $C_a$ . Understanding photosynthesis is, thus, essential when considering global carbon influx into terrestrial ecosystems. Here I go through details of the environmental biology of leaf photosynthesis to illustrate that the  $\mathcal{L}$  function is an approximate constant at any given  $C_a$  and enables us to cut across spatial heterogeneity to quantify the  $C_a$ -stimulated increment of  $P_G$ . I also present equations that are essential to demonstrate the mathematical logic

1 Plants in which the first product of photosynthesis after carbon dioxide fixation is phosphoglycemic acid, which contains three carbon atoms.

behind the property of the  $\mathcal{L}$  function being invariant. In addition, I discuss assumptions and limitations of the  $\mathcal{L}$  function in studying global carbon cycling.

### **Derivation of the $\mathcal{L}$ Function and Its Properties**

Luo and Mooney (1996) derived the  $\mathcal{L}$  function from the well-established Farquhar, von Caemmerer, and Berry (1980) photosynthesis model. Leaf photosynthesis of C<sub>3</sub> plants is usually limited either by ribulose-1,5-bisphosphate (RuBP) regeneration or by ribulose-1,5-bisphosphate carboxylase/oxygenase (Rubisco) activity and described by two equations as:

$$\begin{aligned} P_1 &= J \frac{C_i - \Gamma}{4.5C_i + 10.5\Gamma} \\ P_2 &= V_{\text{cmax}} \frac{C_i - \Gamma}{C_i + K} \end{aligned} \quad (1)$$

where  $J$  is the electron transport rate ( $\mu\text{mol m}^{-2} \text{s}^{-1}$ ), representing light effects on photosynthesis;  $V_{\text{cmax}}$  is the maximum carboxylation rate ( $\mu\text{mol m}^{-2} \text{s}^{-1}$ ), varying with leaf enzyme content which is, in turn, regulated by both species characteristics and nutrient availability in the ecosystem;  $C_i$  is the intercellular CO<sub>2</sub> concentration (ppm) and is regulated by stomata and water status;  $\Gamma$  is the CO<sub>2</sub> compensation point (ppm) in the absence of dark respiration and is a function of temperature; and  $K$  is a coefficient (ppm) associated with enzyme kinetics and varies with temperature. Among all the parameters,  $J$  and  $V_{\text{cmax}}$  are the most variable.  $V_{\text{cmax}}$  ranges from 6 to 194  $\mu\text{mol m}^{-2} \text{s}^{-1}$  among 109 species (Wullschlegel 1993).  $J$  also varies with light, species, and nutrient availability (Field 1983; Harley *et al* 1992; Wullschlegel 1993). High variability of the two parameters makes it difficult to extrapolate leaf-level studies across scales.

To eliminate  $J$  and  $V_{\text{cmax}}$ , Luo and Mooney (1996) defined a leaf-level function ( $\mathcal{L}$ , ppm<sup>-1</sup>) as:

$$\mathcal{L} = \frac{1}{P} \frac{dP}{dC_a} \quad (2)$$

The  $\mathcal{L}$  function denotes the normalized leaf photosynthetic response to a small  $C_a$  change. With an assumption that  $C_i$  is proportional to  $C_a$  as:

$$C_i = \alpha C_a \quad 0 < \alpha < 1 \quad (3)$$

the corresponding  $\mathcal{L}$  functions derived from Equation 2 are:

$$\mathcal{L}_1 = \frac{15\alpha\Gamma}{(\alpha C_a - \Gamma)(\alpha C_a + 10.5\Gamma)} \quad (4)$$

$$\mathcal{L}_2 = \frac{\alpha(K + \Gamma)}{(\alpha C_a - \Gamma)(\alpha C_a + K)}$$

Parameters  $J$  and  $V_{\text{cmax}}$  are eliminated from these equations because  $\mathcal{L}_1$  and  $\mathcal{L}_2$  are a measure of relative responses. Consequently, environmental and biological variation associated with  $J$  and  $V_{\text{cmax}}$  are also eliminated, suggesting that the  $\mathcal{L}$  function is insensitive to light, nutrient environment, and species characteristics but a function of  $\alpha$ ,  $\Gamma$ ,  $K$ , and  $C_a$ . Sensitivity analysis suggests that variation in  $\alpha$ ,  $\Gamma$ , and  $K$  in response to normal environmental changes leads to a variation of 15% or less in predicted values of the  $\mathcal{L}$  function (Luo and Mooney 1996). The lower bound is set by  $\mathcal{L}_1$  when RuBP regeneration limits photosynthesis and the upper bound is set by  $\mathcal{L}_2$  when photosynthesis is Rubisco limited.

The invariant  $\mathcal{L}$  function may become an important scaling parameter in studying global carbon cycling but is subject to experimental tests. Luo *et al* (1996) tested the  $\mathcal{L}$  function with nine sets of experimental data that incorporated photosynthetic responses of 12 species to measurement conditions of light and temperature and to growth in different light, temperature, nitrogen, phosphorus, water stress, and  $\text{CO}_2$  concentration (Figure 1). Absolute rates of leaf photosynthesis differed by more than 10 fold due to differences in species, measurement and growth conditions. However,  $\mathcal{L}$  values derived from these datasets converged into a single narrow range defined by two equations of the  $\mathcal{L}$  function (Figure 1), confirming that  $\mathcal{L}$  was insensitive to differences in photosynthetic capacity among species and between plants acclimated to different growth environments. Differences in the relative control of RuBP regeneration and Rubisco on photosynthesis and the dependence of photosynthesis on measurement temperature may cause a 30% uncertainty in the  $\mathcal{L}$  function at current  $C_a$  (Luo *et al* 1996). In addition, experimental data with *Glycine max* indicated that variation of  $\mathcal{L}$  ( $C_i/C_a$  ratio) from 0.65 to 0.85 hardly affects  $\mathcal{L}$  (K.L. Griffin and Y. Luo, unpublished).

The property that the  $\mathcal{L}$  is an invariant function is rooted in the nature of the biochemical reactions of photosynthesis (Luo and Mooney 1996). Photosynthesis (*ie*, carboxylation of RuBP) and photorespiration (*ie*, oxygenation of RuBP) are both catalyzed by Rubisco (Andrews and Lorimer 1987). The carboxylation/oxygenation ratio is affected by

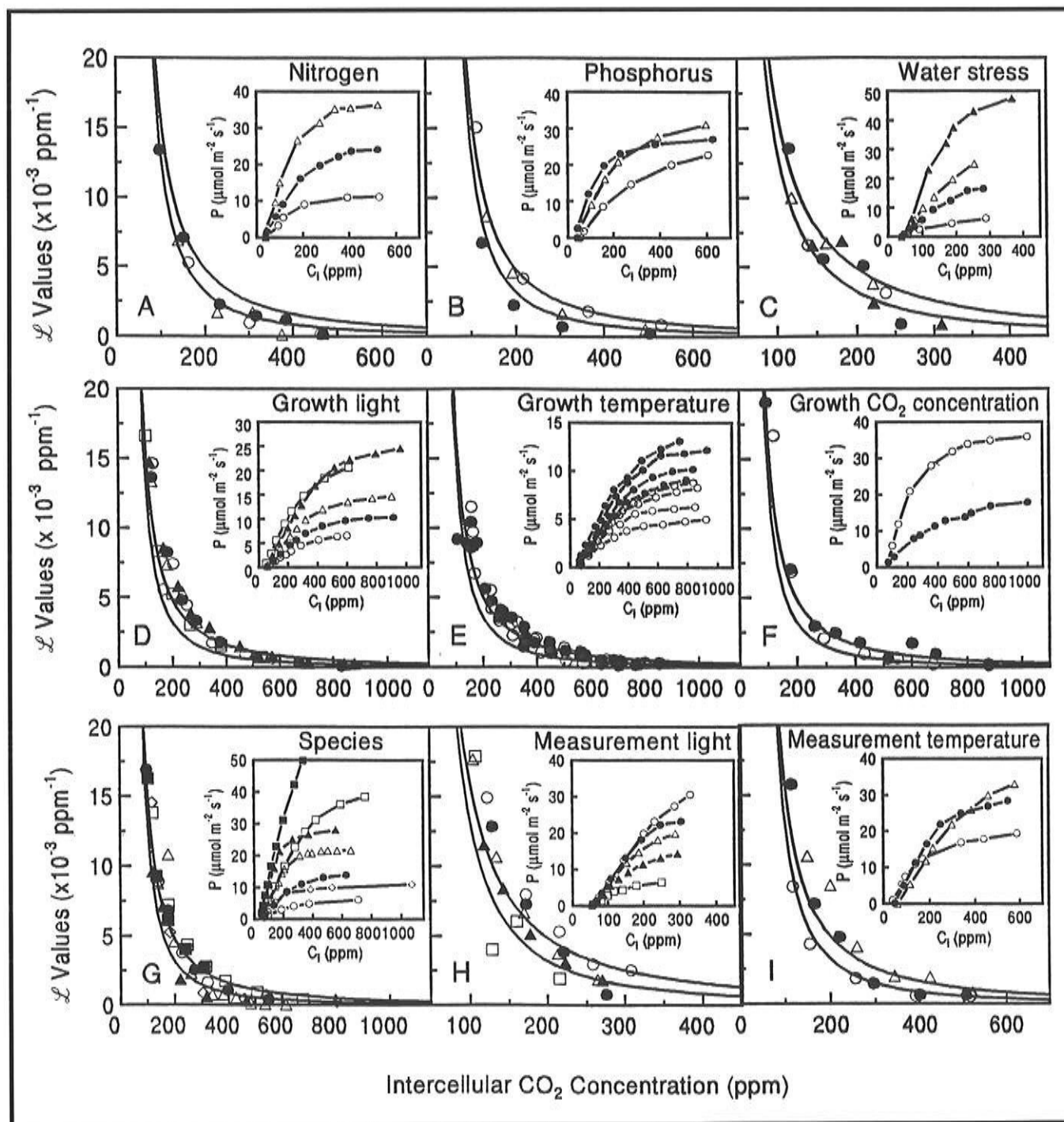


Figure 1 Photosynthetic responses to intercellular CO<sub>2</sub> concentration (inserted figures) and values of the  $\mathcal{L}$  function as affected by: (A) nitrogen for *Triticum aestivum*; (B) phosphorus for *Triticum aestivum*; (C) water stress for *Encelia frutescens*; (D) growth light for *Alocasia macrorrhiza*; (E) growth temperature for *Pinus ponderosa*, (F) growth CO<sub>2</sub> concentration for *Chenopodium album*, (G) seven species: *Castanea sativa*, *Chenopodium album*, *Colocasia esculenta*, *Picea engelmannii*, *Pinus ponderosa*, *Senecio vulgaris*, and *Triticum aestivum*; (H) measurement light for *Phaseolus vulgaris*; and (I) measurement temperature for *Eucalyptus pauciflora*. Solid lines are the predicted  $\mathcal{L}$  function with Equation 4. The lower line is  $\mathcal{L}_1$  (light limitation) and upper line is  $\mathcal{L}_2$  (enzyme limitation). (Redrawn from Luo *et al* 1996).

$\text{CO}_2/\text{O}_2$  ratio, slightly by temperature but not by species or growth conditions (Farquhar *et al* 1980). As  $C_a$  increases, the carboxylation/oxygenation ratio increases, as does the  $\text{CO}_2/\text{O}_2$  ratio.  $\mathcal{L}$  that characterizes the relationship of the carboxylation/oxygenation ratio with the  $\text{CO}_2/\text{O}_2$  ratio, therefore, is a function of  $C_a$  but not species or growth conditions (Luo and Mooney 1996). In cases where photosynthesis is limited by phosphorus (Sharkey 1985), photosynthetic sensitivity to a  $C_a$  change (*ie*,  $\mathcal{L}$ ) may be zero or negative (Luo *et al* 1996) and photosynthetic carbon influx will not be stimulated by an increase of  $C_a$ .

### **Spatial Extrapolation of the $\mathcal{L}$ Function to the Global Scale**

Direct spatial extrapolation of the  $\mathcal{L}$  function from the leaf to the global scale is possible because the  $\mathcal{L}$  function is insensitive to light, nutrient environment, and species characteristics. Ecological difficulties in studying global phenomena lie in the diversity of species characteristics and environmental heterogeneity across different spatial scales (Figure 2). When a parameter we are interested in is independent of interspecific variation and environmental heterogeneity, small-scale measurements can be directly extrapolated to the global scale. Like the atmospheric  $\text{CO}_2$  concentration, which is approximately constant across spatial scales, measurements made at Mauna Loa, Hawaii, are generally used to represent atmospheric  $\text{CO}_2$  concentration all over the Earth's surface.

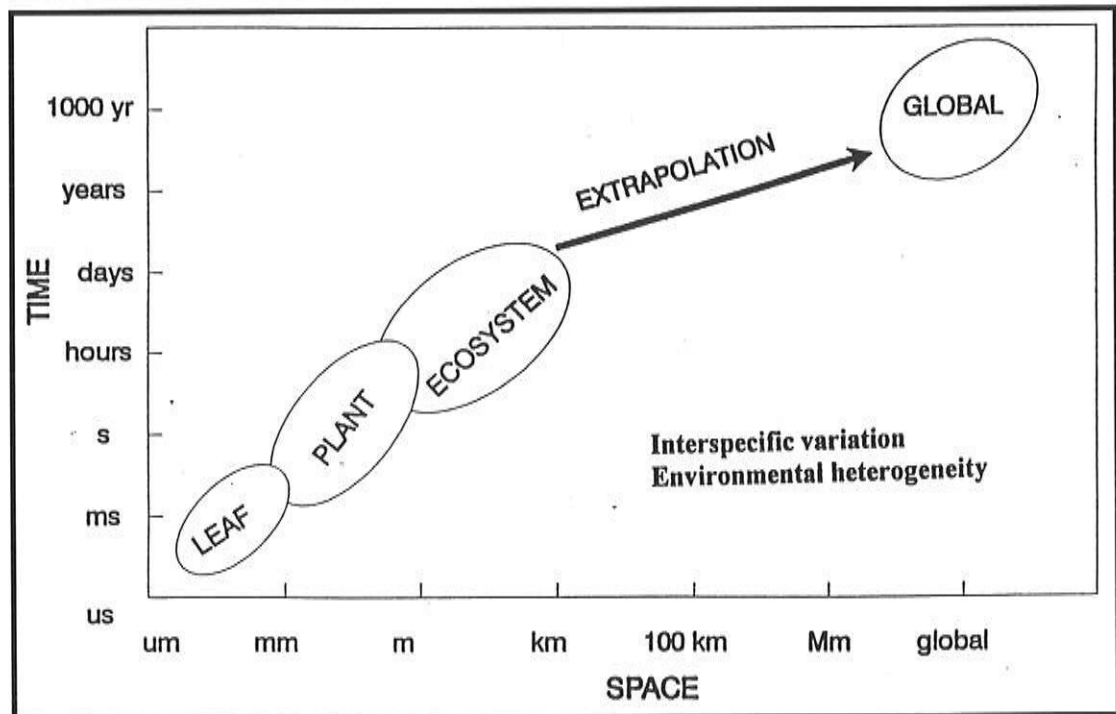


Figure 2 Illustration of major issues involved in global scaling-up studies of biospheric processes. Global change research requires us to address large-scale and long-term issues. However, we can not make any measurements at that large scales but only at leaf, plant or small ecosystem scales. When we extrapolate the small-scale measurements to predict large-scale changes, we encounter two general problems: interspecific variation and environmental heterogeneity. Any methods that can eliminate or diminish their effects on parameters in question will reduce uncertainties in predicting large-scale changes. The  $\mathcal{L}$  function is independent of the two general factors and therefore has the potential to improve precision and reduce uncertainties in predicting global terrestrial carbon sequestration.

Spatial extrapolation of the  $\mathcal{L}$  function is also supported by the mathematical logic. Annual global photosynthetic carbon influx ( $P_G$ , ie, gross primary productivity) is the sum of carbon influx from total leaf area ( $P$ ) within canopies ( $x$ ) over the global surface ( $y$ ) over the period of a year ( $t$ ). Mathematically, it can be expressed as:

$$P_G = \int_{t=\text{year}} \int_{y=\text{globe}} \int_{x=\text{canopy}} P \, dx \, dy \, dt \quad (5)$$

For one unit change in the global atmospheric CO<sub>2</sub> concentration ( $C_a$ , ppm), the rate of  $P_G$  change ( $\text{GtC ppm}^{-1} \text{yr}^{-1}$ ) is:

$$\begin{aligned} \frac{dP_G}{dC_a} &= \int \int \int \frac{dP}{dC_a} \, dx \, dy \, dt \\ &= \int \int \int (\mathcal{L}P) \, dx \, dy \, dt \end{aligned} \quad (6)$$

where  $\mathcal{L}$  is defined by Equation 2. Since  $\mathcal{L}$  is approximately constant at given  $C_a$  for  $C_3$  plants, mathematically, we can move the constant  $\mathcal{L}$  directly from the inside of the triple integrals to the outside in Equation 6. Thus, Equation 6 becomes:

$$\frac{dP_G}{dC_a} = LP_G \quad (7)$$

Equation 7 indicates that the rate of  $P_G$  change relative to  $C_a$  can be calculated simply from  $\mathcal{L}$  and  $P_G$ . It follows that the additional amount of annual photosynthetic carbon influx ( $\Delta P_G$ ,  $\text{GtC yr}^{-1}$ ), stimulated by a yearly increase in atmospheric CO<sub>2</sub> concentration ( $\Delta C_a$ ), can be estimated by:

$$\Delta P_{G,1} = \mathcal{L}_1 P_G \Delta C_a \quad (8)$$

$$\Delta P_{G,2} = \mathcal{L}_2 P_G \Delta C_a$$

where  $P_{G,1}$  and  $P_{G,2}$  are the lower and upper limits of  $\Delta P_G$ , respectively. At  $C_a=357$  ppm in 1993,  $P_G$  ranges from 0.21 to 0.45  $\text{GtC yr}^{-1}$  (Luo and Mooney 1996) with  $C_a=1.5$  ppm and  $P_G=120$   $\text{GtC yr}^{-1}$  (Olson *et al* 1983).

### Assumptions and Limitations of the $\mathcal{L}$ Function

The  $\mathcal{L}$  function can be extrapolated across spatial scales but not necessarily across temporal scales. The basic assumption of the  $\mathcal{L}$  function is that parameters  $J$  and  $V_{cmax}$  do not vary with  $C_a$ . Experimental studies indicate that growth at elevated  $CO_2$  leads to increases or decreases in photosynthetic capacity, *ie*,  $J_{max}$  (maximum  $J$ ) and  $V_{cmax}$  (Bazzaz 1990; Gunderson and Wullschleger 1994; Luo *et al* 1994; Sage 1994). Such adjustments in photosynthetic properties could be incorporated into the prediction of  $\Delta P_G$  by adjusting values of the  $\mathcal{L}$  function as:

$$\mathcal{L}'_1 = \mathcal{L}_1 + \frac{1}{J} \frac{dJ}{dC_a} \quad (9)$$

$$\mathcal{L}'_1 = \mathcal{L}_1 + \frac{1}{V_{cmax}} \frac{dV_{cmax}}{dC_a}$$

Accordingly, Equation 8 will be modified as:

$$\Delta P'_{G,1} = \Delta P_{G,1} + \Delta C_a \int_{t=year} \int_{y=globe} \int_{x=canopy} \left( \frac{P}{J} \frac{dJ}{dC_a} \right) dx dy dt \quad (10)$$

$$\Delta P'_{G,2} = \Delta P_{G,2} + \Delta C_a \int_{t=time} \int_{y=globe} \int_{x=canopy} \left( \frac{P}{V_{cmax}} \frac{dV_{cmax}}{dC_a} \right) dx dy dt$$

Equation 10 embraces concepts of photosynthetic adjustments across various scales from leaf, canopy to vegetation redistribution and growing season shifting. The terms  $(P/J)(dJ/dC_a)$  and  $(P/V_{cmax})(dV_{cmax}/dC_a)$  represent adjustments in leaf photosynthetic parameters  $J$  and  $V_{cmax}$ . The term encompassed by the most inner integral describes adjustments in canopy photosynthetic properties including changes in leaf area index and leaf properties. The term encompassed by the middle integral describes adjustments in spatial distribution of photosynthetic properties, including redistribution of vegetation and changes in leaf and canopy photosynthetic properties. The term encompassed by the outside integral describes adjustments in photosynthetically active seasons. Although Equation 10 provides a conceptual framework for studying photosynthetic acclimation, quantifying adjustments at these temporal and spatial scales requires comprehensive experimental and modeling studies (*eg*, VEMAP members 1995).

Here I provide an example on the potential impact of leaf-level acclimation on global photosynthetic carbon influx. We consider a 10% drop in globally averaged  $J$  and  $V_{\text{cmax}}$ , spreading linearly over time as CO<sub>2</sub> doubles from 350 to 700 ppm. We also assume  $P_G=120 \text{ GtC yr}^{-1}$  at 350 ppm and a 1.5 ppm increase in  $C_a$  per year. Then,  $\Delta P_G'$  would be 0.03% lower than  $\Delta P_G$  each year. Luo and Mooney (1995) have recently compiled published data and found that  $J_{\text{max}}$  and  $V_{\text{cmax}}$  decreased by 1.7% for all 33 species, by 4.1% for a subgroup of 11 crop species, and by 1.1% for a subgroup of 22 wild species with an experimentally doubled CO<sub>2</sub> concentration. Although this dataset does not represent globally averaged  $J$  and  $V_{\text{cmax}}$ , it does illustrate that Equation 10 can be used to incorporate plant- or ecosystem-level adjustments into predictions of global carbon influx.

Global photosynthetic carbon influx estimated by Equation 8 may be lowered by the presence of C<sub>4</sub> plants<sup>2</sup>, whose photosynthesis is less sensitive to a  $C_a$  change than that of C<sub>3</sub> species, and some C<sub>3</sub> plants whose photosynthesis is limited by phosphate regeneration, which desensitizes the CO<sub>2</sub> response (Sharkey 1985; Wullschleger 1993). Baseline  $P_G$  varies by 20-30 GtC yr<sup>-1</sup> (Olson *et al* 1983). When a different  $P_G$  is used,  $\Delta P_G$  could vary by up to 20%.

## **Carbon Residence Time ( $\tau$ ) and Global Terrestrial Carbon Sink**

---

Quantification of terrestrial carbon sequestration requires an estimate of respiration. Biochemical reactions of plant and microbial respiration are much more complex than that of photosynthesis. Our understandings of mechanisms of respiratory responses to environmental changes are extremely limited (Amthor 1991; Raich and Schlesinger 1992). Direct estimation of a marginal change in global respiration ( $R_G$ ) caused by a marginal increase in  $C_a$  as for photosynthesis in Equation 8 is currently not feasible. This section sketches a general idea that carbon residence time can be used to project  $R_G$  from  $P_G$ .

Carbon fixed in photosynthesis goes through various pathways of ecosystem processes and is eventually released back to the atmosphere. Carbohydrate assimilated in photosynthesis is distributed, typically in a form of sucrose, to various plant parts for tissue growth and maintenance (Wardlaw 1990). When sucrose is converted to tissue compounds such as amino acid, lipid, and cellulose, additional biochemical energy is required, leading to breaking down more carbohydrate and releasing carbon dioxide. Maintenance of live plant tissues including uptake of nutrients, turnover of proteins and lipid, supporting electronic gradient between membrane also requires biochemical energy and results in releasing carbon dioxide. About 50% of photosynthetically fixed carbon is released quickly into the atmos-

---

2 Plants in which the first product of photosynthesis after carbon dioxide fixation is oxaloacetic acid, which contains four carbon atoms.

phere through plant growth and maintenance respiration whereas the other half is built into plant tissues and remains in ecosystems for various lengths of duration, depending on lifespan of plant tissues.

Plant tissues will eventually die and become litter. Plant tissue contains various chemical compounds, including carbohydrates, proteins, and lignin. The compounds of sugar and amino acids are easily decomposed by microbes with a mean residence time of a few days (Paul and Clark 1988) but a relatively high growth efficiency (up to 60%). The recalcitrant components of plant litter such as lignin are difficult to be decomposed by microbes with a long residence time and low growth efficiency. Up to 90% of carbon contained in the recalcitrant components is released back to the atmosphere and the rest re-enters the microbial growth-decomposition cycle. The microbial biomass, once dead, can be considered as easily decomposable (cytoplasm) and more resistant (cell walls) components and decomposed to release about 60% and 75% of carbon, respectively, into the atmosphere. A small portion of carbon in the decomposing residues, by-products of decomposition microbes, and microorganisms themselves is incorporated into soil organic matter, which becomes greatly resistant to microbial decomposition with a long residence time (years and decades). A very small portion of carbon may enter into the old organic carbon pool with a carbon residence time of millennial years. Overall, photosynthetically fixed carbon is partitioned into different carbon pools in an ecosystem and then respired into the atmosphere in various lengths of time after fixed in photosynthesis.

The ecosystem carbon processes described above can be characterized by carbon partitioning and residence time in each of the pathways. They can be integrated into calculation of ecosystem carbon residence at regional and global scales (Schimel *et al* 1994), which can be used to project respiration from photosynthesis. If the residence time is for example 10 years, this year's ecosystem respiration is approximately equal to ecosystem photosynthesis 10 years ago. This year's photosynthesis, on the other hand, is that of 10 years ago plus the increment caused by the atmospheric CO<sub>2</sub> increase during the past 10 years. That increment can be quantified by the  $\mathcal{L}$  function and is the amount of carbon sequestered in terrestrial ecosystems. Our preliminary study with this approach indicates that the global terrestrial ecosystems have a potential capacity to sequester about 5 GtC yr<sup>-1</sup>.

In summary, we can use a leaf-level ( $\mathcal{L}$ ) function that is invariant across species and environment to estimate a short-term (yearly), large-scale marginal increment in global photosynthetic carbon influx caused by a marginal increment in atmospheric CO<sub>2</sub> concentration. The carbon processes *post* photosynthesis can be characterized by ecosystem carbon residence time. Linking  $\mathcal{L}$  with residence time yields a terrestrial carbon sequestration model that predicts that global terrestrial ecosystems may have the potential capacity to sequester 5 GtC yr<sup>-1</sup>.

## References

---

- Amthor, J.S. 1991. Respiration in a future, higher-CO<sub>2</sub> world. *Plant, Cell and Environment* 14:13-20.
- Andrews, T.J., and G.H. Lorimer. 1987. Rubisco: structure, mechanisms, and prospects for improvement. Pages 131-218 In *The Biochemistry of Plants, A Comprehensive treatise*, P.K. Stumpf and E.E. Conn, editors, Academic Press, San Diego.
- Bacastow, R., and C.D. Keeling. 1973. Atmospheric carbon dioxide and radiocarbon in the natural carbon cycle: II. Changes from A.D. 1700 to 2070 as deduced from a geochemical model. Pages 86-135 In *Carbon and the Biosphere, Proceedings of the 24th Brookhaven Symposium in Biology*, G.M. Woodwell and E.V. Pecan, editors, AEC Symp. Ser. Vol. 30, Atomic Energy Commission, Upton, NY.
- Bazzaz, F.A. 1990. The response of natural ecosystems to the rising CO<sub>2</sub> levels. *Annual Review of Ecology and Systematics* 21:167-196.
- Ciais, P., P.P. Tans, M. Troler, J.W.C. White, R.J. Francey. 1995. A large northern hemisphere terrestrial CO<sub>2</sub> sink indicated by the <sup>13</sup>C/<sup>12</sup>C ratio of atmospheric CO<sub>2</sub>. *Science* 269:1098-1102.
- Farquhar, G.D., S. von Caemmerer, and J.A. Berry. 1980. A biochemical model of photosynthetic CO<sub>2</sub> assimilation in leaves of C<sub>3</sub> species. *Planta* 149:79-90.
- Field C.B. 1983. Allocating leaf nitrogen for the maximization of carbon gain, leaf age as a control on the allocation program. *Oecologia* 56:341-347.
- Francey, R.J., P.P. Tans, C.E. Allison, I.G. Enting, J.W.C. White, and M. Troller. 1995. Changes in oceanic and terrestrial carbon uptake since 1982. *Nature* 373:326-330.
- Gunderson, C.A. and S.D. Wullschleger. 1994. Photosynthetic acclimation in trees to rising atmospheric CO<sub>2</sub>: A broader perspective. *Photosynthesis Research* 39:369-388.
- Harley, P.C., R.B. Thomas, J.F. Reynolds, and B.R. Strain. 1992. Modelling photosynthesis of cotton grown in elevated CO<sub>2</sub>. *Plant, Cell and Environment* 15:271-282.
- Keeling, C.D., T.P. Whorf, M. Wahlen, and J. van der Plicht. 1995. Interannual extremes in the rate of rise of atmospheric carbon dioxide since 1980. *Nature* 375:666-670.
- Keeling, C.D., J.F.S. Chin, and T.P. Whorf. 1996. Increased activity of northern vegetation inferred from atmospheric CO<sub>2</sub> measurements. *Nature* (in press).
- Luo, Y., C.B. Field, and H.A. Mooney. 1994. Predicting responses of photosynthesis and root fraction to elevated CO<sub>2</sub>: Interactions among carbon, nitrogen, and growth. *Plant, Cell and Environment* 17:1194-1205.
- Luo, Y., and H.A. Mooney. 1995. Long-term studies on carbon influx into global terrestrial ecosystems: Issues and approaches. *Journal of Biogeography* 22:797-803.
- Luo, Y., and H.A. Mooney. 1996. Stimulation of global photosynthetic carbon uptake by increase in atmospheric carbon dioxide concentration. Pages 381-397 in *Carbon Dioxide and Terrestrial Ecosystem*. G.W. Koch and H.A. Mooney, editors. Academic Press, San Diego.
- Luo, Y., D. Sims, R. Thomas, D. Tissue, and J.T. Ball. 1996. Sensitivity of leaf photosynthesis to CO<sub>2</sub> concentration is an invariant function for C<sub>3</sub> plants: A test with experimental data and global applications. *Global Biogeochemical Cycles* 10:209-222.
- Mooney, H.A., P.M. Vitousek, and P.A. Matson. 1987. Exchange of materials between terrestrial ecosystems and the atmosphere. *Science* 238:926-932.
- Olson, J.S., J.A. Watts, and L.J. Allison. 1983. *Carbon in Live Vegetation of Major World Ecosystems*. ORNL-5862, Oak Ridge National Lab., Oak Ridge, TN.
- Paul, E.A., and F.E. Clark. 1989. *Soil Microbiology and Biochemistry*. Academic Press, San Diego, 275 pages.
- Raich, J.W., and W.H. Schlesinger. 1992. The global carbon dioxide flux in soil respiration and its relationship to vegetation and climate. *Tellus* 44B:81-99.

- Sage, R.F. 1994. Acclimation of photosynthesis to increasing atmospheric CO<sub>2</sub>: The gas exchange perspective. *Photosynthesis Research* 39:351-368.
- Sarmiento, J.L., C.L. Quere, and S.W. Pacala. 1995. Limiting future atmospheric carbon dioxide, *Global Biogeochemical Cycles* 9:121-137.
- Schimel, D.S. 1995. Terrestrial ecosystems and the carbon cycle. *Global Change Biology* 1:77-91.
- Schimel, D.S., B.H. Braswell, E.A. Holland, R. McKeown, D.S. Ojima, T.H. Painter, W.J. Parton, and A.R. Townsend. 1994. Climatic, edaphic, and biotic controls over storage and turnover of carbon in soils. *Global Biogeochemical Cycles* 8:279-293.
- Sharkey, T.D. 1985. Photosynthesis in intact leaves of C<sub>3</sub> plants: Physics, physiology, and rate limitations. *Botanical Review* 51:53-105.
- Tans, P.P., I.Y. Fung, and T. Takahashi. 1990. Observational constraints on the global atmospheric CO<sub>2</sub> budget. *Science* 247:1431-1438.
- Tans, P., J.A. Berry, and R.F. Keeling. 1993. Oceanic <sup>13</sup>C/<sup>12</sup>C observations: a new window on ocean CO<sub>2</sub> uptake. *Global Biogeochemical Cycles* 7:353-368.
- VEMAP Members. 1995. Vegetation/ecosystem modeling and analysis project: Comparing biogeography and biogeochemistry models in a continental-scale study of terrestrial ecosystem responses to climate change and CO<sub>2</sub> doubling. *Global Biogeochemical Cycles* 9:407-437.
- Wardlaw, I.F. 1990. The control of carbon partitioning in plants. *New Phytologist* 116:341-381.
- Wullschlegel, S.D. 1993. Biochemical limitations to carbon assimilation in C<sub>3</sub> plants — A retrospective analysis of the A/C<sub>i</sub> curves from 109 species. *Journal of Experimental Botany* 44:907-920.

# Long-Term Response of Torrey Pine to Coastal Climate: Precipitation, Temperature, and Fog

Franco Biondi, Daniel R. Cayan, and Wolfgang H. Berger

**Abstract.** Torrey pine (*Pinus torreyana* Parry ex Carr.) has one of the most limited geographical ranges and population size in the *Pinus* genus; it is present only on Santa Rosa Island and on the coast between San Diego and Del Mar, where our research was conducted. A 168-year chronology (1827-1994) was developed using 28 increment cores extracted from 15 living and 2 dead standing trees at Torrey Pines State Reserve, San Diego, California. Crossdating was possible but not easy, mostly because of faint latewood boundaries in certain years and specimens. Annual tree growth was highly and directly related to precipitation falling between the previous November and the current April. Temperature was not a significant predictor of tree growth. At seasonal scale, tree growth was highly and directly related to winter and spring precipitation, and was also significantly correlated to summer fog. However, when combined with winter and spring precipitation in multiple regression models, summer fog was not a significant predictor of tree growth. Total November-April precipitation explained a larger amount of variance after 1900 (64% in 1900-1949, 70% in 1950-1994) than before 1900 (48% in 1850-1899). The spatial correlation with western North America winter and spring precipitation, as well as with published tree-ring chronologies, indicates a connection with the American Southwest. Global correlation maps with winter sea level pressure and sea surface temperature are consistent with the hypothesis that San Diego precipitation is affected by a southerly displaced North Pacific storm track and by warmer water farther south, both leading to higher transport of lower latitude moisture.

## Introduction

Dendroclimatological studies at coastal sites have been relatively rare in the past because of the widespread belief that trees from such sites are (a) not sensitive to climate variability, (b) not easily datable using dendrochronological techniques, (c) short lived. Recently, Buckley *et al* (1992) and Wiles *et al* (1995) have shown that temperature-sensitive tree-ring records from coastal species can be effectively used to reconstruct climate variability over the last few centuries in the Gulf of Alaska and along the northeastern Pacific Coast.

Farther south along the California borderland, drought-sensitive tree-ring chronologies from near-coastal and interior mountain ranges have been used to reconstruct precipitation (Meko *et al* 1995; Haston and Michaelsen 1994; Michaelsen *et al* 1987; Meko *et al* 1980; Schulman 1947), sea surface temperature (Douglas 1980), fire history (Brown and Swetnam 1994), and El Niño events (Michaelsen 1989). With the exception of Brown and Swetnam (1994), the above-mentioned studies did not incorporate tree-ring records from endemic conifer species (Torrey pine, Monterey pine, bishop pine, Santa Lucia fir, coast redwood, *etc*) growing along the Southern and Central California coast (Barbour and Major

1977). Because the survival of such species within their limited natural distribution is intimately linked to the health and climatic sensitivity of California coastal environments, dendroclimatological studies are useful to quantify the long-term response of coastal ecosystems to climate change.

A typical feature of the U.S. West Coast is the marine fog layer, which can occur throughout the year. Coastal fog is generated offshore, then spread inland by sea breezes, and usually reaches land areas below 250-400 m elevation (Leipper 1994; Filonczuk *et al* 1995). Despite its widespread and frequent occurrence, the relationship between fog and tree growth is not well understood, especially on interannual and longer time scales. We have recently begun investigating the climatic response of endemic conifer species living along the California coast, which in recent decades has experienced rapid urban development. Our objective is to provide information on long-term climate/tree-growth relationships in coastal areas under changing environmental conditions. In this paper we present the dendroclimatology of Torrey pine (*Pinus torreyana* Parry ex Carr.) where it occurs naturally, between La Jolla and Del Mar. We address the following questions:

- Is it possible to crossdate Torrey pine tree rings?
- What is the maximum age of currently living trees?
- What are the most prominent seasonal climatic features that affect Torrey pine growth?
- Is fog beneficial to tree growth?
- Have climate/tree-growth relationships changed over time?

Torrey pine is a five-needle species characterized by long (up to 30 cm) needle-leaves and massive (up to 15-cm long) female cones that can remain attached to the tree for several years (Haller 1986). It has one of the most limited geographical ranges (a few square kilometers) and population size (about 10,000 individuals) in the *Pinus* genus. Its natural distribution is limited to a mainland population on the Pacific Coast between La Jolla and Del Mar, and to a disjunct population 280 km to the northwest on Santa Rosa Island, about 50 km offshore from Santa Barbara (Haller 1986). Torrey pine has persisted in those areas throughout the Holocene (Cole and Liu 1994) and was much more widespread in ancient times (Kellogg *et al* 1927). The two populations have been isolated from each other for several thousand years, but they do not seem to differ genetically (Waters and Schaal 1991), even though morphological and environmental differences do exist (Haller 1986).

## Tree-Ring Records

Field collections took place within Torrey Pines State Reserve and Extension, next to Los Peñasquitos Marsh Natural Preserve between Interstate 5 and Torrey Pines State Beach (Figure 1). The mainland native population of Torrey pines was first protected in 1899 as a city park; it became a reserve in 1921 and has belonged to the California State Park system since 1959 (Hubbs *et al* 1991). Torrey pine is the only overstory species at the study area, usually 10-15 meters in height and open grown, occupying ridgetops, slopes and gullies on eroded marine terraces and sandstone bluffs. The understory varies widely in terms of abundance and species composition, mostly resembling coastal chaparral communities, sometimes with few herbaceous species (Vogl *et al* 1977). The area is characterized by maritime climate with small temperature excursions, limited winter rainfall, and frequent coastal fog. Trees on the most exposed ridges are wind-pruned, and exposure to salt spray varies depending on topography and distance from the shoreline. Despite its ease of access and high biodiversity value, little is known on the life history and ecological relationships of Torrey pine in its natural range.

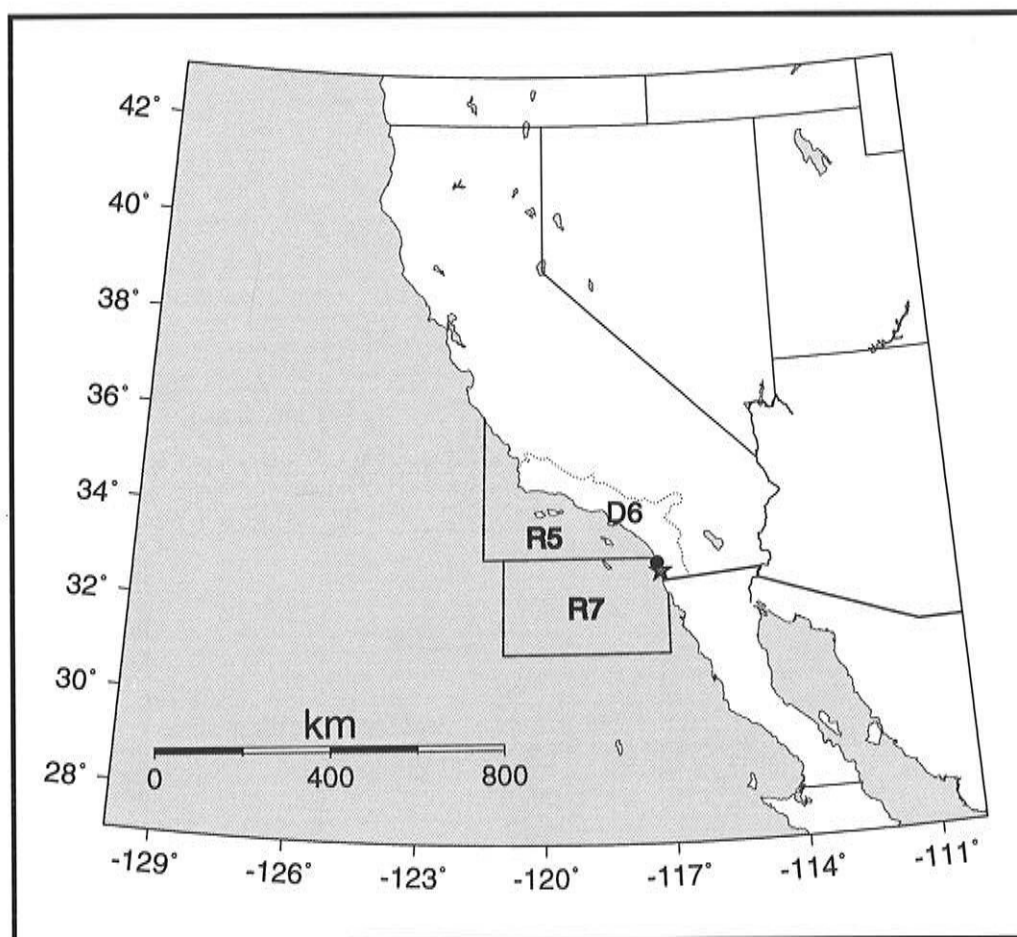


Figure 1. Location of dendroclimatic records. ● = Torrey pine tree-ring chronology; ★ = San Diego precipitation, temperature, and fog; D6 = California Climate Division 6 precipitation and temperature; R5, R7 = fog observations over marine region 5 and 7, respectively.

Dominant trees were sampled by taking two increment cores from the lower stem at about 1 meter above ground level, in a direction parallel to the topographic contour and at about 180 degrees from each other. Wood cores were 4.3 mm wide and less than 50 cm long; all holes were closed and sanitized. Standing trees were selected across the area according to dendrochronological criteria, as first outlined by Douglass (1919). These criteria favor steep, open sites occupied by trees with large branches and flat crown top. Every effort was made to avoid trees affected by non-climatic factors; *eg*, human disturbance, grazing, fire, insect outbreaks, fungi, mistletoe. Information on location, size, and health status of sampled trees was recorded in the field and entered into a computer database for future reference.

All wood samples were transported to the Scripps laboratory, air dried, and glued to wooden mounts after vertically aligning the xylem tracheids. Mounted cores were mechanically sanded, then polished by hand with progressively finer sandpaper until the smallest rings were clearly visible at 10x magnification. Ring patterns were visually crossdated (Douglass 1941; Stokes and Smiley 1968) using a binocular microscope, then ring widths were measured to the nearest 0.001 mm by means of a sliding stage interfaced with an image analysis system. Dating accuracy was numerically verified using the computer program COFECHA (Holmes 1983; Grissino-Mayer *et al* 1996).

## **Climatic Records**

---

Local climatic data came from different sources. Monthly precipitation (1850-1990) and temperature (1852-1990) records for San Diego were obtained from the Global Historical Climatology Network (Vose *et al* 1993). The most recent years of San Diego records (up to December 1994) were taken from the National Climatic Data Center on-line dataset of U.S. Cooperative and National Weather Service stations. Regional averages of monthly precipitation and temperature were provided by California Climate Division 6 time series (1895-1993) distributed by the National Climatic Data Center. Seasonal fog records for San Diego (1948-1990) as well as averaged over two marine regions (1949-1991), one south and one north of San Diego along the Southern California coast (Figure 1), were derived from the dataset compiled by Filonczuk *et al* (1995). Global datasets of sea surface temperature and sea level pressure compiled by Scripps Climate Research Division were used to map correlation fields with the Torrey pine tree-ring chronology.

## Statistical Methods

Ring-width measurements were standardized to remove individual trends as well as age- and size-related differences in growth rates (Cook and Kairiukstis 1990). The Torrey pine tree-ring chronology was produced by means of a statistical model that incorporates both deterministic and stochastic components (Biondi 1992, 1993). The computer program ARSTAN (Grissino-Mayer *et al* 1996) was used for data processing, and the final chronology could be written as follows:

$$\bar{I}_t = (1 - \oplus B) \{ \oplus_{i=1}^{n_t} [\log(w + k) - y]_{it} + \alpha \}$$

- with:  $I_t$  = chronology value at year  $t$   
 $w$  = crossdated ring width  
 $k$  = constant added to avoid taking the logarithm of 0  
 $y$  = modified negative exponential or straight line  
 $n_t$  = number of measured specimens that include year  $t$   
 (in this study,  $4 \leq n_t \leq 25$ )  
 $\oplus_i$  = biweight robust mean (Mosteller and Tukey 1977)  
 of the  $i$ -values,  $i = 1, \dots, n_t$   
 $\alpha$  = difference between 1.000 and the arithmetic mean  
 of the robust-mean chronology  
 $1 - \oplus B$  = first-order autoregressive operator (Box and Jenkins 1976)

The relationship between climate and tree growth was investigated by means of correlation analysis and response-function analysis. Correlation of tree-ring chronologies with annual or seasonal climatic variables is straightforward (Douglass 1914, 1919). Correlation with monthly climatic variables requires more advanced statistical techniques to account for possible collinearity of predictors (Fritts 1991). These techniques are based on multiple regression between the pre-whitened tree-ring index and the principal components of the monthly climatic predictors, as well as on bootstrapped confidence intervals to test significance of each monthly variable (Fritts *et al* 1971; Guiot 1990, 1991). To account for numerical and biological persistence in the tree response to climate, we defined a 14-month dendroclimatic window, going backwards from October of the current growth year to the previous September.

The spatial coherency between Torrey pine and other tree-ring chronologies for western North America was analyzed using the International Tree-Ring Data Bank (NOAA 1992; Figure 2). The data bank is a collection of accurately dated tree-ring records developed by dendrochronologists over many years, and is continuously expanding as new datasets become available. In addition, unpublished chronologies for Southern California were provided by Dave Meko, Laboratory of Tree-Ring Research, University of Arizona, and by Laura Haston, formerly at Geography Department, California State University-Northridge. All tree-ring chronologies began prior to 1800 and ended between 1960 and 1993.

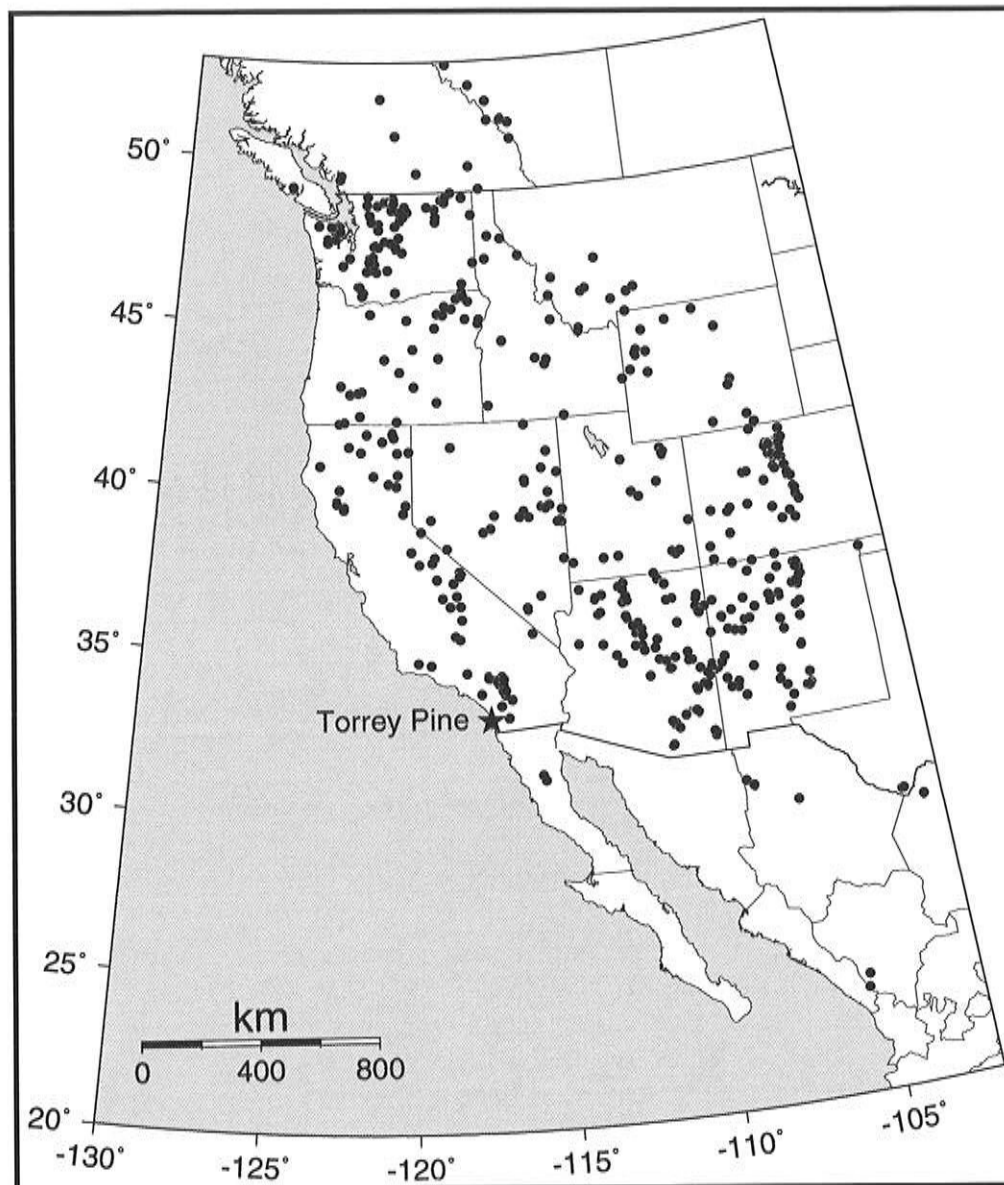


Figure 2. Tree-ring sites in western North America (source: International Tree-Ring Data Bank; NOAA 1992). The period in common between the 585 tree-ring chronologies (●) and the Torrey pine chronology (★) varies from 1827-1960 to 1827-1993.

## Results and Discussion

Torrey pine tree rings could be crossdated, even though faint latewood boundaries in certain years and specimens required careful specimen preparation and long hours of microscope work for correct identification. Based on crossdated series, sampled trees reached a maximum age of 170 years at coring height; *ie*, about 1 meter above ground level. Considering an estimated time of 10-30 years to reach coring height, sampled trees were no older than 200 years, which is almost three times the maximum age reported by Vogl *et al* (1977). The possibility that older trees still exist, albeit unlikely, cannot be ruled out. From the collected samples, we developed a continuous chronology spanning the 1827-1994

period using overlapping segments of well-defined annual rings (Figure 3). Chronology sample depth is maximum in 1917-1978, when the mean index is averaged over 20-25 samples. The early years are based on at least four samples (1827-1838); sample depth rises to ten or more after 1867, and the most recent years are based on at least eighteen samples.

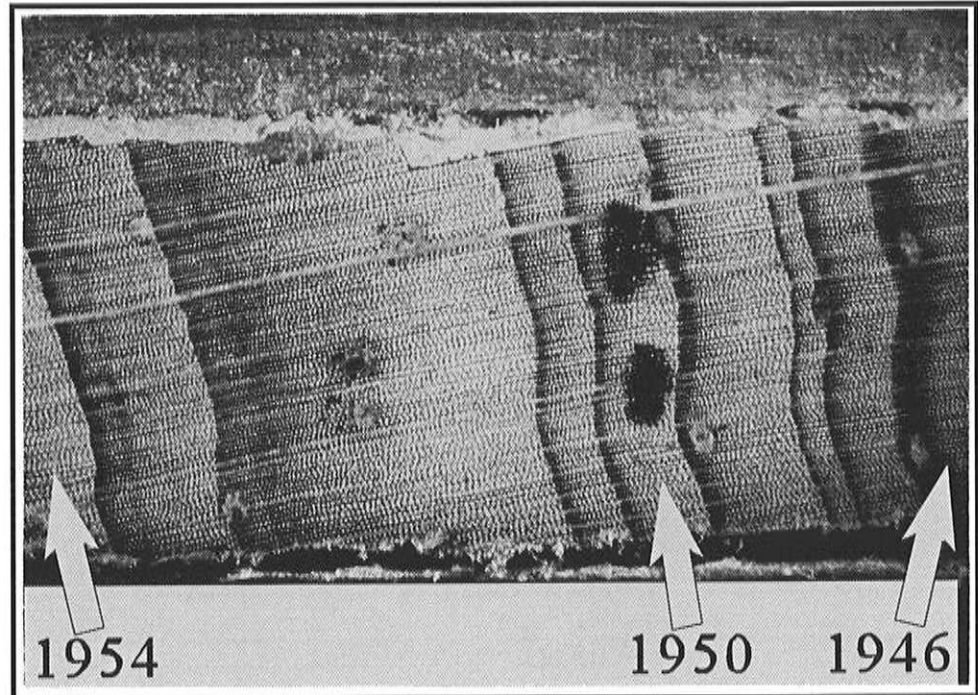


Figure 3. Annual xylem rings of Torrey pine as seen under a binocular microscope after specimen preparation and surfacing.

Response functions based on 28 monthly predictors (14 for precipitation and 14 for temperature) were consistent using either San Diego station data or Climate Division 6 average data. Similarly, response functions based on 12 seasonal predictors (4 each for precipitation, temperature, and fog) were consistent using station data or regional averages. In both cases, however, regression statistics were better using San Diego station data; hence those results are reported in the following paragraphs. The major climatic signal in Torrey pine tree rings consists of winter and spring rainfall, as shown by the significant coefficients for November-April precipitation (Figure 4). Temperature is not a significant predictor of Torrey pine annual growth, and summer fog has a weak, positive association with Torrey pine annual growth (Figure 4). These results were confirmed by linear correlation coefficients between the Torrey pine chronology and climatic time series (Figure 5). From 1850 to 1994, total rainfall from November through April had the highest correlation (0.77,  $n=145$ ) with the Torrey pine tree-ring chronology. Among seasonal variables, winter and spring precipitation had, respectively, the second (0.63,  $n=145$ ) and third (0.43,  $n=145$ ) highest correlation with the tree-ring chronology. The only other seasonal variable significantly correlated (0.37,  $n=43$ ) to Torrey pine annual growth was summer fog. Most likely,

summer fog benefits Torrey pine growth by reducing the evapotranspiration stress during the warmest and driest season of the year. However, when combined with winter and spring precipitation in a multiple regression model, summer fog was not a significant predictor of Torrey pine tree growth.

According to Mallows' *C<sub>p</sub>* criterion (Mallows 1973; SAS Institute 1990), from 1850 to 1994 November-April precipitation is the best predictor of Torrey pine tree growth among all possible combinations of seasonal variables. The consistency of climate/tree-growth relationships through time was then investigated by comparing correlation results between November-April precipitation and Torrey pine annual growth during three non-overlapping periods, 1850-1899, 1900-1949, and 1950-1994

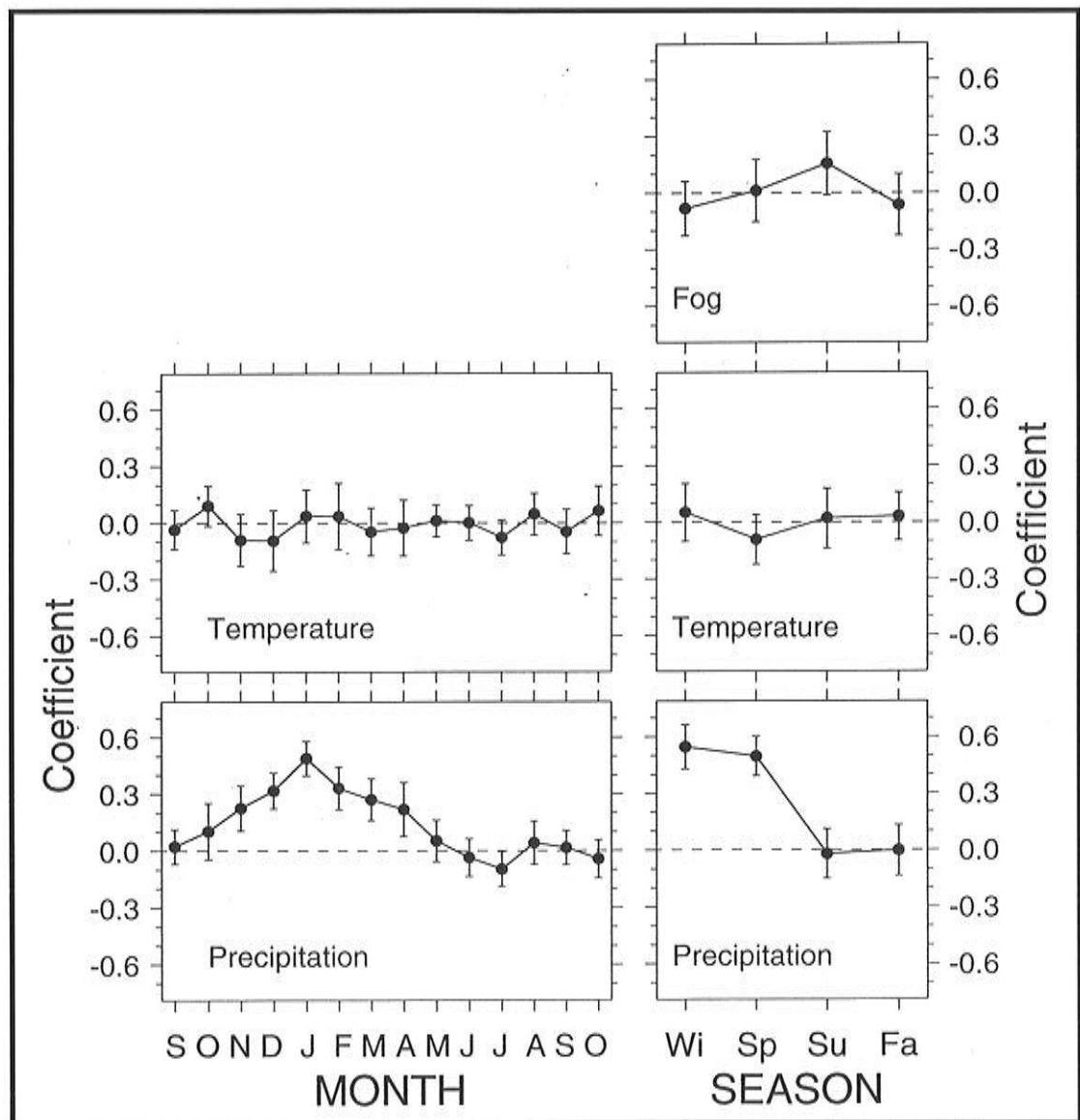


Figure 4. Response functions between Torrey pine tree-ring chronology and San Diego climatic variables. A total of 28 monthly predictors (1892-1990) and 12 seasonal predictors (1950-1990) were decomposed into principal components and randomly selected with replacement to compute bootstrapped confidence intervals.

(Figure 6). The amount of explained variance was higher in the 20th century (64% in 1900-1949, 70% in 1950-1994) than in previous decades (48% in 1850-1899). This difference could be attributed to different factors. Assuming that the tree-ring standardization effectively removed age- and size-related effects on annual growth and that the number of samples used to develop the Torrey pine chronology was large enough throughout the entire period of interest to obscure the effect of time-varying sample depth, temporal differences in climate-tree growth relationships could still be generated by changes in the quality of rainfall data. As an example, the largest value in the whole Torrey pine

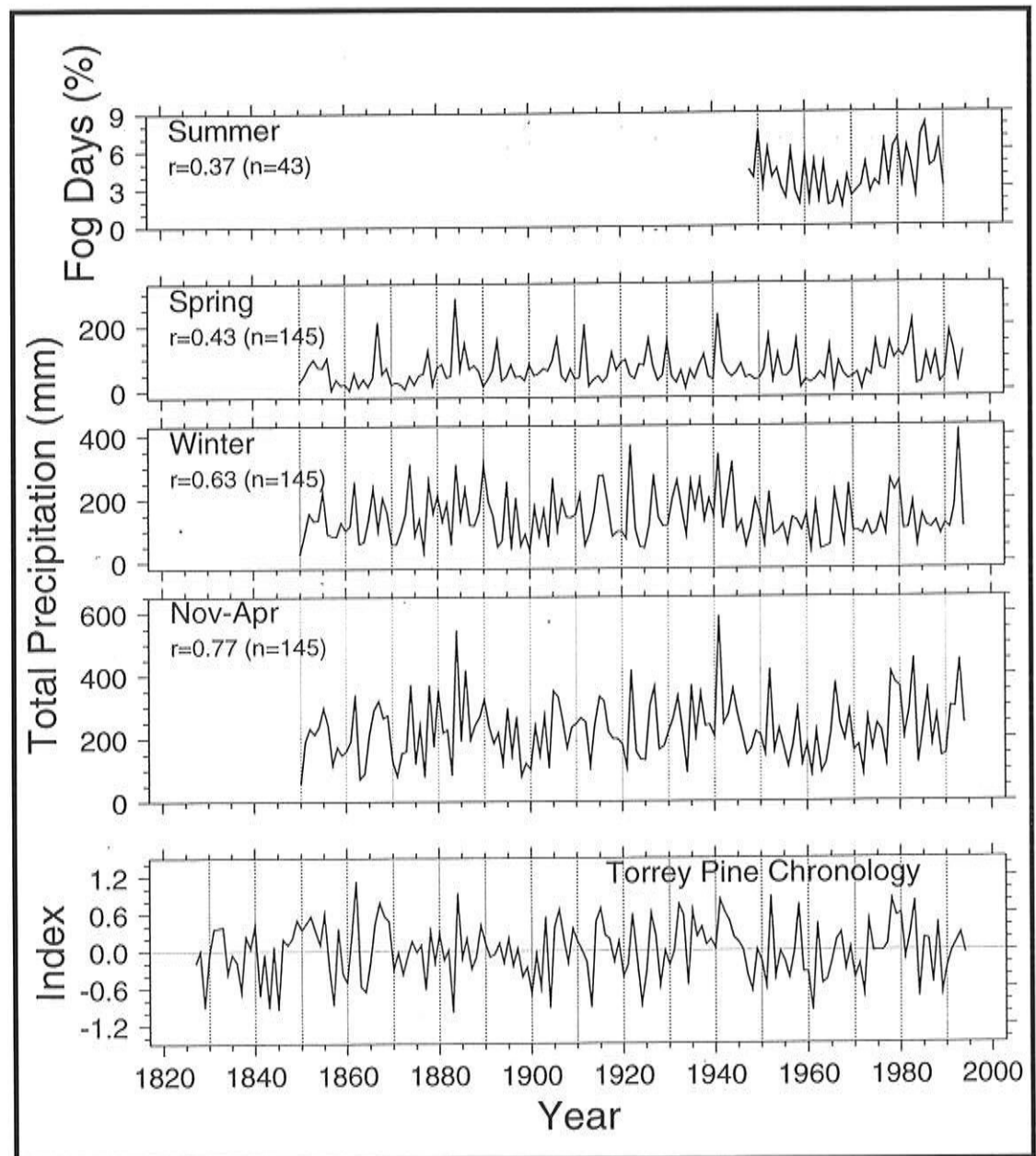


Figure 5. Time-series plots of San Diego dendroclimatic records. The linear correlation ( $r$ ) with the Torrey pine chronology is maximum for total November through April precipitation.

chronology occurs in 1862, which may be one of the wettest winters in recent Southern California history (Engstrom 1996), but is not a very large value in the San Diego precipitation record (Figure 5). The Torrey pine chronology can then provide an estimate of precipitation during the early and pre-instrumental period. As such, it reveals a very dry period in the early and mid-1840s, followed by a wet spell until the early 1850s and by another wet period in the late 1860s (Figure 5).

Spatial correlation between the Torrey pine chronology and seasonal precipitation (1895-1994) over the Climate Divisions identified by NOAA (1983) revealed a connection with the lower half of the West Coast and

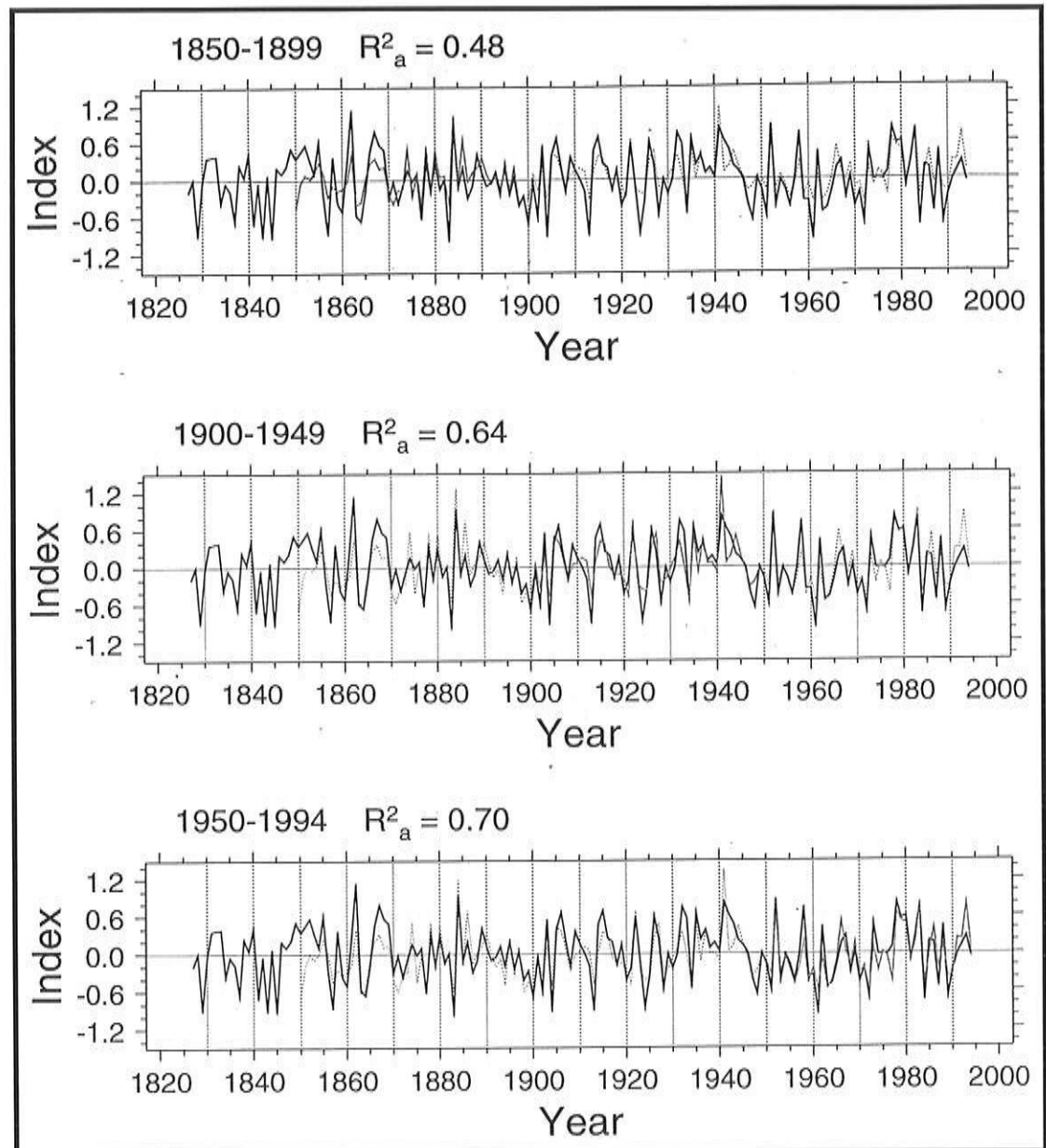


Figure 6. Linear estimates (solid gray line) and predictions (dotted line) of the Torrey pine tree-ring chronology (solid black line) obtained using total November-April precipitation during three adjacent time intervals. The amount of explained variance ( $R^2_a$ ) is lower before 1900 than after 1900.

the American Southwest in winter and with the American Southwest in spring (Figure 7).

Correlation maps with gridded winter sea surface temperature and sea level pressure were consistent using different near-global datasets. Prominent features were a strong positive association with sea surface temperature south of San Diego and in the eastern tropical Pacific, and an equally strong negative association with sea level pressure directly above the California Current, in an area centered approximately over

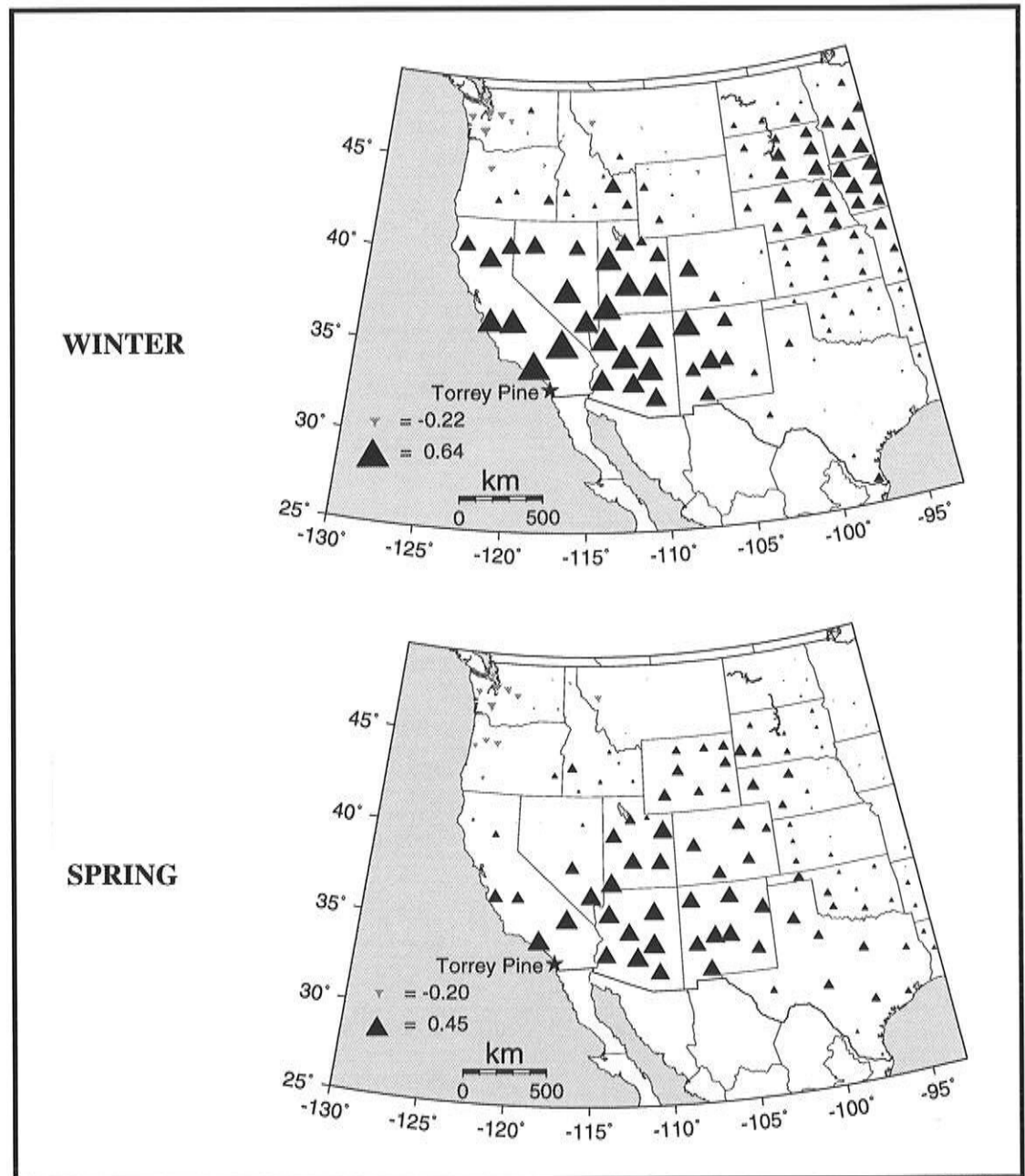


Figure 7. Linear correlation ( $r$ ) between the Torrey pine tree-ring chronology and seasonal precipitation (WINTER and SPRING, 1895-1994) over NOAA/NCDC Climate Divisions for the western U.S. Symbol size for positive (solid, upward triangles) and negative (shaded, downward triangles) correlations is directly proportional to the absolute value of  $r$ .

30-40°N and 120-130°W, just off the Patton Escarpment (Figure 8). These correlation fields indicate that Torrey pine annual growth is favored, on average, by a weakening or a displacement of the high pressure cell that normally develops off Southern California in winter (Duxbury and Duxbury 1991), hence by a southerly displaced winter storm track. Annual tree

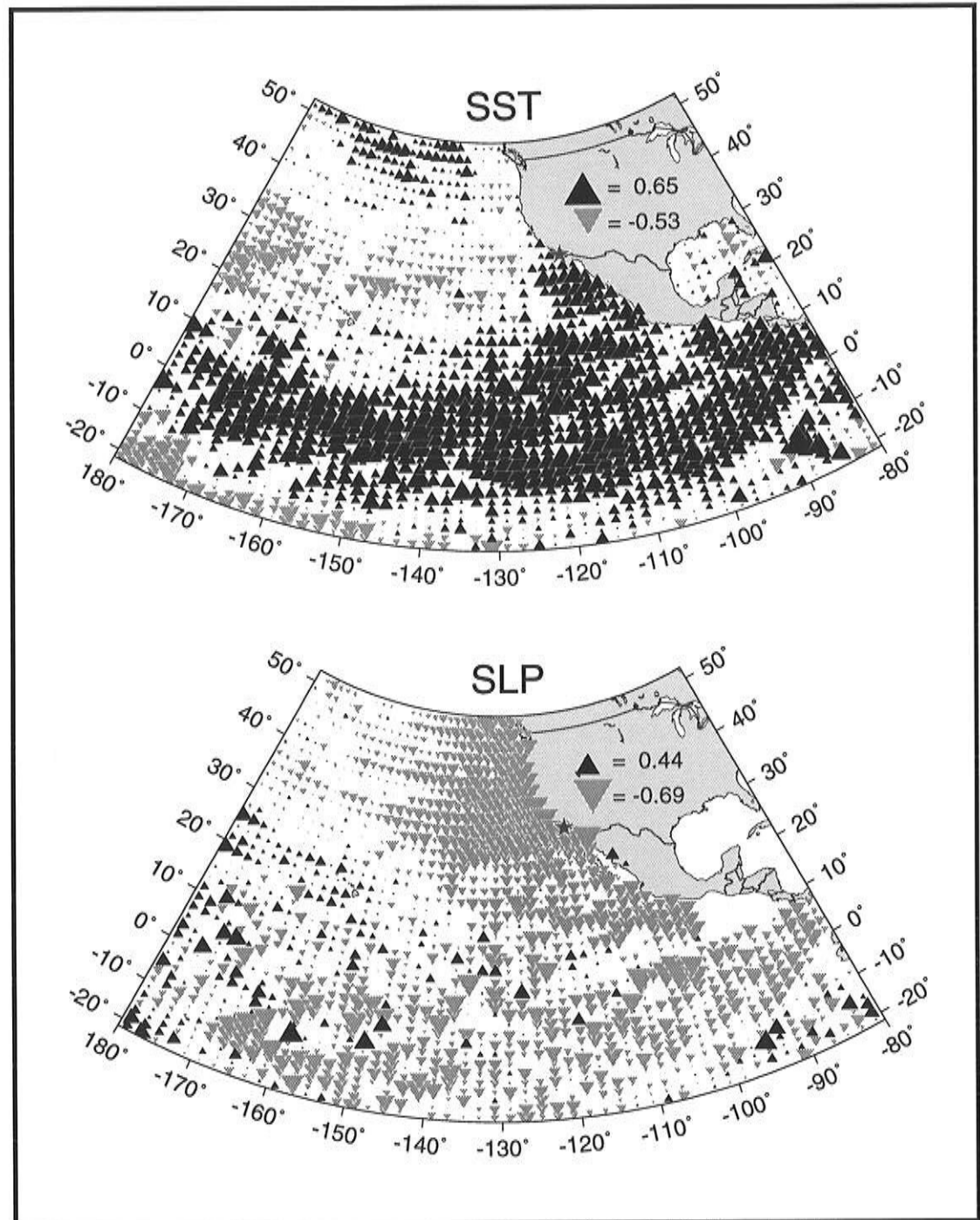


Figure 8. Linear correlation ( $r$ ) between the Torrey pine tree-ring chronology ( $\star$ ) and gridded December to February mean sea surface temperature (SST) and sea level pressure (SLP) in the eastern tropical and subtropical Pacific during 1948-1992. Climate data were obtained from the Comprehensive Ocean-Atmosphere Data Set (COADS). Symbol size for positive (solid, upward triangles) and negative (shaded, downward triangles) correlations is directly proportional to the absolute value of  $r$ .

growth is also favored by the development of warm anomalies in the southern portion of the California Current region and in the eastern tropical Pacific. Both of these patterns indicate that Torrey pine growth is sensitive to moisture transport from the eastern tropical Pacific driven by a southerly extension of the westerlies caused by the lower-than-average pressures off Southern California. Such a mechanism is enhanced by the El Niño-Southern Oscillation (ENSO) phenomenon: during warm events, surface winds and upper-level jets move from the eastern tropical Pacific into the American Southwest, whereas during cold events that airflow is blocked or reversed (Murphree and Reynolds 1995).

The Torrey pine chronology is highly correlated to tree-ring chronologies developed for Southern California and the Colorado Plateau (Figure 9, top). The contoured correlation field shows a pronounced, V-shaped, southwest-to-northeast gradient extending into a large portion of the American Southwest (Figure 9, bottom). Interestingly, the correlation with other regions of the western United States is consistently near zero (Figure 9).

Torrey pine and Southern California are linked to the Colorado Plateau mostly via winter precipitation patterns, as revealed by the spatial correlation between San Diego winter precipitation and tree-ring chronologies (Figure 10, top). On one hand, the high coherency between Torrey pine and tree-ring chronologies much farther inland is remarkable, considering that coastal species are often scarcely sensitive to climate. On the other hand, the extremely good agreement between the correlation maps shown in Figures 9 and 10 (top) is not surprising, considering the previously discussed relationship between winter precipitation and Torrey pine annual growth. In winter, El Niño events are associated with increased rainfall in a region longitudinally stretched from Southern and Baja California to Western Texas and the Southeastern United States (Schonher and Nicholson 1989; Diaz and Kiladis 1992; Stahle and Cleaveland 1993). However, the linkage between Torrey pine and the American Southwest can only partly be attributed to ENSO, as revealed by the correlation maps between the Southern Oscillation Index (SOI, Ropelewski and Jones 1987) and the western North America tree-ring chronologies (Figure 10, bottom). The Colorado Plateau tends to have greater correlations with SOI than Southern California, and some large correlations are also found in the northern portion of the U.S. West Coast. Persistence effects in tree-ring response to climate, as well as other ocean/atmosphere interactions, may play a role in shaping the Southern California/Colorado Plateau connection, as suggested by correlation maps between tree-ring chronologies and previous summer sea surface temperature at coastal stations (Biondi *et al.*, this volume).

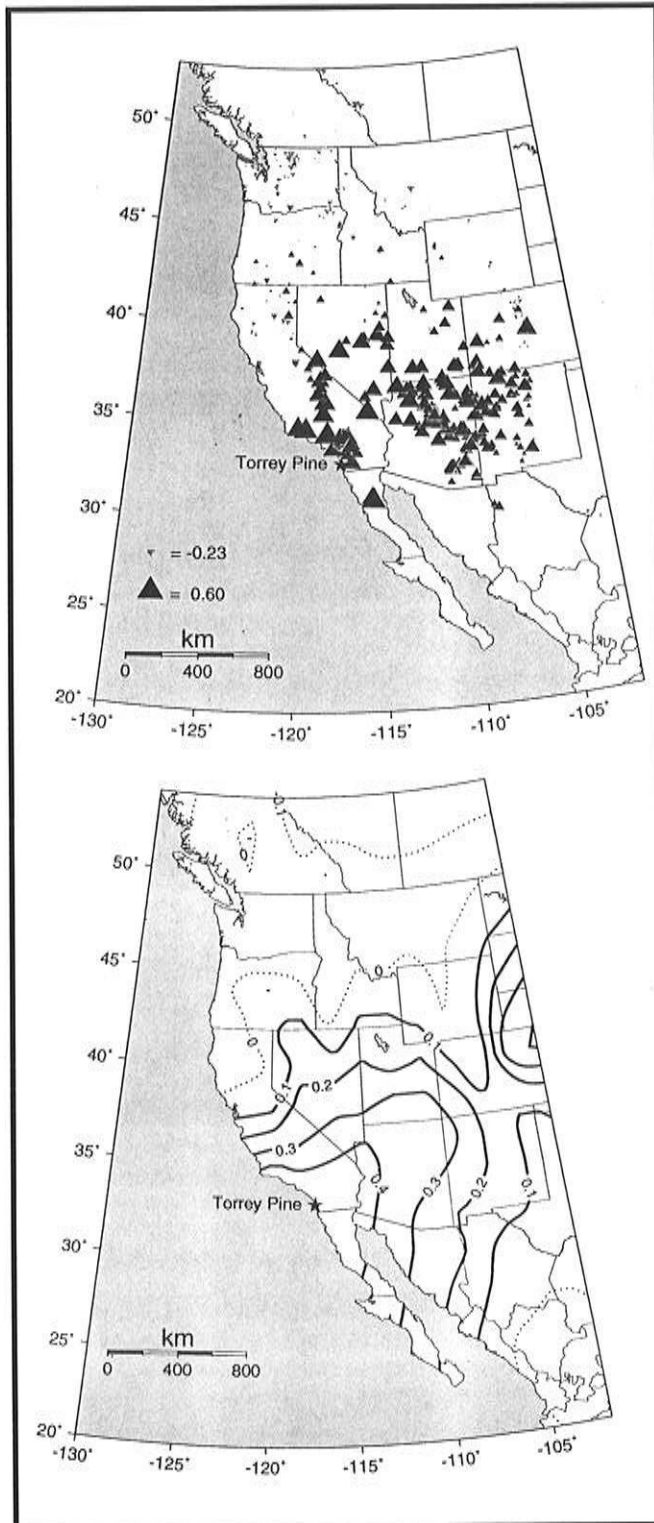


Figure 9. Linear correlation ( $r$ ) between Torrey pine and tree-ring chronologies shown in Figure 3.  
 Top: Point correlations; symbol size for positive (solid, upward triangles) and negative (shaded, downward triangles) correlations is directly proportional to the absolute value of  $r$ .  
 Bottom: Contoured correlation field; contour interval is 0.1 for positive (solid lines) and negative (dotted lines) correlations.

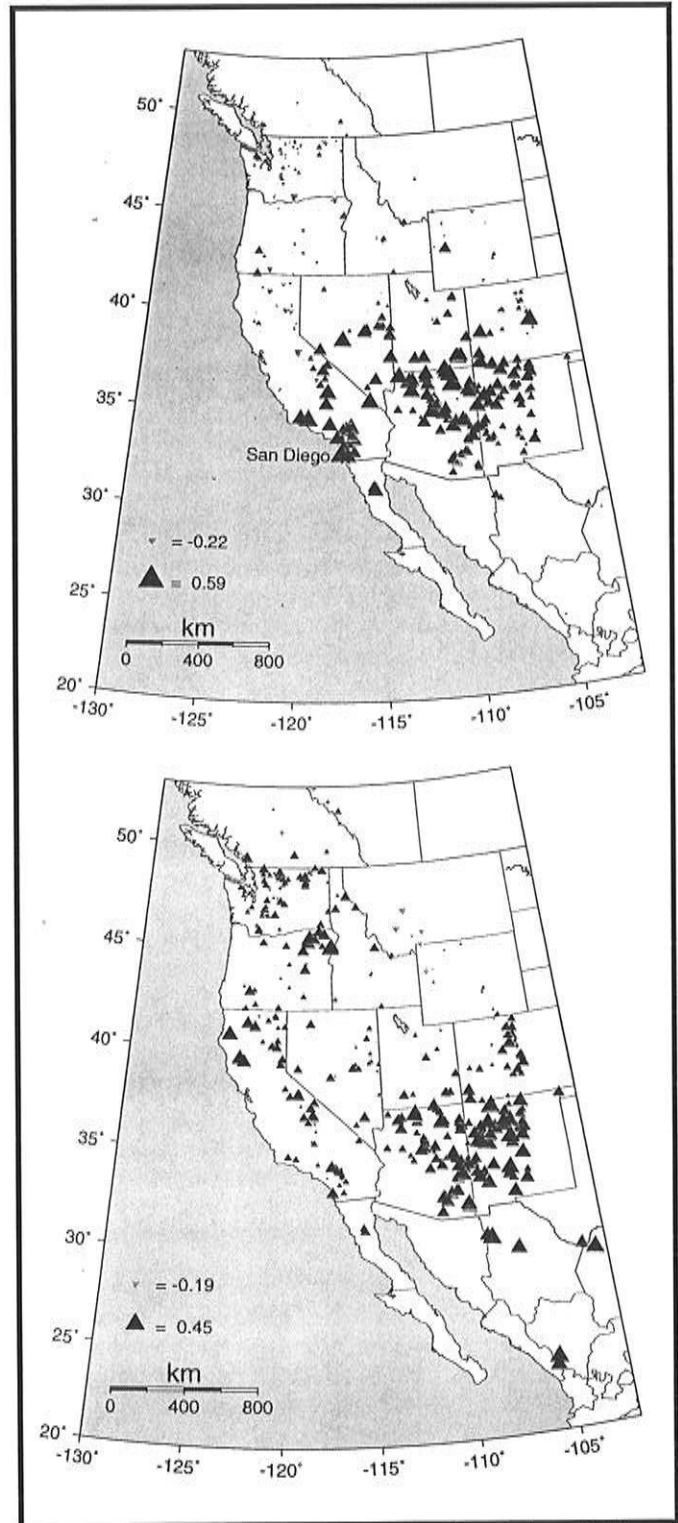


Figure 10. Linear correlation ( $r$ ) between tree-ring chronologies and winter climatic variables. Symbol size for positive (solid, upward triangles) and negative (shaded, downward triangles) correlations is directly proportional to the absolute value of  $r$ .  
 Top: Total DJF precipitation in San Diego (1850-1994).  
 Bottom: Southern Oscillation Index (SOI, 1882-1993; the sign was reversed to make El Niño years positive).

## Conclusion

---

Our study provided evidence that Torrey pine tree rings are datable using dendrochronological techniques, that maximum tree age does not exceed 150-200 years, and that annual growth is highly sensitive to winter and spring precipitation. Summer fog was positively correlated with Torrey pine annual growth, but its predictive ability was minimal when compared with winter and spring rainfall. Large-scale climatic signals in Torrey pine tree rings extend to the California Current region off Southern California and to the eastern tropical Pacific, and show a pronounced gradient from the southern California Coast into the Colorado Plateau. There is little evidence that climate-tree growth relationships have changed over the 20th century. The lower association between tree growth and November-April precipitation in 1850-1899 than in more recent decades may have different causes, including lower quality of rainfall records. The Torrey pine chronology is, then, well suited to provide an estimate of early and pre-instrumental climate records for San Diego.

To complement our results, it would now be desirable to conduct field experiments on the short-term (daily or weekly) response of Torrey pine stem growth to weather variability. Such a study, for instance, could explain why Torrey pine tree rings occasionally show faint latewood boundaries as if, depending on factors internal and external to the tree, xylem growth could slow down but still continue from one growing season to the next. We are also planning to extend this initial dendroclimatic study to other conifer species and sites along the California Coast, and we have already completed the necessary field work (Figure 11).

Resource managers, the public, and the scientific community could benefit from our results. Torrey Pine State Reserve receives an average of one million visitors per year (Mike Wells, *pers comm*). The recreational value alone of conifer species endemic to the California Coast would justify detailed studies on the possible impact of future local and regional climate change on the growth and survival of those species within their natural habitat. Additional results generated by dendrochronological studies of this sort could include age/size equations, which are beneficial to resource managers in assessing the performance of individual trees and stands and in uncovering stand age structure and development.

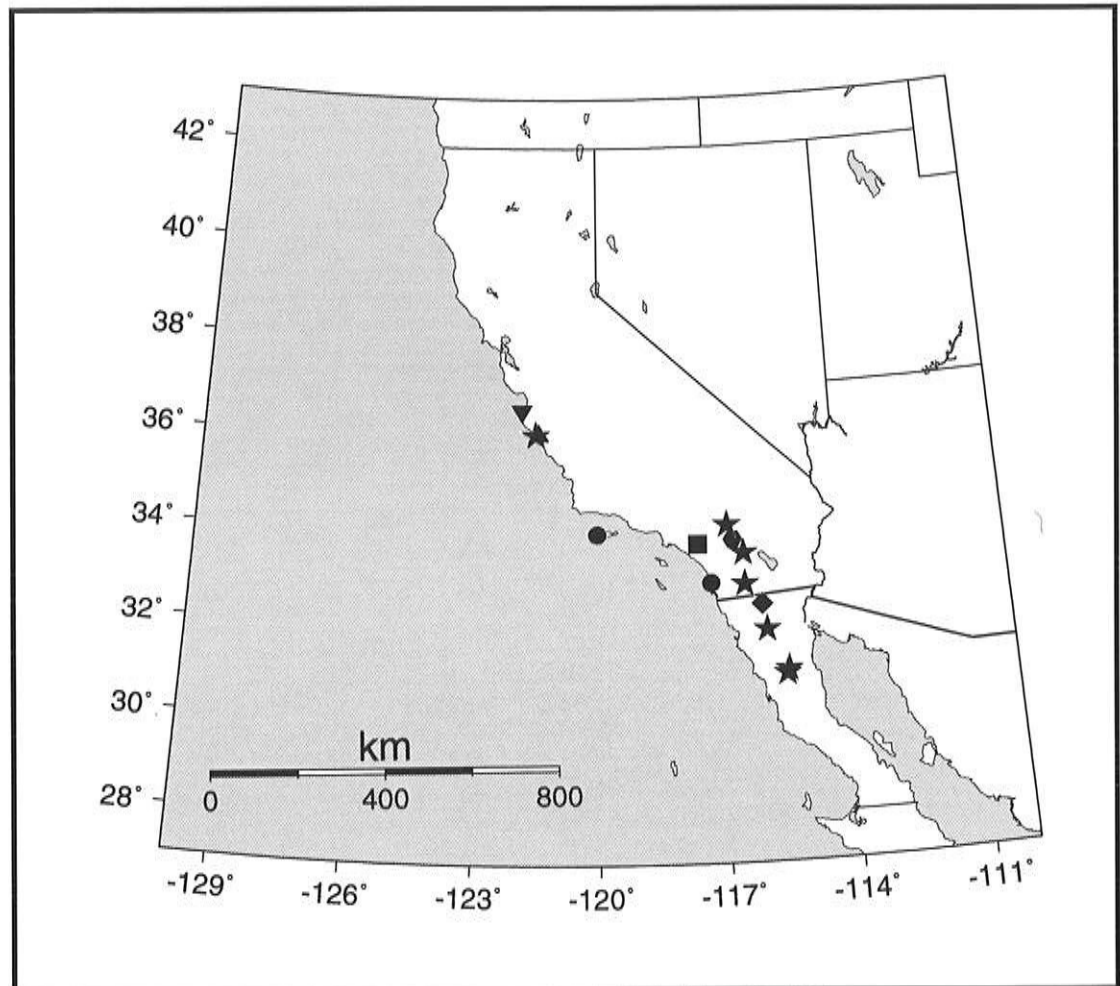


Figure 11. Location of tree-ring sites sampled in Southern and Baja California during 1995-1996.  
 ★ = Jeffrey and ponderosa pine; ● = Torrey pine; \* = limber pine; ◆ = piñon pine;  
 ▲ = sugar pine; ▼ = Monterey pine; ■ = Big-cone Douglas-fir.

## Acknowledgments

We are grateful to the California State Park System for permission to sample within Torrey Pines State Reserve and to Mike Wells for help during field collections. Larry Riddle prepared the poster displayed at PACLIM and provided the climatic data used for statistical analyses. Work supported by National Science Foundation Grant ATM-9509780 to W.H. Berger, D.R. Cayan, F. Biondi, and M.K. Hughes and by a Scripps Post-Doctoral Fellowship to F. Biondi.

## References

---

- Barbour, M.G., and J. Major (eds). 1977. *Terrestrial Vegetation of California*, Wiley, New York.
- Biondi, F. 1992. Development of a tree-ring network for the Italian Peninsula. *Tree-Ring Bulletin* 52:15-29.
- Biondi, F. 1993. Climatic signals in tree-rings of *Fagus sylvatica* L. from the central Apennines, Italy. *Acta Oecologica* 14:57-71.
- Biondi, F., C.B. Lange, W.H. Berger, and M.K. Hughes. 1997. The near-AD 1600 multi-proxy puzzle. In *Proceedings of the Thirteenth Annual Pacific Climate (PACLIM) Workshop*, C.M. Isaacs and V.L. Tharp (eds), Interagency Ecological Program, Technical Report 53. California Department of Water Resources, Sacramento.
- Box, G.E.P., and G.M. Jenkins. 1976. *Time Series Analysis: Forecasting and Control*. Revised Edition. Holden-Day, Oakland.
- Brown, P.M. and T.W. Swetnam 1994. A cross-dated fire history from coast redwood near Redwood National Park, California. *Canadian Journal of Forest Research* 24: 21-31.
- Buckley, B.M., R.D. D'Arrigo, and G.C. Jacoby. 1992. Tree-ring records as indicators of air-sea interaction in the northeast Pacific sector. Pages 35-45 in *Proceedings of the Eight Annual Pacific Climate (PACLIM) Workshop*, K.T. Redmond (ed.), Interagency Ecological Program, Technical Report 31. California Department of Water Resources, Sacramento.
- Cole, K.L., and G.-W. Liu. 1994. Holocene paleoecology of an estuary on Santa Rosa Island, California. *Quaternary Research* 41:326-335.
- Cook, E.R., and L.A. Kairiukstis (eds). 1990. *Methods of Dendrochronology*. Kluwer, Dordrecht.
- Diaz, H.F., and G.N. Kiladis. 1992. Atmospheric teleconnections associated with the extreme phases of the Southern Oscillation. Pages 7-28 in *El Niño: Historical and Paleoclimatic Aspects of the Southern Oscillation*, H.F. Diaz, and V. Markgraf (eds). Cambridge University Press, Cambridge, UK.
- Douglas, A.V. 1980. Geophysical estimates of sea-surface temperatures off western North America since 1671. *California Cooperative Oceanic Fisheries Investigations (CalCOFI) Reports* 21:102-112.
- Douglass, A.E. 1914. A method of estimating rainfall by the growth of trees. Pages 101-121 in *The Climatic Factor*, E. Huntington. Carnegie Institution, Washington.
- Douglass, A.E. 1919. *Climatic Cycles and Tree-Growth*. Carnegie Institution, Washington.
- Douglass, A.E. 1941. Crossdating in Dendrochronology. *Journal of Forestry* 39:825-831.
- Duxbury, A.C., and A.B. Duxbury. 1991. *An Introduction to the World's Oceans*. Third Edition, Wm. C. Brown Publishers, Dubuque, Iowa.
- Engstrom, W.N. 1996. The flood of January, 1862 in Southern California. Page 7 in *Abstracts of the 1996 Southern California Environment and History Conference*, Department of Geography, California State University-Northridge.
- Filonczuk, M.K., D.R. Cayan, and L.G. Riddle. 1995. Variability of marine fog along the California coast. Scripps Institution of Oceanography, SIO Reference No. 95-2. University of California-San Diego, La Jolla.
- Fritts, H.C. 1991. *Reconstructing Large-Scale Climatic Patterns from Tree-Ring Data: A Diagnostic Analysis*. University of Arizona Press, Tucson.
- Fritts, H.C., T.J. Blasing, B.P. Hayden, and J.E. Kutzbach. 1971. Multivariate techniques for specifying tree-growth and climate relationships and for reconstructing anomalies in paleoclimate. *Journal of Applied Meteorology* 10:845-864.
- Grissino-Mayer, H.D., R.L. Holmes, and H.C. Fritts. 1996. The International Tree-Ring Data Bank Program Library Version 2.0 User's Manual. Laboratory of Tree-Ring Research, University of Arizona, Tucson.

- Guiot, J. 1990. Methods of calibration. Pages 165-178 in: *Methods of Dendrochronology*, E. Cook and L. Kairiukstis (eds). Kluwer, Dordrecht.
- Guiot, J. 1991. The bootstrapped response function. *Tree-Ring Bulletin* 51:39-41.
- Haller, J.R. 1986. Taxonomy and relationships of the mainland and island populations of *Pinus torreyana* (Pinaceae). *Systematic Botany* 11:39-50.
- Haston, L., and J. Michaelsen. 1994. Long-term central coastal California precipitation variability and relationships to El Niño-Southern Oscillation. *Journal of Climate* 7:1373-1387.
- Holmes, R.L. 1983. Computer-assisted quality control in tree-ring dating and measurement. *Tree-Ring Bulletin* 43:69-78.
- Hubbs, C.L., T.W. Whitaker, and F.M.H. Reid (eds). 1991. *Torrey Pines State Reserve*. Third Edition. The Torrey Pines Association, La Jolla, California.
- Kellogg, R., J.C. Merriam, C. Stock, R.W. Chaney, and H.L. Mason. 1927. Additions to the palaeontology of the Pacific coast and Great Basin regions of North America. Pages 139-158 in *Contributions to Paleontology*. Carnegie Institute, Washington, DC.
- Leipper, D.F. 1994. Fog on the United States West Coast: a review. *Bulletin of the American Meteorological Society* 75:229-240.
- Mallows, C.L. 1973. Some comments on Cp. *Technometrics* 15:661-675.
- Meko, D.M., C.W. Stockton, and W.R. Boggess. 1995. The tree-ring record of severe sustained drought in the Southwest. *Water Resources Bulletin* 31:789-801.
- Meko, D.M., C.W. Stockton, and W.R. Boggess. 1980. A tree-ring reconstruction of drought in Southern California. *Water Resources Bulletin* 16:594-600.
- Michaelsen, J., L. Haston, and F.W. Davis. 1987. 400 years of central California precipitation variability reconstructed from tree-rings. *Water Resources Bulletin* 23:809-818.
- Michaelsen, J. 1989. Long-period fluctuations in El Niño amplitude and frequency reconstructed from tree rings. Pages 69-74 in *Aspects of Climate Variability in the Pacific and the Western Americas*. D.H. Peterson (ed), Geophysical Monograph 55, American Geophysical Union, Washington.
- Morrison, D.F. 1983. *Applied Linear Statistical Methods*. Prentice-Hall, Englewood Cliffs.
- Mosteller, F., and J.W. Tukey. 1977. *Data Analysis and Regression*. Addison-Wesley, Reading.
- Murphree, T., and C. Reynolds. 1995. El Niño and La Niña effects on the Northeast Pacific: the 1991-1993 and 1988-1989 events. *California Cooperative Oceanic Fisheries Investigations (CalCOFI) Reports* 36:45-56.
- NOAA 1983. Statewide Average Climatic History. *Historical Climatology Series 6-1*. National Climatic Data Center, Asheville, North Carolina.
- NOAA 1992. *International Tree-Ring Data Bank*. National Geophysical Data Center, Boulder, Colorado.
- Ropelewski, C.F., and P.D. Jones 1987. An extension of the Tahiti-Darwin Southern Oscillation Index. *Monthly Weather Review* 115:2161-2165.
- SAS Institute. 1990. *SAS/STAT User's Guide*, Version 6, Fourth Edition, Vol. 2. Cary, North Carolina.
- Schonher, T., and S.E. Nicholson. 1989. The relationship between California rainfall and ENSO events. *Journal of Climate* 2:1258-1269.
- Schulman, E. 1947. *Tree-Ring Hydrology in Southern California*. Laboratory of Tree-Ring Research, Bulletin No. 4. University of Arizona, Tucson.
- Stahle, D.W., and M.K. Cleaveland. 1993. Southern Oscillation extremes reconstructed from tree rings of the Sierra Madre Occidental and Southern Great Plains. *Journal of Climate* 6:129-140.
- Stokes, M.A., and T.L. Smiley. 1968. *An Introduction to Tree-Ring Dating*. University of Chicago Press, Chicago.
- Vogl, R.J., W.P. Armstrong, K.L. White, and K.L. Cole 1977. The closed-cone pines and cypresses. Pages 295-358 in *Terrestrial Vegetation of California*, M.G. Barbour and J. Major (eds). Wiley, New York.

- Vose, R.S., R.L. Schmoyer, P.M. Steurer, *et al.* 1993. The Global Historical Climatology Network: Long-term monthly temperature, precipitation, sea level pressure, and station pressure data. Page 52 in *CDIAC Catalog of Numeric Data Packages and Computer Model Packages*, T.A. Boden, F.M. O'Hara Jr., and F.W. Stoss. ORNL/CDIAC-62, ESD Publ. No. 4008, Oak Ridge, Tennessee.
- Waters, E.R., and B.A. Schaal. 1991. No variation is detected in the chloroplast genome of *Pinus torreyana*. *Canadian Journal of Forest Research* 21: 1832-1835.
- Wiles, G.C., R.D. D'Arrigo, and G.C. Jacoby. 1995. Modeling North Pacific temperature and pressure changes from coastal tree-ring chronologies. Pages 67-78 in *Proceedings of the Eleventh Annual Pacific Climate (PACCLIM) Workshop*, C.M. Isaacs and V.L. Tharp (eds), Interagency Ecological Program, Technical Report 40. California Department of Water Resources, Sacramento.



# Tree-Ring Reconstructions of Winter Climate and Circulation Indices for the Southwestern United States

---

Connie A. Woodhouse

## Introduction

---

A key to understanding the causes for climate variability lies in understanding how atmospheric circulation influences regional climate. The goal of this research is to investigate the long-term relationships between atmospheric circulation and winter climate in the southwestern United States. Patterns of atmospheric circulation are described by circulation indices, and winter climate is defined as number of days with precipitation and mean maximum temperature for the winter wet season, November through March. Records of both circulation indices and climate variables were reconstructed with tree-ring chronologies for the period 1702-1983. The years of the highest and lowest values of circulation indices and climate variables were compared in order to investigate possible spatial and temporal relationships between extremes in circulation and climate.

## Circulation Indices and Reconstructions of Indices

---

In previous research (Woodhouse, in review), I identified some key circulation features influential to climate for the period of instrumental climate records. A set of circulation indices was compiled that described important circulation features, including the Southern Oscillation Index (SOI), a sea surface temperature (SST) index from the equatorial Pacific, a modified Pacific/North American (PNA) index, and two indices that feature a southwestern low pressure center: the Pacific High/Southwestern Low (PHSWL) and the Southwestern Trough (SWTROF) indices (Table 1). The last three indices were derived specifically for this study. Relationships between circulation, as described by the indices, and climate at a network of stations were then examined. To summarize briefly, negative SOI, SWTROF, and PHSWL values and positive SST and PNA values tend to correspond to wet, cool conditions in the Southwest, while positive SOI, SWTROF, and PHSWL values and negative SST and PNA values tend to correspond to warm, dry conditions.

---

In: C.M. Isaacs and V.L. Tharp, Editors. 1997. *Proceedings of the Thirteenth Annual Pacific Climate (PACLIM) Workshop, April 15-18, 1996*. Interagency Ecological Program, Technical Report 53. California Department of Water Resources.

Table 1  
CIRCULATION INDICES

Index	Description	Source	Interval
SOI	Southern Oscillation Index-sea level pressure; Tahiti - Darwin	Climate Analysis Center (CAC)	Winter (Dec, Jan, Feb); Fall-Winter (Sep-Feb)
SST	Sea surface temperature from COADS data 4°N-4°S, 160°-80°W (1930-1979) 5°N-5°S, 190°-90°W (1980-1990)	Kiladis and Diaz (1989) CAC NINO3 index	Winter (Dec, Jan, Feb)
PNA-modified	Pacific North American patterns; a measure of zonality across North America. Location of pressure centers modified after Keables (1992) PNA3 pattern.  $\text{PNA} = 1/3[-Z^*(135^\circ\text{W}, 35^\circ\text{N}) + Z^*(100^\circ\text{W}, 75^\circ\text{N}) - Z^*(70^\circ\text{W}, 30^\circ\text{N})]$	Woodhouse, in press	Winter (Jan, Feb, Mar)
SWTROF	Southwestern trough; measure of intensity of low over the SW, in combination with high pressure over the Gulf of Alaska and the Great Lakes.  $\text{SWTROF} = 1/3[-Z^*(140^\circ\text{W}, 50^\circ\text{N}) + Z^*(115^\circ\text{W}, 35^\circ\text{N}) - Z^*(80^\circ\text{W}, 45^\circ\text{N})]$	Woodhouse, in press	Winter wet season (Nov-Mar); Early/late winter (Nov, Dec, Mar)
PHSWL	Pacific high/southwestern low; measure of intensity of low over the SW, in conjunction with the longitudinal position of the Pacific high.  $\text{PHSWL} = Z^*(115^\circ\text{W}, 35^\circ\text{N}) - \text{longitude of the greatest 500mb height @ } 30^\circ\text{N}, 120^\circ\text{-}160^\circ\text{W}$	Woodhouse, in press	Winter wet season (Nov-Mar); Early/late winter (Nov, Dec, Mar)

\* Z=standardized 500mb height at each grid point.

A network of 86 tree-ring chronologies located in the Southwest was used to reconstruct the circulation indices, using the technique of principal components regression (Fritts 1976; Cook and Kairiukstis 1990). The 86 tree-ring chronologies were transformed into a set of 12 principal component scores. Scores were lagged forward and back one year. This set of lagged and unlagged component scores comprised the set of 36 independent variables used in stepwise regression to reconstruct the circulation indices. Regression models explained from 26% (SST) to 78% (SWTROF, November-March average) of the variation in the circulation indices. Reconstructions were verified statistically and, where possible, validated with independent data. Reconstructed indices extended from 1702 to 1983.

## Climate Reconstructions

The same network of 86 tree-ring chronologies, with two additional ones, was used to reconstruct regional winter climate variables. Climate variables (number of days with precipitation and mean maximum temperature) were reconstructed for each of six regions (California coast; southeastern California and lower Colorado River basin; northern Arizona and New Mexico; southern/central Arizona; central Arizona and New Mexico; and southern Arizona and New Mexico) (Figure 1). As with the reconstructions of indices, a principal components regression technique was used, incorporating lagged and unlagged scores from a principal components analysis on the tree-ring chronologies to generate a set of independent variables for the stepwise regression models. Regression models explained 56-73% of variation in the series of number of precipitation days and 49-79% of variation in the temperature series. As above, reconstructions were verified statistically and validated with independent data.

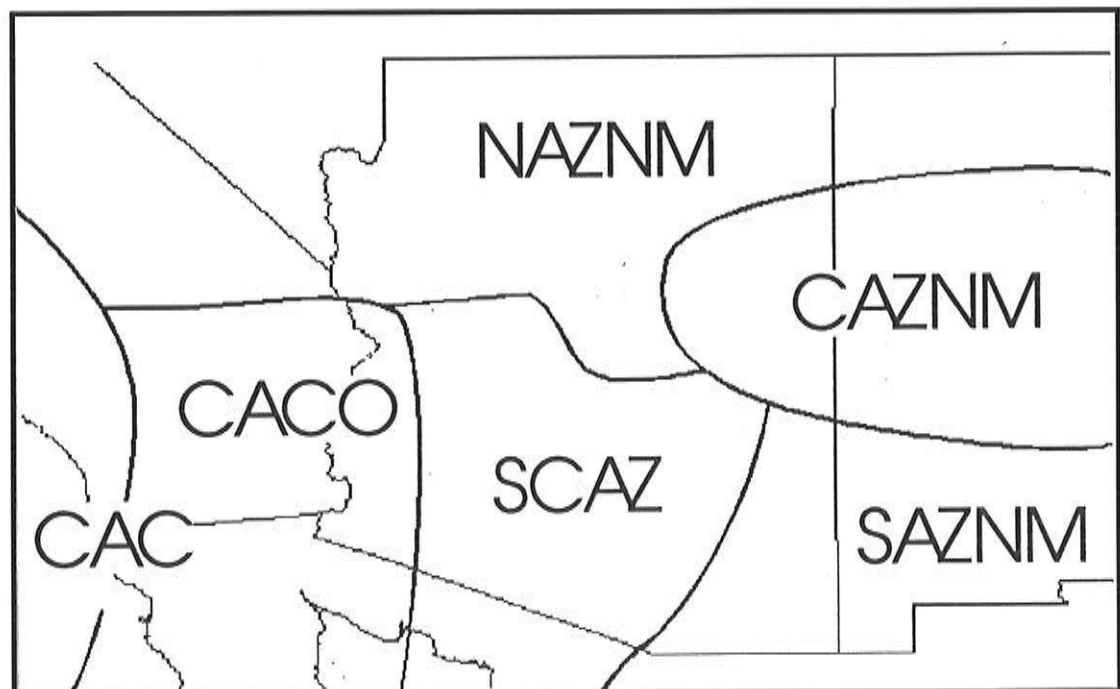


Figure 1 Location of climate regions used in reconstruction of regional climate series.  
CAC = California Coast  
CACO = California and lower Colorado River basin  
NAZNM = Northern Arizona and New Mexico  
SCAZ = South-Central Arizona  
CAZNM = Central Arizona and New Mexico  
SAZNM = Southern Arizona and New Mexico.

## **Principal Components Analysis of Reconstructed Circulation Indices**

A principal components analysis was performed on the set of reconstructed circulation indices. Three components resulted, explaining 83% of total variance and consisting of:

- SOI, SST, and PNA indices
- Two seasonal versions of the SWTROF index
- Two seasonal versions of the PHSWL index.

These groupings suggest that three types of circulation indices may be influential to climate in this area.

## **Time Series Plots of Years of Extreme Values**

Each reconstructed regional climate series and circulation index was ranked, and the years of the highest and lowest 20% of values were identified. Time series plots showing the years of these extreme values for each of the regional climate variables and indices were generated so that relationships could be assessed visually. Plots suggest that:

- For reconstructed numbers of precipitation days and temperature, although there were years of extreme values common to all regions, there were also years when only some of the regions had extreme values. For precipitation day extremes, the two eastern regions (CAZNM, SAZNM) appear to act separately most often. For temperature, the two California regions (CAC, CACO), as well as the two eastern regions, often show years of extreme values in common with each other but not with the other regions. This suggestion of an east/west diagonal division across the study area was also supported by an analysis of the groupings of regions for which the same set of five or more years of extreme values occurred. This split was much more pronounced for the precipitation day series than for the temperature series.
- For reconstructed indices, years of extremes for the SOI/SST/PNA indices occurred fairly consistently over the three centuries, but were most common from 1950 to 1970. Years of extremes for the PHSWL indices were concentrated in the late 1800s and into the 1900s, while years of extreme values for the SWTROF indices were more frequent in the late 1800s and early 1900s.
- Many of the years of extreme values of number of precipitation days and temperature series coincide with years of extremes in one or more of the circulation indices. In some cases, years of extreme values for several of three index types coincide with the same year of an extreme in a climate variable, but frequently only one index type coincided with a year of a climate extreme.

## Distribution of Years of Extreme Values by Century

The number of years of extreme values for reconstructed regional precipitation day and temperature series (Figure 2) and reconstructed circulation indices (Figure 3) was tabulated for each century. The percentage of years of extreme values per century was figured to allow for a comparison between centuries (since the 20th century record is not complete). The values were plotted to assess low-frequency changes in number of extreme values over the past three centuries.

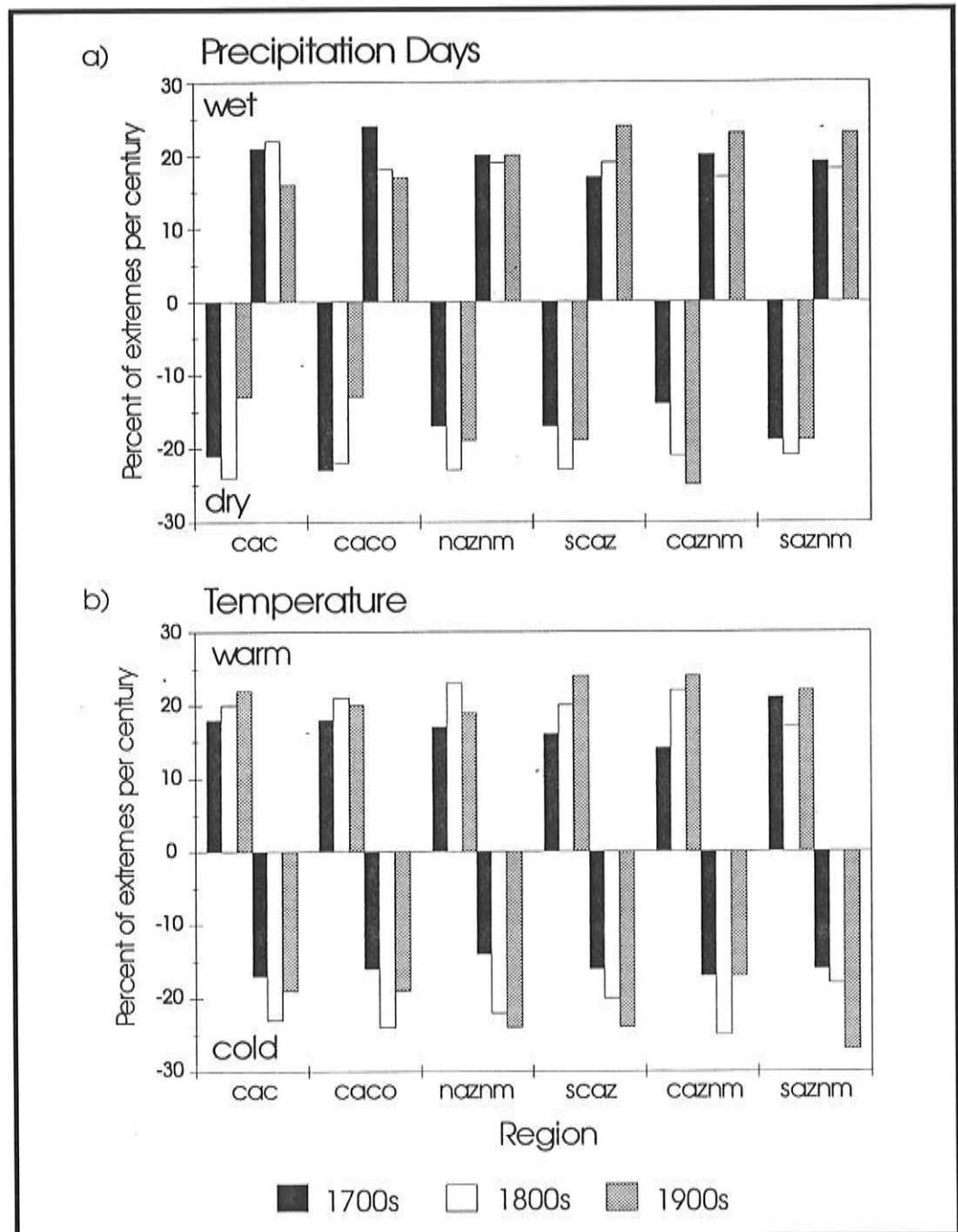


Figure 2 (a) Frequency of years of extreme values (upper and lower 20%) for precipitation day reconstructions. (b) Frequency of years of extreme values (upper and lower 20%) for temperature reconstructions.

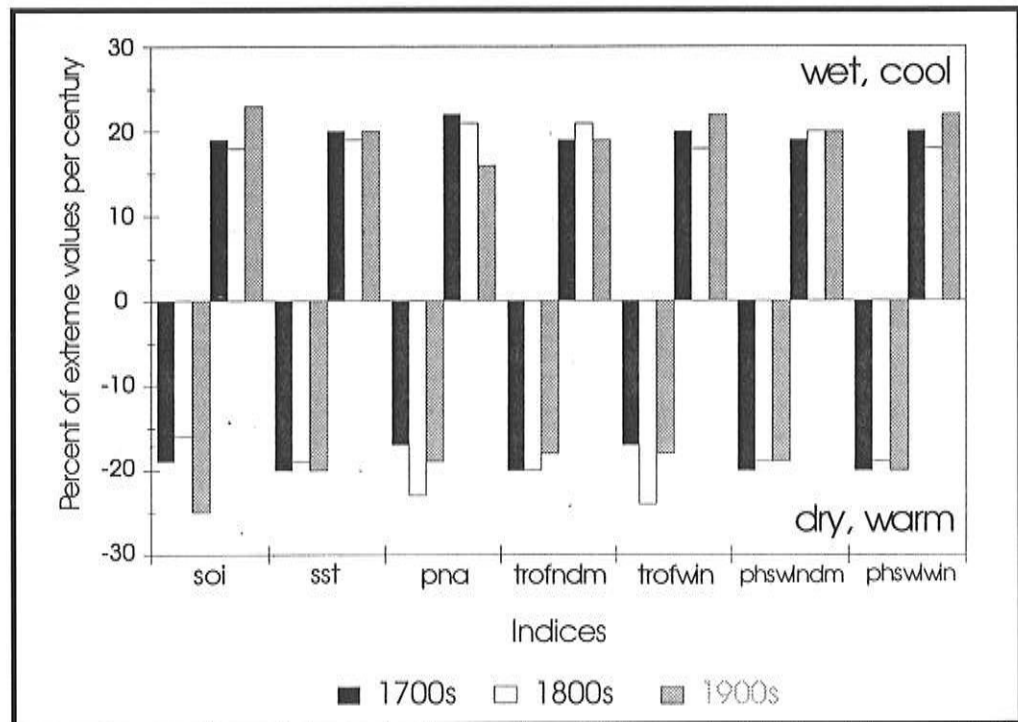


Figure 3 Frequency of years of extreme values (upper and lower 20%) for reconstructed indices. Indices are plotted in the sense that they represent wet/cool and warm/dry conditions.

Results suggest that:

- Years of positive (wet) precipitation day extremes have been more frequent in the 20th century in three eastern regions (SAZNM, CAZNM, SCAZ) but more frequent in the 18th and/or 19th centuries in the two California regions (CAC, CACO). Years of negative (dry) extreme values were also more prevalent in the 18th and especially in the 19th centuries in western and central regions (CAC, CACO, NAZNM, SCAZ).
- Years of warm temperature extremes were more frequent in the 20th century in most regions (except CACO, NAZNM), as were cold extremes in the central and southern regions (NAZNM, SCAZ, SAZNM). In the California regions, years of cold extreme temperature were more frequent in the 19th century.
- For the reconstructed indices, the number of years of extreme SOI values (both warm/dry and cold/wet extremes) is greater in the 20th century than in the previous two centuries. Years of PNA extreme values were more numerous in the previous centuries (18th and 19th centuries for cold/wet extremes, 18th century for warm/dry extremes). Years of warm/dry extremes for the TROF (November-March average) index were more prevalent in the 19th century.

## Summary

---

Reconstructions of regional climate variables (number of days with precipitation and mean maximum temperature) and circulation indices have been produced for the period 1702-1983. A principal components analysis on the reconstructed circulation indices identified three groupings of indices: SOI/SST/PNA indices, SWTROF indices, and PHSWL indices.

An examination of the years of the highest and lowest 20% of values for the climate reconstructions suggests that distribution of years of extreme values has been spatially and temporally variable over the past three centuries. The distribution of years of index extremes has been temporally variable as well.

An analysis of the frequency of years of extreme values by century suggest some possible links between climate extremes and circulation index extremes. The coincidence of an increase in years of SOI extremes in the 20th century and an increase in years of precipitation day extremes in the eastern part of the study area implies a possible relationship, especially during years of wet extremes. A higher frequency of years of warm temperature and low precipitation day extremes in some of the central regions (especially NAZNM) in the 19th century coincides with an increased number of years of warm/dry extremes in the Southwestern trough index, also in that century, suggesting a link. Further research may help elucidate these relationships.

## Acknowledgement

---

This study was funded by the National Biological Service, Agreement CA-8012-2-9001

## Literature

---

- Fritts, H.C. 1976. *Tree Rings and Climate*. Academic Press, New York, 286 pp.
- Cook, E.R., and L.A. Kairiukstis. 1990. *Methods of Dendrochronology: Applications in the Environmental Sciences*. Kluwer Academic Publishers, Dordrecht, 394 pp.
- Kiladis, G.N., and H.F. Diaz. 1989. Global climatic anomalies associated with extremes of the Southern Oscillation. *Journal of Climate* 2:1069-1090.
- Woodhouse, C.A. In review. Winter climate and atmospheric circulation patterns in the Sonoran Desert region, U.S.A. *International Journal of Climatology*.



# The Near-AD 1600 Multi-Proxy Puzzle

Franco Biondi, Carina B. Lange, Malcolm K. Hughes, and Wolfgang H. Berger

**Abstract.** A varve chronology with annual resolution (AD 1117–1992) has been developed recently for Santa Barbara Basin. Varve thickness and water content show an exponential trend consistent with expected patterns in the presence of sediment compaction over time. Annual varve thickness was decomposed into orthogonal components using singular spectrum analysis (SSA) to identify and retrieve inter-decadal oscillations. The first eight SSA eigenfunctions (EOFs) form four oscillatory pairs with periods of ~100, ~58, ~25, and ~12 years respectively, all of them statistically significant. The oscillatory signals retrieved from the marine varves show an abrupt change in frequency and amplitude near AD 1600. The largest contribution to this environmental shift is given by the interdecadal components, the ~25 and the ~12-year oscillation. This suggests a connection with global-scale decadal cycles identified in the subtropical Pacific gyre circulation and, possibly, with solar-driven phenomena. The near-1600 AD event coincides with (a) a similarly sudden change of state in nearby Santa Monica Basin that triggered the onset of anoxic conditions and the preservation of laminated sediments, (b) an extreme drought over the American Southwest, (c) a transformation of the age structure in a number of forest populations throughout Arizona and New Mexico. Total organic carbon burial flux in Santa Barbara Basin varves also shows a marked change after AD 1600. A possible climatic link is proposed that involves pathways for moisture transport in the Southwest at decadal and longer time scales.

## Introduction

High-resolution laminated systems, which include annual couplets in varved marine or freshwater sediments, dust layers within glacial ice, tree rings, and coral bands, are particularly effective in preserving climatic signals at multiple temporal scales through their response to the annual cycle (Baumgartner *et al* 1989). Oceanic basins where varved sediments are presently accumulating are characterized by oxygen-deficient water in contact with the sea floor, because anoxic conditions inhibit the development of benthic communities that would destroy the laminated structure by bioturbation (Calvert 1966). The most extensive and least disturbed record of modern annual varves in the North Pacific is in the central Santa Barbara Basin. Santa Barbara Basin is the northernmost basin of the Southern California Borderland Province, which includes a number of semi-enclosed tectonic basins marked by limited deep-water exchange with the Pacific Ocean (Emery 1960). Santa Barbara Basin is the only such basin that exhibits persistent annual varves (light/dark laminations) throughout the Holocene. Sedimentation rates are of the order of 100 cm/1,000 years and are controlled by a combination of terrigenous sediment supply, surface-water productivity, bacterial activity, and oxygenation of bottom water (Kennett *et al* 1994). The Santa Barbara Basin varve record is an accurate recorder of climate change

---

based on variation in varve thickness, stable isotopes, planktonic microorganisms, sardine fish scale abundance, and other biomarkers (Dunbar 1983; Lange *et al* 1990; Baumgartner *et al* 1992; Schimmelmann *et al* 1992; Lange and Schimmelmann 1994, 1995; Kennett *et al* 1995; Grimm *et al* 1996).

It has been suggested that large climatic shifts have occurred in the past — and may well do so in the future — with transitional periods of only a few decades (Dansgaard *et al* 1993). The sensitivity of Santa Barbara Basin to regional and global changes in climate and the permanent mark that such perturbations leave in the basin's marine sediments have allowed the identification of climate-driven fluctuations in ocean circulation during the past 60,000 years in the North Pacific region that are synchronous with those of the North Atlantic (Behl and Kennett 1996; Kennett and Ingram 1995; Keigwin 1995). With the goal of investigating abrupt and long-lasting environmental changes recorded in Santa Barbara Basin, we present here the inter-decadal variability contained in the varve record over the last millennium. By restricting our focus to this particular frequency band, we emphasize phenomena well within the human life span as a possible aid to long-range forecasting of climatic change.

When dealing with noisy datasets of limited length, singular spectrum analysis (SSA) provides a reliable measure of the information content of a discrete time series at different frequencies (Vautard *et al* 1992). SSA is among the nonlinear mathematical models currently used to search for underlying deterministic properties of climatic and paleoclimatic time series and to investigate the inherently chaotic dynamics of Earth's systems at different time scales (Vautard and Ghil 1989; Tsonis *et al* 1994). As a data-adaptive technique of series decomposition into orthogonal components, SSA has been successfully employed to identify and retrieve low-frequency variability and trends (Ghil and Vautard 1991; Allen and Smith 1994) as well as periodic and quasi-periodic oscillations (Keppenne and Ghil 1992; Ghil 1994; Dettinger *et al* 1995a). In this paper, we apply SSA to the Santa Barbara Basin varve record to separate signal from noise, identify the leading oscillatory modes, and reconstruct their time-varying strength as an indicator of past oscillatory spells.

Oscillations identified in the varve record are compared to published evidence of abrupt events identified in nearby Santa Monica Basin and in forest ecosystems of the American Southwest. Additional unpublished data on total organic carbon burial flux in Santa Barbara Basin varves are also presented. A possible coupling mechanism between oceanic and atmospheric circulation at decadal scales is outlined, based on pathways of moisture transport from the tropics to the American Southwest.

## Varve Record

We used X-radiography of sediment slabs for documenting the sediment structure, for varve counting, and for cross-correlating with previously collected Santa Barbara Basin cores (Lange and Schimmelmann 1995). A complete set of X-radiograph contact prints and negatives that spans the period AD 1100-1993 is kept on file at the Geosciences Research Division, Scripps Institution of Oceanography. A dark band on an X-radiograph contact print indicates strong absorption of X-rays due to relatively higher density of terrigenous mineral content of a particular sediment layer (winter to early spring subannual lamina); more porous subannual laminae, relatively poor in minerals, appear lighter in the X-radiograph contact print (summer deposition of biogenic material). The dark and light laminae pairs represent single years of deposition and are regarded as annual varves (Soutar and Crill 1977). Varves are counted from top to bottom of a slab on each contact print and the varve thickness is measured to the nearest 0.1 mm using a hand lens with an integrated scale. Varve thickness is the mean of two measurements taken near the left and right margins of an X-radiograph contact print. The final chronology is averaged over two to three separate cores taken from different sites within the deepest portion of the basin (Figure 1; Schimmelmann *et al* 1990; Lange and Schimmelmann 1995; Lange *et al* in press).

Soutar and Crill (1977) constructed the original varve chronology for Santa Barbara Basin, AD 1820-1970. In subsequent publications (Schimmelmann *et al* 1990, 1992; Lange and Schimmelmann 1995;

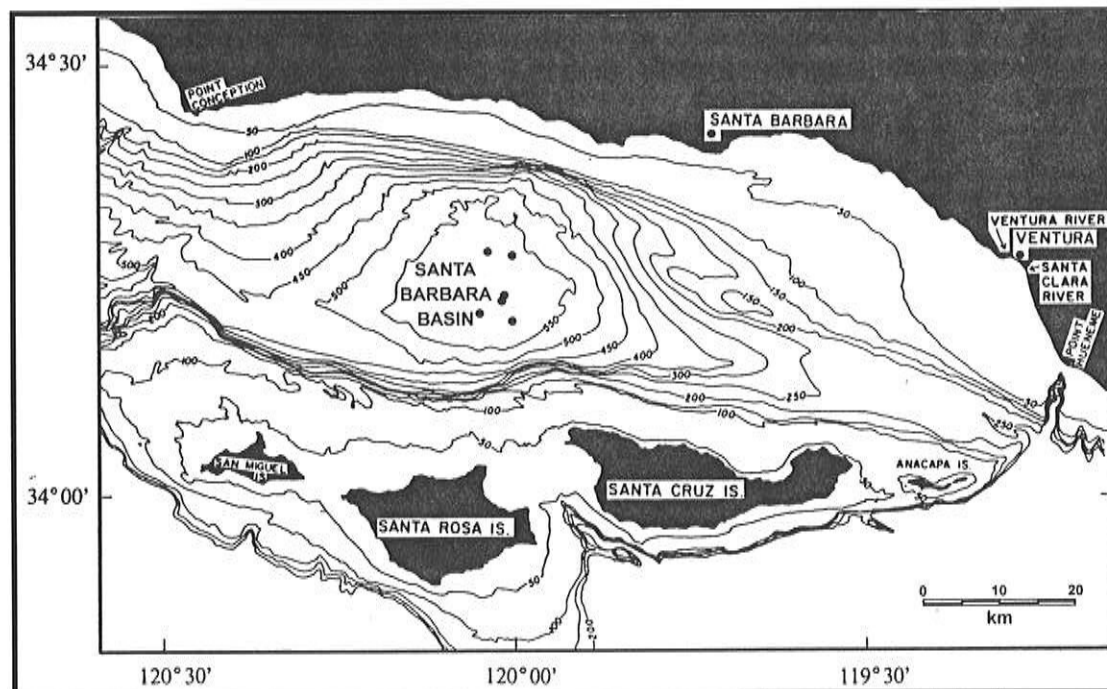


Figure 1. Varve collection sites (●) and bathymetry (thin lines, 50-m contour interval) of Santa Barbara Basin. Land masses (solid black) encompassing the basin are the Southern California Coast to the north and the Channel Islands to the south.

---

Schimmelmann and Lange, in press) the original chronology has been revised and extended to about AD 1400. We have recently obtained additional X-radiographs of high quality from three sediment cores located in the southeastern area of the central basin at depths greater than 580 meters. The revised chronology presented here, AD 1117-1992, is based on our detection and discounting of thin gray layers that may lead to faulty varve counts, as well as on varve count comparisons and cross-matching among the three new cores and those collected at various times since 1985 (Figure 1). We estimate the accuracy of the time scale to be  $\pm 1$  year for the last century and  $\pm 2$  years down to AD 1800. Dating accuracy deteriorates with sediment depth, but calendar year assignment most likely remains within  $\pm 10$  years at AD 1100. This error level is still negligible compared to the accuracy of most paleoclimatic time series derived from marine sediments and subjected to interpolation to obtain the equally-spaced time intervals required for statistical processing (Yiou *et al* 1994).

Pore-water content was determined according to the procedure described by Schimmelmann *et al* (1990). Sectioned samples of 1-2 mm intervals were weighed wet and then re-weighed with a precision of  $\pm 0.2$  mg after freeze-drying to calculate pore-water content. Pore-water content, reported in percent dry weight on a salt-free basis, is influenced by many factors, such as mineral composition, grain size distribution, and organic matter constituents. X-radiograph images were used in combination with water content determinations to assign precise dates to the sectioned sample intervals. Because of changes in varve thickness, samples used to compute water content could refer to a single year or parts thereof or to multiple years, and certain years could be covered by more than one sample or by no sample at all. Hence, the yearly varve water content was given by the average of all water content samples covering that year. Years covered by no sample were considered missing.

## **Time Series Methods**

---

Singular spectrum analysis is a form of principal component analysis applied to the autocovariance matrix of the time series (Vautard and Ghil 1989). The matrix dimension ( $M$ ) is called "window length" or "embedding dimension". Because SSA concentrates in the first one or two components all variability on time scales longer than the window length, it is also possible to filter a time series for selected frequencies simply by changing  $M$  (Vautard *et al* 1992). SSA requires no curve fitting or prewhitening, nor does it rely on prescribed sines and cosines to identify periodic behavior. Rather, SSA gives the principal axes of an  $M$ -dimensional sequence of vectors obtained by progressively lagging the original time series up to lag  $M$ . As classical principal component analysis (Preisendorfer 1988), SSA provides the amount of variance explained by

each orthogonal component, whose time-varying strength and phase can be computed in the same units as the original series (Dettinger *et al* 1995b). Because of this, Vautard and Ghil (1989) used SSA to identify intermittent oscillations in  $\delta^{18}\text{O}$  series from deep-sea sediment cores. SSA decomposition assumes that the process under study is at least weakly stationary, but results are robust to deviations from the stationarity assumptions (Vautard *et al* 1992).

We employed SSA as a nonlinear trend-removal algorithm to account for the non-climatic exponential increase of varve thickness and water content with decreasing sediment age. Because SSA does not allow missing observations, missing water content values were estimated by means of cubic spline interpolation (de Boor 1981). The definite integrals of the spline over each year were constrained to equal the observed annual totals (SAS Institute 1993). An SSA window length of 150 years was selected to isolate inter-decadal oscillations from lower-frequency signals. Given the length of our record ( $N=876$  years) and the minimum number of replicates needed to compute the eigenspectrum, it is customary to limit the window length to less than  $N/3$  (Vautard *et al* 1992). Lowering the cut-off time to 130 and 110 years had little impact on the results.

The overall time-series trend identified by the combination of slow-varying SSA eigenfunctions was compared to a natural exponential function,  $y = \alpha e^{\beta x} + k$ , where  $y$  is varve thickness,  $\alpha$  and  $\beta$  are the exponential parameters,  $x$  represents years, and  $k$  is the horizontal asymptotic value of  $y$ . Least squares estimates of the parameters were obtained using the Marquardt iterative method (Marquardt 1963), which regresses the model residuals onto the partial derivatives of the model with respect to the parameters until the estimates converge (SAS Institute 1990). The overall trend was subtracted from the raw data to obtain detrended time series, which were then SSA-processed for identifying significant oscillatory modes. Signal-to-noise separation of the eigenspectrum was performed according to significance tests based on red-noise assumptions and Monte Carlo simulation (Allen and Smith 1994, *in press*; Breitenberger *in press*; Dettinger *et al* 1995a). Oscillatory modes were identified by eigenvalue pairs whose EOFs were in quadrature with each other and whose principal components had a single power peak of the same frequency (Vautard *et al* 1992). The time-varying strength of the reconstructed components — series of length  $N$  corresponding to a given set of eigenelements — highlighted location and duration of oscillatory spells (Keppenne and Ghil 1992).

---

## Results

---

The exponential trend for annual thickness ( $y = 0.00003e^{0.00565x} + 1.2638$ ) and for water content ( $y = 0.00072e^{0.00515x} + 63.6674$ ) were monotonically increasing (Figure 2). As explained in the following paragraphs, the exponential trend fitted to the water content effectively removes all variability at periods longer than 150 years, thereby suggesting that dewatering is responsible for the exponential-type decrease in varve thickness with increasing sediment age. Even though the high-frequency variability of the water content may contain climatic signals, ascribing its overall exponential trend to sediment compaction is consistent with studies of depositional processes in marine basins (Hamilton 1976; Cowie and Karner 1990; Audet 1995). There is no evidence for a trend or a discontinuity in the variance of the water content, hence dewatering cannot be responsible for the sudden change in variability seen in the varve thickness series. The water content per unit thickness (Figure 2) had a monotonically decreasing trend ( $y = -0.00028e^{0.00351x} + 0.528$ ), which suggested that compaction not only lowered water percentage and sediment thickness, but also reduced porosity, thereby diminishing the water percentage per unit thickness over time.

A total of 168 water content values, which were missing in the observed series, were estimated prior to singular spectrum analysis. In each varve series — water content, thickness, and their ratio — variability on time scales longer than 150 years was concentrated in the first two SSA components. The sum of the first two reconstructed components quantified the overall trend and followed closely the non-climatic exponential trend, with the notable exception of a sinusoidal swing in varve thickness from about 1600 to about 1900 (Figure 2). Pairs of residual series obtained by exponential and SSA detrending were highly correlated ( $r \geq 0.92$ ). The exponential trend effectively removed all variability with periods longer than 150 years from the water content series but not from the other two series. In other words, water content was the only variable to behave strictly as if its rate of change at a particular time was proportional to the amount of the variable at that time. Because of our interest in higher-frequency oscillations, the trend was subtracted from the raw data, and because the exponential trend did not account for low-frequency variability in every variable, only the SSA-detrended series were considered for further analysis. After detrending, identification of oscillatory modes was limited to the varve thickness series to avoid the risk of numerical artifacts introduced by estimation of missing values in the water content series.

The hypothesis that the detrended varve record was purely a red-noise series was rejected by Monte Carlo simulation. A total of 2500 surrogate red-noise time series were randomly generated according to the following first-order autoregressive, or AR(1) model fitted to the varve thickness series:

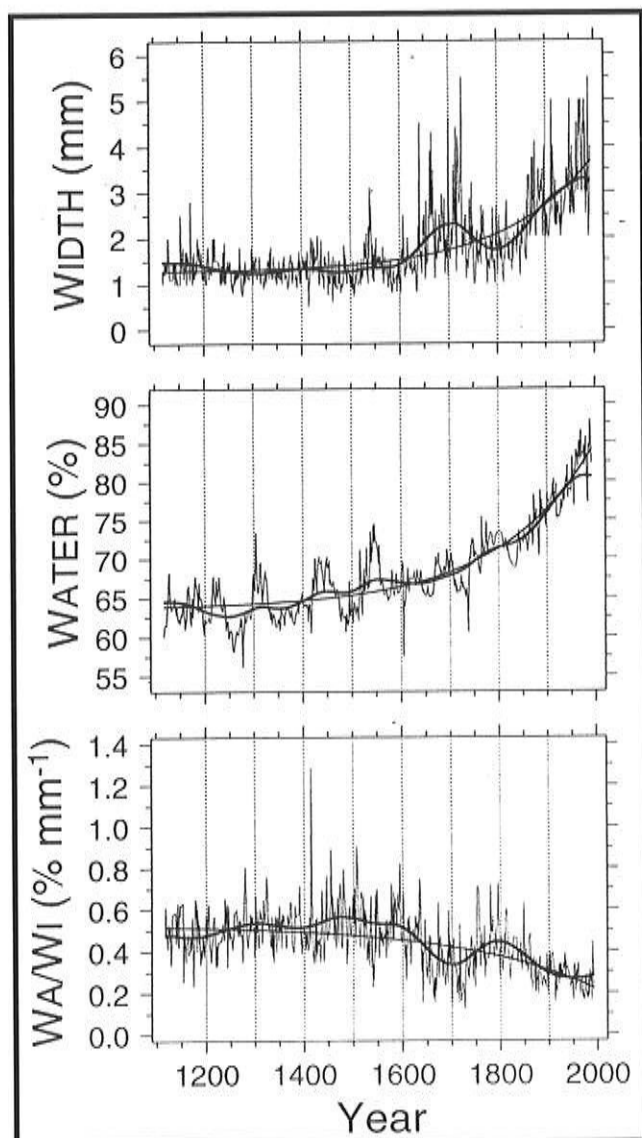


Figure 2. Annual varve width, water content and water content per unit width (Wa/Wi) in Santa Barbara Basin, AD 1117-1992. The reconstructed SSA components with periods longer than 150 years (heavy solid line) can be compared with a natural exponential function (monotonic solid line).

$$y_t = 0.3307 y_{t-1} + 0.4834 \varepsilon_t$$

with  $\varepsilon_t$  being an independent, standard normal forcing. The first seven eigenvalues were significant at the 99% level, and eigenvalues eight and nine were significant at the 90% level (Figure 3). Because we used two-sided confidence intervals, the first seven eigenvalues fell in the upper 0.5% of the Monte Carlo distribution. Simulation using 100 surrogate time series gave very similar results. The combination of the first nine eigenvalues of the varve series is equivalent to a low-pass filtered version ("Signal") of the detrended series (Figure 4). The signal series summarizes nonlinear oscillations whose period is shorter than 150 years and that are significant under red-noise assumptions. As defined, the signal accounts for 25% of the total variance; the remaining components (75% of the variance) are indistinguishable from autocorrelated noise.

The signal series highlighted a change in time series properties near AD 1600. This shift was also visible in the original (Figure 2) and in the detrended (Figure 4) varve thickness, as a combination of higher variability and higher frequency in the recent half of the record. No similar shift was visible in the water content or in the water to thickness ratio (Figure 2). The maximum entropy spectrum (Penland et al 1991; Figure 5) of detrended thickness is smooth and dominated by red noise, whereas the signal series

has three sharp spectral peaks, the highest of which corresponds to 12-year oscillations. Another sharp peak occurs at 25-year periods, and the third one is centered on the 76-year period, but with power densities greater than one spanning the 65- to 92-year interval. Each leading eigenvalue presents a single power peak, and the first eight eigenvalues are organized in four oscillatory pairs with frequencies of ~100, ~58, ~25, and ~12 years respectively (Figure 6). The strong quadrature of the first three pairs of EOFs is superior to the quadrature shown by EOFs seven and eight; EOF nine has the same ~12-year frequency as components seven and eight. The number of significant eigenvalues is well within the power of SSA, which is usually able to identify about  $M/10$  significant components before lumping oscillations together (Dettinger *et*

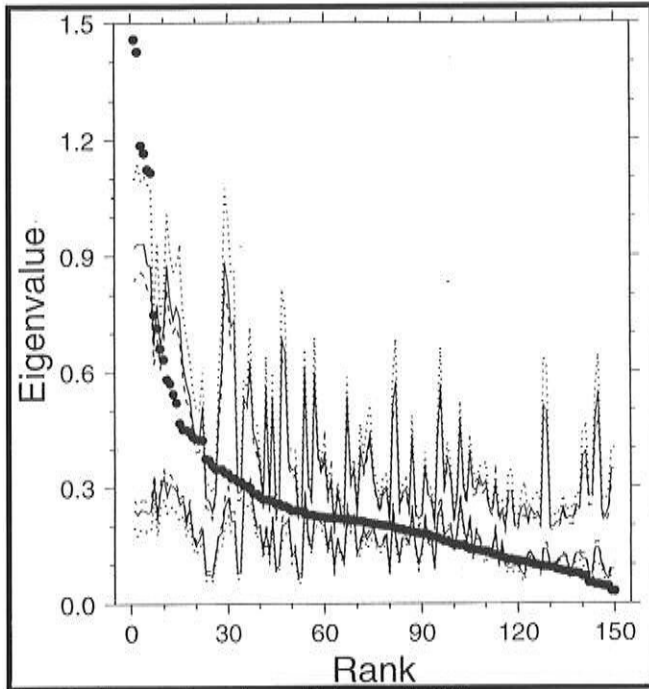


Figure 3. Eigenspectrum of varve thickness with 90% (dashed lines), 95% (solid lines), and 99% (dotted lines) confidence intervals computed from 2500 Monte Carlo simulations of red-noise surrogate series whose eigenspectra were projected against an SSA fixed basis.

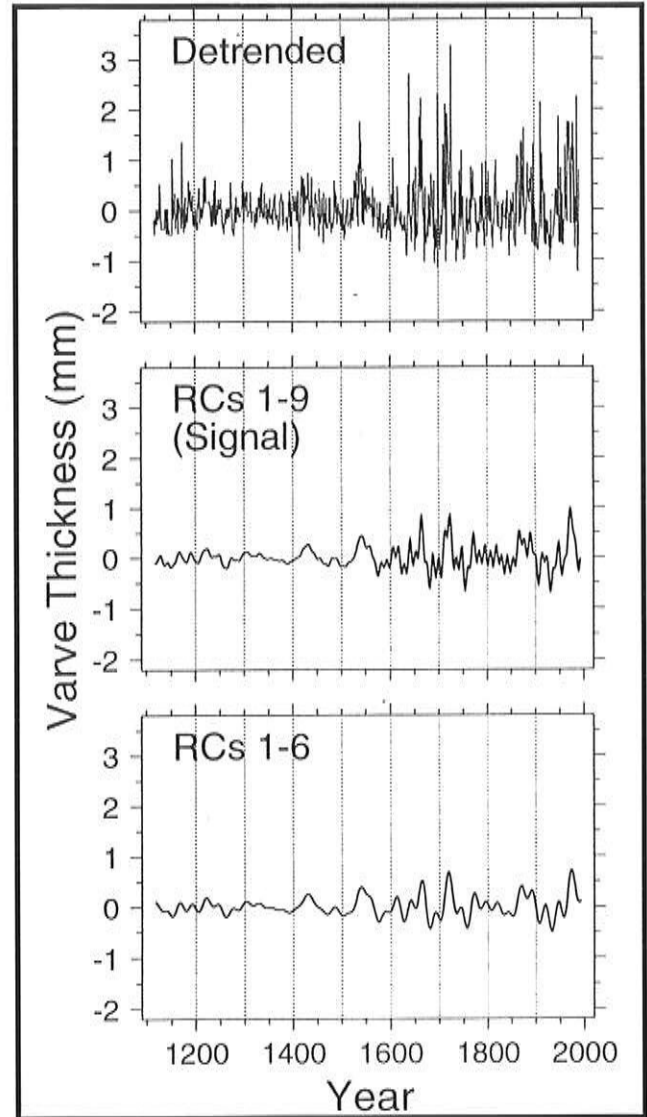


Figure 4. Detrended varve thickness and its filtered version obtained by adding the SSA components (RCs) 1 to 9 ("Signal") and 1 to 6.

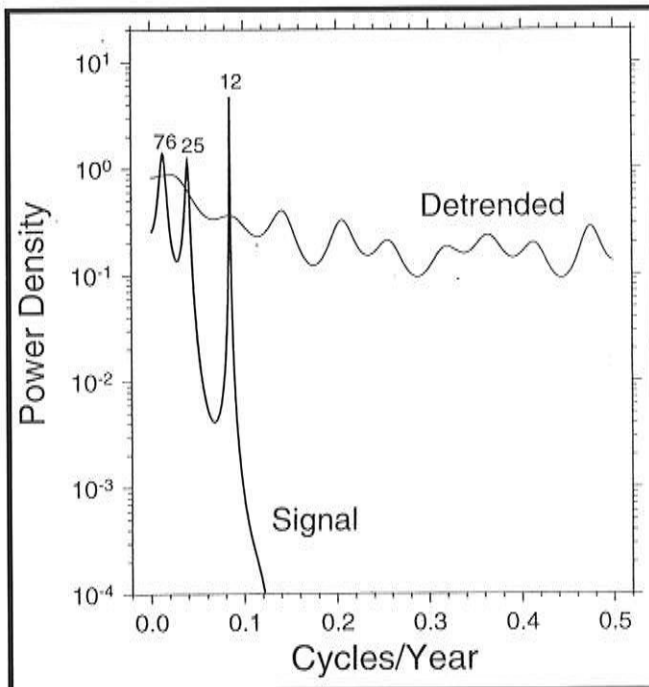


Figure 5. Maximum entropy spectrum of detrended varve thickness (thin line) and of its first nine eigenelements ("Signal", thick line; values below  $10^{-4}$  were ignored). The period (years) of spectral peaks greater than one is shown above each peak.

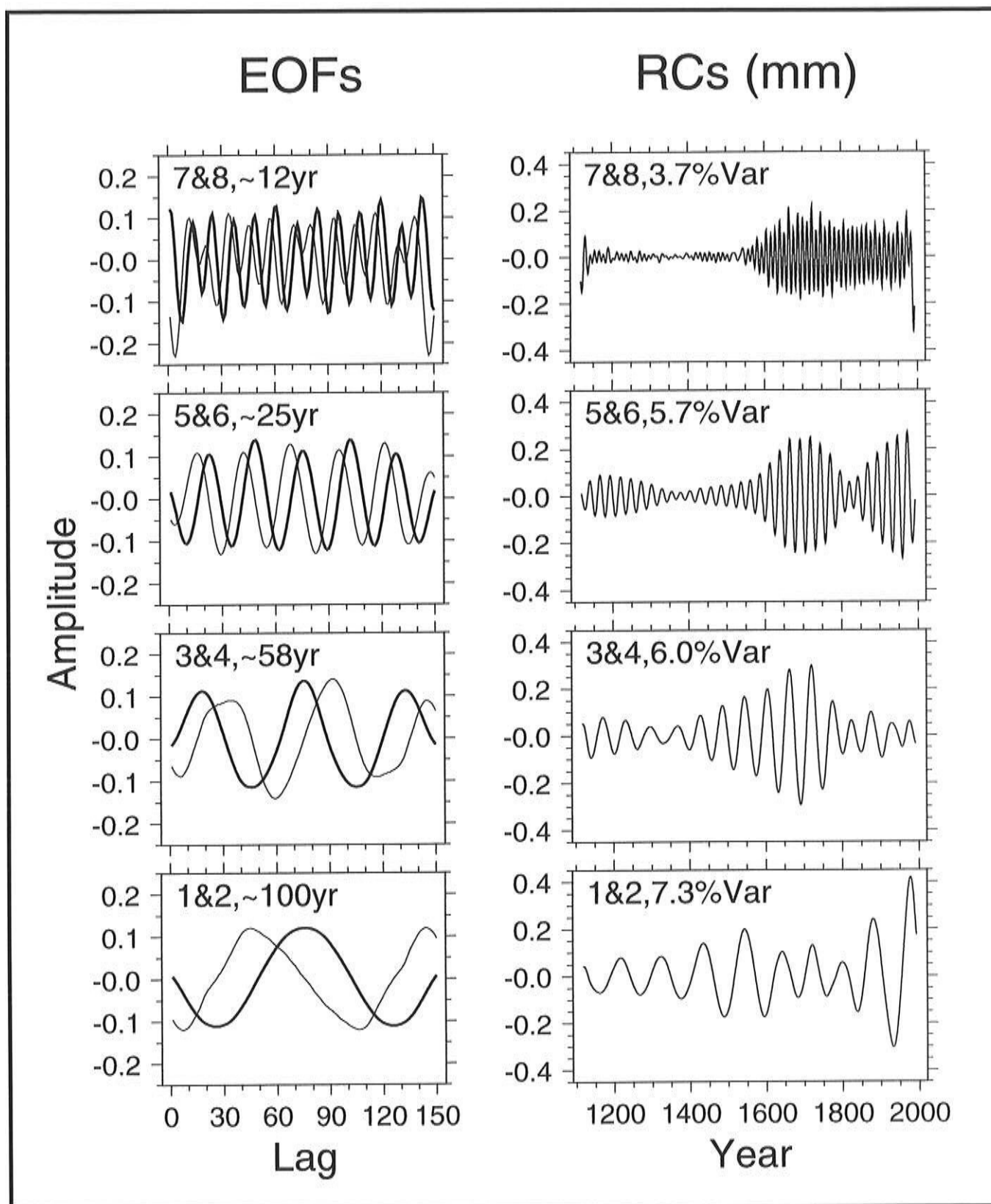


Figure 6. Leading SSA eigenfunctions of detrended varve thickness plotted by oscillatory pair (thick line: even-number eigenfunctions). The reconstructed components were combined by pair to show the time-varying strength of the nonlinear oscillatory modes identified in the varve record.

---

*al* 1995b). For  $M=80$ , oscillations with periods of ~58, ~25, and ~12 years are captured by EOFs 1&2, 3&4, and 7&8 respectively. Even though decadal-scale oscillations account for little variance when  $M=150$ , their identification is robust to changes in  $M$  with regard to the respective eigenvalue order and the shape of the eigenvector.

The time-varying strength of the four oscillatory modes (Figure 6) presents remarkable changes over time, especially at the interdecadal scale. The amount of variance explained by pair one to four is 7.3, 6.0, 5.7, and 3.7% respectively. The amplitude of ~100-year oscillations has increased over the last century, and the ~58-year mode reaches maximum intensity between AD 1600 and 1800, but the most dramatic changes involve interdecadal frequencies. The ~25-year and ~12-year oscillations are dampened and negligible before AD 1600, but have undergone much stronger swings since that time (Figure 6). The negative peak at both ends of RCs 7&8 is absent in the corresponding principal components. Component nine presents the same type of post-1600 shift as RCs 7&8. As indicated by the combination of reconstructed components one to six and one to nine (Figure 4), the shift in amplitude and frequency of the filtered varve series is more evident when the ~12-year oscillations are included.

## Discussion

---

The combined amplitude of the first nine SSA eigenelements of varve thickness highlighted a major, long-lasting, decadal-scale environmental shift in the marine sediments near AD 1600. The temporal location and duration of oscillatory spells in the Santa Barbara Basin record shows remarkable changes at the interdecadal scale. Interdecadal oscillatory modes were "turned on" around the end of the sixteenth century in a rather abrupt fashion, and have remained in an excited state until the present. In the following paragraphs, we argue that the near-AD 1600 event was not a local phenomenon, rather it was likely to have climatic implications. Evidence for the climatic sensitivity of the Santa Barbara Basin varves has already been published for both long (Kennett and Ingram 1995; Behl and Kennett 1996) and short (Soutar and Crill 1977; Lange *et al* 1990; Schimmelmann *et al* 1990, 1992) time scales.

As detailed in the Results, the time-series patterns of water content (Figure 2) do not support the hypothesis that sediment compaction was responsible for the abrupt change in the variance of the varve thickness. In other words, there is no evidence for a trend or a discontinuity in the variance of the water content, which appears smaller rather than larger in the most recent layers. The minimum varve thickness we measured (0.5 mm) is five times our measurement resolution, hence the change in variance over time cannot be an artifact caused by the measuring scale. With regard to the applicability of singular spectrum analysis to

nonstationary processes, one should consider that stationarity is defined by properties of the underlying process, which cannot be identified from a single realization of it (Myers 1989). In other words, it is impossible to say if the Santa Barbara Basin varve series is generated by a stationary process or not, even though the raw data appear “nonstationary”. As a result, the variability with periods greater than 150 years could be identified and removed, but it cannot be correctly ascribed, in whole or in part, to the trend of a nonstationary process or to ultra-low frequency oscillations of a stationary process.

At least two global physical mechanisms with interdecadal periodicity could be responsible for the Santa Barbara Basin varve patterns. First, the subtropical Pacific gyre circulation is characterized by a ~20 year cycle in the latitudinal distribution of heat content anomalies (Latif and Barnett 1994). The reconstructed strength of the ~25-year oscillatory mode could suggest that the Pacific gyre circulation was much more stable during the first half of the second millennium than in recent centuries. Second, solar irradiance is dominated by the 11-year cycle (Lean 1991) and recent studies have found a strong correlation between solar irradiance and Northern Hemisphere temperature anomalies from 1610 to 1800 (Lean *et al* 1995; Rind and Overpeck 1993). The ~12-year oscillatory mode found in the varve record is reminiscent of solar-driven phenomena, even though the relatively low statistical significance of the 12-year eigenvalues assigns modest influence to solar forcing. The near-absence of the 12-year oscillation before AD 1600 cannot be compared with reconstructed solar irradiance, whose record goes back to AD 1600 (Lean *et al* 1995). However, the absence of any relationship with the Maunder Minimum (AD 1645-1715) cautions against accepting solar variability as a controlling factor of the Santa Barbara Basin varve record. Interaction between the above-mentioned mechanisms cannot be ruled out: for instance, a small change in the phase of the North Pacific gyre interdecadal oscillation could greatly modify its resonance with the solar cyclic input, which in turn could either dampen or enhance the amplitude of decadal-scale oscillations.

A close relationship exists between changes in sea surface water temperature, oxygenation of bottom waters, and lamination of marine sediments in Santa Barbara Basin over the last 60,000 years (Kennett and Ingram 1995; Behl and Kennett 1996). If the near-AD 1600 shift visible in the last 1000 years of the Santa Barbara Basin varve record has any climatic relevance, it should be synchronous with similar long-lasting changes in nearby basins. Marine sediments from Santa Monica Basin, which lies just south of Santa Barbara Basin along the inner Continental Borderland of southern California (Emery 1960), also show a permanent change of state beginning at about AD 1600 (Christensen *et al* 1994). Since that time, the laminated structure of the sediments has been preserved, whereas it was destroyed by bioturbation in deeper, older

sediments. The onset of lamination — a proxy for near-anoxic conditions in bottom waters — occurs around AD 1600 in the deepest portion of the basin and has spread to increasingly lower depths ever since (Figure 7). This concurrence rejects the alternative explanation that decadal-scale oscillations in Santa Barbara Basin were modified by a local shift in sediment supply and storage, as would be produced, for instance, by eliminating a temporary reservoir for terrigenous sediment.

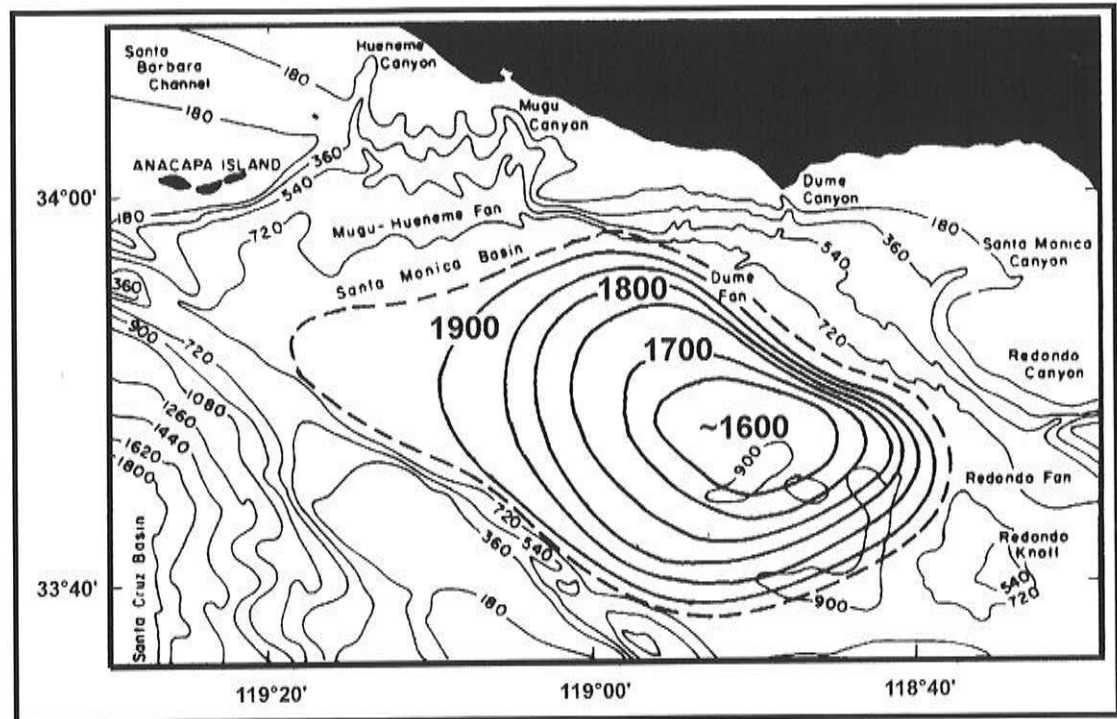


Figure 7. Bathymetry (thin lines, 180-m contour interval) and initiation time (thick lines, 50-year contour interval) of non-bioturbated sediments in Santa Monica Basin, California (modified from Christensen *et al* 1994).

Lange *et al* (1990) and Behl and Kennett (1996) have proposed that changes in the circulation off California are linked with the climate of the North Pacific by way of atmospheric forcing. If the Santa Barbara record is tied to large-scale atmospheric circulation in the North Pacific, then terrestrial proxy climatic records used to reconstruct atmospheric phenomena should contain a near-1600 marker in western North America. Tree-ring reconstructions of different hydrological variables for the American Southwest do show a near-AD 1600 extreme drought of decadal-scale duration (Stockton and Jacoby 1976; Rose *et al* 1982; Grissino-Mayer *in press*). The last quarter of the 1500s was characterized by extreme sustained drought in the Upper Colorado River Basin, in the Northern Rio Grande Climatic Division, and in the Sacramento River Basin (Meko *et al* 1995). Annual total flow of the Colorado River at Lee Ferry, Arizona (Figure 8) and of the Green River at Green River, Utah (Stockton 1976), annual total precipitation (July-July) in Northwestern New Mexico (Figure 9), and July Palmer Drought Severity Index (Figure 10) in Northern New Mexico all point to the years before AD 1600 as the period of most extreme drought over the Colorado Plateau during the

last millennium. The same negative peak is shown by a 50-year weighted average of tree-ring reconstructed November-to-May precipitation (AD 985-1970) for the Northwestern Plateau Climatic Division of New Mexico (D'Arrigo and Jacoby 1991).

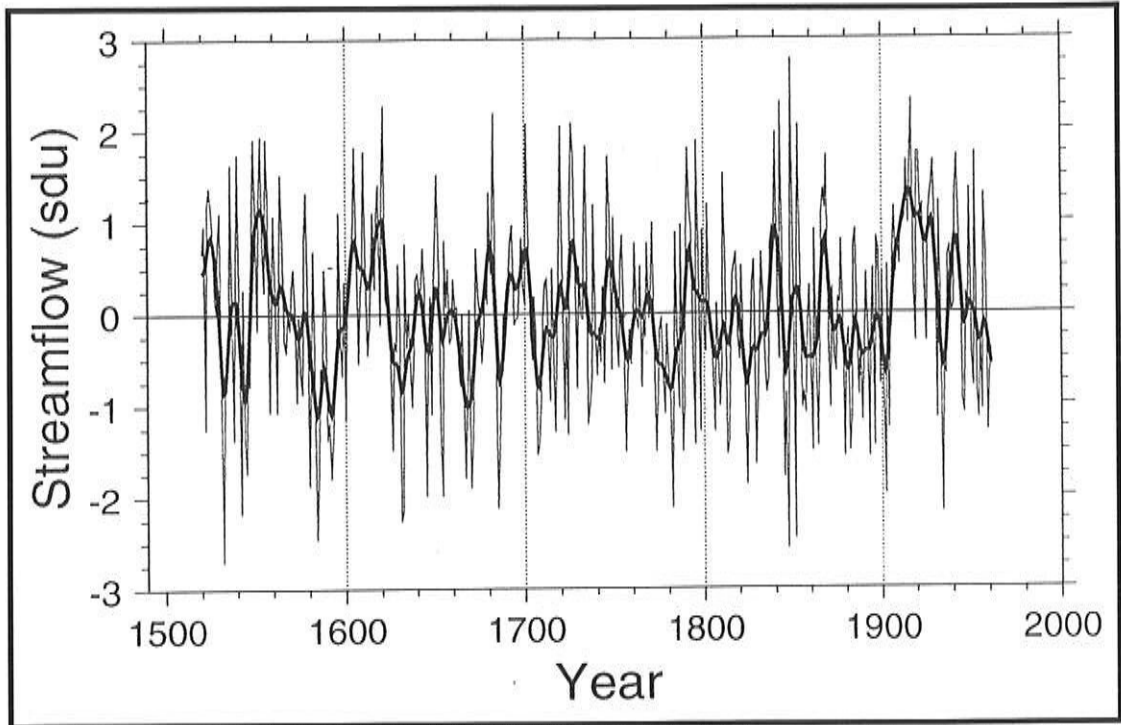


Figure 8. Tree-ring reconstructed Colorado River flow (1520-1961) at Lee Ferry, Arizona (modified from Stockton and Jacoby 1976). The annual series (thin line) is overlaid with a 10-year spline (thick line) to represent decadal-scale variability. sdu: standard deviation unit.

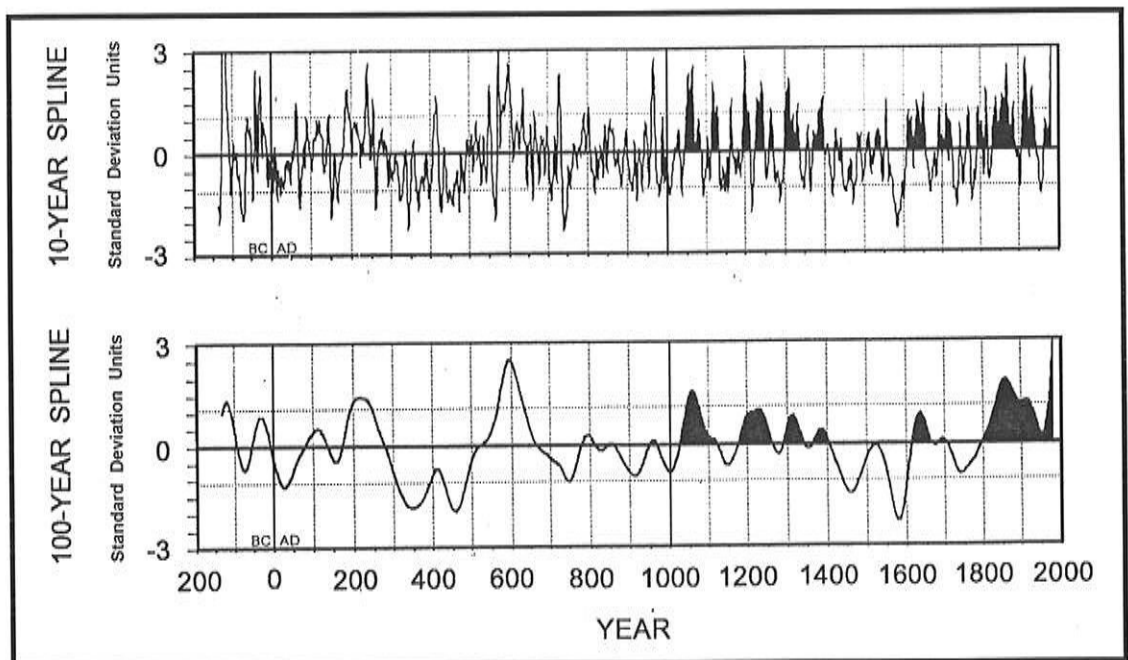


Figure 9. Tree-ring reconstructed annual (July<sub>t-1</sub> to July<sub>t</sub>) precipitation for northwestern New Mexico (modified from Grissino-Mayer, in press).

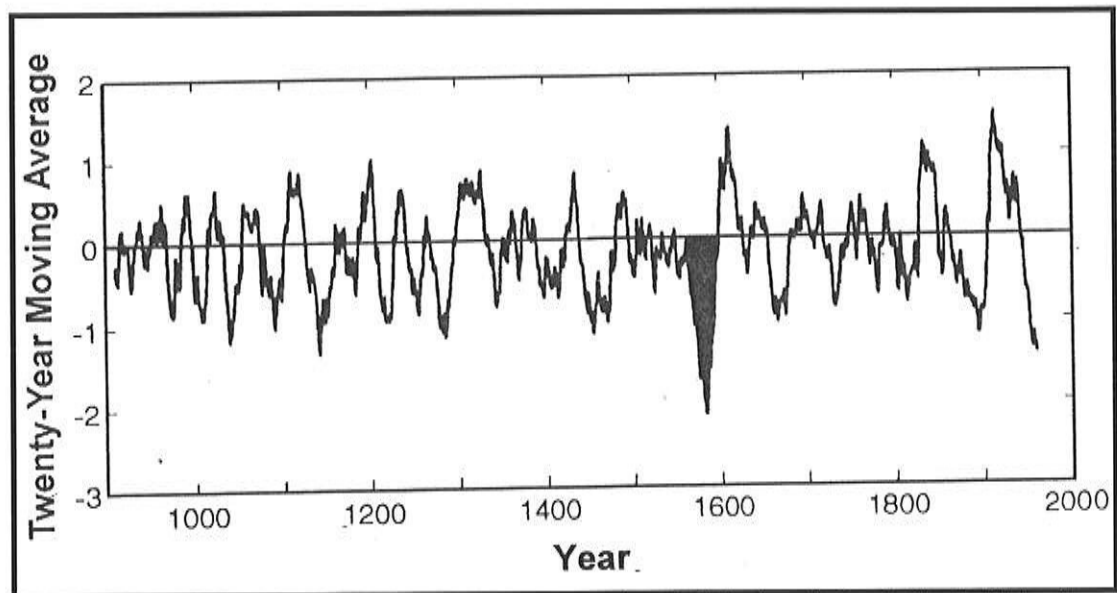


Figure 10. Tree-ring reconstructed July Palmer Drought Severity Index (900-1970), Northern Rio Grande Climatic Division, New Mexico (modified from Rose *et al* 1982).

At about AD 1600, near-shore basins off California entered and remained locked in a different state, but there is no evidence in the cited dendrochronological literature of a structural difference in the variability of the record before and after AD 1600. It is possible that terrestrial environments experienced extreme stress and then recovered, but it is also possible that the standardization methods used in tree-ring analysis for removing non-climatic variability (Cook and Kairiukstis 1990) may, to some degree, suppress changes in the amplitude of periodic and quasi-periodic oscillatory modes. Cook *et al* (1995) have discussed restrictions on the length of oscillations that can be reconstructed from tree-ring series. Those restrictions are less relevant when tree-ring chronologies are composed of several long (*ie*,  $\geq 150$  years) specimens, such as in the semi-arid southwestern United States, but the ability of tree-ring chronologies to reproduce changes in the amplitude of oscillatory modes has not yet been formally investigated. Work by Swetnam and Brown (1992) on tree age distributions in Arizona and New Mexico indicates a change of state in forest age structure. Based on a large number of sampled trees and sites, the population structure of three widespread coniferous species was greatly modified around AD 1600. Even though trees much older than 400 years exist, the vast majority of the old individuals still alive originated after AD 1580 (Figure 11), revealing a remarkable shift in age structure caused by either a decrease in mortality rates, an increase in regeneration rates, or both (Swetnam and Brown 1992). In turn, the difficulty in finding moisture-sensitive trees that originated before AD 1600 has constrained most tree-ring reconstructions (*eg*, Fritts 1976, 1991) to the last four centuries, making it even harder to detect any structural change in the amplitude of low-frequency oscillations.

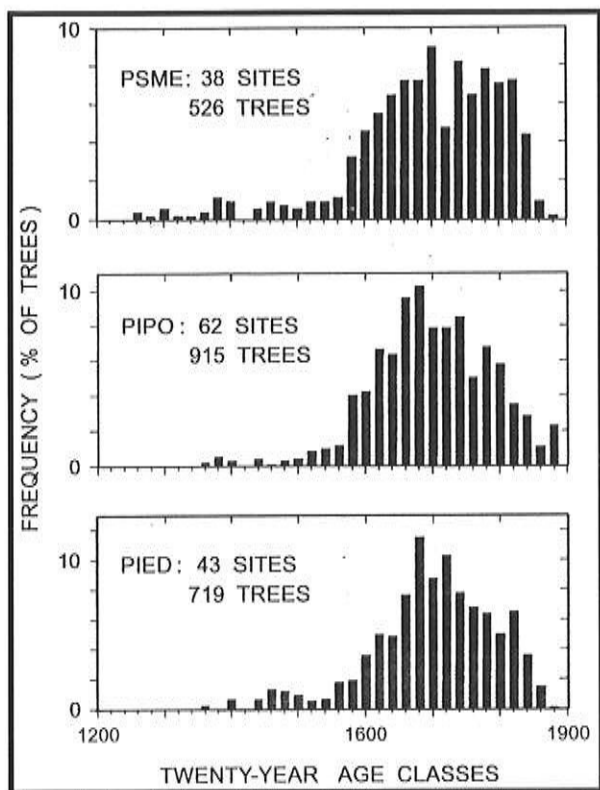


Figure 11. Age structure of old trees in Arizona and New Mexico, as derived from the innermost tree-ring date (modified from Swetnam and Brown 1992). Histogram bars are plotted on first year of age class (i.e. the 1600 bar represents the 1601-1620 age class). PSME: *Pseudotsuga menziesii*; PIPO: *Pinus ponderosa*; PIED: *Pinus edulis*.

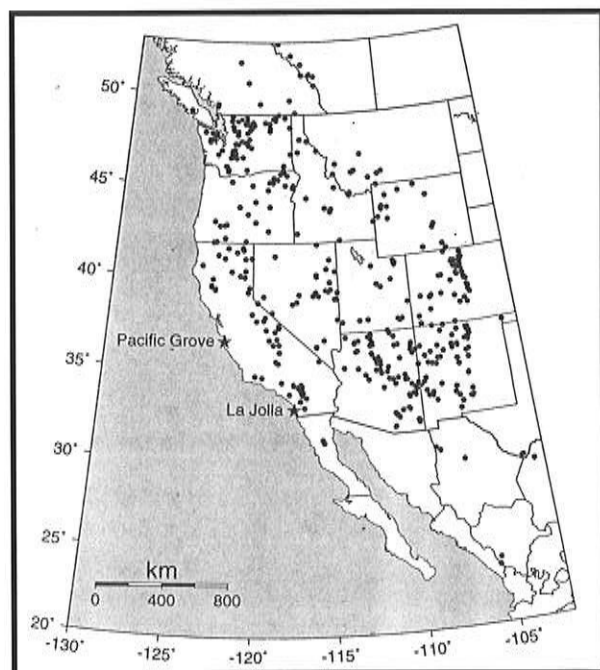


Figure 12. Location of 586 tree-ring chronologies (solid dots) for western North America (source: International Tree-Ring Data Bank, NOAA 1992) with respect to the coastal sea surface temperature stations of La Jolla (1917-1994) and Pacific Grove (1919-1994). All tree-ring chronologies begin before 1900 and end between 1960 and 1994.

Recent evidence from submerged and re-exposed tree stumps at Mono Lake and other sites in the Sierra Nevada points to long droughts at about AD 900-1100 and AD 1200-1350 (Stine 1994). Those patterns are consistent with tree-ring reconstructions of decadal- to centennial-scale wet and dry periods developed using high-elevation sites in the south-central Sierra Nevada (Graumlich 1993) and White Mountains of California (LaMarche 1974; Hughes and Graumlich 1996). To reconcile the apparent discrepancy in timing of prolonged, extreme droughts in the Colorado Plateau and in the Sierra Nevada, it is possible to hypothesize that the precipitation regimes of the two regions are controlled by different — possibly overlapping — mechanisms at decadal and longer time scales, especially with regard to the coupling of atmospheric and oceanic circulation. An intriguing representation of this hypothesis is provided by the correlation between tree-ring chronologies for western North America (NOAA 1992) and the previous summer mean sea surface temperature at two California coastal stations (Walker *et al* 1995), La Jolla and Pacific Grove (Figures 12 and 13). Those two stations have long time series (from the late 1910s to the present) and are commonly used to summarize latitudinal differences in the variability of the California Current (Hayward *et al* 1994). The spatial correlation pattern for the La Jolla station (Figure 13, top) is characterized by a pronounced dipole between the American Northwest and Southwest, with negative correlations in the former (including most of the Sierra Nevada) and positive correlations in the latter. This mode is extremely similar to the spatial correlation between the same tree-ring chronologies and either the winter precipitation in San Diego (1850-1994) or the San Diego tree-ring chronology for Torrey pine (1827-1994; Biondi *et al*, this volume). The spatial correlation pattern for the Pacific Grove station (Figure 13, bottom) is not so well defined as the one for La Jolla. Positive correlations are scattered along the western and

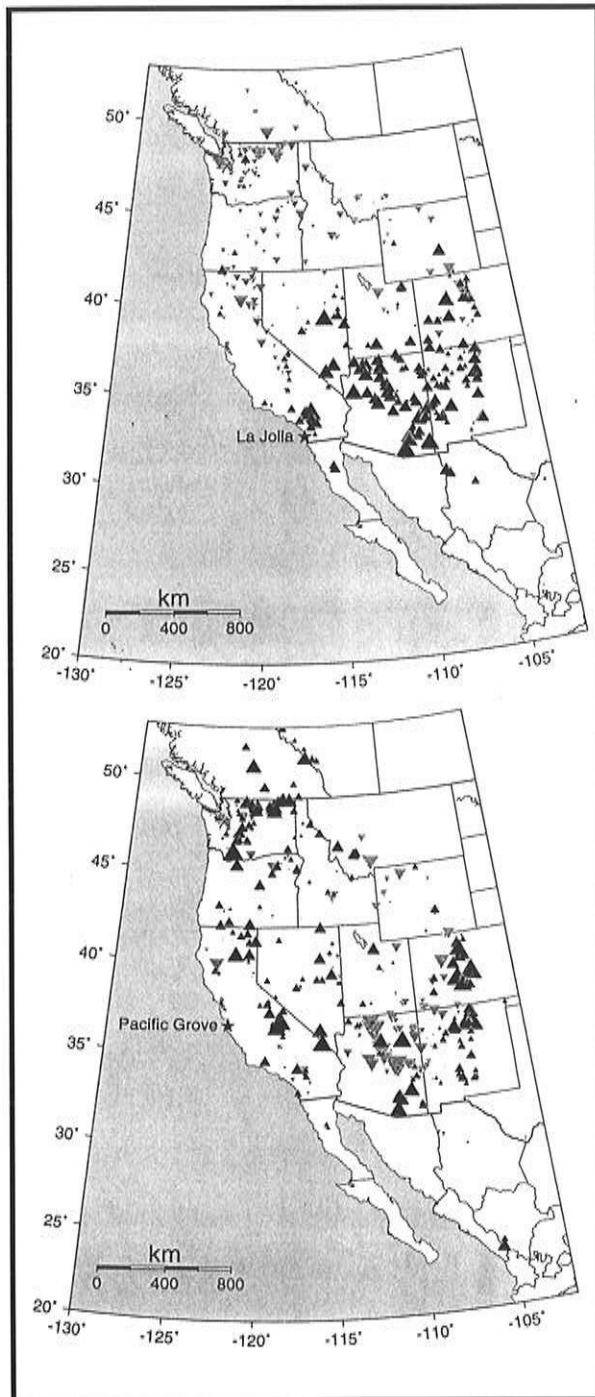


Figure 13. Linear correlation ( $r$ ) between tree-ring chronologies and mean sea surface temperature during the previous summer (June-August) at: (top) La Jolla ( $r$  from  $-0.374$  to  $0.499$ ), and (bottom) Pacific Grove ( $r$  from  $-0.576$  to  $0.647$ ). Symbol size for positive (solid, upward triangles) and negative (shaded, downward triangles) correlations is directly proportional to the absolute value of  $r$ .

eastern edges of the Cordillera and in the Sierra Nevada, while negative correlations tend to concentrate in north-central Arizona. Interestingly, the maps presented in Figure 13 are independent of each other because the correlation between sea surface temperature at Pacific Grove and La Jolla is only 0.1 in the summer, whereas it is 0.6-0.8 in the other seasons.

Changes in climate regime between different regions of California are mostly related to the different impact of the Pacific maritime airstream and to the relative importance of tropical versus subtropical Pacific circulation (Emery and Hamilton 1985; Yarnal and Diaz 1986). Schonher and Nicholson (1989) have already pointed out that annual rainfall (previous July through current June) over California presents a regionally specific response to El Niño-Southern Oscillation (ENSO) events, which are large-scale phenomena with 3-6 year periodicity (Trenberth and Shea 1987). From 1950 to 1982, ENSO has been strongly associated with higher rainfall in southern California (the driest portion of the state), but has had little impact in the Sierra Nevada (Schonher and Nicholson 1989). ENSO, which is probably the most prominent interannual climate fluctuation on Earth (Philander 1990; Latif *et al* 1994), is commonly described as an oscillation between a warm (El Niño) and a cold (La Niña or El Viejo) state of the tropical Pacific Ocean, accompanied by significant circulation anomalies that extend to the global atmosphere and ocean (Zebiak and Cane 1987; Ropelewski and Halpert 1989; Tourre and White 1995). In the winter, El Niño conditions are associated with increased rainfall not only in southern California but also in the Colorado River Basin and Northern Rio Grande Basin, spanning a region longitudinally stretched from southern and Baja California to western Texas and the south-eastern United States (Diaz and Kiladis 1992; Stahle and Cleaveland 1993).

If a large-scale mechanism could link decadal-scale productivity and sedimentation rates off southern California with southwestern prolonged droughts, it should involve the coupling of atmospheric and oceanic circulation as expressed by pathways of moisture transport from the Pacific to the American Continent at decadal and longer time scales. The wintertime Pacific circulation is dominated by a deep low-pressure system in the north (the Aleutian Low) and by a weaker high-pressure system in the south centered over 30°N and 130°W, just off the Patton Escarpment, directly above the California Current. An intensification of the Aleutian Low and a strengthening of the subtropical jet and zonal westerlies are common midlatitude responses to ENSO, but they can also vary on decadal time scales (Trenberth and Hurrell 1994; Miller *et al* 1994). A general coincidence was reported by Emery and Hamilton (1985) between low sea surface temperature anomalies along the American West Coast and weak North Pacific atmospheric circulation. This is confirmed by the high correlation between indices of North Pacific atmospheric circulation and winter sea surface temperature at Pacific Grove and La Jolla. The wintertime correlation between (a) the Pacific North American index (Wallace and Gutzler 1981), and (b) the Central North Pacific index (Cayan and Peterson 1989) with sea surface temperature at Pacific Grove is (a) 0.79 (n=37), and (b) -0.57 (n=72); the correlation with sea surface temperature at La Jolla is (a) 0.73 (n=39), and (b) -0.58 (n=77).

The mountain arc described by the Transverse Mountains and by the southern Sierra Nevada represents the southern edge of the area influenced by the Aleutian Low; just south of those mountains, along the U.S.-Mexico border, lies the southernmost route for low-level westerlies to cross the Cordillera (Bryson and Hare 1974). Moisture transport from the eastern tropical Pacific to Southern California and the Colorado Plateau can only take place if the winter high-pressure cell over the California Current is displaced or weakened, allowing the westerlies to extend into the tropical region of anomalous sea surface temperature (Horel and Wallace 1981). Additionally, the summer monsoon that brings precipitation from July through September to northwestern Mexico and the southwestern United States is closely linked to sea surface temperatures in the Gulf of California (Stensrud *et al* 1995). Lower-than-normal summer through winter temperatures in the California Current region would then hamper the transport of Pacific moist air by leading to formation of higher-than-normal air pressures off Southern California. Prolonged dry and wet spells in the American Southwest could be associated with extended periods of, respectively, lower and higher sea surface temperature anomalies in the California Current region, which in turn would correspond to a period of, respectively, higher and lower upwelling and productivity in near-shore basins.

---

## Conclusion

---

The varve thickness analysis presented here has uncovered an abrupt environmental change in Santa Barbara Basin around AD 1600. That decadal-scale event may be related to (a) a similarly sudden change of state in the nearby Santa Monica Basin that triggered the onset of anoxia and the preservations of laminated sediments, (b) an extreme drought and a transformation of forest age structure over most of the American Southwest. Our understanding of the physical processes and forcing mechanisms involved in the formation of Santa Barbara Basin varves would be improved by the analysis of geochemical parameters. For instance, total organic carbon burial flux in Santa Barbara Basin varves (A. Schimmelmann, *pers. comm.*) also shows a marked change around AD 1600 (Figure 14).

The greater variability of varve thickness and total organic carbon burial flux in recent centuries points to a “world of extremes”, where oceanic productivity and/or circulation has undergone large interdecadal swings. On the other hand, the terrestrial events may be explained by a pulse-like, decadal-scale climatic anomaly because published tree-ring records do not indicate a change from one oscillatory pattern to another. A possible climatic link between oceanic and terrestrial records should involve pathways for moisture transport from the Pacific to the American Southwest at decadal and longer time scales. At those time scales, the interplay between the Aleutian low pressure system, the California

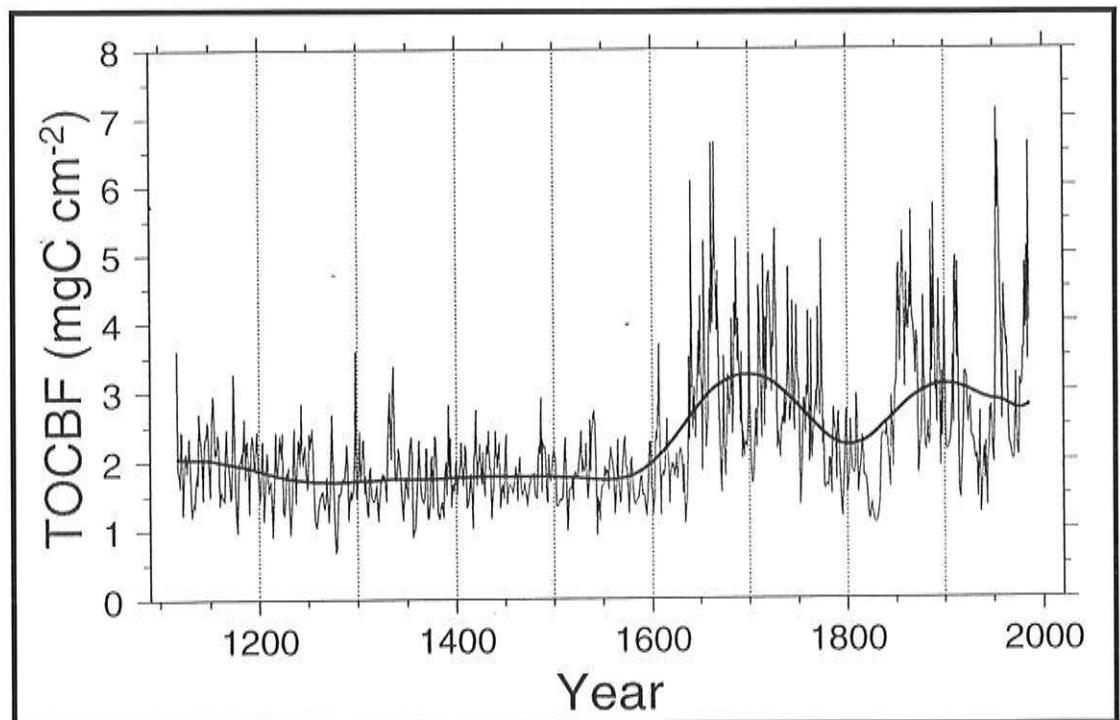


Figure 14. Total organic carbon burial flux (TOCBF) in Santa Barbara Basin varves (AD 1117-1986; data courtesy of A. Schimmelmann). The annual series (thin line) is overlaid with the reconstructed SSA components with periods longer than 150 years (thick line).

Current, ENSO, and the Mexican monsoon could be responsible for both changing sedimentation rates in the Santa Barbara Basin and precipitation patterns in the American Southwest.

Further research is needed on different subjects, including the danger of losing information on amplitudes of oscillatory modes when tree-ring records are standardized and averaged in a mean chronology. Detecting a shift from one decadal-scale precipitation regime to another would require tree-ring chronologies based on trees about 1000 years of age and older. Work to reprocess a large set of suitable tree-ring specimens has commenced (Hughes and Graumlich 1996; Hughes *et al* in press). In the meantime, to account for such uncertainties, we entertain the hypotheses that oceanic and terrestrial evidence of a near-AD 1600 multi-year anomaly may be (a) linked by a pulse-like climatic event that changed the sensitivity of the marine basins, (b) connected by a climatic shift in the oceanic systems that has sporadic effects on the terrestrial ones, (c) a chance coincidence.

---

## Acknowledgments

We are grateful to Arndt Schimmelmann for sharing his unpublished data and to Dan Cayan for providing advice on climatic patterns. We also thank Mike Dettinger and Eric Breitenberger for donating the public domain software used for singular spectrum analysis and for kindly answering our questions on methodological details. Work supported by National Science Foundation Grants OCE-9301438 and ATM-9509780, as well as by a Scripps Post-Doctoral Fellowship to F. Biondi.

---

## References

- Allen, M.R., and L.A. Smith. 1994. Investigating the origins and significance of low-frequency modes of climate variability. *Geophysical Research Letters* 21:883-886.
- Allen, M.R., and L.A. Smith. In press. Monte Carlo SSA: detecting irregular oscillations in the presence of coloured noise. *Journal of Climate*.
- Audet, D.M. 1995. Mathematical modelling of gravitational compaction and clay dehydration in thick sediment layers. *Geophysical Journal International* 122:283-298.
- Baumgartner, T.R., J. Michaelsen, L.G. Thompson, G.T. Shen, A. Soutar, and R.E. Casey. 1989. The recording of interannual climatic change by high-resolution natural systems: tree-rings, coral bands, glacial ice layers, and marine varves. Pages 1-14 in *Aspects of Climate Variability in the Pacific and the Western Americas*. D.H. Peterson (ed.), Geophysical Monograph 55, American Geophysical Union, Washington, D.C.
- Baumgartner, T.R., A. Soutar, and V. Ferreira-Bartrina. 1992. Reconstruction of the history of Pacific sardine and northern anchovy populations over the past two millennia from sediments of the Santa Barbara Basin, California. *California Cooperative Oceanic Fisheries Investigations (CalCOFI) Reports* 33:24-40.
- Behl, R.J., and J.P. Kennett. 1996. Brief interstadial events in the Santa Barbara basin, NE Pacific, during the past 60 kyr. *Nature* 379:243-246.

- 
- Biondi, F., D.R. Cayan, and W.H. Berger. In press. Long-term response of Torrey pine to coastal climate: precipitation, temperature, and fog. In *Proceedings of the Thirteenth Annual Pacific Climate (PACLIM) Workshop*. C.M. Isaacs, and V.L. Tharp (eds.), Interagency Ecological Program for the Sacramento-San Joaquin Estuary, Technical Report 53. Department of Water Resources, Sacramento.
- Breitenberger, E. In press. Sea ice and its relationship with large-scale atmospheric circulation, Ph.D. Thesis, University of Alaska - Fairbanks.
- Bryson, R.A., and F.K. Hare. 1974. The climates of North America. Pages 1-47 in *Climates of North America*. R.A. Bryson, and F.K. Hare (eds.), World Survey of Climatology, Vol. 11. Elsevier, Amsterdam.
- Calvert, S.E. 1966. Origin of diatom-rich, varved sediments from the Gulf of California. *Journal of Geology* 76:546-565.
- Cayan, D.R., and D.H. Peterson. 1989. The influence of north Pacific atmospheric circulation on streamflow in the west. Pages 375-397 in *Aspects of Climate Variability in the Pacific and the Western Americas*, D.H. Peterson (ed.). Geophysical Monograph 55, American Geophysical Union, Washington.
- Christensen, C.J., D.S. Gorsline, D.E. Hammond, and S.P. Lund. 1994. Non-annual laminations and expansion of anoxic basin-floor conditions in Santa Monica Basin, California Borderland, over the past four centuries. *Marine Geology* 116:399-418.
- Cook, E.R., and L.A. Kairiukstis (eds.). 1990. *Methods of Dendrochronology*. Kluwer, Dordrecht.
- Cook, E.R., K.R. Briffa, D.M. Meko, D.A. Graybill, and G. Funkhouser. 1995. The "segment length curse" in long tree-ring chronology development for paleoclimatic studies. *The Holocene* 5:229-237.
- Cowie, P.A., and G.D. Karner. 1990. Gravity effect of sediment compaction: examples from the North Sea and the Rhine Graben. *Earth and Planetary Science Letters* 99:141-153.
- Dansgaard, W., S.J. Johnsen, H.B. Clausen, D. Dahljensen, *et al* 1993. Evidence for general instability of past climate from a 250-kyr ice-core record. *Nature* 364:218-220.
- D'Arrigo, R.D., and G.C. Jacoby. 1991. A 1000-year record of winter precipitation from northwestern New Mexico, USA: a reconstruction from tree-rings and its relation to El Niño and the Southern Oscillation. *The Holocene* 1:95-101.
- de Boor, C. 1981. *A Practical Guide to Splines*. Springer-Verlag, New York.
- Dettinger, M.D., M. Ghil, and C.L. Keppenne. 1995. Interannual and interdecadal variability in United States surface-air temperatures, 1910-87. *Climatic Change* 31:35-66.
- Dettinger, M.D., M. Ghil, C.M. Strong, W. Weibel, and P. Yiou. 1995. Software expedites singular-spectrum analysis of noisy time series. *EOS*, Transactions of the American Geophysical Union 76:12,14,21.
- Diaz, H.F., and G.N. Kiladis. 1992. Atmospheric teleconnections associated with the extreme phases of the Southern Oscillation. Pages 7-28 in *El Niño: Historical and Paleoclimatic Aspects of the Southern Oscillation*, H.F. Diaz, and V. Markgraf (eds.). Cambridge University Press, Cambridge, UK.
- Dunbar, R.B. 1983. Stable isotope record of upwelling and climate from Santa Barbara Basin, California. Pages 217-246 in *Coastal Upwelling, its Sedimentary Record*. Part B: Sedimentary Records of Ancient Coastal Upwelling, J. Thiede, and E. Suess (eds.). Plenum, New York.
- Emery, K.O. 1960. *The Sea Off Southern California: A Modern Habitat of Petroleum*. Wiley, New York.
- Emery, W.J., and K. Hamilton. 1985. Atmospheric forcing of interannual variability in the northeast Pacific Ocean: Connections with El Niño. *Journal of Geophysical Research* 90:857-868.
- Fritts, H.C. 1976. *Tree Rings and Climate*. Academic Press, London.
- Fritts, H.C. 1991. *Reconstructing Large-Scale Climatic Patterns from Tree-Ring Data: A Diagnostic Analysis*. University of Arizona Press, Tucson.
- Ghil, M. 1994. Cryothermodynamics: The chaotic dynamics of paleoclimate. *Physica D* 77:130-159.

- Ghil, M., and R. Vautard. 1991. Interdecadal oscillations and the warming trend in global temperature time series. *Nature* 350:324-327.
- Graumlich, L. J. 1993. A 1000-year record of temperature and precipitation in the Sierra Nevada. *Quaternary Research* 39:249-255.
- Grimm, K. A., C. B. Lange, and A. S. Gill. 1996. Biological forcing of hemipelagic sedimentary laminae: Evidence from ODP Site 893, Santa Barbara Basin, California. *Journal of Sedimentary Research* 66:613-624.
- Grissino-Mayer, H.D. In press. A 2129-year reconstruction of precipitation for northwestern New Mexico, USA. In *Proceedings of the International Conference on Tree Rings, Environment and Humanity*, J.S. Dean, D.M. Meko, and T.W. Swetnam (eds.).
- Hamilton, E.L. 1976. Variations of density and porosity with depth in deep-sea sediments. *Journal of Sedimentary Petrology* 46:280-300.
- Hayward, T.L., A.W. Mantyla, R.J. Lynn., P.E. Smith, and T.K. Chereskin. 1994. The state of the California Current in 1993-1994. *CalCOFI Reports* 35:19-35.
- Horel, J.D., and J.M. Wallace. 1981. Planetary scale atmospheric phenomena associated with the Southern Oscillation. *Monthly Weather Review* 109:813-829.
- Hughes, M.K., and L.J. Graumlich. 1996. Multimillennial dendroclimatic studies from the western United States. Pages 109-124 in *Climatic Variations and Forcing Mechanisms of the Last 2000 Years*, P.D. Jones, R.S. Bradley, and J. Jouzel (eds.). NATO ASI Series, Vol. 141. Springer-Verlag, Berlin.
- Hughes, M.K., R. Touchan, and P.M. Brown (in press). A multimillennial network of giant sequoia chronologies for dendroclimatology. In *Proceedings of the International Conference on Tree Rings, Environment and Humanity*, J.S. Dean, D.M. Meko, and T.W. Swetnam (eds.).
- Keigwin, L.D. 1995. The North Pacific through the millennia. *Nature* 377:485-486.
- Kennett, J.P., J.G. Baldauf, et al 1994. *Proceedings of the Ocean Drilling Program*, Initial Reports, Vol. 146 (Part 2); College Station, Texas.
- Kennett, J. P., J. G. Baldauf, and M. Lyle (eds.). 1995. *Proceedings of the Ocean Drilling Program*, Scientific Results, Vol. 146 (Part 2); College Station, Texas.
- Kennett, J.P., and B.L. Ingram. 1995. A 20,000-year record of ocean circulation and climate change from the Santa Barbara basin. *Nature* 377:510-514.
- Keppenne, C.I., and M. Ghil. 1992. Adaptive filtering and prediction of the Southern Oscillation Index. *Journal of Geophysical Research* 97:20449-20454.
- LaMarche, V.C. Jr. 1974. Paleoclimatic inferences from long tree-ring records. *Science* 183:1043-1048.
- Lange, C. B., and A. Schimmelmann. 1994. Seasonal resolution of laminated sediments in Santa Barbara Basin: Its significance in paleoclimatic studies. Pages 83-92 in *Proceedings of the Tenth Annual Pacific Climate (PACLIM) Workshop*, K.T. Redmond and V.L. Tharp (eds), Interagency Ecological Program, Technical Report 36. California Department of Water Resources.
- Lange, C.B., and A. Schimmelmann. 1995. X-radiography of selected, predominantly varved intervals at Hole 893A. Pages 333-346 in *Proceedings of the Ocean Drilling Project*, Scientific Results, J.P. Kennett, J.G. Baldauf, and M. Lyle (eds.), Vol. 146 (Part 2). College Station, Texas.
- Lange, C.B., S.K. Burke, and W.H. Berger. 1990. Biological production off southern California is linked to climatic change. *Climatic Change* 16:319-329.
- Lange, C.B., A. Schimmelmann, M.K. Yasuda, and W.H. Berger (in press). Paleoclimatic significance of marine varves off southern California. In *Southern California Climate: Trends extremes of the past 2,000 years*, P. Wigand, P., and M. Rose (eds.), Los Angeles County National History Museum, Los Angeles, California.
- Latif, M., and T.P. Barnett. 1994. Causes of decadal climate variability over the North Pacific and North America. *Science* 266:634-637.
- Latif, M., T.P. Barnett, M.A. Cane, M. Flügel, N.E. Graham, H. von Storch, J.-S. Xu, and S.E. Zebiak. 1994. A review of ENSO prediction studies. *Climate Dynamics* 9:167-179.

- 
- Lean, J. 1991. Variations in the sun's radiative output. *Reviews of Geophysics* 29:505-535.
- Lean, J., J. Beer, and R. Bradley. 1995. Reconstruction of solar irradiance since 1610: Implications for climate change. *Geophysical Research Letters* 22:3195-3198.
- Marquardt, D.W. 1963. An algorithm for least squares estimation of nonlinear parameters. *Journal of the Society of Industrial and Applied Mathematics* 11:431-441.
- Meko, D.M., C.W. Stockton, and W.R. Boggess. 1995. The tree-ring record of severe sustained drought in the Southwest. *Water Resources Bulletin* 31:789-801.
- Miller, A.J., D.R. Cayan, T.P. Barnett, N.E. Graham, and J.M. Oberhuber. 1994. Interdecadal variability of the Pacific Ocean: model response to observed heat flux and wind stress anomalies. *Climate Dynamics* 9:287-302.
- Myers, D.E. 1989. To be or not to be...stationary? That is the question. *Mathematical Geology* 21:347-362.
- NOAA. 1992. *International Tree-Ring Data Bank*. National Geophysical Data Center, Boulder, Colorado.
- Penland, C., M. Ghil, and K. Weickmann. 1991. Adaptive filtering and maximum entropy spectra with application to changes in atmospheric angular momentum. *Journal of Geophysical Research* 96:22659-22671.
- Philander, S.G. 1990. *El Niño, La Niña, and the Southern Oscillation*. Academic Press, San Diego.
- Preisendorfer, R.W. 1988. *Principal Component Analysis in Meteorology and Oceanography*. Elsevier, Amsterdam.
- Rind, D., and J. Overpeck. 1993. Hypothesized causes of decade-to-century climate variability: Climate model results. *Quaternary Science Review* 12:357-374.
- Ropelewski, C.F., and M.S. Halpert. 1989. Precipitation patterns associated with the high index phase of the Southern Oscillation. *Journal of Climate* 2:268-284.
- Rose, M.R., W.J. Robinson, and J.S. Dean. 1982. Dendroclimatic reconstruction for the southeastern Colorado Plateau. Final Report to Dolores Archaeological Project, University of Colorado.
- SAS Institute. 1990. *SAS/STAT User's Guide*, Version 6, Fourth Edition, Vol.2. Cary, North Carolina.
- SAS Institute. 1993. *SAS/ETS User's Guide*, Version 6, Second Edition. Cary, North Carolina.
- Schimmelmann, A., and C.B. Lange. In press. Tales of 1001 varves — Review of Santa Barbara Basin sediment studies. In *Palaeoclimatology and Palaeoceanography from Laminated Sediments*, A.E.S. Kemp (ed.). Geological Society Special Publication, The Geological Society, London.
- Schimmelmann, A., C.B. Lange, and W.H. Berger. 1990. Climatically controlled marker layers in Santa Barbara Basin sediments and fine-scale core-to-core correlation. *Limnology and Oceanography* 35:165-173.
- Schimmelmann, A., C.B. Lange, W.H. Berger, A. Simon, S.K. Burke, and R.B. Dunbar. 1992. Extreme climatic conditions recorded in Santa Barbara Basin laminated sediments: the 1835-1840 *Macoma* event. *Marine Geology* 106:279-299.
- Schonher, T., and S.E. Nicholson. 1989. The relationship between California rainfall and ENSO events. *Journal of Climate* 2:1258-1269.
- Soutar, A., and P.A. Crill. 1977. Sedimentation and climatic patterns in the Santa Barbara Basin during the 19th and 20th centuries. *Geological Society of America Bulletin* 88:1161-1172.
- Stahle, D.W., and M.K. Cleaveland. 1993. Southern Oscillation extremes reconstructed from tree rings of the Sierra Madre Occidental and Southern Great Plains. *Journal of Climate* 6:129-140.
- Stensrud, D.J., R.L. Gall, S.L. Mullen, and K.W. Howard. 1995. Model climatology of the Mexican monsoon. *Journal of Climate* 8:1775-1794.
- Stine, S. 1994. Extreme and persistent drought in California and Patagonia during mediaeval time. *Nature* 369:546-549.

- Stockton, C.W. 1976. Long-term streamflow reconstruction in the Upper Colorado River Basin using tree rings. *Colorado River Basin Modeling Studies*, C.G. Clyde, D.R. Falkenberg, and J.P. Riley (eds.). Utah Water Research Laboratory, Utah State University, Logan.
- Stockton, C.W., and G.C. Jacoby. 1976. Long-Term Surface Water Supply and Streamflow Levels in the Upper Colorado River Basin. *Lake Powell Research Project*, Bulletin No. 18, Institute of Geophysics and Planetary Physics, University of California-Los Angeles.
- Swetnam, T.W., and P.M. Brown. 1992. Oldest known conifers in the southwestern United States: Temporal and spatial patterns of maximum age. *Old-Growth Forests in the Southwest and Rocky Mountain Regions*, M.R. Kaufmann, W.H. Moir, and R.L. Bassett (tech. coords.). USDA For. Serv. Gen. Tech. Rep. RM-123, Fort Collins, Colorado.
- Toure, Y.M., and W.B. White. 1995. ENSO signals in global upper-ocean temperature. *Journal of Physical Oceanography* 25:1317-1332.
- Trenberth, K.E., and J.W. Hurrell. 1994. Decadal atmosphere-ocean variations in the Pacific. *Climate Dynamics* 9:303-319.
- Trenberth, K.E., and D.J. Shea. 1987. On the evolution of the Southern Oscillation. *Monthly Weather Review* 115:3078-3096.
- Tsonis, A.A., G.N. Triantafyllou, J.B. Elsner, J.J. Holdzkom II, and A.D. Kirwan Jr. 1994. An investigation of the ability of nonlinear methods to infer dynamics from observables. *Bulletin of the American Meteorological Society* 75:1623-1633.
- Vautard, R., and M. Ghil. 1989. Singular spectrum analysis in nonlinear dynamics, with applications to paleoclimatic time series. *Physica D* 35:395-424.
- Vautard, R., P. Yiou, and M. Ghil. 1992. Singular spectrum analysis: A toolkit for short, noisy chaotic signals. *Physica D* 58:95-126.
- Walker, P.W., C.L. Fey, and D.M. Newton. 1995. Surface water temperatures, salinities and densities at shore stations: United States West Coast. Data Report, SIO Reference 95-30, University of California, San Diego.
- Wallace, J.M., and D.S. Gutzler. 1981. Teleconnections in the 500 mb geopotential height field during the Northern Hemisphere winter. *Monthly Weather Review* 109:784-812.
- Yarnal, B., and H.F. Diaz. 1986. Relationships between extremes of the Southern Oscillation and the winter climate of the Anglo-American Pacific coast. *Journal of Climatology* 6:197-219.
- Yiou, P., M. Ghil, J. Jouzel, D. Paillard, and R. Vautard. 1994. Nonlinear variability of the climatic system from singular and power spectra of Late Quaternary records. *Climate Dynamics* 9:371-389.
- Zebiak, S.E., and M.A. Cane. 1987. A model of El Niño-Southern Oscillation. *Monthly Weather Review* 115:2262-2278.



# Some Perspectives on the Late Quaternary Paleoclimate of Beringia

Cary J. Mock and Patricia M. Anderson

**Abstract:** Analyses of the modern summer synoptic climatology of Beringia illustrate that the region cannot be treated as a homogeneous climatic unit as a result of different circulation controls that operate over the region. GCM (general circulation model) simulations and information from the modern synoptic climatology were used to infer the summer paleosynoptic climatology of the region since the last glacial maximum. Implications of surface climatic responses for the late Quaternary were compared with available proxy data, mostly from fossil pollen records. Results indicate that surface climatic responses differ spatially over Beringia, mostly as a result of variations in circulation controls such as the East Asian trough and Pacific subtropical high that are superimposed within external controls such as insolation and ice sheet size. Variations in these climatic controls offer important implications in assessing the vegetation histories of western Beringia versus eastern Beringia.

## Introduction

Comparisons between GCM (general circulation model) simulations and proxy evidence of late Quaternary paleoclimates are at times complicated as a result of spatially heterogeneous climatic patterns suggested by the latter (*eg*, Mock and Bartlein 1995). Beringia, with its borders defined as from the Alaska/Canada border westward to the Indigirka River in Siberia (Figure 1), is a key region for studying late Quaternary paleoclimatic changes in the Arctic as a result of a growing body of modern and fossil records, particularly palynological ones (Bartlein *et al* 1991). Differences in the temporal and spatial variability of vegetation histories within Beringia may be explained by changes in atmospheric circulation controls, which create more heterogeneous surface climatic responses spatially as compared to larger-scale controls such as incoming insolation. This paper examines the summer synoptic climatology of Beringia since the last glacial maximum around 18,000 years ago (18 ka, radiocarbon years), using available GCM simulations as well as information from the modern synoptic climatology of the region. Proxy data, mostly from fossil pollen evidence, provided additional information on surface paleoclimatic responses.

## Modern Summer Synoptic Climatology of Beringia

Composite difference maps of 500-mb heights, representing atmospheric circulation that causes abnormal temperature and precipitation anomalies at selected representative stations, were examined to determine the circulation controls that govern surface summer climate. In this paper,

In: C.M. Isaacs and V.L. Tharp, Editors. 1997. *Proceedings of the Thirteenth Annual Pacific Climate (PACCLIM) Workshop, April 15-18, 1996*. Interagency Ecological Program, Technical Report 53. California Department of Water Resources.

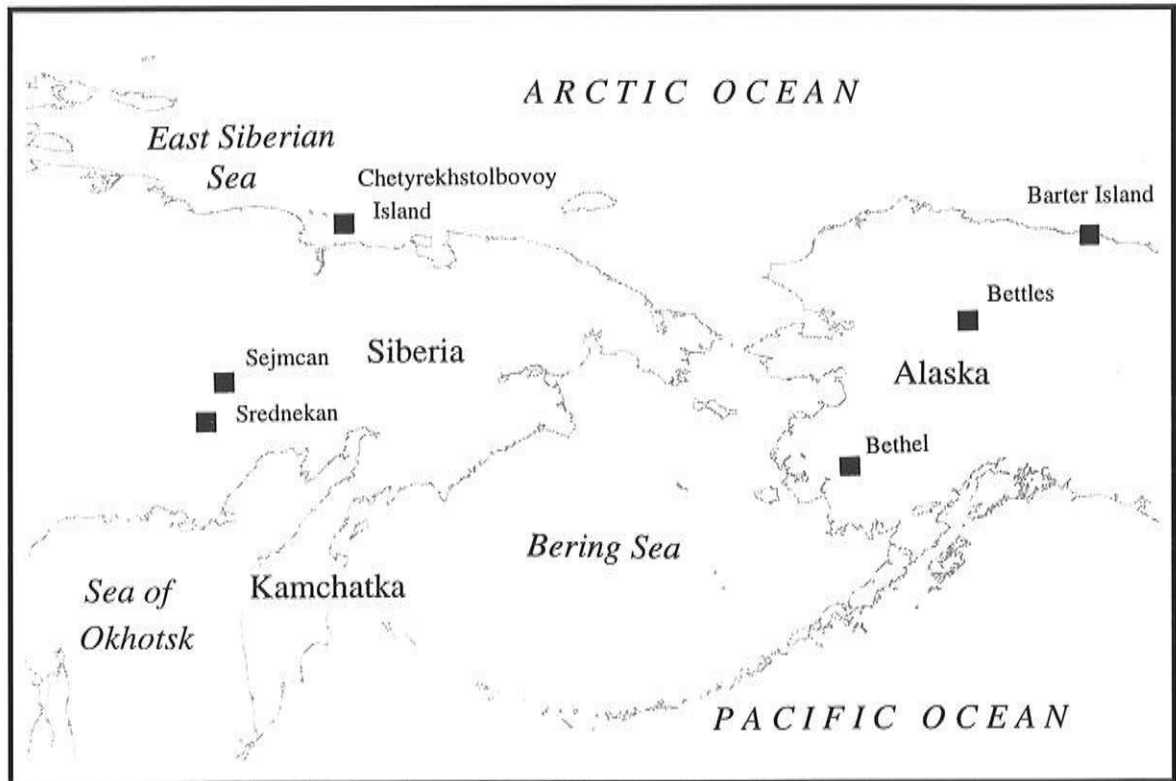


Figure 1. Beringia and locations within the region as mentioned in the text.

discussion is focused on sea-level composites for July temperature and 500-mb composites for July precipitation, as these height levels represent the clearest assessments of the synoptic climatology of the region. Circulation values for the months that have values greater than the 75th percentile were averaged. A similar procedure was conducted for months with values less than the 25th percentile, with the differences between the two extremes representing the composite differences (eg, Klein and Kline 1984). Negative anomalies on the maps represent increased cyclonic and counterclockwise flow around centers, and positive anomalies represent increased anticyclonic and clockwise flow around centers.

Sea-level composite difference maps of July temperature for selected sites in Beringia show some similarities and some differences (Figure 2). Positive anomalies located off the coast of Kamchatka are associated with increased southerly winds and warmer temperatures for western Beringia, as shown in the examples for Chetyrekhtolbovoy Island and Sejmcan. A reversal of anomaly signs suggests a weaker area of high pressure as compared to normal and, thus, increased frequency of northerly winds and colder temperatures for these locations. Although anomalies are generally weak over most of northern Asia, the negative and positive signs suggest that the pattern of ridges and troughs plays an important role in summer temperature variations as well, perhaps determining the mean position of the arctic front (Krebs and Barry 1970). Along the north coast of Alaska, as shown in the example for Barter Island, southerly flow around the Pacific subtropical high to the south

plays a major role in governing temperature variations. However, the example for Bettles, Alaska, is typical for most sites south of the North Slope. Anomaly patterns suggest that a weakened Pacific subtropical high and a strengthened anticyclone over the Beaufort Sea enable increased easterly winds and thus warmer temperatures. A reversal of anomaly signs implies that increased westerly winds bring colder temperatures to the area.

The synoptic situations favoring precipitation differ from temperature by exhibiting more spatial variability in atmospheric circulation from site to site (Figure 3). First considering western Beringia, the 500-mb composite difference map for Chetyrekhtolbovoy Island July precipitation illustrates negative heights along northwestern Beringia that represent the East Asian trough, with positive anomalies adjacent and to the south representing northward shifts of the subtropical anticyclones. The East Asian trough is also clearly evident for Srednekan, but positive anomalies are mostly absent as a result of the trough being generally displaced farther southward due to the location of Srednekan. The trough enables

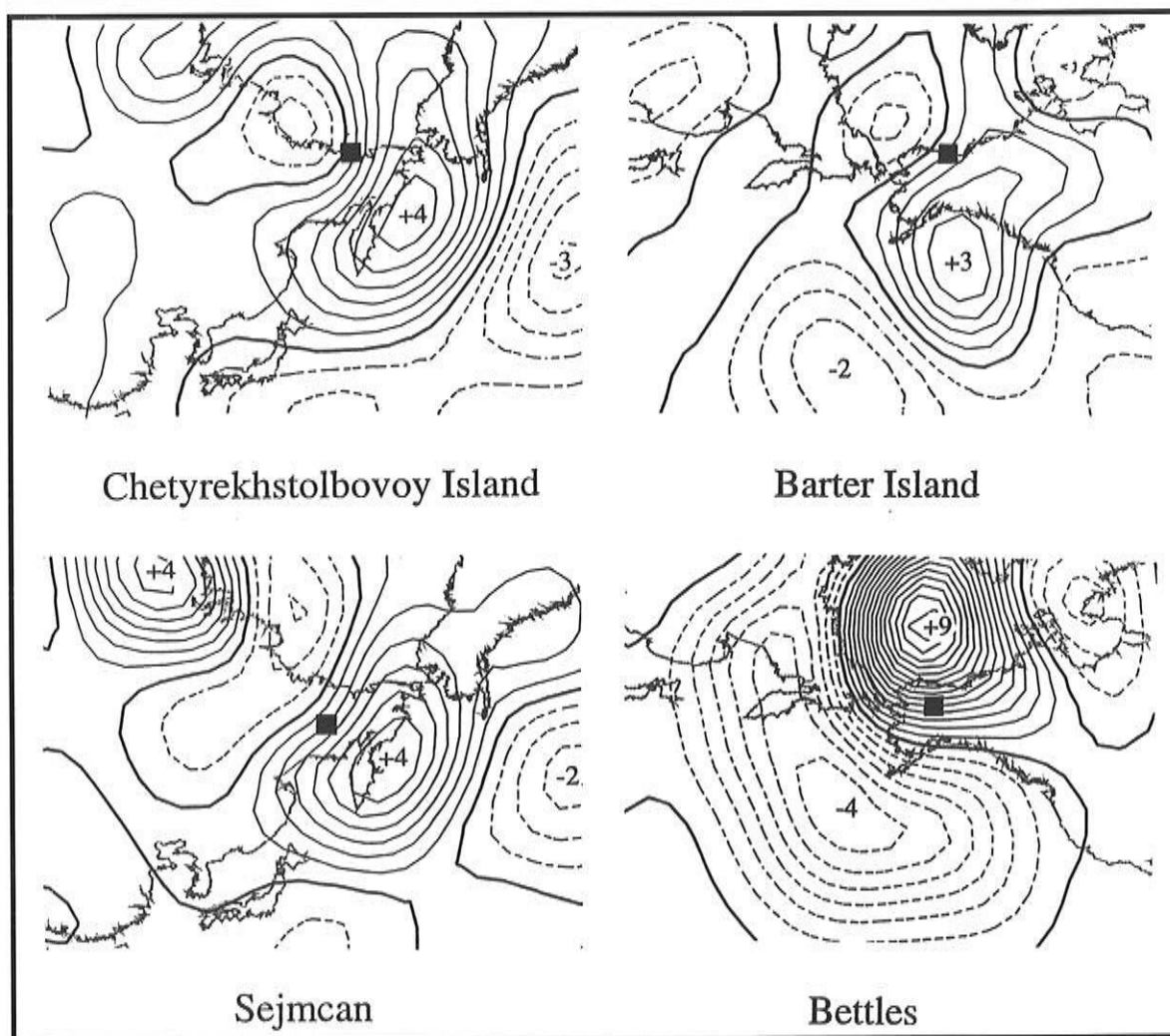


Figure 2. Sea-level pressure composite difference maps (mb) of July temperature for selected stations.

higher precipitation by allowing cyclogenesis to occur in the region, and perhaps also by retaining and steering storms coming from the west and southwest.

The 500-mb composite difference maps for Bettles and Bethel July precipitation both show that higher precipitation results from negative height anomalies centered to the north-northwest of their respective locations. This eastward extension of the East Asian summer trough allows storms from the East Siberian Sea to enter the region (Moritz 1979). However, the Bethel 500-mb composite map differs from that of Bettles by illustrating higher positive anomalies south of Alaska. These anomalies, representing a stronger and/or expanded Pacific subtropical high, combined with the zone of negative anomalies to the north, increases the frequency of westerly winds and storms into Bethel. Bettles, which is farther inland, is not affected as much by the subtropical high as a result of numerous mountain ranges impeding moisture coming directly from the Pacific. Therefore, negative anomalies over the Beaufort Sea are more important for enabling higher precipitation to occur at Bettles.

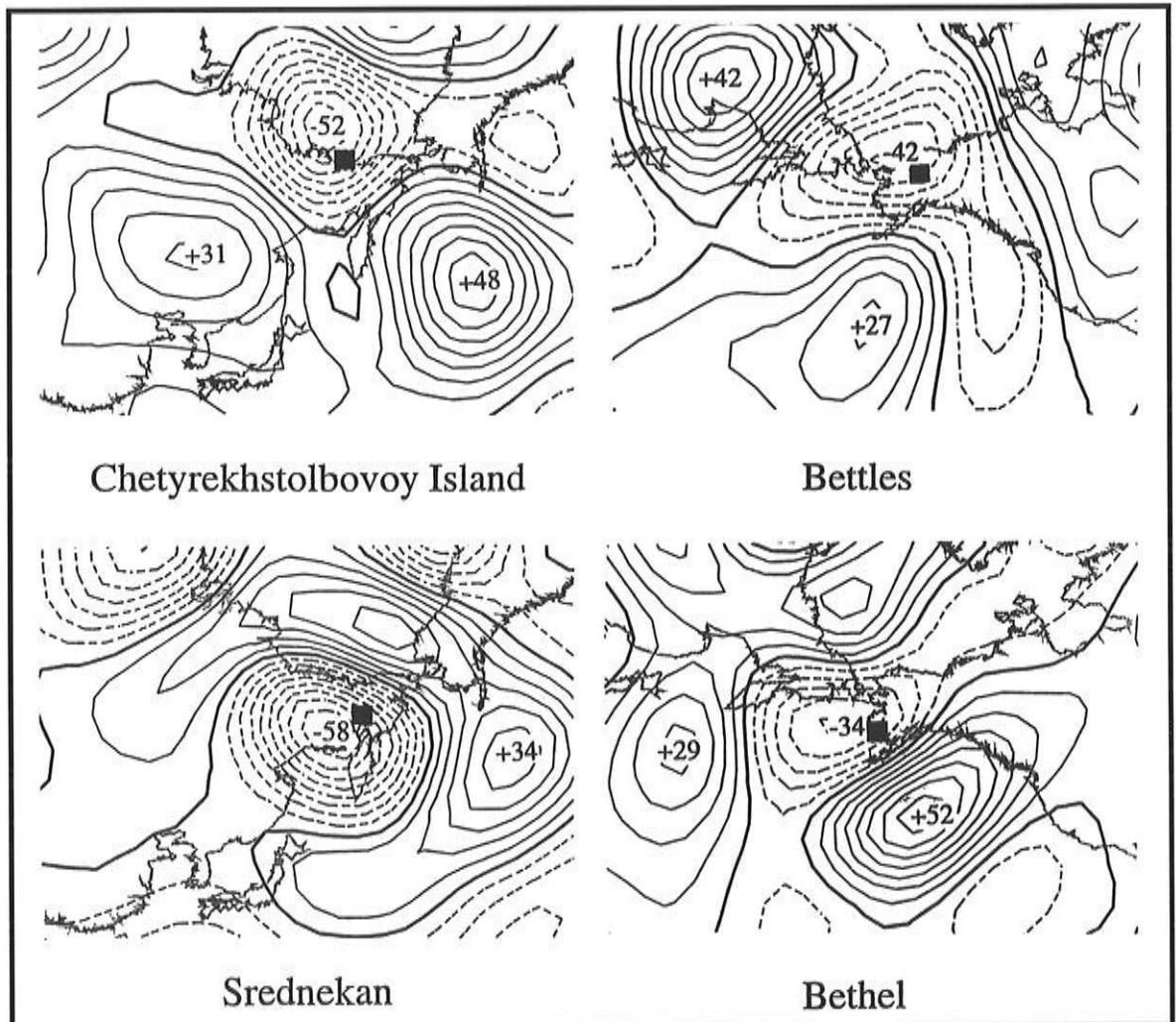


Figure 3. 500-mb composite difference maps (geopotential meters) of July precipitation for selected stations.

## Summer Synoptic Climatology of Beringia Since the Last Glacial Maximum

---

General circulation models have some problems in simulating spatial patterns of temperature and precipitation, particularly the latter, at smaller spatial scales. These problems are the result of the models' limited grid-size resolution and portrayal of topographic features such as the Alaska and Brooks ranges, as well as the coastline of Beringia. However, GCMs have been proven to simulate large-scale synoptic patterns of paleoclimates fairly well for the mid-latitudes (COHMAP Members 1988). Therefore, this discussion focuses mostly on the synoptic patterns from the GCMs, since some uncertainty still remains in the simulations of surface climatic anomalies for Beringia, particularly for precipitation. The GCM simulations discussed come from both NCAR CCM 0 and NCAR CCM 1 (National Center for Atmospheric Research Community Climate Model), and simulations of both GCMs were conducted in roughly 3000-year intervals (COHMAP 1988; Kutzbach *et al* 1993; COHMAP Members, personal communication). Time periods are broadly summarized for discussion (Table 1) as the last glacial maximum (18-12 ka), the late glacial (12-9 ka), and the early-mid Holocene (9-5 ka).

GCM simulations for July atmospheric circulation around the last glacial maximum imply positive pressure anomalies over northern Siberia and negative pressure anomalies over much of the north Pacific Ocean. The positive anomalies suggest increased anticyclonic flow around western Beringia, which would create drier conditions relative to today (Table 1). The negative anomalies suggest a weaker Pacific subtropical high, thus preventing a strong, moist southwesterly flow over most of Alaska. Nearby ice sheets throughout Beringia would still, however, keep temperatures lower as compared to today. The weaker Pacific subtropical high during summer would also contribute to lower temperatures for Alaska. Overall, the paleoclimatic analyses suggest colder and drier summers, and these conditions correspond well with the implications of herb tundra that was prevalent over much of the region (Anderson and Brubaker 1994).

Model simulations from NCAR CCM 1 imply that negative pressure anomalies were predominant over most of Beringia during the late glacial. Synoptic interpretation, based on modern synoptic climatic reasoning, suggests that such widespread negative pressure anomalies would create widespread wetter and colder conditions than today. Such conditions during the late glacial, however, did not occur as suggested by fossil pollen and lake-level evidence — conversely most proxy data suggest the opposite (Anderson and Brubaker 1994; M. Edwards personal communication). Results from NCAR CCM 0 also show negative pressure anomalies prevalent over most of Beringia, but it also indicates anticyclonic flow over Alaska. The anticyclone over Alaska, would suggest stronger easterly flow, causing warmer and drier conditions compared to today.

These results are more consistent with the implications of a *Populus* woodland that indicate drier and warmer conditions (Anderson and Brubaker 1994). Thus perhaps the NCAR CCM 0 simulation better reflects the summer synoptic climatology during the late glacial. A stronger East Asian trough may have been prevalent during this time over western Beringia, but the subtropical high to the south may have also been stronger, so precipitation anomalies are inconclusive (Table 1). Temperatures throughout Beringia were generally warming from the full glacial due to the increased tilt of the earth's axis and timing of perihelion, but a stronger East Asian trough over western Beringia may have prevented summer temperatures from being above normal.

Both GCM simulations show a strengthening of the Pacific subtropical high during the early-mid Holocene, and the East Asian trough over western Beringia weakened to about as strong as today. These synoptic conditions suggest similar precipitation conditions in western Beringia as at present, perhaps consistent with vegetation reconstructions that indicate the establishment of the modern larch/pine forests by the early Holocene (Lozhkin *et al* 1993). A stronger Pacific subtropical high may cause increased summer precipitation for southern and central Alaska, and these conditions may have been more conducive for the spread and changes of spruce forests during this time. GCM simulations suggest positive temperature anomalies as a result of the orbital factors. The simulations also show that as the Holocene progressed, summer temperature and precipitation lowered toward values that are prevalent today.

Table 1  
SUMMARY OF SUMMER SYNOPTIC CLIMATOLOGY OF WESTERN AND EASTERN BERINGIA AS ANALYZED FROM GCM SIMULATIONS AND MODERN SYNOPTIC CLIMATOLOGY

Climatic descriptions are relative to present-day conditions.

Period	Western Beringia	Eastern Beringia
Last Glacial Maximum (18-12 Ka)	Increased ridging; colder and drier.	Weaker subtropical high; colder and drier.
Late Glacial (12-9 Ka)	Gradual strengthening of subtropical high and East Asian trough, but location of the latter is uncertain; warming from full glacial and approximately equal precipitation compared to today.	Generally negative sea-level pressure anomalies, but an anticyclone over Alaska; warmer and drier.
Early to Mid-Holocene (9-6 Ka)	Conditions progress more toward present-day, but still stronger subtropical high; warmer.	Stronger Pacific subtropical high; warmer and wetter.

## Conclusions

---

Modern synoptic climatic analyses show that the circulation controls that govern temperature and precipitation variations differ within the region — thus Beringia cannot be treated as a homogeneous unit climatically. Some climatic controls that affected paleoclimates in Beringia in the late Quaternary most likely differed as compared to those in the modern, but similarities in the circulation controls most likely also held true in the past and can provide an explanation of spatial heterogeneous paleoclimatic responses (Mock and Bartlein 1995). Analyses of the synoptic climatology of Beringia since the last glacial maximum suggest that changes in different circulation controls did occur, and these changes may help explain spatial variations in the vegetation histories of taxa, as the histories in western Beringia versus eastern Beringia are quite different. Some disagreements between GCM results, implications from paleoclimatic proxy data, and reasoning from modern synoptic climatology are still evident — this mostly deals with the problem of interpreting processes at different spatial scales. The continued refinement of GCMs, growing network of paleoclimatic proxy data, and the application of RCMs (regional climate models) will help resolve these problems.

## Bibliography

---

- Anderson, P.M., and L.B. Brubaker. 1994. Vegetation history of North Central Alaska: A mapped summary of late Quaternary pollen data. *Quaternary Science Reviews* 13:71-92.
- Bartlein, P.J., P.M. Anderson, M.E. Edwards, and P.F. McDowell. 1991. A framework for interpreting paleoclimatic variations in eastern Beringia. *Quaternary International* 10-12:73-83.
- COHMAP Members. 1988. Climatic changes of the last 18,000 years: observations and model simulations. *Science* 241:1043-1052.
- Lozhkin, A., P.M. Anderson, W.R. Eisner, L.G. Ravako, D.M. Hopkins, L.B. Brubaker, P.A. Colinvaux, and M.C. Miller. 1993. Late Quaternary lacustrine pollen records from Southwestern Beringia. *Quaternary Research* 39:314-324.
- Klein, W.H., and J.M. Kline. 1984. The synoptic climatology of monthly mean surface temperature in the United States during winter relative to the surrounding 700 mb height field. *Monthly Weather Review* 112:433-448.
- Krebs, J.S., and R.G. Barry. 1970. The arctic front and the tundra-taiga boundary in Eurasia. *Geographical Review* 60:548-554.

- Kutzbach, J.E., P.J. Guetter, P.J. Behling, and R. Selin. 1993. Simulated climatic changes: results of the COHMAP climate-model experiments. Pages 24-93 in *Global Climates since the last Glacial Maximum*. H.E. Wright, Jr., J.E. Kutzbach, T. Webb III, W.F. Ruddiman, F.A. Street-Perrott, and P.J. Bartlein, editors. University of Minnesota Press, Minneapolis.
- Mock, C.J., and P.J. Bartlein. 1995. Spatial variability of late-Quaternary paleoclimates in the western United States. *Quaternary Research* 44:425-433.
- Moritz, R.E. 1979. *Synoptic climatology of the Beaufort Sea Coast of Alaska*. Occasional Paper No. 30, Institute of Arctic and Alpine Research, Boulder, Colorado, 176 pp.

# **Addendum I: Paleoclimate and the Solar-Insolation / Tidal-Resonance Climate Model**

---

Thor Karlstrom

In climate research, instrumental observations of the past 100 or so years drive speculation on climatic process and global changes in atmospheric circulation. Likewise in paleoclimate research, generally less precise but much longer time series provide the basis for speculation on ultimate cause(s) and the resulting temporal and spatial patterns of longer term climate change. Recent papers (Karlstrom 1995, 1996) provide detailed analyses of more than 40 high-resolution time series culled from the extensive paleoclimate literature that appear to define cyclical elements of the Solar-Insolation/Tidal-Resonance Climate Model. This model was earlier referred to as the Milankovitch/Pettersson Climatic Theory (Karlstrom 1961 cf).

This paper provides comparable analyses of an additional 20 or so, evidently supportive, climate and volcanic time series. The tree-ring, historical, pollen, cultural, time-frequency, and hydrologic records range in length from 400 to 90,000 years and spatially from Alaska to Tierra del Fuego. Included are records from both Old World and New World sites. The temporally defined cycles range in wavelength from decades to 10s of thousands of years.

Procedures of analysis and presentation are discussed in previous papers. These differ from those of most paleoclimatic researchers:

- By placing subdivision boundaries at chronostratigraphic Point Boundaries marking inferred warm/dry culminations rather than at conventional (approximate) transitional positions to increase precision in temporal definition and correlation of both longer- and shorter-term events (Karlstrom 1961; Ray and Karlstrom 1968).
- By procedures in presentation of percent-frequency pollen and other types of similar records that contrast the inferred warmer/drier indices from inferred cooler/wetter indices by subtracting the former from the latter components (Hevly and Karlstrom 1974).
- By plotting, at various levels of smoothing, the selected paleoclimatic records on common time scales to graphically judge degree and sign of correlation and to facilitate cyclical analyses of both primary and secondary trends.

- By half-cycle smoothing and differencing (derivatives) of those records based on equal-interval sampling as a direct test of correlation with the theoretically dated Solar Insolation/Tidal Resonance Model (Karlstrom 1995).

The coefficient of correlation (R) shown on most of the figures is simply the percent of apparent match between paleoclimatic trends and turning points of the theoretical cycle or resonance indicated by wavelength in years within the accompanying parentheses.

## **Paleoclimate Time Series**

---

Figure 1 summarizes the highest resolution data available relating to climate, hydrology, and cultural history of the Anasazi on the Colorado Plateaus. The striking correlation between longer-term climatic change (from tree-rings), inferred hydrology (from Point Boundary analysis of Southwest alluvial chronostratigraphy), and the number and distribution of tree-ring dated surface sites (crude proxy for population size and movement) suggests strong influence on prehistoric cultural evolution in the region. These results are generally in keeping with both previously and subsequently published interpretations (Karlstrom *et al* 1976; Euler *et al* 1979; Berry 1982; Breternitz 1988; Gumerman 1988; Hevly 1988; Karlstrom 1988; Petersen 1988, Plog *et al* 1988; Orcutt 1991; Dean and Funkhouser 1994). As noted by J.S. Dean (personal communication, 1996) two papers now in press<sup>1</sup> provide tree-ring and alluvial reconstructions that bear an uncanny resemblance to my climatohydrologic model. Alternative nonclimatic or behavioral interpretations of cultural adaptation are also addressed in Gumerman (1988) and most recently elaborated by Dean (1996) in the form of a conceptual model interrelating low- and high-frequency changes in environment with demographic and behavioral adaptations of the prehistoric Anasazi over the past 2000 years. A similar pattern of cyclical change (the 139-year Event Cycle) may be reflected historically in Egyptian dynastic changes back to mid-Holocene time (see Figure 22, below).

Figures 2-5 are European historical and tree-ring proxy records of climate that when analyzed by half-cycle smoothing predominantly record in-phase relations with the 139-year Event Cycle (Figure 2) and with the 278-year Subphase Cycle (Figures 4 and 5). Figure 3 suggests that the irregular higher frequency trends of some bioclimatic records may be largely reproduced by plotting the fractional subharmonics to the differing seasons of recurrence.

---

1 One on tree-ring data from New Mexico by Grissino-Mayer and the other on dated alluvium in Colorado by Force and Howell.

Figure 6 contains time-frequency diagrams of historical floods and frosts in China that suggest strong in-phase relations of floods with the 278-year Subphase Cycle and of frosts with its 2/1 (139-year) and 6/1 (34.33-year) resonances. The nearly one-to-one phasing of frosts with the 6/1 resonance (Brückner Cycle) is particularly impressive.

Figures 7-10 are pollen and isotope records from the Midwest (Figures 7 and 8), Alaska (Figure 9) and the Southwest (Figure 10) that show common Late Glacial and Postglacial trends and a moderate to strong tendency to oscillate in phase with the secondary 3336-year Substage Cycle.

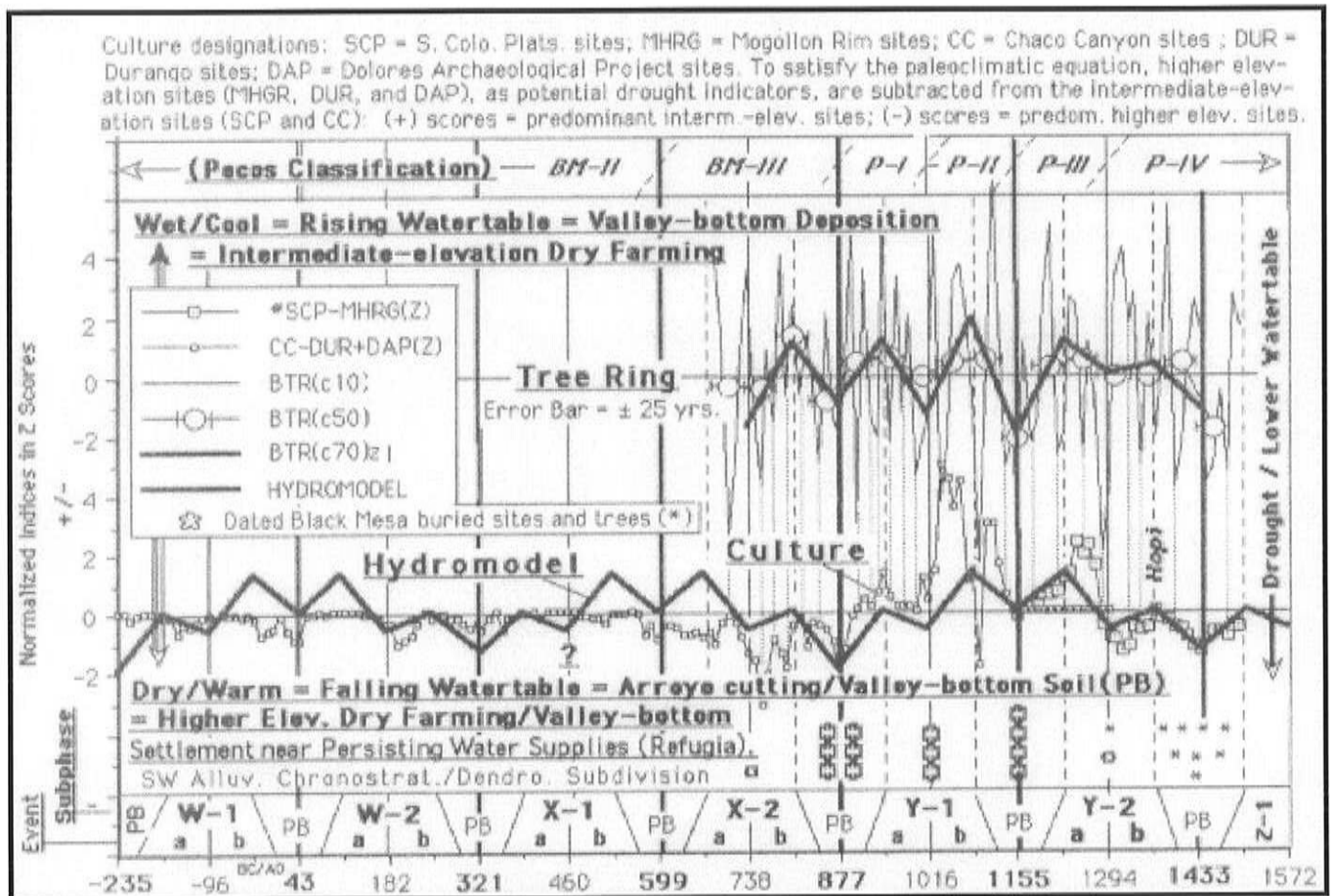


Figure 1 Colorado Plateaus dendroclimate, hydrology, and culture on timescale of the 139-year Event Cycle and its 2/1(69.5-year) resonance.

Decadal tree-ring indices from Berry (1982); 50-year and half-cycle smoothing. Tree-ring and radiocarbon-dated buried sites and trees and chronostratigraphic subdivision from Karlstrom (1976a, 1988); PB = clustering of basal contact dates. Tree-ring-dated surface sites from Euler *et al* (1979), Berry (1982), and Breternitz *et al* (1986). Note striking parallels between longer-term tree-ring trends, inferred hydrology and number of dated sites (population proxy).

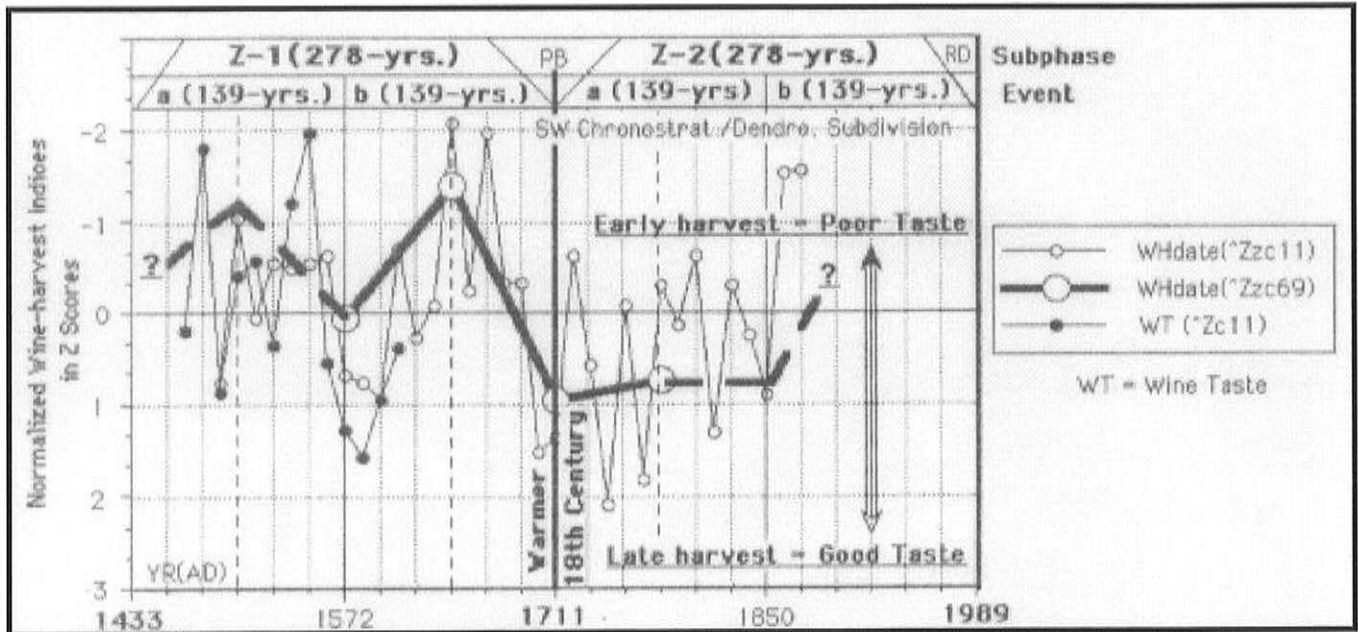


Figure 2 Northern European historical wine-harvest dates and quality on timescale of the 278-year Substage Cycle and its 2/1 (139-year) and 6/1 (23.166-year) resonances.

Annual wine indices from Laderie (1971). Strong tendency for oscillations in phase with the 139-year Event Cycle. Note, however, the irregularities in the higher frequency trends that apparently are largely reproducible by plotting the seasonality of the fractional subharmonics, as shown in Figure 3.

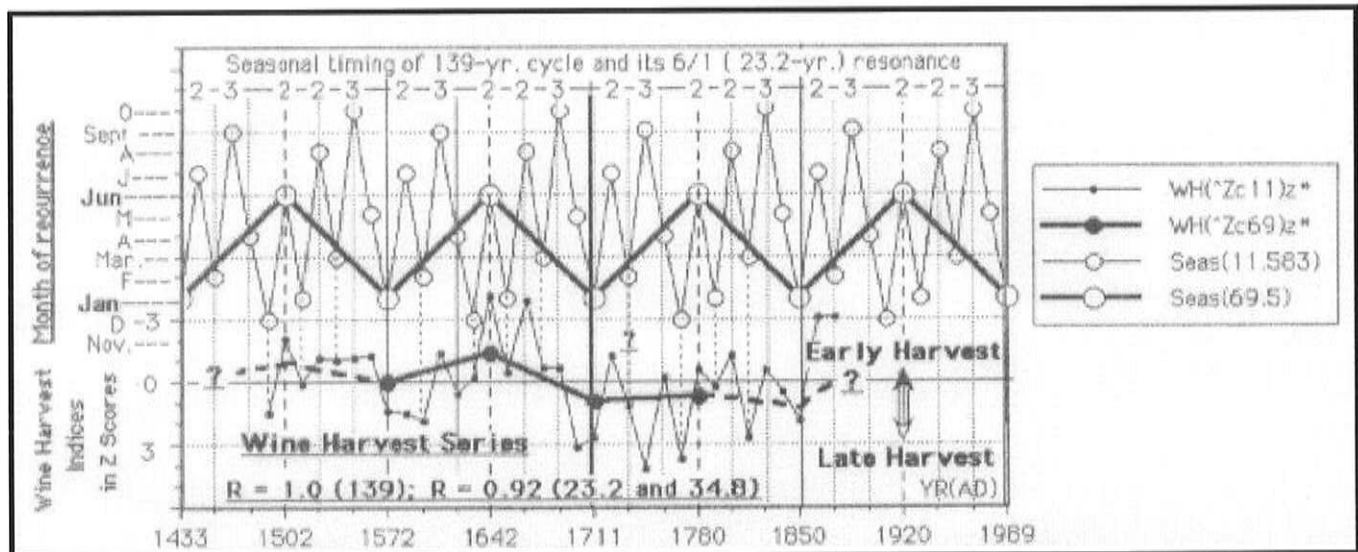


Figure 3 Correlation of Laderie's (1971) wine-harvest series with seasonal timing of the 139-year Cycle and its 2/1 (69.5-year) and 6/1 (23.166-year) resonances.

Smoothing as before centered on cycle turning points. Two-point cycle = 23.2 years; three-point cycle = 34.8 years. The resulting seasonal higher frequency series of 2/3/2/2/3-point cycles repeat in all Event Cycles and appear to have a strong expression in the higher frequency components of the wine-harvest record. The climatic dynamics involved remain obscure, but the largely replicated pattern does suggest that resonance forcing at differing seasons may explain part of the irregularities in some higher frequency bioclimate records.

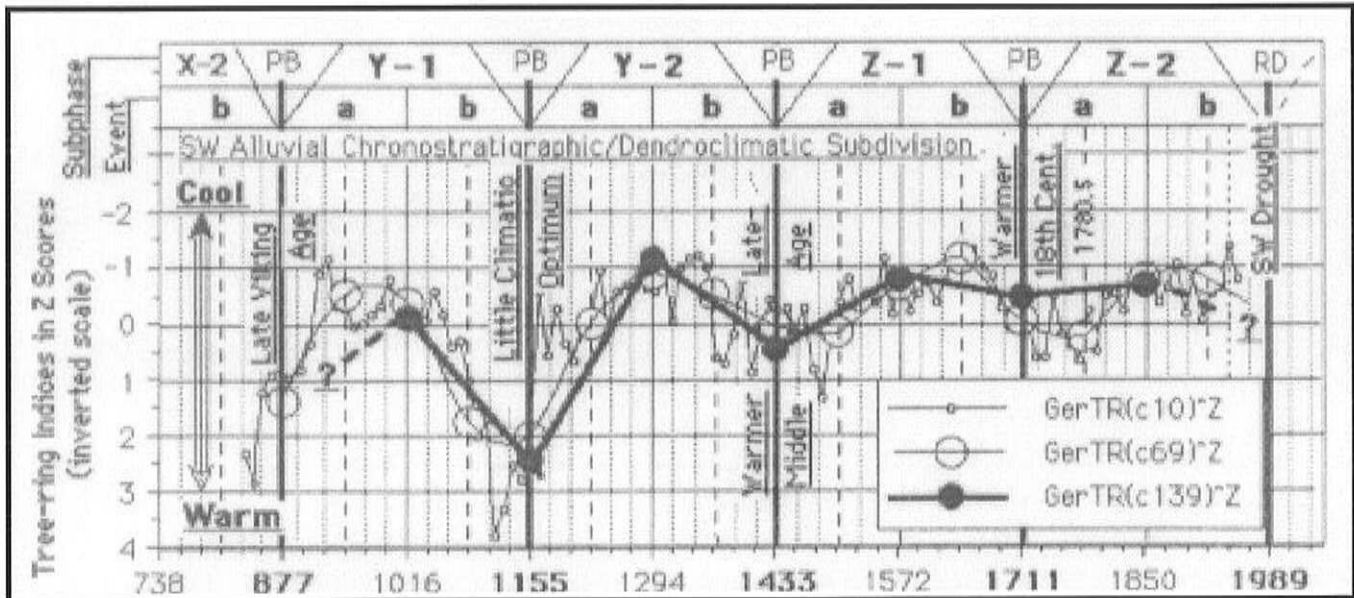


Figure 4 German tree-ring record on timescale of the 139-year Event Cycle and its 2/1 (69.5-year) and 6/1 (23.17-year) resonances.

Annual tree-ring indices from Ladurie (1971). Half-cycle smoothing as before. In contrast to the comparably smoothed North American Southwest dendroclimatic records that reveal the regionally robust 139-year Event Cycle (Figure 23), this German record shows the strongest tendency to oscillate in phase with the longer-term 278-year Subphase Cycle, suggesting differing response functions and/or regional atmospheric dynamics. Of the higher frequency components, the 6/1 (23.17-year) resonance apparently provides the best fit for the decadal fluctuations. That temperature may have been the limiting factor on tree growth in Germany is suggested by its northerly location as well as by other European evidence that centers the warmer "Little Climatic Optimum" in the 12th century and the warmer "Late Middle Age" in the 15th century. The tree record further suggests a warmer interval in the 18th century, or again compatible with that of the Southwest, including the short anomalously warm interval around AD 1780 present in some of the Southwest dendroclimatic records (Figure 23-2, -3, and -8). PB= Point Boundary.

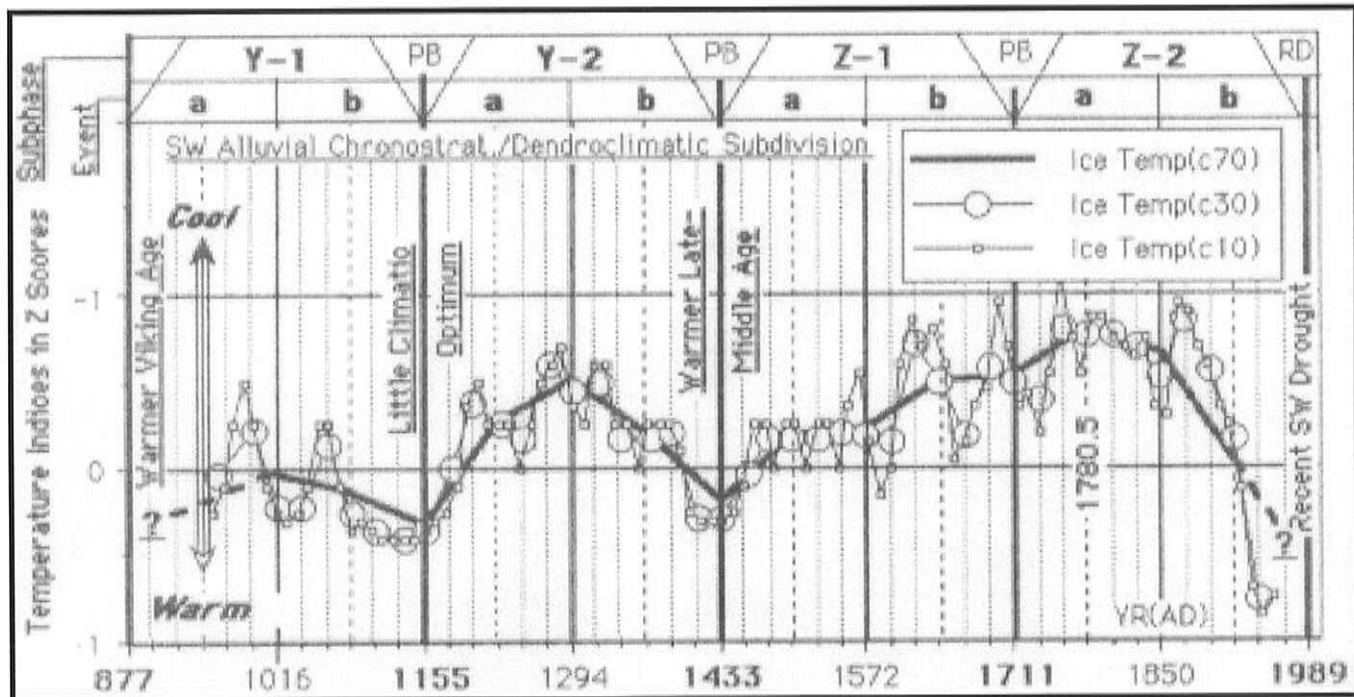


Figure 5 Iceland temperature record on timescale of the 139-year Event Cycle and its 2/1 (69.5-year) and 6/1 (23.166-year) resonances.

Ten-year temperature indices from Bergthorsen (1969). Half-cycle smoothing as before. Note the strong tendency to oscillate in phase with the 278-year Subphase Cycle, and the lesser tendencies with the 139-year Event Cycle and its 2/1 (69.5-year) and 6/1 (23.17-year) resonances. Compare with the shorter wine harvest record (Figure 2) and with the German tree-ring record (Figure 4), both of which appear to share common cyclical timings though with differing amplitudes. These differences may, in part, reflect differing regional climates, differing response functions and lags, or imperfections (nonclimatic noise) in these differing types of proxy records. The Medieval Warm period (MWP) placed from about AD 900 to 1300 by Lamb (1977) appears to combine several separate warmer intervals as recorded in higher resolution records from Europe, the Southwest, and elsewhere. For apparent post-AD 1700 correlation with Sunspot indices, see Figure 12 in Karlstrom (1995).

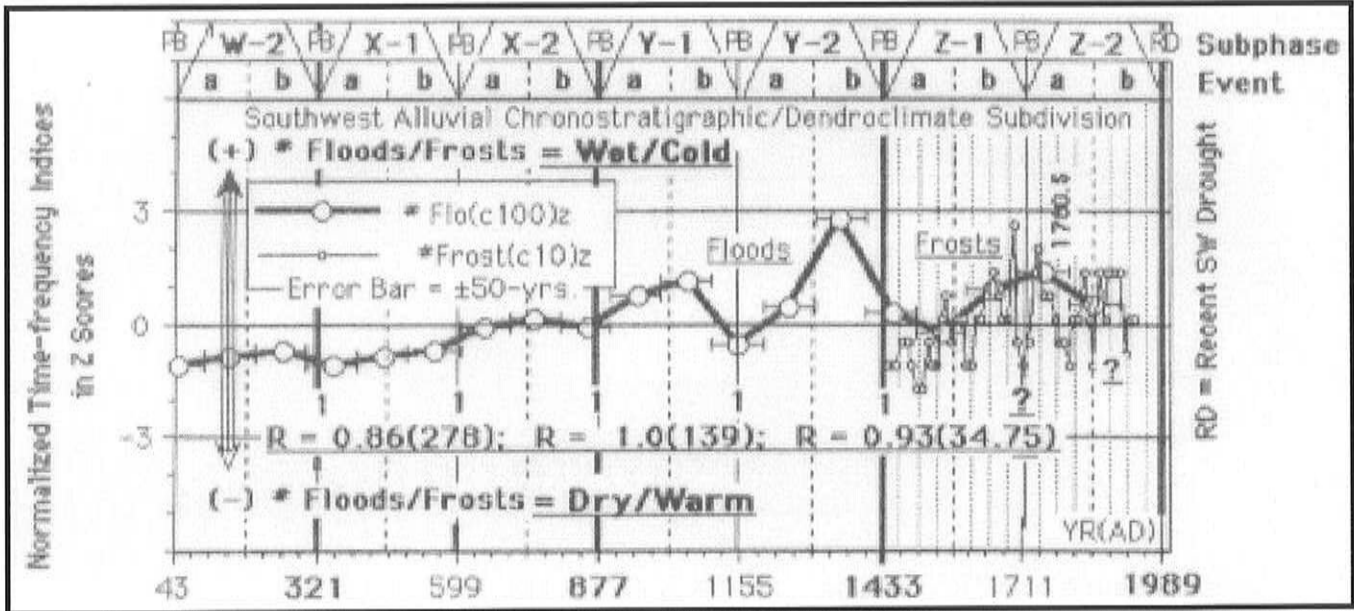


Figure 6 Chinese historical records of the frequency of floods (centered in 100-year intervals) and of frosts (centered in 10-year intervals) on timescale of the 278-year Subphase Cycle and its 2/1 (139-year) and 8/1 (34.75-year) resonances.

Indices from Bradley (1985: Floods p. 393; Frosts p. 383). Strong tendency for the century-smoothed flood record of northern China to oscillate in phase with the 278-year Subphase Cycle; equally strong tendency for the decadal frost record of central and southern China to oscillate in phase with its 2/1 (139-year) and 8/1 (34.75-year = Brückner Cycle) resonances. Note also the anomalously warm interval around AD 1780, which also appears in the German tree-ring record (Figure 4) and in some of the Southwest tree-ring records (Figure 23). The apparent strong correlation with the Brückner Cycle is particularly impressive. A similar cycle appears to be more mildly expressed back to AD 700 in a decadal tree-ring record of the southern Colorado Plateaus (Figure 24).

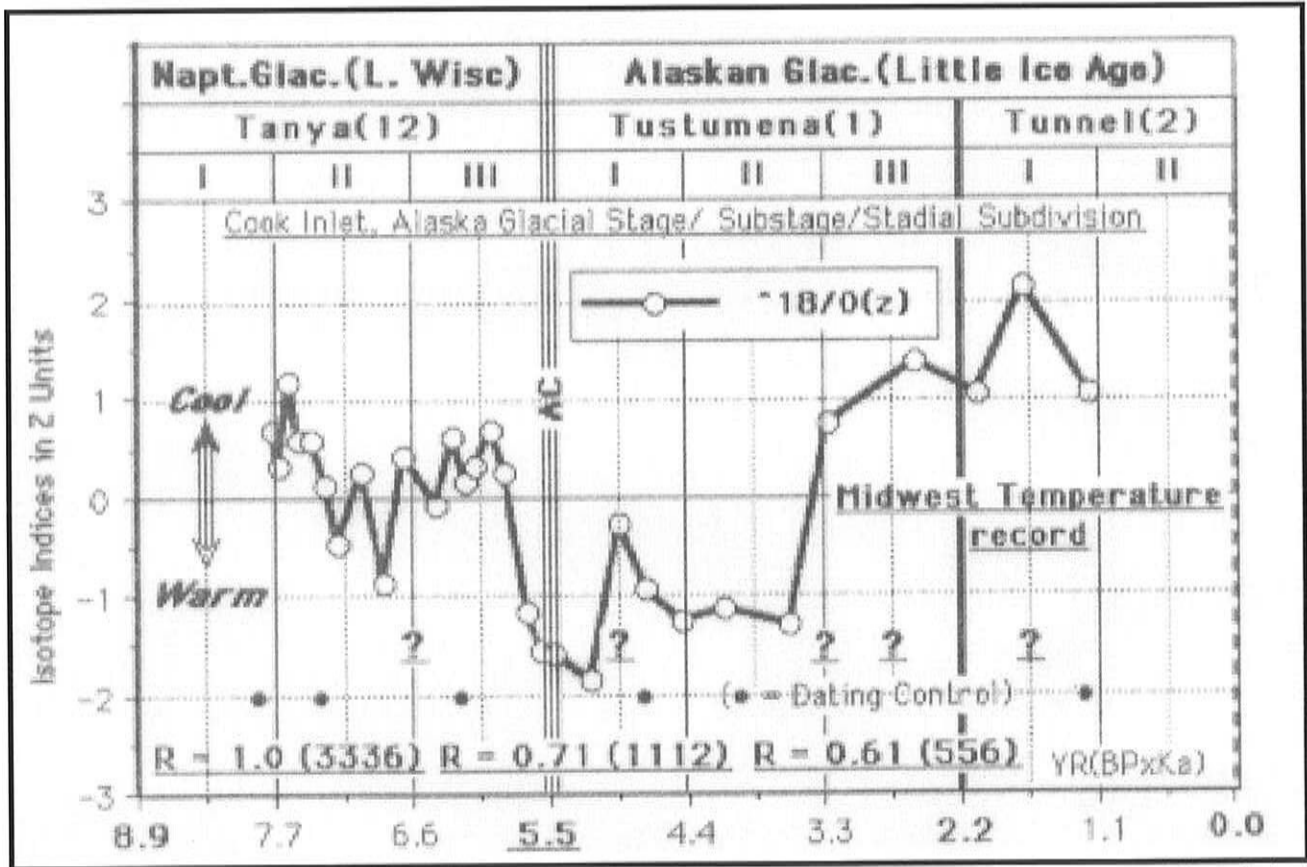


Figure 7 Midwest isotope record of the Holocene (speliotem calcite) on timescale of the 1112-year Stadial Cycle and its 2/1 (556-year) Phase Cycle.

U/Th-dated oxygen-isotope (temperature) indices from Dorale *et al* (1992). The record clearly places the warmest postglacial interval in the Midwest between 5000 and 6000 years ago, or contemporaneous with that in Europe (late Atlantic) and the western United States (Allithermal culmination = AC). The speliotem record also suggests a strong tendency to oscillate in phase with the Substage Cycle, a weaker tendency with the Stadial Cycle, and a very weak, or insignificant, tendency with the Phase Cycle due partly to sample spacing being too wide.

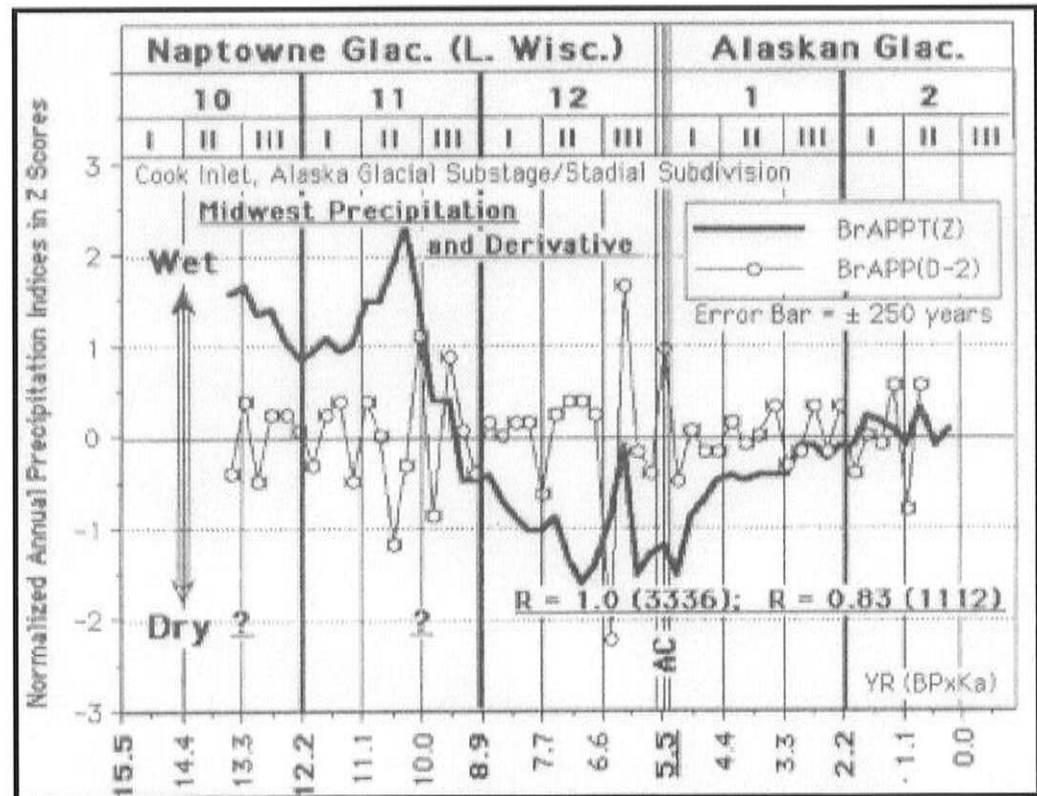


Figure 8 Pollen-derived precipitation record from the Midwest on timescale of the 3336-year Substage Cycle and its 3/1 (1112-year) Stadal resonance.

Annual precipitation indices from Webb and Bryson (1972) replotted in 500-year intervals. Strong tendencies to oscillate in phase with the Substage and Stadal cycles. This precipitation record, combined with the speliotherm temperature record (Figure 7) strongly suggests that at least in part of the Midwest, the Allithermal marks the driest and the warmest interval in postglacial time, similar to that in the western United States.

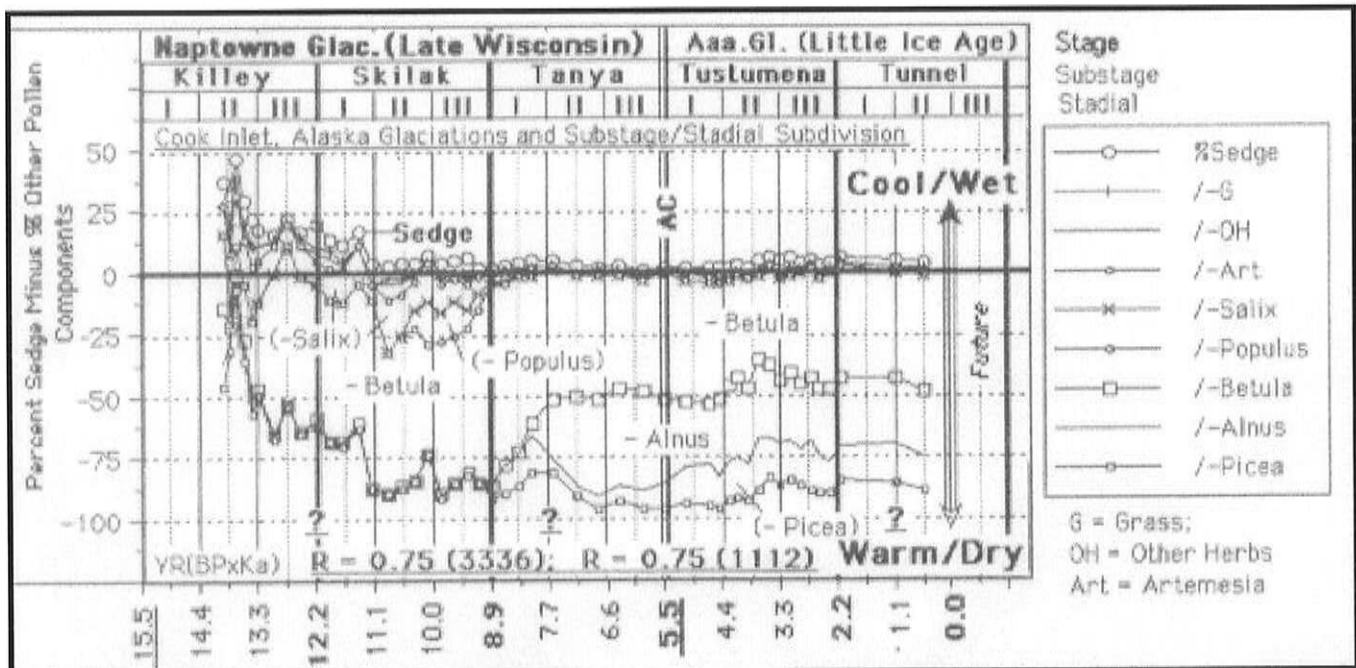


Figure 9 Bioclimatic record of Sithylemenkat Lake, northern Alaska (N66°) on timescale of the 1112-year Stadal Cycle and its 2/1 Phase (556-year) resonance.

Dated pollen indices from Anderson *et al* (1990). This high-latitude record, though somewhat complacent, seems to replicate middle latitudes Northern Hemisphere records in placing the warmest/driest postglacial interval between 5000 and 6000 years ago. This result, however, does not agree with the general palynological consensus that the warmest postglacial interval in Alaska is marked by the Populus maximum about 10,000 years ago. The Lake record also suggests a fairly strong tendency to oscillate in phase with the Substage and Stadal cycles.

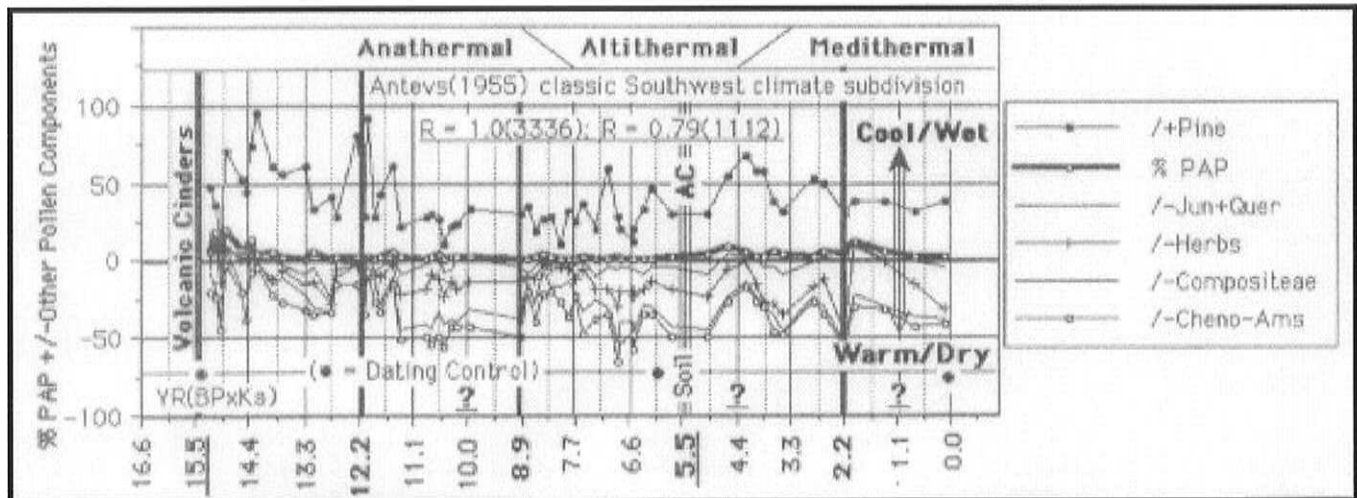


Figure 10 Bioclimatic record (15,500 YBP-present) of Walker Lake, Arizona, on timescale of the 1112-year Stadal Cycle and its 2/1 (556-year) resonance.

Pollen indices after Hevly (1989). Strong tendency for oscillations in phase with the Substage Cycle and a fairly strong tendency with its 3/1 Stadal Cycle. Although the Altithermal Culmination is seemingly well defined by pollen plus an associated soil suggesting lowest postglacial lake levels, an earlier, equally warmer and drier interval is suggested by pollen between 11,000 and 9,000 years ago, or near the end of the early Holocene (Southwest Anathermal and European Late Glacial) and essentially coincident with the local Precessional Solar Maximum 9/10 (Figure 26).

Figures 11-14 are Southern Hemisphere pollen and glacial records that suggest generally in-phase relations with Southern Hemisphere precessional insolation trends (which trends are 180 degrees out-of-phase with counterpart trends in the Northern Hemisphere), but also a moderate-to-strong tendency for secondary oscillations to phase with their Northern Hemisphere counterparts.

Figures 15-17 are Pluvial records that again appear to record out-of-phase primary climatic trends across the Equator but also again suggest moderate to strong in-phase relations of the superposed secondary oscillations in both hemispheres with the global tidal-resonance model.

Figures 18-20 are the longest pollen records from the Northwest (Figure 18), Southwest (Figure 19) and Midwest (Figure 20) that show some regional variability in generally similar primary trends but also moderate to strong tendencies of secondary trends to oscillate in phase with the Substage Cycle and tidal-resonance model.

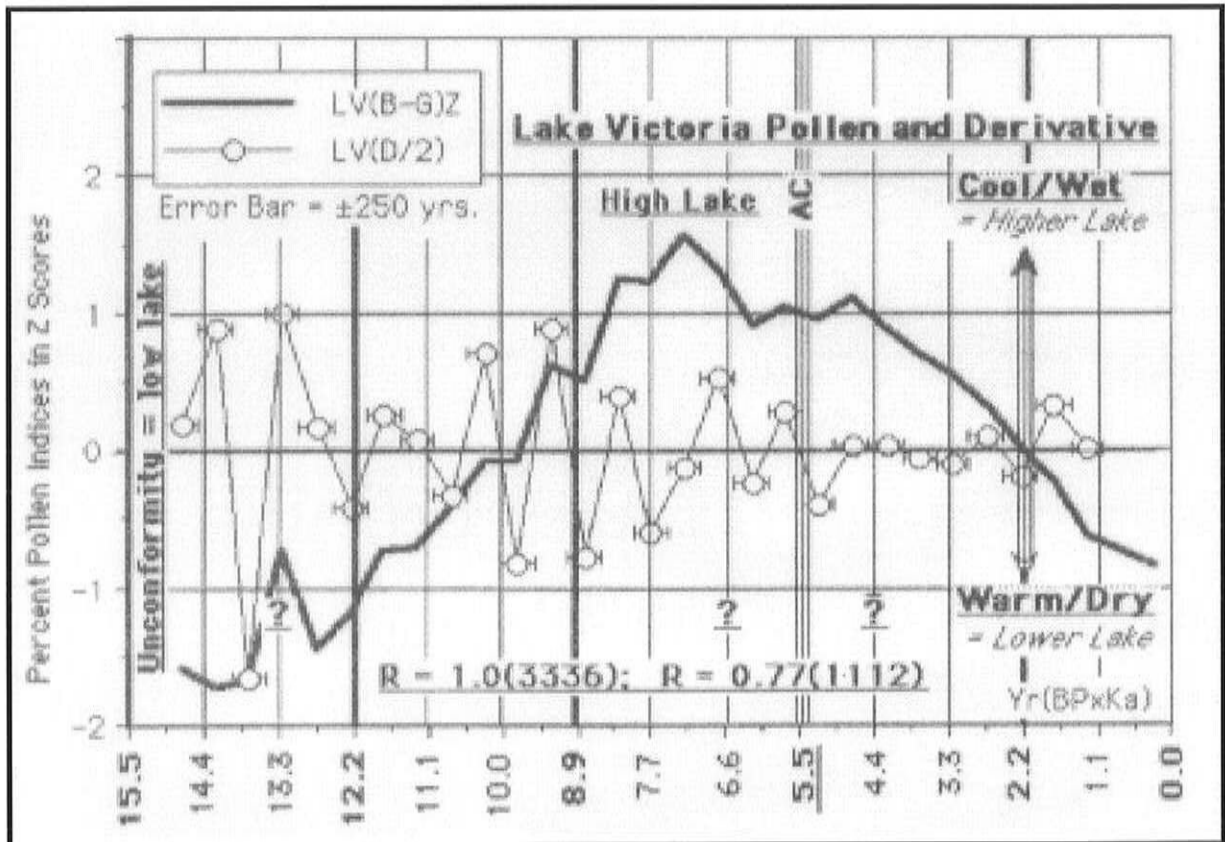


Figure 11 Lake Victoria pollen record on timescale of the 1112-year Stadal Cycle.

Pollen indices from Kendall (1969) replotted in centered 500-year intervals. Very strong tendency to oscillate in phase with the Substage Cycle; lesser but significant tendency with the Stadal Cycle. Note that the Allithermal Culmination (AC = maximum postglacial warm/dry) of the middle to upper latitudes of the Northern Hemisphere occurs here south of the Equator near the apex of a primary wetter/cooler maximum coincident with Precessional Minimum 10, which is displaced about 10,000 years from its Northern Hemisphere counterpart (Figure 26).

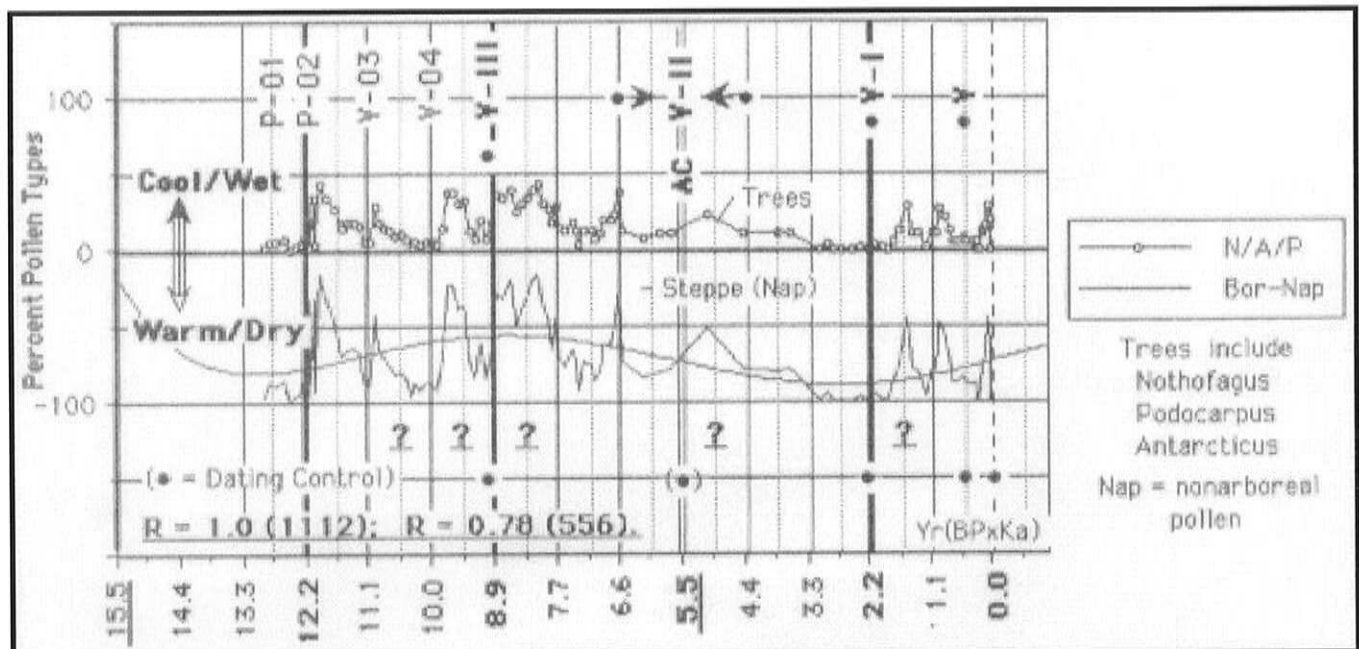


Figure 12 Bioclimatic record of La Mission Bog, Argentina, on timescale of the 1112-year Stadal Cycle and its 2/1 (556-year) Phase resonance.

Pollen indices and correlation with dated volcanic ash from Auer (1968) (Karlstrom 1968). As dated, strong tendency to oscillate in phase with the Stadal Cycle; lesser but significant tendency with the Phase Cycle. Primary trends seem to parallel that of the S60° Latitude insolation curve, including the post-2000-YBP slight upward trend that apparently reflects increased influence of Obliquity insolation at these higher latitudes (S55° L). Compare with Figures 11 and 26. V=volcanic ash; P=pumice. Also see Figure 27.

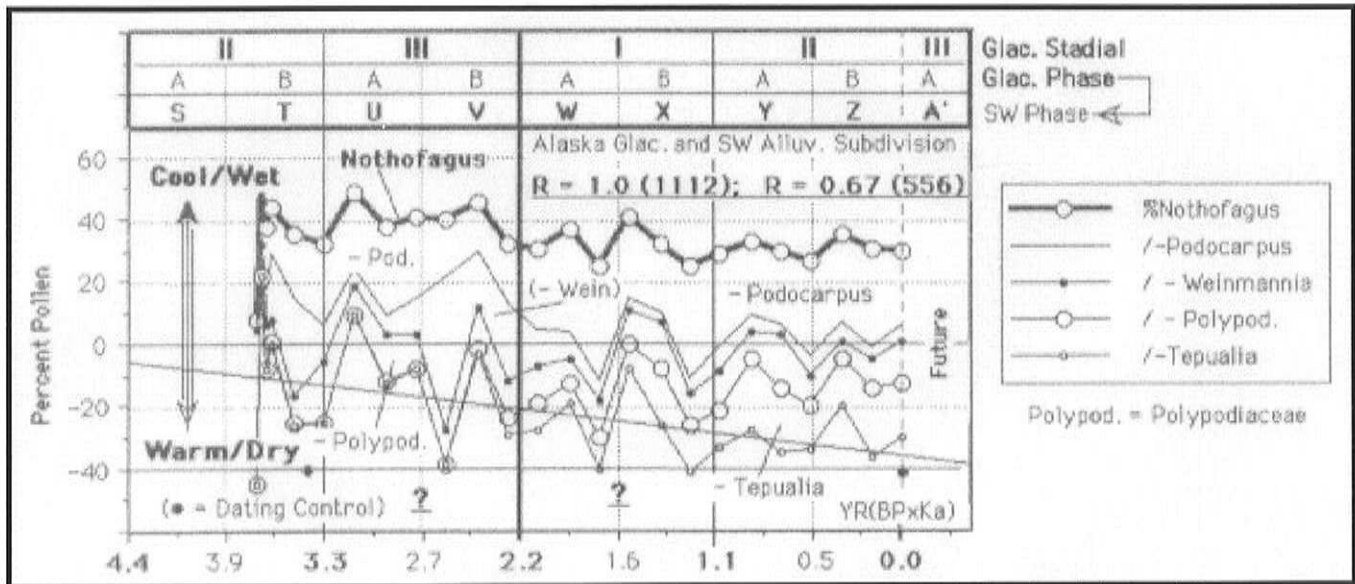


Figure 13 Bioclimatic record of Lago I Bog, Laguna de San Rafael area, Chile, on timescale 1112-year Stadal Cycle and its 2/1 (556-year) Phase resonance.

Pollen indices from Heusser (1960). Very strong tendency to oscillate in phase with the Stadal Cycle; a lesser, perhaps insignificant, tendency with the Phase Cycle. Note the primary warming/drying trend to the present, which parallels the local Precessional insolation trends near S45° latitude. These in turn are opposed to those in the counterpart Northern Hemisphere latitudes and with the correlative Little Ice Age (Figures 18, 19, 21, 26).

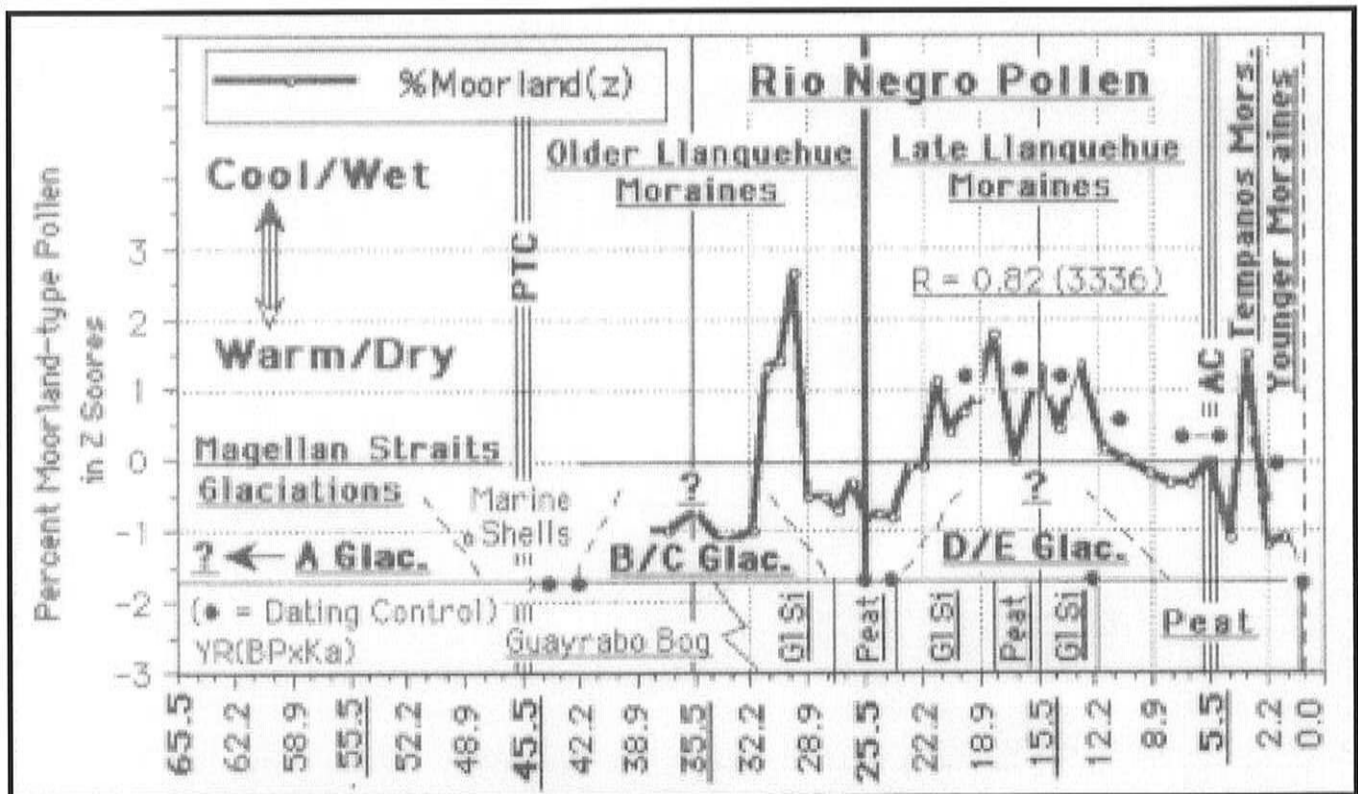


Figure 14 Correlation of Chile Pollen, Bog Stratigraphy, and dated glacial events on timescale of the 3336-year Substage cycle.

Pollen indices from Villagren (1988). Dating of Late Llanquihue moraines after Porter (1981). Dating of Magellan Straits glaciations and bog chronostratigraphy after Clapperton *et al* (1995). Dating of Tempanos and younger moraines from data in Muller (1960) as discussed in Karlstrom (1966). Strong pollen tendency for in-phase relations with the Substage Cycle. The convergent pollen, bog chronostratigraphic and dated glacial sequences are internally consistent in recording wetter climates and glaciations between 45,000, 25,000, and 12,000 years ago, or compatible with direct correlation with the precession-dominated insolation trends of the Southern Hemisphere. These are offset about 10,000 years from counterpart precessional and glacial trends in the Northern Hemisphere (Figures 21 and 26). GI Si=Glaciolacustrine silt = glaciation. Peat = nonglacial interval.

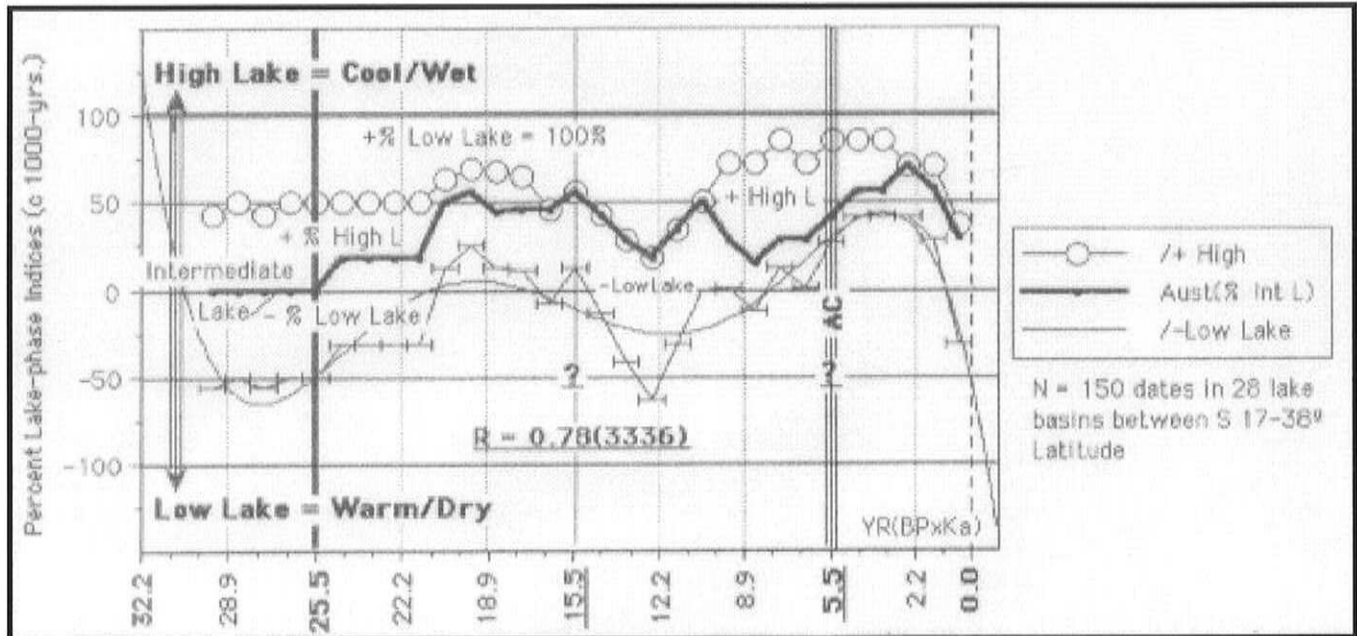


Figure 15 Time-frequency diagram of Australian lake phases (% high/intermediate/low) on timescale of the 3336-year Substage Cycle.

Lake-phase indices from Street and Grove (1979). Fairly strong tendency to oscillate in phase with the 3336-year Substage Cycle. This record seems to provide an additional example of a Southern Hemisphere climatic record suggesting precessional controls 180 degrees out of phase with Northern Hemisphere counterparts, as exemplified by the Southwest Lake record (Figure 16). For other records suggesting opposing primary climatic trends in the two hemispheres, see Figure 26. In the Northern Hemisphere, the Allthermal Culmination (AC) marks the turning point between postglacial warming/drying and trends toward cooler/wetter climate; in the Southern Hemisphere, it is seemingly closely associated with a cool/wet maximum with warming/drying trends to the present. Note the secondary cool/wet peak at about 20,000 years ago that appears to correlate with comparable secondary trends in other Southern Hemisphere records and with opposing secondary trends in Northern Hemisphere records as shown in Figure 26.

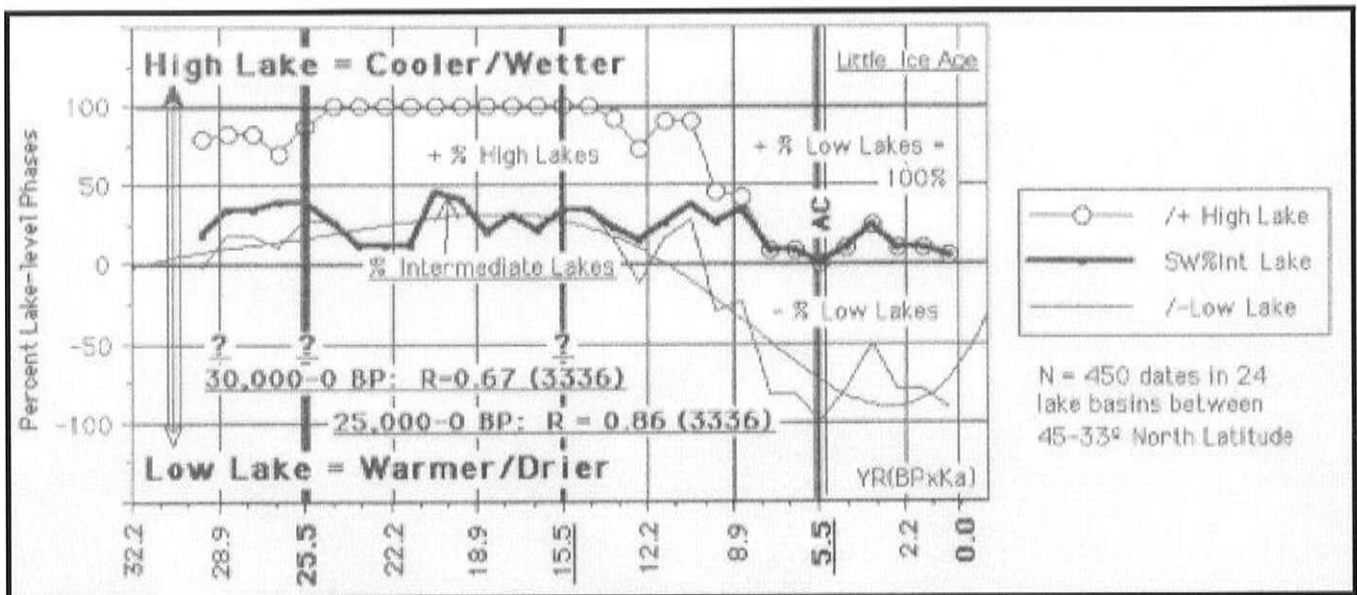


Figure 16 Time-frequency diagram of North American Southwest dated lake-level phases (% high/intermediate/low) on timescale of the 3336-year Substage Cycle.

Lake-level indices from Street and Groves (1979). Weak or insignificant tendency to oscillate in phase with the Substage Cycle, but a much stronger tendency in the post-25,000-YBP part of the curve controlled by a larger number of dates. More notable is the general trend of the dataset that suggests wetter/cooler climate around 20,000 years ago and warmest/driest climate around 5500 years ago, or generally consistent with regional pollen records (Hevly and Karlstrom 1974; Karlstrom 1995; this paper).

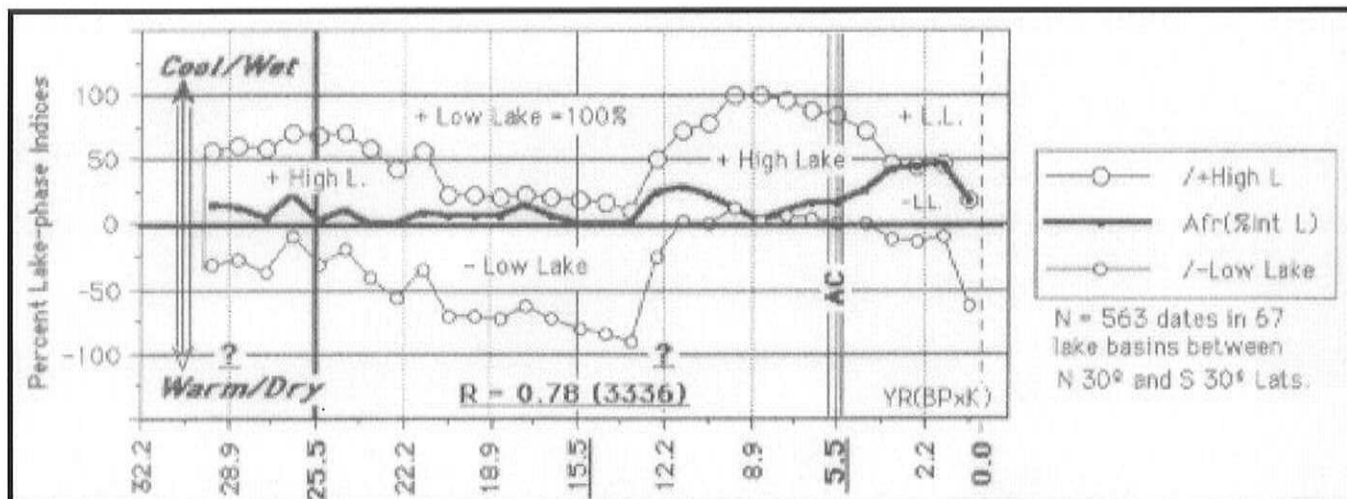


Figure 17 Time-frequency diagram of African lake phases (% high/intermediate/low) on timescale of the 3336-year Substage Cycle.

Lake-phase indices from Street and Grove (1979). Diagram is unsuitable as a test of the Precessional-insolation control model in that it mixes dates from lake basins both north and south of the Equator. As earlier suggested (Karlstrom 1966) and further supported by evidence presented in this paper, whereas longer-term climatic trends (presumably determined by Precessional insolation) were in opposition across the Equator, higher frequency climatic components (presumably modulated by tidal resonances) were globally synchronous. Therefore, it seems significant that the Equator-straddling African dataset shows a fairly strong tendency to oscillate in phase with the Substage Cycle while showing a mixture of both Southern and Northern Hemisphere primary trends, suggesting a predominance of Northern Hemisphere dates in the early part and a predominance of Southern Hemisphere dates in the later part of the record.

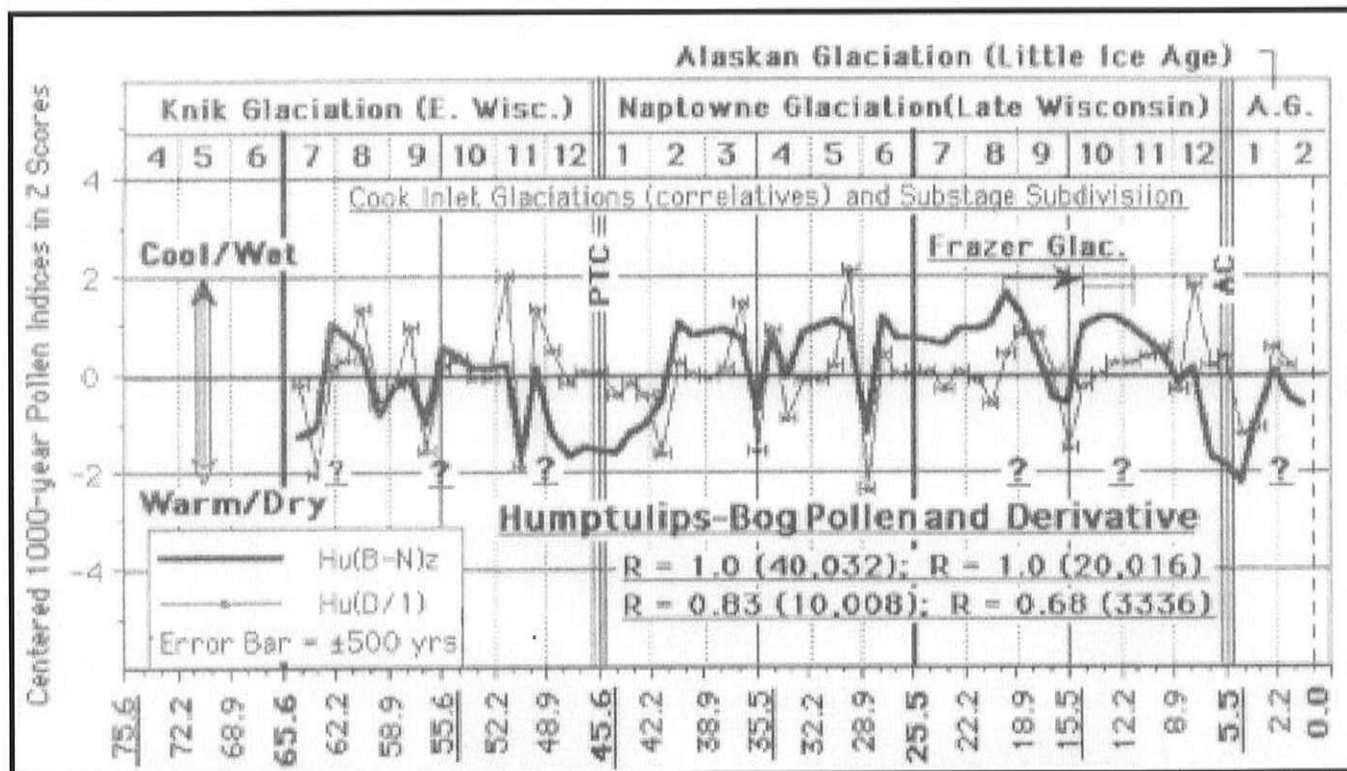


Figure 18 Bioclimatic record of Humptulips Bog, Washington, on timescale of the 3336-year Substage Cycle and its x3 (10,008-year), x6 (20,016-year), and x12 (40,032-year) super harmonics.

Pollen indices from Heusser (1965) replotted in 1000-year intervals. Strong tendency for oscillations in phase with the 3x, 6x, and 12x superharmonics; weak, or insignificant, tendency with the base Substage Cycle, but a stronger tendency (0.79) in the post-45,000-year (more firmly dated) part of the record. B=Boreal, N=Nonarboreal components. PTC=Port Talbot Culmination. AC= Allthermal Culmination. Note that the apparent coolest/wettest interval (about 20,000 years ago) occurred several thousand years before maximum extension of ice lobes of the Frazer Glaciation in the nearby Juan de Fuca Straits and Puget Sound trough.

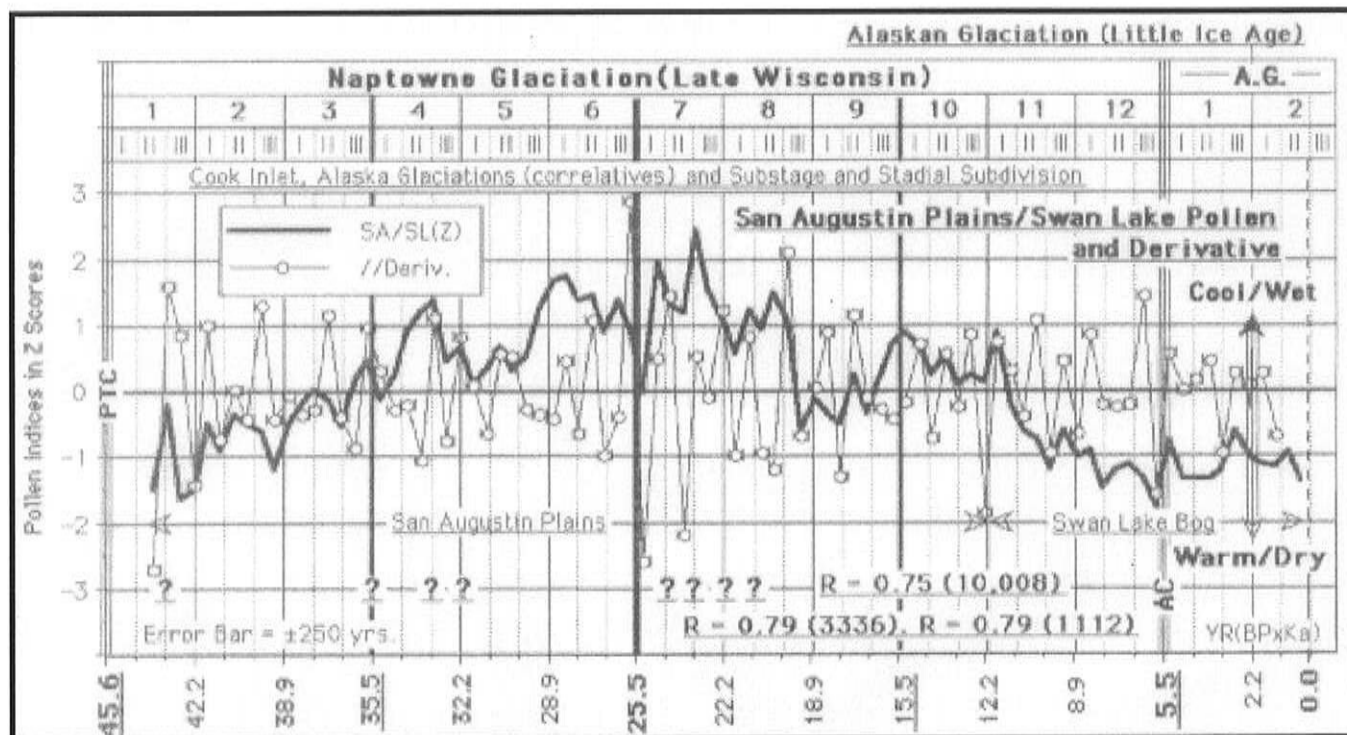


Figure 19 Southwest bioclimatic record on timescale of the 3336-year Substage Cycle and its 3/1 (1112-year) Stadal Resonance.

Pollen indices (Boreal-Nonboreal) replotted in 500-year intervals from data of the San Augustin region (Cisby *et al* 1964) and of the Swan Lake Bog, southern Idaho (Bright 1968). Fairly strong tendencies for oscillations in phase with the Substage and Stadal cycles. The combined record suggests cooler/wetter climate in the Southwest about 23,000 years ago, or thousands of years before maximum extensions of continental ice during the Last Glacial Maximum (LGM=late Wisconsin). However, the outermost belts of transecting moraines of this age date oldest in Ohio (about 21,000 YBP) and progressively younger in Illinois (about 28,000 YBP), in Iowa (about 14,000 YBP), and in North Dakota (about 12,000 YBP), presumably because of westward-shifting ice centers. Which is the LGM?

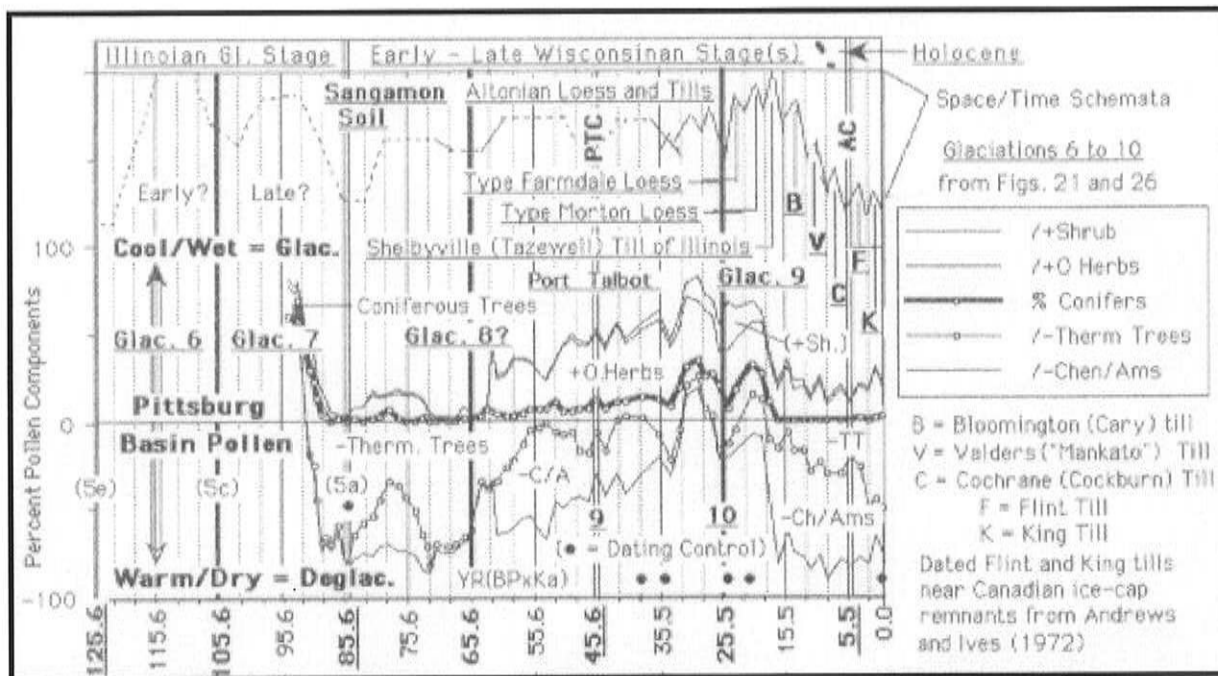


Figure 20 Bioclimatic record of the Pittsburg Basin, Illinois, on timescale of the 10,008-year Cycle and its 3/1 (3336-year) Substage Resonance.

Pollen indices from Grüger (1972). Beyond the radiocarbon-controlled part, the record is fine-tuned to the "standard" marine record of the Equatorial Pacific (Figure 25a), which places the thermophylous-tree maximum and the Sangamon Soil as correlatives of 5a (85,000 YBP) rather than of 5e (125,000 YBP) in the "standard" Equatorial Atlantic marine record (Figure 25b), as generally assumed. This alternative correlation seems more consistent with uniform depositional rates and obviates the presumption of a major unconformity in the pollen record for which there is no direct evidence. Dating of the classic morphostratigraphic substages in designated type localities suggests correlation with the  $\pm 3300$ -year cycle (Karlstrom 1961, 1976b) and also, as shown above, with secondary oscillations in the pollen record. Note that the PTC coincides with a minor thermophylous-tree maximum at the apex of Precessional Minimum 9 and correlative glaciations (Figure 21).

Figure 21 shows correlation of opposing high-resolution glacial records of the Northern and Southern Hemispheres with marine chronostratigraphy, precessional trends, and latitudinal displacement of the Caloric Equator and associated Intertropical Convergence Zone (ITCZ)

Figures 22-26 are previously published figures (Karlstrom 1995) slightly modified for ready comparison with the additional paleoclimatic time series presented in this Addendum.

Figures 27 and 28 are time-frequency diagrams of global and North American volcanic activity and correlation with the tidal resonance model.

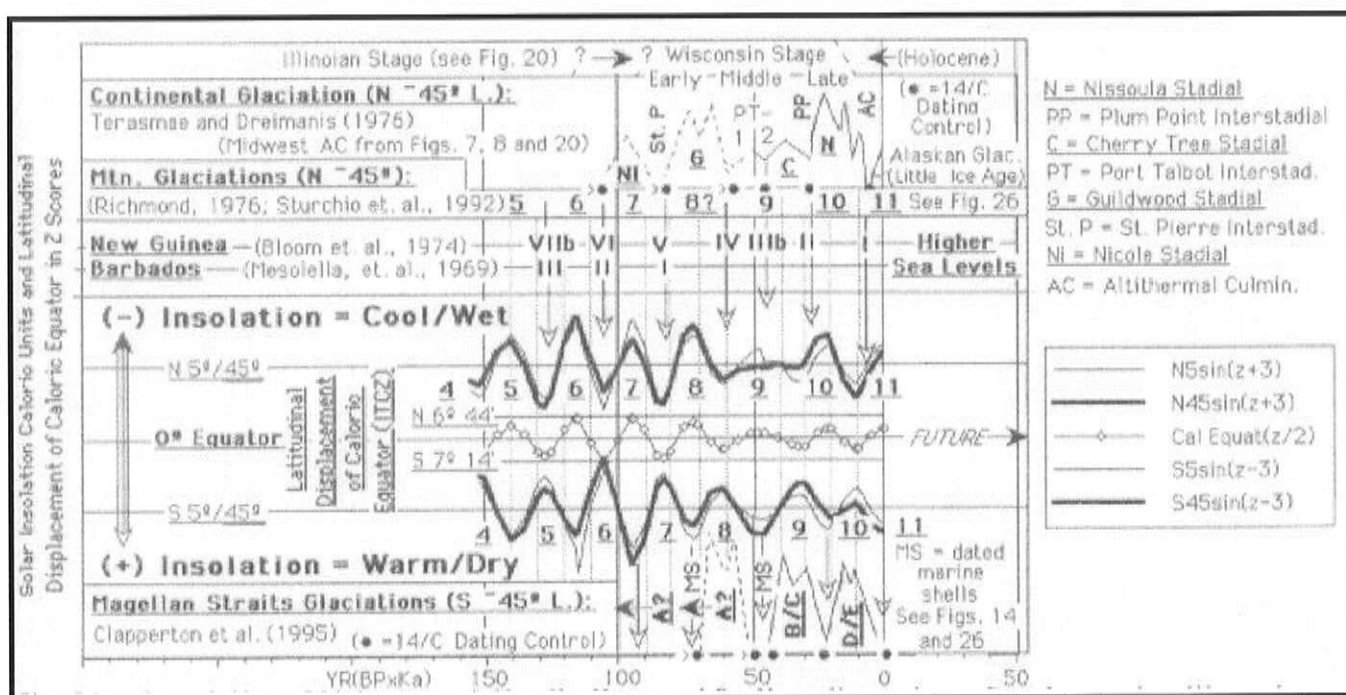


Figure 21 Correlation of highest resolution Northern and Southern Hemisphere glacial records with marine chronostratigraphy (glaceoestatic sea levels) and, in turn, with opposing hemispheric precessional trends and latitudinal displacements (in degrees) of the Caloric Equator and associated Intertropical Convergence Zone (ITCZ).

Richmond (1976) and Terasmae and Dreimanis (1976) see a remarkable coincidence between their glacial chronostratigraphies and that of the dated sea level records. This supports the concept of glacioeustasy but not necessarily that of inter-hemispheric climatic synchrony. This is because the much greater volume of glacial ice in the Northern Hemisphere can mask opposing meltwater trends in the interconnected oceans of the Southern Hemisphere (Karlstrom 1966). Clapperton *et al* (1995) see no clear-cut correlation of their Southern Hemisphere glacial record with that of the Northern Hemisphere. However, their B/C and D/E glacial complexes, as broadly dated between 45,000 years, 25,000 years, and the present, most closely correlate with the local Southern Hemisphere precessional trends, which in turn are displaced 10,000 years from their Northern Hemispheric counterparts and correlative continental glacial events. Insolation curves after Milankovitch (1941). Alternate N-S displacement of the Caloric Equator and reversing insolation gradients may serve to force or facilitate modulation of changing summer circulation patterns in the two hemispheres. Note the apparent absence in lower Southern Hemisphere of the Northern Hemisphere Alaskan Glaciation due to opposing precessional trends. (Also Figure 13).

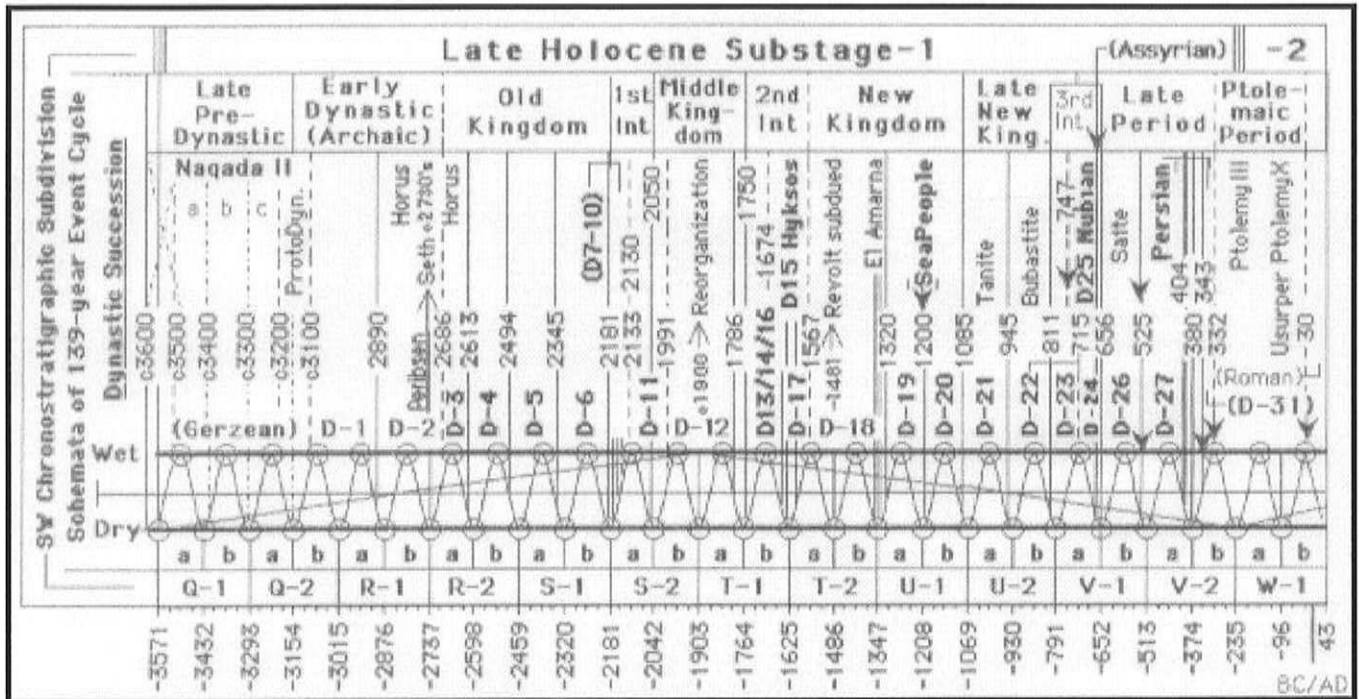


Figure 22 Correlation of Egyptian Dynastic History with schemata of the 139-year Event Cycle.

Reconstruction of dynastic record from James (1979), who notes that the dating is approximate and increasingly so toward the beginning of the record. Most dated boundaries (solid lines) fall within the dry epicycles; the remaining few (dashed lines) fall within the wet epicycles, suggesting that environmental stress (lower Nile levels) played a contributory role in dynastic succession. If so, empirical evidence for the Event Cycle is extended back to the mid-Holocene. Similarly, instrumental temperature evidence of its about-70-year half cycle is projected back to the mid-Holocene through correlation with dated beach ridges of Lake Michigan (Delcourt *et al* 1996). Modified from Figure 11 in Karlstrom (1995).

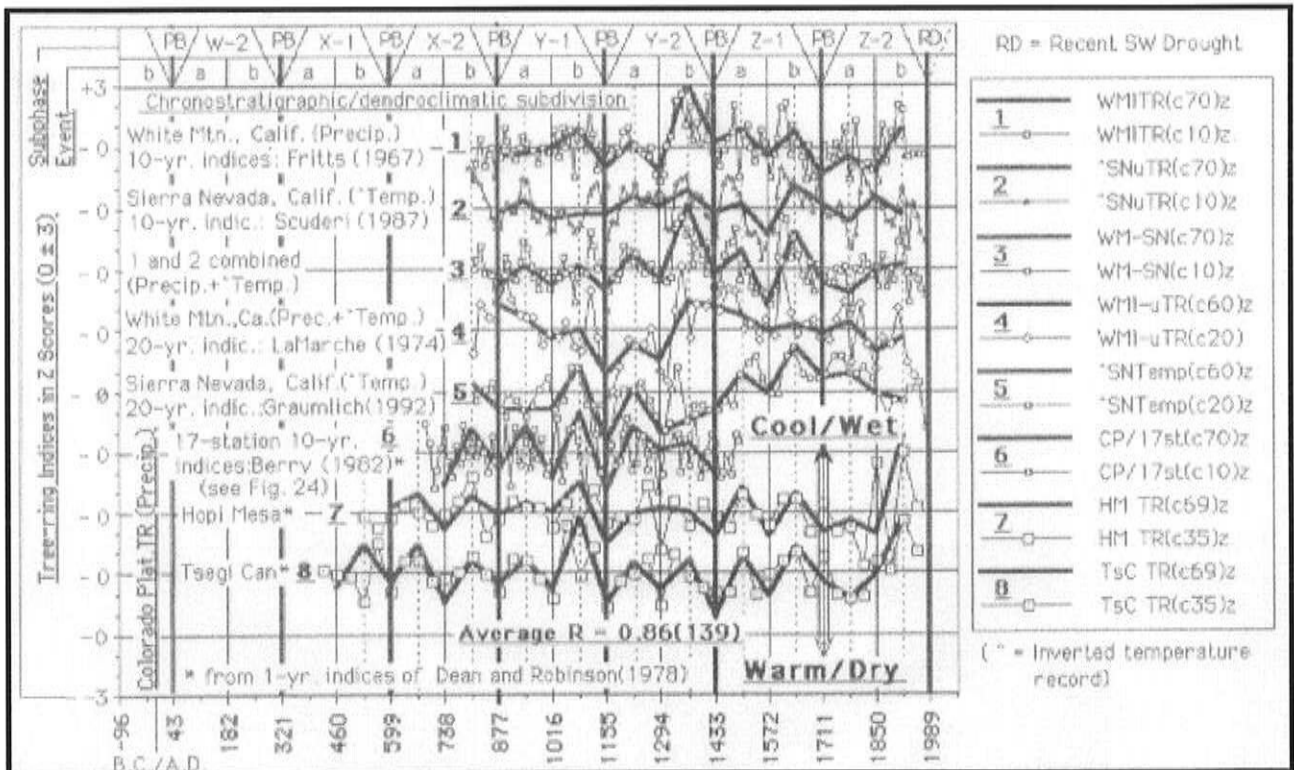


Figure 23 Summary evidence for a dendroclimatic cycle in phase with the 139-year Event Cycle.

Half-cycle smoothing positioned on cycle turning points. Trend correlations, temperature and precipitation, range from 0.75 to >0.90, or within the upper range of tree-ring/climate calibrations. This suggests that the cycle is real, regionally robust, and related to changing atmospheric dynamics and patterns. Similar half-cycle analyses of other records may define different regional patterns and responses, advancing understanding of climatic/biologic process. Modified from Figure 10 in Karlstrom (1995). PB=Point Boundary (clustering of Southwest basal alluvial dates) from Karlstrom (1988).

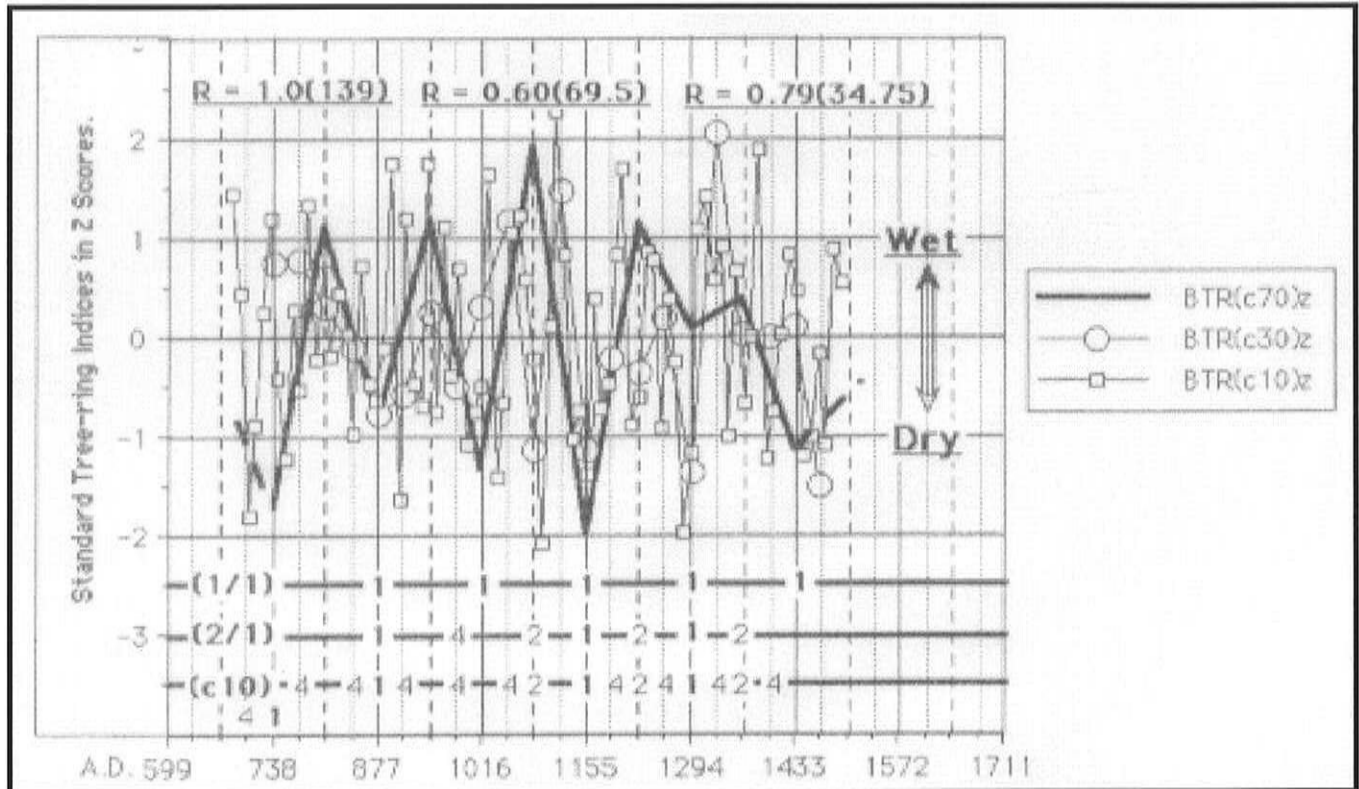


Figure 24 Dendroclimate record of the southern Colorado Plateaus on timescale of the 139-year Event Cycle and its 2/1 (69.5-year) and 4/1 (35-year) Resonances.

Seventeen-station decadal tree-ring indices from Berry (1982). Half-cycle smoothing as before. Very strong precipitation response to the Event Cycle; lesser but significant response to the 4/1 (34.75-year = Brückner Cycle) resonance. Figure same as Figure 6 in Karlstrom (1995).

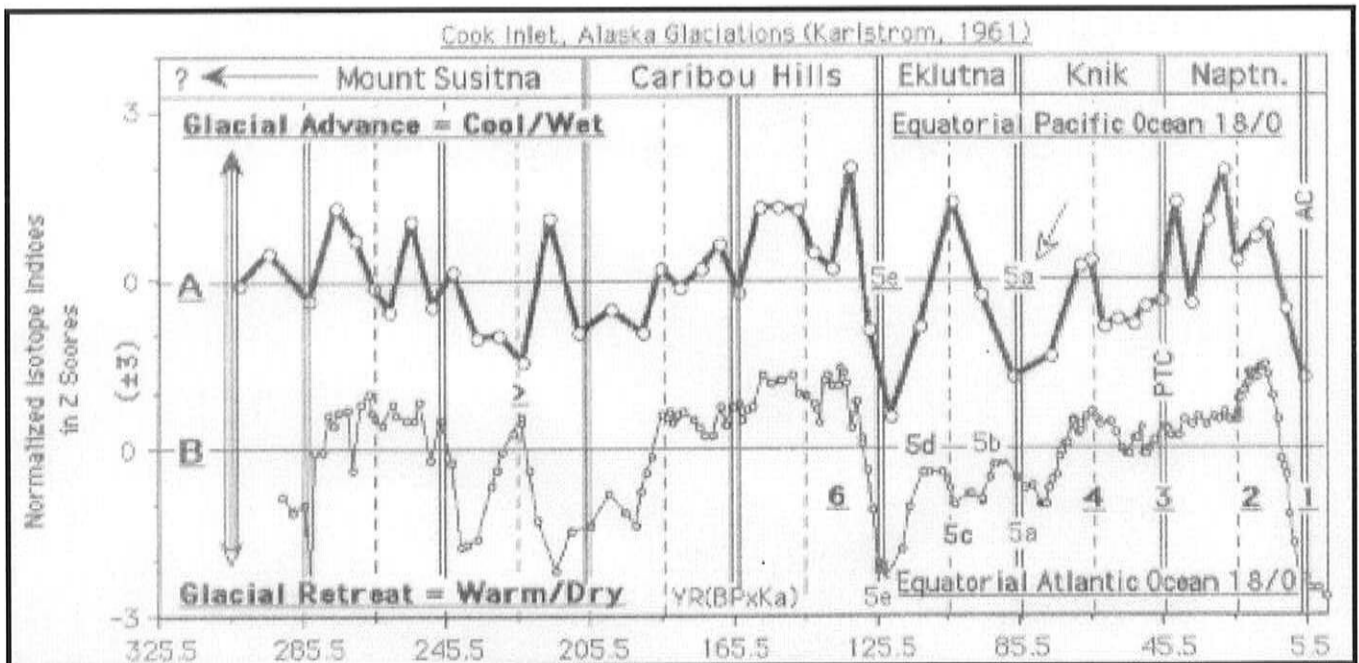


Figure 25 Two "standard" Marine Ice Age chronologies on timescale of the Obliquity Insolation Cycle (about 40,000 years) and its 2/1 about 20,000 years) Resonance assuming a response lag of about 4500 years (Karlstrom 1961).

Equatorial Pacific record from Chuey *et al* (1987); the Equatorial Atlantic record from Martinson *et al* (1987). Both are fine-tuned to the Milankovitch Climate Model assuming corresponding response lags. The curves differ mainly in (1) out-of-phase relations about 225,000 years ago and (2) relative glacial amplitudes in the past 125,000 years, suggesting either heterogeneities in the marine record or remaining difficulties with dating procedures and sample mixing. Note the tendency for in-phase oscillations with the Obliquity 2/1 (about 20,000 year) Resonance. Modified from Figure 28 in Karlstrom (1995).

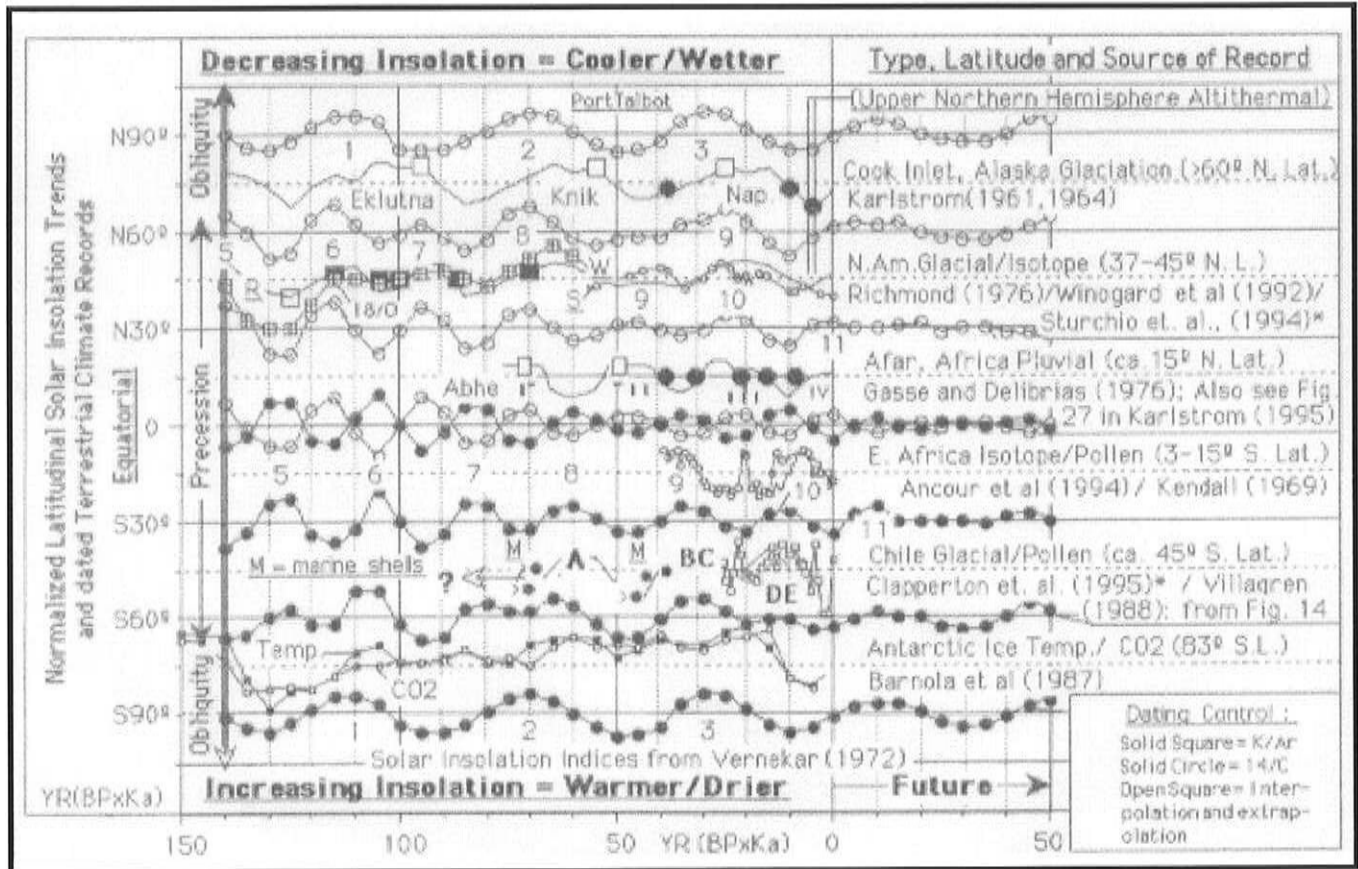


Figure 26 Latitudinal control of terrestrial climate records.

These dated records seem to parallel more closely the local latitudinal insolation trends than the records at other latitudes. If these climate records are representative of their respective latitudinal belts, the conventional concept of interhemispheric climatic synchrony must be reassessed as a basis for Ice Age correlations and resulting global paleoclimatic reconstructions (Karlstrom 1961). Modified from Figure 29 of Karlstrom (1995): \* = added record.

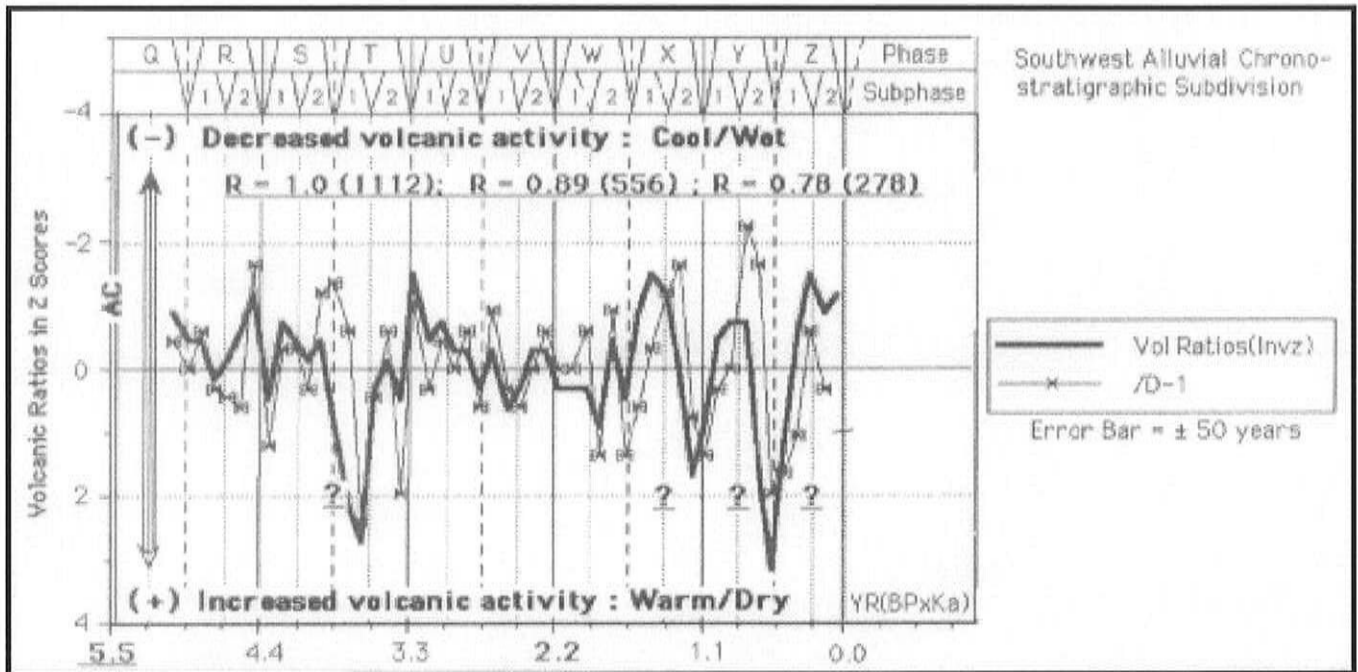


Figure 27 Time-frequency diagram and derivative of dated volcanic events on timescale of the 1112-year Stadal Cycle and its 2/1 (556-year) and 4/1 (278-year) resonances.

Volcanic-ratio indices from Bryson and Goodman (1980) converted to Z Scores. Strong tendency for intervals of increased volcanism to phase with drought (warm/dry) intervals of the Subphase (278-year) Cycle and stronger tendencies with its x2 (556-year) and x4 (1112-year) superharmonics. These correlations strongly suggest that tidal resonances and associated increased rate of Earth's spin play a role in triggering volcanic activity and minimize the importance of transitory cooling (and warming) of the atmosphere by volcanic ejecta as a causal factor in longer-term climate change. From his pioneer work on South American pollen, Veni Auer (1966) early suggested the correlation between volcanism and warmer climate. Time-frequency analyses of dated volcanic events culled from the radiocarbon literature through 1972 suggest similar statistical relationships between volcanism and warm climate in North America and globally through common correlation with the tidal model (Figure 28). Bryson and Goodman's selected global dataset thus apparently provides independent support for these correlations. To predict local volcanic events solely by tidal intensity, however, is highly uncertain because of the statistical nature of the correlation and because of the triggering mechanism that requires endogenous processes near threshold conditions.

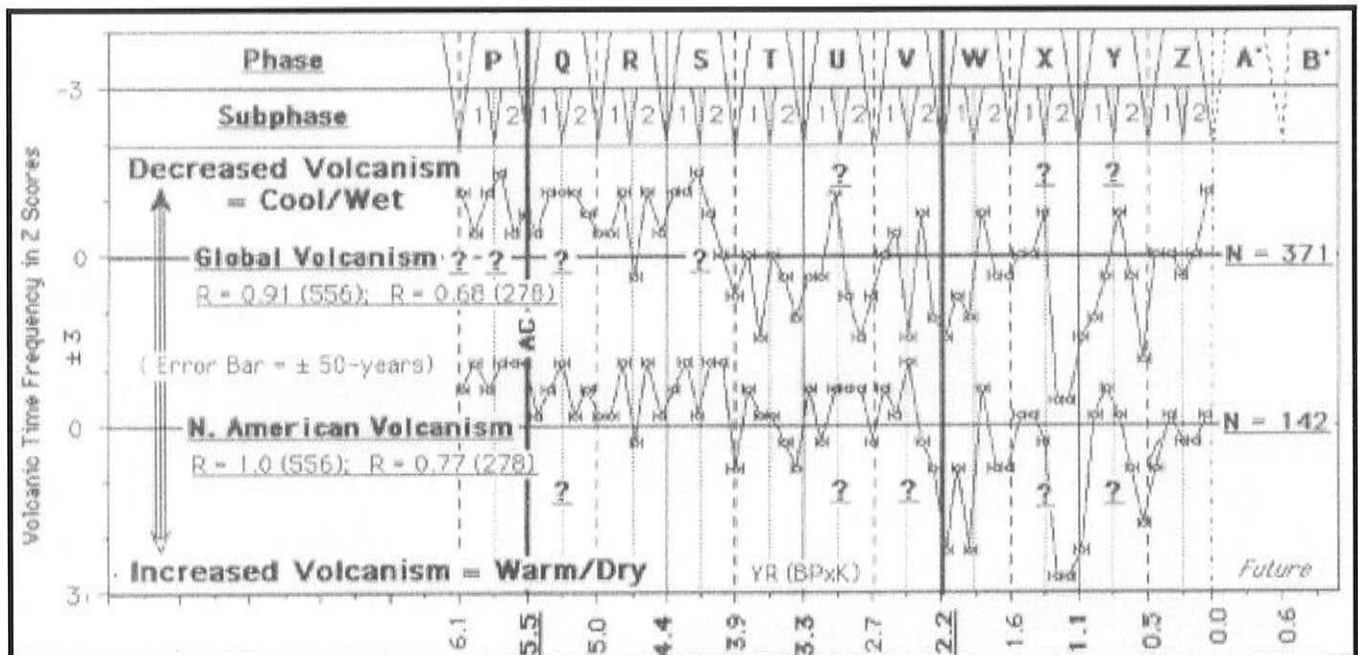


Figure 28 Time-frequency diagrams of global and North American volcanic activity on timescale of the 556-year Phase Cycle and its 2/1 (278-year) Resonance.

Volcanic indices from Figure 7 in Karlstrom (1975); 100-year class intervals centered in centuries. Note strong tendency for increased volcanic activity during the warm/dry epicycles of the Phase Cycle and the lesser tendencies during those of the Subphase Cycle.

## Summary

---

Detailed cyclical analyses of the additional Northern and Southern Hemisphere terrestrial time series presented in this paper provide an expanded database that substantially fortifies and extends previous interpretations and correlations with the Solar-Insolation/Tidal-Resonance Model. However, in the absence of an accepted climatic theory and a fuller understanding of the climatic dynamics and atmospheric circulation patterns involved, it is necessary to assume that the presented empirical correlations represent in some fashion direct cause-and-effect relationships and, further, that the expanded database is sufficient to generally satisfy the fundamental requirement of latitudinal representativeness. With these caveats in mind, I conclude the following:

- Longer-term “Ice Age” changes were out of phase across the Equator and evidently modulated by Precessional-insolation trends, which in the Northern Hemisphere are 180 degrees out of phase with those in the Southern Hemisphere. The supporting data run counter to the conventional assumption of interhemispheric synchrony and parallel glacial records and suggest that major revisions are required in the derived concepts of global atmospheric circulation dynamics and patterns. Theoretically, there appears to be no apparent reason why, if the Northern Hemisphere glaciers responded directly to summer half-year insolation (the Milankovitch mechanism), the glaciers and associated hydrologic processes in the Southern Hemisphere were not similarly controlled by the opposing local summer-insolation trends. Interconnected ocean bodies explain why the greater volumes of continental ice in the Northern Hemisphere generally dominated the marine meltwater and glacioeustatic records of both hemispheres. In contrast, the terrestrial climatic records suggest that the current (nominal) atmospheric circulation barrier between hemispheric air masses created by the oscillating Intertropical Confluence Zone persisted throughout the time of record.
- In contrast to the above longer-term climatic trends, superposed secondary oscillations (those less than several thousands of years in duration) were synchronous across the Equator and evidently were modulated by tidal resonances generated essentially simultaneously throughout the global atmosphere.
- Detailed analysis of a bioclimatic record (Figure 3) suggests that differing seasonal timings of fractional higher frequency atmospheric resonances contribute to fluctuational variability present in some bioclimatic time series.
- The longest pollen records (Figures 18-20) suggest a terrestrial cycle of about 10,000 years, comparable in length to that recently noted in higher resolution marine records.

- The correlation of increased global volcanic activity with warmer/drier epicycles of the Tidal-Resonance Model strongly suggests that tidal stressing of the lithosphere played a triggering role in volcanic frequency and minimizes the importance of transitory cooling (and local warming) by volcanic ejecta as a causal factor in longer-term climate changes. To predict local volcanic events solely by tidal intensity, however, is highly uncertain because of the statistical nature of the correlation and because of the presumed triggering mechanism that requires endogenetic processes near threshold conditions.
- The Solar-Insolation/Tidal-Resonance Model appears to satisfy temporal and spatial similarities and differences in paleoclimatic records not explained by other climate models. It is a viable scientific hypothesis in that it remains empirically testable by continued cyclical analyses of scores of other high-resolution records available in the extensive international paleoclimatic literature. Further testing should concentrate on the distribution of records improving uniformity of global coverage — particularly in upper latitudes to satisfy dominant Obliquity controls and along the Equator to satisfy past displacements of the Caloric Equator and associated Intertropical Convergence Zone. These longer-term Equatorial displacements along with changing insolation gradients (Figure 21) are potentially important mechanisms for driving or modulating seasonal atmospheric circulations patterns in the two hemispheres.
- When sufficient supporting data are accumulated, it will be possible to significantly improve (within limits of sampling interval and dating resolution) the dating and correlation of secondary cycles by fine-tuning to the theoretical tidal-resonance model. This model is primarily built on the celestial-mechanics calculations of Pettersson (1914) as cyclically extended by Stacey (1963, 1967) and continues to provide a best fit for the paleoclimatic records presented in this and previous papers. Additional celestial-mechanics analyses of tidal-force changes are required to assess the general validity of the Pettersson-Stacey calculations and to define the higher-frequency components of planetary perturbations.

## Acknowledgments

---

The results of my research on paleoclimate have been tempered in the crucible of vigorous discussions with numerous colleagues over the course of many years. Early on, I am particularly indebted to my U.S. Geological Survey colleagues, the late L.L. Ray, W. Bradley, H.W. Coulter, John Hack, Al Chidester, and Robert R. Sutton; to many others, including the late J Harlen Bretz, Kritiof Fryxel, Rudy Edmond, Ernst Antevs, V. Auer, Carl Lindroth, Eric Hultén, Alexis Dreimanis, and David Bloomenstock; to George Ball, Robert Rausch, and W.C. Mahany; and also to Rhodes Fairbridge for his insightful, eclectic, and extensive contributions to paleoclimatic research. Later on, special acknowledgment is due my colleagues (Jeffrey S. Dean, Robert C. Euler, George J. Gumerman, and Richard H. Hevly) in the "Gang of Five" for provocative ideas and comradeship during our 15 years of joint field research on environment and prehistoric culture of the Colorado Plateaus. I also thank Jeff Dean, Dick Hevly, and Eric Karlstrom for reading and commenting on an earlier version of this paper. Any errors in data selection, analysis, and interpretation remain my own. Finally, I acknowledge the professionalism and assistance of Caroline Isaacs and Vera Tharp, editors of the PACLIM Workshop, who have greatly facilitated the publication of my most recent research results.

## Bibliography

---

- Ancour, A-M, C. Hillaire-Marchel, and R. Bonnefille. 1994. Late Quaternary biomass changes from  $^{13}\text{C}$  measurements in a highland peat bog from Equatorial Africa (Barundi), *Quat. Research* 41:225-233.
- Anderson, P.N., R.E. Reanier, and L.B. Brubaker. 1990. A 14,000-year Pollen Record from Sithylemenkat Lake, North-Central Alaska. *Quat. Research* 33:400-404
- Andrews, J.T., and J.D. Ives. 1972. Late glacial and postglacial events (<10,000 BP) in the eastern Canadian Arctic with particular reference to the Cockburn Moraines and break-up of the Laurentide ice sheet. Pages 149-174 in *Acta Univ. Oul. Series A, No. 3, Geol. No. 1*. Y. Vasaari, H. Hyvarinen, and S. Hicks, editors.
- Antevs, E. 1955. Geologic-climatic dating in the West. *Am. Antiquity*, 20:317-335
- Auer, V. 1958. *The Pleistocene of Fuego-Patagonia, Pt. II: The History of the Flora and Vegetation*. Pub. Inst. Geogr., Univ Helsinkiensis 30, Helsinki.
- Auer, V. 1966. Climatic variations in Fuego-Patagonia. Pages 37-55 in *Pleistocene and Post-pleistocene climatic variation in the Pacific area*. D.L. Blumenstock, editor. Bishop Museum Press Honolulu.
- Barnola, J.M., D. Raymond, Y.S. Korotkevich, and C. Lorius. 1987. Vostock ice core provides 160,000 year record of atmospheric CO<sub>2</sub>. *Nature* 329:4-10.
- Bergthorsen, P. 1969. An estimate of drift ice and temperature in Iceland in 1000 years. *Jour. of Jokull* 19:94-101.
- Berry, M.S. 1982. *Time/Space and Transition in Anasazi Prehistory*. Univ. of Utah Press, Salt Lake City. 147 pp.
- Bloom, A.L. et al. 1974. Quaternary sea level fluctuations on a tectonic coast: New  $^{230}\text{Th}/^{234}\text{U}$  dates from the Huon peninsula, New Guinea. *Quat. Research* 4:185-205
- Bradley, R.S. 1985. *Quaternary Paleoclimatology*. Allen and Unwin, Boston.

- Breternitz, D.A. 1986. *Dolores Archaeological Program: Final Synthetic Report*. U.S. Department of the Interior, Bureau of Reclamation, Engineering and Research Center, Denver.
- Bright, R.C. 1968. Pollen and seed stratigraphy of Swan Lake, southeastern Idaho: Its relationship to regional vegetations history. *Jour. Idaho State Univ. Mus. Tebiwa*, 9
- Bryson, R.A., and B.M Goodman. 1980. Volcanic activity and climatic changes. *Science* 207:1041-1044.
- Chuey, J.M., D.K. Rea, and N.G. Piasias. 1987. Late Pleistocene paleoclimatology of the central Equatorial Pacific: A quantitative record of eolian and carbonate deposition. *Quat. Research* 38:323-33.
- Clapperton, C.M., D.E. Sudgen, D.S. Kaufman, and R.D. McCulloch. 1995. The last glaciation in central Magellan Strait, southernmost Chile. *Quat. Research* 44:133-148.
- Clisby, K., and P.B. Sears. 1956. San Augustin Plains — Pleistocene climatic changes. *Science* 124:537-539.
- Clisby K.H., F. Foreman, and P.B. Sears. 1962. Palynology-diastrorphism-erosion. Pages 28-30 in Internat. Pollen Conf. field excursion, Pleistocene palynology of the southwest: Tuscon, Arizona.
- Dean, J.S. 1996. Demography, environment and subsistence stress. Pages 25-56 in *Resource Stress, Economic Uncertainty and Human Response in the Prehistoric Southwest*. J.A. Tainer and B. Tainer editors. Workshop Proceedings XXIV, Santa Fe Institute Studies in the Sciences of Complexity, Addison-Wesley Publishing Company, Advanced Book Program, Reading, MA.
- Dean, J.S., and W.J. Robinson. 1978. Expanded tree-ring chronologies for the southwest United States. *Chronology Series III, Laboratory of Tree-ring Research*. Univ. of Arizona, Tucson. 58 pages.
- Dean J.S., and G.S. Funkhouser. 1994. Dendroclimatic reconstructions for the southern Colorado Plateau. Pages 85-104 in *Climate Change in the Four Corners and Adjacent Regions: Implications for Environmental Restoration and Land-Use Planning*, W.J. Waugh, editor. Proceedings of Workshop , Campbell College Center, Mesa State College, Grand Junction, Colorado, Sponsored by U.S. Department of Energy, Grand Junction Projects Office, Desert Research Institute, U.S. Bureau of Land Management, Mesa State College.
- Delcourt, P.A., W.H. Petty, and H.R. Delcourt. 1996. Late-Holocene formation of Lake Michigan beach ridges correlated with a 70-year oscillation in global climate. *Quat. Research* 45:321-326.
- Dorale, J.A. 1992. A high resolution record of Holocene climate change in speleothem calcite from Cold Water Cave, Northeast Iowa. *Science*, 258:1626-1630.
- Euler, R.C., G.J. Gumerman, T.N.V. Karlstrom, J.S. Dean, and R.H. Hevly. 1979. The Colorado Plateaus: Cultural dynamics and paleoenvironment. *Science* 205:1089-1101.
- Force, E.L., and W. Howell. In press. Holocene depositional history and Anasazi occupation of McElma Canyon, southwestern Colorado. *Arizona State Museum Archaeological Series*.
- Fritts, H.C. 1963. Tree-ring analysis (dendroclimatology). Pages 1008-1026 in *The Encyclopedia of Atmospheric Sciences and Astrogeology*. R.W. Fairbridge, editor. Reinhold Publishing, New York.
- Gasse, F., and G. Delibrious. 1976. Les Lacs de L'afar Centrol (Ethiopie et F. T. A. I.). Pages 529-575 in Shoji Horie, Ed. *Paleoclimatology of Lake Biwa and the Japanese Pleistocene* 4.
- Graumlisch, L.J. 1992. A 1000-year record of climatic variability in the Sierra Nevada, California: Handout, Am. Quat. Assoc. 12th Biennial Meeting, August 24-26, Univ. of Calif., Davis.
- Grissino-Mayer, H.D. In press. A 2129-year annual record of drought for northwestern New Mexico, USA. *Tree-Rings, Environment and Humanity*. J.S. Dean, D. Mako, and T.W. Swetman, editors. Proceedings of the International Conference, Tucson, Arizona, May 17-21, 1994. *Radiocarbon*.
- Grüger, E. 1972. Late Quaternary vegetation development in south-central Illinois. *Quat. Research* 2:217-231.
- Gumerman, G.E., Ed. 1988. *The Anasazi in a Changing Environment*. Cambridge Univ. Press, London.
- Heusser, C.J. 1960. Late-pleistocene environments of the Laguna de San Rafael area. Chile. *The Geographical Review*, L. 4:555-577.

- Heusser, C.J. 1965. A Pleistocene phytogeographic sketch of the Pacific Northwest and Alaska. Pages 469-483 in *The Quaternary of the United States*. H.E. Wright and B.G. Frey, editors. Princeton Univ. Press, Princeton, NJ.
- Hevly, R.H. 1988. Prehistoric vegetation and paleoclimates on the Colorado Plateaus. Pages 92-118 in *The Anasazi in a Changing Environment*, J.G. Gumerman, editor. Cambridge Univ. Press, Cambridge, GB.
- Hevly, R.H. 1989. Post-15,500 BP Pollen of Walker Lake, Arizona. (Preliminary manuscript).
- Hevly, R.H., and T.N.V. Karlstrom. 1974. Southwest paleoclimate and continental correlations. Pages 257-295 in *Geology of Northern Arizona and Notes on Archaeology and Paleoclimate*. T.N.V. Karlstrom, G. Swann, and R.L. Eastwood, editors. Geol. Soc. of America Field Guide 1. Rocky Mountain Meeting, Flagstaff, AZ.
- James, T.G.H. 1979. *Introduction to Ancient Egypt*. Farrar Straus Giroux, New York, in association with the British Museum Publication Limited, London. 286 pp.
- Karlstrom, T.N.V. 1961. The glacial history of Alaska: Its bearing on paleoclimatic theory. *Annals New York Academy of Science* 95, Article 1:290-340.
- Karlstrom, T.N.V. 1964. Quaternary geology of the Kenai Lowland and glacial history of the Cook Inlet Region, Alaska. *U.S. Geological Survey Professional Paper* 443. 69 pp.
- Karlstrom, T.N.V. 1966. Quaternary glacial record of the North Pacific region and worldwide climatic change. Pages 153-182 in *Pleistocene and Post-Pleistocene Climatic Variations in the Pacific Area*. D.J. Blumenstock, editor. Bishop Museum Press, Honolulu.
- Karlstrom, T.N.V. 1975. Cenozoic Time-stratigraphy of Colorado Plateaus, Continental Correlations and some Paleoclimatic Implications. Handout, Symposium on Quaternary Stratigraphy, York University, Toronto, May 1975.
- Karlstrom, T.N.V. 1976a. Stratigraphy and paleoclimate of the Black Mesa Basin. *U.S. Geological Survey Circular* 778:18-22.
- Karlstrom, T.N.V. 1976b. Quaternary and upper Tertiary time-stratigraphy of the Colorado Plateaus, continental correlations and some paleoclimatic implications. Pages 275-282 in *Quaternary Stratigraphy of North America*. W. C. Mahany, editor. Bowden, Hutchinson and Ross, Stroudsburg, PA.
- Karlstrom, T.N.V. 1988. Alluvial chronology and hydrologic change of Black Mesa and nearby regions. Pages 45-91 in *The Anasazi in a Changing Environment*. G.J. Gumerman, editor. School of American Research Advance Seminar Book, Cambridge Univ. Press, London.
- Karlstrom, T.N.V. 1995. A 139-year dendroclimatic cycle, cultural/environmental history, sunspots and longer-term cycles. Pages 137-159 in *Proceedings of the Eleventh Annual Pacific Climate (PACLIM) Workshop, April 19-22, 1994*. C.M. Isaacs and V.L. Tharp, editors.. Interagency Ecological Program, Technical Report 40. California Department of Water Resources.
- Karlstrom, T.N.V. 1996. The QBO, El Niño, and Tidal Resonance Model. Pages 241-253 in *Proceedings of the Twelfth Annual Pacific Climate (PACLIM) Workshop, May 2-5, 1995*. C.M. Isaacs and V.L. Tharp, editors. Interagency Ecological Program, Technical Report 46. California Department of Water Resources.
- Karlstrom, T.N.V., G.J. Gumerman, and R.C. Euler. 1976. Paleoenvironmental and cultural correlates in the Black Mesa region. Pages 149-161 in *Papers on the Archaeology of Black Mesa, Arizona*. G.J. Gumerman and E.C. Euler, editors. Southern Illinois University Press, Carbondale.
- Kendall, R.L. 1969. An ecological history of the Lake Victoria Basin. *Ecological Monographs* 39:121-176.
- Ladure, E.L. 1971. *Times for Feast and Times of Famine: A History of Climate Since the Year 1000*. Doubleday, NY.
- Lamarche, V.C. Jr. 1974. Paleoclimatic inferences from long tree-ring records. *Science* 183:1043-1048.
- Lamb, H.H. 1977. *Climate: Present, Past and Future, Vol. 2, Climate History and the Future*. Methuen, London.

- Martinson, D.G., N.G. Pisias, J.D. Hays, J. Imbrie, T.C. Moore Jr., and N.J. Shackleton. 1987. Age dating and the orbital theory of the Ice Ages: Development of a high-resolution 0 to 300,000-year chronostratigraphy. *Quat. Research* 27:1-29.
- Mesoella, K.J. 1969. The astronomical theory of climatic change, Barbados data. *Jour. Geology* 2:250-274.
- Milankovitch, M. 1941. *Canon of Insolation and the Ice-age Problem*. Translated from German by Israel Program for Scientific Translation, Jerusalem. Available from U.S. Department of Commerce, Springfield, Virginia.
- Muller, E.H. 1960. Glacial geology of the Laguna San Rafael area. *Am. Geog. Soc. Southern Chile Expedition 1959*. Tech. Report (Mimeo).
- Orcutt, J.D. 1991. Environmental variability and settlement changes on the Pajarito Plateau, New Mexico. *American Antiquity*, 56:315-332.
- Petersen, K.L. 1988. *Climate and the Dolores River Anasazi*. University of Utah Anthropological Papers 113, University of Utah Press, Salt Lake City.
- Pettersson, O. 1914. Climatic variations in historic and prehistoric time. *Svenska hydrogr. Biol. Komm. Skrifter* 5.
- Plog, F., G.J. Gumerman, R.C. Euler, J.S. Dean, R.H. Hevly, and T.N.V. Karlstrom. 1988. Anasazi adaptive strategies: The model predictions and results. Pages 230-276 in *The Anasazi in a Changing Environment*. G.J. Gumerman, editor. Cambridge Univ. Press, Cambridge, GB.
- Porter, S. 1981. Pleistocene glaciation in the southern Lake district of Chile. *Quat. Research* 16:263-292.
- Ray, L.L., and T.N.V. Karlstrom. 1968. Theoretical concepts in time-stratigraphic subdivision of glacial deposits. Pages 115-119 in *Means of Correlation of Quaternary Succession*. R.B. Morrison and H.E. Wright Jr., editors. Univ. of Utah Press, Salt Lake City.
- Richmond, G.M. 1976. Pleistocene stratigraphy and chronology in the mountains of western Wyoming. Pages 353-379 in *Quaternary Stratigraphy of North America*. W.C. Mahany, editor. Dowden, Hutchinson and Ross, Stroudsburg, PA.
- Scuderi, L.A. 1987. Glacial variations in the Sierra Nevada, California, as related to a 1200-year tree-ring chronology. *Quat. Research* 27:220-231.
- Stacey, C. 1963. Cyclical measures: Some tidal aspects concerning equinoctial years. *Annals New York Academy of Science* 105, Article 2:421-460.
- Stacey, C. 1967. Earth motions and time and astronomic cycles. Pages 335-340 and 999-1003 in *The Encyclopedia of Atmospheric Sciences and Astrogeology*. R. Fairbridge, editor. Reinhold Publishing, New York.
- Street, F.A., and A.T. Grove. 1979. Global maps of lake-level fluctuations since 30,000 yr B.P. *Quat. Research* 12:83-118.
- Sturchio, N.C., K.L. Pierce, M.T. Murrell, and M.L. Sorey. 1994. Uranium-series ages of Travertine and timing of the last glaciation in the northern Yellowstone area, Wyoming-Montana. *Quat. Research*, 42:265-277.
- Terasmae, J., and A. Dreimanis. 1976. Quaternary stratigraphy of southern Ontario. Pages 51-63 in *Quaternary Stratigraphy of North America*. W.C. Mahany, editor. Dowden, Hutchinson and Ross, Stroudsburg, PA.
- Vernekar, A.D. 1972. Long period global variations of incoming solar radiation. *Meteorological Monographs* 12. Whole monograph: 19 pages + 170 unnumbered pages.
- Villagrén, C. 1988. Late Quaternary vegetation of southern Isla Grande de Chilo, Chile. *Quat. Research* 29:294-306.
- Webb III, T., and R.A. Bryson. 1972. Late- and postglacial climatic changes in the northern midwest USA: Quantitative estimates derived from fossil pollen spectra by multivariate statistical analysis. *Quat. Research* 2:70-115.
- Wingard, I.J., T.B. Coplen, J.M. Landwehr, A.C. Riggs, K.B. Ludwig, B.J. Szabo, P.T. Kolegar, and K.M. Revesz. 1992. Continuous 500,000-year climate record from vein calcite in Devils Hole, Nevada. *Science* 258:255-260.

# **ABSTRACTS 1996**

Listed Alphabetically by First Author



### **Recurrence of Highstands of Great Salt Lake, Utah**

---

Genevieve Atwood  
Department of Geography, University of Utah

Great Salt Lake is the largest closed-basin lake in the western hemisphere. Great Salt Lake and the Great Salt Lake Desert have a drainage basin of about 23,000 square miles that covers portions of four states and is affected by more than one weather system. The lake has risen 10 feet above its historical average elevation twice in the last 150 years, flooding 750 square miles of low-lying land in and adjacent to Wasatch Front communities. The first rise crested in the early 1870s, about 25 years after the Mormon pioneers had settled near the shore of the lake. The 1870s highstand was not measured at that time, but later measurements of the shoreline formed by the 1870s highstand indicate that the stillwater lake elevation was 7212 feet above sea level. Weather records for the drainage basin during this period are fragmentary but suggest that the lake rose in response to a 4- or 5-year wet cycle. In the mid-1870s, the lake began a general decline that lasted until 1963, when the lake reached its historical low level of 4191 feet above sea level. Consumptive use of water in the drainage basin contributed to the lake's decline, but its importance was overestimated and led most planners and developers to conclude that the lake would never rise again to its 1870s flood levels.

From 1963 to 1982, the lake rose about 10 feet to near its historical average. A 4-year wet cycle began over the drainage basin of the Great Salt Lake in 1982. The lake rose dramatically and crested in 1986 and 1987 with an elevation of the main body of the lake equal to that of the 1870s highstand. The 1980s flooding of Great Salt Lake disrupted lifelines and industries on the lake and cost public and private entities hundreds of millions of dollars.

Defining the flood hazard associated with expected highstands of Great Salt Lake requires knowledge of the morphology of the lake bed to define at what elevations the lake will tend to stabilize plus knowledge of weather patterns, wind durations, and velocities to determine flooding from lake set-up and wave run-up.

Also needed, and lacking, is an understanding of the recurrence of the various highstand elevations that should be expected. The historical record is too short to determine recurrence. Prehistoric lake level fluctuations can be studied by shorelines, lagoonal deposits, and other features formed during highstands and by sediment cores. Decision-makers want to know: (1) how to tell when a 4- to 6-year wet cycle has begun, (2) the expected highstand elevation that has a recurrence interval on the order of 100 years — an event that should be of concern to major construction on the lakebed, and (3) the expected highstand elevation that has a recurrent interval on the order of several hundred years. Highstands with recurrence intervals on the order of thousands of years are not considered useful for most planning purposes.

### **The Near-1600 AD Multi-Proxy Puzzle**

---

Franco Biondi, C.B. Lange, W.H. Berger, and M.K. Hughes  
Scripps Institution of Oceanography, University of California  
La Jolla, California

A newly-developed chronology of annual varve thickness (AD 1117-1992) from the Santa Barbara Basin has been decomposed into orthogonal components using singular spectrum analysis (SSA) to identify and retrieve interdecadal oscillations. SSA eigenfunctions (EOFs) 1-8 form four oscillatory pairs with periods of ~100, ~58, ~25, and ~12 years respectively, all of them above the noise floor and in strong quadrature, with the possible exception of EOFs 7-8. Based on 2500 simulated series and on two-sided confidence intervals, EOFs 1-7 are significant at the 99% level and EOFs 8-9 are significant at the 95% level; EOFs 8-9 are significant at the 95% level using a one-sided test. The deterministic oscillatory signals retrieved from the marine varves show an abrupt change in frequency and amplitude near AD 1600. The largest contribution to this environmental shift is given by the interdecadal components, especially the ~25 and the ~12-year oscillation, suggesting a connection with global-scale decadal cycles identified in the subtropical Pacific gyre circulation and, possibly, with solar-driven phenomena. The near-1600 AD event coincides with (a) a similarly sudden change of state in the nearby Santa Monica Basin that triggered the onset of laminations in the marine sediments, (b) an extreme drought over most of the American Southwest. Total organic carbon burial flux in Santa Barbara Basin varves also shows a marked change around AD 1600 and seems highly correlated with detrended varve thickness. It is now our purpose to investigate further the time series properties of geochemical parameters derived from Santa Barbara Basin varves and to refine our understanding of the physical mechanisms that link oceanic circulation and atmospheric processes in the Eastern Pacific on decadal to centennial timescales.

### **Salmon Migration and Extreme Climatic Events at Various Scales**

---

D.J. Blackbourn  
Canada Department of Fisheries and Oceans

Strong associations between the nearshore migration of two groups of British Columbia salmon and environmental variables are discussed. Both cases have considerable biological, commercial, and biopolitical importance. In these associations, the responses vary continuously over a wide range of oceanographic data. The salmon appear to control the temporal but not the spatial scale nor the intensity of the response.

In one case, Fraser River sockeye seem to spatially adjust their final southward migration route to move inside Vancouver Island in a negative response to offshore SSTs, if the latter are above about 15°C. However, if the SST anomaly occurs too close to shore, the response of the salmon is more complex and they may be delayed and/or forced to travel west of the island at unusual depths.

In the second example, southern British Columbia coho salmon that spawn in the fall in rivers in Georgia Strait (east of Vancouver Island) are found in their final summer inside or outside the strait. In years in which salinity of the strait

in the previous winter/spring has been low, a small fraction are caught inside. The nature of this association is a mystery and bears no obvious relationship to the timing of the major physical and biological changes in the strait and in the coho salmon.

### **The Effects of Climate and Man on the Bering Sea Ecosystem: Developing a Context**

---

Robert C. Francis  
School of Fisheries, University of Washington, Seattle

The Bering Sea is one of the most productive marine ecosystems on the planet. Despite a variety of recent protections for marine mammals, birds, and fish resources, some species of the Bering Sea and adjacent regions have undergone large and sometimes sudden population fluctuations. As part of an NRC study to assess the current scientific understanding of the Bering Sea, a new view of how sequential change occurs in marine ecosystems has begun to develop. One thing is clear, most ecosystem issues arise in response to no single cause. In the case of the Bering Sea, climate forcing along with some long-term effects of exploitation by man appear to have led to current conditions. The scenario developed by the NRC committee presents a very different view of cause and effect than that normally employed in fishery management organization.

### **Historic 1000-Year Storms of California**

---

Jim Goodridge  
Mendocino, California

This is a study of 46 California storm events where the return period was 1000 years or more, based mainly on an analysis of daily rainfall records. The period of time covered in this study is from the major flood of 1862 up to 1995. This study describes a dataset compiled originally for drainage engineering studies. The basic data of this study consist of tabulated daily rainfall records from 3000 California rainfall records. Depth duration frequency studies were prepared for each record. The record length averaged 35 years of data for each station. The statistically smoothing procedure is discussed. Maps of lines of equal return period were prepared for each storm event with a 1000-year return period. The storm events with high return periods were distributed in a random pattern over the entire state. Five hundred and forty daily rainfalls in excess of 10 inches in one day were shown to be distributed on the windward slopes of orographic barriers. It was concluded that one million dollars in damage resulted from each rainfall station reporting the highest ever rainfall during a storm.

### **The Global Paleoflood Database Project**

---

Katherine K. Hirschboeck, M.L. Wood, F. Ni, and V.R. Baker  
Laboratory of Tree-Ring Research, University of Arizona, Arizona

In certain environments, excessive flood events have left behind datable century-to-millennium-aged geomorphic indicators of their occurrence and magnitude on the landscape. These paleorecords of large floods provide us with one of the best indicators of the occurrence of past hydrologic extremes, as well as indirect

evidence of the extreme rainfall events that generated the floods. The Global Paleoflood Database project has been initiated to compile various types of paleoflood information and incorporate it into a flexible-but-structured database that will allow regional and global analyses and comparisons.

The objectives of the GDP are: (1) to compile a global database of existing paleoflood information and establish a central repository for future submissions of paleoflood data; (2) to supplement the paleoflood data with complementary information from the gaged record; (3) to assemble a bibliographical database of paleoflood literature cross-referenced with the databases; (4) to establish an Internet and World Wide Web forum for communication among paleoflood researchers; and (5) to identify areas where future collection and analysis should be directed to adequately represent paleoflood extremes in climatically-sensitive regions of the world. The ultimate goal of the project is to provide a repository and communication forum to facilitate and stimulate research about climate variability and hydrological extremes through the accelerated sharing of paleoflood information. As this repository evolves, it will serve as a platform for examining the long-term patterns, processes, and causes of extreme streamflow and precipitation events throughout the world.

### **Radiocarbon Record of Abrupt Oceanographic Changes in the Santa Barbara Basin Over the Past 20,000 Years**

---

B. Lynn Ingram and James P. Kennett  
Department of Geography, University of California, Santa Barbara

Radiocarbon dating by accelerator mass spectrometry of coexisting planktonic and benthic foraminifers separated from Santa Barbara Basin sediments were used to provide a chronology for the upper 70 meters of core from Ocean Drilling program Hole 893A. The  $^{14}\text{C}$  chronology allows a determination of the age of the Younger Dryas (YD) in Santa Barbara Basin, and provides evidence for changes in ocean circulation in the eastern Pacific over the past 20,000 years. The YD event is represented in the Santa Barbara Basin by a climatic change based on oxygen isotopic shifts measured in planktonic and benthic foraminifers, and occurs in a non-laminated interval within laminated sediments at a depth of 17.60 to 20.40 mbsf. The event was dated using six planktonic foraminifer samples. The calibrated radiocarbon age for the initiation of the YD in Santa Barbara Basin is 12,970 year BP, coincident with that in North Atlantic deep-sea cores, glacial deposits in New Zealand, and ice core records. The radiocarbon age for the termination of the YD in the Santa Barbara Basin is poorly constrained due to a 1300-year radiocarbon plateau, falling between 11,000 and 12,300 years before the present. Assuming a constant sedimentation rate in the core, the termination age would be 11,220 years BP, with a duration of 1750 years. During the YD, the planktonic-benthic age difference averaged 90 years, compared with an average value of 470 years in younger and older sediments. The age decrease of surface-to-bottom waters during the YD may reflect a change in source of Pacific Intermediate Water, with a greater proportion originating from a more proximal source.

---

## **Climatic Impacts on Terrestrial Vegetation as Deduced from Leads and Lags in Atmospheric Carbon Dioxide and Temperature Signals**

---

Charles D. Keeling and Timothy Whorf  
Scripps Institution of Oceanography, La Jolla, California

Observations of atmospheric CO<sub>2</sub> suggest that climatic variability affects the global carbon cycle on all time scales that can be explored using existing records. We will discuss interannual variations on time scales longer than El Niño events which appear to reflect imbalances between the uptake and release of CO<sub>2</sub> by vegetation and soils, the former expressed as net primary production (NPP), and the latter by heterotrophic respiration (HR). Both the seasonally-adjusted concentration of atmospheric CO<sub>2</sub> and the amplitude of its seasonal cycle are affected by these imbalances. The annual average difference in NPP and HR causes interannual variations in the seasonally-adjusted concentration while variation in the annual sum causes variations in the amplitude of the seasonal cycle (the latter relationship, because the drawdown phase of the seasonal cycle depends mainly on NPP, the return phase on HR). The phase relationship between interannual signals in amplitude and concentration should, therefore, be related to how variations in NPP and HR have affected both signals. We have found that quasi-decadal variations in the amplitude of the seasonal cycle in atmospheric CO<sub>2</sub> lag similar variations in the seasonally-adjusted concentration by about 2 years. We have also found that quasi-decadal variations in air temperature are nearly in phase with these variations in atmospheric CO<sub>2</sub> as we have reported previously at PACLIM meetings. It follows that NPP and HR on the decadal time scale were in balance at times of nearly simultaneous quasi-decadal maxima and minima in CO<sub>2</sub> and temperature, while a quarter of the decadal cycle (about 2 years) after a decadal maximum, NPP maximally-exceeded HR; and about 2 years after a decadal minimum, HR similarly exceeded NPP. Because the observed quasi-decadal amplitude signal, as described above, also has lagged temperature by about 2 years, decadal maxima in amplitudes have evidently occurred approximately when NPP has maximally exceeded HR, and vice versa. We suggest that changes in the length of the growing season of plants at higher latitudes may account for these relationships.

---

## **Modeling and Predicting Intertidal Variations of the San Francisco Bay Salinity Field**

---

Noah Knowles, Climate Research Division, SIO-UCSD, La Jolla  
Daniel R. Cayan, Climate Research Division, SIO-UCSD, La Jolla  
David H. Peterson, USGS, WRD, Menlo Park, CA  
R.J. Uncles, Plymouth Marine Laboratory, Plymouth PL1 3DH, UK

An intertidal model of current velocities and salinity distributions in the San Francisco Bay estuary (Uncles and Peterson, 1995) is introduced and shown to reproduce available Bay salinity observations on daily to interannual time scales with reasonable accuracy. The UP model is distinguished by its coarse resolution and its use of tidally-averaged physics, which enable it to simulate variations in the baywide salinity field on a longer timescale than was previously feasible.

A simulation of the salinity distribution from 1930 through 1990 provides a historical context for an examination of the Bay's response to unusually wet and

dry water years. The behavior of the North Bay is shown to be relatively straightforward, responding quickly to changes in Delta outflow: high flows produce low salinity and vice-versa. The modeled South Bay response is more subtle, with dependence on the outflow's recent history as well as concurrent local and Delta flows.

A calibration of model parameters with respect to observed salinities yields a more realistic simulation throughout the Bay and provides further insight into Bay dynamics. Salinities landward of Carquinez Strait are shown to be highly sensitive to mixing processes in the strait and San Pablo Bay. Calibration results also indicate that estuarine circulation in this region may be considerably stronger than theory suggests.

The UP model's economic computational requirements and baywide domain offer the prospect of using the it as a forecasting tool. To this end, a predictive scheme is explored wherein a freshwater inflow prediction is developed from winter/spring runoff and snowpack. The predicted runoff serves as input to the estuarine model, providing ESP-type salinity estimates days and months in advance. The model's forecast capabilities show particular promise in dry years such as 1994, when low inflows allow tidal mixing to dominate the dynamics, and the UP model's dynamical accuracy yields an effective salinity prediction. In wetter years such as 1995, the salinity is more dependent on the hydrological details, but the model still permits an accurate prediction of the year-end salinity rise.

---

### **Preliminary Evidence Linking Regional Climate Variability to a Recent and Dramatic Collapse of the Mexican Sardine Fishery**

---

Daniel Lluch-Cota, Salvador Lluch-Cota, and Daniel Lluch-Belda  
Centro de Investigaciones Biológicas del Noroeste, S.C., La Paz, BCS, Mexico

The Gulf of California has been the most important region for the Mexican pelagic fishery since the mid 1970s, mainly because of the Monterey sardine landings. From 1976/1977 the catch increased from 25,000-30,000 t to a maximum of 290,000 t in 1988/1989. However, in the next two seasons the fishery collapsed to less than 120,000 t in 1988/1989 and 7,500 t in 1993/1994. After this event, the catch recovered to 100,000 t in 1993/1994 season. The fact that the effort level did not change markedly during the 1984-1991 period, strongly suggests that these variations were caused mainly by environmental factors. The Gulf of California sardine population inhabits the region near the large Islands of the Central Gulf given that there exist high productivity and low temperature conditions through the year. During winter the sardine expands its distribution in order to spawn over the Sonora-Sinaloa coastal seasonal upwelling region. Considering that an optimal set of environmental conditions for the spawning has been suggested for other sardine populations around the world, we analyzed the spawning extension as a function of both a local wind derived upwelling index and sea surface temperature. We found that the period in which the fishery increased is related to low levels of upwelling activity as well as to a sustained decrease in sea surface temperatures. Further, the onset of the collapse corresponded to the highest level of upwelling activity since the beginning of the fishery. It is suggested that reproductive success, and so next year's population biomass, partially depends on the sardine's habitat availability of an

adequate set of environmental conditions; identified here as a combination of optimal levels of both temperature and upwelling activity.

---

### **Potential Global Terrestrial Carbon Sink is 2.5 Times “Missing Sink”**

---

Yiqi Luo

Biological Sciences Center, Desert Research Institute, Reno, Nevada

I have recently developed a global terrestrial carbon sequestration model which uses two driving parameters to bound terrestrial carbon sink associated with an increase in atmospheric CO<sub>2</sub> concentration (C<sub>0</sub>). The first parameter is a leaf-level function (L), the normalized photosynthetic response to a small change in C<sub>a</sub>, which has been found to be an invariant function of C<sub>0</sub>, independent of almost all biological and environmental factors. The invariance of L enables us to cut across spatial heterogeneity of biotic and abiotic variables to quantify the Ca-induced increment of global photosynthetic carbon influx (P<sub>G</sub>). The second parameter is the global mean residence time (τ<sub>G</sub>) of photosynthetically-fixed carbon, which is used to project global respiration (R<sub>G</sub>), that is the return of carbon to the atmosphere through biology, from P<sub>G</sub>. If τ<sub>G</sub> is, for example, 10 years, this year's R<sub>G</sub> is approximately equal to P<sub>G</sub> 10 years ago. This year's P<sub>G</sub>, on the other hand, is that of 10 years ago plus the increment caused by the C<sub>0</sub> increase during the past 10 years. That increment can be quantified by and is the potential carbon sink in global terrestrial ecosystems. This model estimates that τ<sub>G</sub> is 17.7 years and the global carbon sink is 5.0 GtC yr<sup>-1</sup>, approximately 2.5 times “missing sink.”

---

### **The Regional Response of Salmon Populations to Climate Variability in the Northeast Pacific**

---

Nathan Mantua, Bob Francis, and Patricia Dell'Arciprete

University of Washington, JISAO, Seattle

As part of the Integrated Assessment of the Dynamics of Climate Variability, Impacts, and Policy Response Strategies in the Pacific Northwest project, we have examined relationships between historical climate indices and salmon production in the northeast Pacific. The primary goal of our study is to identify the regional and species-specific responses of Pacific salmon to large-scale climate forcing. We have separated the salmon production records into 10 geographical regions: Western, Central, and Southeast Alaska; Northern, Exterior, and Interior British Columbia; Washington Coast, Puget Sound, Oregon; and California.

Statistical analysis techniques were applied to identify the coherent salmon population responses to climate variability. Our preliminary results demonstrate that when salmon production is high in Alaska, it tends to be high in Puget Sound and low in California and Oregon. The opposite-signed relationships are also evident.

Salmon production in the British Columbia and Washington Coast regions tend to have less obvious connections to large-scale climate indices than those in Alaska, Puget Sound, California, and Oregon. Interestingly, salmon production in Puget Sound is well correlated with that in Alaska and poorly correlated with

that in neighboring regions. We also find that linkages to the El Niño/Southern Oscillation are most evident at the latitudinal extremes of our salmon production regions, in the sense that warm (cold) ENSO years are generally poor (good) salmon production years in California and Oregon and good (poor) salmon production years in Alaska. We offer some possible mechanisms by which these relationships may be driven.

### **A Decadal Change in the North Pacific Thermocline and Gyre-Scale Circulation**

Arthur J. Miller, Daniel R. Cayan, and Warren B. White  
Scripps Institution of Oceanography, La Jolla, California

A cooling of the thermocline at 250-400m depth from the early 1970s to the early 1980s in the North Pacific Ocean is identified in observations and in a numerical simulation. The observed change in the thermocline has gyre scale and is intensified in the western part of the basin north of 20°N. In an ocean model, forced by observed wind stress and heat flux anomalies from 1970-1988, a similar change in thermocline structure occurs. The model current fields reveal that the North Pacific subpolar gyre strengthened by about 10/% from the early 1970s to the early 1980s in the sense that the Kuroshio/Oyashio extension and the subpolar gyre return flow were increased. The model thermocline cooling and concomitant circulation changes were driven by a decadal-scale change in basin-scale wind stress curl forcing (Ekman pumping) with the response being nearly in Sverdrup balance over much of the eastern half of the basin.

### **Synoptic Climatology of Beringia Since the Last Glacial Maximum**

Cary J. Mock  
Department of Geography, University of Oregon, Eugene, Oregon

Beringia, comprised of Alaska and eastern Siberia, generally north of 60°N, provides unique opportunity for understanding past climatic variations since around 18 ka. Numerous new proxy data sites have been added to the paleoclimatic data network over the past several years, particularly fossil pollen and lake-level evidence. The output of paleoclimatic simulations from several different versions of general circulation models and unexploited modern climatic data are also available. This study examines the synoptic paleoclimatology of Beringia by comparing results from both GCMs and proxy data with one another, augmented by using information from modern synoptic climatology. Although boundary conditions since the late Pleistocene obviously differ dramatically when compared to today, some aspects of atmospheric circulation from the modern record provide an understanding of the synoptic climatic controls that predominated in the past. Results suggest that synoptic climatic features, such as the East Asian trough, the Siberian high, and the Pacific subtropical high, may explain some spatially heterogeneous paleoclimatic patterns as suggested by proxy data, including differences in the vegetation histories between western and eastern Beringia.

---

## **The Large-Scale Context for Recent Precipitation Extremes in Western North America**

---

Tom Murphree

Naval Postgraduate School, Monterey, California

Extreme events in regional-scale precipitation may be explained, to a large extent, by basin or hemispheric-scale variations of the climate system. I have examined these variations during several recent periods of unusual precipitation in western North America. My focus was on periods of high precipitation, lasting one to several weeks (for example, the heavy rains in Arizona during early 1993, in California during early 1995, and in the Pacific Northwest during late 1995). Preliminary analyses suggest that many of these precipitation extremes were part of larger-scale disturbances with origins in several distant upwind areas. The most important of these disturbances were intraseasonal variations in: (1) tropical cyclone activity in the eastern Indian Ocean and western Pacific; (2) cold surge activity in eastern Asia; and (3) El Niño and La Niña processes in the tropical Pacific. There are also indications that sea surface temperature anomalies in the nearby northeastern Pacific may have contributed to the precipitation extremes induced by these larger-scale disturbances.

---

## **Fisheries Catastrophes in Slow Motion: Wind Stress and Sustainable Development**

---

Richard H. Parrish

Southwest Fisheries Science Center, Pacific Grove, California

Analyses of the variations of the Japanese and California sardine and mackerel fisheries and the North American albacore fishery suggest that the principal time scale of the population variability of these stocks is decadal or regime scale. productive periods have lasted up to two decades and have occurred at intervals of 40 to 60 years. Climatic analyses of the CEOS's version of the COADS dataset clearly demonstrate regime-scale climatic variations in sea surface temperature, atmospheric pressure patterns, and wind indices which are proxies for turbulent mixing, Ekman transport, and wind stress curl.

Major climatic changes appear to be primarily associated with basinwide, regime-scale variation in the intensity and position of the winter atmospheric pressure patterns in the North Pacific. this basin-scale variation in wind stress, in association with regional scale features, results in greatly altered air/sea interactions which control the oceanic circulation. Areas particularly affected by the regime-scale variation include the Oyashio-Kuroshio mixing area east of northern Honshu, the Kuroshio extension region, and the northern California Current to Gulf of Alaska region.

There is evidence that population declines of major stocks of North Pacific pelagic fishes are associated with regime changes which alter the productivity of feeding grounds of these stocks. the failure of fisheries management regimes to reduce exploitation rates to compensate for the decreased productivity has led to fishery collapses with resultant long-term reductions in fishery yields.

## **Seasonal Streamflow Forecasting in Australia Using the Southern Oscillation Index**

---

Thomas C. Piechota and John A. Dracup

Civil and Environmental Engineering Department, UCLA, Los Angeles, California

Previous studies have shown that climate variability in Australia is strongly linked to the El Niño/Southern Oscillation (ENSO). Extreme droughts in Australia occur when the Southern Oscillation Index is strongly negative. In this study, the potential of using the SOI to forecast seasonal streamflow in eastern Australia is investigated. A probabilistic streamflow forecast is made from an optimal linear combination of climatology, persistence, SOI Phase, and Linear Discriminant Analysis forecasts. This is referred to as a consensus model approach and is used by the Australian Bureau of Meteorology to make seasonal probabilistic forecast of precipitation.

The climatology forecast is based on the natural probabilities of receiving below normal (30%), normal (40%), or above normal conditions (30%). The persistence forecast uses the previous 3-month average streamflow value to make a probabilistic forecast of the next seasons streamflow. The influence of ENSO in the generation of streamflow is accounted for in the SOI Phase and LDA forecast models. The SOI Phase model uses the strength and trend in the previous months SOI to forecast the next season's streamflow, and the LDA model evaluates the shift in the SOI during below normal, normal, and above normal streamflow conditions. The optimal linear combination of the four models is the forecast that minimizes the mean square error (Half-Brier score) and is the forecast with the best skill.

This modeling approach is used on 10 unimpaired streamflow stations from eastern Australia for the period 1927-1992. In general, the persistence model is most useful in the austral winter (July-September). The SOI phase and LDA models also provide valuable information in the winter. During years of high (positive) SOI values, there is a high probably of receiving normal or above normal streamflow. Conversely, there is a high probably of receiving below normal streamflow when the SOI is strongly negative. Preliminary results suggest that this approach may give water resource planners and managers valuable information for the design and allocation of water supplies.

## **ENSO Connections to Western Canada, the U.S. And Mexico**

---

Kelly T. Redmond

Western Regional Climate Center, Desert Research Institute, Reno, Nevada

Previous studies have shown that ENSO has significant associations with the winter climate of the western United States. The status of ENSO is portrayed, for this purpose, by the Tahiti minus Darwin Southern Oscillation Index. Maximal correlation occurs at a lag of about 4 months (SOI leading climate). Positive summer/autumn SOI is followed by wet and cool winters in the Pacific Northwest, and dry and warm winters in the Desert Southwest. Negative summer/autumn SOI is followed by the opposite pattern. A gridded precipitation dataset (Mike Hulme, Climatic Research Unit, East Anglia) is used to extend these analyses to western Canada, southern Alaska and northwest Mexico. The relationship

earlier seen for the southwest U.S. extends well into Mexico, and the opposing relationship seen in the Pacific Northwest extends well into western Canada. The latter relationship is nearly centered on the Columbia River Basin, whose runoff shows the same relationship. Relationships for both centers of action, as measured by correlation and split sample techniques, are strongly significant. The relationship noted over the Columbia River Basin gives way to an opposing, but weaker, relationship along the Pacific Coast from the Queen Charlotte Islands northward toward Yakutat and westward toward Kodiak Island. Although relationships derived from gridded values do not pass significance tests in this region, those derived from some individual station data do. These surface-based results are consistent with results of upper air analyses. In the Desert Southwest, extreme events (number of days exceeding selected thresholds of rain or snow) are also significantly related to the phase of ENSO.

### **The Top Ten California Floods of the 20th Century**

---

Maurice Roos, Chief Hydrologist

California Department of Water Resources, Sacramento, California

This paper is a review of the 10 biggest floods during this century in northern and central California, starting with the 1970 flood which was the pattern for design of the Sacramento River Flood Central Project, and ending with the 1995 floods. There are regional differences in exposure to storm-bearing winds which affect the extent of precipitation in a given area. The most feared general floods are those caused by a slow-moving weather system with a long southwestern fetch over the ocean, extending from Hawaii. Although heavy rains are usually widespread in these flood events, the brunt of the storm will be concentrated in different areas. For example, the December 1964 storm hit the north coast region hardest, while the February 1986 storm was worst in a broad band from the north San Francisco Bay through the north central Sierra. Orographic lifting is a strong factor in heavy rain production. Snow levels during a storm are another factor. Snowmelt floods are only a problem in the southern Sierra.

### **Southern California's "Flood of the Millennium" Occurred Ca. 1605 AD: Historical and Multi-Proxy Evidence for Large-Scale Atmospheric Forcing**

---

Arndt Schimmelmann and C.B. Lange

Biogeochemical Laboratories, Indiana University, Bloomington, Indiana

A distinct 1- to 2-cm thick flood deposit found in the Santa Barbara Basin with a varve-date of AD 1605±5 years testifies to an intensity of precipitation that remains unmatched for later periods when historic or instrumental records can be compared against the varve record. The 1605±5 event correlates well with Enzel's finding of a Silver Lake playa perennial lake at the terminus of the Mojave River (14C-dated AD 1560±90; Enzel 1992, *The Holocene* 2:11-18), in relative proximity to the rainfall catchment area draining into the Santa Barbara Basin. According to Enzel, such a persistent flooding of Silver Lake playa occurred only once during the last 3,500 years and required a sequence of floods, each comparable in magnitude to the largest floods in the modern record. To gain confidence in dating of the 1605±5 event, we compare Southern California's sedimentary evidence against historical reports and multi-proxy time-series that

indicate unusual events or are sensitive to changes in atmospheric circulation patterns. To name a few, tree-rings near Santa Barbara recorded very high precipitation for 1604, on top of a high 11-year average for 1601 to 1611 (Haston and Michaelsen 1994, *Journal of Climate* 7:1373-1387). Devastating drought conditions during the 1590s in Mexico City changed in 1604 and 1607 to such severe flooding that a drainage canal was excavated out through the northern part of the basin (O'Hara and Metcalfe 1995, *The Holocene* 5:485-490). Between 1599 and 1608, northern Italy experienced its densest cluster of severe and great winters in recorded history (since 1406; Camuffo and Enzi 1992, in: *Climate Since A.D. 1500*, p. 143-154). Overall, the first decade of the 17th century was marked by a rapid cooling of the Northern Hemisphere, with some indications for global coverage. A very large 1601 volcanic eruption recorded in Greenland Crête ice core acidity (Hammer et al. 1980, *Nature* 288:230-235) and 1604 marking a 270-year minimum of D14C (Stuiver and Braziunas 1993, *The Holocene* 3:289-305) seem to be linked to the observations, although no consensus has been reached about underlying causal mechanisms. We speculate about changes in atmospheric circulation over North American that may have been responsible for climate anomalies around 1605 AD.

### **Interdecadal Variability in North Pacific Wind and SST**

---

Franklin B. Schwing, Roy Mendelssohn, and Richard Parrish  
Pacific Fisheries Environmental Group, Pacific Grove, California

From an analysis of historical observations over the last half century, areas of the North Pacific (e.g., California-Alaska Currents, Kurishio-Oyashio Currents) exhibit clear regional variability on decadal time scales. Fisheries and other biological components also fluctuate on similar time scales, suggesting a coupling between climate variability and ecosystem structure (population size and range, feeding patterns, species composition). In the California Current, for example, SST has warmed and equatorward wind stress has increased south of Monterey. However, the region north of Monterey features a cooling tendency that coincides with increasing equatorward stress off northern California and increasing poleward stress off the Pacific Northwest. Cross-shelf differences in SST and wind are noted as well, particularly off the northwestern United States.

No clear systemwide relationship between SST and local coastal wind is seen in the California Current on interannual and longer scales. We examine the large-scale seasonal fluctuations in the wind field and its derivatives (e.g., wind curl, wind mixing) over the North Pacific in the decades prior to and following the 1976 climate shift, as a possible forcing mechanism for West Coast temperature variability. A complex interaction of spatially as well as temporally varying Ekman advection, wind mixing, and direct heating appears to be responsible for the long-term fluctuations in SST in the northeast Pacific.

The wintertime intensification of the Aleutian Low produced anomalous eastward wind stress south of 40°N and rotated stress in the Gulf of Alaska to the northwest. The resulting anomalous (1976-85 relative to 1966-75) winter Ekman surface flow was divergent (upwelling favorable) over the central North Pacific, but convergent off the western North American and eastern Asian coasts. Regions of anomalous surface divergence (convergence) are strongly correlated with anomalously cool (warm) SST in winter. Summer wind and SST anomalies

are not spatially correlated. SST winter anomalies appear to propagate in a manner consistent with the large-scale ocean circulation, resulting in a summer distribution of SST anomalies that is determined from late-fall and winter atmospheric anomalies. One example is the cool anomaly off the Pacific Northwest, which appears to be advected into the region from the central North Pacific via the West Wind Drift.

### **Increasing Evidence of Severe, Persistent, and Widespread Drought in the Western United States During Medieval Time**

---

Scott Stine  
California State University, Hayward, California

Evidence from an increasing number of sites in the western United States indicates that severe and persistent drought characterized much of the region during upper Medieval times. At previously described localities in the central Sierra Nevada, water levels in lakes, rivers, and marshes dropped lower than at any time during the past 150 years, permitting trees to colonize the emergent lands. Ring counts and radiocarbon dates from relict stumps of these trees point to two desiccation events — AD ~900-1120, and ~1200-1350 [Stine, *Nature*, v. 369, 546-549 (1994)]. Similar evidence, of identical antiquity, has now been found in the northern Sierra at Independence Lake [Lindstrom, *J. Ca. and Gr. Bsn. Anth.*, v. 12, 146-157 (1990)]; east of the sierra at Walker Lake; and in the southern Sierra at Owens Lake, where rooted shrub stumps and artifacts of the "Rose Spring" type litter the artificially exposed playa. Drought in the Sierra at these times is corroborated by the dendroclimatic record [Graumlich, *Quat. Ros.*, v. 39, 249-255 (1993)] [D. Graybill, pers. com., 1991)].

In the northern Rocky Mountains, D. Love (pers. com. 1996) reports drowned tree trunks, with a death date of ~AD 1350, rooted on the floor of Jenny Lake in the Tetons; and L. Hadley (pers. com., 1996) described contemporaneous evidence of desiccation-induced vegetation change from packrat middens in Yellowstone. Still farther east, in the sands of Nebraska and eastern Colorado, dunes that had been anchored for thousands of years lost their vegetation and became mobile during upper Medieval time, burying soils and damming the South Platte River [Madole, *Geol.*, v. 22, 483-485] [J. Swinehart, pers. com. 1995]. These new records contribute to a lengthening list of sites from the Americas (southern and northern Andes, Yucatan, central Mexico) and beyond, that point to a marked Medieval Climatic Anomaly.

### **A Detailed 2,000-Year Late Holocene Pollen Record from the Lower Pahranaagat Lake, Southern Nevada, USA**

---

Peter E. Wigand, Martha L. Hemphill, and Sikha (Manna) Patra  
Quaternary Sciences Center, Desert Research Institute, Reno, NV 89506

Analysis of 266 pollen samples from the upper two-thirds of a 15-m long, 10-cm diameter set of overlapping cores retrieved from Lower Pahranaagat Lake (elevation 975 m), Lincoln County, Nevada, gives us a rare, continuous, record of vegetation change at an interval of every 14 years over the last 3.8 ka. Each sample averaging ~3.8 years of pollen with ~10.4-year gaps between each sample outlines a record of alternating dry and wet periods with rapid onsets and

terminations. During this period increasing *Pinus* (pine) pollen values with respect to *Juniperus* (juniper) pollen values indicate that pinyon pine is now more abundant in the southern Great Basin than at any time since the beginning of the "Neoglacial" ~4.0 ka. This is due not only to a shift from harsher winters about 2.0 k, in part evidenced by the decline of juniper dominance in the woodland, but also to an increase in summer shifted rainfall which has favored seedling survival during the summer.

Additional evidence of periods of summer shifted rainfall is seen in the expansion of grasses (reflected in *Poaceae* pollen) preceding expansions of piñon pine without coincident expansions of winter rainfall-loving species such as sagebrush and juniper. Expansion of piñon at this time is also indicated in pollen records from the Carson Sink of the north-central Great Basin (Lead Lake, NV) and of grasses in pollen records from the northern Great Basin, e.g., Diamond Pond, Nevada. Periodic increases in the values of sagebrush (*Artemisia*) pollen, sometimes coincident with increases in juniper pollen, reflect intervals of cooler climate. Occasional, sometimes severe, drought is marked by increased bur sage (*Ambrosia*-type) and saltbush (*Chenopodiaceae*) pollen and decreased regional conifer pollen. Drier climate between 3.0 and 2.5 ka, 2.4 and 2.0 ka are eclipsed by the severe droughts of the last 2 ka. In particular, the droughts between 1.9 and 1.6 ka and 0.9 and 0.3 ka have little parallel during the late Holocene in southern Nevada. The ratio of aquatic to littoral pollen types indicates generally deeper water conditions ~1.6 to 1.3 ka and more variable, but predominately more marshy, conditions during most of the last 1.3 ka. Accompanying geomorphic investigations suggest that the sudden shift from lake to marsh conditions may be linked to the impact of extreme rainfall events that eroded a spillway through the alluvial fans that impound the lake during the early portion of the Late Holocene.

### **Daily Rainfall Along the U.S. Pacific Coast Appears to Conform to a Square-Root-Normal Probability Distribution**

---

Raymond C. Wilson

U.S. Geological Survey, Menlo Park, California

Daily rainfall data from 24 Pacific coastal stations, from San Diego to Cape Flattery with >40 year records, were examined during a study of the influence of regional climatic variations on rainfall thresholds for initiating landslides. Statistical analysis of the data disclosed an unexpected result — the square root of the daily rainfall closely approximates a normal distribution function. In fact, while the fit-to-daily rainfall data provided by the conventional log-normal distribution is fair,  $r^2 = 0.83$  to  $0.90$ , the fit from a square-root normal distribution is significantly better,  $r^2 = 0.98$  to  $0.999$ . This greater precision enables meaningful, quantitative comparisons of rainfall records from gages in different locations, and provides a sharper tool for delineating both spatial and temporal variations in precipitation. Several examples of the use of the square-root-normal distribution to explore variations in precipitation along the U.S. Pacific Coast will be discussed, including such effects as orographic enhancement, rain shadows, and the increase in storm frequency with geographic latitude.

---

## Poster Presentations

---

### **Butte Valley, California: A Pollen and Paleomagnetic Record for the Past 3 MA**

---

David P. Adam and A.P. Roberts

California Academy of Sciences, Golden Gate Park, San Francisco

A 102 m core recovered by the U.S. Geological Survey from Butte Valley, Siskiyou County, California, has yielded long records of paleomagnetic and pollen data. Initial interpretation of the record was based on an assumption of uniform sedimentation rates based on the position of the Brunhes/Matuyama boundary at 65 m depth, and produced an estimated age for the base of the section of 1 MA. More detailed analyses have led us to reject this model in favor of a new model in which sedimentation rates were much slower prior to the Brunhes/Matuyama boundary; this new model makes much better sense in terms of the paleomagnetic reverse record observed below 65 m in the core. Our new estimate of the age of the base of the Butte Valley core is about 3 MA, making the Butte Valley core span about the same time interval as the Tule Lake core, about 50 km to the east.

The lithology of the Butte Valley core indicates that the valley has become less lacustrine through time; lake sediments comprise a larger fraction of the section toward the base of the core than toward the top. We attribute this tendency to a drop in the regional water table caused by the incision of the Klamath Gorge just to the north of Butte Valley.

Comparison of the Butte Valley and Tule Lake pollen records indicate generally similar vegetation development in the two basins, but with some differences as a result of the position of Butte Valley closer to the Cascade Range than Tule Lake is. The slow sedimentation rate in the lower part of the Butte Valley core has resulted in rather long intervals between sample points in the lower part of the section.

### **Geomorphic Evidence for an Extreme Climate Episode in the American Southwest (Young Dryas)**

---

Roger Y. Anderson and B.D. Allen

Department of Earth and Planetary Sciences, University of New Mexico, Albuquerque

Eolian and shoreline landforms in the Estancia Basin in central New Mexico were generated and shaped during the large and abrupt changes in climate that occurred at the glacial termination and during the younger Dryas (YD) climatic episode. Gypsum dunes which were generated from sediments on the desiccated floor of the lake basin, after ~11,000 radiocarbons BP, were reshaped into a prominent beach ridge after a lake returned and quickly rose ~10 meters above the lake floor, to an elevation of 1862 meters. A minimum age for the gypsum beach ridge is 9650 radiocarbons BP, as determined by radiocarbon dating of shell material in channel-fill sediments within deltaic deposits at the same shoreline elevation. The age window for the beach ridge corresponds approximately to the radiocarbon age plateau associated with the YD event, the YD lake was sustained at the 1862 m elevation or some unknown interval of time, after which

the lake abruptly fell in elevation and disappeared. The rise and fall of the lake had a minimal effect on the dune field, with significant reworking restricted to the downwind, eastern side of the lake, where dunes were reorganized into linear shoreline features. Within the dune field, the dunes have largely retained their complex dune forms, including barchan shapes, indicating that the lake rose and fell rapidly, having little time to reshape dune forms within the gypsum dune field. The preservation of fragile eolian landforms, under conditions where their survival is unexpected, is consistent with evidence from other regions for extremely abrupt changes in climate during the YD climate episode.

### **Long-Term Response Of Torrey Pine (Southern California) to Coastal Climate: Precipitation, Temperature, and Fog**

---

Franco Biondi, D.R. Cayan, L.G. Riddle, and W.H. Berger  
Scripps Institution of Oceanography, University of California, La Jolla, California

Torrey pine (*Pinus torreyana* Parry ex Carr.) has one of the most limited geographical ranges and population size in the *Pinus* genus; it is present only on Santa Rosa Island and on the coast between San Diego and Del Mar, where our research was conducted. A 168-year chronology (1827-1994) was developed using 28 increment cores extracted from 15 living and 2 dead standing trees at Torrey Pines State Reserve, San Diego, California. Crossdating was possible but not easy, mostly because of faint latewood boundaries in certain years and specimens. Annual tree growth was highly and directly related to precipitation falling between the previous November and the current April. Temperature was not a significant predictor of tree growth. At seasonal scale, tree growth was highly and directly related to winter and spring precipitation, and was also significantly correlated to summer fog. However, when combined with winter and spring precipitation in multiple regression models, summer fog was not a significant predictor of tree growth. Total November-April precipitation explained a larger amount of variance after 1900 (64% in 1900-1949, 70% in 1950-1994) than before 1900 (48% in 1850-1899). The spatial correlation with western North America winter and spring precipitation, as well as with published tree-ring chronologies, indicates a connection with the American Southwest. Global correlation maps with winter sea level pressure and sea surface temperature are consistent with the hypothesis that San Diego precipitation is affected by a southerly displaced North Pacific storm track and by warmer water farther south, both leading to higher transport of lower latitude moisture.

### **Correlation of Paleoclimate Records from Upper Klamath Lake and from the Continental Margin Off California**

---

J.P. Bradbury, W.E. Dean, J.G. Rosenbaum, and R.L. Reynolds  
U.S. Geological Survey, Denver, Colorado

A 12.8 m piston core from Upper Klamath Lake, Oregon contains a high-resolution paleoclimate record of the past 40 kyr based on diatoms, geochemistry, pollen, and sediment magnetic properties. Age controls are provided by radiocarbon dating and tephrochronology. Abrupt fluctuations in abundances of planktic diatoms with different seasonal adaptations between 35 and 19 ka suggest alternating warm and cold climate regimes. The warm intervals correspond to eutrophic lake

conditions. The fluctuations in diatom abundance correspond to fluctuations in the input of glacial flour, inferred from magnetic and geochemical properties. Full glacial diatom assemblages are dominated by reworked Pliocene species and taxa that today bloom under the ice in north-temperate oligotrophic lakes. During the full glacial, magnetic properties indicate maximum flux of glacially-derived sediment. Post-glacial climates after 13 ka produced a seasonally shallower, eutrophic lake that gave way to encroaching marshes by 8 ka. Marsh development with anoxic sediments reached a maximum between 7 and 5 ka, with sediment organic-carbon concentrations as high as 48 weight percent.

Marine cores collected from within the oxygen minimum zone on the continental slope off northern and central California contain intervals of laminated sediments between intervals of bioturbated sediment in sections deposited between about 50 and 25 ka (i.e. during oxygen-isotope stage 3). Enhanced preservation of organic matter and elevated concentrations of molybdenum in the laminated sediments suggest that bottom waters were severely oxygen-depleted and perhaps anoxic when these sediments were deposited. The organic-rich, laminated sediments further imply that the California current system was more productive at that time. The laminated sediments, and peaks in percent organic carbon and molybdenum, may correspond to peaks in abundance of eutrophic diatoms in the core from Upper Klamath Lake, but there is not as yet sufficient age control for the marine cores to confirm this correlation. In contrast to the inferred high organic productivity on the California margin during oxygen-isotope stage 3, marine full-glacial organic productivity was the lowest of anytime during the past 50 kyr. The climate and hydrology of the western U.S. is controlled by seasonal interactions of the North Pacific high, the Aleutian Low, and the western U.S. Low. These major atmospheric circulation systems control the California current upwelling system as well as the location and intensity of storm tracks bringing precipitation to the western U.S.

### **Decadal Variability of Snow in the Western U.S.**

---

Dan Cayan, Scripps Institution of Oceanography and U.S. Geological Survey  
Larry Riddle, Scripps Institution of Oceanography

Much of the water supply in the western United States is derived from snowmelt runoff. For example, it is estimated that 75% of the annual discharge of most of the major streams in the western U.S. is from melting mountain snowpack (Palmer 1988). Topography plays a strong role — the heaviest snow accumulations are at middle-to-high elevation mountain sites, usually with exposures to the west or southwest. In the Sierra Nevada, the primary water-bearing region for California, most snowmelt is derived from snowpack accumulated during winter storms at elevations above 1300 meters. Regional precipitation is very seasonal; most locations west of the Rocky Mountains have a winter maximum and a summer minimum. Combined with the annual temperature cycle, this seasonality produces a spring maximum in snow accumulation, so that most snowcourses attain their climatological maximum snow water equivalent (SWE) at about the beginning of April. Snowcourse observations are generally collected on or about the first of the month during the winter and spring. The greatest frequency of sampling over the historical period is for April 1.

How much variability occurs in the snow accumulation? A survey of historical snowcourse records over the western states indicates the coefficient of variation (CV) of April 1 SWE ranges from 20% to well over 100%. For the 200 snowcourses used in this study, 45 had a CV >50%, while only 23 had a CV <25%. This level of variability is comparable to that of seasonal precipitation over this region (Granger 1977; Chanagnon et al 1991). Snowpack accumulations are coherent over scales of at least a few hundred kilometers; Aguado (1990) showed in California that for 28 snowcourses across the Sierra Nevada Mountains, over 80% of the variance of SWE was accounted for by a single principal component.

Although mountain snow accumulations have been routinely monitored for several years to gauge water supplies, these measurements have not been fully exploited as a climate dataset. A comprehensive study of short period climate variability of snowpack in the West has not been undertaken, but there are noteworthy regional examples. In examining snowcourse records in the Rocky Mountains, Chanagnon et al (1991) demonstrated that spring snow accumulation serves as a regional climatic indicator; Chanagnon et al (1993) derived effects of synoptic atmospheric circulation patterns and a tendency for out-of-phase multi-year shifts in snow accumulation and associated circulation patterns over the central part of the northern and southern Rocky Mountains. Concerning El Niño, Redmond and Koch (1991) demonstrated that snowfall in Oregon is significantly biased, with a low in years with a low SOI (Southern Oscillation Index) relative to those with a high SOI; and Cayan and Webb (1992) derived the pattern of SWE over the western United States in conjunction with the SOI.

Both precipitation and temperature affect the snowpack, but their aggregate impacts are not entirely clear. There does not appear to be a strong temperature/snow relationship over the entire region (Walsh et al 1982; Leathers and Robinson 1993; Karl et al 1993). However, anomalous temperature impacts are evident in Sierra Nevada spring runoff variations (Aguado et al 1992; Cayan et al 1993). Also, winter temperature trends appear to be involved in a decades-long change in the fraction of runoff occurring in late spring and summer runoff found in the Sierra Nevada and many other snowmelt-driven streams over the western United States (Roos 1987, 1991; Wahl 1992; Aguado et al 1992; Dettinger and Cayan 1995). Its dependence on temperature makes snow a key diagnostic in climate change scenarios (eg, Gleick 1987; Roos 1989; Lettenmaier and Gan 1990; Dettinger and Jeton in press). Temperature and precipitation are not well correlated during the cool seasons in the West (Zhao and Khalil 1993; Cayan and Peterson 1993), so their individual influences on snowpack should be separable.

### **Issues**

In view of the above, the purpose of this study is to examine a network of mountain snowcourses over the western United States to examine the following issues associated with snow accumulation. These issues include: the way in which the space/time structure of the decadal (>7-year period) variability at high elevation snow accumulation is revealed by mountain snowcourse snow water equivalent (SWE) records (1930-1989); the consistency of SWE variability when compared to other hydrological measures (eg, temperature, precipitation, and streamflow); the

relationship of SST variability to large-scale fields of atmospheric circulation and SST; and a comparison of decadal SWE variability to that of the ENSO timescale.

### **Data**

For several decades, the U.S. Department of Agriculture Soil Conservation Service has archived snow observations (depth and water content) at several hundred mountain snowcourses in the western United States (Stafford 1959; Work and Beaumont 1959). Throughout the West, many snowcourses were established in the mid-to-late 1930s in response to the early 1930s western drought.

Snowcourses are commonly sited in sheltered alpine meadows so that drifts, blowing snow, and excessive sublimation are minimized. More recently, many automated snow sensor observations are available over the western region; these records are limited to the last 10-15 years and may have errors in measuring seasonal accumulation of snow, so they are not employed in the present study. Most snowcourses are monitored at the beginning (on or about the first of the month) and sometimes the middle of each of the substantial snow-covered months, usually from January or February through May or June. Here, we use the first-of-the-month snowcourse samples because mid-month samples are generally not available over the complete record. Snowcourses cover a large range of elevation, from less than 1000 meters to over 3000 meters. Most of the lowest snowcourses are in the Oregon and Washington coastal ranges; most of the highest ones are in the southern Sierra Nevada in California or the southern Rocky Mountains.

The 200 snowcourses employed are from a network of more than 2000 snowcourses in the 11 western states of the conterminous United States (Palmer 1988; State of California 1991). Data from Alaska were not used in the present study because Alaska has relatively short records and because British Columbia sites were not available. Many snowcourses in this network are sited in very close proximity, so anomalous variability at a particular site is likely redundant with that of neighboring stations (Aguado 1990). The 200 snowcourses were selected to provide a relatively complete record (most of them span 1930-1989, and none begin later than 1940). The stations were culled to provide a relatively uniform spatial sample: the following mix of sites was included: 5 from Washington, 29 from Oregon, 21 from California, 3 from Arizona, 9 from Nevada, 25 from Utah, 32 from Idaho, 27 from Montana, 19 from Wyoming, 26 from Colorado, and 4 from New Mexico. Other studies (Aguado 1990; Changnon et al 1991) have demonstrated much regional coherence of the spring snow accumulation within networks of the snowcourses in California and the Rocky Mountain states, respectively, so results of this study are not likely to be very sensitive to this choice of stations.

Most snowcourses attain their climatological maximum snow water equivalent at about the beginning of April. Snowcourse observations are generally collected on or about the first of the month during the winter and spring; the April 1 sampling tends to be the period with the greatest frequency of sampling over the historical period. However, some low elevation sites and some of the southernmost sites experience maxima as early as February 1, and some of the

high-elevation sites have maxima delayed until May. Of the 200 snowcourses used in this study, 149 had climatological maximum first-of-the-month values on April 1; 29 had maxima on March 1; 19 had maxima on May 1, and 3 had maxima on February 1.

April 1 observations are the primary data used in the present study, but observations from the other months are also used to track the seasonal evolution of the snow. April 1 is the most commonly sampled period over the duration of record, probably because maximum snow accumulation at most stations is reached in early April. The seasonal progression of snow accumulation at representative locations is shown later in the regional SWE composites. Snow depth is generally measured concurrently with SWE at each snowcourse. At the 200 snowcourses include here, April 1 snow depth and SWE are high correlated; nearly all (199) have correlation coefficients exceeding 0.8; many (160) have correlations of 0.909, and several (84) have correlations exceeding 0.95.

Atmospheric circulation is represented by Northern Hemisphere sea level pressure (SLP) from 1899 to present, obtained from NCAR and the NOAA Climate Analysis Center. The SLP data are monthly averages over a 10° longitude by 5° latitude "diamond grid" since December 1946.

SST is from the GISST adjusted and filled global anomaly set (Parker and Jackson) from about 1900 to present. In addition, we have augmented the SST with a set of gridded land temperatures obtained from Henry Diaz and Jon Eischied (NOAA, Boulder, CO).

Streamflow is from a set of about 60 USGS stream gauge records, as described in Cayan and Webb (1992).

## **Conclusions**

A major portion (about 55%) of the decadal SWE variability is expressed in two EOFs; a northwest pattern (Washington, Oregon, Idaho, Montana, and western Wyoming); and a southwest/northwest opposition pattern (California, Nevada, Utah, and southwestern Colorado out of phase with northern Idaho and Montana). The northwest pattern has had three or four major rhythms since 1930; the opposition pattern has had two broad maxima in the late 1930s to early 1940s and in the early 1980s. Interestingly, the decadal/spatial patterns of EOFs 1 and 2 have very strong resemblance to the spatial patterns of EOFs 1 and 2 of ENSO-filtered SWE.

Decadal SWE fluctuations over the western United States are produced by regional/basin-scale atmospheric circulation patterns, with major features over the North Pacific. The relationship to decadal SST anomalies produced surprisingly strong correlations with global features; in particular, the opposition pattern exhibits marked correlations with tropical SST over the Pacific and the Indian Ocean basins. Although these decadal analyses are based on a painfully short (60-year) record, there is support for a true physical mechanism in the form of analogous linkages on the ENSO time scale. The correlation pattern on the ENSO scale with SST produces a nearly identical pattern. Further, the temporal variability (PC) of the second SWE decadal EOF is quite closely coherent with that of a global precipitation mode (rooted in the Sahel, among

other regions) that is associated with global SST, as has been noted by several authors. Thus, it appears that a part of the low-frequency precipitation variability in western North America is associated with a global low-frequency climate mode.

## References

- Aguado, E. 1990: Elevational and latitudinal patterns of snow accumulation departures from normal in the Sierra Nevada. *Theor. Appl. Climatol.* 42:177-185.
- Aguado, E., D. Cayan, L. Riddle, and M. Roos. 1992: Climatic fluctuations and the timing of West Coast Streamflow. *J. Climate* 5:1468-1483.
- Cayan, D. R., and R.H. Webb. 1992. El Niño/Southern Oscillation and streamflow in the western United States. Pages 29-68 in *El Niño: Historical and Paleoclimatic Aspects of the Southern Oscillation*. H Diaz and V. Markgraf, editors. Cambridge Univ. Press.
- Changnon, D., T.B. McKee, and N.J. Doesken. 1991: Hydroclimatic variability in the Rocky Mountains. *Water Resources Bulletin* 27:733-743.
- Changnon, D., T.B. McKee, and N.J. Doesken. 1993: Annual snowpack patterns across the Rockies: long-term trends and associated 500 mb synoptic patterns. *Monthly Weather Review* 121:633-647.
- Dettinger, M.D., and D.R. Cayan. 1995. Large-scale atmospheric forcing of recent trends toward early snowmelt runoff in California. *J. Climate* 8:606-623.
- Gleick, P.H., 1987. The development and testing of a water balance model for climate impact assessment: Modeling the Sacramento Basin. *Water Resources Res.* 23:1049-1061.
- Granger, O.E. 1977: Secular fluctuations of seasonal precipitation in lowland California. *Mon. Wea. Rev.* 105:386-397.
- Jeton, A.E., M.D. Dettinger, and J.L. Smith. 1996. Potential Effects of Climate Change on Streamflow, Eastern and Western Slopes of the Sierra Nevada, California and Nevada. USGS Water Resources Investigations Report 95-4260. 44 pp.
- Karl, T.R., P.Y. Groisman, R.W. Knight, and R.H. Heim Jr. 1993: Recent variations of snow cover and snowfall in North America and their relation to precipitation and temperature variations. *J. Climate* 6:1327-1344.
- Leathers, D.J., and D.A. Robinson. 1993. The association between extremes in North American snow cover and United States temperatures. *J. Climate* 6:1345-1355.
- Lettenmaier, D.P., and T.Y. Gan. 1990. Hydrologic sensitivities of the Sacramento-San Joaquin River basin, California, to global warming. *Water Resources Res.* 26:69-86.
- Palmer, P.L. 1988: The SCS snow survey water supply forecasting program: current operations and future directions. *Proceedings of Western Snow Conference*, Kalispell, Montana. pp. 43-51.
- Redmond, K.T., and R.W. Koch. 1991. Surface climate and streamflow variability in the western United States and their relationship to large scale circulation indices. *Water Resources Research* 27:2381-2399.
- Roos, M. 1987. Possible changes in California snowmelt patterns. *Proc. Fourth Pacific Climate Workshop*, Pacific Grove, CA. 141-150.
- Roos, M. 1989. Possible climate change and its impact on water supply in California. *Oceans '89 Conference*, Seattle, Washington.
- Stafford, H.M. 1959: History of snow surveying in the West. *Proceedings of the Western Snow Conference*. pp. 1-12.

- State of California. 1991. 1991 California Snow Survey Measurement Schedule. California Cooperative Snow Surveys, Department of Water Resources, Hydrology Branch, Sacramento. 55 pp.
- Wahl, K.L. 1992. Evaluation of trends in runoff in the western United States. Managing Water Resources during Global Change. Proc. American Water Resources Association 28th Annual Conf. and Symp., Reno, NV, Amer. Water Resource Association. pp. 701-710.
- Walsh, J.E., D.R. Tucek, and M.R. Peterson. 1982. Seasonal snow cover and short term climatic fluctuations over the United States. *Mon. Wea. Rev.* 110:1474-1485.
- Work, R.A., and R.T. Beaumont. 1958. Basic data characteristics in relation to runoff forecast accuracy. Proceedings of Western Snow Conference, Bozeman, Montana. pp. 45-53.
- Zhao, W., and M.A.K. Khalil. 1993. The relationship between precipitation and temperature over the contiguous United States. *J. Climate* 6:2322-2336.

### **Geochemical Characteristics of Sediments on the Peru and California Margins**

W.E. Dean, M.A. Arthur, and J.V. Gardner  
U.S. Geological Survey, Denver, Colorado

Sedimentary characteristics of Holocene muds deposited under an intense oxygen-minimum zone (OMZ) on the Peru margin were mapped by submersible and studied in surface-deployed box, gravity, and piston cores and submersible-deployed push cores on two transects over depths of 75 to 1000 meters across the Peru margin (12° and 13.5°S) on two cruises in 1982 and 1992. The organic matter on the Peru margin is almost entirely marine as confirmed by rock-Eval pyrolysis and isotopic composition of organic carbon (OC). OC and trace-metal concentrations are highest (up to 16 wt. % OC) in sediments where intermediate water masses in the core of the oxygen minimum zone (OMZ) with low dissolved oxygen concentrations (<5-10µM) impinge on the continental slope at depths of 75 to 450 m. Oxygen concentration is the primary control on organic matter preservation, but sediment transport and reworking by strong bottom currents exerts a secondary control on organic-matter preservation. High concentrations of OC and metals also were observed in inner shelf (<100 m) sediments where the sediment surface commonly is covered by thick mats of *Thioploca* (sulfur oxidizing bacteria), suggesting that the bacterial mats also may play direct and/or indirect roles in OC and metal concentration, accumulation, and preservation. Q-mode factor analyses of major- and trace-element concentrations in surface sediment samples delineate three dominant element associations: (1) an organic association (OC, Mo, Cd, V, Ni, Cu, and Zn); (2) a phosphate association (Ca, P, Sr, U, Y); and (3) a clastic association (Al, Mn, Ti, Li, Gga, n, Ba, Nd, Th, and Sc). The clastic association was dominant in the 13.5°S transect, whereas the OC-metal association dominated on the 12°S transect. On both transects, phosphorite (carbonate fluorapatite, CFA) is most abundant on the upper slope between 300-500 m. On the 13.5°S transect, a glauconite element association (Fe, K, and Cr) occurs on the slope below 450 m to at least 1000 m where the surface sediments consist of nearly pure medium-size glauconite sands. No glauconite was found on the 12°S transect.

Sedimentary characteristics of Holocene muds deposited under an intense oxygen-minimum zone (OM) off California were studied in surface-deployed gravity and piston cores collected on the continental slope from the Oregon

border on the north to the Mexican border on the south. Based on geochemical evidence, sediments on the southern California slope overall contain the most abundant H-rich, sapropelic marine organic matter as judged by Rock-Eval pyrolysis, OC content, and carbon isotopes. The southern California margin sediments also have the highest overall concentrations of phosphorus (P/Al ratio), CaCO<sub>3</sub>, and Barium (Ba/Al). This suggests that today productivity is greatest on the southern California margin. Concentrations of biogenic silica also are highest in surface sediments off northern California, suggesting that diatom productivity is highest there. The high carbonate productivity on the southern California margin appears to be a continuation of conditions established during late glacial times. The phosphate concentration in sediments on the California margin, as measured by the P/Al ratio, is 100 to 1000 times less than that in sediments on the Peru margin, which is why phosphate deposits are forming on the Peru margin and not on the California margin.

### **The Instrumental Record of Climate Variability in the Pacific Northwest: Laying the Foundations for an Integrated Assessment of Climate Impacts**

Patricia Dell'Arciprete, N. Mantua, and R.C. Francis  
University of Washington, Fisheries Research Institute, Seattle

As one of the foundations for the "Integrated Assessment of the Dynamics of Climate Variability, Impacts, and Policy Response Strategies in the Pacific Northwest" project, we have assembled historical records of the marine and terrestrial environment in the Pacific Northwest region. Our longest continuous time series extends back to the late 19th century.

Our goals include objectively identifying spatially coherent climate variability at seasonal, interannual, and interdecadal time scales. Ultimately, we hope to quantify the potential for climate predictability at the aforementioned range of time scales. Preliminary results suggest that there are strong decadal and interannual oscillations in Pacific Northwest climate that are well captured by snowpack, wintertime air temperature, streamflow, and sea surface temperature in Puget Sound and along the coast of Washington State and British Columbia. As noted in previous studies, teleconnections to the El Niño/Southern Oscillation are evident in Pacific Northwest climate records, though less directly than is commonly stated. Nonetheless, teleconnections to ENSOs yield a promising mechanism for making seasonal to interannual climate predictions for the Pacific Northwest region. We are also encouraged by the potential for decadal-scale predictability associated with the longer-time-scale oscillations of the North Pacific climate system. Many of our best climate records were obtained via the PACLIM data base, and we strongly encourage participants in this workshop to maintain and update these valuable climate records.

### **Uranium/Calcium Variations in the Reef Coral *Porites lobata***

Stewart J. Fallon, Eric M. Cathcart, Sarah C. Gray, and Ellen Druffel  
Marine and Environmental Science, University of San Diego

There are several proxy techniques available to reconstruct SST from coral aragonite such as  $\delta^{18}\text{O}$  and Sr/Ca. Recent studies have shown that the ratio of U/Ca in coral aragonite varies in conjunction with  $\delta^{18}\text{O}$ , Sr/Ca, and the SST of

the water. The purpose of this study is to test the robustness of the U/Ca tracer from several different areas in the Pacific and under varying local conditions. *Porites lobata* corals were collected in Fiji and Hawaii from "open ocean" sites and sites influenced by stream runoff. Although the Fijian corals are young (~5 years old), the cores collected from Hawaii are from large coral heads that appear to encompass 100 years of continuous growth.

Two of the corals from Fiji were analyzed for U/Ca by isotope dilution ICP-MS and compared to  $\delta^{18}\text{O}$  and the IGOSS NMC weekly SST dataset. At the open-ocean site, the U/Ca and  $\delta^{18}\text{O}$  appear to change in phase with SST. The U/Ca measurements for the site range from 0.85 to 1.25  $\mu\text{mol U/mol Ca}$ ; the  $\delta^{18}\text{O}$  ranges from  $-4.5$  to  $-5.5\text{‰}$ ; and the temperature ranges from 26 to 30°C. The inshore site shows more variation in the magnitude of the  $\delta^{18}\text{O}$  signal ( $-3.8$  to  $-5.1\text{‰}$ ) than does the open ocean site and does not always correlate with the instrumental record. Preliminary U/Ca measurements from the two sites in Hawaii range from 0.8 to 1.3  $\mu\text{mol U/mol Ca}$ , which is consistent with measurements made by other workers. Analysis of a 15-year time series of U/Ca from the two Hawaiian sites will be presented.

### **Correlation of Laminated Late Pleistocene Sediments from the Open Continental Slope Off Central California**

---

James V. Gardner

US Geological Survey, Menlo Park, CA

Eighteen out of 46 deep-sea cores recently collected in water depths between 500 and 1000 m along the central California continental margin contain subbottom intervals of laminated sediment. Correlations with 9 AMS 14C-dated cores in the area indicate the laminated sequences occur during three intervals; late Pleistocene Oxygen-Isotope Stage 3 (OIS-3) at about 35 to 40 ka, OIS-2 at about 25, and 15 ka. The similarities of the central California laminations in appearance, composition, and age with varves found off northern California (Gardner and Hemphill-Haley, 1986; Hemphill-Haley and Gardner, 1994; Anderson et al., 1987; 1989) suggest that the central California laminations are also varves. Varve-preserving conditions prevailed at four different times during the last 40 ka along the California margin. The oldest intervals occurred at about 39 ka and roughly coincide with the timing of Dansgaard-Oeschger cycle 12 (DO-12) and Heinrich Event HE-4. The next interval of varves occurred at about 36 ka, coinciding with DO-8 and HE-3, followed at about 25 ka (AMS 14C dated) by similar conditions that coincide with DO-4 and He-2. The youngest varve-preserving conditions occurred at about 15 ka (AMS 14C dated) and coincide with HE-1. During these times of varve-preserving conditions, the oxygen-minimum zone must have been depleted in dissolved oxygen to the degree that precluded benthic bioturbation. This condition could be met either with the dissolved oxygen content of Pacific Intermediate Water being much lower than today, with coastal upwelling being much more intense than occurs today, or both. Our data suggest both mechanisms contributed to the low values of bottom-water dissolved oxygen during the varve-preserving conditions. We speculate that atmospheric changes in the North Atlantic during Heinrich Events were teleconnected to the North Pacific and altered atmospheric and oceanographic conditions there.

Digital image-processing techniques were used to display 8-bit gray-scale profiles of each varve sequence in order to correlate them to one another. Three OIS-2 sequences can be correlated down to individual hemicycles (light or dark layer). Two OIS-3 sequences can similarly be correlated. Individual varve hemicycle thicknesses were compiled to investigate a possible El Niño signal, reasoning that a typical El Niño generates heavy winter rainfall (thick dark layer) along the central California coast and a major reduction in spring and summer upwelling (thin light layer). The thickness (or thinness) of each seasonal laminae should be a reflection of the "strength" of each of these seasonal processes. Spectral analyses of the varve thicknesses did not reveal a consistent El Niño periodicity of 3 to 7 years. In fact, a periodic pattern has been found in only one core so far. This preliminary result suggests that the El Niño/Southern Oscillation may be a rather recent condition, at least in its effect along the central California margin.

The highest correlation occurs between dark-laminae thickness and light-laminae thickness. This correlation suggests that heavy winter rainfall and intense spring upwelling were the most common seasonal climates during those times that marine varves were preserved. However, heavy winter rainfall followed by intense spring upwelling is not a common seasonal succession in today's climate patterns along the U.S. west coast. Today's El Niño conditions typically have heavy winter rainfall followed by weak spring upwelling (thick-dark laminae and thin-light laminae) whereas today's La Niña conditions typically have relatively light winter rainfall followed by relatively intense upwelling (thin dark laminae and thick light laminae).

### **Potential Insolation Maps of the H.J. Andrews Experimental Forest**

---

David Greenland

Department of Geography, University of Oregon, Eugene

Potential clear-sky radiation receipt is modeled for the slopes of the H.J. Andrews Experimental Forest Long-Term Ecological Research site in the foothills of southern Cascade mountains of central Oregon. The modeling method developed by Williams is selected and applied to the forest area for the times of the solstices and equinox as well as mid-month times in January, February, April, and May to completely characterize the seasonal change of potential radiation of the location. The method uses an  $82 \times 111$  point grid with a 120 m spacing interval. Resulting maps reveal areas of the forest with extremely steep gradients of potential radiation. These steep gradients have higher absolute values in summer compared to winter. The south-facing slopes which have the highest potential radiation values tend to be at the highest elevations. There are places that receive no direct radiation as far into the year as February. Standard deviation values of potential radiation across the Andrews show the maximum spatial variability to occur in February. There is a decrease in the ratio of diffuse to direct plus diffuse potential radiation from 0.66 at December 22 to 0.23 at June 21. It seems that Lookout Creek approximately divides the Andrews Forest into an area of relatively high potential radiation to the north of the creek and relatively lower potential radiation values to the south of the creek. Potential radiation values seem to be associated with the Andrews GIS data layers of debris flows and predominant tree species zones.

## **Calibration of a Climate Model for Northwestern Mexico**

---

D.E. Jones and R.G. Craig

Department of Water Resources Research Institute, Kent State University, Ohio

We have extended an existing statistically-based climate model of the western United States to provide solutions for northwestern Mexico. Daily data for the 11 northernmost states of Mexico were obtained from national archives in Mexico City and supplied to us through the courtesy of Julio Betancourt (USGS). Maximum temperature, minimum temperature, and precipitation from over 1839 stations are included. Stations with continuous records from 1961 to 1985 were chosen (giving a total of 416) and the 2552 stations with the highest percentages of reporting days were subset for use in calibrating a modified version of the local climate model of Stamm and Gettleman (1995), which predicts monthly maximum temperature and monthly average precipitation from a suite of 22 independent variables.

This version of the LCM did not include two of the original independent variables, and added new ones. Also, both the arithmetic mean value and standard deviation were predicted for five variables: monthly maximum temperature, monthly minimum temperature, monthly temperature range, monthly total precipitation and monthly log (total precipitation).

Independent and dependent variable sets are related through a multiple linear regression analysis. The strength of the relationship for each dependent variable is assessed by use of a multiple correlation coefficient ( $R^2$ ). Both mean monthly maximum temperature and mean monthly minimum temperature have high  $R^2$  values, with that of the minimum temperature being slightly higher. Range of temperature is not as easy to predict. Transforming precipitation degraded the strengths of relationship rather than improving it. Mean values are more precisely predicted than standard deviation. Of the standard deviation, that of precipitation is most precisely predicted.

### **Addendum:**

#### **Paleoclimate and the Solar Insolation/Tidal Resonance Climate Model**

---

Thor Karlstrom  
Seattle, Washington

In climate research instrumental observations of the past 100 years drive speculation on climatic process and global changes in atmospheric circulation. Likewise in paleoclimate research, less precise but much longer time series provide the basis for speculation on ultimate cause(s) and the resulting temporal and spatial patterns of longer term climate change. Recent papers (Karlstrom 1995, 1996) provide detailed analyses of more than 40 high-resolution time series culled from the extensive paleoclimate literature that appear to define cyclical elements of the Solar Insolation/Tidal Resonance Climate Model (Karlstrom 1961 cf.). This paper provides comparable analyses of an additional 20, evidently supportive, climate time series. These tree-ring, historic, pollen, and pluviochronostratigraphic records range in length from 400- to 65,000-years, and spatially from Alaska to Tierra del Fuego, and include both Old World and New World sites. The temporally-defined cycles rang in wavelength from

decades to tens of thousands of years. The presented evidence seemingly fortified previous conclusions that (1) longer term "Ice Age" changes (presumably modulated by Precessional Insolation) were out-of-phase across the Equator, and (2) the superposed complex pattern of secondary cycles (presumably phased by tidal resonances in the atmosphere) were globally synchronous. Analysis of a bioclimate record suggests that differing seasonal timings of fractional higher frequency cycles may contribute to fluctuational variability in biologic time series. The longest pollen records suggest a terrestrial cycle of about 10,000 years, or comparable to that recently noted in higher resolution marine records. When the accumulated number of supportive records is deemed adequate the correlation of secondary cycles can be appreciably improved (within limits of dating uncertainties) by fine-tuning to the theoretical Tidal Model.

### **Diatom, Silicoflagellate and Radiolarian Fluxes in Santa Barbara Basin, California**

Carina B. Lange, F.M.H. Reid, A.L. Weinheimer, L. Riddle, and R. Thunell  
Scripps Institution of Oceanography, University of California, La Jolla

Seasonal fluctuations in the total particle, biogenic opal, diatom, silicoflagellate and radiolarian fluxes were observed in a sediment trap deployed at 540 m in Santa Barbara Basin, California from 12 August 1993 to 11 August 1994. Biogenic opal content varied from about 8.6 to 31.8% of the total mass flux, and CaCO<sub>3</sub> content varied between 5.6 and 57.9%. Diatoms were the main contributor to the opal fraction (mean daily flux of ca.  $4.35 \times 10^5$  valves m<sup>-2</sup>d<sup>-1</sup>) followed by radiolarians (ca.  $6.3 \times 10^3$  skeletons m<sup>-2</sup>d<sup>-1</sup>) and silicoflagellates (ca.  $1.3 \times 10^3$  skeletons m<sup>-2</sup>d<sup>-1</sup>). The biogenic particle composition of the opaline fraction reflected the hydrology patterns of the area with a combination of California Current and California Countercurrent water masses. Diatoms yielded three flux maxima in February, April-May and June 1994. Species composition associated with the flux peaks differed, probably reflecting different sources. *Bacteriastrium furcatum*, resting spores of *Chaetoceros radicans* and a composite of *C. concavicornis*, and resting spores of *C. radicans* and *C. vanheurckii* dominated the diatom assemblages, respectively. In total, 142 diatom taxa were identified. Diatom diversity was lowest during times of highest fluxes. Silicoflagellates peaked in December 1993 with *Dictyocha fibula* as the main contributor.

Total radiolarian flux peaked in October 1993 and during the diatom peak of February 1994. Warm, surface dwelling fauna from the west and/or south contribute most to the October peak. Fauna of less certain origin constitute the February peak. Relative abundance of warm fauna was high beginning in Augusts 1993 peaking in December, and tapering off for the duration of the time series. Conversely, the percentage of deep-living intermediate radiolarians initially was low and increased with time, peaking in May and June 1994. Radiolarian diversity closely resembles total radiolarian flux with high flux and diversity coinciding, in contrast to the diatoms.

## **Long-Term Changes in Phytoplankton Chlorophyll *a* Concentration and Community Composition and Their Relationship to Climate**

---

Peggy W. Lehman

Department of Water Resources, Sacramento

The years after 1977 were characterized by low phytoplankton chlorophyll *a* concentrations and a shift in phytoplankton community composition in the upper San Francisco Bay estuary. The long-term changes reflected interannual variation that was associated with changes in water year type. Water year types are associated with changes in the ENSO climatic signal and patterns of change were consistent with the increase in the frequency and intensity of ENSO events after 1977. For climate to be the driving force for changes in phytoplankton, it must affect mechanisms that control phytoplankton biomass and community composition. The influence of climate on environmental factors was examined using 19 years of physical, chemical, and phytoplankton data collected monthly at 16 stations throughout the estuary. Covariance analysis was used to extract the environmental variation associated with the ENSO climatic signal, and this variation was summarized using principal component analysis. Correlations between the principal component axes and phytoplankton community composition and chlorophyll *a* concentration suggest mechanisms by which climate contributes to long-term changes in phytoplankton communities.

## **Temporal and Spatial Variability of Streamflow in California During the Past 100 Years: An Indicator of Jet Stream Shift and Moisture Source Change**

---

Hong-Chun Li and T-L Ku

University of Southern California, University Park, Los Angeles

We have analyzed streamflow variations recorded at 15 USGS gaging stations in California during the past 90 years or so. The anomalies (departures from the 1960-1990 mean discharge) of streamflow on annual-to-decadal time scales are strongly correlated with precipitation anomalies in each drainage basin. The temporal variations of the 5-year running averages of these records clearly show high/low runoff cycles with a frequency of about 113 years, representing a decadal climate (precipitation) variability. High runoff periods (wet climate) centered around 1982, 1969, 1956, 1940, and 1915. Low runoff periods (dry climate) centered around 1989, 1976, 1962, 1946, and 1932. In addition, the intensity of streamflow during the high runoff periods reveal different spatial patterns. For example, runoff around 1956 was much stronger at the northern California stations than at the southern California stations. In 1993, all stations (four) in southern California showed very high runoff while the other stations showed weakly increased runoff. Although the causes of the decadal climate (precipitation) variability are presently not known with certainty, the use of streamflow records may help us understand the relative strength of moisture sources and shift of the jet stream in atmospheric circulation. Precipitation regimes in California are influenced by three moisture sources: northwesterly flow (polar front) related to the Pacific/North America anomaly, southwesterly flow controlled by the tropic ENSO pattern, and southeasterly flow governed by the summer monsoon. A preliminary assessment shows that variations of California runoff on decadal time scale, but not on annual time scale, are strongly correlated with ENSOs. This implies that the northwesterly flow may be blocked by the subtropical high-pressure system with descending, dry air in

mid-latitude zones when the Southern Oscillation is strong, causing drought in California. When the Southern Oscillation is weak, the northwesterly flow can penetrate farther south and the El Niño event can bring more precipitation from the equatorial Pacific to California. Summer monsoon mainly affects the climate and streamflow in southern California. Strong runoff in 1969 and 1993 recorded by gaging stations in the south may indicate the strengthening of the summer monsoon.

### **Late Glacial Millennial Scale Hydrological Events in Western Great Basin, California and Nevada**

---

Jo C. Lin, W.S. Broecker, S.R. Hemming, I. Hajdas, R.I. Dorn, T. Liu,  
R.F. Anderson, F.M. Phillips, G.I. Smith and G. Bonani  
Lamont-Doherty Earth Observatory of Columbia University, Palisades, New York

The timing of the last major pluvial event and of six distinct desiccation events in Great Basin during late glacial to deglacial period has been investigated through  $^{14}\text{C}$  and U-Th age determinations and  $^{14}\text{C}$  age determinations. U-Th isochron ages of tufas formed on shorelines suggest that the last pluvial event was synchronous in Lake Lahontan and Searles Lake at about 16,500 calendar years B.P. (i.e. between 13,500 and 14,000 radiocarbon years B.P.). Radiocarbon measurements on subvarnish organic matter are consistent with an age of 14,000 radiocarbon years, suggesting that this pluvial event was possibly linked with Heinrich Event #1, the last of a series of major iceberg discharges into the North Atlantic Ocean. The U-Th age determination on six evaporite samples within seven mud-salt interbedded layers in Searles Lake (Lower Salt Unit) suggests close correlation of the millennial-scale climates recorded in Greenland ice cores (Dansgaard-Oeschger events) and Searles Lake between 23,000 years and 35,000 calendar years BP.

Hydrological conditions in the Searles Lake drainage basin appear to have responded to the climate forcing responsible for the millennial-scale climate fluctuations in northern polar region during late glacial time. Dust events in Greenland and hydrological anomalies in the Great Basin point to dramatic changes in zonal atmospheric circulation and to more efficient moisture transport from the tropics to mid-latitudes during each cold phase of the Dansgaard-Oeschger cycles. Geographical distribution of the areas impacted by the last of these events bears a resemblance to that for ENSO-related precipitation anomalies.

### **Uncommonly Cold Half-Decade in the Colorado Front Range**

---

Mark Losleben  
Mountain Research Station, University of Colorado, Nederland

Niwot Ridge is located in the Front Range of Colorado, just to the west of the Denver/Boulder metropolitan area. The instrumented records of over four decades, from two of these sites, C1 at 3300 m and D1 at 3749 m, show an uncommonly cold period beginning in 1981 and continuing through 1985. The cold period is more pronounced at D1, where the average annual temperature is 2.5°C colder than the 44-year annual average.

This cooling is particularly interesting because it occurs without similar cooling just 27 km to the east, and it occurs during a period of general warming in North America. Therefore, in an effort to understand the process(es) causing this cooling, other parameters such as solar radiation, precipitation, and pressure grid anomalies, as well as the temporal and spatial distribution of the colder temperatures, are examined.

### **A Comparison of the Paleosecular Variation Record from Late Pleistocene Lake Estancia with Other Records from Western North America**

H.D. Rowe, B.D. Allen, J.W. Geissman, and R.Y. Anderson  
Geology and Geophysics, Rice University, Houston, Texas

A detailed record of paleosecular variation of the geomagnetic field has been constructed from sediments of latest Pleistocene Lake Estancia. The record reveals millennial-scale paleosecular variation broadly consistent with observations in other contemporaneous records from western North America. This record also contains prominent submillennial-scale variations. Strong agreement among several paleosecular variation curves from western North Americas indicates that these records may be useful for the correlation of sedimentary sequences throughout a large region. The Estancia record, tied to an accurate geochronology, contributes to the construction of a high-fidelity "master curve" for western North America. It is hoped that future records of paleosecular variation may "tie into" this master curve with minimal absolute age dating.

### **Tempus Fugit! PACLIM Data Sets Need Update**

Gary D. Sharp  
California State University, Monterey Bay, Seaside, California

The AGU Geophysical Monograph Volume 55 was a timely and valued product that justified PACLIM's very existence. Looking into the patterns and trends of those, and other time series, questions abound. Where are we now? What has the recent decade's notable variability done to presumed trends in these, now fore-shortened, records? Keeping pace with the extreme weather events of the recent fifteen years has been hectic, and a sure change from the previous few decades' relative monotony. With the broad spectrum of agency and institutional science interests pitching for ever more limited funds, the glitzy doomsday climate warming scenarios appear to have won the day. Is the fundamental message wrong? Would warming be bad? Would cooling be worse? History tells the tale. I would be loath to stop anything that would sustain a general global warming, within reason. Historically, humans thrive during warm, wet periods and suffer tremendous problems during cool, dry epochs-particularly when these are punctuated by warm, wet years with pestilence and disease having created havoc within debilitated societies. The 19976 climate shift and related ecosystem changes over great sections of the globe have begun clear signs of reversal. The Pacific sardine has come and gone again, anchoveta and an array of Peruvian fauna that were prevalent in the 1950s and 1960s are back, and under intense exploitation, once again. The Gulf of Alaska has also warmed and cooled. Perhaps more than ever, the messages from PACLIM need to be brought to the public. Are there any prognostic symptoms in the scope? If so, where?

Opportunities to reflect on the observational basis of most of the climate predictions and trends still come up short of answers, primarily due to inconsistencies between the records, and questions about the presumed causes and effects. It is time for PACLIM participants to readdress their data sets, and bring them up to date.

### **Response of Whitebark Pine Krummholz Leader Release to 20th Century Climate Change in the Sierra Nevada, California**

---

Jacqueline J. Shinker and J.C. King

Laboratory of Tree-Ring Research, University of Arizona, Tucson

Treeline can often sensitively reflect short-term changes in climate. We are particularly interested in whitebark pine (*Pinus albicaulis*) because (1) it is an important tree in the subalpine forests of the Sierra Nevada, and (2) it changes growth form from shrub-like krummholz to upright tree in response to environmental change. At its elevational limits, conditions such as heavy snowpack and icy winds prevent the whitebark pine krummholz from growing above the snowpack. However, given milder conditions, a krummholz will send up one or more vertical stems or leaders. We use cross sections of krummholz leaders at the point where the stem emerges from the top of the krummholz canopy to determine the calendar year in which vertical release occurred. We compare the dates of release to the 20th century climate data from records at Yosemite Valley and Tuolumne Meadows. We find a sharp increase in the number of stem releases during the late 1940s and early 1950s. This corresponds to a steady increase in average June through August temperature seen in the climate record. keyword: dendrochronology, treeline, krummholz

### **A Model Linking Climate to Growth and Dispersal of Saguaro**

---

Lella Shiozawa and R. Craig

Department of Geology, Kent State University, Ohio

Saguaro (*Carnegie gigantea*) is the defining species of the Sonoran Desert, a species whose distribution has changed dramatically during the Holocene and which may be sensitive to future climate change including that associated with a greenhouse effect. To evaluate potential changes in Saguaro distribution, we have developed (in cooperation with the USGS Desert Laboratory) a simulation model that uses high-resolution Monte Carlo solutions of climate and a set of rules for saguaro survival, growth, dispersal, establishment, and mortality. We base our climate solutions on a modified version of the Local Climate model of Stamm and Gettleman (1995) which has been supplemented by calculation of standard deviations as the standard error of the prediction from the regression equations and is solved at a grid resolution of 15 km throughout the Sonoran Desert, including the states of Arizona, Sinaloa, and Sonora.

Using the recently published Plant Atlas of the Sonoran Desert (Turner, et al., 1995) we have identified grid cells in which saguaro are known to occur and extracted LCM solutions of temperature and precipitation for each month at those points. Ranking these, we classify the suitability of the climate in all grid cells according to the calculated 6 and 0 percentile values. Growth rate depends on height and climate state. Precipitation exceeding the 6 percentile range leads

to growth at a slower rate and if precipitation is less than the 0 percentile value, no growth occurs. Height of an exemplar plant in each cell is incremented annually and a height of 2 meters signals dispersal of seeds to adjacent cells. Successful completion of the seedling state (at 100 mm height) requires all months in the 10-year period following germination to lie within the 6% to 94% climate bounds. Random mortality occurs at a height-dependent rate (Pierson, 1995, personal communication).

The model illustrates several phenomena consistent with field observations: (1) elevation-dependent survival, growth, and spreading; (2) geographically varying growth and spreading rates, higher in the more humid east, and (3) spreading from established locations at rates consistent with paleoclimate data. Simulations extending for hundreds of years of stable climate show the dynamic nature of the population.

### **Pandora Moth Outbreaks in Central Oregon: A Dendrochronological Study**

---

James H. Speer, T.W. Swetnam, A. Youngblood, and B. Wickman  
Laboratory of Tree-Ring Research, University of Arizona, Tucson, Arizona

Pandora moth is a frequent defoliator of ponderosa pine in the forests of central Oregon; however, there have been no long-term studies of this insect and its effects on the forest ecosystem. We used dendrochronological techniques to examine timing and intensity of the defoliation through its effect on radial growth. Historical records document the occurrence of past defoliation events in 1893 (Carolin 1968) and 1920-25 (Keen 1937) that show up clearly in the host trees as periods of reduced growth. These reduced growth signatures are a proxy for past defoliation events. We identified 17 episodes of reduced growth over the past 500 years in a site collected in the Deschutt National Forest.

### **Monte Carlo Simulation of Streamflow of the Salt River, Arizona**

---

Marina Timofeyeva and Rachael Craig  
Department of Geology, Kent State University, Ohio

Water resources evaluations for climate change scenarios (such as a greenhouse effect) need to represent both the expected change and the uncertainty in that change. Since water resources such as streamflow and reservoir levels depend on a variety of factors each subject to significant uncertainty, it is desirable to formulate methods of representing that uncertainty in the forcing factors and from this determine the uncertainty in the response variable. We report here progress in the representation of the uncertainty in climate input upon the uncertainty in the resulting estimated hydrologic response. Our simulations are the first to link a stochastic Local Climate Model that is a modified version of that reported by Stamm and Gettleman (1995) and a Snow and Surface Hydrology model based on that of Orndorff (1994). For illustration, we use a 5 km × 5 km grid over an area of 30,805 km<sup>2</sup> which contains the drainage of the Salt River, Arizona. This river forms a critical water supply for the greater Phoenix area, and the utility of the water supply is dependent upon wintertime snowfall and timing of snowmelt.

The results of the LCM are monthly mean maximum daily temperature (TMAX) and total monthly precipitation (PREC). We also derive standard deviations for

TMAX and log (LPREC) as the standard error of the regression of the canonical correlation model. Together they form the spatially-varying parameters of frequency distributions of TMAX (normal) and PREC (lognormal) at each point of a grid. Monte Carlo perturbation of the climate using these parameters provides stochastic input into a mainly deterministic SSHM. Results of the SSHM with this stochastic input are long-term monthly runoff over each grid cell, and discharges for specified drainage which can be compared to observed discharge at the same point.

Comparison of modeled with observed streamflow at Roosevelt Lake shows that mean discharges are very close to the observed values, but the standard deviation of discharge is different. Observed standard deviations are more than an order of magnitude larger than the modeled ones. Analysis of standard deviation of precipitation at 14 stations within the solution domain has shown long-term variations from one 10-year period to another of factors of 2× to 5×. One explanation for the discrepancies in the discharges may be the need to define boundary conditions for solution of the LCM that corresponds to the same time period being tested rather than an average period. Another possible improvement could be to treat standard deviation of TEMP and PREC as further dependent variables in the LCM. We have implemented the second of these two methods.

### **100 Years of Biogenic Silica Flux to the Santa Barbara Basin and Its Relationship to Climate**

Amy L. Weinheimer, D.R. Cayan, C.B. Lange, and Aida Martinez  
Scripps Institution of Oceanography, University of California, La Jolla

Santa Barbara Basin varved sediment is an invaluable resource for reconstructing the ocean/atmosphere of the northeast Pacific. Although various time scales can be studied, we focus on annual resolution of the past century to establish relationships between the biological record preserved in the sediment and instrumental records of the region. These relationships will ultimately be applied to a longer biological record from the SBB for high-resolution modeling of paleoclimate.

The annual total, warmwater, and deep-living radiolarian accumulations to SBB sediments from 1875-1991 were tabulated from two cores. The resulting time series from the two cores are similar and capture several aspects of climate and circulation of the California Current System. For example, fluxes of total land percent warm radiolarians closely resemble regional low frequency (decadal) SST. Deep-living radiolarians and resting spores of upwelling diatoms, indicative of strong southerly transport in the California Current and upwelling, fluctuate at low frequency and exhibit low relative abundance in the late 1980s-1990, similar to the drop observed by others (Roemmich and McGowan, 1995) in zooplankton within the Southern California Bight. Additionally, we have constructed an index with the warm and deep-living fauna, which reflects seasonal atmospheric circulation over the North Pacific.

**Tree-Ring Reconstructions of Winter Climate and  
Circulation Indices for the Southwestern United States:  
Climate Extremes and Their Relationship to Circulation Patterns**

---

Connie A. Woodhouse

Laboratory of Tree-Ring Research, University of Arizona, Tucson

The goal of this research is to investigate the influence of atmospheric circulation on winter climate in the southwestern United States. Previous research of this author identified the key circulation features influential to climate for the period of modern climate records. A set of circulation indices was generated that described important circulation features, including the Southern Oscillation Index, a sea surface temperature index from the equatorial Pacific, a modified Pacific North American index, and two indices that feature a southwesterly low pressure center; the Pacific high/southwestern low and Southwestern trough indices. The spatial and temporal relationships between circulation, as described by the indices and climate (precipitation and temperature) were examined.

In the next phase of research, a network of 75 tree-ring chronologies located throughout the Southwest was used to reconstruct regional winter climate for southern California, Arizona, and western New Mexico. The climate variables reconstructed for the winter season (November-March) were: total precipitation, number of rainy days, and average maximum temperature for each of six regions. Regression models explained 42-71% of the variance in the regional climate series. Reconstructed climate series extend from 1702 to 1983.

In the final stage of this research, the network of tree-ring chronologies has been used to reconstruct the circulation indices. The tree-ring chronologies explain variances in the indices ranging from  $r^2_{adj} = 0.26$  for the winter sea surface temperature index to  $r^2_{adj} = 0.78$  for the Southwestern Trough index. Reconstructed regional climate series and circulation indices were ranked and years of highest and lowest values were compared. Results show that years of climate extremes often coincide with extremes in one or more of the ENSO-related indices (SOI, SST, and/or PNA) and with one or the other of the two southwestern low indices. An examination of the groupings of regions with extreme values in a given year shows that the influence of these circulation features during extreme years is spatially variable. Reconstructed climate and circulation indices both suggest that the 1800s included more dry extremes than the 1700s or 1900s.

## **Appendix A**

# **AGENDA**

---

Thirteenth Annual Pacific Climate (PACLIM) Workshop  
Asilomar Conference Center, Pacific Grove, California  
April 14-17, 1996

PACLIM is a multidisciplinary workshop broadly focused on climate phenomena occurring in the eastern Pacific and western Americas. Its purpose is to understand the climate effects in this region by bringing together specialists from diverse fields including both physical and biological sciences. Time scales range from weather to paleoclimate.

Convened at the Asilomar Conference Center, the atmosphere of the Workshop is intentionally informal, and room and board are provided for the participants. The Workshop is organized by a committee of representatives from several organizations, but historically it has been spearheaded by U. S. Geological Survey scientists. Held annually, the Workshop has benefited from funding and other forms of support from several agencies (public and private).



# AGENDA

Thirteenth Annual Pacific Climate (PACLIM) Workshop  
Asilomar Conference Center, Pacific Grove, California  
April 14-17, 1996

Asilomar Meal Schedules  
Breakfast 7:30-9:00 am  
Lunch 12:00-1:00 pm  
Dinner 6:00-7:00 pm

---

## Sunday Evening

April 14, 1996

Moderator: Don Cayan

- 7:00-7:10      Welcome and Announcements
- 7:10-7:25      The Global Paleoflood Database Project  
K.K. Hirschboeck, M.L. Wood, F. Ni, and V.R. Baker  
Laboratory of Tree-Ring Research  
University of Arizona, Tucson, Arizona
- 7:25-7:45      Recurrence of Highstands of Great Salt Lake, Utah  
Genevieve Atwood, University of Utah
- 7:45 —        SOCIAL GATHERING

---

## Monday Morning

### Invited Talks Extreme Events and Uncommon Episodes

April 15, 1996

Moderator: Caroline Isaacs

- 8:30-9:15      Southern California's "Flood of the Millennium" Occurred Ca. 1605 AD:  
Historical and Multi-Proxy Evidence for Large-Scale Atmospheric Forcing  
Arndt Schimmelmann and C.B. Lange, Indiana University, Bloomington, Indiana
- 9:15-10:00     Salmon Migration and Extreme Climatic Events at Various Scales  
D.J. Blackbourn, Department of Fisheries and Oceans, Canada
- 10:00-10:15    BREAK
- 10:15-11:00    The Large Scale Context for Recent Precipitation Extremes in  
Western North North America  
Tom Murphree, Naval Postgraduate School, Monterey, California
- 11:00-11:45    Historic 1000-Year Storms of California  
Jim Goodridge, Mendocino, California
- 12:00-1:30     LUNCH

---

## Monday Afternoon

### Invited Talks Extreme Events and Uncommon Episodes

April 15, 1996

Moderator: Dan Cayan

- 1:30-2:15      The Top Ten California Floods of the 20th Century  
Maurice Roos, California State Hydrologist, Sacramento

2:15-2:55	Two-Minute Poster Presentations
2:55-3:25	BREAK
3:25-3:45	Modeling and Predicting Intertidal Variations of the San Francisco Bay Salinity Field Noah Knowles, D. Cayan, D.H. Peterson, and R. Uncles U.S. Geological Survey, Menlo Park, California
3:45-4:05	Daily Rainfall Along the U.S. Pacific Coast Appears to Conform to a Square-Root Normal Probability Distribution Raymond C. Wilson, U.S. Geological Survey, Menlo Park, California
4:05-5:00	POSTERS
5:00-7:00	DINNER

---

<b>Monday Evening</b>	<b>Invited Talk</b>	<b>April 15, 1996</b>
	<b>Extreme Events and Uncommon Episodes</b>	

---

7:30-8:15	Increasing Evidence of Severe, Persistent, and Widespread Drought in the Western United States during Medieval Time Scott Stine, California State University, Hayward
-----------	--

---

<b>Tuesday Morning</b>	<b>April 16, 1996</b>
------------------------	-----------------------

---

Moderator: David Blackkbourn

8:30-8:50	Fisheries Catastrophes in Slow Motion: Wind Stress and Sustainable Development Richard H. Parrish, Pacific Fisheries Environmental Group Southwest Fisheries Science Center, Pacific Grove, California
8:50-9:10	The Regional Response of Salmon Populations to Climate Variability in the Northeast Pacific Nathan Mantua, B. Francis, and P. Dell'Arciprete, University of Washington, Joint Institute for the Study of the Atmosphere and Oceans, Seattle, Washington
9:10-9:30	Preliminary Evidence Linking Regional Climate Variability to a Recent and Dramatic Collapse of the Mexican Sardine Fishery Daniel Lluch-Cota, Salvador Lluch-Cota, and Daniel Lluch-Belda CIB-NOR, S.C. Fisheries Research Group
9:30-9:50	Interdecadal Variability in North Pacific Wind and SST Franklin B. Schwing, R. Mendelsohn, and R. Parrish Pacific Fisheries Environmental Group, Pacific Grove, California
9:50-10:30	BREAK
10:30-10:50	The Effects of Climate and Man on the Bering Sea Ecosystem: Developing a Context Robert C. Francis, School of Fisheries, University of Washington, Seattle, Washington
10:50-11:10	A Decadal Change in the North Pacific thermocline and Gyre-Scale Circulation Arthur J. Miller, Daniel R. Cayan, and Warren B. White Scripps Institution of Oceanography, La Jolla, California
11:10-11:30	Potential Global Terrestrial Carbon Sink is 2.5 Times "Missing Sink" Yiqi Luo, Biological Sciences Center, Desert Research Institute, Reno, Nevada
11:30-11:50	Climatic Impacts on Terrestrial Vegetation as Deduced from Leads and Lags in Atmospheric Carbon Dioxide and Temperature Signals Charles D. Keeling and T. Whorf, Scripps Institution of Oceanography, La Jolla, California

12:00-1:30 LUNCH

---

**Tuesday Afternoon** **April 16, 1996**

---

Moderator: John Dracup

- 1:30-1:50 ENSO Connections to Western Canada, the U.S. and Mexico  
Kelly T. Redmond  
Western Regional Climate Center, Desert Research Institute, Reno, Nevada
- 1:50-2:10 Seasonal Streamflow Forecasting in Australia Using the Southern Oscillation Index  
Thomas C. Piechota and J. A. Dracup  
Civil and Environmental Engineering Department, UCLA, Los Angeles, California
- 2:10-2:30 Climate and West Coast Sea Surface Temperature Variability  
John McGowan, L. Dorman, and D. Cayan  
Scripps Institution of Oceanography, La Jolla, California
- 2:30-4:30 POSTERS

---

**Tuesday Evening** **Invited Talk** **April 16, 1996**

---

Introduction: Gary Sharp

- 7:30-8:15 The Salinas River Flood, 1995  
J. Oliver and Rikk Kvitek, Moss Landing Laboratories, Monterey, California

---

**Wednesday Morning** **April 17, 1996**

---

Moderator: Peter Wigand

- 8:30-8:50 Radiocarbon Record of Abrupt Oceanographic Changes in Santa Barbara Basin Over the Past 20,000 Years  
B. Lynn Ingram and J.P. Kennett, University of California, Santa Barbara, California
- 8:50-9:10 The Near-1600 AD Multi-Proxy Puzzle  
Franco Biondi, C.B. Lange, W.H. Berger, and M.K. Hughes  
Scripps Institution of Oceanography, La Jolla, California
- 9:10-9:30 Synoptic Climatology of Beringia Since the Last Glacial Maximum  
Cary J. Mock, Department of Geography, University of Oregon, Eugene, Oregon
- 10:00-10:15 BREAK
- 10:15-10:35 Anoxic Episodes in the California Bight: A Historic Change in Santa Monica Basin and Earlier Episodes  
Lowell D. Stott, University of Southern California, Los Angeles, California
- 10:35-10:55 Comparison of the Timing of Severe Drought Events in the Northern and Southern Great Basin as Indicated in Pollen Records  
Peter E Wigand, Quaternary Sciences Center, Desert Research Center, Reno, Nevada
- 10:55 am CLOSING
- 12:00-1:30 LUNCH



**POSTER PRESENTATIONS**

---

Thirteenth Annual Pacific Climate (PACLIM) Workshop  
Asilomar Conference Center, Pacific Grove, California  
April 14-17, 1996



## POSTER PRESENTATIONS

Thirteenth Annual Pacific Climate (PACLIM) Workshop  
Asilomar Conference Center, Pacific Grove, California  
April 14-17, 1996

Butte Valley, California: A Pollen and Paleomagnetic Record for the Past 3 Ma.

David P. Adam and A.P. Roberts  
California Academy of Sciences, Golden Gate Park, San Francisco, California

Geomorphic Evidence for an Extreme Climate Episode in the  
American Southwest (Younger Dryas)

Roger Anderson and B.D. Allen, Earth and Planetary Sciences Department  
University of New Mexico, Albuquerque, New Mexico

Long-term response of Torrey pine (Southern California) to Coastal Climate:  
precipitation, temperature, and fog.

Franco Biondi, D.R. Cayan, L.G. Riddle, and W.H. Berger  
Scripps Institution of Oceanography, University of California, La Jolla, California

Correlation of Paleoclimate Records from Upper Klamath Lake and from the  
Continental Margin Off California

J.P. Bradbury, W.E. Dean, J.G. Rosenbaum, and R.L. Reynolds  
U.S. Geological Survey, Denver, Colorado

Decadal Variability of Snow in the Western United States

Daniel R. Cayan, Scripps Institution of Oceanography and U.S. Geological Survey  
Larry Riddle, Scripps Institution of Oceanography

Geochemical Characteristics of Sediments on the Peru and California Margins

Walter E. Dean, M.A. Arthur, and J.V. Gardner, U.S. Geological Survey, Denver, Colorado

The Instrumental Record of Climate Variability in the Pacific Northwest:

Laying the Foundations for an Integrated Assessment of Climate Impacts  
Patricia Dell'Arciprete, N. Mantua, and R.C. Francis, University of Washington,  
School of Fisheries, Fisheries Research Institute, Box 357980, Seattle, Washington

Uranium/Calcium Variations in the Reef Coral *Porites lobata*

Stewart J. Fallon, E.M. Cathcart, S.C. Gray, and E. Druffel  
Marine and Environmental Science, University of San Diego, San Diego, California

Correlation of Laminated Late Pleistocene Sediments from the  
Open Continental Slope Off Central California

James V. Gardner  
U.S. Geological Survey, Menlo Park, California

Potential Insolation Maps of the H.J. Andrews Experimental Forest

David Greenland, Department of Geography, University of Oregon, Eugene, Oregon

The Global Paleoflood Database Project

Katherine K. Hirschboeck, M.L. Wood, F. Ni, and V.R. Baker  
Laboratory of Tree-Ring Research, University of Arizona, Tucson, Arizona

Calibration of a Climate Model for Northwestern Mexico

David Jones and R.G. Craig, Department of Geology and Water Resources  
Research Institute, Kent State University, Kent, Ohio

Addendum: Paleoclimate and the Solar Insolation/Tidal Resonance Climate Model

Thor Karlstrom, Seattle, Washington

- Diatom, Silicoflagellate and Radiolarian Fluxes in Santa Barbara Basin, California  
Carina Lange, F.M.H. Reid, A.L. Weinheimer, L.G. Riddle, and R. Thunell  
Scripps Institution of Oceanography, University of California, La Jolla, California
- Long-Term Changes in Phytoplankton Chlorophyll *a* Concentration and  
Community Composition and Their Relationship to Climate  
Peggy W. Lehman, Department of Water Resources, Sacramento, California
- Temporal and Spatial Variability of Streamflow in California during the  
Past 100 Years: An Indicator of Jet Stream Shift and Moisture Source Change  
Hong-Chun Li and T-L Ku, Department of Earth Science,  
University of Southern California, University Park, Los Angeles, California
- Late Glacial Millennial Scale Hydrological Events in  
Western Great Basin, California and Nevada  
Jo C. Lin, W.S. Broecker, S.R. Hemming, I. Hajdas, R.I. Dorn, T. Liu,  
R.F. Anderson, F.M. Phillips, G.I. Smith and G. Bonani  
Lamont-Doherty Earth Observatory of Columbia University, Palisades, New York
- Uncommonly Cold Half-Decade in the Colorado Front Range  
Mark Losleben, Mountain Research Station, University of Colorado, Nederland, Colorado
- A Comparison of the Paleosecular Variation Record from Late Pleistocene  
Lake Eestancia with Other Records from Western North America  
H.D. Rowe, B.D. Allen, J.W. Geissman, and R.Y. Anderson  
Geology and Geophysics, Rice University, Houston, Texas
- Tempus Fugit! PACLIM Data Sets Need Update  
Gary D. Sharp, Cooperative Institute for Research in the Integrated  
Ocean Sciences, California State University, Monterey Bay, Seaside, California
- Response of Whitebark Pine Krummholz Leader Release to  
20th Century Climate Change in the Sierra Nevada, California  
Jacqueline J. Shinker and J.C. King, Laboratory of Tree-Ring Research  
University of Arizona, Tucson, Arizona
- A Model Linking Climate to Growth and Dispersal of Saguaro  
Leila Shiozawa and R.G. Craig, Department of Geology, Kent State University, Kent, Ohio
- Pandora Moth Outbreaks in Central Oregon: A Dendrochronologic Study  
James H. Speer, T.W. Swetnam, A. Youngblood, and B. Wickman  
Laboratory of Tree-Ring Research, University of Arizona, Tucson, Arizona
- Monte Carlo Simulation of Streamflow of the Salt River, Arizona  
Marina Timofeyeva and R.G. Craig  
Department of Geology, Kent State University, Kent, Ohio
- 100 Years of Biogenic Silica Flux to the Santa Barbara Basin and  
Its Relationship to Climate  
Amy L. Weinheimer, D.R. Cayan, C.B. Lange, and A. Martinez  
Scripps Institution of Oceanography, La Jolla, California
- Tree-Ring Reconstructions of Winter Climate and Circulation Indices for the  
Southwestern United States: Climate Extremes and Their Relationship to  
Circulation Patterns  
Connie A. Woodhouse, Laboratory of Tree-Ring Research,  
University of Arizona, Tucson, Arizona

**Appendix C**  
**ATTENDEES**

---

Thirteenth Annual Pacific Climate (PACLIM) Workshop  
Asilomar Conference Center, Pacific Grove, California  
April 14-17, 1996



## ATTENDEES

Thirteenth Annual Pacific Climate (PACLIM) Workshop  
Asilomar Conference Center, Pacific Grove, California  
April 14-17, 1996

David Adam  
California Academy of Sciences  
224 Edgehill Drive  
San Carlos, CA, USA 94070  
Phone: 415/591-7726  
david@quercus.org

Bruce D. Allen  
University of New Mexico  
Dept Earth and Planetary Sciences,  
Albuquerque, NM, USA 87131  
Phone: 505/277-0075  
Fax: 505/277-8843  
allenb@triton.unm.edu

Roger Y. Anderson  
University of New Mexico  
Dept Earth and Planetary Sciences  
Albuquerque, NM, USA 87131  
Phone: 505/277-1639  
Fax: 505/277-8843  
ryand@unm.edu

Genevieve Atwood  
University of Utah  
30 U Street  
Salt Lake City, UT, USA 84103  
Phone: 801/534-1896  
Fax: 801/534-1896

Franco Biondi  
SIO-GRD-UCSD  
UCSD, Mailcode 0215-GRD  
La Jolla, CA, USA 92093-0215  
Phone: 619/534-7174  
Fax: 619/534-0784  
fbiondi@ucsd.edu

David Blackburn  
Canada Dept Fisheries&Oceans  
Pacific Biological Station  
Nanaimo, BC, Canada V9R5K6  
Phone: 604/756-7089  
Fax: 604/756-7138  
blackbournd@pbs.dfo.ca

Randall Brown  
CA Dept. of Water Resources  
3251 S Street  
Sacramento, CA, USA 95816  
Phone: 916/227-7531  
Fax: 916/227-7554  
rbrown@water.ca.gov

Andrea Brunelle  
Northern Arizona University  
Northern Arizona Univ, Box 5694  
Flagstaff, AZ, USA 86011  
Phone: 520/523-1276  
arb@dana.ucc.nau.edu

Richard Casey  
Ocean Research Intl  
650 Loring St  
San Diego, CA, USA 92109  
Phone: 619/483-6507

Daniel R. Cayan  
SIO-CRD, 0224 UCSD  
LaJolla, CA, USA 92093-0224  
Phone: 619/534-4507  
Fax: 619/534-8561  
cayan@seaair.ucsd.edu

Francisco Chavez  
Monterey Bay Aquar. Res. Inst.  
PO Box 628, 7700 Sandholdt Road  
Moss Landing, CA, USA 95039-0628  
Phone: 408/775-1709  
Fax: 408/775-1645  
chfr@mbari.org

Annette Ciccateri  
Ocean Research Intl  
650 Loring St  
San Diego, CA, USA 92109  
Phone: 619/483-6507

Rachael Craig  
Kent State Univ  
Kent State Univ  
Kent, OH, USA 44242  
Phone: 216/672-7987  
Fax: 216/672-7949  
rcraig@gilbert.kent.edu

Robert Curry  
P.O. Box 770  
Soquel, CA, USA 95064  
Phone: 408/582-4098  
Fax: 408/426-9604

Walt Dean  
USGS  
Box 25046, DFC, MS939  
Denver, CO, USA 80225  
Phone: 303/236-5760  
Fax: 303/236-0459  
wdean@usgs.gov

Pat Dell'Arciprete  
School of Fisheries, Fish.Res.Ins.  
University of Washington 357980  
Seattle, WA, USA 98115  
Phone: 206/685-1616  
Fax: 206/685-7471  
patricia@u.washington.edu

John A. Dracup  
Dept. Civ & Env Eng.  
5732 Boelter Hall, UCLA  
P.O. 951593  
LosAngeles, CA, USA 90024-1593  
Phone: 310/825-2176  
Fax: 310/206-7245  
dracup@seas.ucla.edu

Robert Dull  
UC Berkeley, Dept Geography  
501 Earth Sciences Bldg, UC  
Berkeley, CA, USA 94705  
Phone: 510/643-8108  
Fax: 510/642-3370  
robert@pollen1.berkeley.edu

Stewart Fallon  
Univ San Diego  
3323 Oliphant St  
San Diego, CA, USA 92106  
Phone: 619/260-4600 X-2833  
sfallon@pwa.acusd.edu

Robert C. Francis  
University of Washington  
FRI, Box 357980, Univ of Washington  
Seattle, WA, USA 98195  
Phone: 206/543-7345  
Fax: 206/685-7471  
rfrancis@fish.washington.edu

James V. Gardner  
USGS  
345 Middlefield Rd, MS 999  
Menlo Park, CA, USA 94025  
Phone: 415/354-3087  
Fax: 415/354-3191  
jim@octopus.wr.usgs.gov

Don Gautier  
USGS  
Box 25046, DFC, MS960  
Denver, CO, USA 80225  
Phone: 303/236-5740  
Fax: 303/236-8822  
gautier@bpgsvr.cr.usgs.gov

James D. Goodridge  
PO Box 970  
Mendocino, CA, USA 95460  
Phone: 707/937-4709  
Fax: 707/937-5436

David Greenland  
Dept Geography, Univ Oregon  
Eugene, OR, USA 97403-1251  
Phone: 541/346-4541  
Fax: 541/346-2067  
greenlan@oregon.uoregon.edu

Martha L. Hemphill  
Quaternary Sciences Center  
Desert Research Institute  
PO Box 60220  
Reno, NV, USA 89506  
Phone: 702/673-7407  
Fax: 702/673-7397  
hemphill@maxey.dri.edu

Steve Holets  
Pacific Gas & Electric Co  
77 Beale St, Rm 1651  
San Francisco, CA, USA 94177  
Phone: 415/973-4530  
Fax: 415/973-1521

Lynn Ingram  
Dept Geography, UC Berkeley  
Dept Geography, Univ California  
Berkeley, CA, USA 94720  
Phone: 510/643-1474  
ingram@violet.berkeley.edu

Caroline Isaacs  
USGS  
345 Middlefield Rd, MS 999  
Menlo Park, CA, USA 94025  
Phone: 415/354-3014  
Fax: 415/354-3224  
cisaacs@octopus.wr.usgs.gov

Barb Johnson  
USGS  
Box 25046, DFC, MS934  
Denver, CO, USA 80225  
Phone: 303/236-5715  
Fax: 303/236-8822  
barb@bpgsvr.cr.usgs.gov

Thor Karlstrom  
USGS - Retired  
4811 SW Brace Pt Dr  
Seattle, WA, USA 98136  
Phone: 206/938-7087

Charles D. Keeling  
SIO, UCSD  
LaJolla, CA, USA 92093-0220  
Phone: 619/534-4230 X11  
Fax: 619/534-8814  
cdkeeling@ucsd.edu

Tim Klett  
USGS  
Box 25046, DFC, MS960  
Denver, CO, USA 80225  
303/236-5740  
Fax: 303/236-8822  
tklett@bpgsvr.cr.usgs.gov

Noah Knowles  
SIO/CRD, MC 0224  
La Jolla, CA, USA 92093-0224  
Phone: 619/534-2764  
Fax: 619/534-8561  
nknowles@sdcc3.ucsd.edu

Rikk Kvitek  
Moss Landing Marine Laboratories  
P.O. Box 950  
MossLanding, CA, USA 95039  
Phone: 408/633-7251  
Fax: 408/633-5642

John Laurmann  
Environmental Policy Forum, Stanford Univ  
3372 Martin Rd  
Carmel, CA, USA 93923  
Phone: 408/625-6696

Peggy W. Lehman  
Dept of Water Resources  
3251 S Street  
Sacramento, CA, USA 95816  
Phone: 916/227-7551  
Fax: 916/227-7554  
plehman@water.ca.gov

Hong-Chun Li  
University of Southern California  
Department of Earth Sciences, USC  
Los Angeles, CA, USA 90089-0740  
Phone: 213/740-6736  
Fax: 213/740-8801  
hli@earth.usc.edu

Jo Chiu-Fang Lin  
Geography, UC Berkeley  
Dept Geography, UC  
Berkeley, CA, USA 94720  
Phone: 510/642-1281  
Fax: 510/642-3370  
jolin@violet.berkeley.edu

Daniel Lluch-Cota  
CIB-NOR, S.C. Fisheries Research Group  
P.O. Box 128  
LaPaz, BCS, Mex 23000  
Phone: 11253633  
Fax: 11253625  
slluch@cibnor.conacyt.mx

Salvador Lluch-Cota  
CIB-NOR, S.C. Fisheries Research Group  
P.O. Box 128  
La Paz, BCS, Mex 23000  
Phone: 11253633  
Fax: 11253625  
slluch@cibnor.conacyt.mx

Mark Losleben  
Mountain Research Station  
University of Colorado  
818County Rd 116  
Nederland, CO, USA 80466  
Phone: 303/492-8842  
Fax: 303/492-8842  
markl@culter.colorado.edu

Yiqi Luo  
Desert Research Institute  
Biological Sciences Center  
Reno, NV, USA 89512  
Phone: 702/674-7562  
Fax: 702/673-7485  
yluo@maxey.dri.edu

Nathan Mantua  
Univ. Washington, JISAO  
Univ. Washington, JISAO  
Box 354235  
Seattle, WA, USA 98195-4235  
Phone: 206/616-5347  
Fax: 206/616-5346  
mantua@atmos.washington.edu

Arthur J. Miller  
Scripps Institution of Oceanography  
CRD-0224, SIO-UCSD  
La Jolla, CA, USA 2093-0224  
Phone: 619/534-1868  
Fax: 619/534-8561  
ajmiller@ucsd.edu

Cary Mock  
University of Oregon  
Department of Geography,  
Eugene, OR, USA 97403  
Phone: 541/346-0466  
Fax: 541/346-2067  
cmock@oregon.uoregon.edu

Tom Murphree  
NPS Meteorology  
Naval Postgraduate School  
Monterey, CA, USA 93943-5114  
Phone: 408/656-2723  
Fax: 408/656-3061  
murphree@osprey.met.nps.navy.mil

John Oliver  
Moss Landing Marine Laboratories  
P.O. Box 950  
MossLanding, CA, USA 95039  
Phone: 408/633-7250  
Fax: 408/633-5642

Richard Parrish  
PFEG NMFS NOAA Pacific Fisheries Env. Grp.  
1352 Lighthouse Ave  
Pacific Grove, CA, USA 93950  
Phone: 408/648-9033  
Fax: 408/648-8440

Thomas Piechota  
UCLA Civil & Env. Eng.  
3066 Engineering I  
Los Angeles, CA, USA 90024-1593  
Phone: 310/206-8612  
Fax: 310/206-7245  
piechota@seas.ucla.edu

Mitchell J. Power  
Northern Arizona University  
Bilby Research Center  
616W. Tombstone Ave.  
Flagstaff, AZ, USA 86001  
Phone: 520/774-9464  
Fax: 520/523-7423  
mjp3@dana.ucc.nau.edu

Kelly Redmond  
Western Regional Climate Center  
PO Box 60220  
Reno, NV, USA 89506-0220  
Phone: 702/677-3139  
Fax: 702/677-3243  
krwrcc@sage.dri.edu

Larry Riddle  
CRD/SIO/UCSD/0224  
La Jolla, CA, USA 92093-0224  
Phone: 619/534-1869  
Fax: 619/534-2240  
lriddle@ucsd.edu

Maurice Roos  
Calif Dept Water Resources  
PO Box 219000, 3310 El Camino Ave, Suite200  
Sacramento, CA, USA 95821-9000  
Phone: 916/574-2625  
Fax: 916/574-2767  
mroos@water.ca.gov

Harold Rowe  
Rice University  
Dept Geology and Geophysics, Rice University,  
MS-126, 6100 MainSt  
Houston, TX, USA 77005  
Phone: 713/666-4193  
Fax: 713/285-5214  
hrowe@rice.edu

Arndt Schimmelm  
Dept. Geological Sciences  
Indiana Univ  
Bloomington, IN, USA 47405-1403  
Phone: 812/855-7645  
Fax: 812/855-7961  
aschimme@indiana.edu

Frank Schwing  
PFEG NMFS Pacific Fisheries Environmental  
Group  
1352 Lighthouse Ave  
Pacific Grove, CA, USA 93950  
Phone: 408/648-9034  
Fax: 408/648-8440  
fschwing@pfe.noaa.gov

Gary Sharp  
California State University, Monterey Bay  
100 Campus Center, Bldg 3754  
Seaside, CA, USA 93955-8001  
Phone: 408/582-3840  
Fax: 408/582-3656  
gary\_sharp@monterey.edu

Jacqueline J. Shinker  
University of Arizona  
Laboratory of Tree-Ring Research  
1433 E. Elm Street  
Tucson, AZ, USA 85719  
Phone: 520/323-6083  
Fax: 520/621-6464  
shinkerj@geo.arizona.edu

Leila Shiozawa  
Kent State Univ, Dept Geology  
510 Jeanette Dr.  
Richmond Heights, OH, USA 44143  
Phone: 216/486-0227  
Fax: 216/672-7949  
leila@gilbert.kent.edu

Lawrence H. Smith  
U.S. Geological Survey, WRD  
2800 Cottage Way, Rm. W-2233  
Sacramento, CA, USA 95825  
Phone: 916/979-2615x395  
Fax: 916/979-2668  
lhsmith@usgs.gov

James H. Speer  
Laboratory of Tree-Ring Research  
LTRR, University of Arizona  
Tucson, AZ, USA 85721  
Phone: 520/621-6463  
Fax: 520/621-8229  
jspeer@ltrr.arizona.edu

John Stamm  
California State University, Monterey Bay  
ESSP 100 Campus Center  
Seaside, CA, USA 93955-8001  
Phone: 408/582-3743  
john\_stamm@monterey.edu

Scott Stine  
California State University, Hayward  
1450 Acton Crescent  
Berkeley, CA, USA 94702  
Phone: 510/841-6940  
Fax: 510/841-1430  
swstine@aol.com

Lowell D. Stott  
University of Southern California  
Dept Earth Sciences  
University of Southern California  
Los Angeles, CA, USA 90089-0740  
Phone: 213/740-5120  
Fax: 213/740-8801  
stott@usc.edu

Robert N. Swanson  
Climatological Consulting Corp  
1216 Babel Ln  
Concord, CA, USA 94518  
Phone: 510/676-2228  
Fax: 510/676-2228

Jonathon Swinchatt  
EarthVision, Inc  
52 Cook Hill Rd  
Cheshire, CT, USA 6410  
Phone: 203/250-9311  
Fax: 203/699-0865  
swinchatt@aol.com

Sus Tabata  
Inst Ocean Sciences  
PO Box 6000, 9860 West Saanich Road Sidney,  
BC, Canada V8L4B2  
Phone: 604/363-6573  
Fax: 604/363-6746  
tabata@ios.bc.ca

Marina Timofeyeva  
Kent State Univ, Dept Geology  
6600 Alpha Dr., Apt. 211  
Kent, OH, USA 44240  
Phone: 216/673-0593  
Fax: 216/672-7987  
marina@gilbert.kent.edu

G. James West  
USBR  
3429 Oyster Bay  
Davis, CA, USA 95616  
Phone: 916/979-2478  
Fax: 916/979-2450  
jwest@2mp700.mp.usbr.gov

Peter E. Wigand  
Quaternary Sciences Center, Desert Research  
Institute 7010 Dandini Blvd, PO Box 60220  
Reno, NV, USA 89506  
Phone: 702/673-7387  
Fax: 702/673-7397  
pwigand@maxey.dri.edu

Raymond C. Wilson  
USGS  
345 Middlefield Road, MS 998  
Menlo Park, CA, USA 94025  
Phone: 415/329-4892  
Fax: 415/329-5390  
rwilson@mojave.wr.usgs.gov

Michelle Lee Wood  
Laboratory of Tree-Ring Research, Univ Ariz  
105 West Stadium, Univ Arizona  
Tucson, AZ, USA 85721  
Phone: 520/621-9731 or 6469  
Fax: 520/621-8229  
mlwood@ltr.arizona.edu

Connie Woodhouse  
Lab. Tree-Ring Research  
Univ. Arizona  
Tucson, AZ, USA 85721  
Phone: 520/621-9732 or 520/621-8229  
grad7@ccit.arizona.edu

James R. Young  
So Cal EdPO Box 800, 2244 Walnut Grove Avenue  
Rosemead, CA, USA 91770  
Phone: 818/302-9191  
Fax: 818/302-9730  
youngjr@sce.com



